AgriLIFE RESEARCH & EXTENSION
Texas A&M System

TEXAS A&M UNIVERSITY

COLLEGE OF AGRICULTURE
AND LIFE SCIENCES

TR-350
2009

Texas A&M University – Lake Granbury and Bosque River Assessment

Final Scientific/Technical Report

November 26, 2008

Texas Water Resources Institute Technical Report
April 2009

Texas Water Resources Institute
make every drop count

AgriLIFE RESEARCH
Texas A&M System

Texas A&M University – Lake Granbury and Bosque River Assessment

Final Scientific/Technical Report
November 26, 2008

DOE Award Number: DE-FG02-06ER64255

Recipient: Texas Agricultural Experiment Station, Bryan, Texas (as of Jan 1, 2008, the agency name changed to: Texas AgriLife Research)

Project Director: Dr. C. Allan Jones, Director, Texas Water Resources Institute

Texas Water Resources Institute
make every drop count

3. Executive Summary:

The "Texas A&M University – Lakes Granbury and Waco, and Bosque River Assessment" project was developed to address two separate water quality issues in Central Texas. Prior work in each waterbody has identified major water quality concerns and laid the ground work for the activities conducted in this project. Lake Granbury and the Bosque River both serve vital roles in the Brazos River watershed. Lake Granbury is a reservoir constructed on the main stem of the Brazos River in Hood County, Texas and provides a potable water supply for over 250,000 area residents, cooling water for a natural gas fired and a nuclear power plant, vital flood control for the city of Waco and a critical economic stimulus for the city of Granbury and surrounding areas. The Bosque River, also in the Brazos River watershed plays a vital role in Central Texas as well; it feeds Lake Waco and supplies water for 200,000 Central Texans.

Lake Granbury has experienced recent toxic blooms of *Prymnesium parvum* (Golden algae) that have resulted in massive fish kills and concerns about general water quality. Lake Waco, a reservoir constructed on the main stem of the Bosque River, has viable *P. parvum* populations, but does not experience harmful blooms. Thus, comparisons between Lakes Granbury and Waco allow for comparisons of environmental conditions leading to bloom formation. Both Lake Granbury and Lake Waco are critical to this region as being primary water supplies, sources of revenue and recreational hotspots. This project addressed these water quality issues by providing critical information about the relationships between the contaminants (Golden algae and nutrients) and environmental factors in the respective watersheds. In Lakes Granbury and Waco, various plankton, nutrient and water quality samples were collected at fixed-location stations, and high-resolution spatial maps were generated using an on-board dataflow technology of various plankton and water quality parameters. Linkages between the toxic Golden algae blooms and environmental conditions were examined. In addition, a numerical model of Lake Granbury was developed and continues to be refined. Bloom forming processes were investigated with this model.

In the Bosque River, elevated nutrient levels have lead to increased aquatic vegetation growth and subsequent taste and odor problems in Lake Waco. This project enlists physically based computer modeling to determine the nutrient and sediment removal capabilities of implementing recommended Best Management Practices (BMPs) throughout the watershed. Results of this project indicate areas where specific management strategies will provide the most pollutant control for the cost to implement the practice.

Each project is focused on addressing specific water quality issues in a specific water body, but each will provide valuable information that can be used to correct water quality concerns in other watersheds with similar problems. Ultimately, the project will result in improved water quality for consumptive, recreational, and industrial uses and will help to sustain the economic stimulus resulting from these water bodies.

4. Project Goals and Accomplishments:

Task 1: Water Quality Program for Lake Granbury, Texas

Objectives:

- To conduct monthly system-wide sampling of Lake Granbury using a newer technology, Dataflow, where measured parameters include chlorophyll *a*, dissolved organic matter, transparency, photosynthetically active radiation, conductivity, and temperature.
- To conduct monthly fixed-station sampling in Lake Granbury where surface water measurements include inorganic nutrients (NO_3^-, NO_2^-, NH_4^+, PO_4^{3-}, SiO_2), total and dissolved organic carbon, phytoplankton biomass and community composition, coliform bacteria concentration, and toxicity; and profile data include various water quality parameters (DO, pH, temperature, conductivity, turbidity, oxidation-reduction potential).
- To investigate potential temporal and spatial linkages between *P. parvum*, coliform bacteria, toxicity, and the physicochemical environment using multivariate statistics.
- To further develop a numerical model that is designed to explore factors that influence *P. parvum* demographics.

Accomplishments:

The data records for Lakes Granbury and Waco span September 2006 through August 2008, and September 2007 through August 2008, respectively, which corresponds to the initiation of the project in 2006 and the expansion of the project in 2007.

- *High-Resolution Spatial Mapping*

  We measured spatial patterns of water quality in Lakes Granbury and Waco (see Appendix A) at monthly intervals with Dataflow, a high-speed, flow-through measurement apparatus developed for mapping physicochemical parameters in shallow aquatic systems (Madden and Day 1992). We used this integrated instrument system to concurrently measure chlorophyll *a*, dissolved organic matter, transparency, salinity, and temperature from a boat running closely spaced transects. Measurements were taken at 4-second intervals from ~20 cm below the surface. An integrated GPS was used to simultaneously plot sample positions, allowing geo-referencing of all measurements for each variable.

  GPS and dataflow information were used to create highly detailed contour maps of water quality parameters in relation to physiographic features. We also collected discrete water samples from the flow-through system during our continuous sampling for laboratory analysis of multiple parameters that were used to calibrate the dataflow unit. In addition to these samples, we measured profiles of water quality parameters that include dissolved oxygen and temperature to determine the degree of stratification of the water column.

High-resolution spatial maps are provided in Appendix E for Lake Granbury, and Appendix G for Lake Waco. The maps are as follows:

- *Sampling of Fixed Stations*

During each Dataflow trip we sampled fixed-location stations, which enabled us to characterize the plankton seasonal succession pattern (phytoplankton and zooplankton) and determine seasonal changes in various water quality parameters (inorganic nutrients, toxicity, pH, temperature, dissolved oxygen, Secchi depth). We sampled 20 fixed-position stations in Lake Granbury (Figure A1) and 10 stations in Lake Waco (Figure A2).

Estimates of total phytoplankton biomass and biomasses of higher taxa were achieved by measuring concentrations of phytopigments. Quantification of phytopigments followed Pinckney et al. (1998). Briefly, filters containing phytopigments were sonicated in 100% acetone (3 ml) for 30 seconds and then extracted in the dark for 20-24 h at -20° C. Extracts were filtered (0.2 µm) and injected (300 ul) into an HPLC system equipped with reverse-phase C_{18} columns in series (Rainin Microsorb-MV, 0.46 x 10 cm, 3mm, Vydac 201TP, 0.46 x 25cm, 5mm). A nonlinear binary gradient, adapted from Van Heukelem et al. (1994), was used for pigment separations. Solvent A consisted of 80% methanol and 20% ammonium acetate (0.5M adjusted to pH 7.2), and Solvent B was 80% methanol and 20% acetone. Absorption spectra and chromatograms were acquired using a Shimadzu SPD-M10av photodiode array detector, where pigment peaks were quantified at 440 nm.

Using the measured phytopigment concentrations, biomasses of higher phytoplankton taxa were estimated with CHEMTAX. CHEMTAX is a matrix factorization program that enables the user to estimate the abundances of higher taxonomic groups from concentrations of pigment biomarkers (Mackey et al. 1997, Wright et al. 1996). The program uses a steepest descent algorithm to determine the "best fit" of an unknown sample to an initial estimate of pigment ratios for targeted algal taxa. The taxa used in the analysis were cyanobacteria, euglenophytes, chlorophytes, prymnesiophytes, cryptophytes and diatoms, which were selected because of their prevalence in Lakes Granbury and Waco.

Enumeration of *P. parvum* population density was performed using a settling technique (Utermöhl 1958). A 0.5-1 ml subsample was taken out of a well-mixed sample (preserved using glutaraldehyde, 3% v/v). Subsamples were settled for a 24 h period, then counted using an inverted, phase-contrast, light-microscope (400x, Leica Microsystem Inc.). Depending on the density of material in the samples, a range of 15-50 randomly selected fields of view were counted per sample, which resulted in ~200 *P. parvum* cells counted per sample.

While examining the phytoplankton samples for *P. parvum* cells, we observed other phytoplankton species present and the condition of cells. Specifically, we looked for the presence of other HAB species common to Texas lakes (e.g., multiple cyanobacteria that will include *Microcystis*, *Anabaena* and *Cylindrospermopsis*), for signs of algal pathogens (e.g., remains of lysed cells and

presence of parasitic fungi), and took note of the dominant taxonomic groups present in each sample.

Our sampling also included enumeration of zooplankton and bacteria. Zooplankton were collected using a 12-liter Schindler trap, concentrated to 50 ml and preserved in 2% buffered formalin. Subsamples, ~10 ml, were settled for a 24 h period, then counted using an inverted, phase-contrast, light-microscope (40x and 200x, Leica Microsystem Inc.). For each individual counted, geometric shapes were determined that best corresponded to the shape of the zooplankter and dimensions were measured that enabled calculation of the individual's biovolume (Wetzel and Likens 1991). Identification was to the taxonomic level of genus. For bacteria (Lake Granbury only), samples were preserved using paraformaldehyde and prepared for enumeration by adding a fluorescent DNA stain (Rigler 1966) to 1 mL of sample, then filtered through a 25 mm diameter black filter (Hobbie et al. 1977). Counts were performed using epifluorescent microscopy and our enumeration technique resulted in ~100 to ~300 cells counted per sample.

Samples for nutrient analyses were filtered through Whatman GF/F filters (pore size ~0.7 μm) and frozen for transport to the laboratory. Using autoanalyzer methodology (Armstrong and Sterns 1967, Harwood and Kuhn, 1970), analyses included nitrate (NO_3), nitrite (NO_2), ammonia (NH_4), orthophosphate (PO_4) and silicate (SiO_3).

Since toxins produced by *P. parvum* under various physiological states are not fully understood, standards for measuring concentrations of toxins are not available at this time. Toxicity can be estimated, however, using other methods. In previous studies, researchers commonly employed an *in vitro* hemolytic assay (Johannson and Granéli 1999, Barriero et al. 2005, Uronen et al. 2005) or non-standardized *in vivo* bioassays to assess biological effects of *P. parvum* cultures under nutrient limitation. In our previous research (see Roelke et al., 2007), ambient toxicity was evaluated rigorously using a standardized 24 h static acute toxicity assay with the fathead minnow (*P. promelas*) model and a standardized 10 day static renewal chronic toxicity test with a cladoceran (*D. magna*) model, generally following standardized aquatic toxicology methodology (US EPA 1994, 2002).

Samples were collected from Lakes Granbury and Waco and transported to the laboratory where toxicity tests were initiated within 24 hrs. To evaluate toxicity relationships among treatment combinations, ambient samples were diluted using a 0.5 dilution series with reconstituted hard water (RHW), which was performed according to US EPA recommendations (US EPA 2002). This dilution approach is routinely used to evaluate water quality of surface waters because it allows for assessment of relative extracellular toxicity among samples if an undiluted ambient sample is acutely toxic.

For each *P. promelas* toxicity test sample from each experimental unit, three replicate chambers with 7 organisms per chamber were used to assess toxicity at each dilution level. *D. magna* bioassays followed established US EPA protocols

(US EPA 1994). RHW, was prepared according to standard methods (APHA 1998), and used as control treatment water for all toxicity assays. Alkalinity (mg/L as $CaCO_3$) and hardness (mg/L as $CaCO_3$) of RHW was measured potentiometrically and by colorimetric titration, respectively, before initiation of acute studies (APHA 1998). Specific conductance (µS/cm), pH and dissolved oxygen (mg/L) of RHW was measured before toxicity testing. All toxicity tests were performed in climate controlled chambers at 25 ±1°C with a 16:8 hour light-dark cycle. Less than 48 h old fathead minnow larvae were fed newly hatched *Artemia* nauplii two hours before initiation of testing (US EPA 2002). *D. magna* were fed a Cerophyll®/green algae suspension daily, which was prepared according to methods reported previously (Brooks et al. 2004, Dzialowski et al. 2006). LC_{50} values for fathead minnow toxicity tests were estimated as percentage of ambient sample using Probit (Finney 1971) or Trimmed Spearman Karber (Hamilton et al. 1977) techniques, as appropriate.

Contour plots of fixed station data are provided in Appendices B and C for Lake Granbury, and Appendix F for Lake Waco.

- *Statistical analysis*

  For the Lake Granbury data, regressions were performed comparing dissolved organic carbon, total bacteria, fecal coliform bacteria, *E. coli* and *P. parvum* using fixed station data (stations 1 through 10) that spanned September 2006 to August 2007 (our first analysis). This corresponded to a period spanning an intense, lake-wide *P. parvum* bloom, and all stations included in the analysis were located along the main body of the lake. Fixed station data (stations 1 through 10, stations A through J) spanning September 2006 to August 2008 were used in our second analysis. This period spanned a *P. parvum* bloom year and a non-bloom year, and included data from stations located along the main body of the lake and from locations within coves of long hydraulic residence time.

  Regressions are provided in Appendix D.

- *Numerical model*

  A seasonally forced 1-D model was constructed that predicts both summer and winter blooms of P. parvum under varying modeling conditions. In each situation, the model predicts that blooms will occur in association with declines in phosphates, nitrates and salinity levels. Work will continue to refine the model as more data are collected.

  A more detailed description of the model can be found in Section 7 and Appendixes H and I at the end of this report.

References

American Public Health Association, American Water Works Association, Water Environment Foundation (1998) Standard Methods for the Examination of Water and Wastewater, 20th ed. American Public Health Association, Washington, DC, USA.

Armstrong FA, Sterns CR (1967) The measurement of upwelling and subsequent biological processes by means of the Technicon Autoanalyzer and associated equipment. Deep-Sea Res I 14:381-389.

Barreiro A, Guisande C, Maneiro I, Lien TP, Legrand C, Tamminen T, Lehtinen S, Uronen P, Granéli E (2005) Relative importance of the different negative effects of the toxic haptophyte Prymnesium parvum on Rhodomonas salina and Brachionus plicatilis. Aquat Microb Ecol 38:259-267.

Brooks BW, Stanley JK, White JC, Turner PK, Wu KB, La Point TW (2004) Laboratory and field responses to cadmium in effluent-dominated stream mesocosms. Environ Toxicol Chem 24:464-469.

Dzialowski EM, Turner PK, Brooks BW (2006) Physiological and reproductive effects of β-adrenergic receptor antagonists on Daphnia magna. Arch Environ Contam Toxicol 50:503-510.Harwood JE, Kuhn AL (1970) A colorimetric method for ammonia in natural waters. Water Res 4:805-811.

Finney DJ (1971) Probit Analysis, 3rd ed. Cambridge University Press, London, 333 p.

Hamilton MA, Russo RC, Thurston RV (1977) Trimmed Spearman-Karber method for estimating median lethal concentrations in toxicity bioassays. Environ Sci Tech 117:714-719; correction 12:417(1978).

Hobbie, J. E., R. J. Daley and S. Jasper. 1977. Use of nuclepore filters for counting bacteria by fluorescence microscopy. Applied and Environmental Microbiology. 33: 5: 1225-1228.

Johansson, N., and E. Granéli. 1999. Influence of different nutrient conditions on cell density, chemical composition and toxicity of Prymnesium parvum (Haptophyta) in semi-continuous cultures. J. Exp. Mar. Biol. Ecol. 239: 243-258.

Mackey M, Mackey D, Higgins H, Wright S (1997) CHEMTAX—a program for estimating class abundances from chemical markers: application to HPLC measurements of phytoplankton. Mar Ecol Prog Ser 144: 265-83.

Madden, C.J. and J.W. Day, Jr. 1992. An instrument system for high speed mapping of chlorophyll-a and physico-chemical variables in surface waters. Estuaries 15:421-427.

Pinckney JL, Paerl HW, Harrington MB, Howe KE (1998) Annual cycles of phytoplankton community structure and bloom dynamics in the Neuse River Estuary, North Carolina. Mar Biol 131:371-82.

Roelke D.L., R. Errera, R. Kiesling, B.W. Brooks, J.P. Grover, L. Schwierzke, F. Ureña-Boeck, J. Baker, J.L. Pinckney. 2007. Effects of nutrient enrichment on Prymnesium parvum population dynamics and toxicity: Results from field experiments, Lake Possum Kingdom, USA. Aquatic Microbial Ecology. 46:125-140.

U.S. Environmental Protection Agency (1994) 10-day Chronic Toxicity Test Using Daphnia magna or Daphnia pulex. EPA SOP#2028. Environmental Response

Team, United States Environmental Protection Agency, Washington, DC.

U.S. Environmental Protection Agency (2002) Methods for measuring the acute toxicity of effluents and receiving waters to freshwater and marine organisms. EPA-821-R-02-012. United States Environmental Protection Agency, Washington, DC.

Uronen P, Lehtinen S, Legrand C, Kuuppo P, Tamminen T (2005) Haemolytic activity and allelopathy of the haptophyte Prymnesium parvum in nutrient-limited and balanced growth conditions. Mar Ecol Prog Ser 299:137-148.

Utermöhl H (1958) Zur Vervollkominnung der quantitativen phytoplankton methodik. Mitteilumgen Internationale Verejnigung für Theoretische und Angewandte Limnologie. 9:1-38.

Van Heukelem L, Lewitus AJ, Kana TM, Craft NE (1994) Improved separations of phytoplankton pigments using temperature-controlled high performance liquid chromatography. Mar Ecol Prog Ser 114:303-13.

Wetzel RG, Likens GE (1991) Limnological Analysis. Springer-Verlag, New York.

Wright S, Thomas D, Marchant H, Higgins H, Mackey M, Mackey D (1996) Analysis of phytoplankton of the Australian sector of the Southern Ocean: comparisons of microscopy and size frequency data with interpretations of pigment HPLC data using the 'CHEMTAX' matrix factorization program. Mar Ecol Prog Ser 144:285-298.

Task 2: Best Management Practice – Benefit Verification Infrastructure Improvement Plan for the Bosque River Basin

Objectives:

- To evaluate the Bosque River watershed using the Soil and Water Analysis Tool (SWAT), a physically based computer model, to isolate what locations of the watershed will yield the greatest reductions in pollutant loading from implementing recommended BMPs.
- To analyze a suite of BMPs as recommended by an established scientific advisory committee, and assess the potential pollutant loading reductions for each of the practices.
- To produce a document that details the description, general overview of where the application of the practice is most feasible, what implementation and operation costs can be expect and what potential pollutant removal rate can be expected for each of the recommended BMPs.

Accomplishments:

- The document that describes the recommended BMPs has been published as Texas Water Resources Institute, Technical Report 309 "Descriptions and Expectations of Recommended BMPs for Improving the Bosque River Watershed." This report is currently available online at: http://twri.tamu.edu/project-info/EnvironmentalInfrastructures/
- The report that describes the SWAT modeling analysis and the environmental impacts of implementing selected BMPs has been published as Texas Water Resources Institute, Technical Report 313 "Bosque River Environmental Infrastructure Improvement Plan: Phase II BMP Modeling Report". The report also identified areas of the watershed that will likely result in the greatest decrease in nutrient removal as a result of implementing selected management practices. This report is currently available online at: http://twri.tamu.edu/project-info/EnvironmentalInfrastructures/

5. Summary of Project Activities:

Task 1: Water Quality Program for Lakes Granbury and Waco, Texas

The overarching objective of this research was to further the understanding of factors that influence demographics of *Prymnesium parvum* in Lake Granbury, TX, with an emphasis on bloom initiation and toxicity, and to explore potential relationships between incidences of *P. parvum* blooms and coliform bacteria. Research coupled system-wide high-resolution spatial mapping, fixed-station sampling, and statistical and numerical modeling. Additional information can be gleaned by comparing data from other lakes. As mentioned previously, Lake Waco has viable populations of *P. parvum*, but blooms do not occur there. Specific research objectives were:

- To conduct monthly system-wide sampling of Lakes Granbury and Waco using a newer technology, Dataflow, where measured parameters include chlorophyll *a*, dissolved organic matter, transparency, conductivity, and temperature.
- To conduct monthly fixed-station sampling in Lakes Granbury and Waco where surface water measurements include inorganic nutrients (NO_3^-, NO_2^-, NH_4^+, PO_4^{3-}, SiO_2), total and dissolved organic carbon, phytoplankton biomass and community composition, zooplankton biomass and community composition, and profile data including various water quality parameters (DO, pH, temperature, conductivity, turbidity, oxidation-reduction potential). At Lake Granbury, total and fecal coliform bacteria concentration, as well as *E. coli,* was sampled.
- To investigate potential temporal and spatial linkages between *P. parvum*, coliform bacteria, and the physicochemical environment using multivariate statistics on the Lake Granbury data.
- To further develop a numerical model that is designed to explore factors that influence *P. parvum* demographics.

Preliminary Findings (Figures can be found in the Appendices)

For Lake Granbury, multivariate statistics will be performed on the data matrix when the third year of sampling is completed (second year for 'lettered' stations). This will enable interannual variability to be accounted for in our analyses. For Lake Waco, multivariate statistics will also be performed on the data matrix when the second year of sampling is completed, which again will interannual variability to be accounted for in our analyses.

There are some noteworthy trends in the data presented in this report, however. The intense *P. parvum* bloom and associated toxicity that occurred in Lake Granbury in 2006 did not reoccur in 2007 (Figures B1-3, C1-3). In addition, the bloom in 2006 was patchy in its population density (Figures E2-3), although it was monospecific throughout the lake. The bloom was terminated by very high inflows late in the spring of that year. The high inflows reduced population density of *P. parvum* and lowered salinity throughout the lake (Figures B6, C6). It may be that in 2007 salinities were too low for *P. parvum* to gain a selective advantage over other phytoplankton during the historic period of bloom initiation. Population densities below bloom proportions (10^4 to 10^5 cells liter^{-1}) were present in Lake Granbury throughout the entire period of sampling, however.

Interestingly, *P. parvum* was present in Lake Waco at population densities very similar to those in Lake Granbury (Figures F1-2). Population densities were higher in the winter months when *P. parvum* historically blooms in other Texas lakes. Toxicity was

not detected in Lake Waco (Figure F3).

Some water quality parameters were very similar between the two lakes, and others were not. For example, pH and temperature showed very similar temporal trends in the two lakes (Figures B4-5, C4-5, F4-5), where pH ranged between 7 and 9 a range over which prymnesins are know to produce toxic effects. Salinity, however, was lower in Lake Waco (<0.3 psu) compared to Lake Granbury (as high as 1.5 psu during 2007) (Figures B5, C6, F6). Similarly, Sechhi depth and turbidity were greater (deeper light penetration) in Lake Waco relative to Lake Granbury (Figures B7-8, C7-8, F7-8).

Zooplankton biomass (cladocerans, copepods adults, rotifers and protozoan) appeared lower in Lake Waco compared to Lake Granbury (Figures B9-10, 12-13, C9-10, 12-13, F9-10, 12-13). On the other hand, nutrient concentrations (PO_4 and DIN) were slightly higher in Lake Waco compared to Lake Granbury (Figures B14-15, C14-15, F14-15). It may be that the plankton community composition in Lake Granbury during 2007 was configured in such a way that nutrients resided in organisms more so than in Lake Waco.

For Lake Granbury, trends between dissolved organic carbon, bacteria (total, fecal coliform, *E. coli*) and *P. parvum* are still being analyzed (Figures B2, 16-19, C2, 16-19, D1-12). The simple regressions we provide here show very poor relationships between these parameters, suggesting that causative factors between *P. parvum*, bacteria and potentially leaky septic systems may not be significant. However, only the second year in this data record comprises locations from coves where the hydraulic residence time is much greater than the open water sections of the lake. *P. parvum* did not bloom this past year, likely due to low salinity. It may be that during a bloom year the linkage between *P. parvum*, bacteria and potentially leaky septic systems is significant in the coves. Ongoing sampling may address this question.

This research, coupled to findings from previous research, will increase the understanding of *P. parvum* blooms in Texas, and better enable the development of mitigation and management strategies aimed at preventing harmful blooms.

Task 2: Best Management Practice – Benefit Verification Infrastructure Improvement Plan for the Bosque River Basin

Hypothesis**:** The SWAT model can be employed as an initial step in selecting ideal locations for implementing BMPs to reduce pollutant loading and predict what pollutant load reductions to expect from implementing these practices in the Bosque River watershed.

Approach**:** Information compiled by a scientific advisory committee formed to advise research and implementation activities in the Bosque River watershed was used to guide the approach used in this research and to provide guidance on the validation and calibration of the SWAT model prior to assessing BMP implementation in the watershed. This information included previously collected and verified spatial data sets such as, soils, historical water quality and flow, nutrient application rates, land use and land cover and historical rainfall measurements. The scientific advisory committee also provided a

listing of BMPs that they felt were most feasible for implementation in the Bosque River watershed and applicable implementation criteria (slope, soil types, land uses, etc.) to use in selecting the best implementation sites for selected BMPs.

After the model was set up, calibrated and validated using these data sets, BMP modeling ensued. Each BMP was modeled by implementing the practice in all feasible locations in the watershed according to their implementation criteria and were evaluated to determine what pollutant (sediment and nutrients) load reductions could be expected from implementing those practices in the watershed. Not all practices listed by the scientific advisory committee and described in the BMP Description document (Technical Report 309) could be accurately represented in the model, so expected pollutant reductions could not be developed for all practices. Table 1 presents expected load reductions from specific BMPs implemented in all possible areas of the watershed over a 30 year period; in other words, a best case scenario for BMP implementation.

Table 1: Long-term (30 years) annual average percent reduction at the watershed outlet (load into Lake Waco), with BMPs implemented in all possible areas of the watershed (high, medium, and low priority subwatersheds)

Type of BMP	**Sediment**	**TN**	**TP**	**length (km) or area (km^2) of BMP implementation**
Streambank stabilization	34.6	0.9	4.0	245 km*
gully plug	5.3	4.8	4.9	959 km**
Recharge structures	37.2	24.4	29.6	1302 km**
Conservation tillage	3.0	3.1	-3.3	432 km^2
Terrace	17.2	18.5	27.0	432 km^2
Contour	9.6	10.20	15.60	432 km^2
Grazing management	7.4	5.3	4.0	2820 km^2
Manure incorporation	0.0	1.7	20.9	88 km^2
Filter strip	9.4	15.5	25.7	499 km^2
Removal of current PL-566 structures	-9.3	-15.2	-16.9	

*length of main channel in the subbasins considered
**length of tributary channels within the subbasins considered

Despite all BMPs not being modeled, the outcomes of the project were not adversely affected. Results from the modeling effort clearly show what pollutant removal rates can be expected from implementing specific BMPs in feasible areas of the watershed. Of the practices evaluated, all but Conservation Tillage yielded reductions in pollutant loading. The increase in total phosphorous realized through the usage of conservation tillage is a result of the decrease in soil mixing and increased amount of organic material near the soil surface thus enabling more nutrient loss during runoff events.

Conclusions**:** The results of this project demonstrate that properly located installation of selected BMPs can result in significant reductions of nutrients and sediment loads. Additionally, the watershed's evaluation has resulted in the identification of priority areas in the watershed that have the greatest potential for reducing pollutant loading through the implementation of selected BMPs.

6. Product Descriptions:

Task 1: Water Quality Program for Lake Granbury, Texas

a. Publications/presentations:

Papers:

Errera, R.M., D.L. Roelke, R. Kiesling, B.W. Brooks, J.P. Grover, L. Schwierzke, F. Ureña-Boeck, J.W. Baker, J.L. Pinckney. 2008. The effect of imbalanced nutrients and immigration on Prymnesium parvum community dominance and toxicity: Results from in-lake microcosm experiments, Texas, USA. Aquatic Microbial Ecology. 52: 33-44.

Roelke D.L., R. Errera, R. Kiesling, B.W. Brooks, J.P. Grover, L. Schwierzke, F. Ureña-Boeck, J. Baker, J.L. Pinckney. 2007. Effects of nutrient enrichment on Prymnesium parvum population dynamics and toxicity: Results from field experiments, Lake Possum Kingdom, USA. Aquatic Microbial Ecology. 46:125-140.

Baker, J.W., J.P. Grover, B.W. Brooks, F. Ureña-Boeck, D.L. Roelke, R.M. Errera, R. Kiesling. 2007. Growth and toxicity of Prymnesium parvum (Haptophyta) as a function of salinity, light and temperature. Journal of Phycology. 43:219-227.

Grover, J.P., J.W. Baker, F. Ureña-Boeck, B.W. Brooks, R. Errera, D.L. Roelke, R.L. Kiesling. 2007. Laboratory tests of ammonium and barley straw extract as agents to suppress abundance of the harmful alga Prymnesium parvum and its toxicity to fish. Water Research. 41: 2503-2512.

Presentations:

Grover, J.P., J.W. Baker, D.L. Roelke, and B.W. Brooks. 2008. Mathematical models of population dynamics of Prymnesium parvum. Great Plains Limnology Conference / Oklahoma-Texas Aquatic Research Group meeting, September 25-27, Oklahoma University Biological Station, Willis, Oklahoma.

Grover, J., D. Roelke, B. Brooks, R. Kiesling. 2008. Advancing the understanding of Prymnesium parvum blooms in Texas. Texas Parks and Wildlife, Golden Algae Research Workshop, Buda, Texas, March 14, 2008.

Grover, J., Jason W. Baker, Daniel L. Roelke, Bryan W. Brooks. Mathematical models of population dynamics of Prymnesium parvum in inland waters. OTARG 2008

Roelke, D., B. Brooks, J. Grover. 2008. Golden Algae bloom dynamics and thoughts on management strategies for reservoirs. Granbury Town Hall Meeting, Granbury, Texas, February 20, 2008.

Roelke, D., Leslie Schwierzke, Bryan Brooks, James Grover, Reagan Errera, Theodore Valenti Jr., James Pinckney. Factors influencing Prymnesium

parvum population dynamics in subtropical lakes: The potential role of cyanobacterial allelopathy. TAPMS 2008

Roelke, D., Leslie Schwierzke, Bryan Brooks, James Grover, Reagan Errera, Theodore Valenti Jr. , James Pinckney. Factors influencing Prymnesium parvum population dynamics in subtropical lakes: The potential role of cyanobacterial allelopathy. OTARG 2008

Errera, RM, Pinckney, J, Roelke, DL. Pigment composition of the Texas strain of Prymnesium parvum during log, stationary, and senescent growth phases. 4th Annual HAB Symposium 2007

Gable, G., Roelke, D., J. Grover, B. Brooks, S. Davis, A.-M. Gable, J. Baker, F. Ureña-Boeck, M. Lahousse. 2007. Water quality, P. parvum and fecal coliform monitoring for Lake Granbury, TX. Texas River and Reservoir Management Society.

Gable, G., Roelke, D., J. Grover, B. Brooks, S. Davis, A.-M. Gable, J. Baker, F. Ureña-Boeck, M. Lahousse. 2007. Water quality, P. parvum and fecal coliform monitoring for Lake Granbury, TX. Granbury Town Hall Meeting, Granbury, Texas.

Grover, J., D. Roelke, B. Brooks, S. Davis, G. Gable, A.-M. Gable, J. Baker, J. Stanely, F. Ureña-Boeck, M. Lahousse. 2007. Water quality research for Lake Granbury, TX. Granbury Town Hall Meeting, Granbury, Texas, May 22, 2007.

Roelke, D., J. Grover, B. Brooks, S. Davis, G. Gable, A.-M. Gable, J. Baker, F. Ureña-Boeck, M. Lahousse. 2007. Water quality research for Lake Granbury, TX. Texas Parks and Wildlife, TX Harmful Algal Bloom Workshop, College Station, Texas, March 9, 2007.

Roelke, D., J. Grover, B. Brooks, S. Davis, G. Gable, A.-M. Gable, J. Baker, F. Ureña-Boeck, M. Lahousse. 2007. Water quality research for Lake Granbury, TX. Granbury Town Hall Meeting, Granbury, Texas, February 13, 2007.

Valenti, T., B. Brooks, M. Lahousse, L. Dobbins, J. Grover, D.L. Roelke. 2007. Influences of pH on ambient toxicity of the harmful alga Prymnesium parvum to aquatic life. Society of Environmental Toxicology and Chemistry. Milwaukee, Wisconsin. November 11 – 15, 2007.

Valenti, T., Mieke Lahousse, Susan James, Daniel Roelke, James Grover, Bryan Brooks. Potential factors influencing the pH-dependent aquatic toxicity of Prymnesium parvum Carter (golden algae). SETAC-Houston

Errera, R.M., D.L. Roelke, R.L. Kiesling, B.W. Brooks, J.P. Grover, F. Ureña-Boeck, J. Pinckney. 2006. The role of inorganic nutrients and barley straw extract in the invasion and inhibition of Prymnesium parvum. Aquatic Sciences Meeting, ASLO. Victoria, Canada. June 4-9.

b. Websites: Information from this project, as well as other projects in the watershed, is available online at: http://lakegranbury.tamu.edu. A general project description, a list of collaborators, funding agencies, news stories, technical reports and quarterly progress reports are all available at this site.

c. Networks or collaborations fostered: Thru this and previous projects conducted in the Lake Granbury Watershed, continued collaboration and support has been received from the following groups:

Texas Water Resources Institute
Texas AgriLife Research
Texas AgriLife Extension Service
Texas Commission on Environmental Quality
Brazos River Authority
USDA Natural Resources Conservation Service
Texas Parks and Wildlife Department
Baylor University
University of Texas at Arlington
Hood County, Texas

d. Technologies/Techniques: N/A

e. Inventions/Patent Applications: N/A

f. Other Products: N/A

Task 2: Best Management Practice – Benefit Verification Infrastructure Improvement Plan for the Bosque River Basin

a. Publications: Two reports were developed under this task of the project; they are:

- "Descriptions and Expectations of Recommended BMPs for Improving the Bosque River Watershed." This report was published by the Texas Water Resources Institute as Technical Report 309 and is currently available online at: http://bosque-river.tamu.edu/reports.php
- "Bosque River Environmental Infrastructure Improvement Plan: Phase II BMP Modeling Report." This report was published by the Texas Water Resources Institute as Technical Report 313 and is available online at: http://bosque-river.tamu.edu/reports.php

b. Websites: Information from this project is available online at: http://twri.tamu.edu/project-info/EnvironmentalInfrastructures/. A general project

description, a list of collaborators, funding agencies, technical reports and quarterly progress reports are all available at this site.

c. Networks or collaborations fostered: Thru this and previous projects conducted in the Bosque River Basin, continued collaboration and support has been received from the following groups:

    Texas Water Resources Institute
    U.S. Army Corps of Engineers
    Texas AgriLife Research
    Texas AgriLife Extension Service
    Texas Institute for Applied Environmental Research
    Blackland Research and Extension Center
    Texas A&M University Spatial Sciences Laboratory
    Brazos River Authority
    USDA Natural Resources Conservation Service
    Texas State Soil and Water Conservation Board
    Texas Farm Bureau
    The City of Waco

d. Technologies/Techniques: N/A

e. Inventions/Patent Applications: N/A

f. Other Products: N/A

7. Computer Modeling:

Task 1: Water Quality Program for Lake Granbury, Texas

a. Model description, key assumptions, version, source, and intended use

Briefly, 0- and 1-dimensional models were constructed in which the population dynamics of *P. parvum* were coupled to those of nutrients (nitrate, phosphate). A suite of five 0-dimensional models was developed, which differed in the number of algal populations competing with *P. parvum* (0, 1, or 4) and whether the competitor types included cyanobacteria exerting allelopathic effects on *P. parvum*. A single 1-dimensional model was developed, with no additional algal populations competing with *P. parvum*. All models take input data from observations of lake conditions (temperature, irradiance, salinity, zooplankton grazing, dilution by flows, nutrient supply) and produce predicted dynamics of *P. parvum* population density, densities of other algal populations (if present), and dissolved concentrations of nitrate and phosphate.

Thorough descriptions of the models are provided in appendices to this report. **Appendix 1. Modeling Overview** summarizes the documentation and electronic files provided; **Appendix 2. Draft Modeling Manuscript** is a manuscript that has been submitted to the *Journal of the American Water Resources Association* for publication in the special collection on "golden algae" to be published in conjunction with an upcoming symposium on the topic; **Electronic Appendix** is a CD containing (1) Microsoft Word documents summarizing various versions and model runs, including all of those used in composing the draft manuscript; (2) Microsoft Excel files containing all input and output data summarized in these documents; and (3) source code for all programs used.

b. Performance criteria for the model related to the intended use

These are fully summarized in the appendices. Briefly, the models constructed here take input data from observations of lake conditions (temperature, irradiance, salinity, zooplankton grazing, dilution by flows, nutrient supply) and produce predicted dynamics of *P. parvum* population density, densities of other algal populations (if present), and dissolved concentrations of nitrate and phosphate. One year of observational data from Lake Granbury was available to use as input and simulations of dynamics over multiple years were obtained by repeating these inputs as an annual cycle. Simulations quickly converged to annually periodic dynamics that were taken as predictions. These predictions were then compared to observations of *P. parvum* population densities taken at the same time the input data were collected. Three error metrics were used for quantitative comparison of predictions and observations, which measure the performance of the models in predicting the magnitude and timing of *P. parvum* population density during winter, the period of time when fish-killing blooms occur in Texas lakes.

These models can also be modified to accept input data from multiple years or from other lakes when these become available, to enable more extensive predictions of *P. parvum* dynamics.

c. Test results to demonstrate the model performance criteria were met (e.g. code verification/validation, sensitivity analyses, history matching with lab or field data, as appropriate)

These are fully summarized in the appendices. Sensitivity analyses were conducted for all model parameters using the comparison of predicted and observed dynamics described above.

d. Theory behind the model, expressed in non-mathematical terms

Population dynamics of *P. parvum* and other, competing algae are modeled as functions of physical factors such as temperature, irradiance, and salinity, and as functions of dissolved nitrate and phosphate concentration. Dynamics of these nutrients are coupled to population growth, so that large populations deplete nutrients leading to competition within and between populations. All algal populations suffer losses due to flow (washout from the habitat), grazing by zooplankton, and sinking in the case of diatoms. Some models also assume that a cyanobacterial population, competing with *P. parvum*, produces a toxin that reduces the growth rate of *P. parvum*.

e. Mathematics to be used, including formulas and calculation methods

These are fully summarized in the appendices. Zero-dimensional models were based on coupled ordinary differential equations similar to those used in many water quality models that simulate algal and nutrient dynamics (Thomann and Mueller, 1987; Chapra, 1997). A well-tested $4^{th}/5^{th}$ order Runge-Kutta algorithm with adaptive step size was used for numerical simulations based on these differential equations (Press et al., 1986). This algorithm was coded in Fortran 77, and compiled with the Digital Visual Fortan compiler, version 6. One-dimensional models were based on partial differential equations (reaction-diffusion-advection equations), numerically simulated with the MacCormack algorithm, as modified by Chapra (1997). This algorithm was again coded in Fortran 77, and compiled with the Digital Visual Fortan compiler, version 6.

f. Whether or not the theory and mathematical algorithms were peer reviewed, and if so, include a summary of theoretical strengths and weaknesses

The basic theoretical frameworks and numerical algorithms used are fairly conventional, and thus are now well reviewed. The specific implementations for these models have not been reviewed. As noted, a draft manuscript describing the zero-dimensional models has been submitted for publication, thus this set of implementations is now being reviewed.

g. Hardware requirements

All models were written in Fortran 77 and compiled with the Digital Visual Fortran compiler, version 6. Numerical work was done on several IBM PC type computers with Pentium 4 or higher processors. However, the program code is portable to a wide range of hardware for which Fortran compilers are available. The programs use only simple ASCII text files for input and output and thus can be used on a wide range of hardware enabling use of this file format.

h. Documentation (e.g. users guide, model code)

These are fully summarized in Appendices 8 and 9.

Task 2: Best Management Practice – Benefit Verification Infrastructure Improvement Plan for the Bosque River Basin

a. Model description

The SWAT model is a hydrologic/water quality model developed by the U.S. Department of Agriculture-Agricultural Research Service and is also one of the models within the U.S. Environmental Protection Agency's Better Assessment Science for Integrated Point and Nonpoint Sources program. SWAT is a physically based, distributed, continuous scale model that operates on a daily time-step. The model has the capability to simulate a variety of land management practices and has been used to assess water resources and pollution problems across a wide range of spatial scales at locations around the world. SWAT is distributed in the sense that it divides the watershed/river basin into a number of subwatersheds based on topography and a user-defined threshold drainage area (minimum area required to begin a stream). Each subwatershed is then further divided into Hydrologic Response Units (HRUs), which are a unique combination of soil, landuse, and land management. HRUs are the smallest landscape component of SWAT and are used for computing the hydrologic processes in the watershed. Major components in the model include hydrology, weather, erosion, soil temperature, crop growth, nutrients, pesticides, and agricultural management. A complete review of SWAT including historic developments and applications can be found in Gassman et al. (2007) and a detailed description of the components and mathematical equations representing the processes can be found in Neitsch et al. (2005). The study used SWAT2005 version and the ArcView Geographic Information System interface (AVSWAT-X), an upgrade of AVSWAT (Di Luzio et al., 2004a) with added SEA extension (Di Luzio et al., 2004b) to process and manage SSURGO (soil survey geographic) soil dataset to derive the required inputs.

b. Performance criteria

SWAT has a built in range of applicable parameters that ensure that model simulations are conducted within reasonable parameters. The parameters modeled and adjusted in this study are presented in Tables 2, 3, and 4 of Tuppad and Srinivasan, 2008 (Technical Report 313). Mean, standard deviation, coefficient of determination (R^2), and Nash-Sutcliffe modeling efficiency (NS_e) were used to evaluate model predictions during calibration and validation. R^2 is the ratio of the explained variation to the total variation and it denotes the strength of the linear association between observed and predicted values. NS_e is a measure of relative model efficiency, developed as a sum of squares. Possible values of NS_e range from - ∞ to 1 and a value of 1 means that modeled results are a perfect match to recorded data. NS_e uses the mean of observed values and, therefore, may not be appropriate for non-normal data;

however, it gives a measure of deviation of predicted values from the perfect fit (1:1) line.

c. Test results

SWAT was validated and calibrated for application in the Bosque River watershed using 45 years of flow data collected at two sites in the river. Sediment and nutrient were also calibrated and validated using data collected at these same sites, but only 3 years of data were available at one site and 6 years of data were available at the other. Model performance statistics for flow, sediment, and nutrients during calibration and validation period are reported in Tables 6, 7, 8 of Tuppad and Srinivasan, 2008 (Technical Report 313).

d. Model theory

The Soil and Water Assessment Tool (SWAT) is a river basin or watershed scale model that was developed by Dr. Jeff Arnold of the USDA ARS to predict the impacts of land management practices on water, sediment and chemical yields in complex watersheds with varying soils, land uses over extended periods of time. SWAT is a physically based model meaning that it uses watershed specific data regarding soils, weather, topography, vegetation and land use management to represent the watershed. Under this approach, watersheds that have no monitoring data available can effectively be modeled and the impacts of management changes on water quality can easily be quantified. The SWAT model employs readily available data that can be obtained from government agencies reducing or eliminating the need for costly localized data acquisition. The SWAT model is also extremely efficient computationally; it can simulate a very large basin with a wide array of management practice implemented over a long time period (i.e. 30 yrs or more).

e. Mathematics

A complete review of SWAT including historic developments and applications can be found in Gassman et al. (2007) and a detailed description of the components and mathematical equations representing the processes can be found in Neitsch et al. (2005).

f. Literature review

There have been numerous reviews of the SWAT model in various forms and fashions. Gassman et al. (2007) provides one of the more extensive reviews of the model, its theory, applications, and future uses. This paper can be used as one of the more comprehensive reviews of the model. One of the strengths of SWAT as indicated by several reference papers available at http://www.brc.tamus.edu/swat/ is that it is more user friendly than other available models and handles the loading and routing of sediment and nutrients better than other models while is ability to predict storm events has been considered a weakness by some.

g. Hardware requirements

- Personal computer using a Pentium IV processor or higher, which runs at 2 gigahertz or faster

- 1 GB RAM minimum
- 500 megabytes free memory on the hard drive for minimal installation and up to 1.25 gigabyte for a full installation (including sample datasets and US STATSGO data)

h. Documentation

SWAT Documentation available online at:
http://www.brc.tamus.edu/swat/doc.html

References

Di Luzio, M., R. Srinivasan, J. G. Arnold. 2004a. A GIS-Coupled Hydrological Model System for the Water Assessment of Agricultural Nonpoint and Point Sources of Pollution. Transactions in GIS 8(1): 113-136.

Di Luzio, M., J. G. Arnold, R. Srinivasan. 2004b. Integration of SSURGO maps and soil parameters within a geographic information system and nonpoint source pollution model system. Journal of Soil and Water Conservation 59(4): 123-133.

Gassman, P. W., M. R. Reyers, C. H. Green, and J. G. Arnold. 2007. The Soil and Water
Assessment Tool: Historical Development, Applications, and Future Research Directions.
Transaction of the ASABE 50(4): 1211-1250.

Neitsch, S. L., J. G. Arnold, J. R. Kiniry, J. R. Williams, and K. W. King. 2002. Soil and Water Assessment Tool, Theoretical documentation, Version 2000. (TWRI Report No. TR-191, GSWRL 02-01, BRC 02-05). College Station: Texas A&M AgriLife Texas Water Resources Institute. Available at http://www.brc.tamus.edu/swat/.

Tuppad, P. and R. Srinivasan. 2008. Bosque River Environmental Infrastructure Improvement Plan: Phase II BMP Modeling Report. Texas Water Resources Institute Technical Report 313.

Appendix A

Locations of fixed-stations

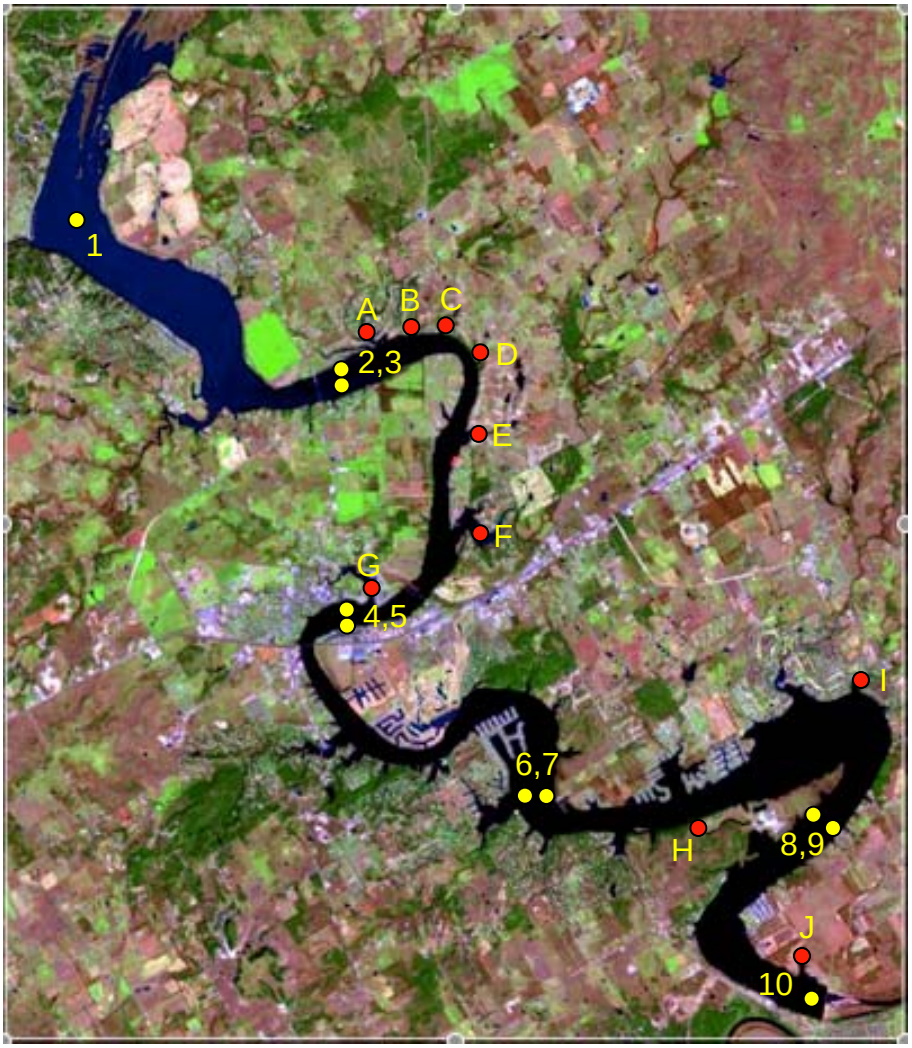

Figure A1. Fixed station locations for Lake Granbury

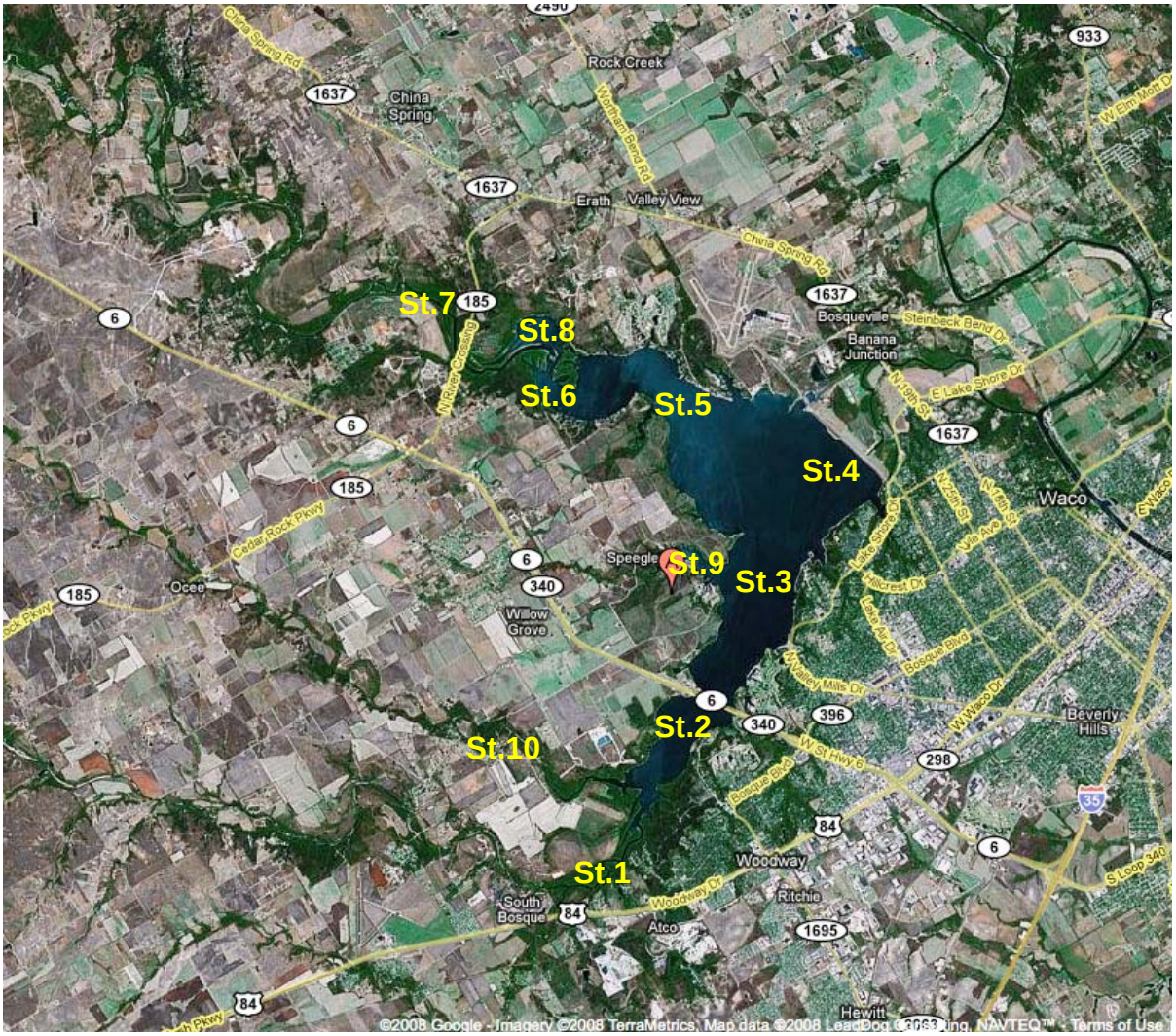

Figure A2. Fixed station locations for Lake Waco

Appendix B

Lake Granbury

Fixed station data from the head and dam of the reservoir (stations 1 and 10), and deep water locations (stations 3, 5, 6, 8), i.e., over the historic river channel.

The data collection involved monthly trips over a period from September 2006 to August 2008.

Figures B-1 through B-3 - Chlorophyll a, P. parvum, toxicity
Figures B-4 through B-8 – pH, temperature, salinity, Secchi depth, turbidity
Figures B-9 through B-13 – Cladoceran, copepod adult and nauplii, total rotifers, protozoan
Figures B-14 through B-15 – Phospahate, dissolved inorganic nitrogen
Figures B-16 through B-19 – Dissolved organic carbon, total bacteria, fecal coliform, E. coli

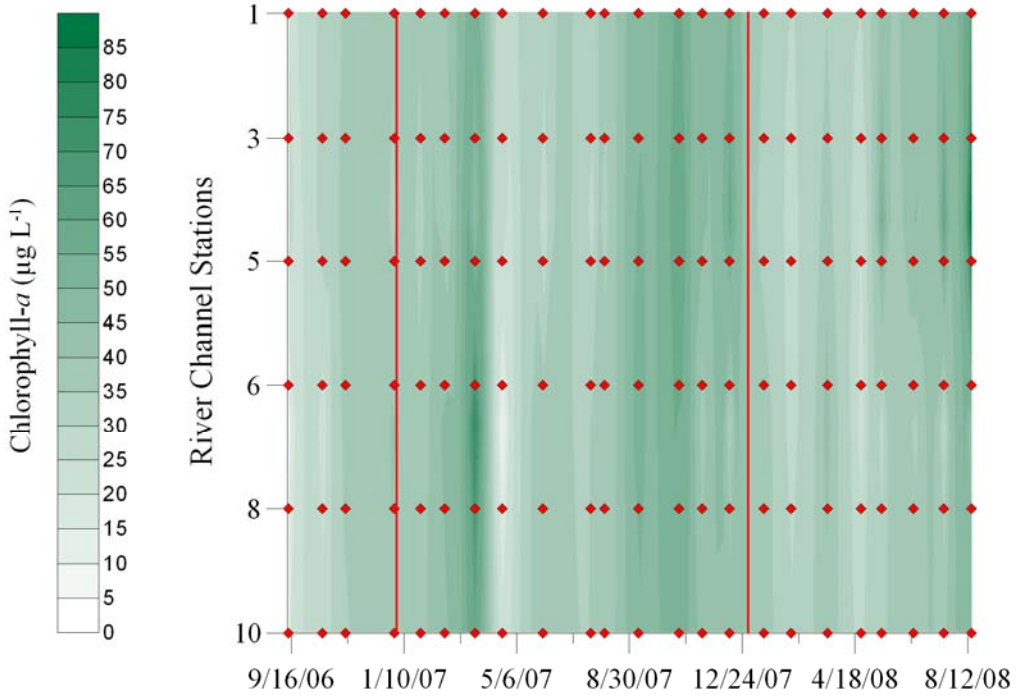

Figure B1. Phytoplankton biomass approximated using chlorophyll *a* for a period spanning September, 2006 through August, 2008 for deep water stations, i.e., over historic river channel.

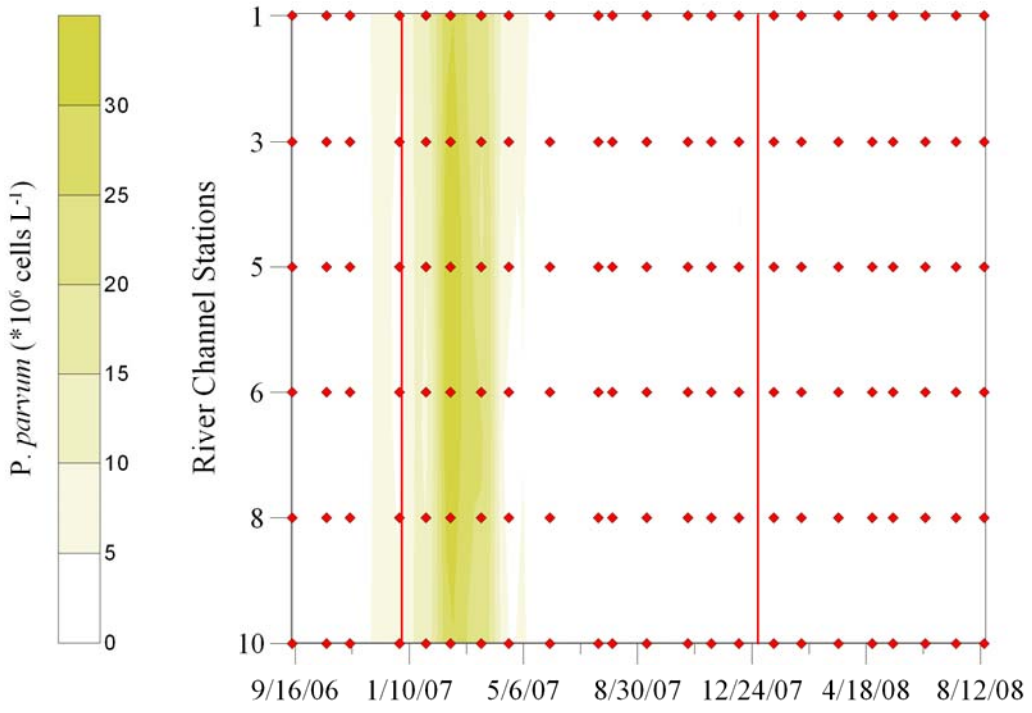

Figure B2. *Prymnesium parvum* population density for a period spanning September, 2006 through August, 2008 for deep water stations, i.e., over historic river channel.

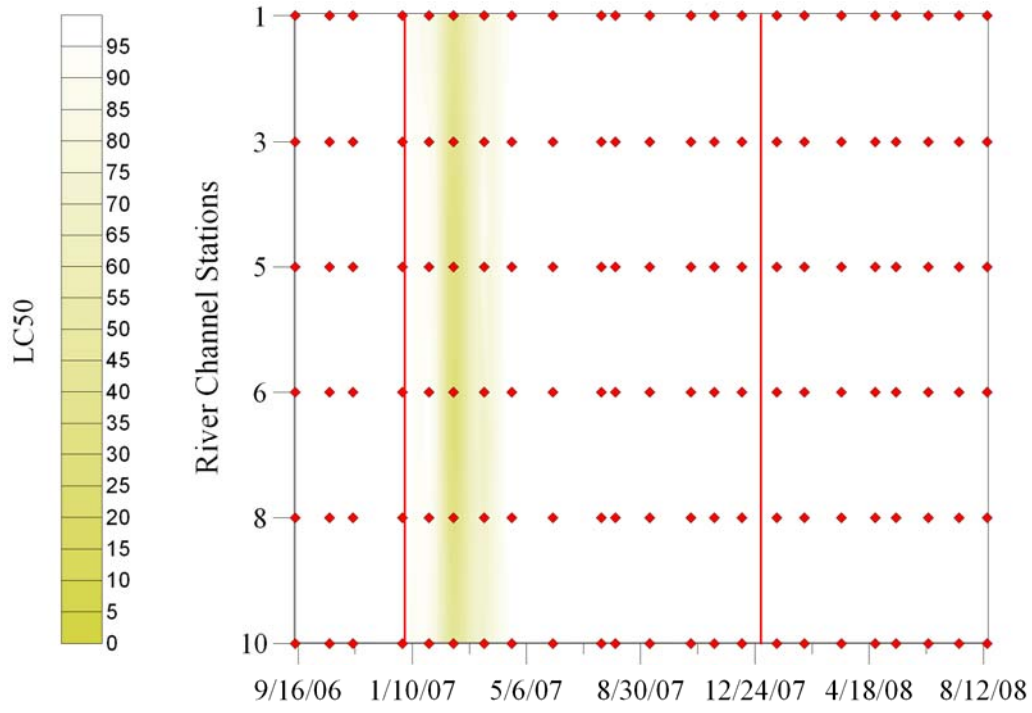

Figure B3. Ambient toxicity estimated using fish bioassays for a period spanning September, 2006 through August, 2008 for deep water stations, i.e., over historic river channel.

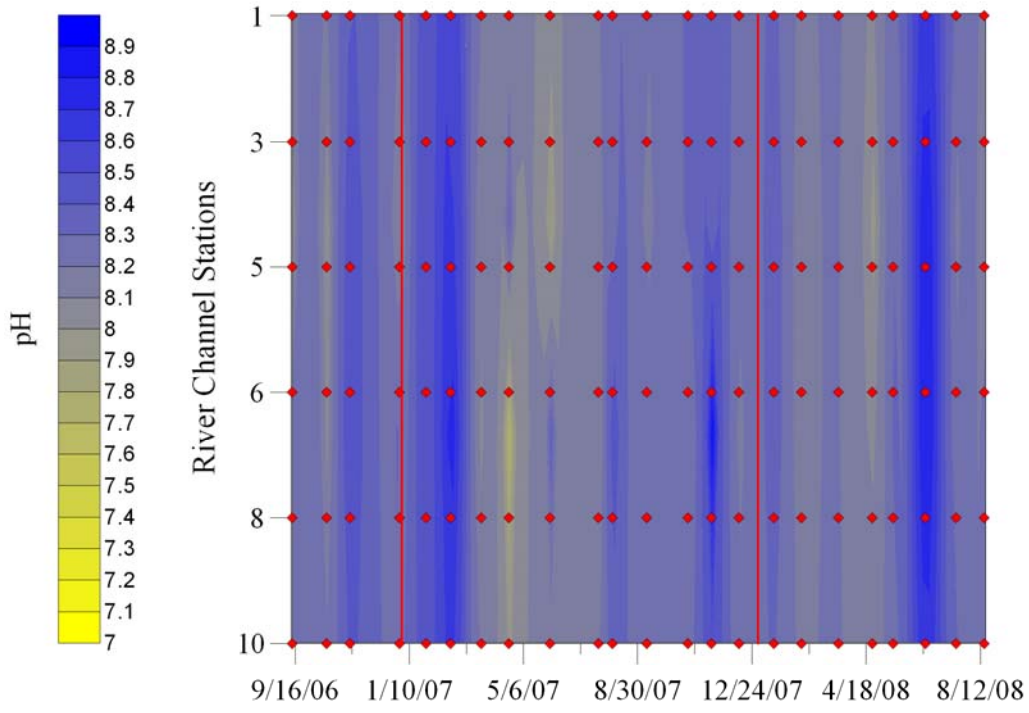

Figure B4. Surface water pH for a period spanning September, 2006 through August, 2008 for deep water stations, i.e., over historic river channel.

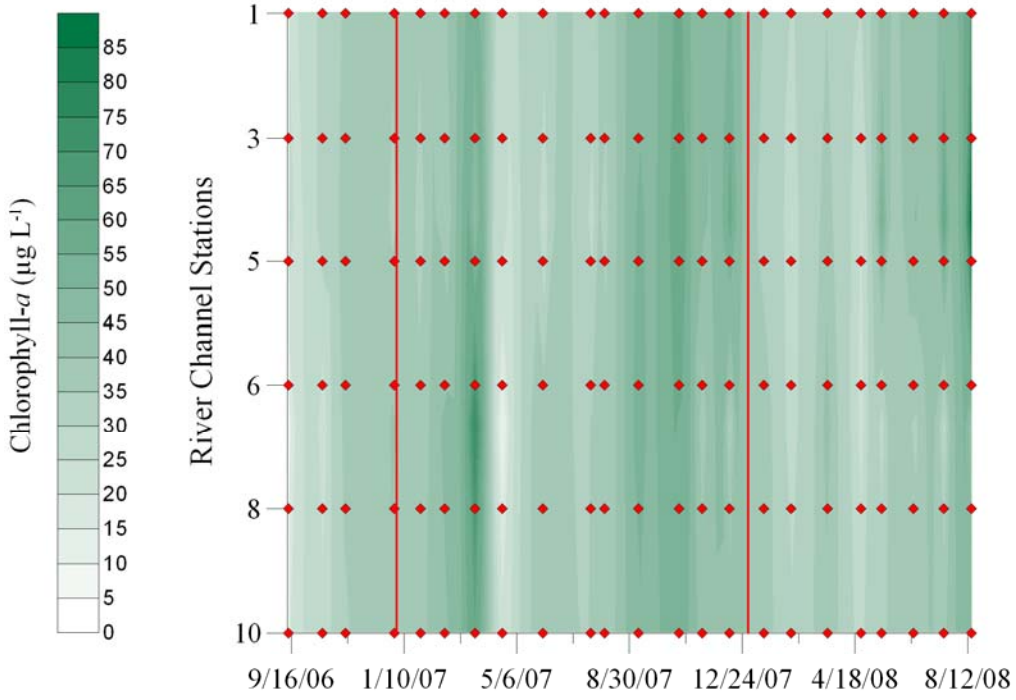

Figure B1. Phytoplankton biomass approximated using chlorophyll *a* for a period spanning September, 2006 through August, 2008 for deep water stations, i.e., over historic river channel.

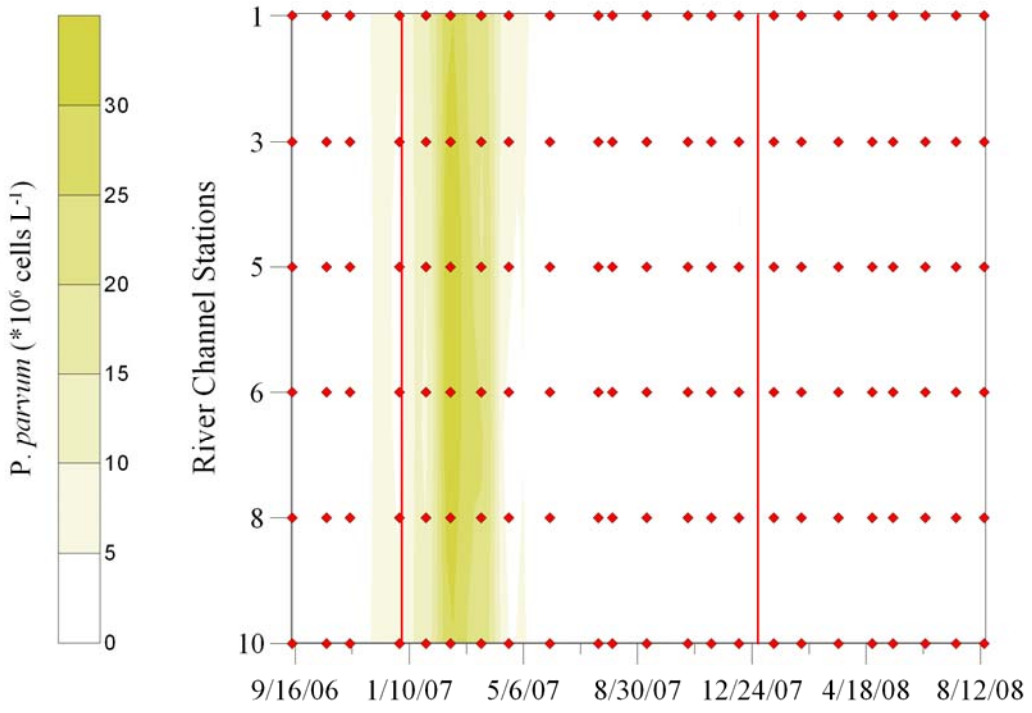

Figure B2. *Prymnesium parvum* population density for a period spanning September, 2006 through August, 2008 for deep water stations, i.e., over historic river channel.

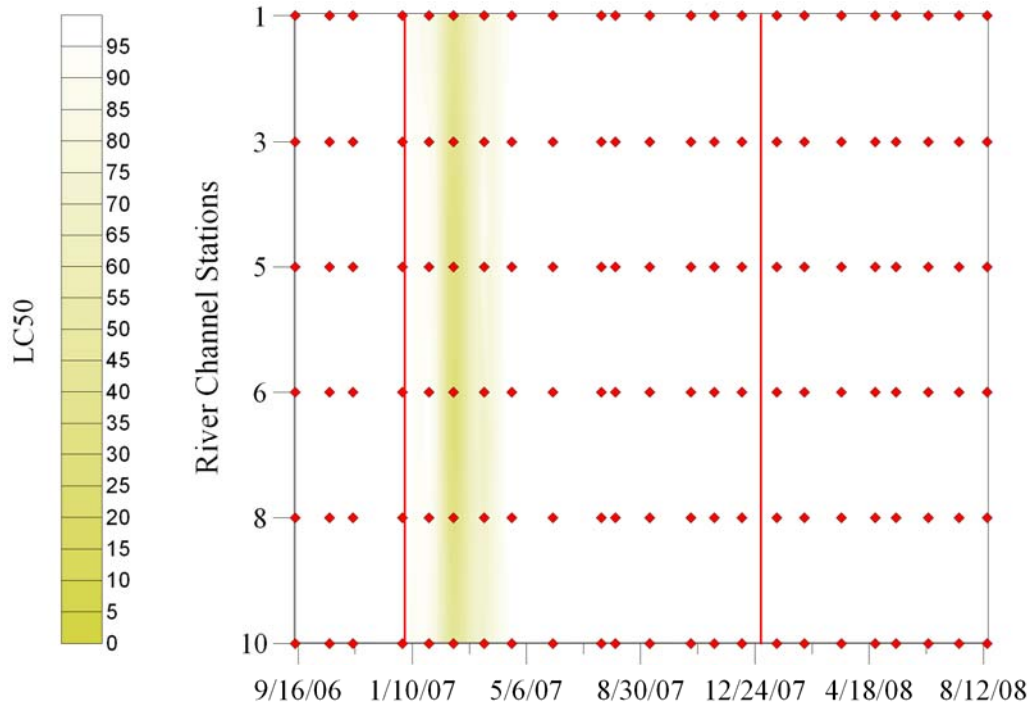

Figure B3. Ambient toxicity estimated using fish bioassays for a period spanning September, 2006 through August, 2008 for deep water stations, i.e., over historic river channel.

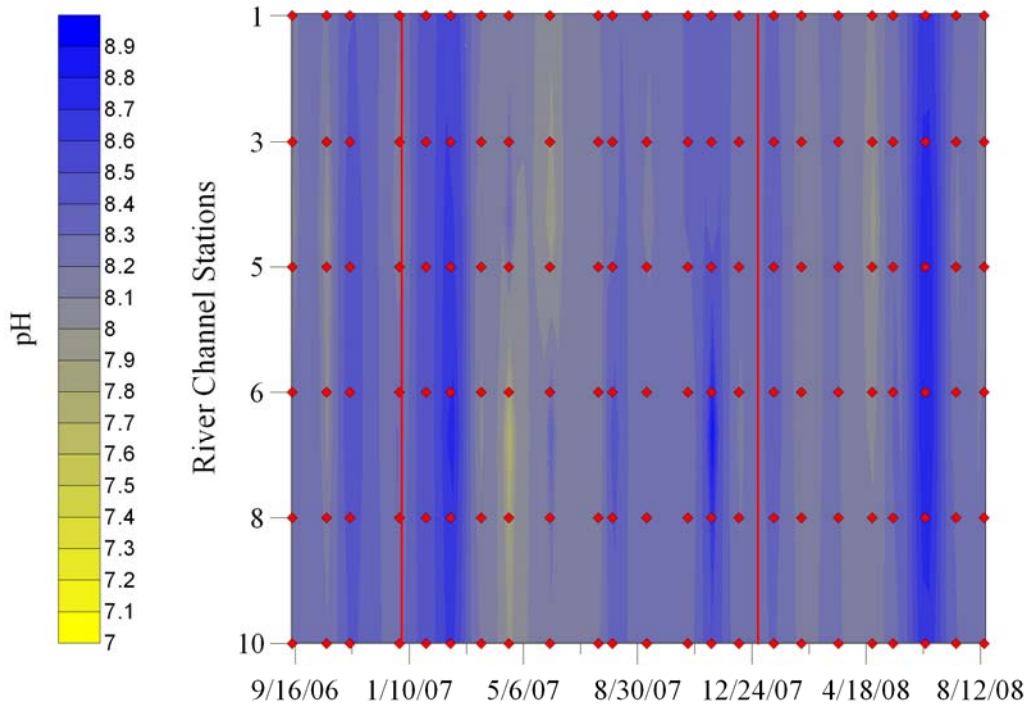

Figure B4. Surface water pH for a period spanning September, 2006 through August, 2008 for deep water stations, i.e., over historic river channel.

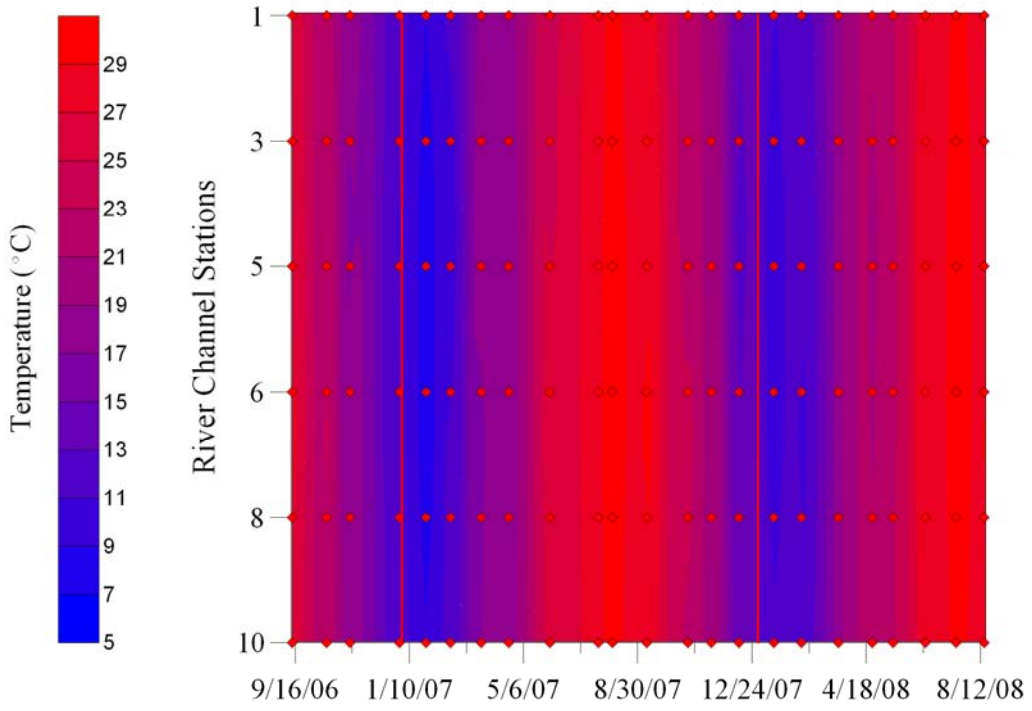

Figure B5. Surface water temperature for a period spanning September, 2006 through August, 2008 for deep water stations, i.e., over historic river channel.

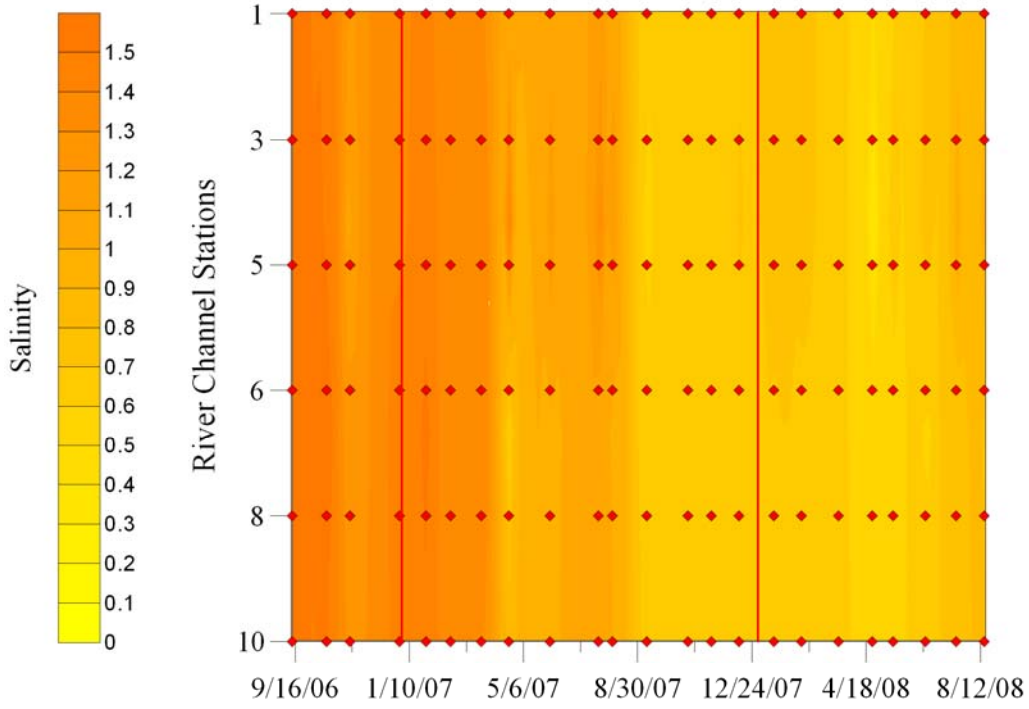

Figure B6. Surface water salinity for a period spanning September, 2006 through August, 2008 for deep water stations, i.e., over historic river channel.

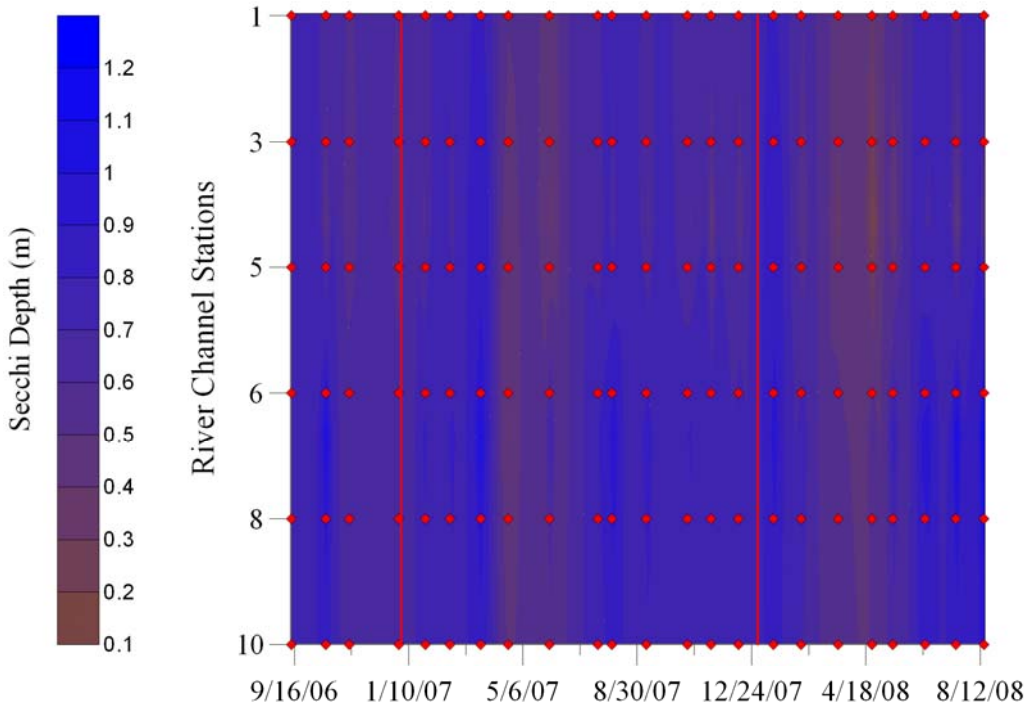

Figure B7. Secchi depth for a period spanning September, 2006 through August, 2008 for deep water stations, i.e., over historic river channel.

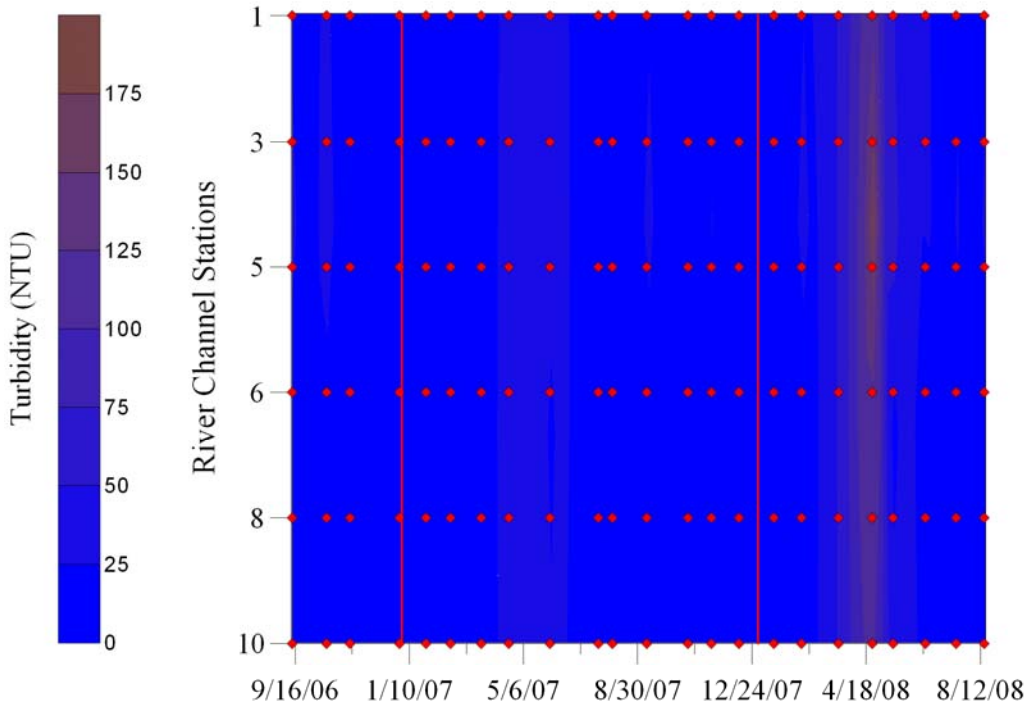

Figure B8. Surface water turbidity for a period spanning September, 2006 through August, 2008 for deep water stations, i.e., over historic river channel.

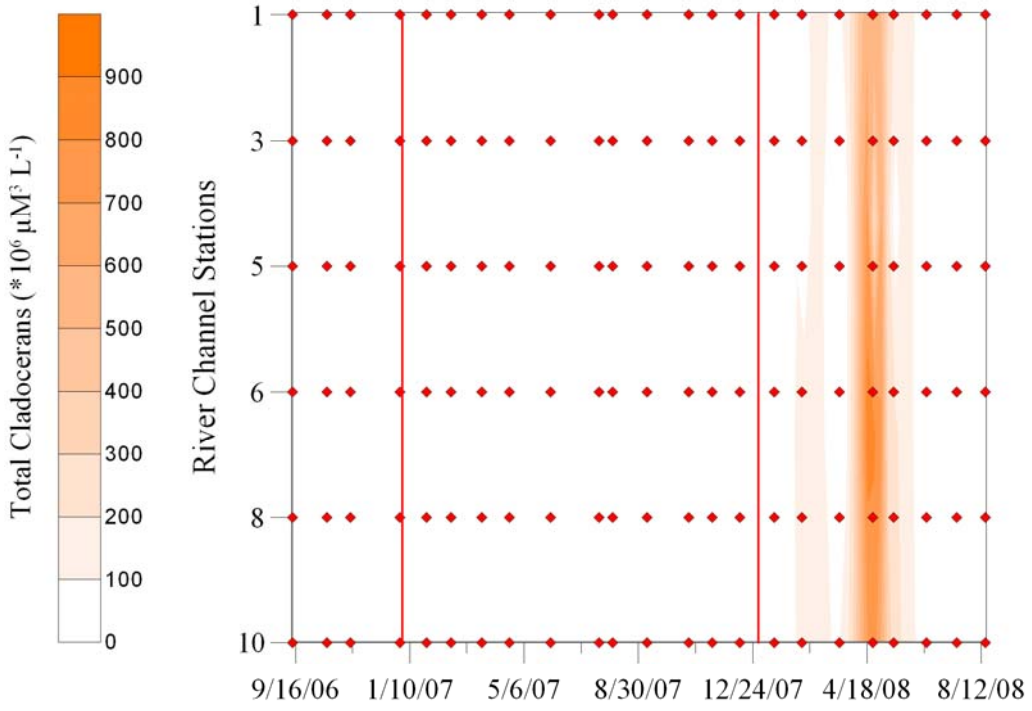

Figure B9. Total cladoceran biovolume for a period spanning September, 2006 through August, 2008 for deep water stations, i.e., over historic river channel.

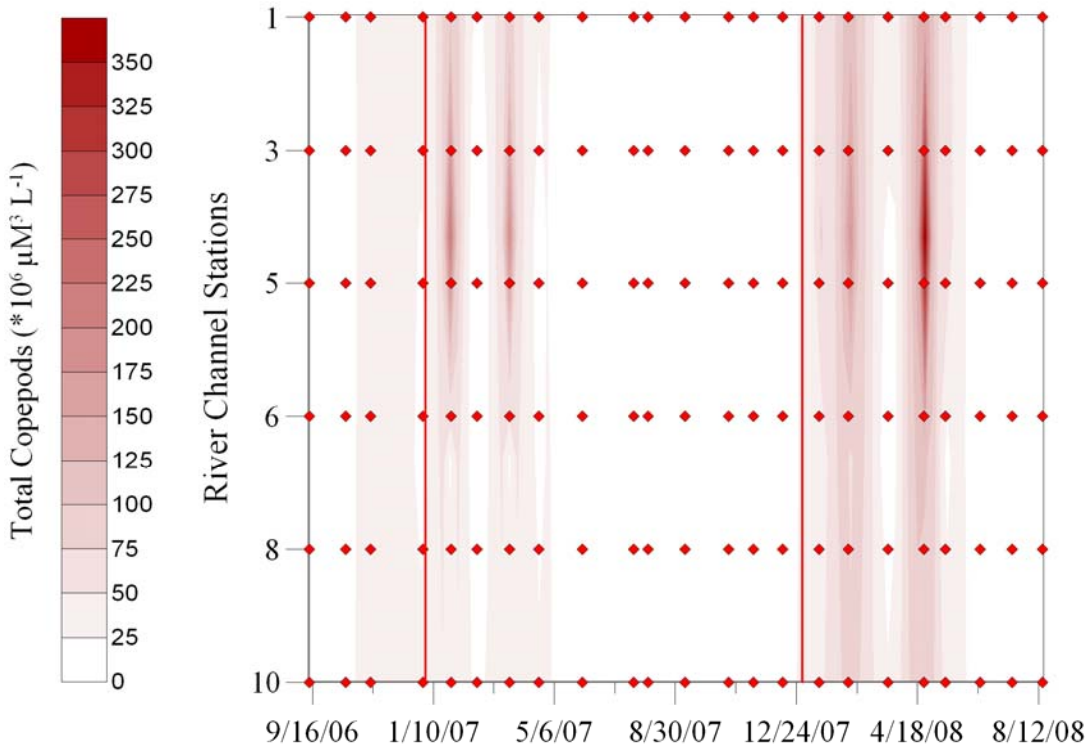

Figure B10. Total copepod biovolume for a period spanning September, 2006 through August, 2008 for deep water stations, i.e., over historic river channel.

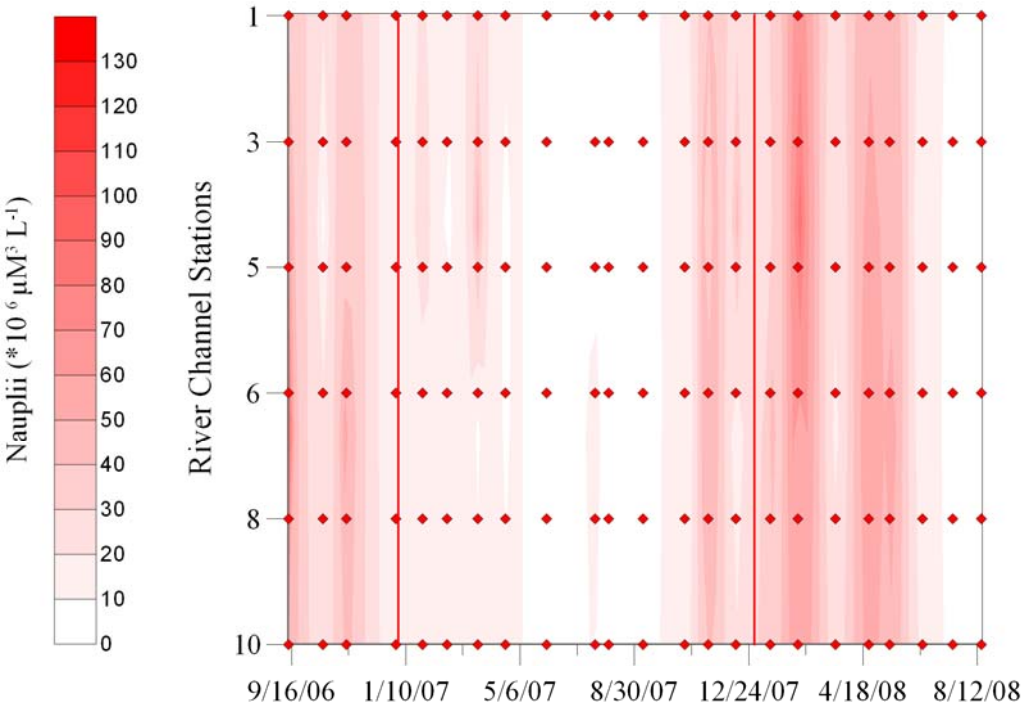

Figure B11. Total copepod nauplii biovolume for a period spanning September, 2006 through August, 2008 for deep water stations, i.e., over historic river channel.

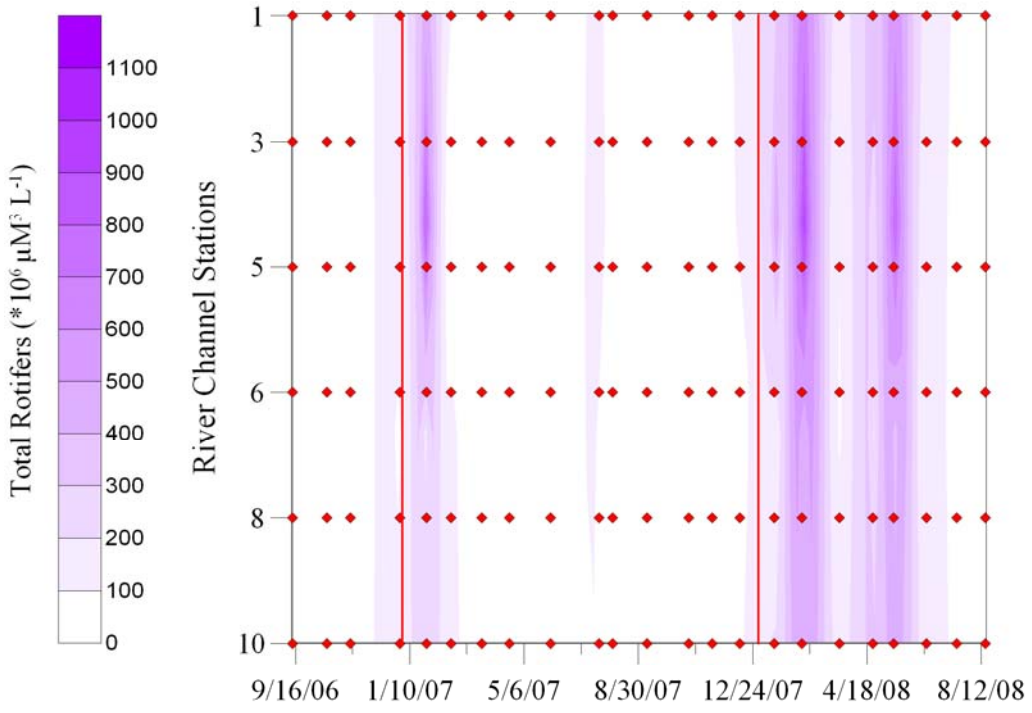

Figure B12. Total rotifer biovolume for a period spanning September, 2006 through August, 2008 for deep water stations, i.e., over historic river channel.

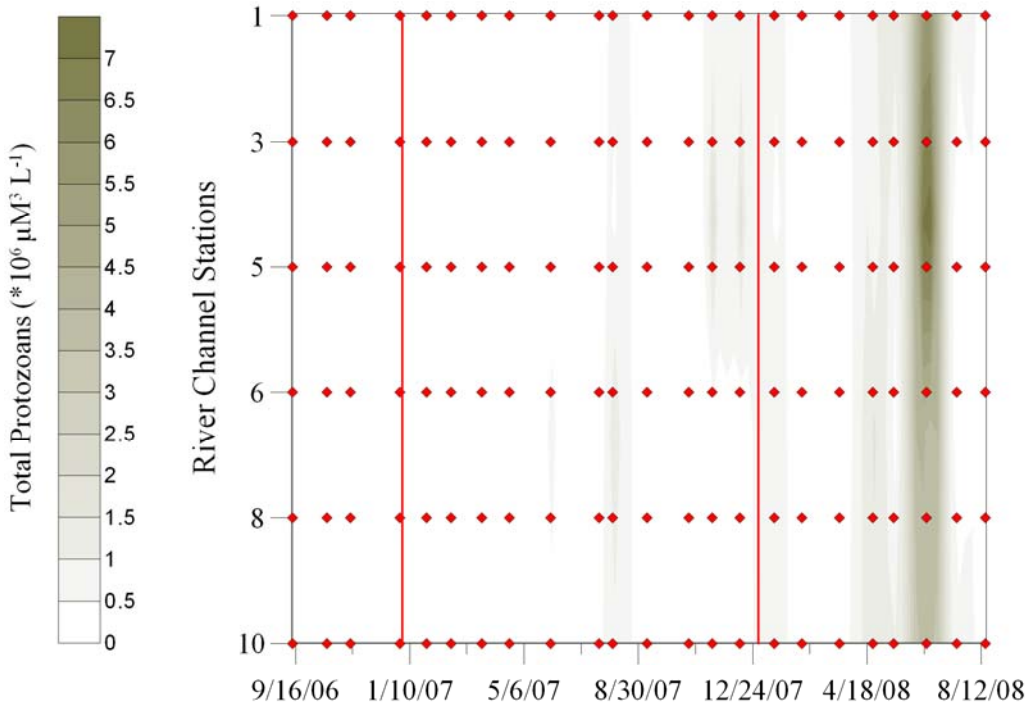

Figure B13. Total protozoan biovolume for a period spanning September, 2006 through August, 2008 for deep water stations, i.e., over historic river channel.

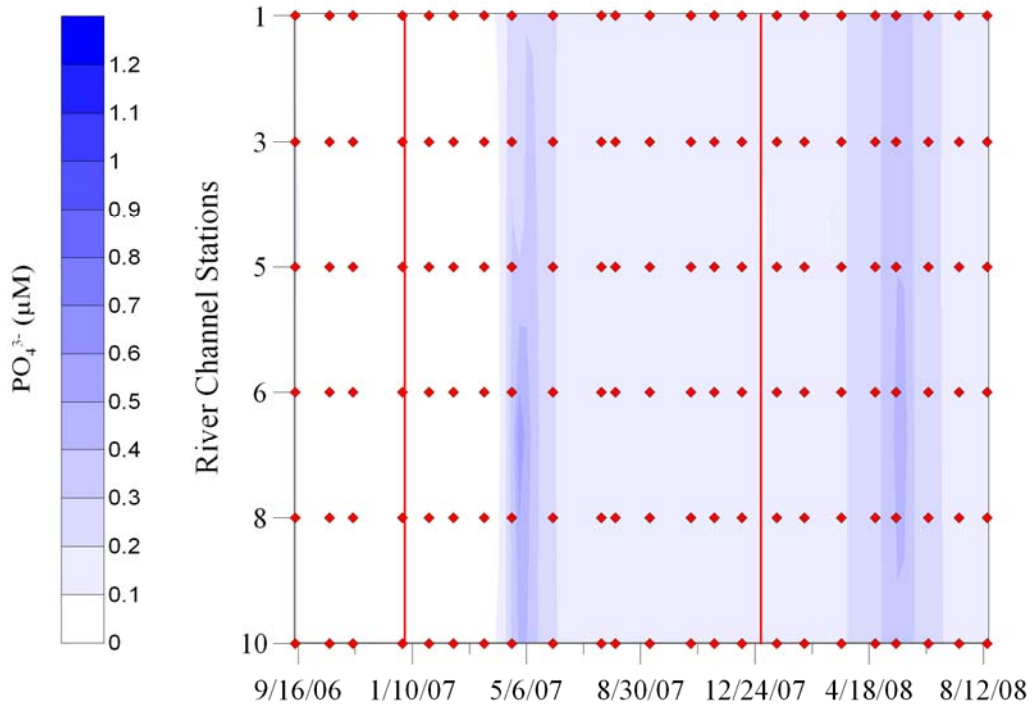

Figure B14. Phosphorus concentration for a period spanning September, 2006 through August, 2008 for deep water stations, i.e., over historic river channel.

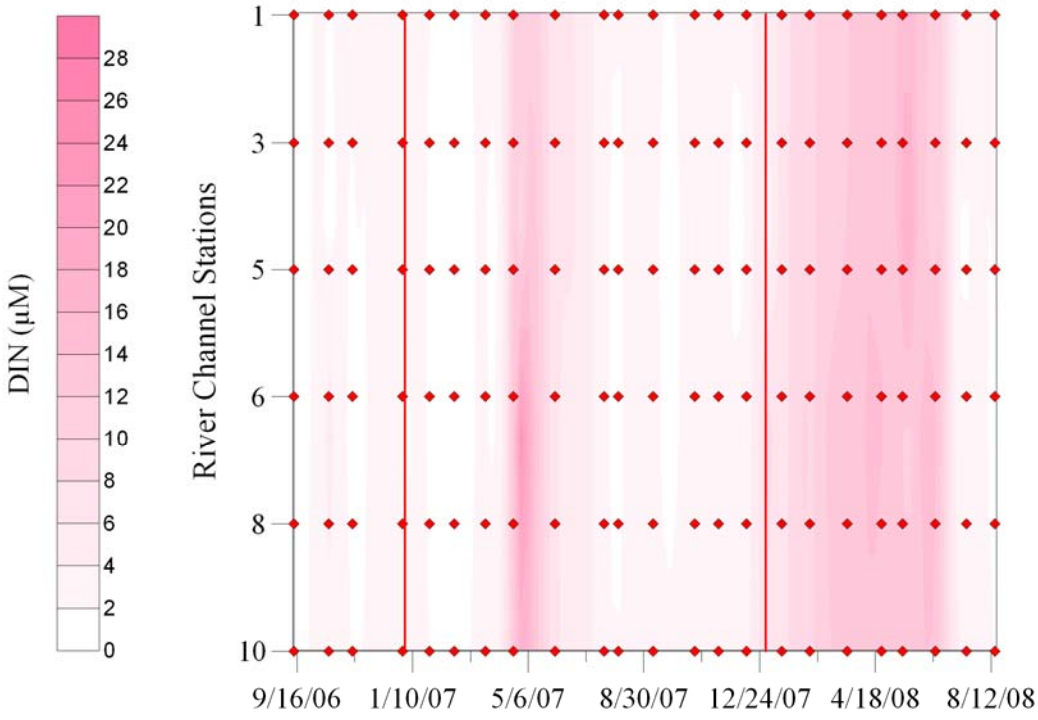

Figure B15. Dissolved inorganic nitrogen concentration for a period spanning September, 2006 through August, 2008 for deep water stations, i.e., over historic river channel.

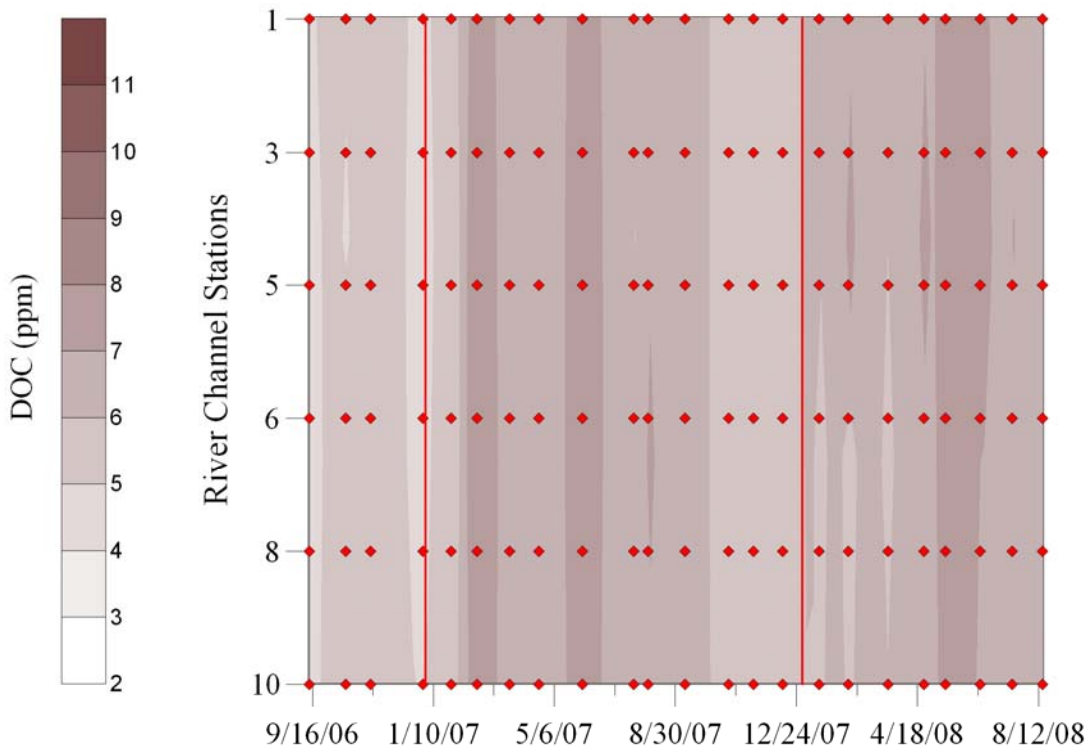

Figure B16. Dissolved organic carbon concentration for a period spanning September, 2006 through August, 2008 for deep water stations, i.e., over historic river channel.

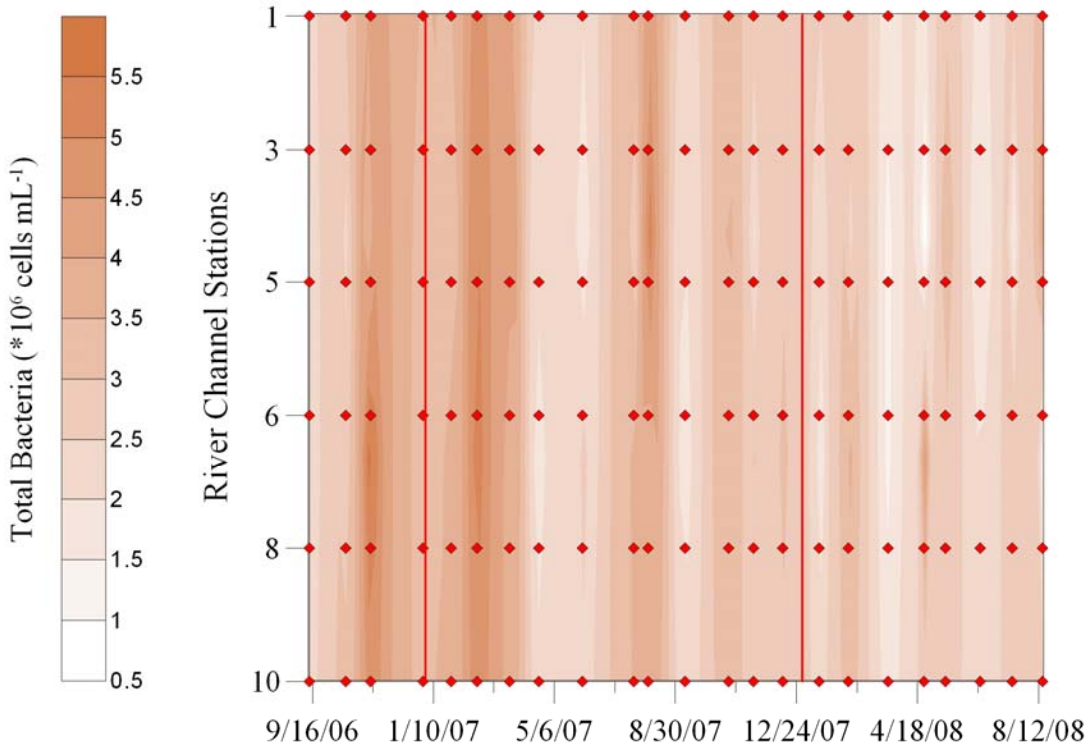

Figure B17. Total bacteria cell concentration for a period spanning September, 2006 through August, 2008 for deep water stations, i.e., over historic river channel.

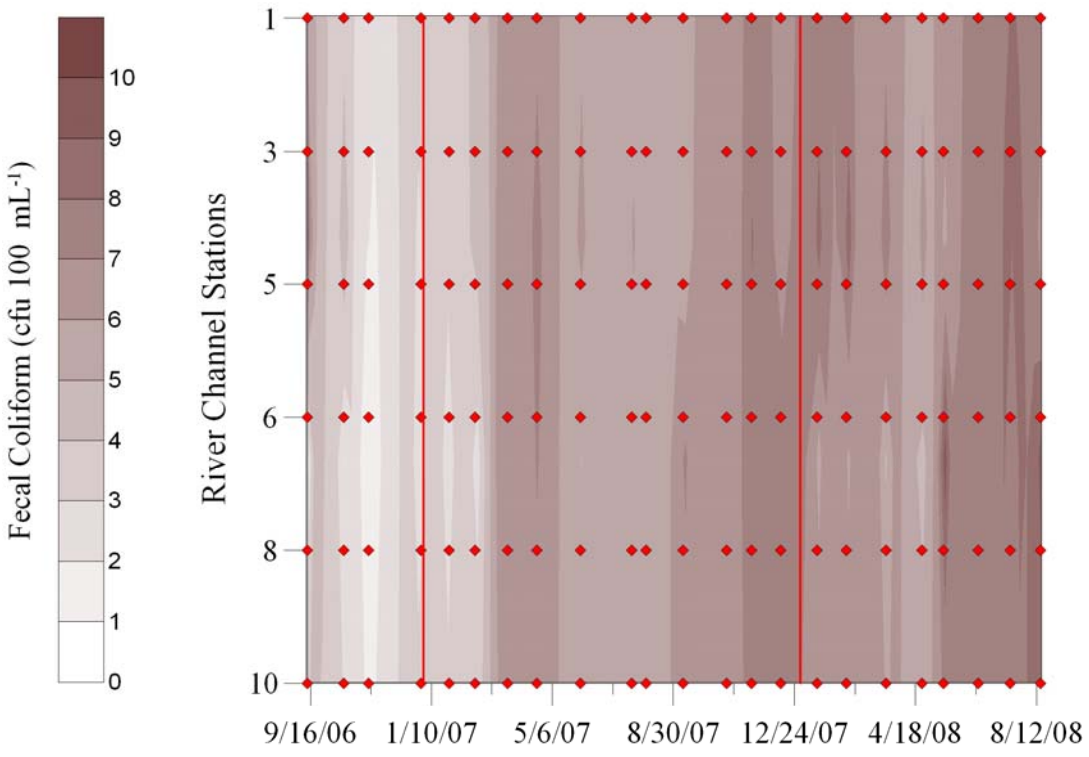

Figure B18. Fecal bacteria concentration for a period spanning September, 2006 through August, 2008 for deep water stations, i.e., over historic river channel.

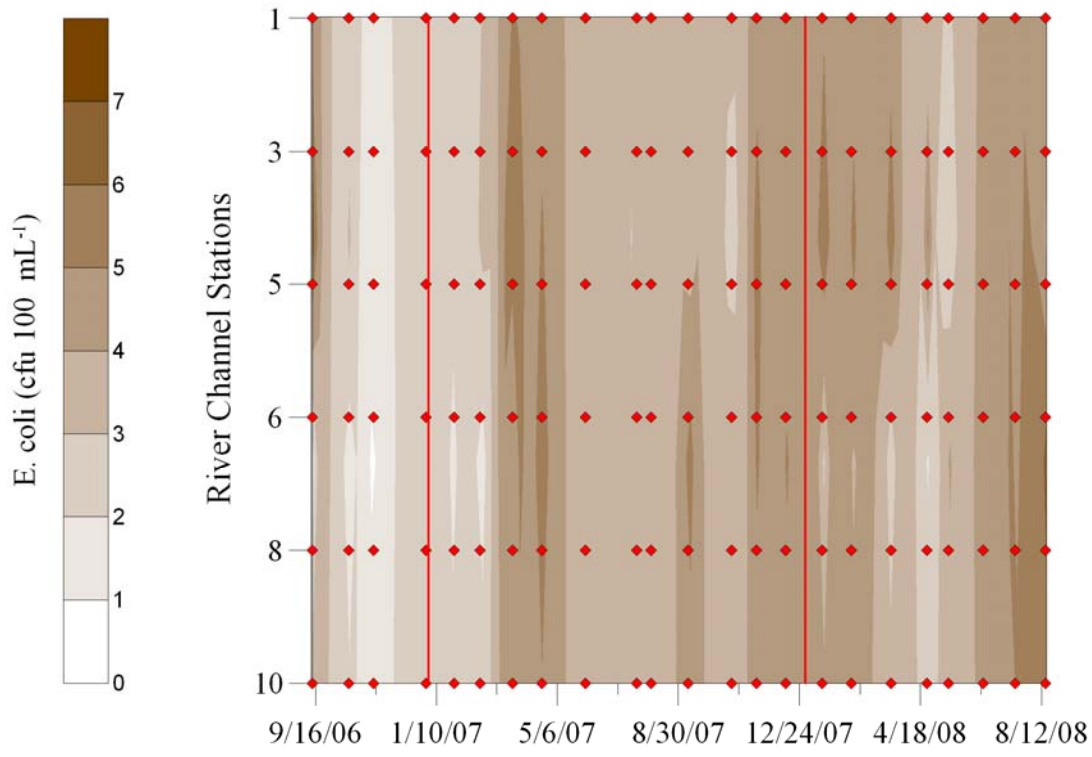

Figure B19. *E. coli* concentration for a period spanning September, 2006 through August, 2008 for deep water stations, i.e., over historic river channel.

Appendix C

Lake Granbury

Fixed station data from the head and dam of the reservoir (stations 1 and 10), and shallow water locations (stations 2, 4, 7, 9), i.e., submerged banks adjacent to the historic river channel.

The data collection involved monthly trips over a period from September 2006 to August 2008.

Figures C-1 through C-3 - Chlorophyll a, P. parvum, toxicity
Figures C-4 through C-8 – pH, temperature, salinity, Secchi depth, turbidity
Figures C-9 through C-13 – Cladoceran, copepod adult and nauplii, total rotifers, protozoan
Figures C-14 through C-15 – Phospahate, dissolved inorganic nitrogen
Figures C-16 through C-19 – Dissolved organic carbon, total bacteria, fecal coliform, E. coli

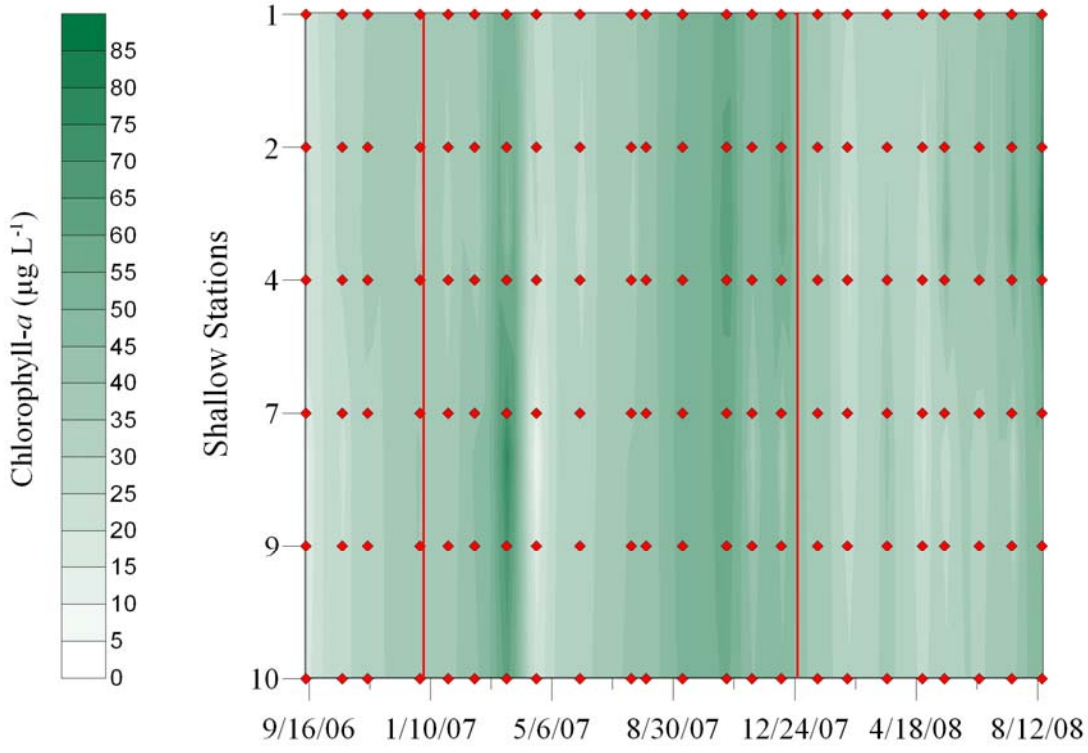

Figure C1. Phytoplankton biomass approximated using chlorophyll *a* for a period spanning September, 2006 through August, 2008 for shallow water stations, i.e., opposite bank from historic river channel.

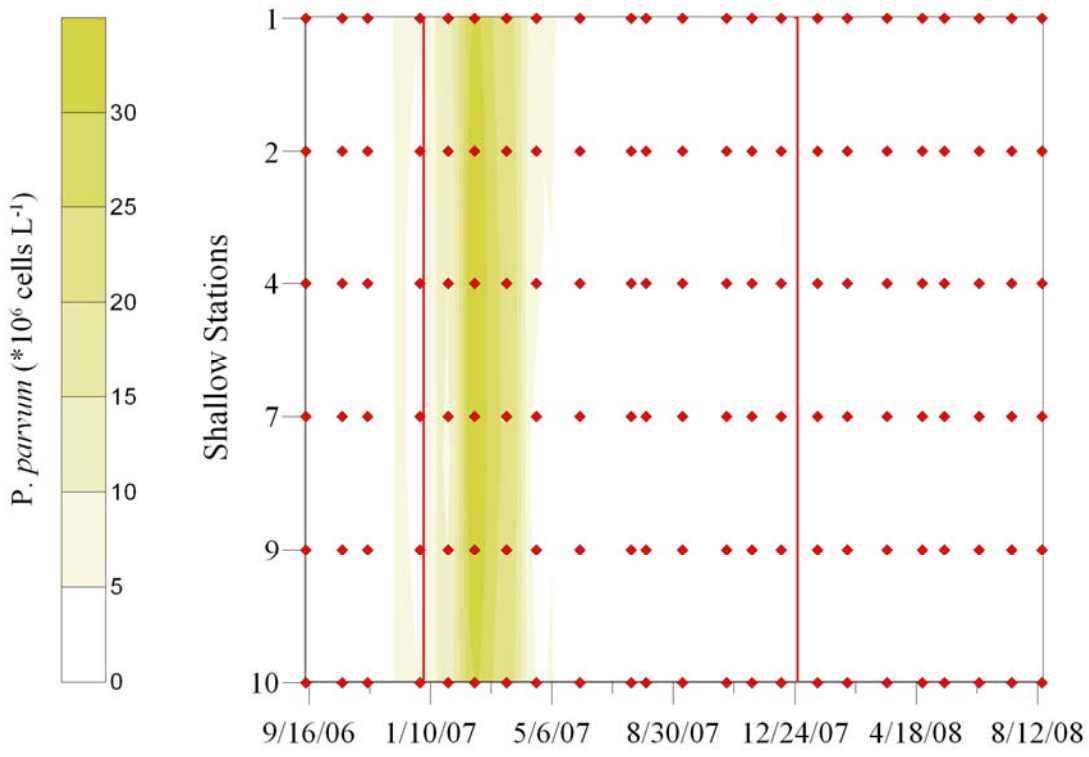

Figure C2. *Prymnesium parvum* population density for a period spanning September, 2006 through August, 2008 for shallow water stations, i.e., opposite bank from historic river channel.

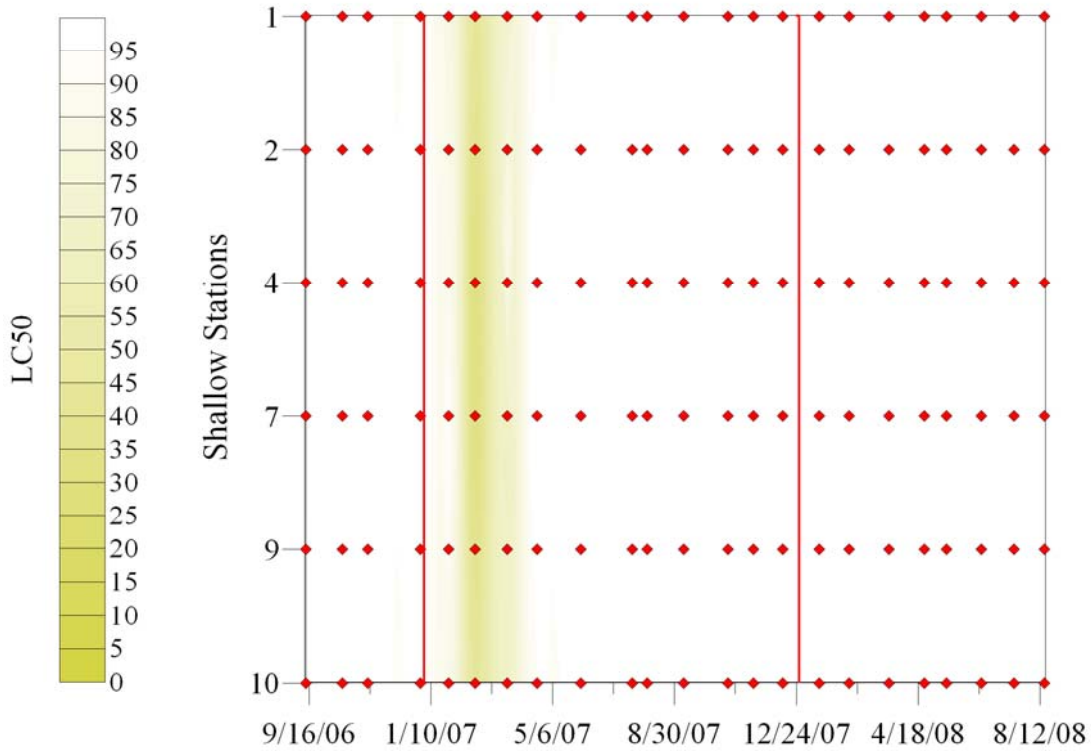

Figure C3. Ambient toxicity estimated using fish bioassays for a period spanning September, 2006 through August, 2008 for shallow water stations, i.e., opposite bank from historic river channel.

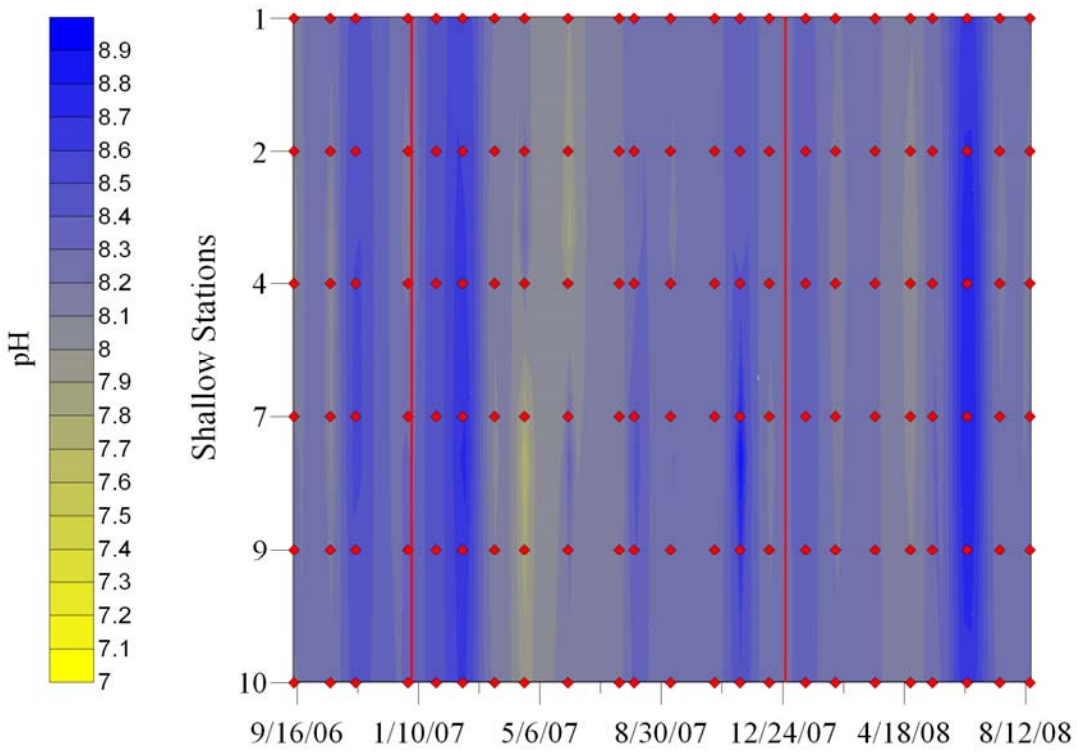

Figure C4. Surface water pH for a period spanning September, 2006 through August, 2008 for shallow water stations, i.e., opposite bank from historic river channel.

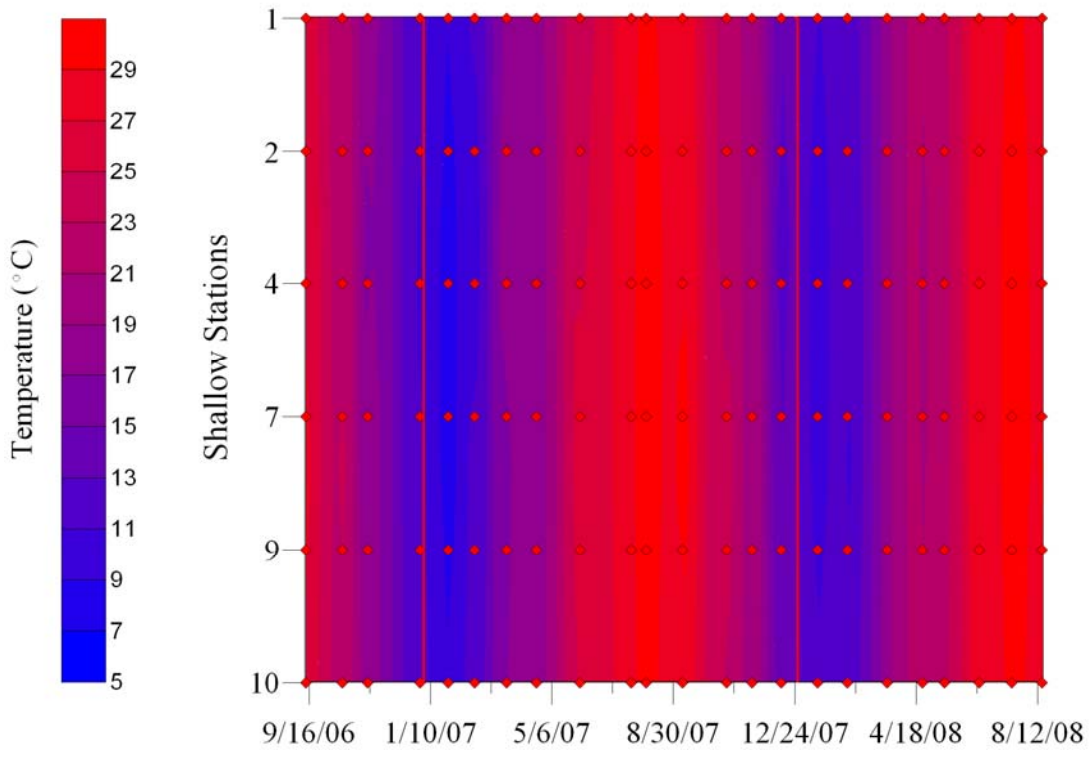

Figure C5. Surface water temperature for a period spanning September, 2006 through August, 2008 for shallow water stations, i.e., opposite bank from historic river channel.

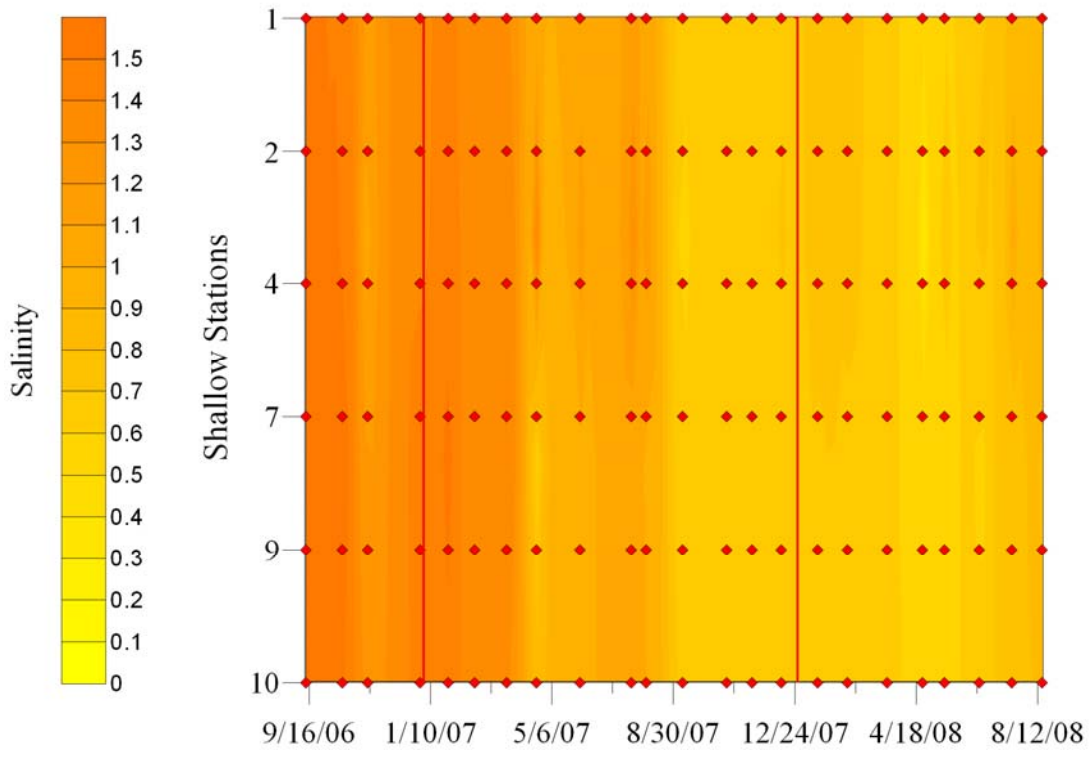

Figure C6. Surface water salinity for a period spanning September, 2006 through August, 2008 for shallow water stations, i.e., opposite bank from historic river channel.

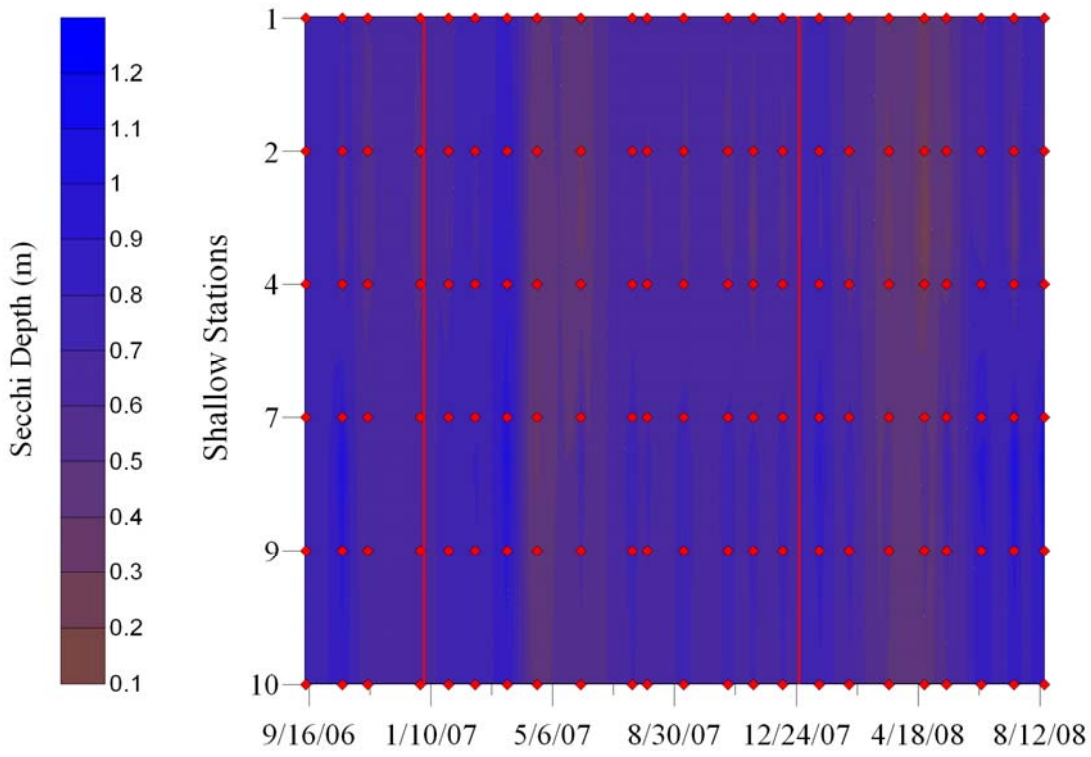

Figure C7. Secchi depth for a period spanning September, 2006 through August, 2008 for shallow water stations, i.e., opposite bank from historic river channel.

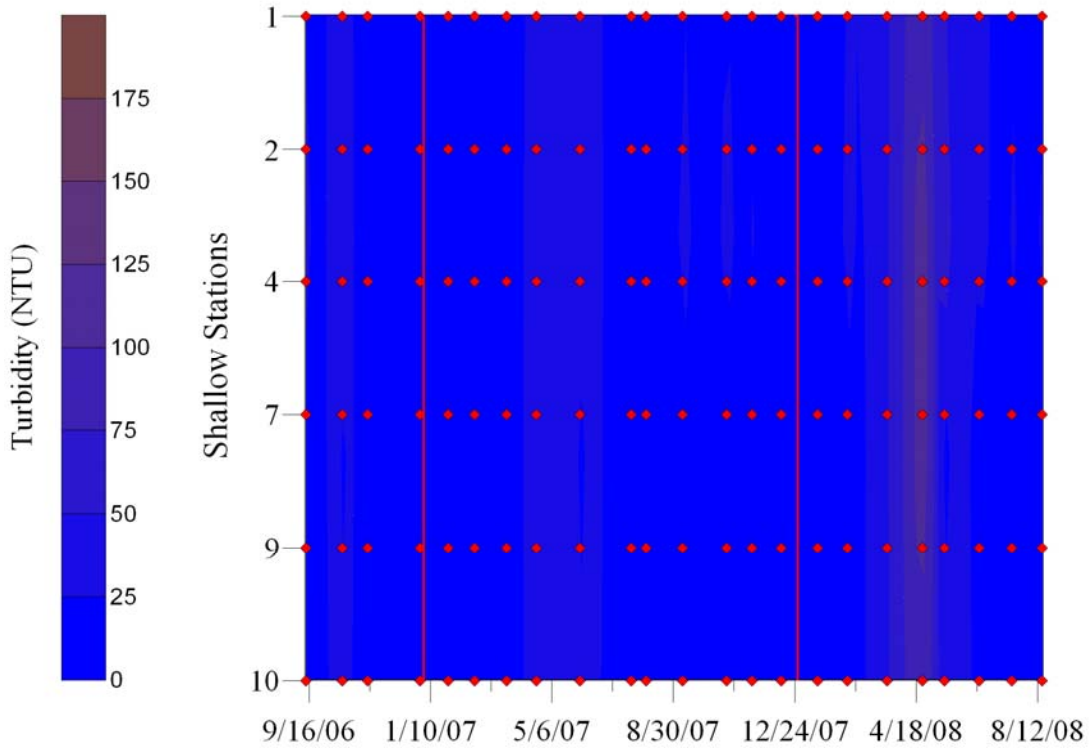

Figure C8. Surface water turbidity for a period spanning September, 2006 through August, 2008 for shallow water stations, i.e., opposite bank from historic river channel.

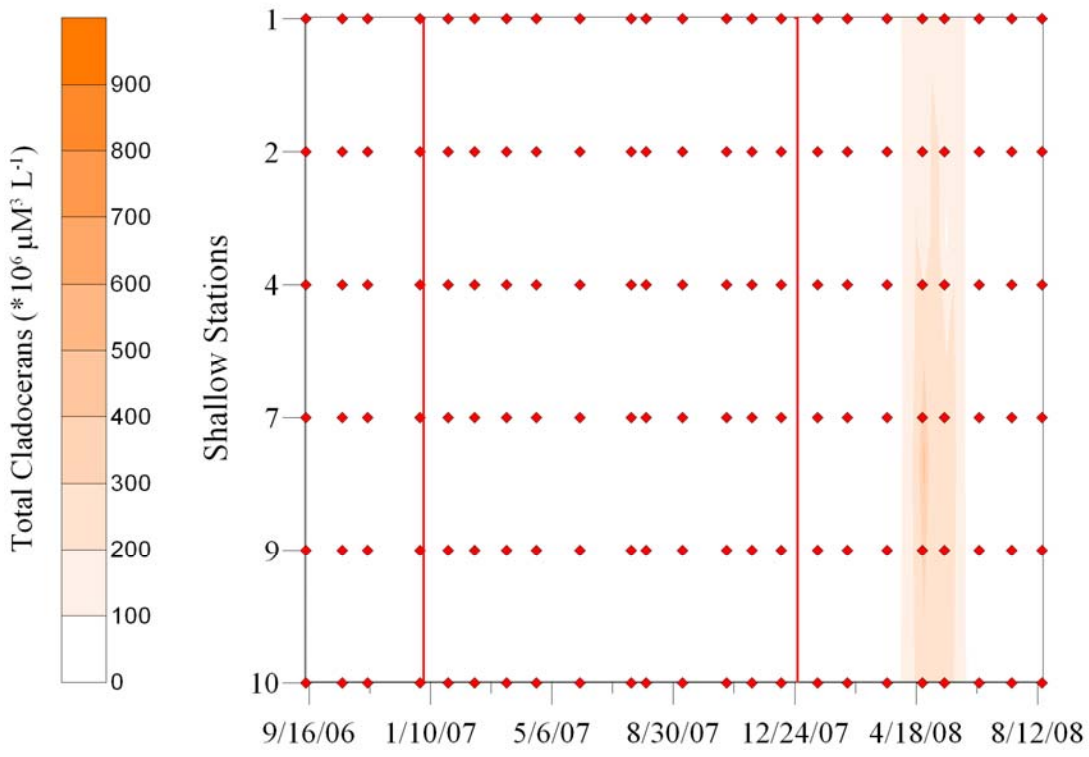

Figure C9. Total cladoceran biovolume for a period spanning September, 2006 through August, 2008 for shallow water stations, i.e., opposite bank from historic river channel.

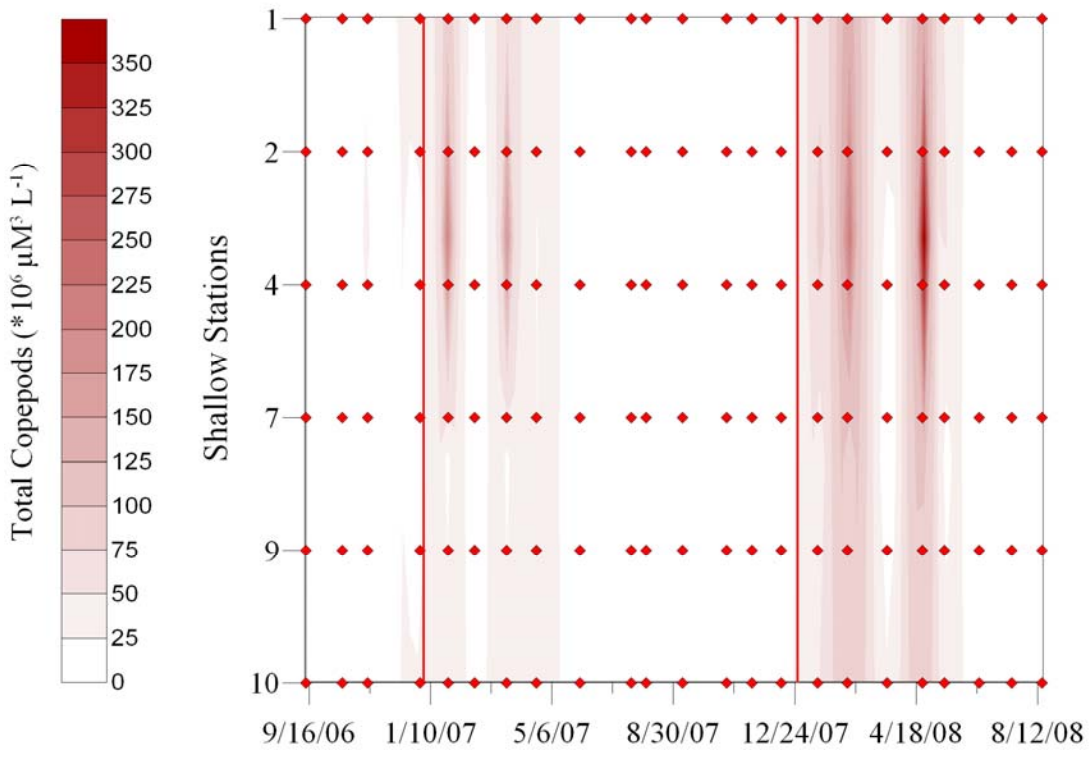

Figure C10. Total copepod biovolume for a period spanning September, 2006 through August, 2008 for shallow water stations, i.e., opposite bank from historic river channel.

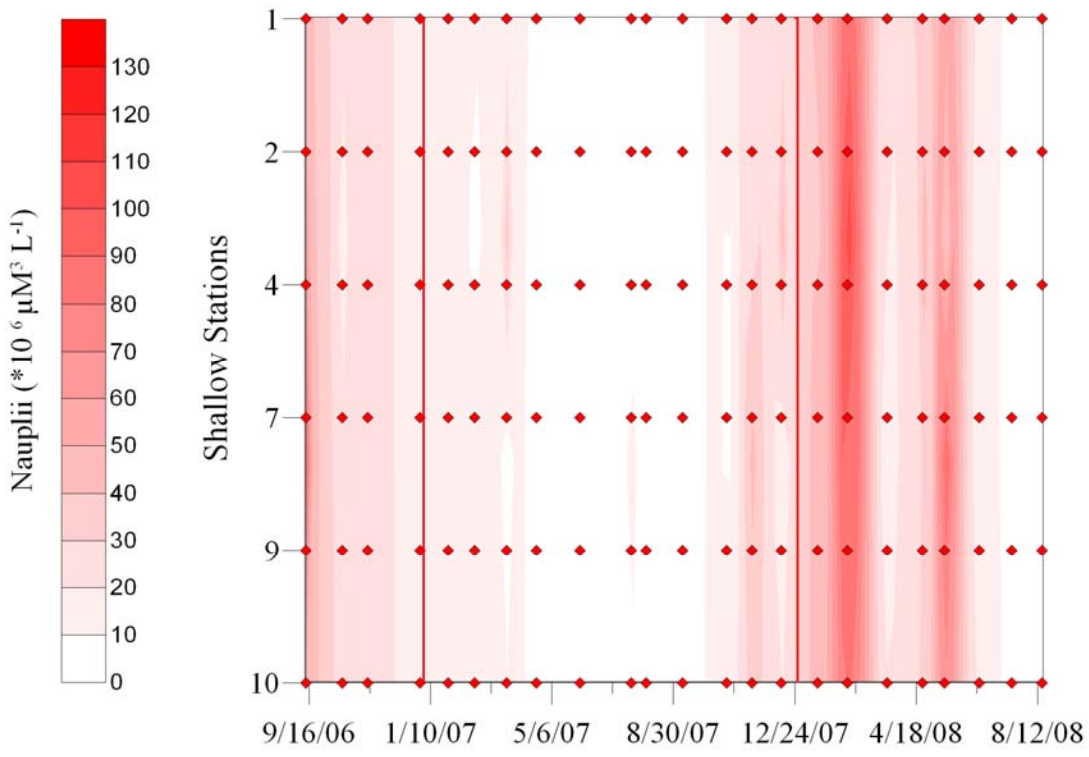

Figure C11. Total copepod nauplii biovolume for a period spanning September, 2006 through August, 2008 for shallow water stations, i.e., opposite bank from historic river channel.

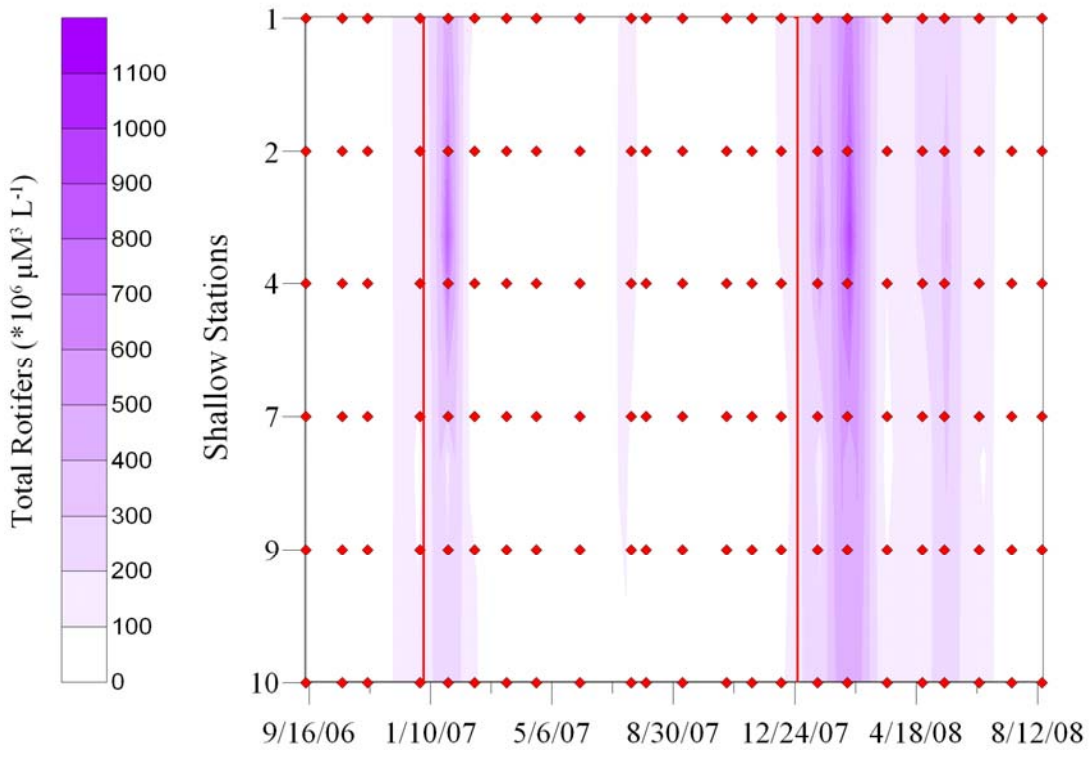

Figure C12. Total rotifer biovolume for a period spanning September, 2006 through August, 2008 for shallow water stations, i.e., opposite bank from historic river channel.

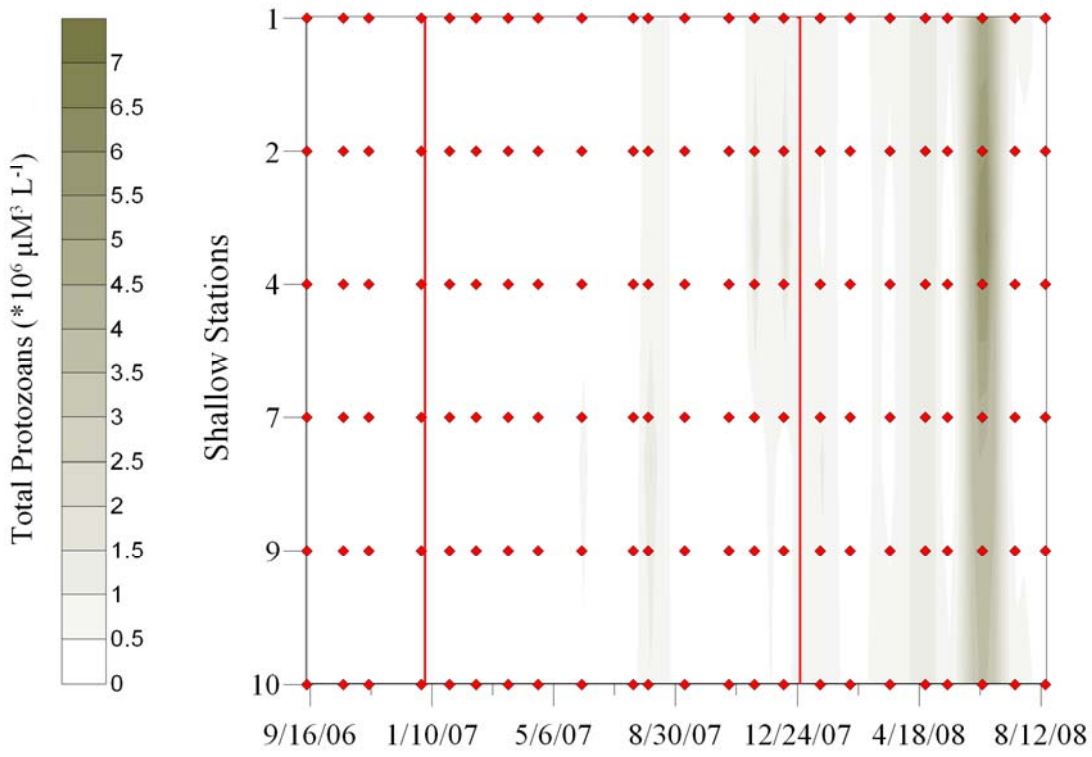

Figure C13. Total protozoan biovolume for a period spanning September, 2006 through August, 2008 for shallow water stations, i.e., opposite bank from historic river channel.

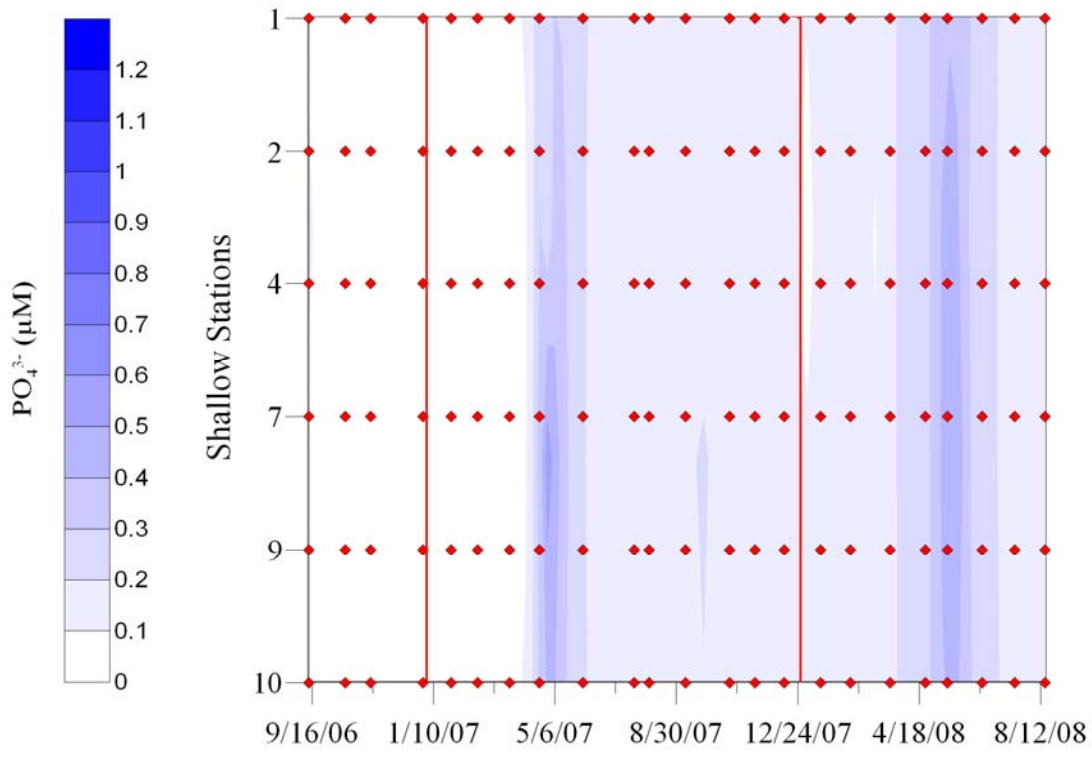

Figure C14. Phosphorus concentration for a period spanning September, 2006 through August, 2008 for shallow water stations, i.e., opposite bank from historic river channel.

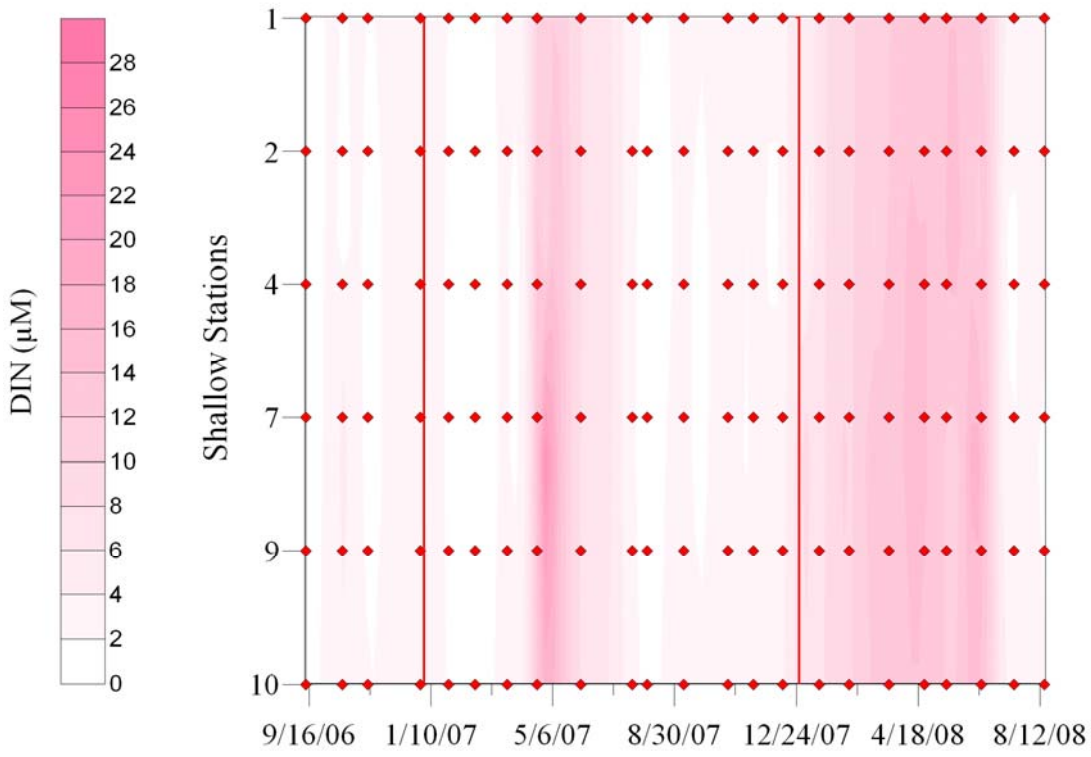

Figure C15. Dissolved inorganic nitrogen concentration for a period spanning September, 2006 through August, 2008 for shallow water stations, i.e., opposite bank from historic river channel.

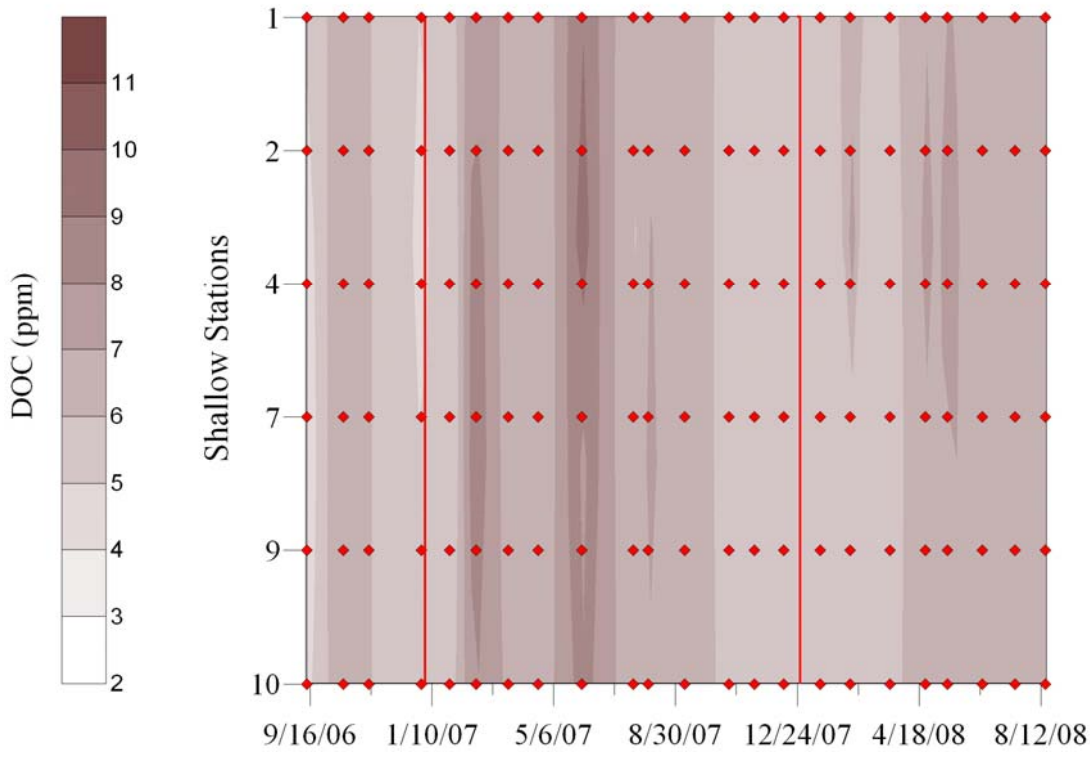

Figure C16. Dissolved organic carbon concentration for a period spanning September, 2006 through August, 2008 for shallow water stations, i.e., opposite bank from historic river channel.

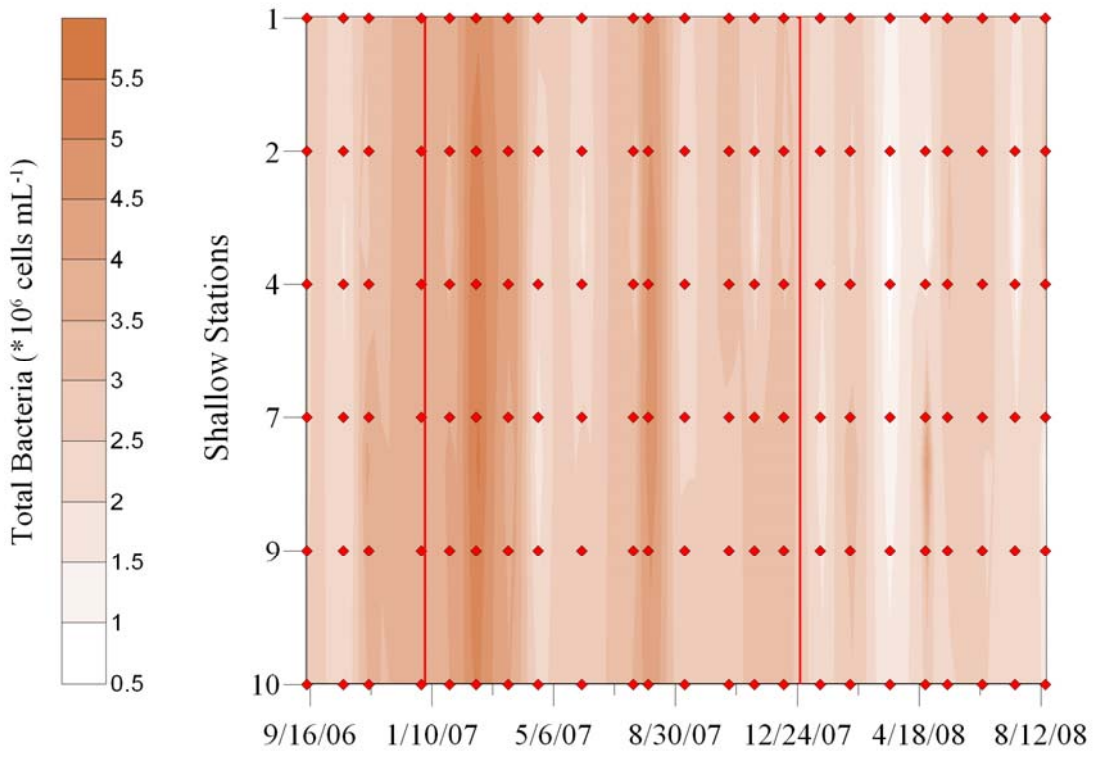

Figure C17. Total bacteria cell concentration for a period spanning September, 2006 through August, 2008 for shallow water stations, i.e., opposite bank from historic river channel.

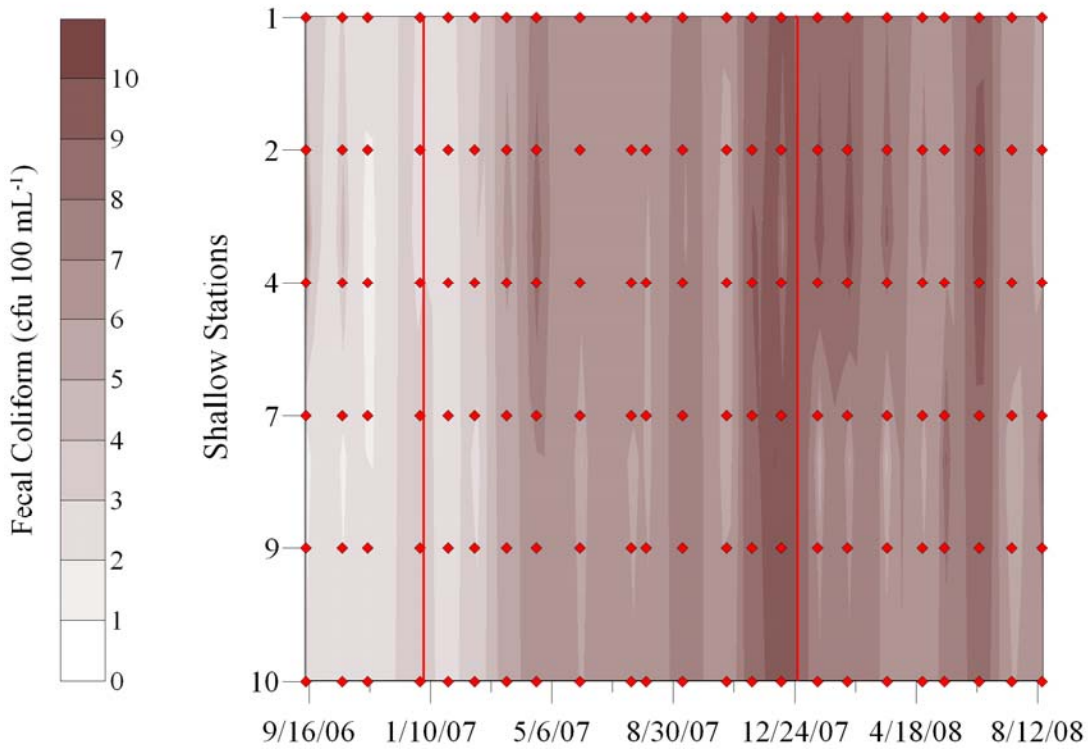

Figure C18. Fecal bacteria concentration for a period spanning September, 2006 through August, 2008 for shallow water stations, i.e., opposite bank from historic river channel.

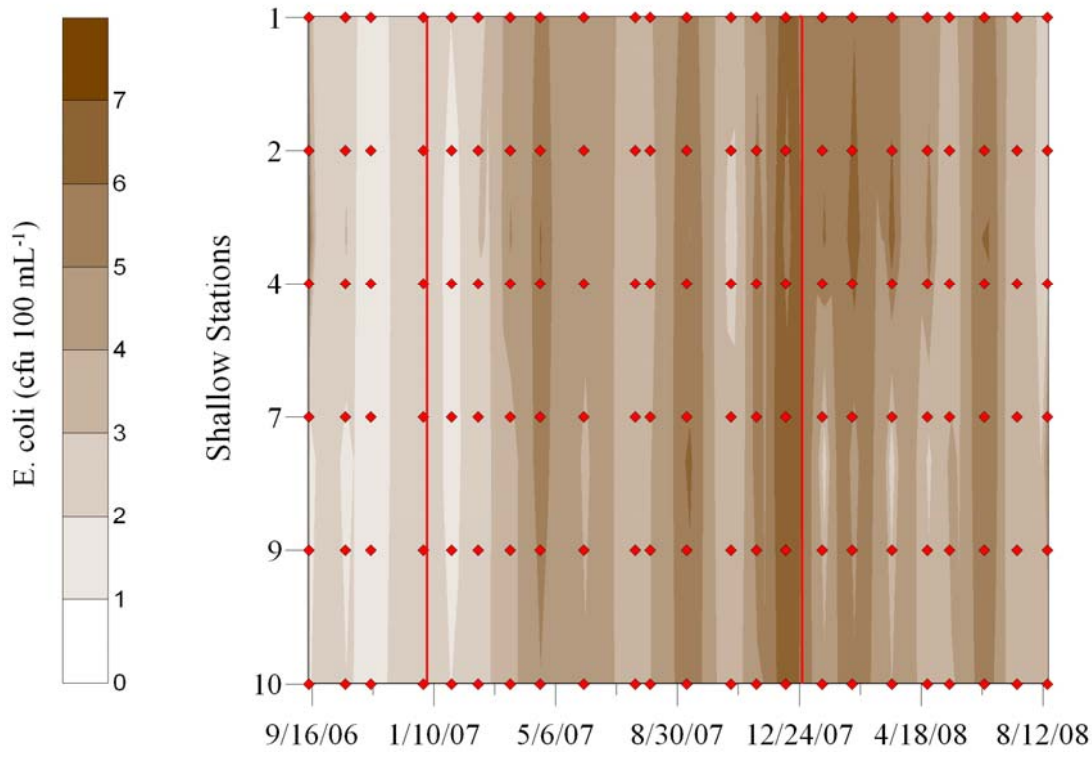

Figure C19. *E. coli* concentration for a period spanning September, 2006 through August, 2008 for shallow water stations, i.e., opposite bank from historic river channel.

Appendix D

Lake Granbury

Regressions comparing dissolved organic carbon, total bacteria, fecal coliform bacteria, *E. coli* and *P. parvum*.

Fixed station data (stations 1 through 10) spanning September 2006 to August 2007 were used in the first analysis, a period spanning an intense, lake-wide *P. parvum* bloom.

Fixed station data (stations 1 through 10, stations A through J) spanning September 2006 to August 2008 were used in the second analysis, a period spanning a *P. parvum* bloom year and a non-bloom year.

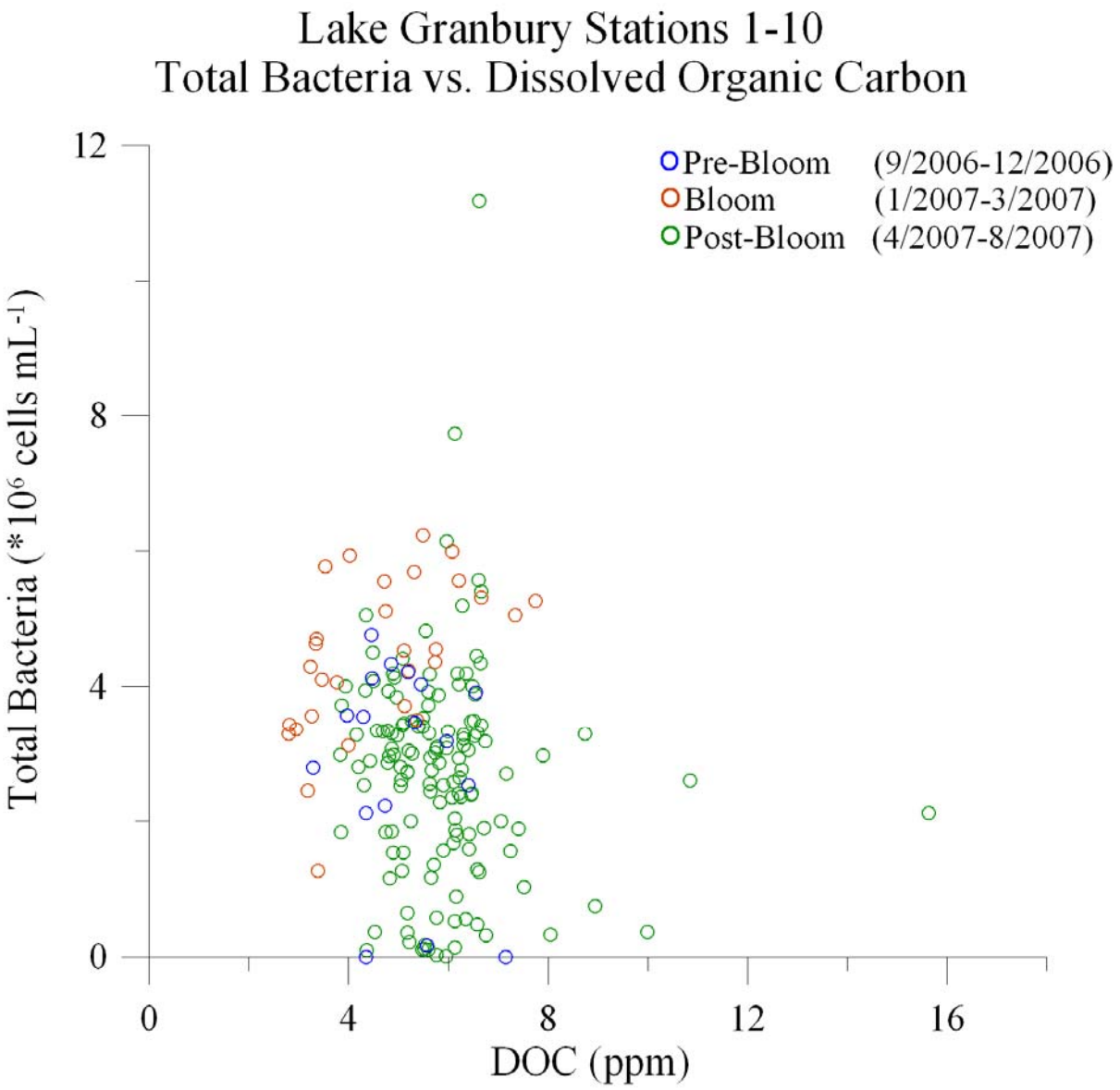

Figure D1. Regression of total bacteria and dissolved organic carbon from open-lake, fixed locations (stations 1 through 10) from Lake Granbury during the *P. parvum* bloom year spanning September 2006 through August 2007.

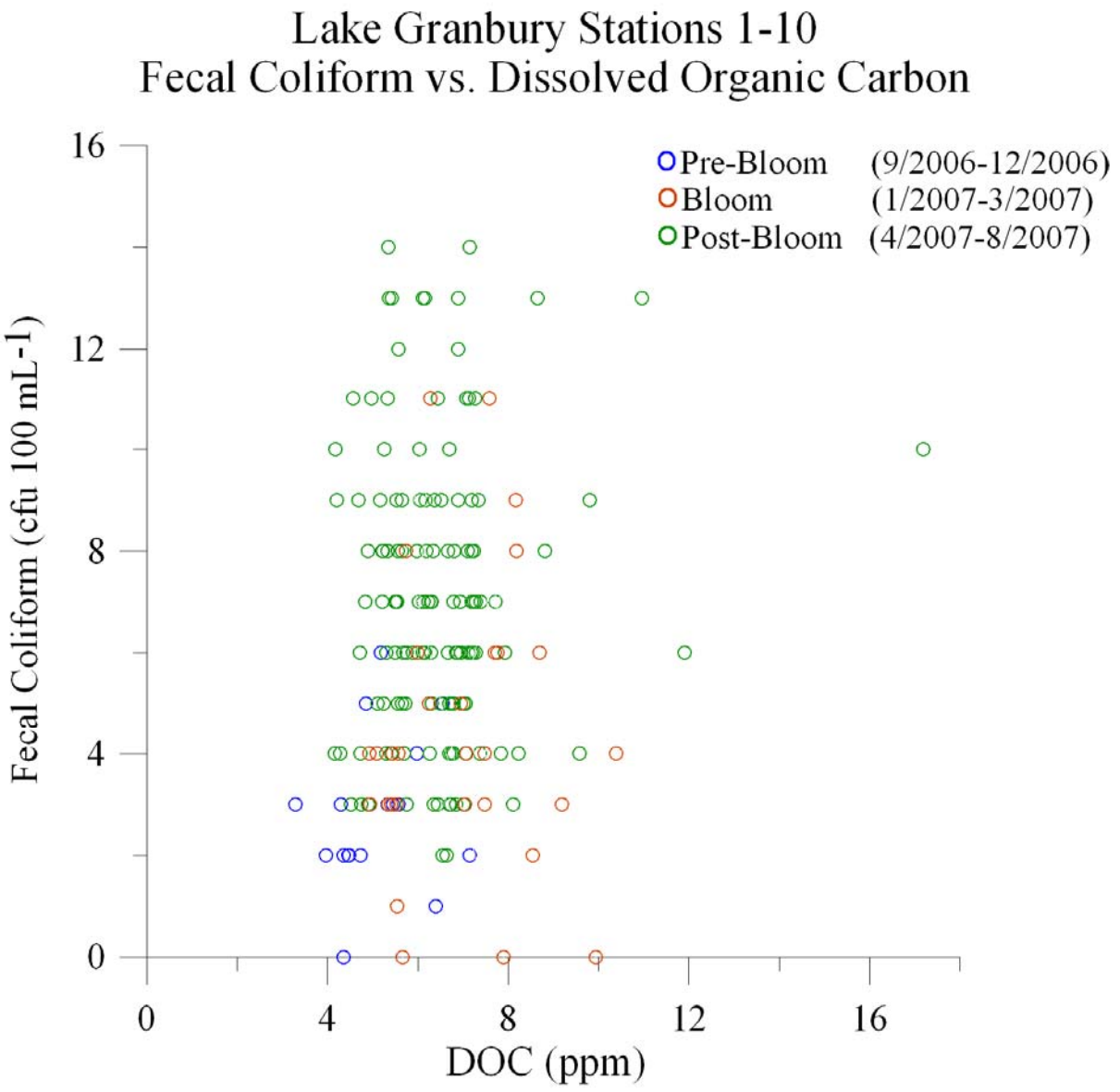

Figure D2. Regression of fecal coliform bacteria and dissolved organic carbon from open-lake, fixed locations (stations 1 through 10) from Lake Granbury during the *P. parvum* bloom year spanning September 2006 through August 2007.

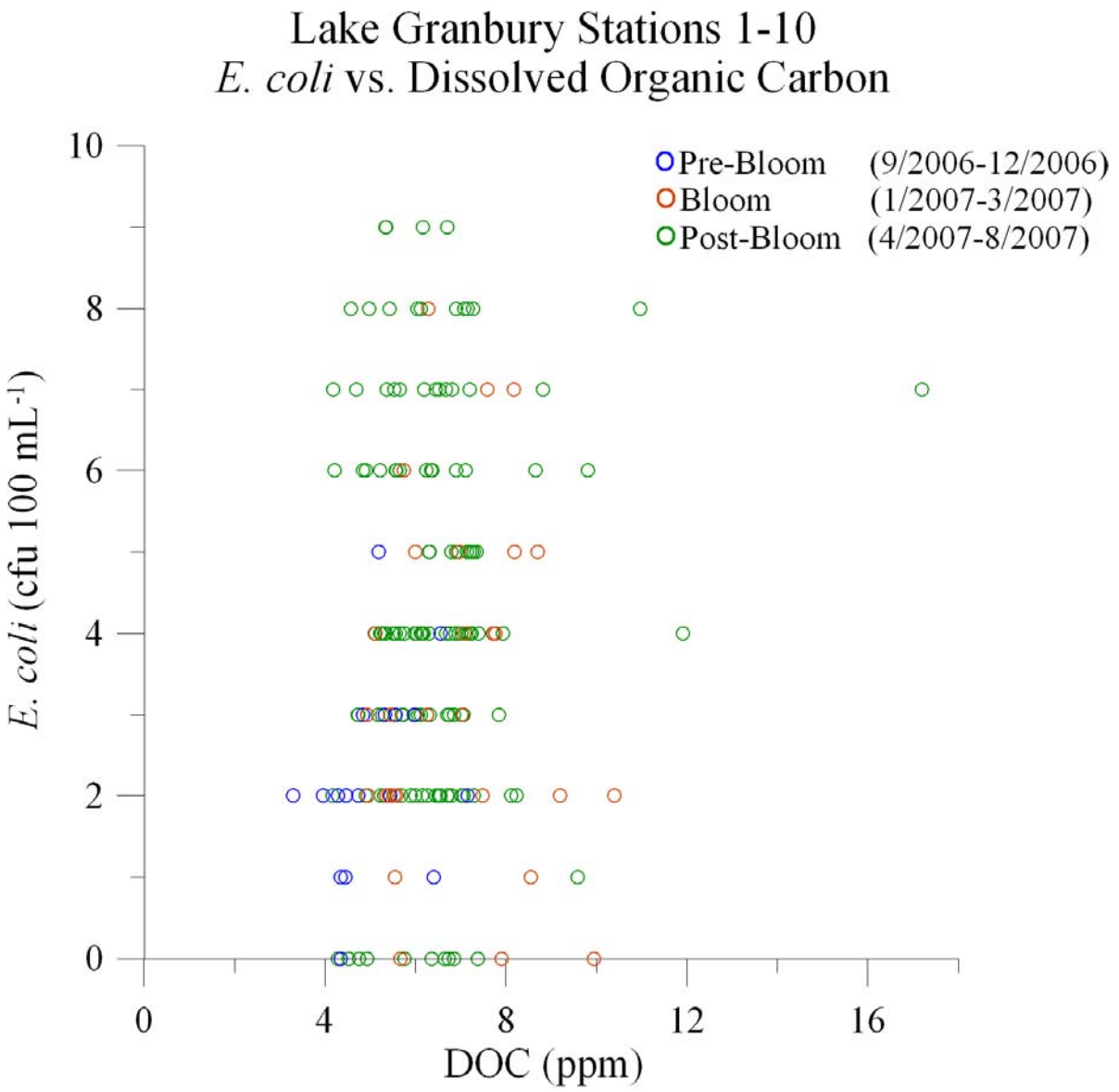

Figure D3. Regression of *E. coli* and dissolved organic carbon from open-lake, fixed locations (stations 1 through 10) from Lake Granbury during the *P. parvum* bloom year spanning September 2006 through August 2007.

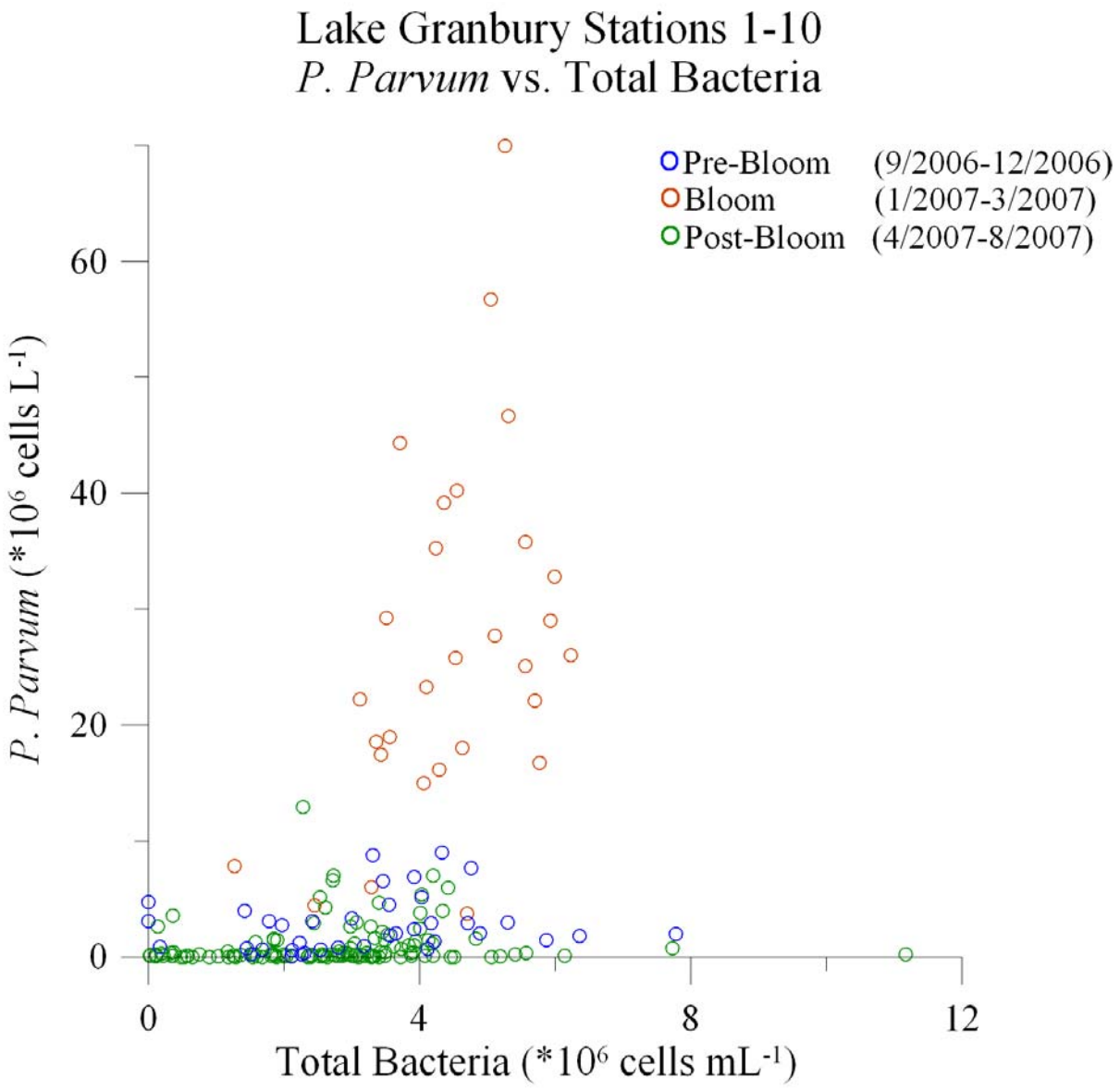

Figure D4. Regression of *P. parvum* and total bacteria from open-lake, fixed locations (stations 1 through 10) from Lake Granbury during the *P. parvum* bloom year spanning September 2006 through August 2007.

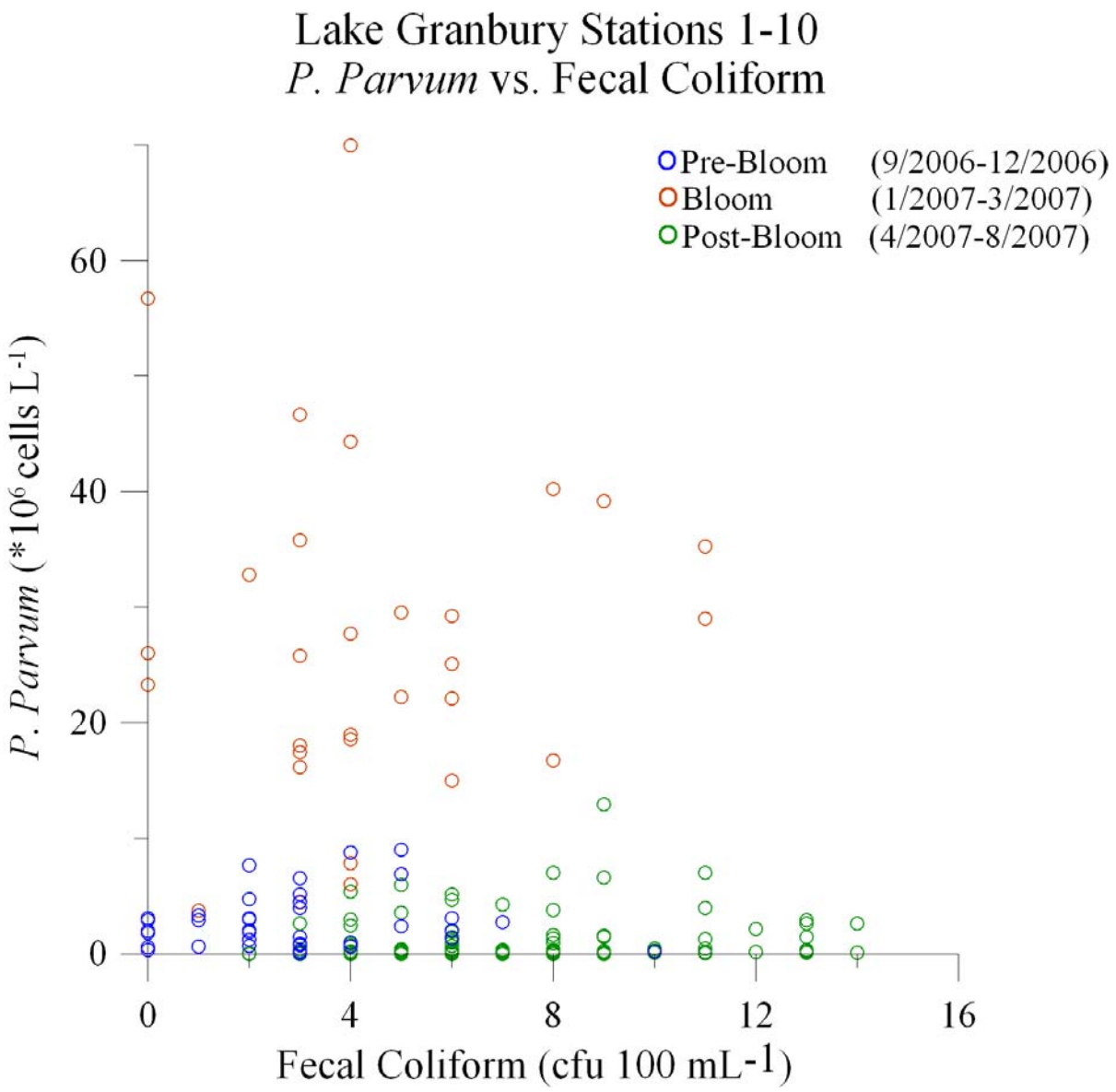

Figure D5. Regression of *P. parvum* and fecal coliform bacteria from open-lake, fixed locations (stations 1 through 10) from Lake Granbury during the *P. parvum* bloom year spanning September 2006 through August 2007.

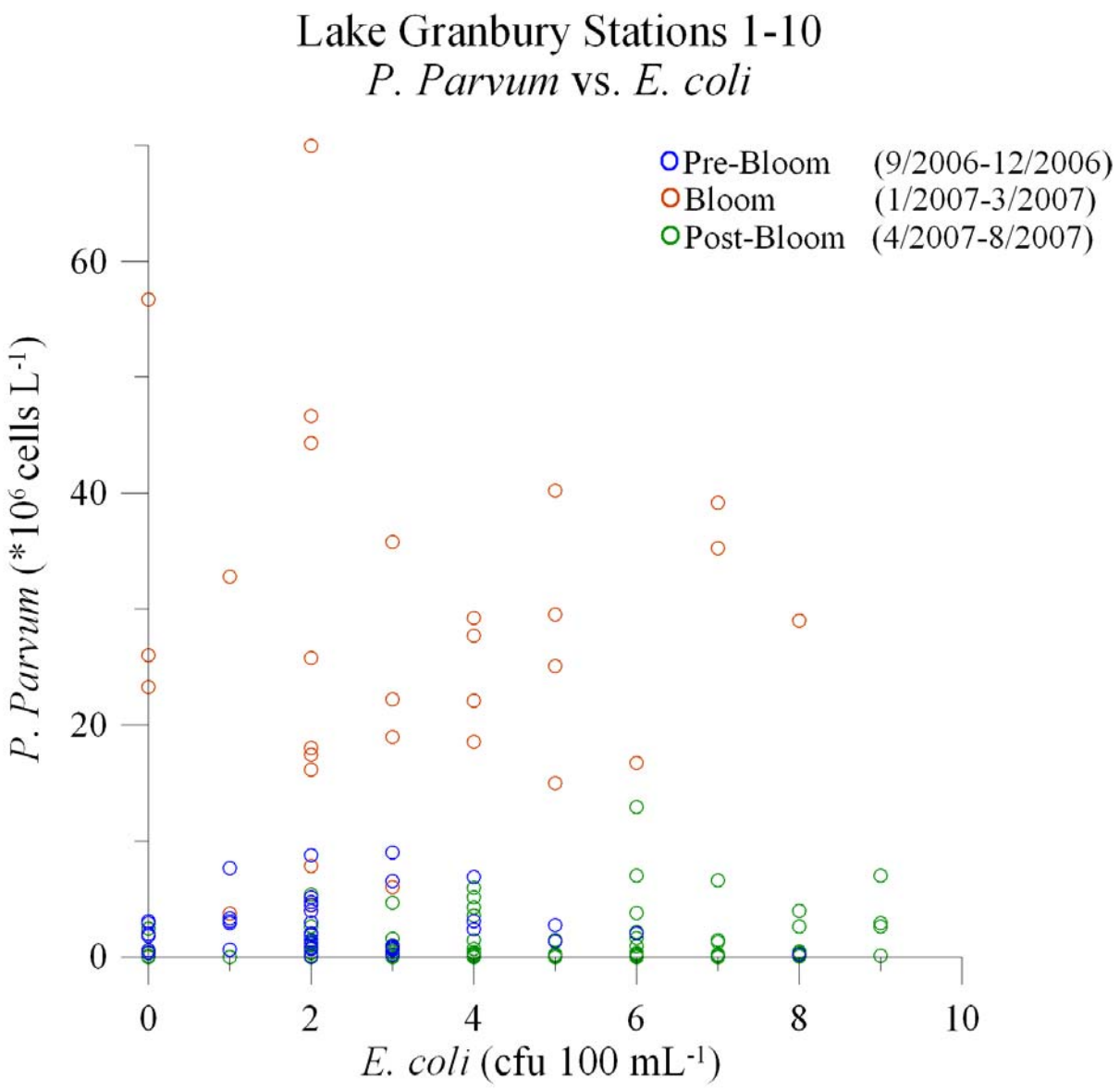

Figure D6. Regression of *P. parvum* and *E. coli* from open-lake, fixed locations (stations 1 through 10) from Lake Granbury during the *P. parvum* bloom year spanning September 2006 through August 2007.

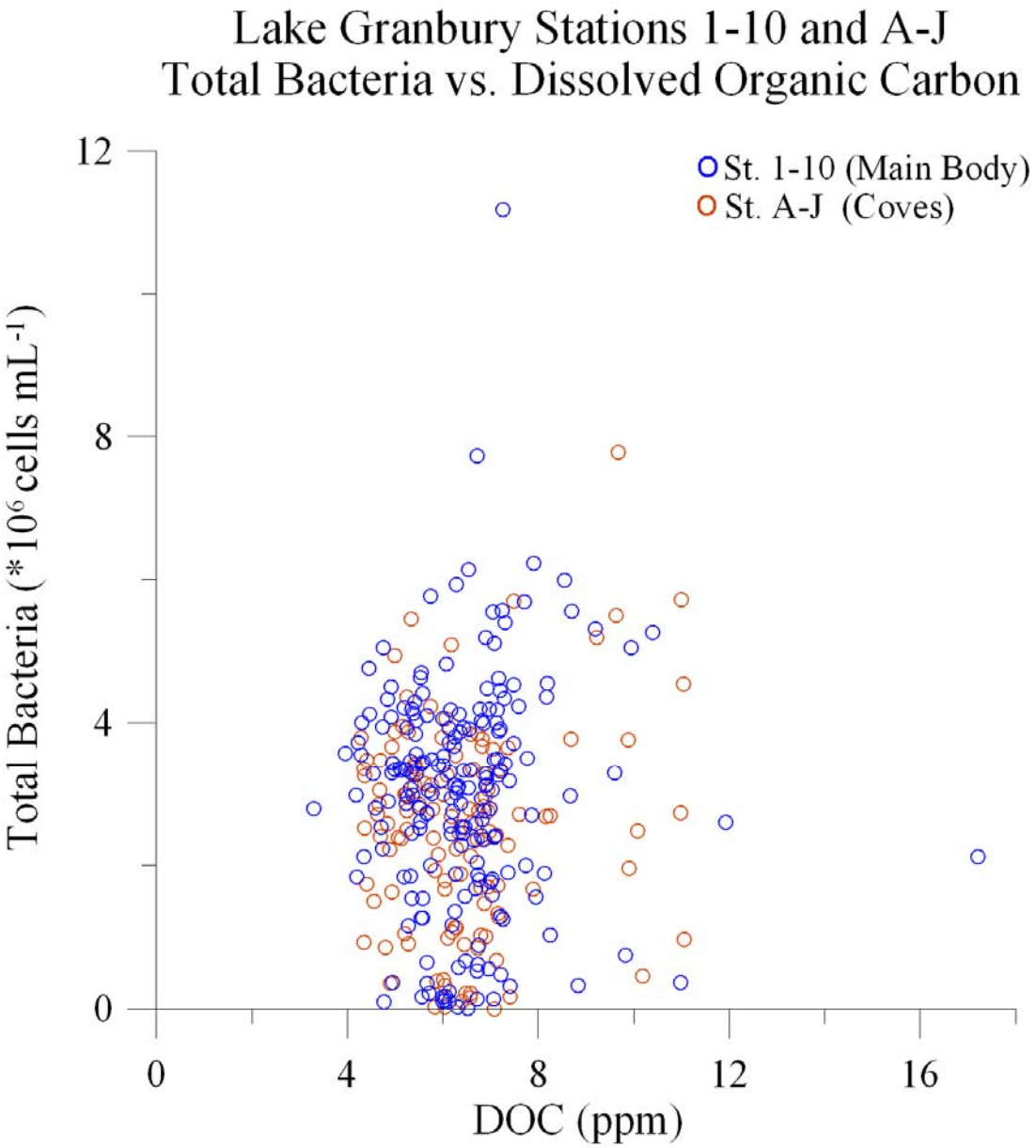

Figure D7. Regression of total bacteria and dissolved organic carbon from open-lake and cove locations (stations 1 through 10, stations A through J) from Lake Granbury during the *P. parvum* bloom year spanning September 2006 through August 2007, and during the non-bloom year spanning September 2007 through August 2008.

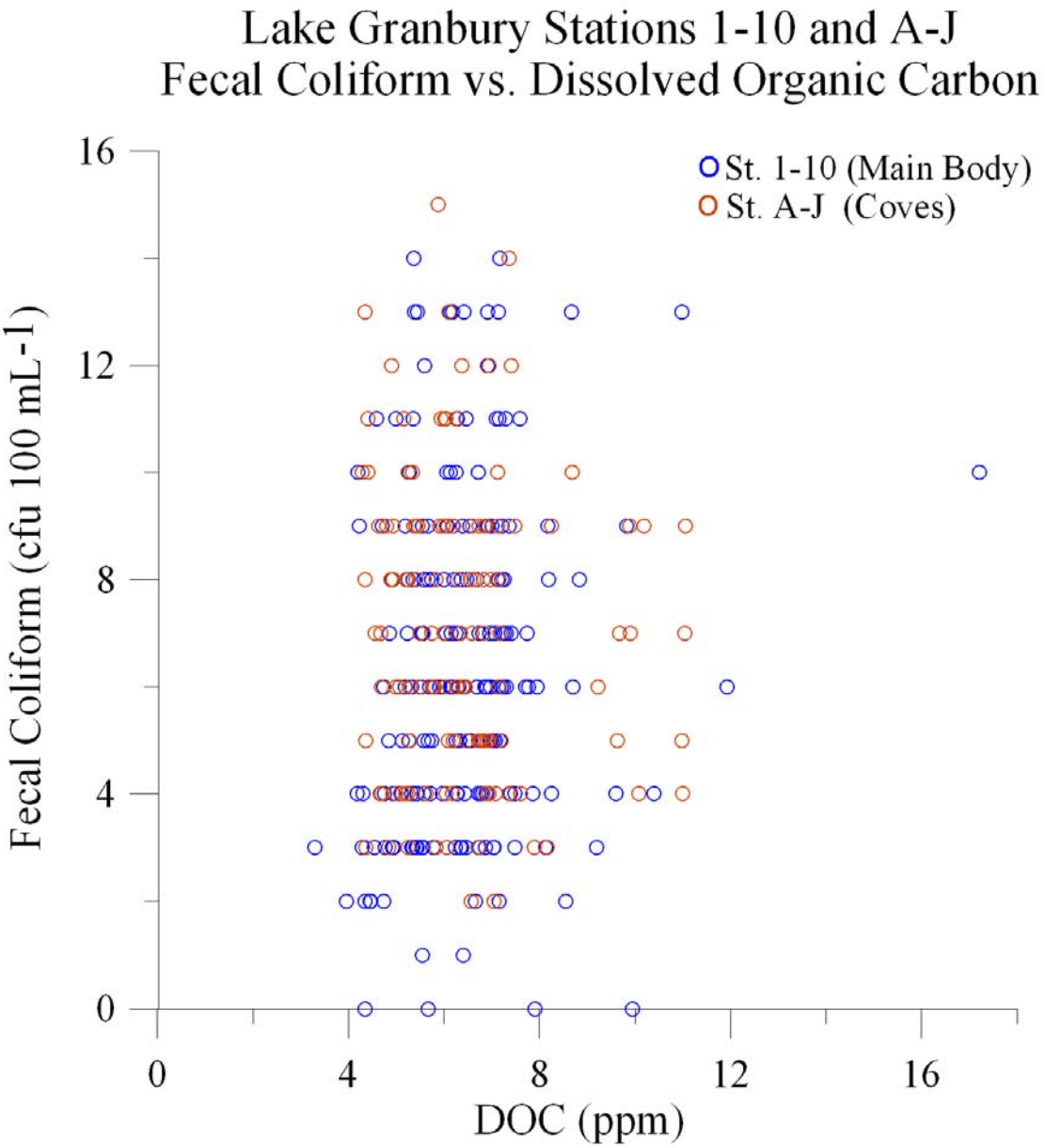

Figure D8. Regression of fecal coliform bacteria and dissolved organic carbon from open-lake and cove locations (stations 1 through 10, stations A through J) from Lake Granbury during the *P. parvum* bloom year spanning September 2006 through August 2007, and during the non-bloom year spanning September 2007 through August 2008.

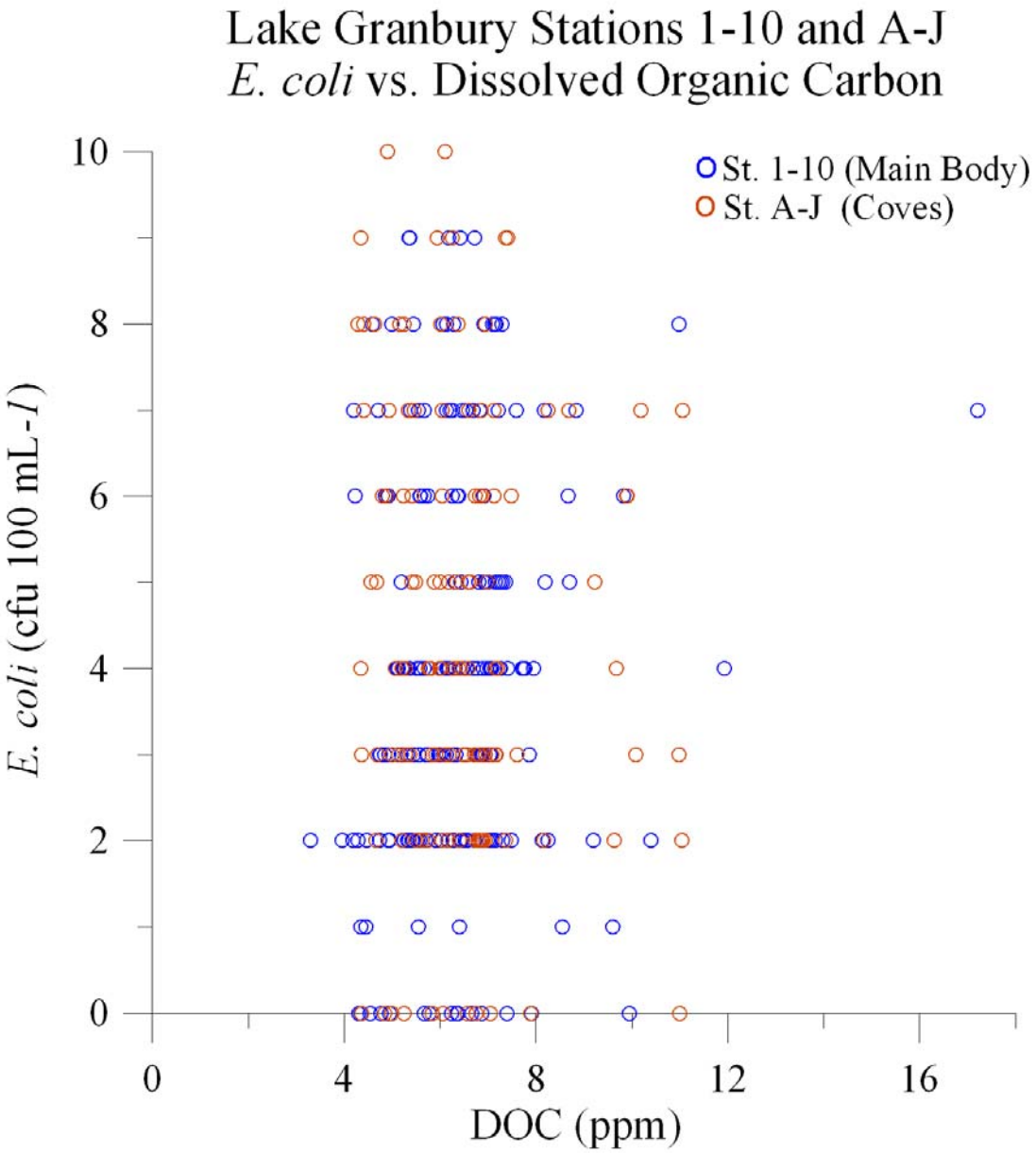

Figure D9. Regression of *E. coli* and dissolved organic carbon from open-lake and cove locations (stations 1 through 10, stations A through J) from Lake Granbury during the *P. parvum* bloom year spanning September 2006 through August 2007, and during the non-bloom year spanning September 2007 through August 2008.

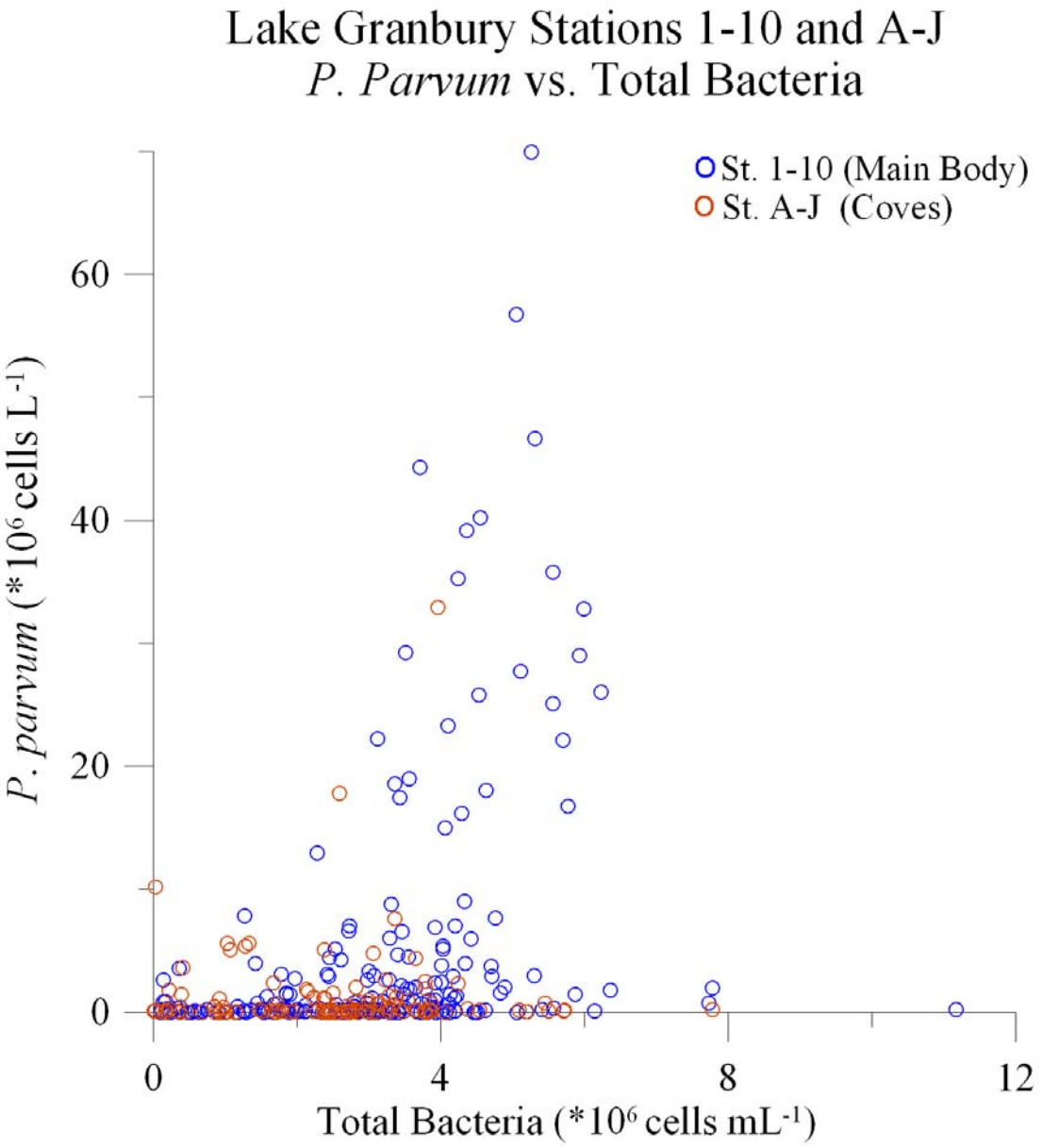

Figure D10. Regression of *P. parvum* and total bacteria from open-lake and cove locations (stations 1 through 10, stations A through J) from Lake Granbury during the *P. parvum* bloom year spanning September 2006 through August 2007, and during the non-bloom year spanning September 2007 through August 2008.

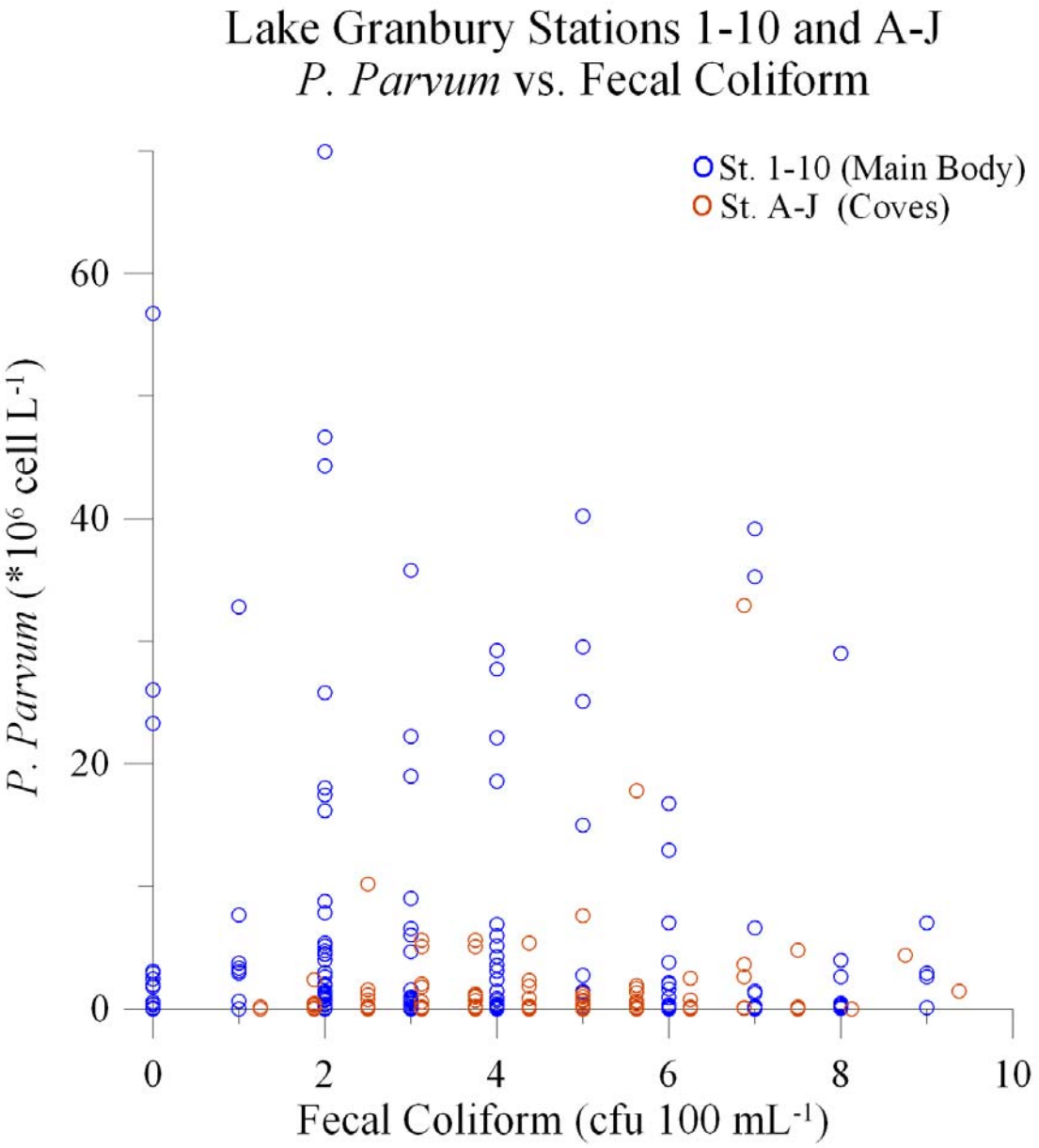

Figure D11. Regression of *P. parvum* and fecal coliform bacteria from open-lake and cove locations (stations 1 through 10, stations A through J) from Lake Granbury during the *P. parvum* bloom year spanning September 2006 through August 2007, and during the non-bloom year spanning September 2007 through August 2008.

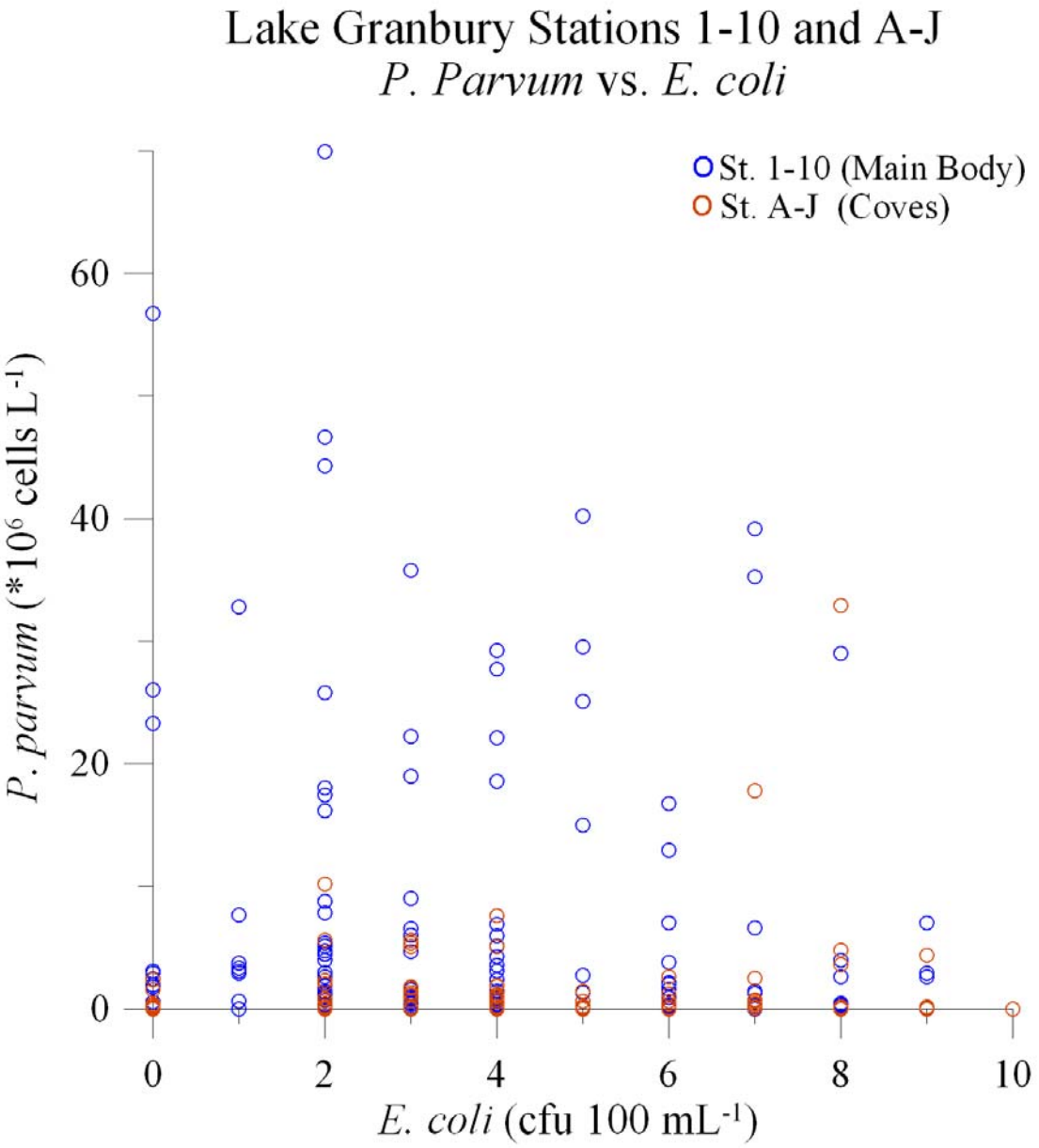

Figure D12. Regression of *P. parvum* and *E. coli* from open-lake and cove locations (stations 1 through 10, stations A through J) from Lake Granbury during the *P. parvum* bloom year spanning September 2006 through August 2007, and during the non-bloom year spanning September 2007 through August 2008.

Appendix E

Dataflow maps for Lake Granbury

Monthly sampling from September 2006 through August, 2008. Note, early in the data record transects were not system wide due to troubles encountered while sampling. Months were no data flow maps are presented indicate that on-board instrument troubles prevented collection of flow-through data, ot that some of the sensors in the dataflow were malfunctioning.

Figures E-1 through E-16 - Chlorophyll *a*
Figures E-17 through E-33 - Salinity
Figures E-34 through E-50 - Temperature
Figures E-51 through E-74 - pH
Figures E-65 through E-81 - Turbidity
Figures E-82 through E-98 - Dissolved Organic Carbon

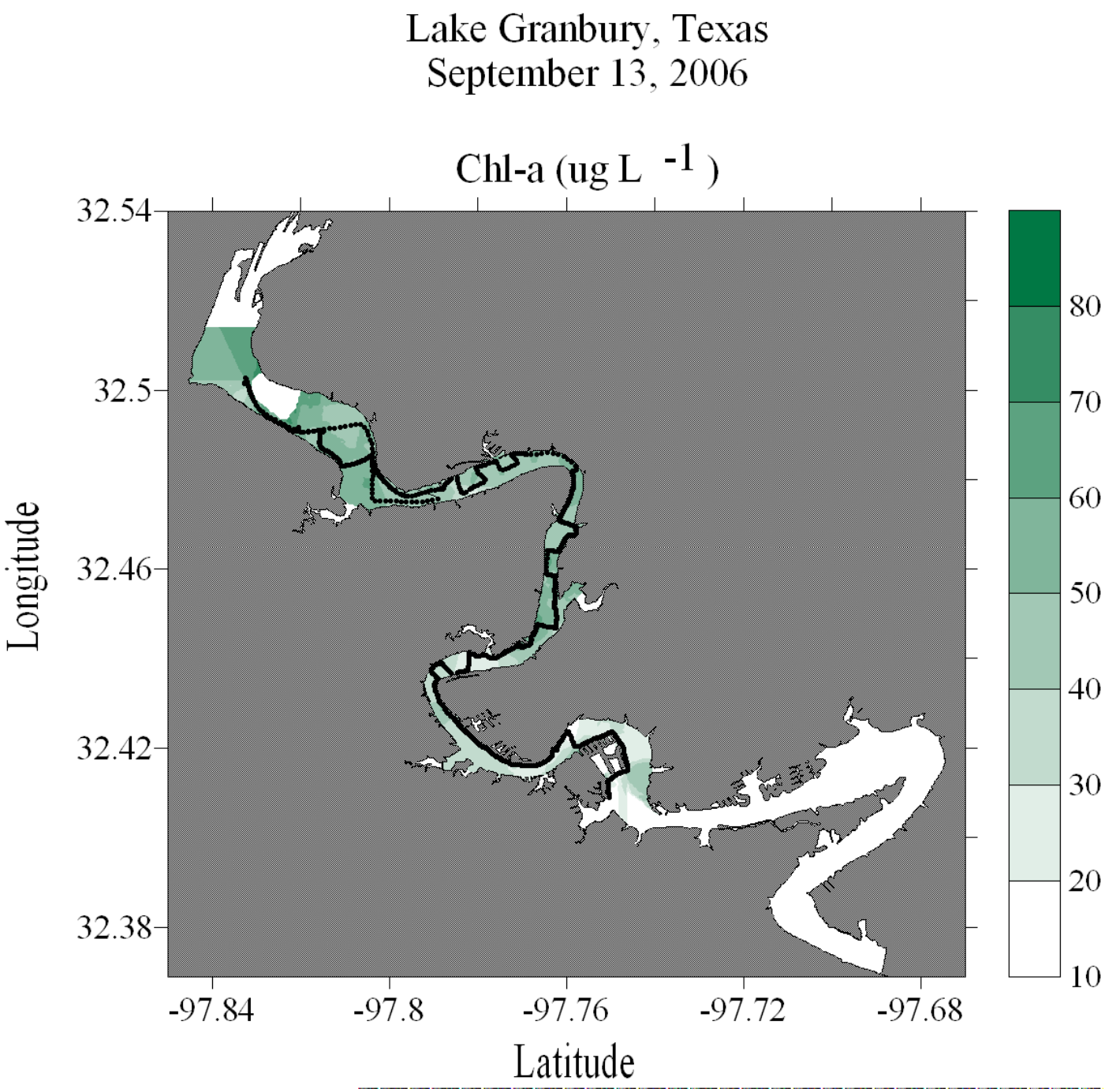

Figure E-1. Chlorophyll *a* dataflow map for Lake Granbury

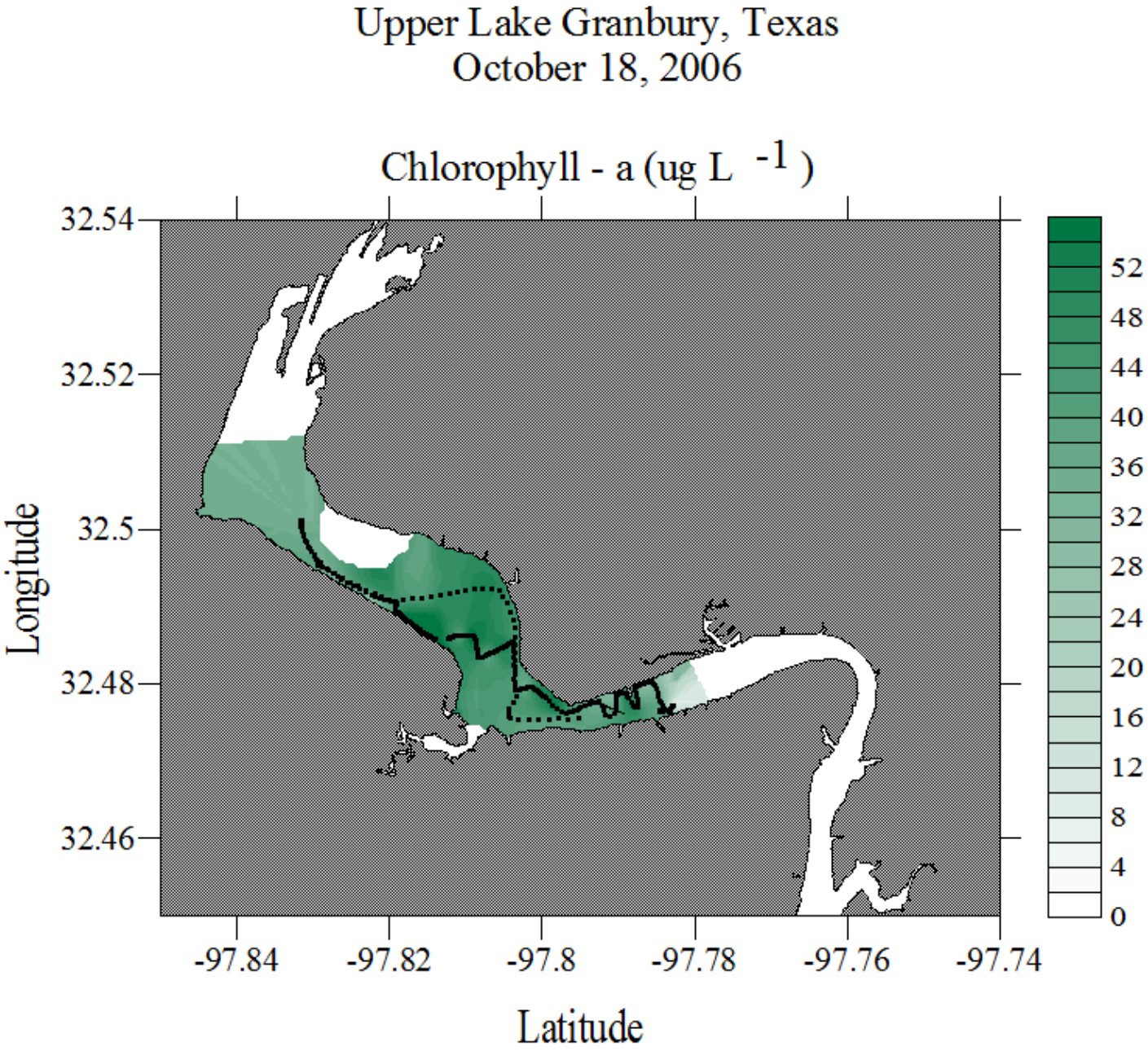

Figure E-2. Chlorophyll *a* dataflow map for Lake Granbury

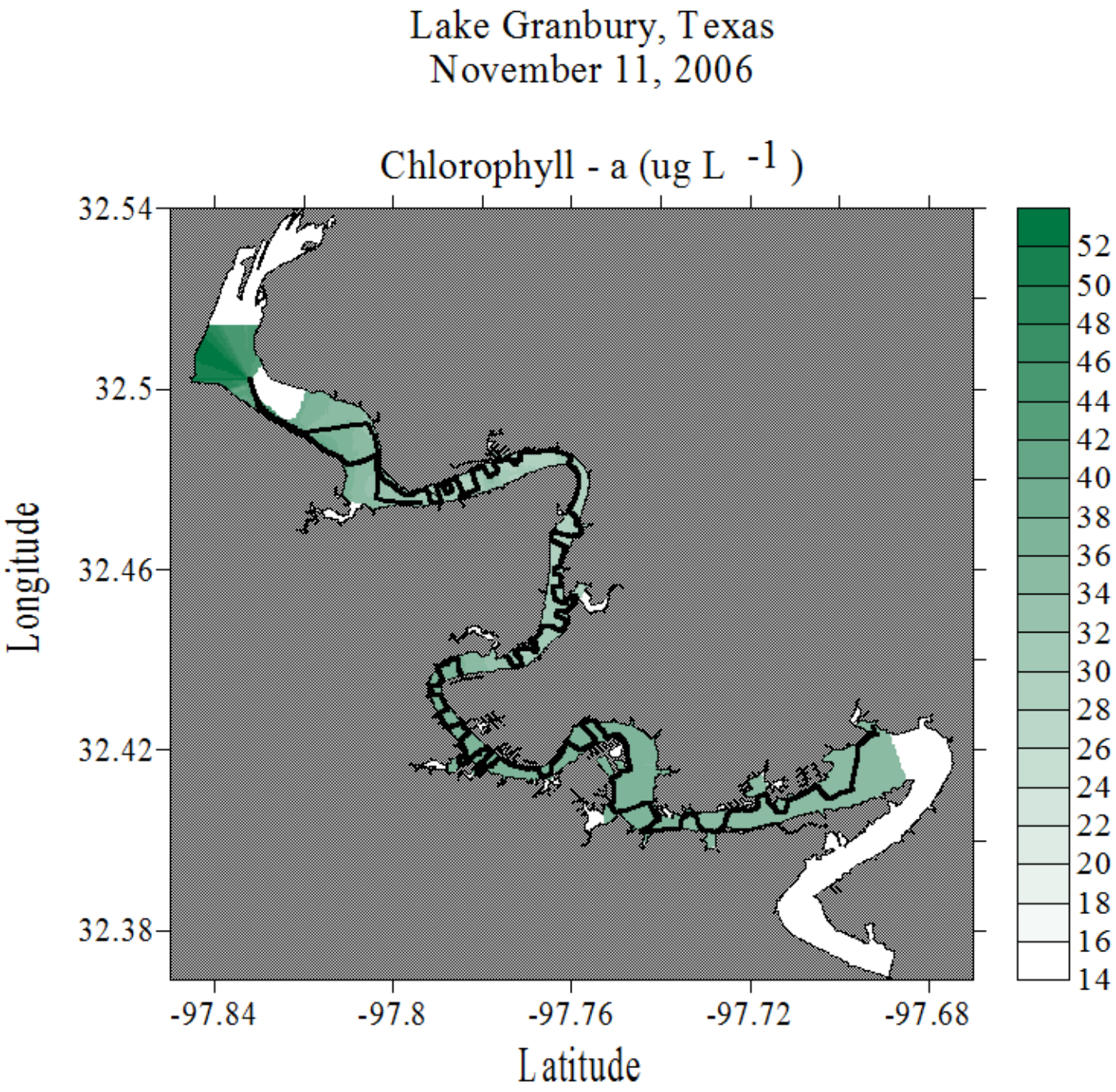

Figure E-3. Chlorophyll *a* dataflow map for Lake Granbury

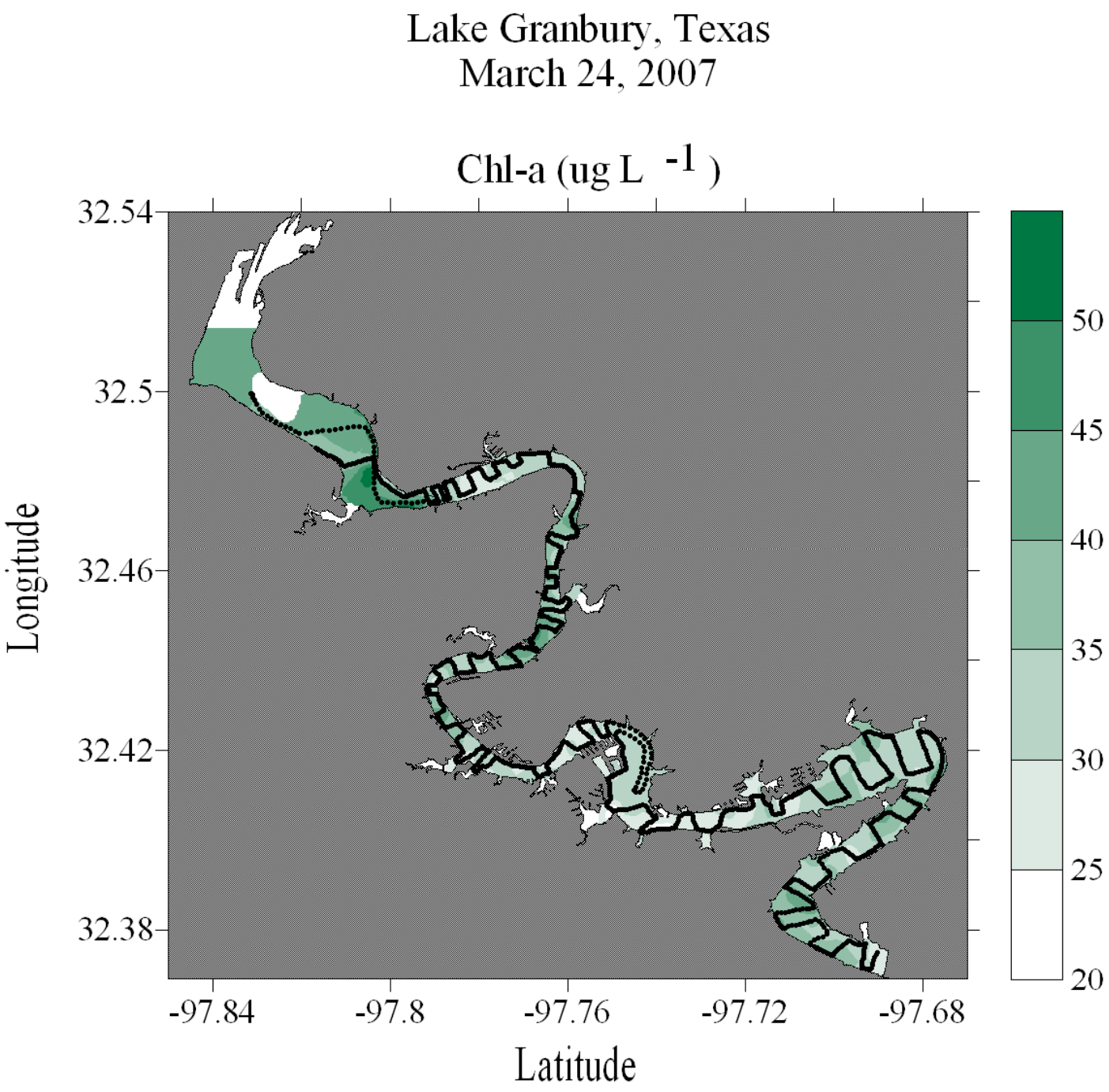

Figure E-4. Chlorophyll *a* dataflow map for Lake Granbury

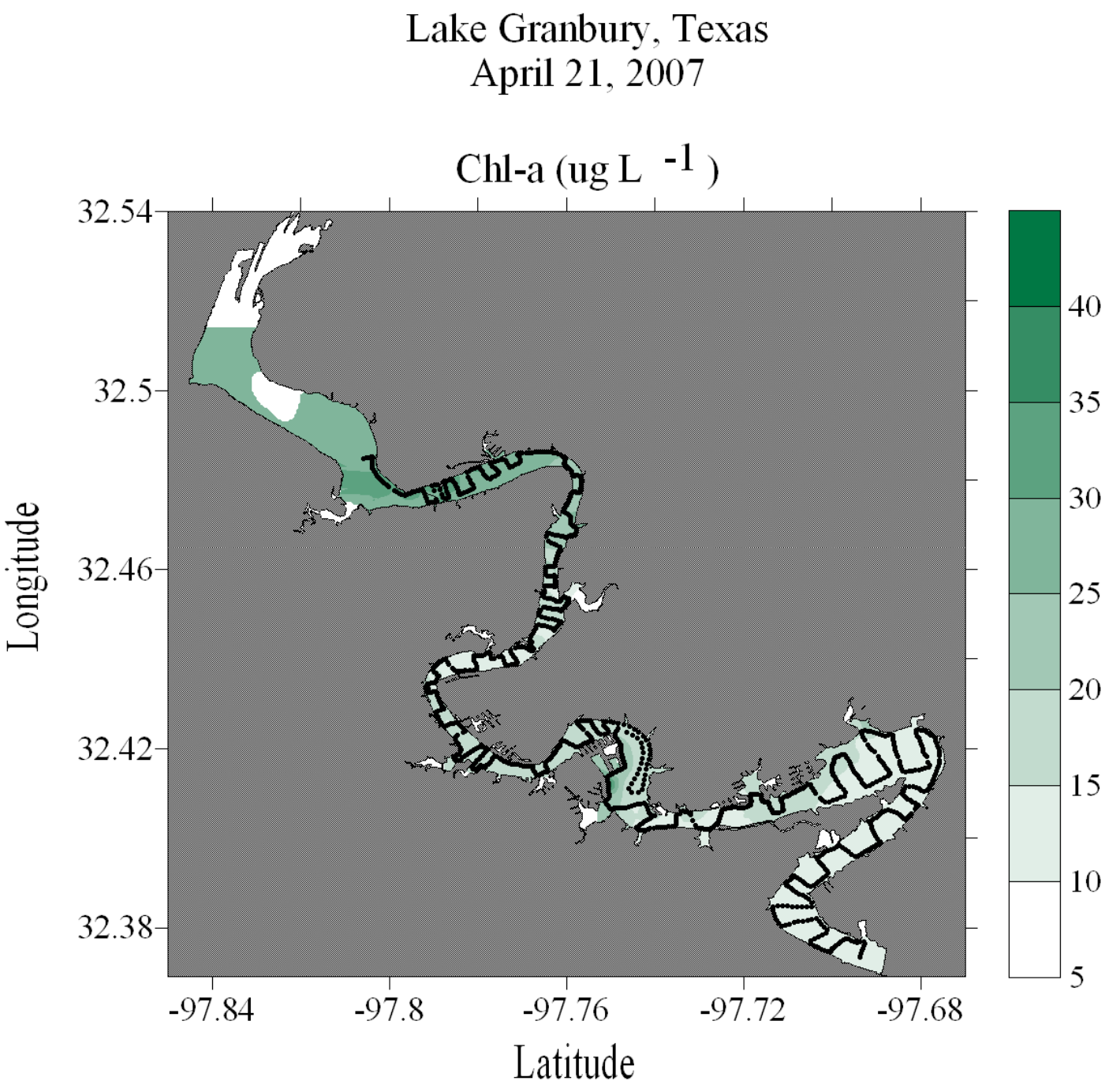

Figure E-5. Chlorophyll *a* dataflow map for Lake Granbury

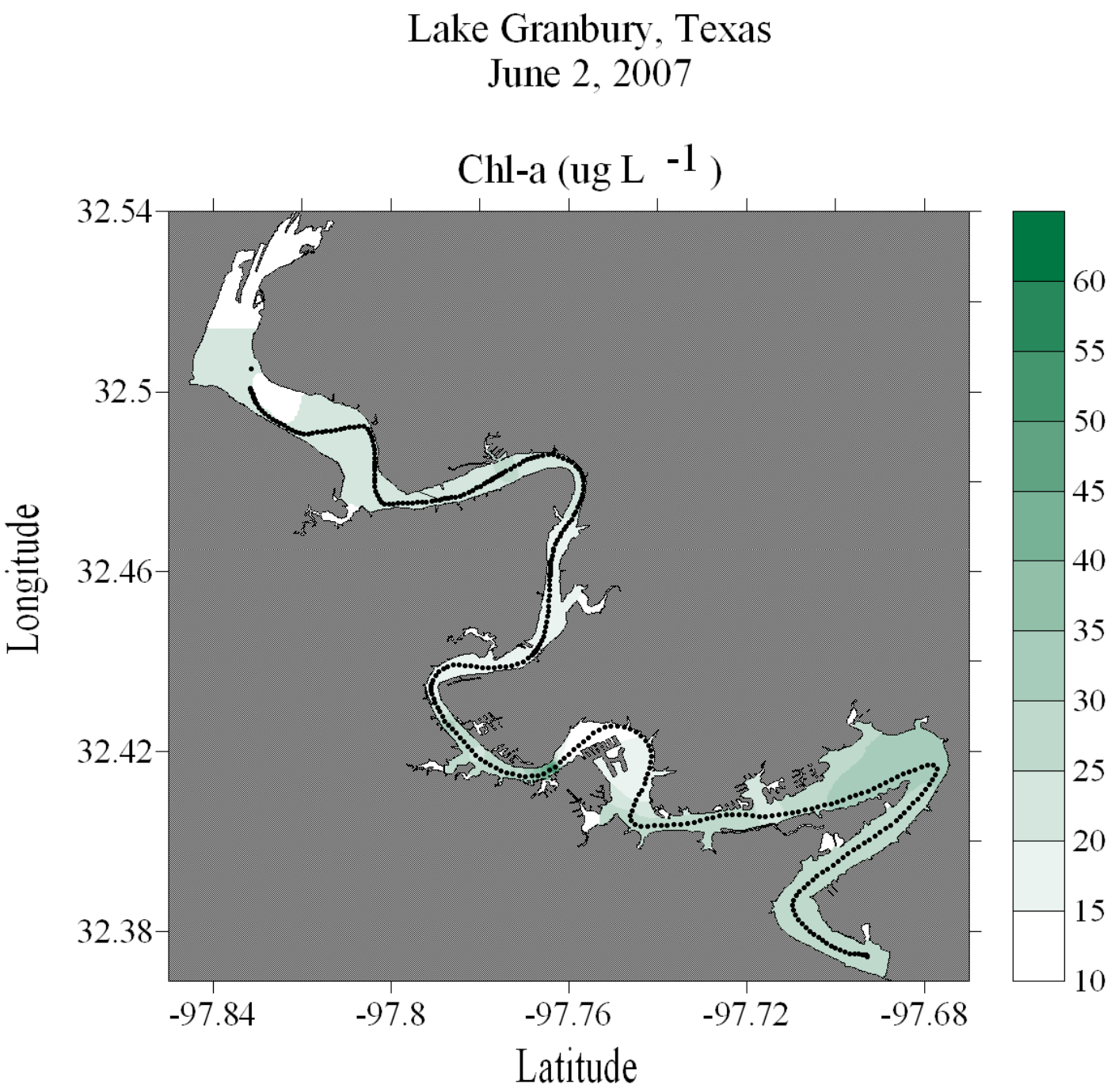

Figure E-6. Chlorophyll *a* dataflow map for Lake Granbury

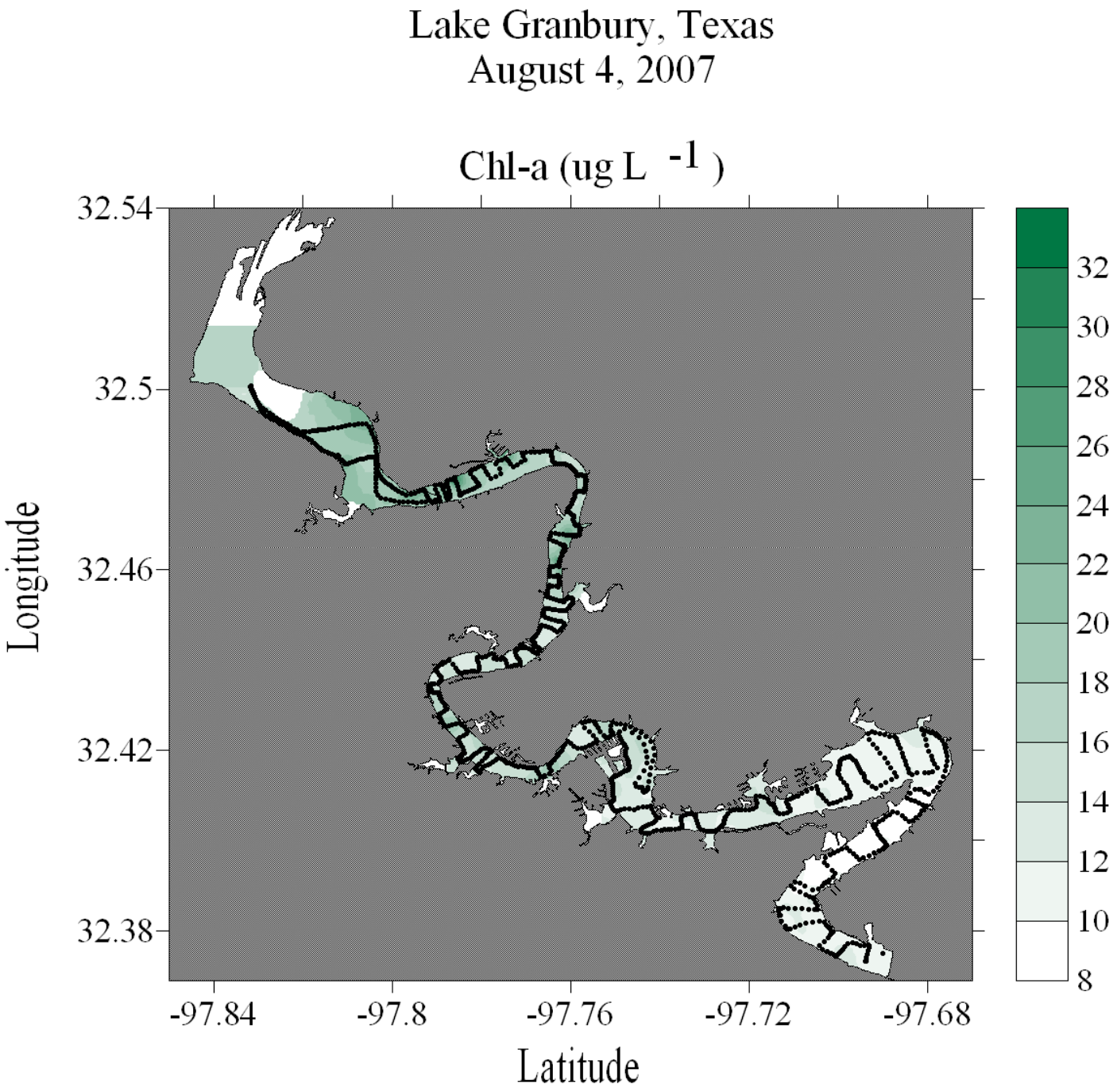

Figure E-7. Chlorophyll *a* dataflow map for Lake Granbury

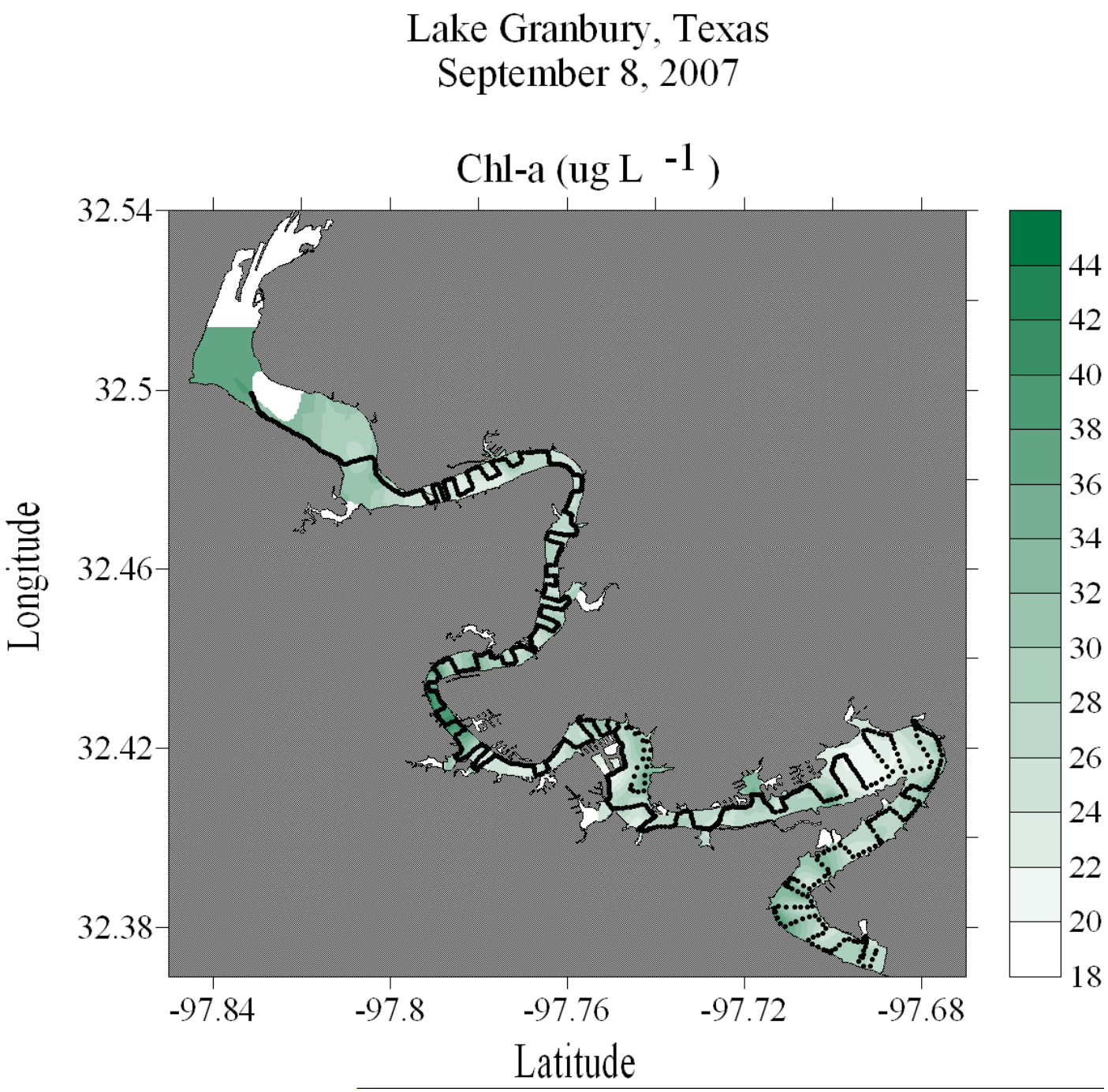

Figure E-8. Chlorophyll *a* dataflow map for Lake Granbury

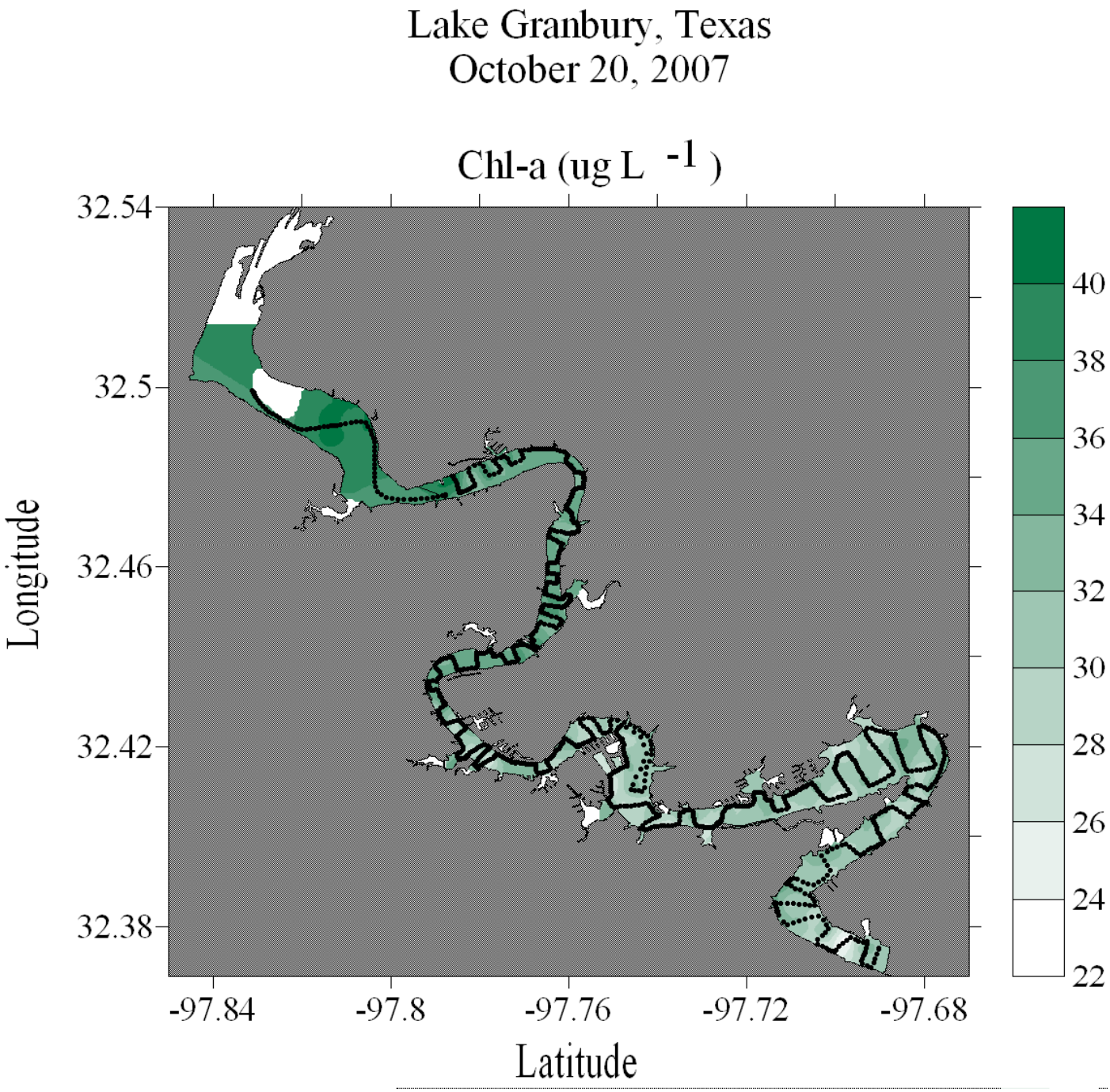

Figure E-9. Chlorophyll *a* dataflow map for Lake Granbury

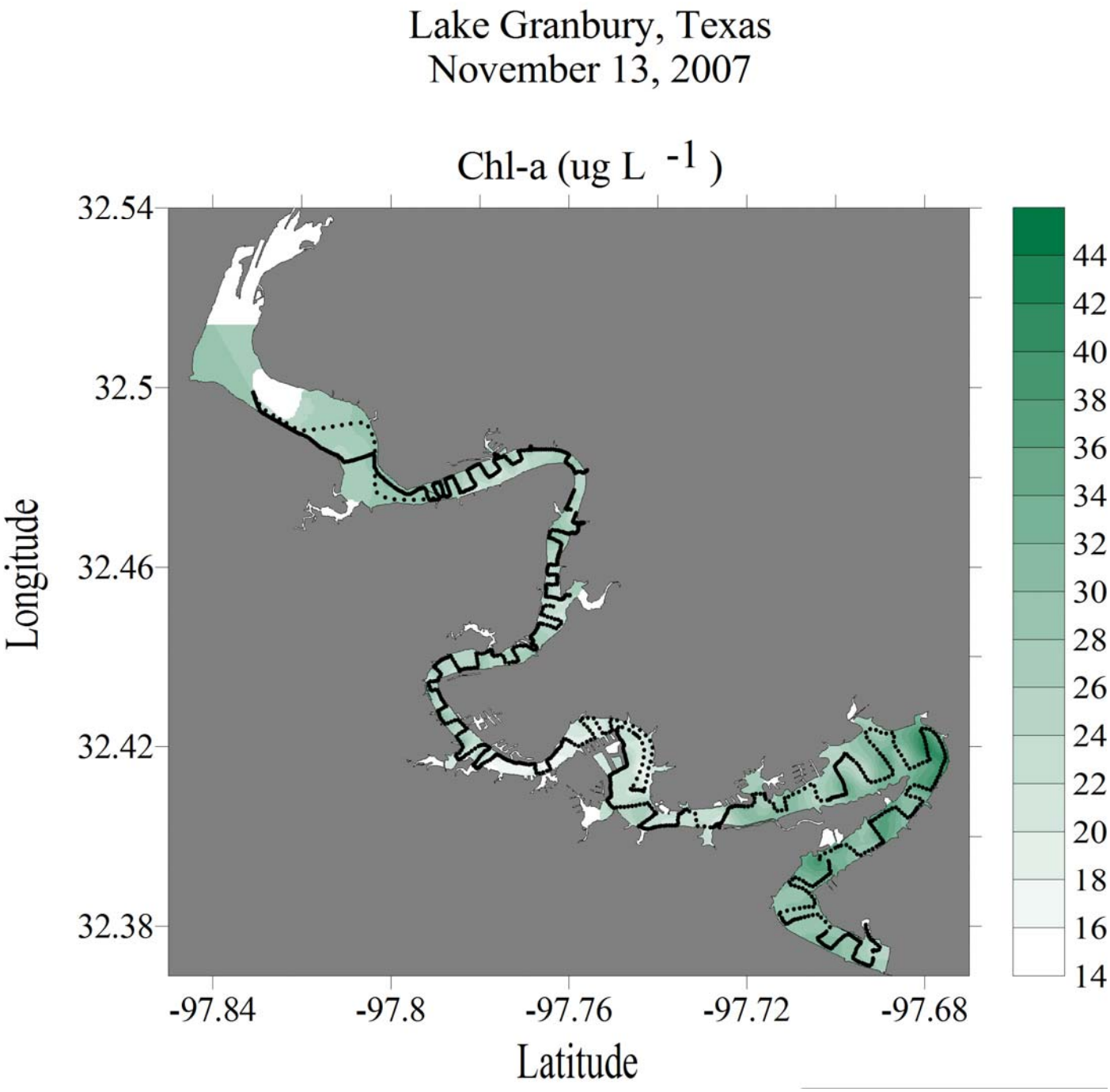

Figure E-10. Chlorophyll *a* dataflow map for Lake Granbury

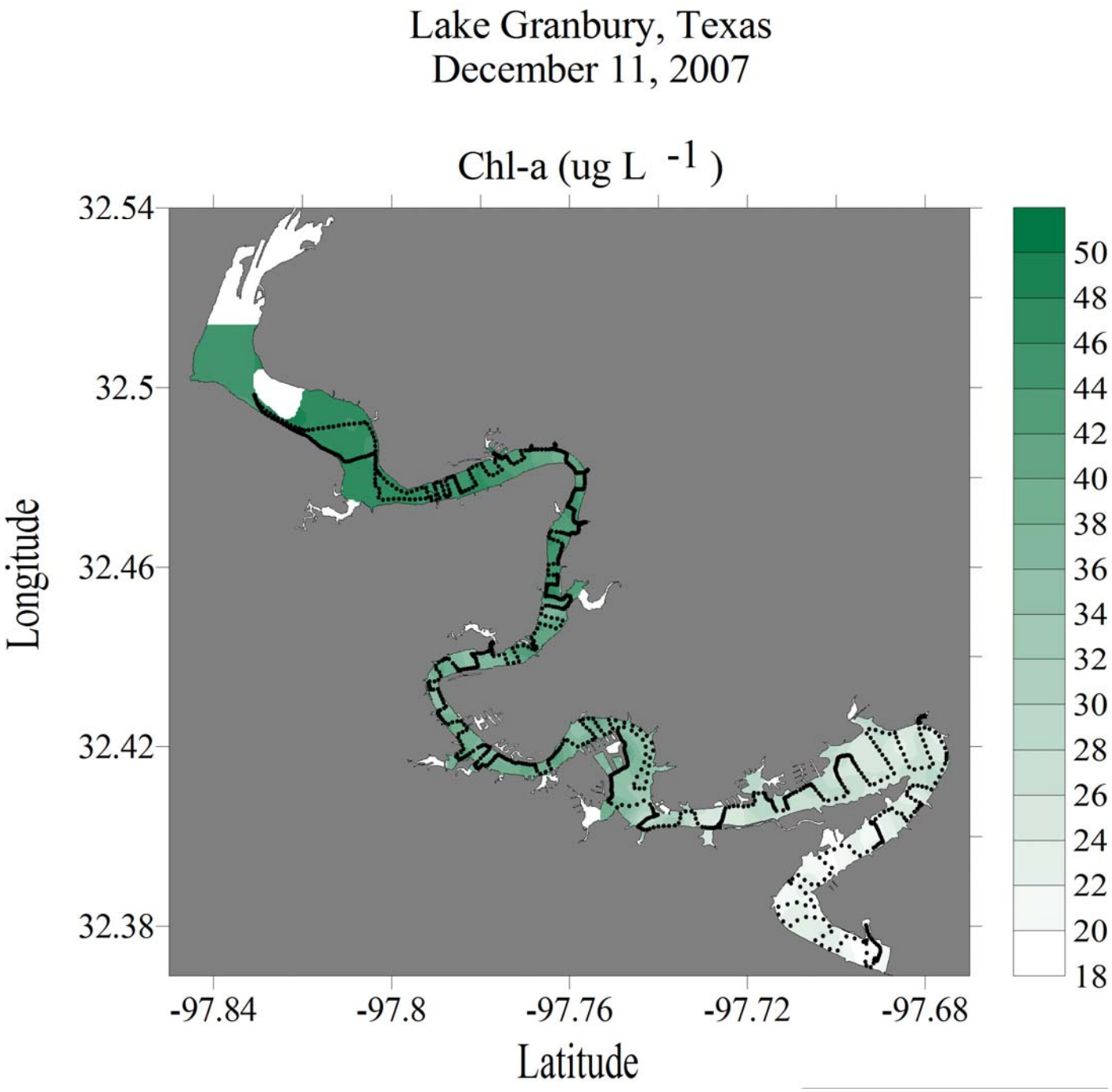

Figure E-11. Chlorophyll *a* dataflow map for Lake Granbury

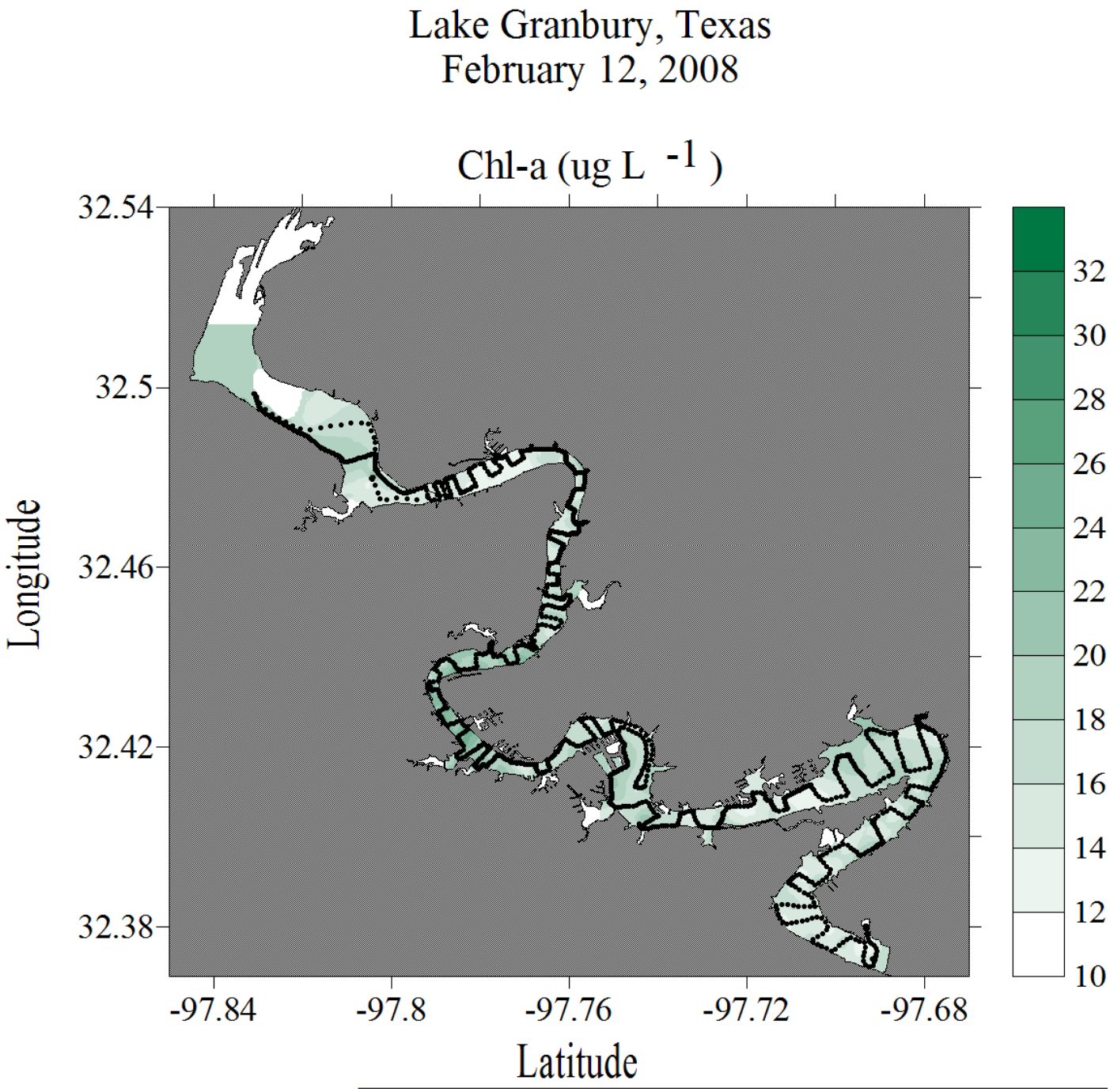

Figure E-12. Chlorophyll *a* dataflow map for Lake Granbury

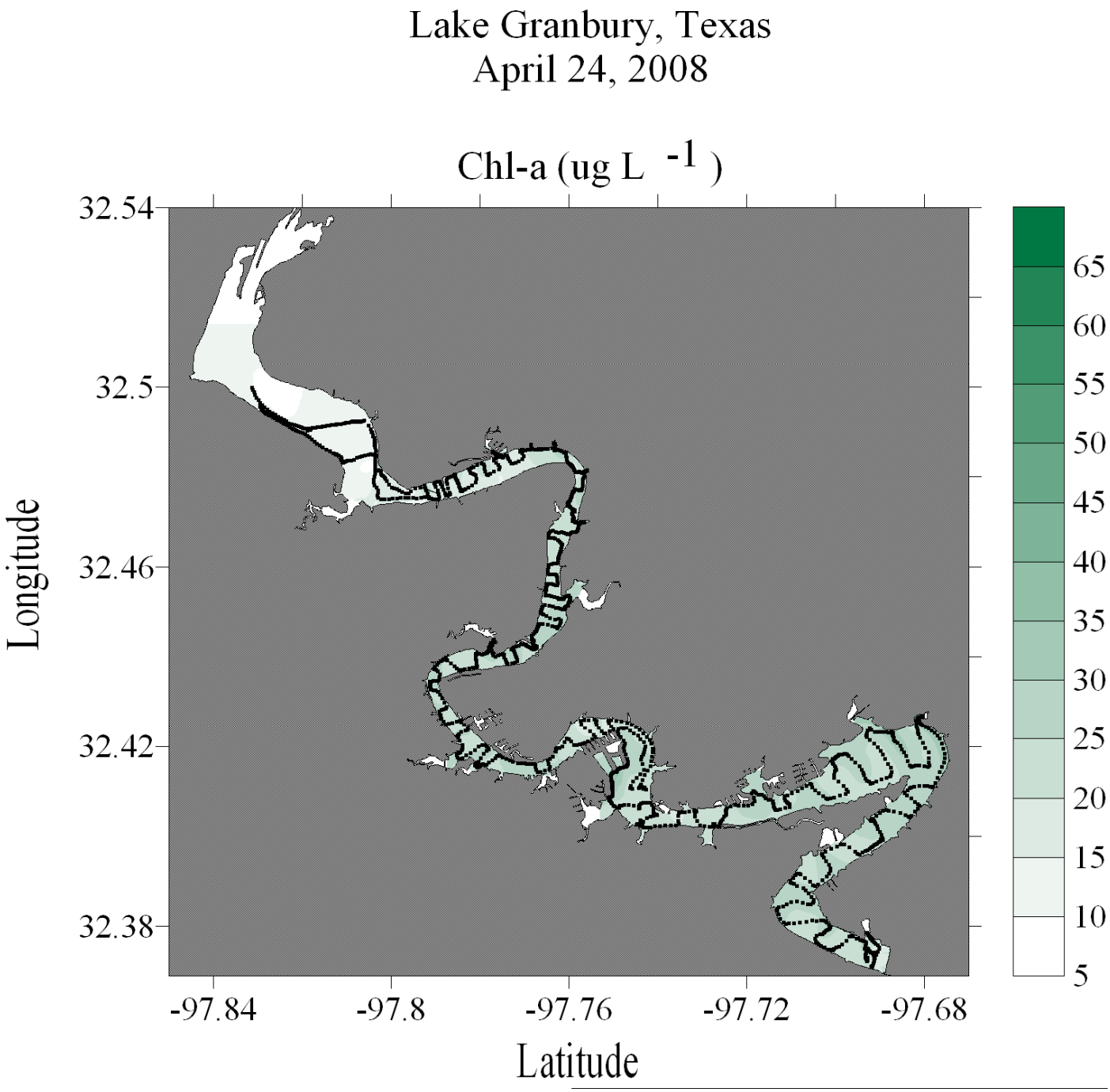

Figure E-13. Chlorophyll *a* dataflow map for Lake Granbury

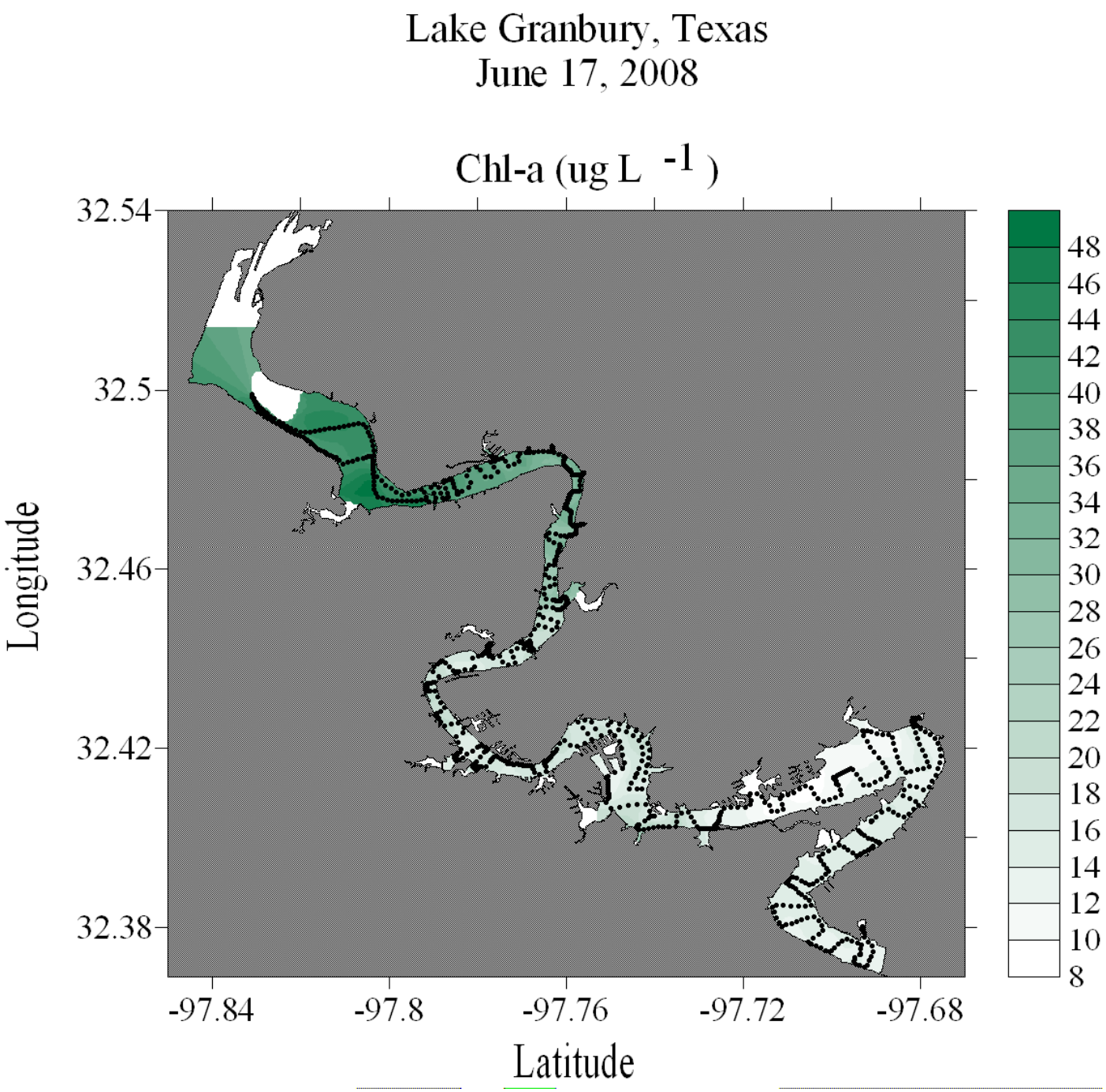

Figure E-14. Chlorophyll *a* dataflow map for Lake Granbury

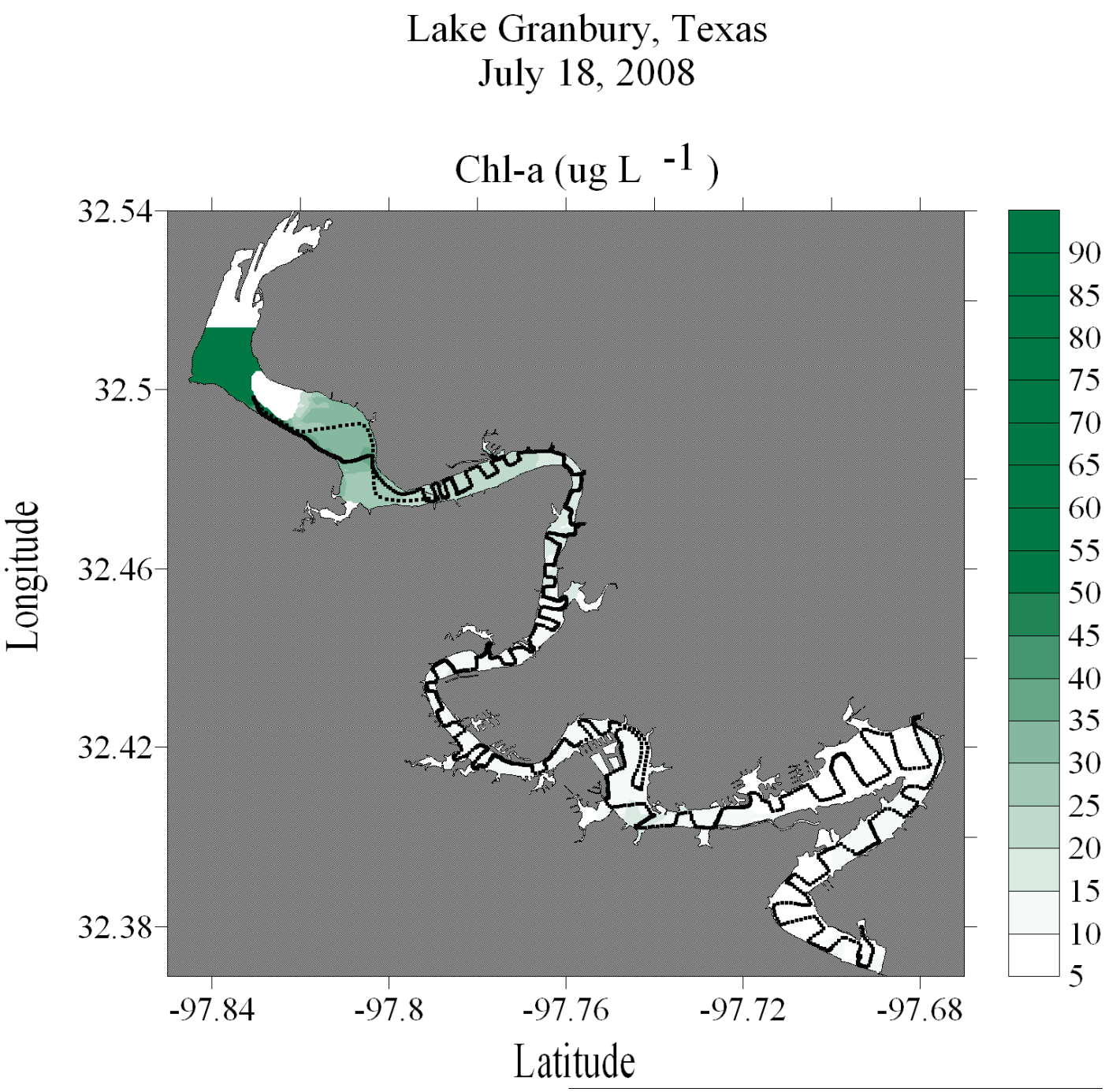

Figure E-15. Chlorophyll *a* dataflow map for Lake Granbury

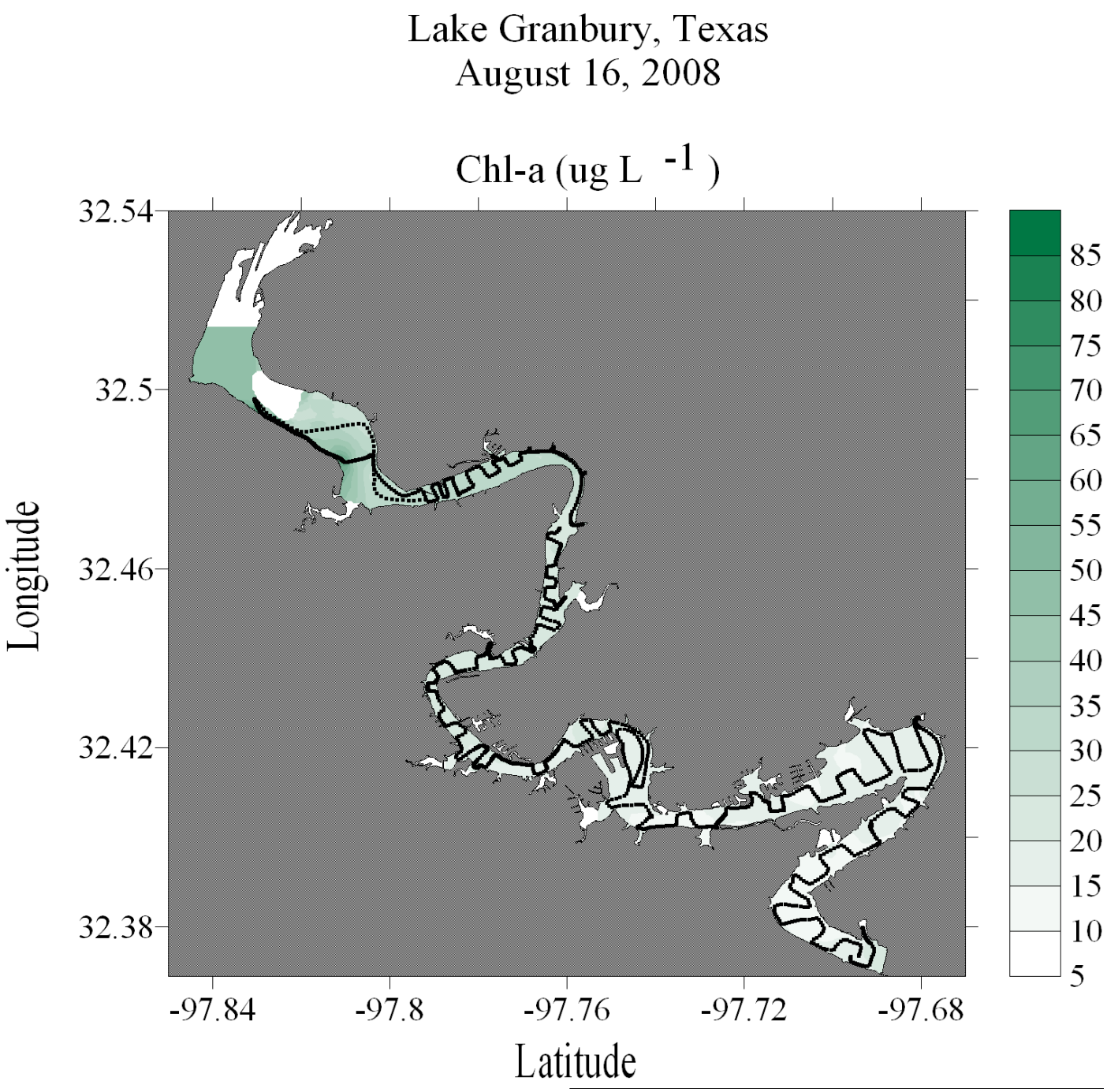

Figure E-16. Chlorophyll *a* dataflow map for Lake Granbury

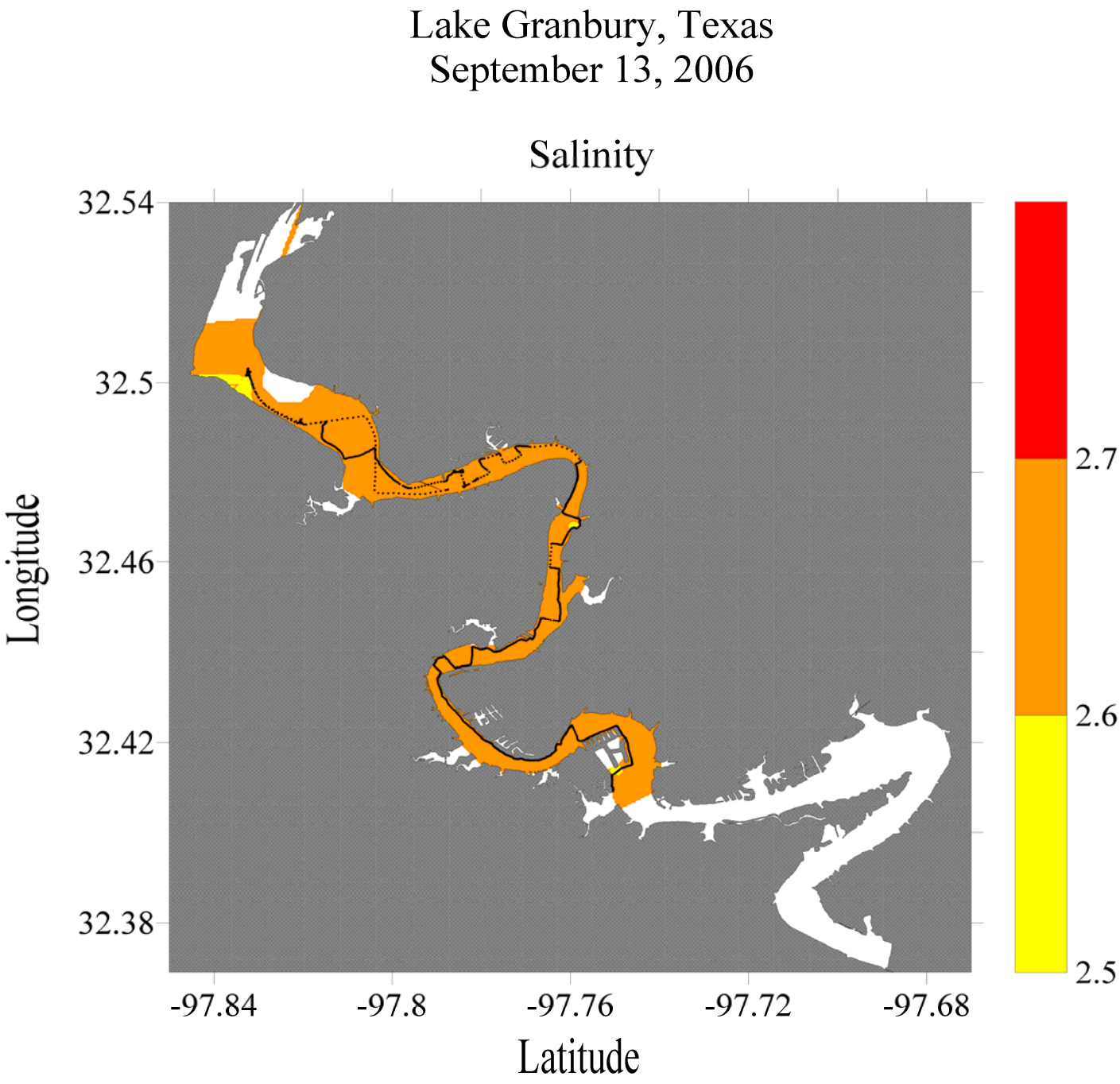

Figure E-17. Salinity dataflow map for Lake Granbury

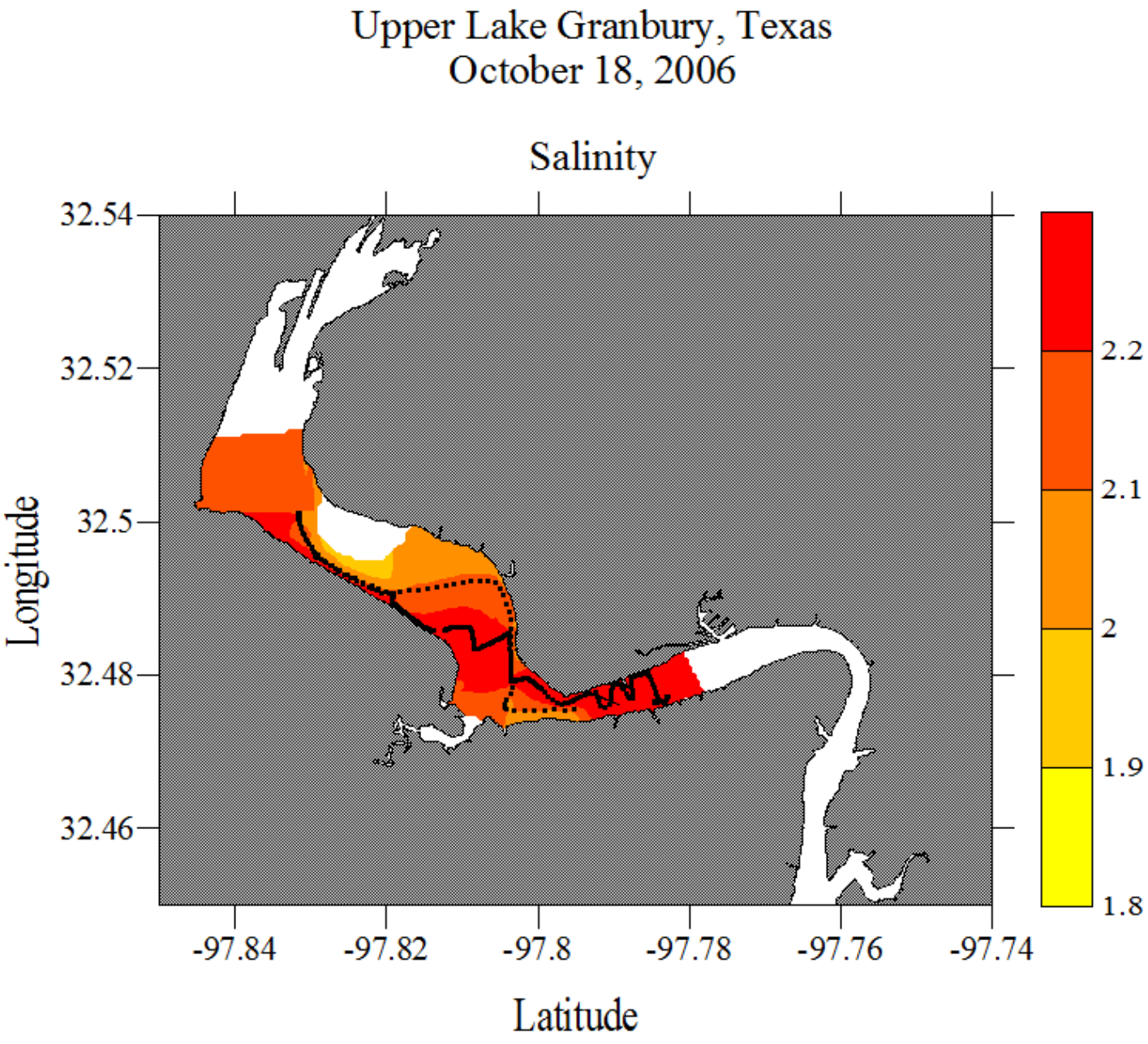

Figure E-18. Salinity dataflow map for Lake Granbury

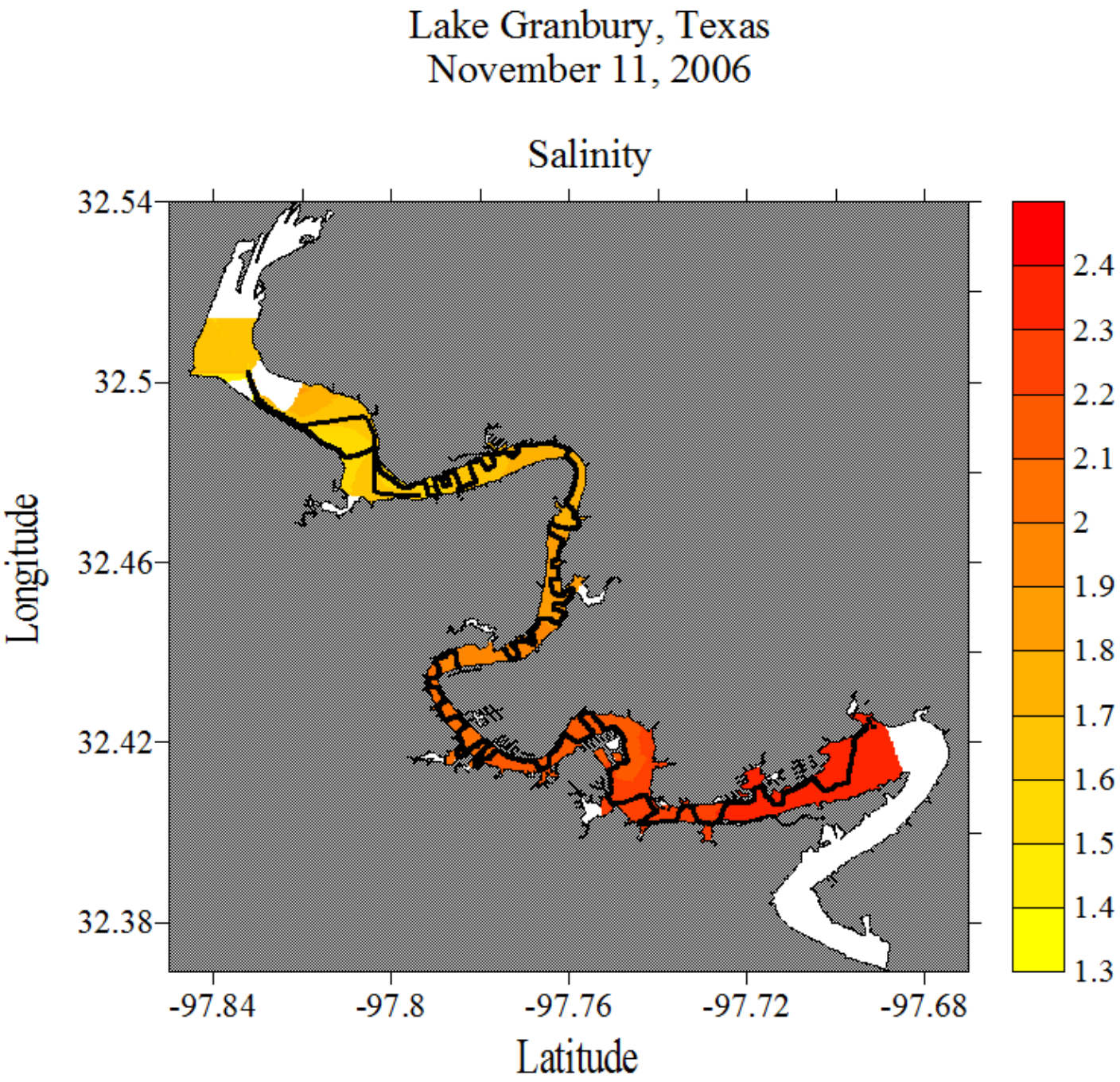

Figure E-19. Salinity dataflow map for Lake Granbury

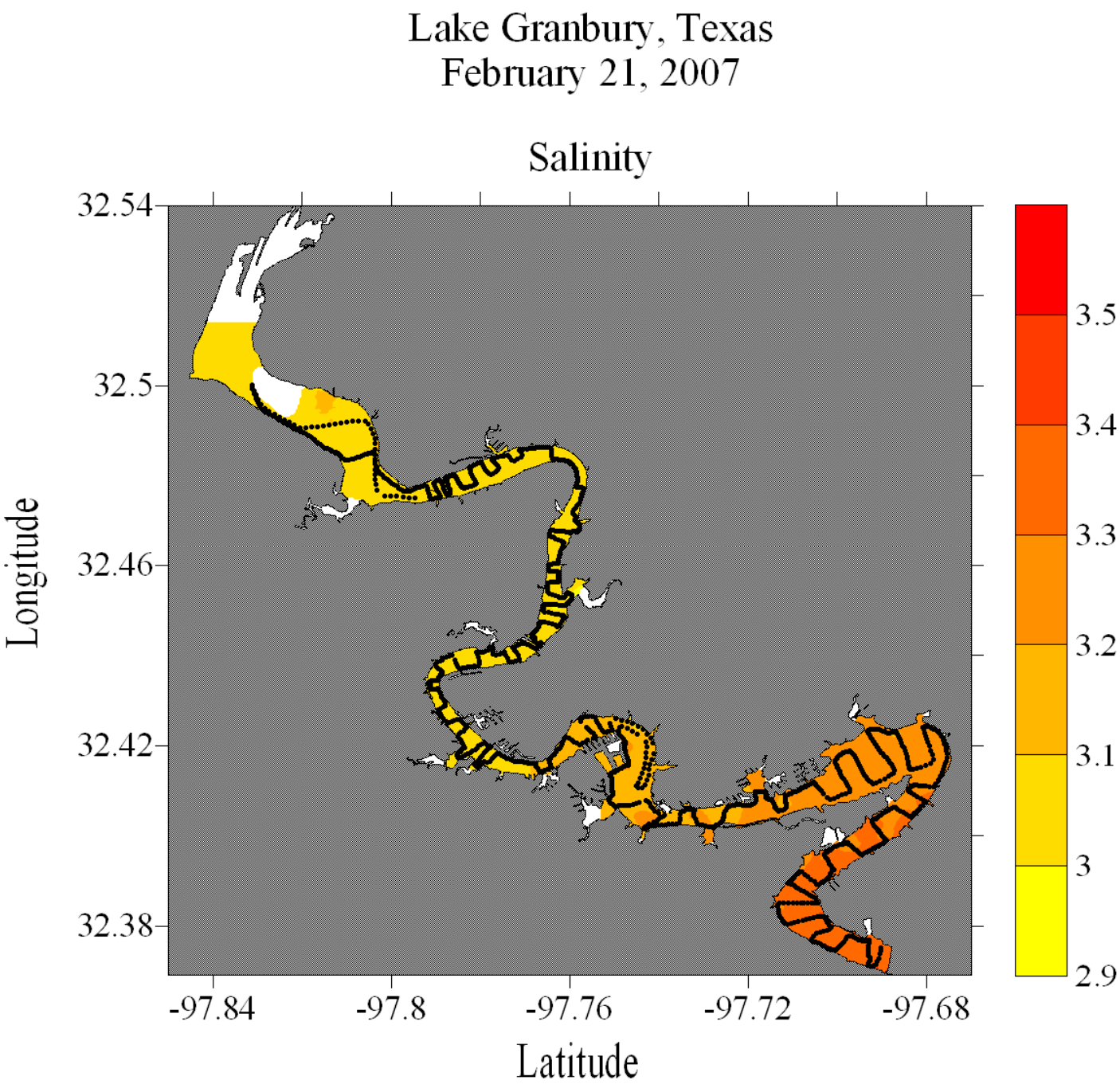

Figure E-20. Salinity dataflow map for Lake Granbury

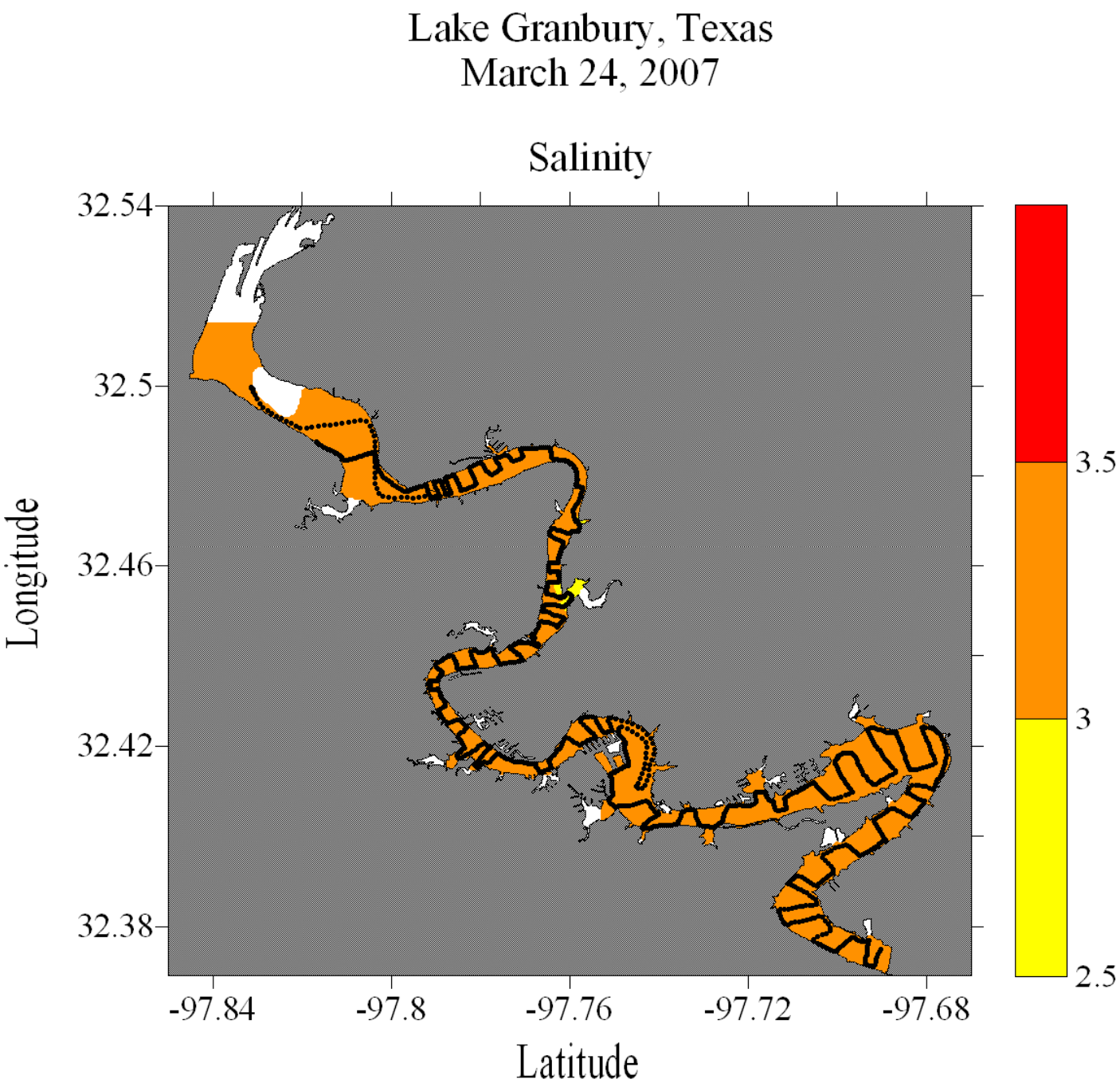

Figure E-21. Salinity dataflow map for Lake Granbury

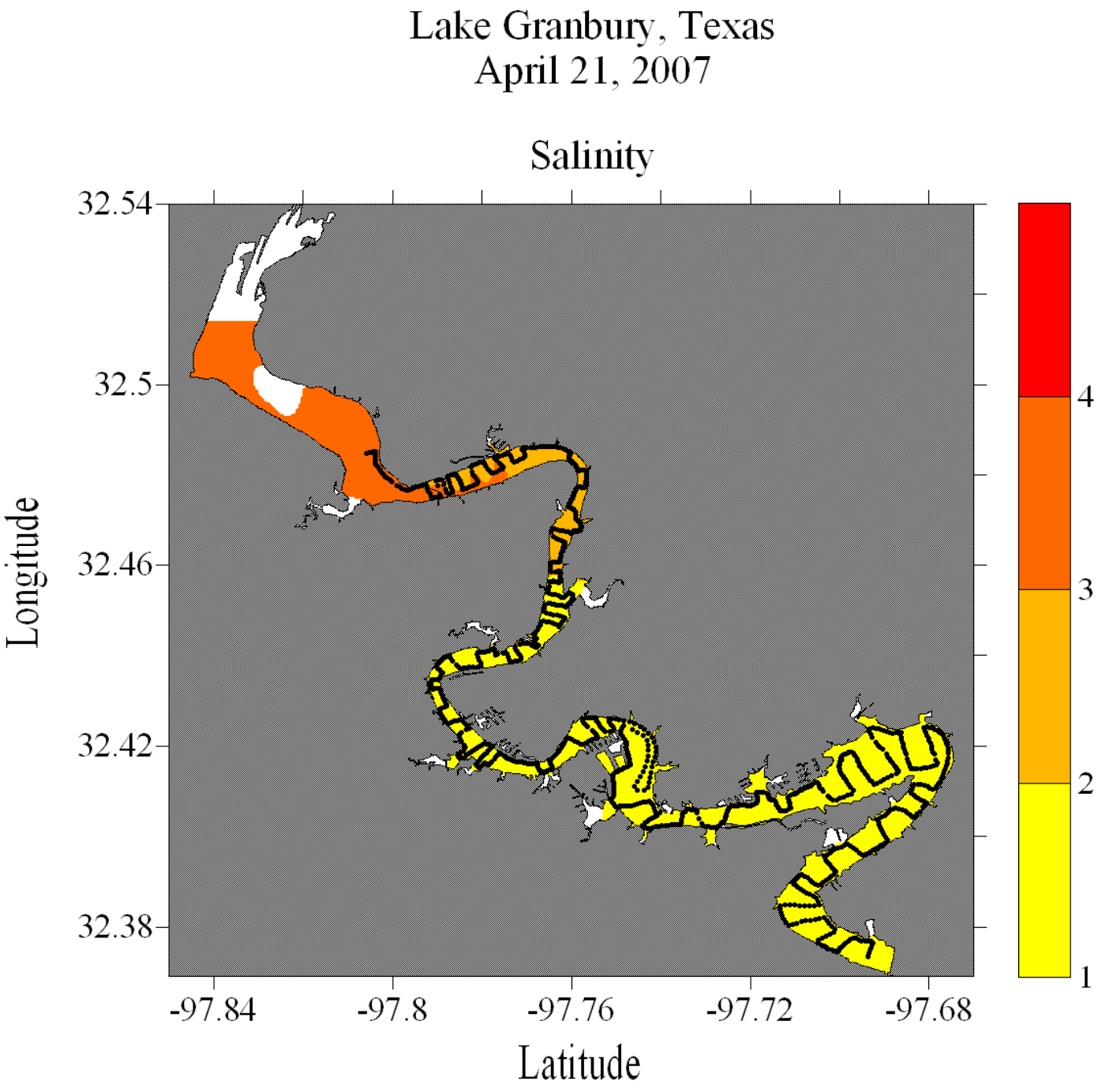

Figure E-22. Salinity dataflow map for Lake Granbury

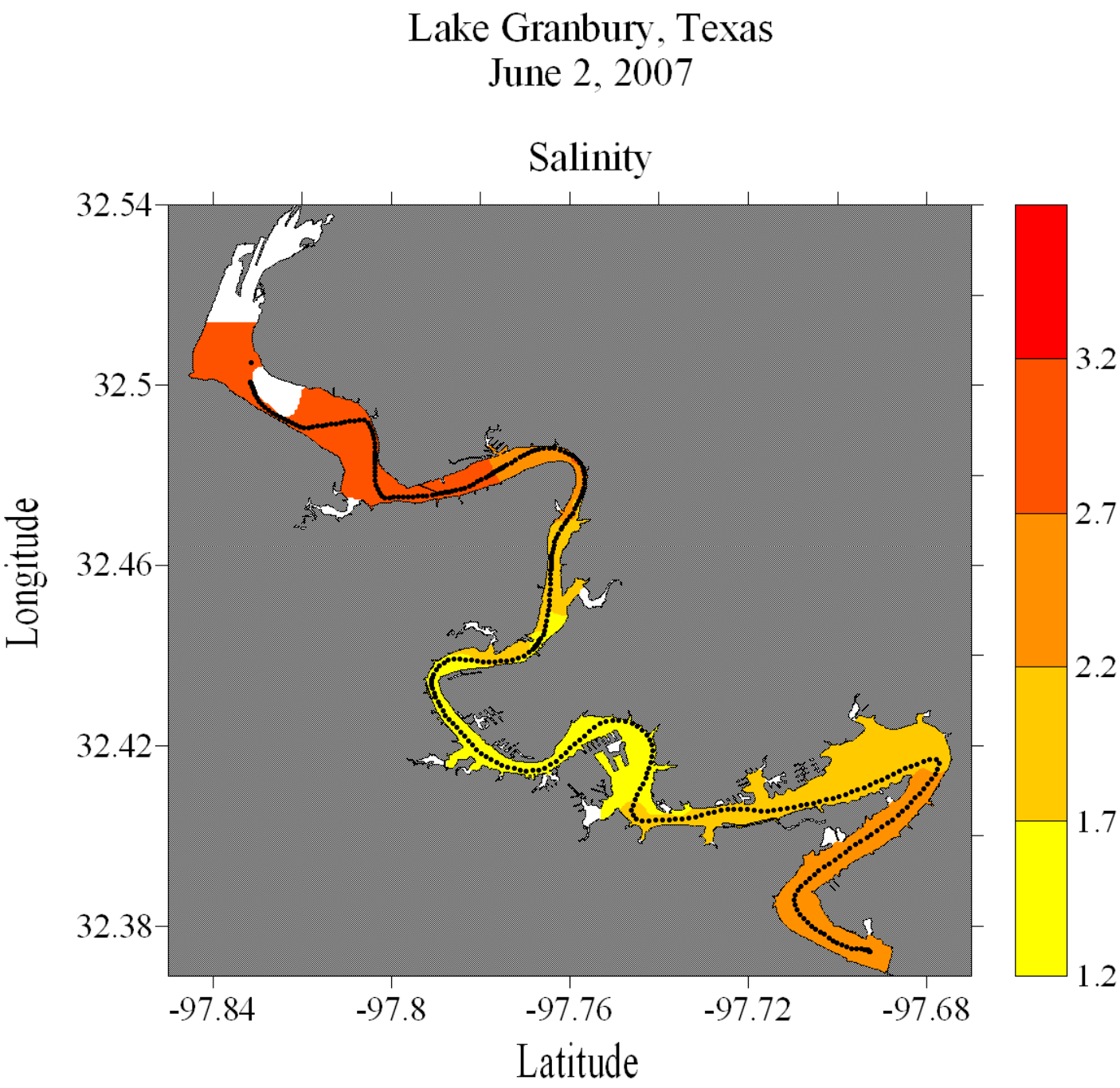

Figure E-23. Salinity dataflow map for Lake Granbury

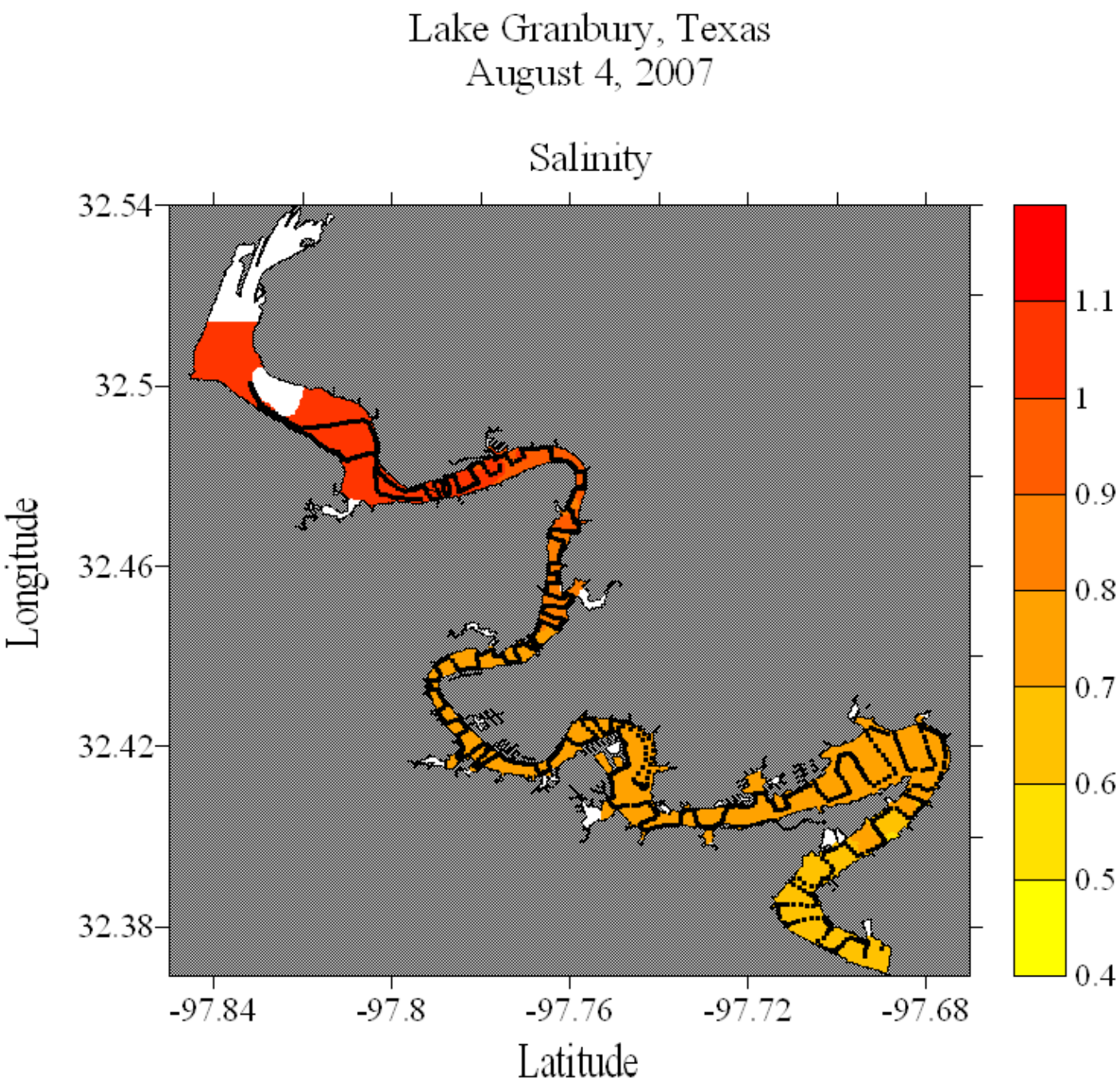

Figure E-24. Salinity dataflow map for Lake Granbury

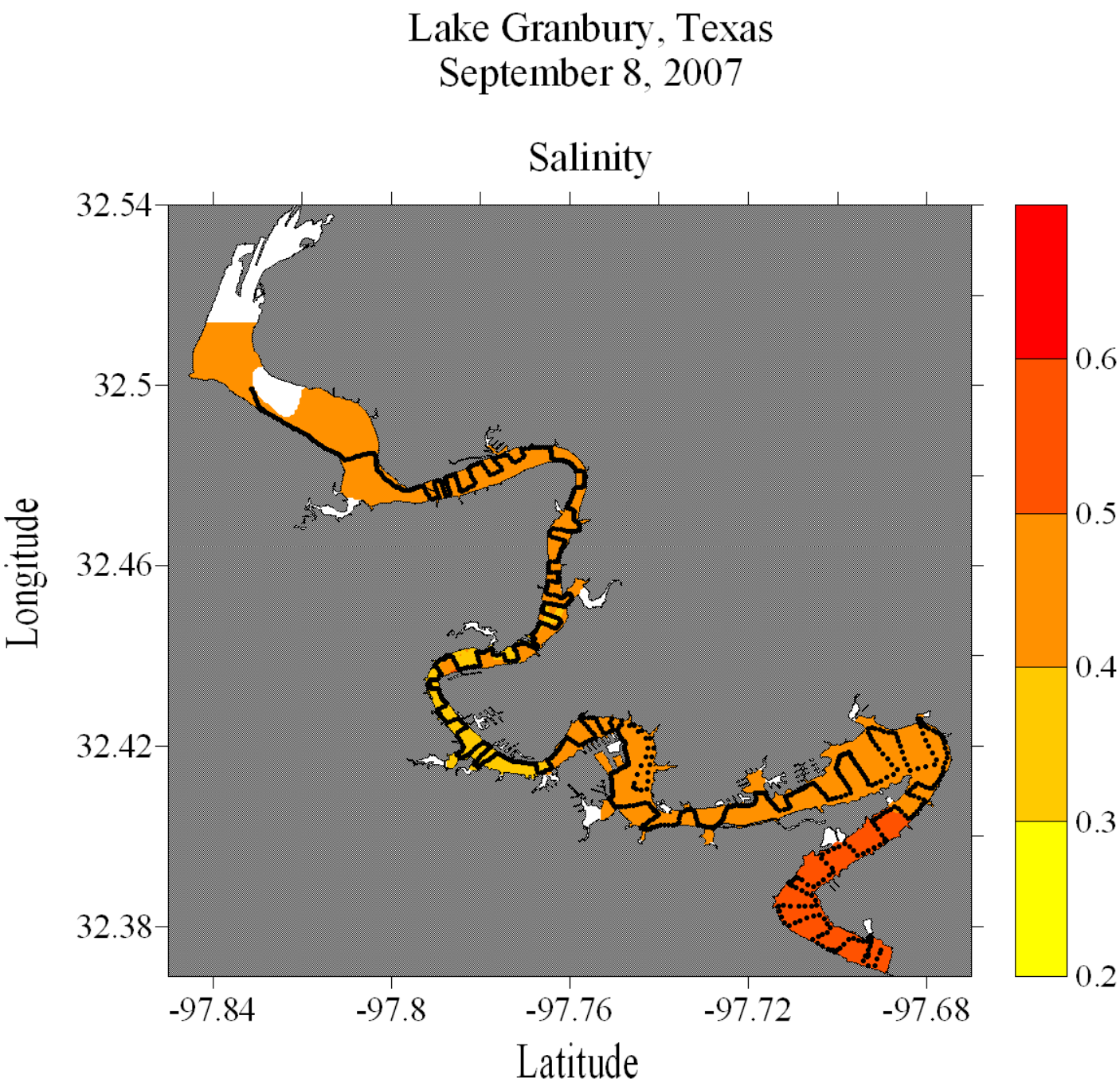

Figure E-25. Salinity dataflow map for Lake Granbury

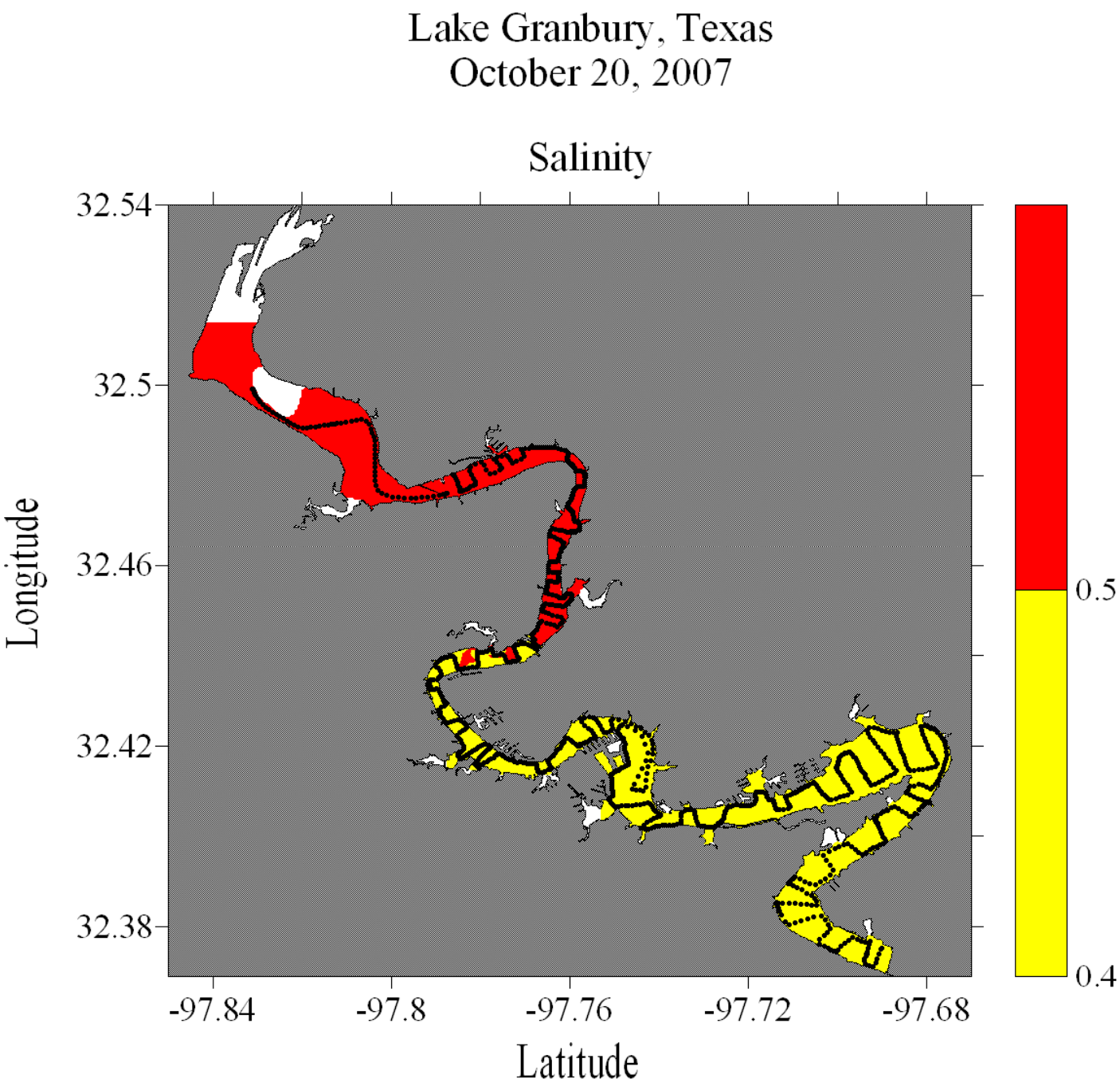

Figure E-26. Salinity dataflow map for Lake Granbury

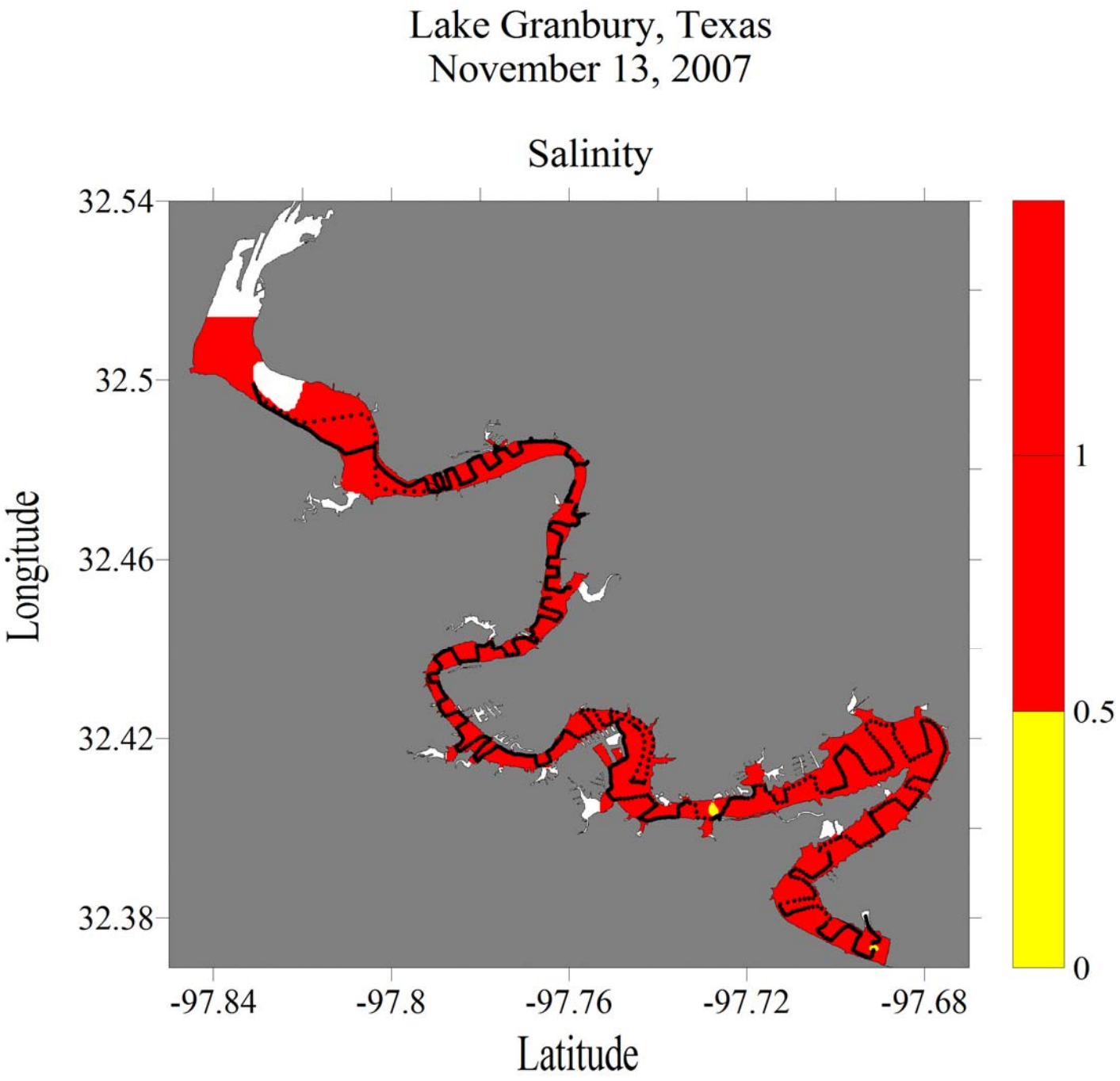

Figure E-27. Salinity dataflow map for Lake Granbury

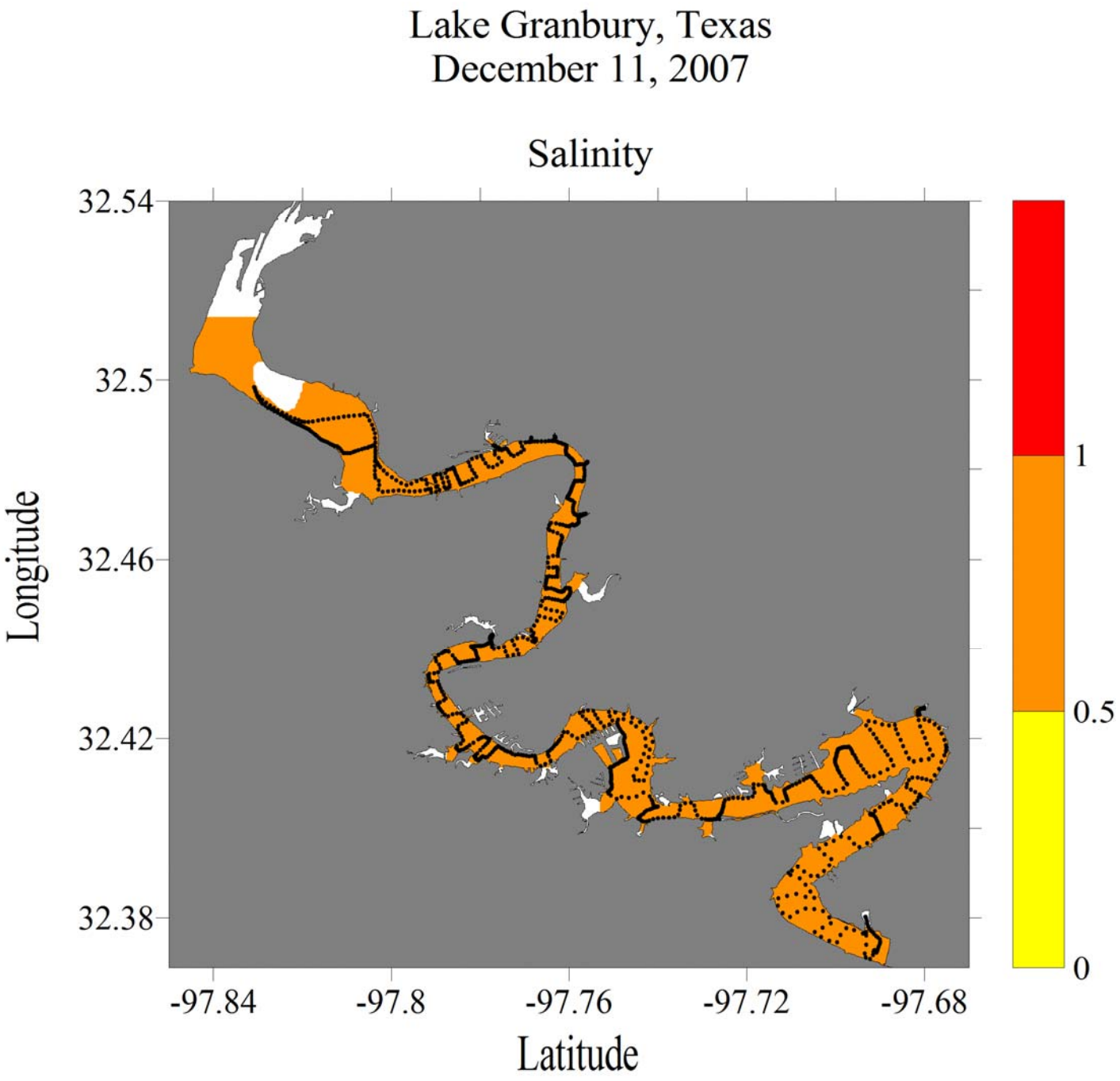

Figure E-28. Salinity dataflow map for Lake Granbury

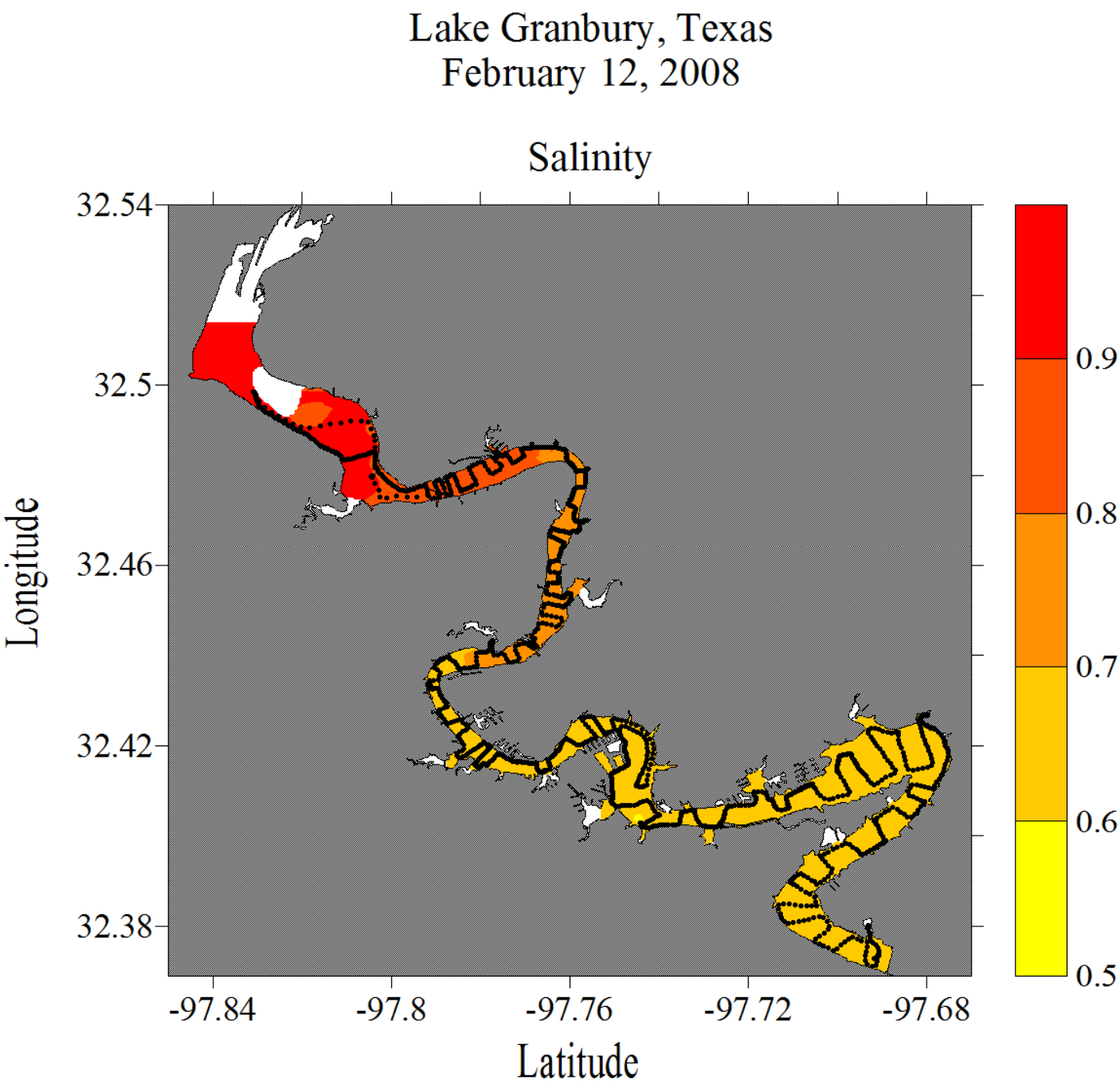

Figure E-29. Salinity dataflow map for Lake Granbury

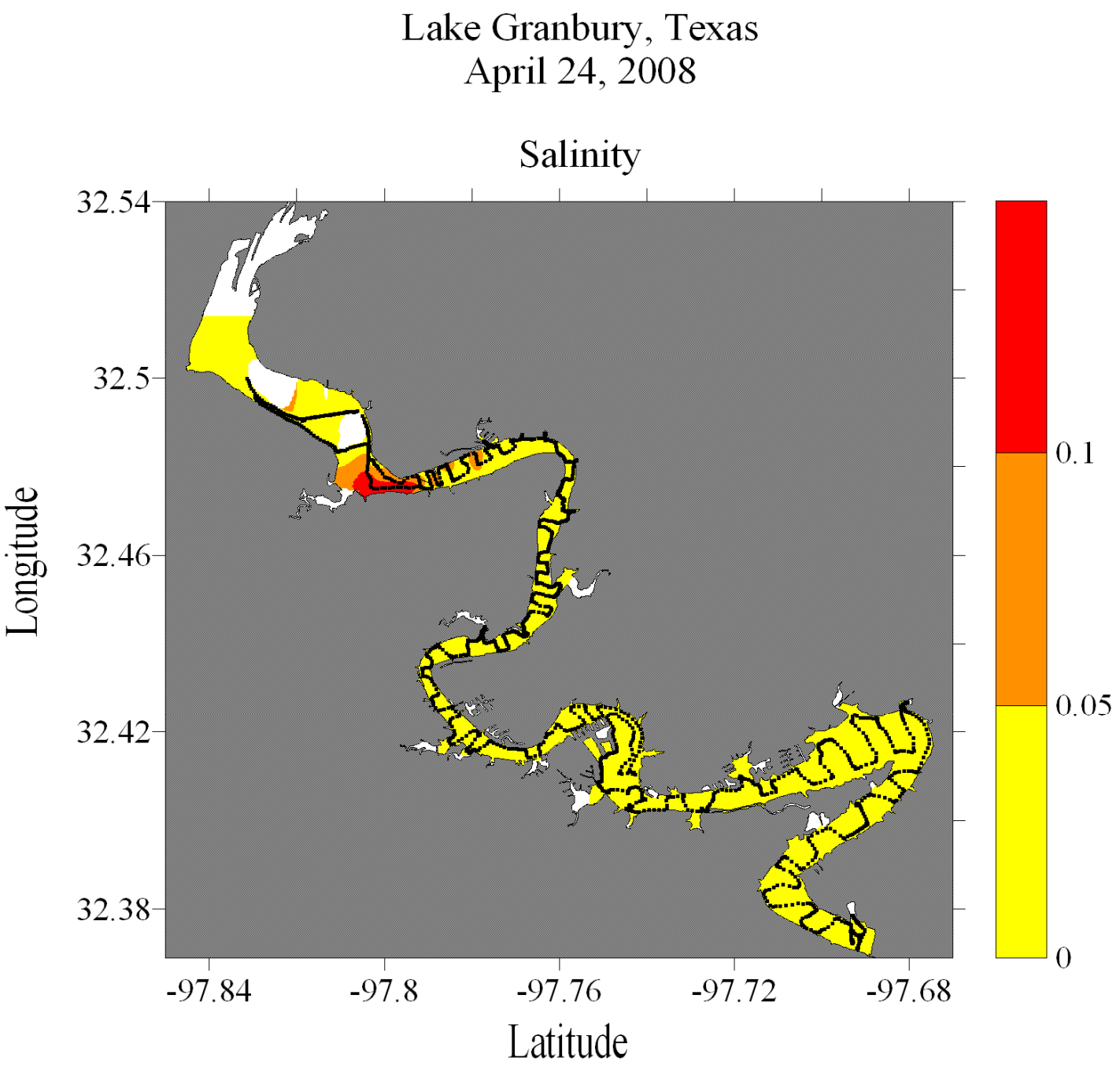

Figure E-30. Salinity dataflow map for Lake Granbury

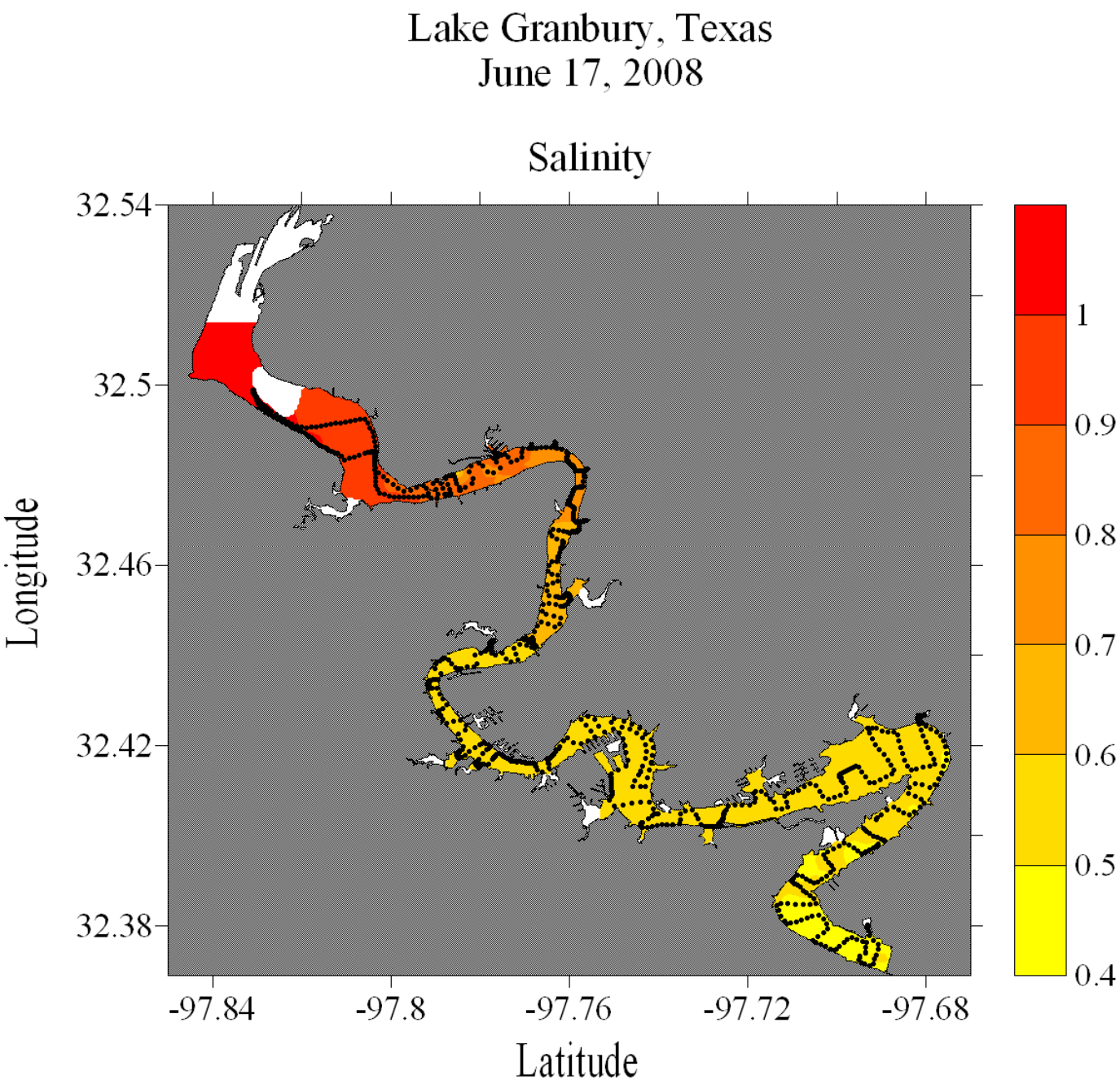

Figure E-31. Salinity dataflow map for Lake Granbury

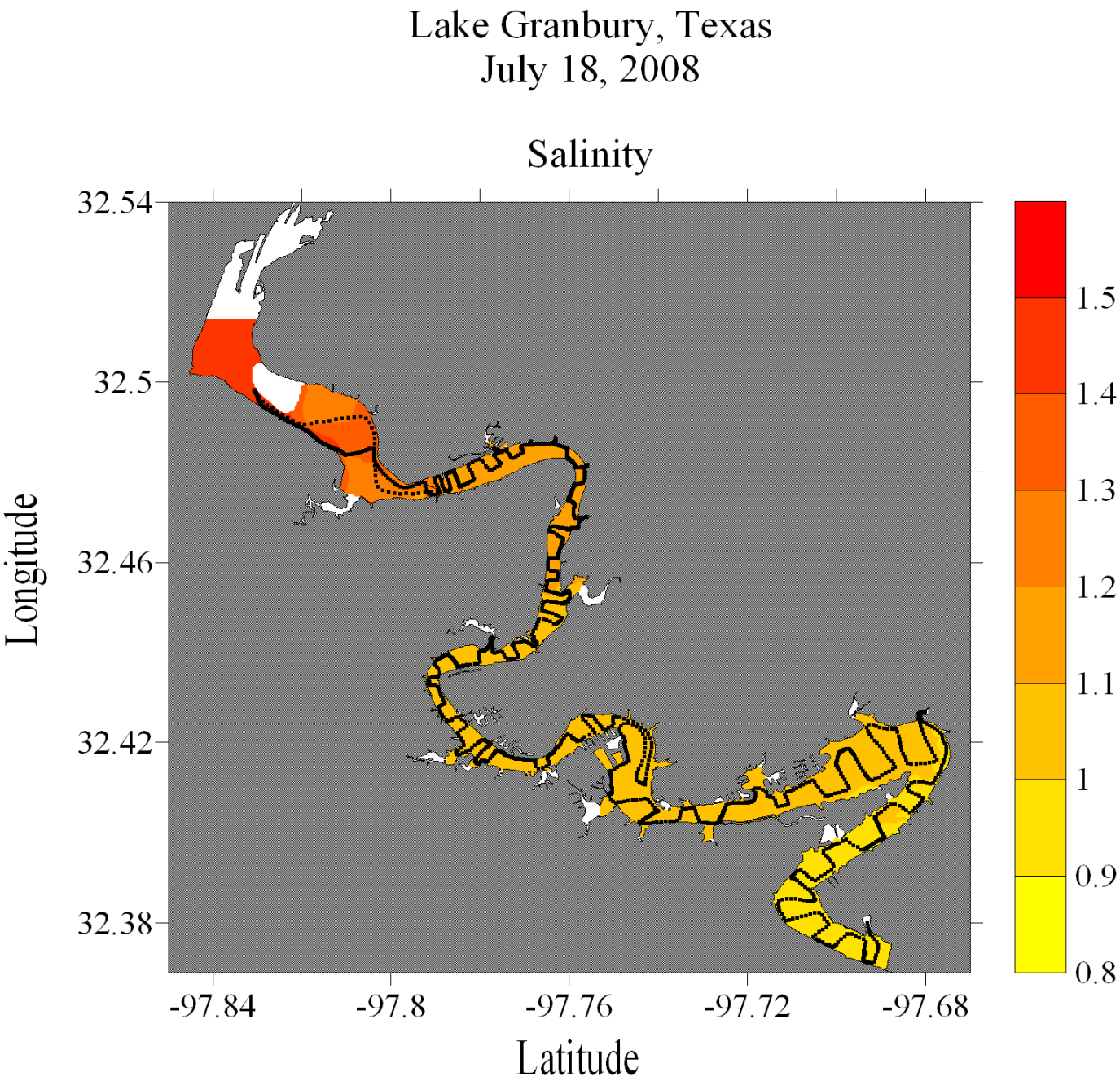

Figure E-32. Salinity dataflow map for Lake Granbury

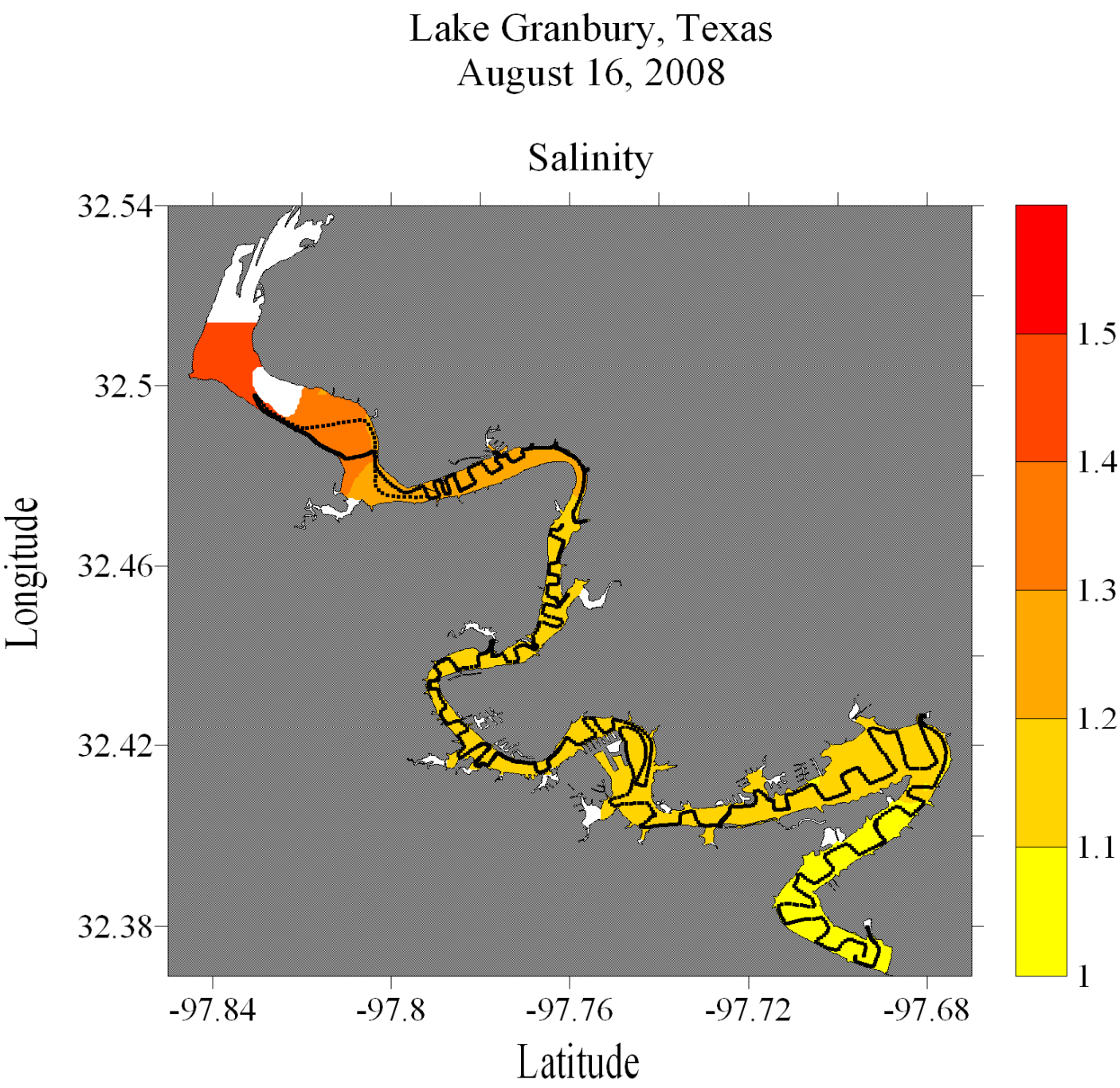

Figure E-33. Salinity dataflow map for Lake Granbury

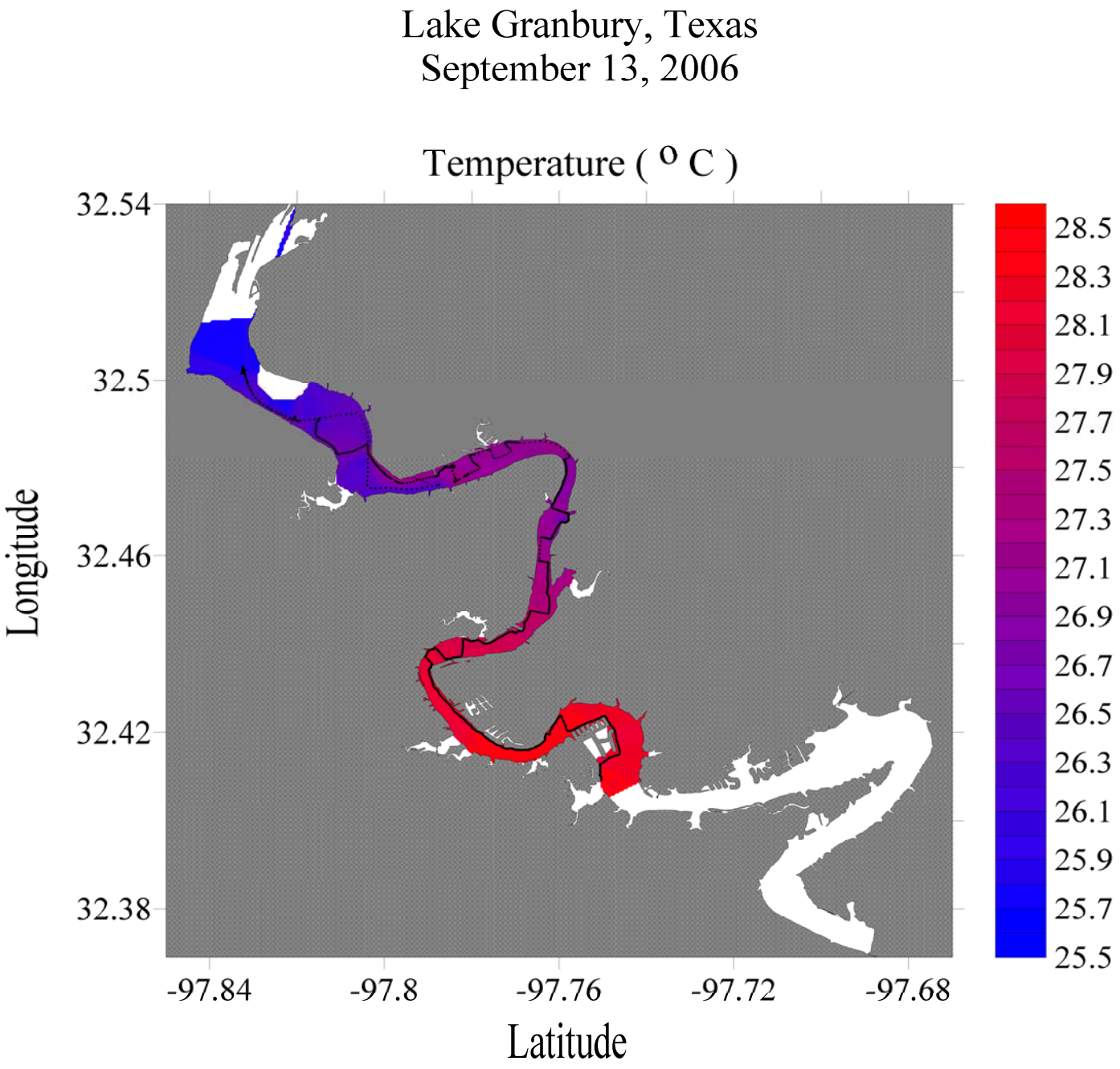

Figure E-34. Temperature dataflow map for Lake Granbury

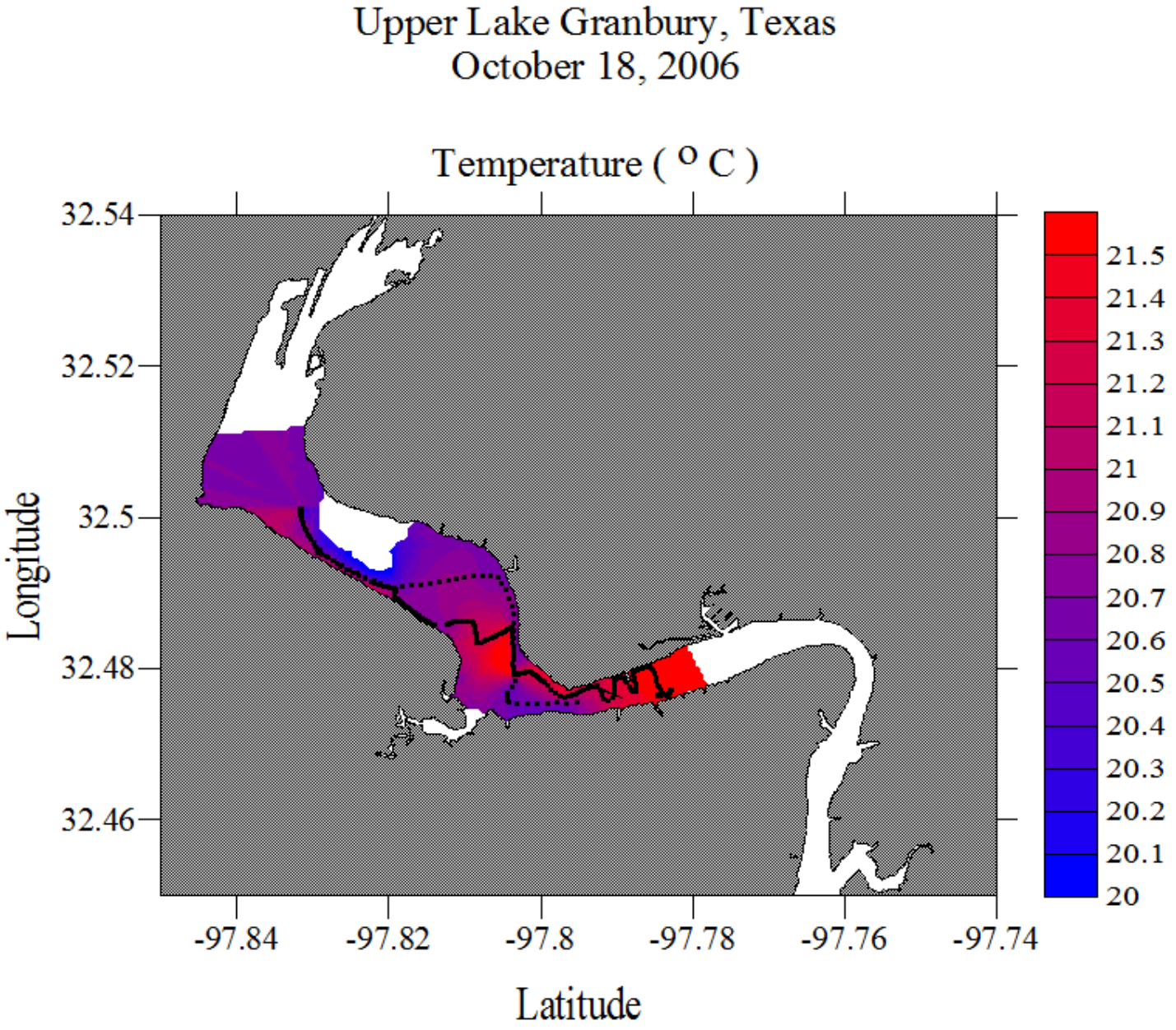

Figure E-35. Temperature dataflow map for Lake Granbury

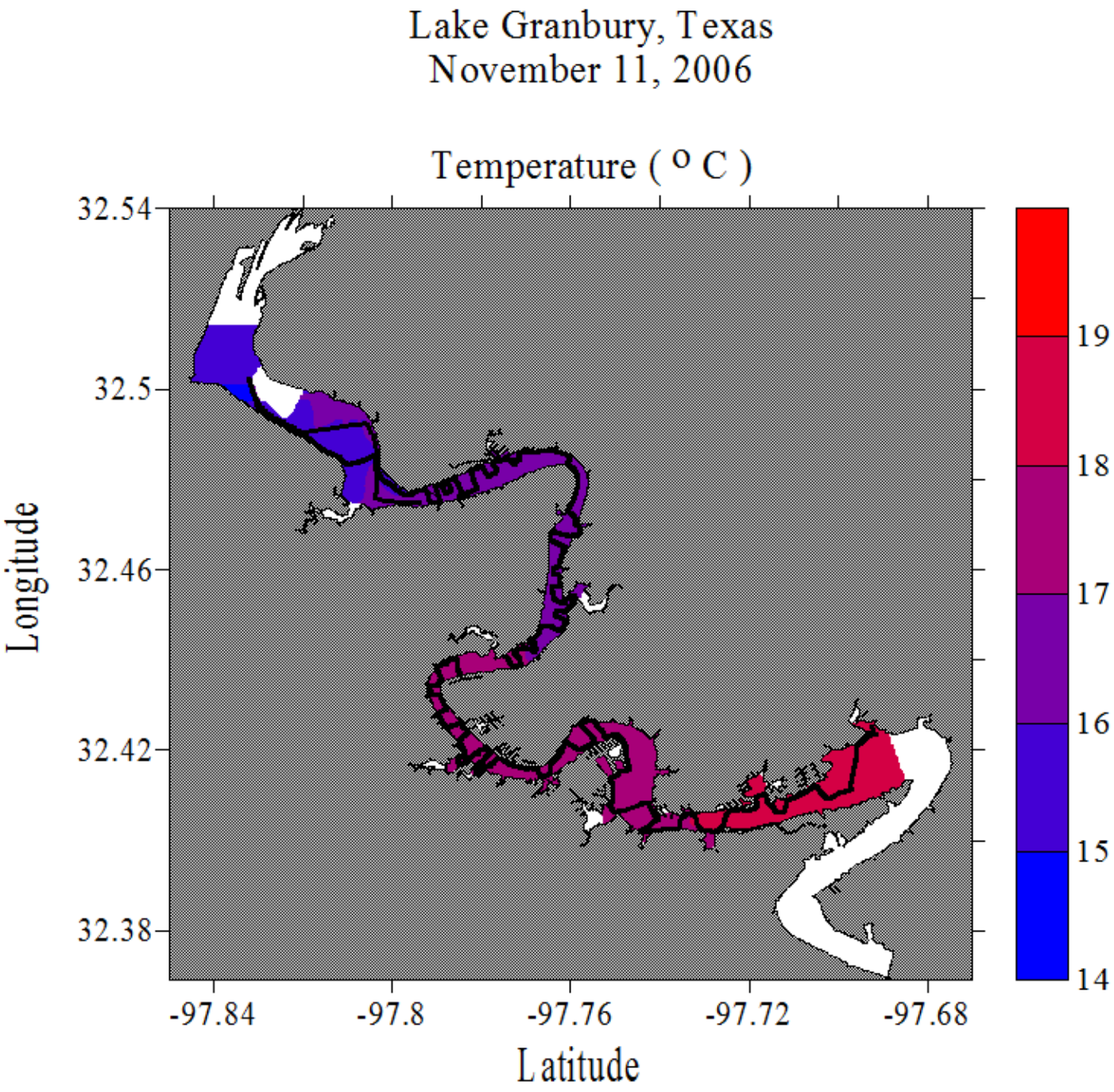

Figure E-36. Temperature dataflow map for Lake Granbury

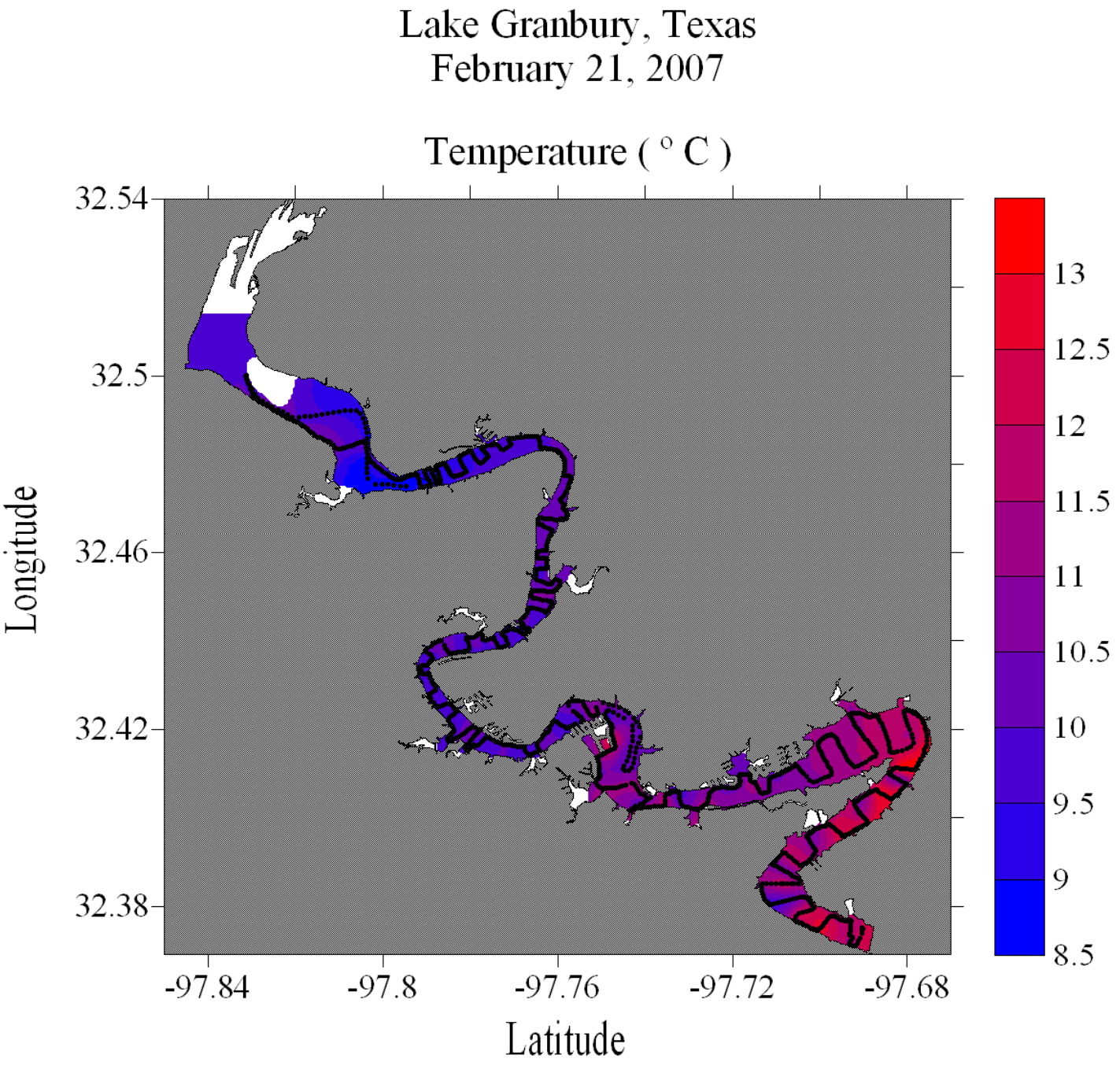

Figure E-37. Temperature dataflow map for Lake Granbury

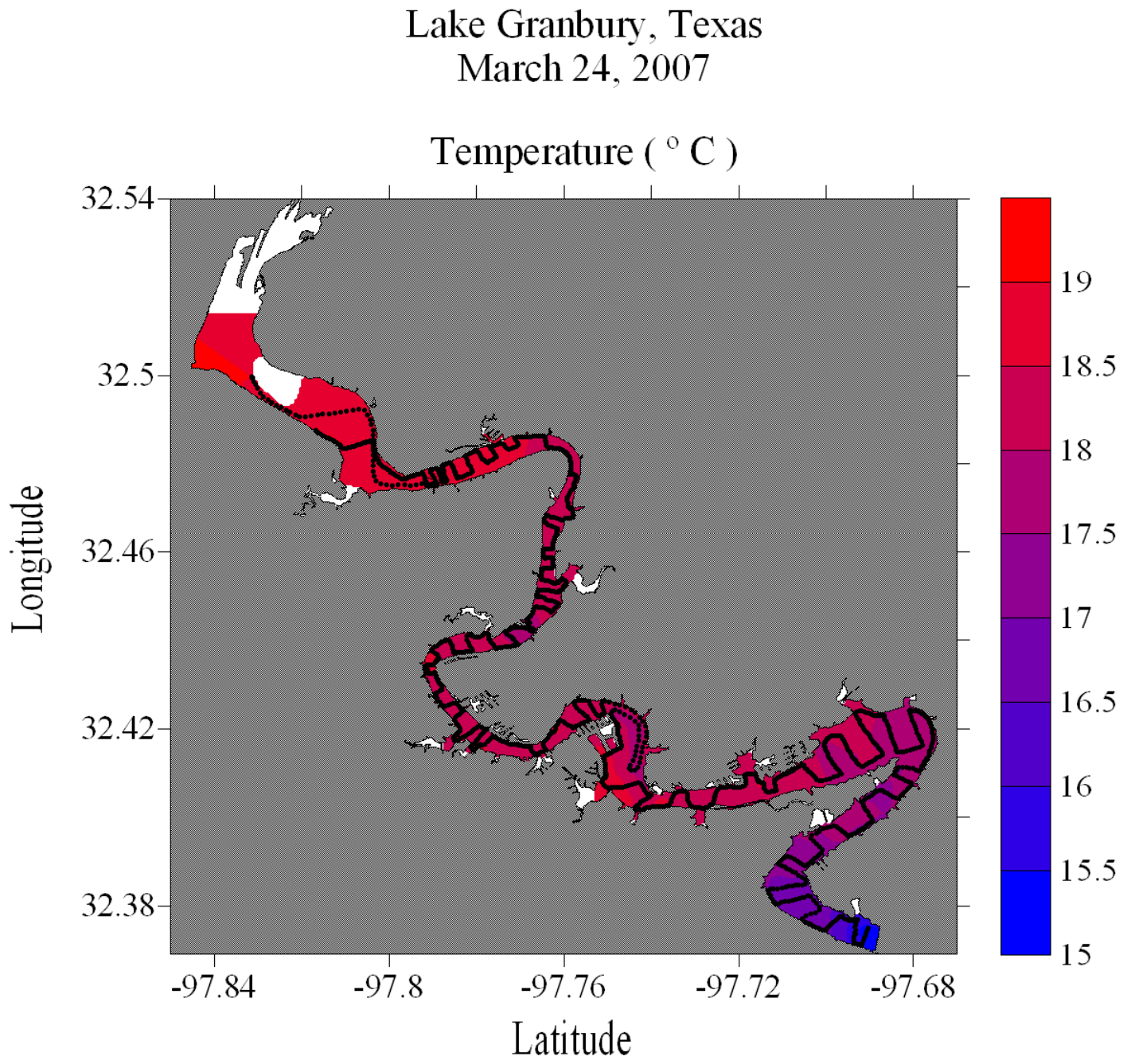

Figure E-38. Temperature dataflow map for Lake Granbury

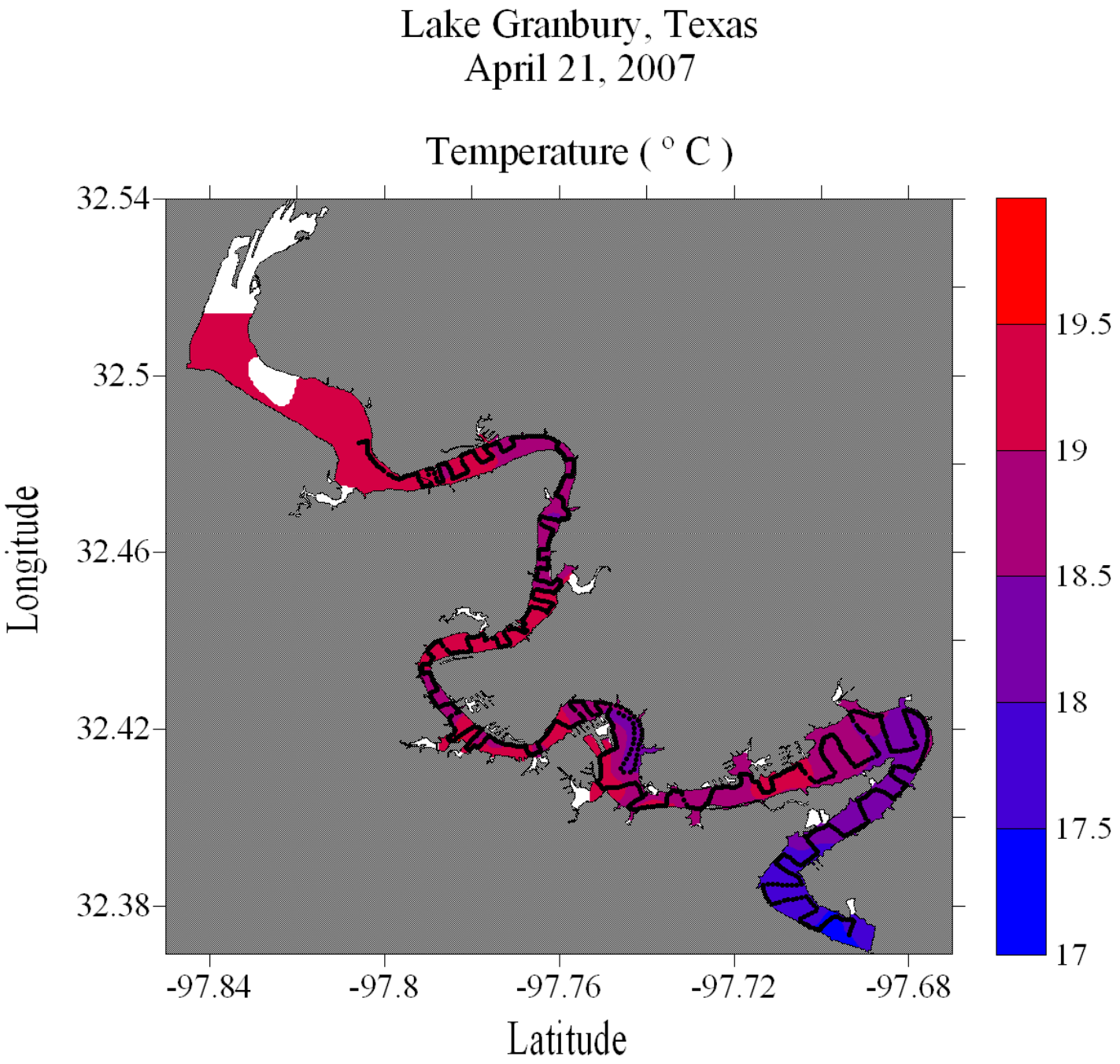

Figure E-39. Temperature dataflow map for Lake Granbury

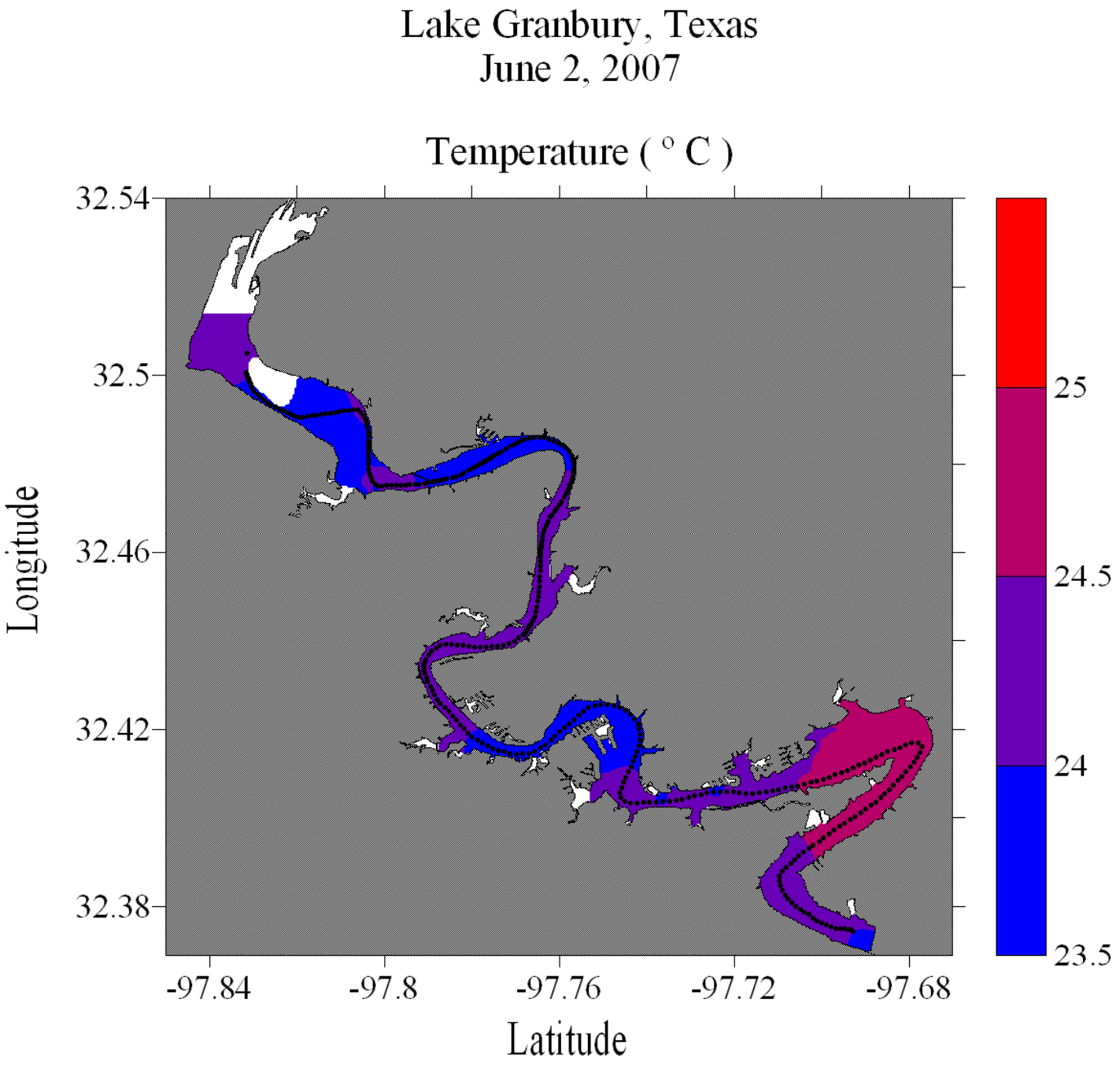

Figure E-40. Temperature dataflow map for Lake Granbury

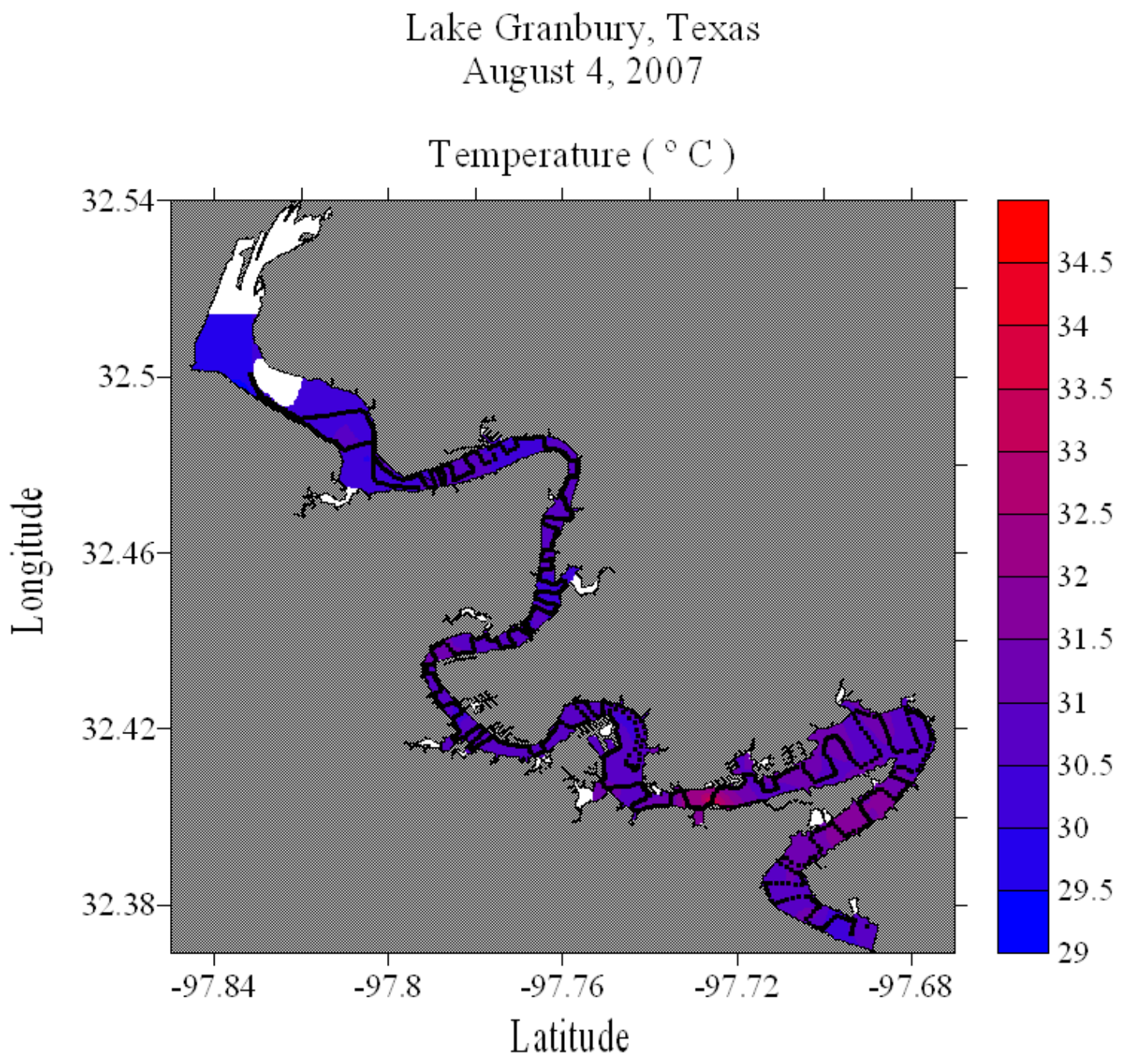

Figure E-41. Temperature dataflow map for Lake Granbury

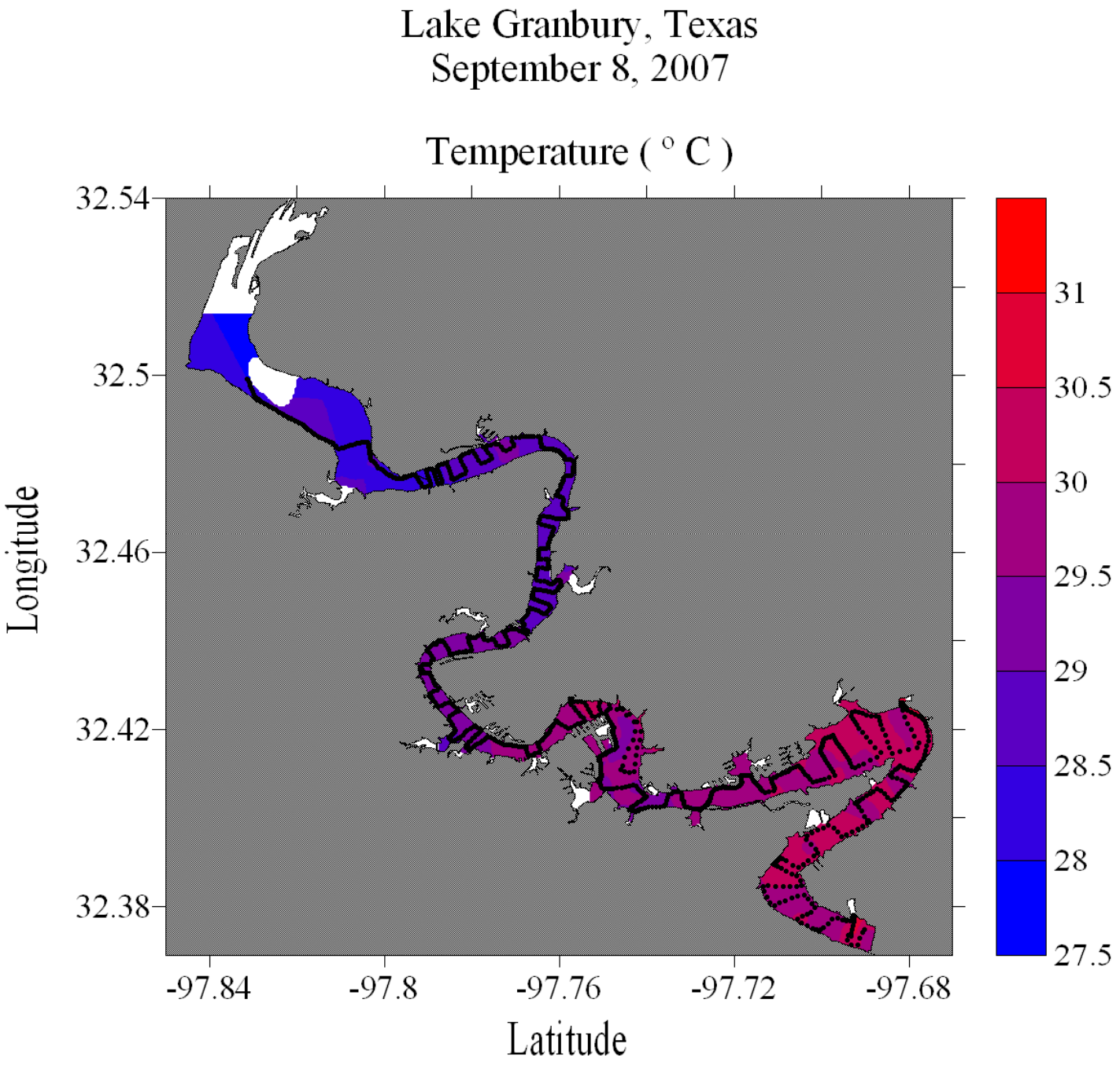

Figure E-42. Temperature dataflow map for Lake Granbury

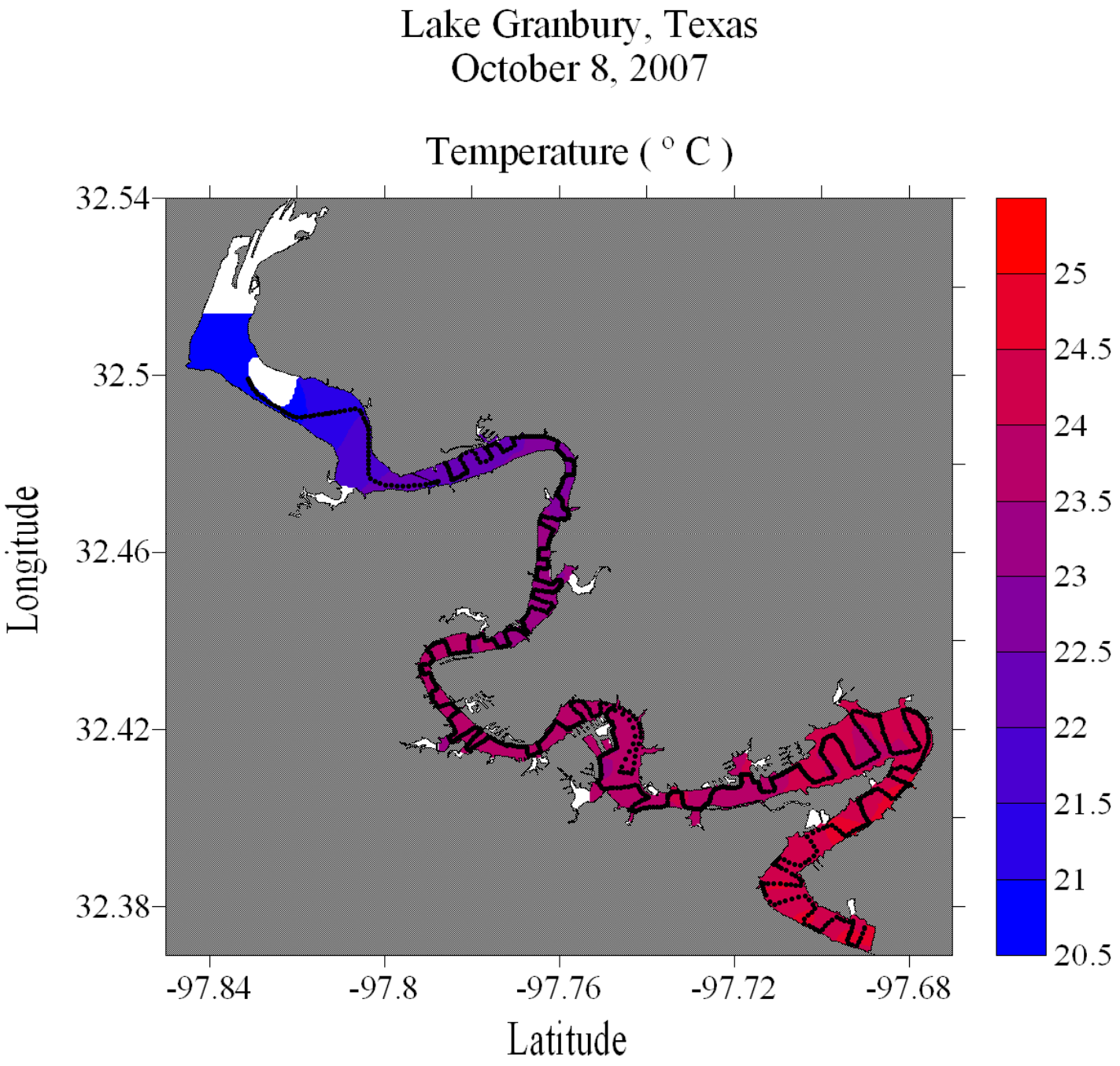

Figure E-43. Temperature dataflow map for Lake Granbury

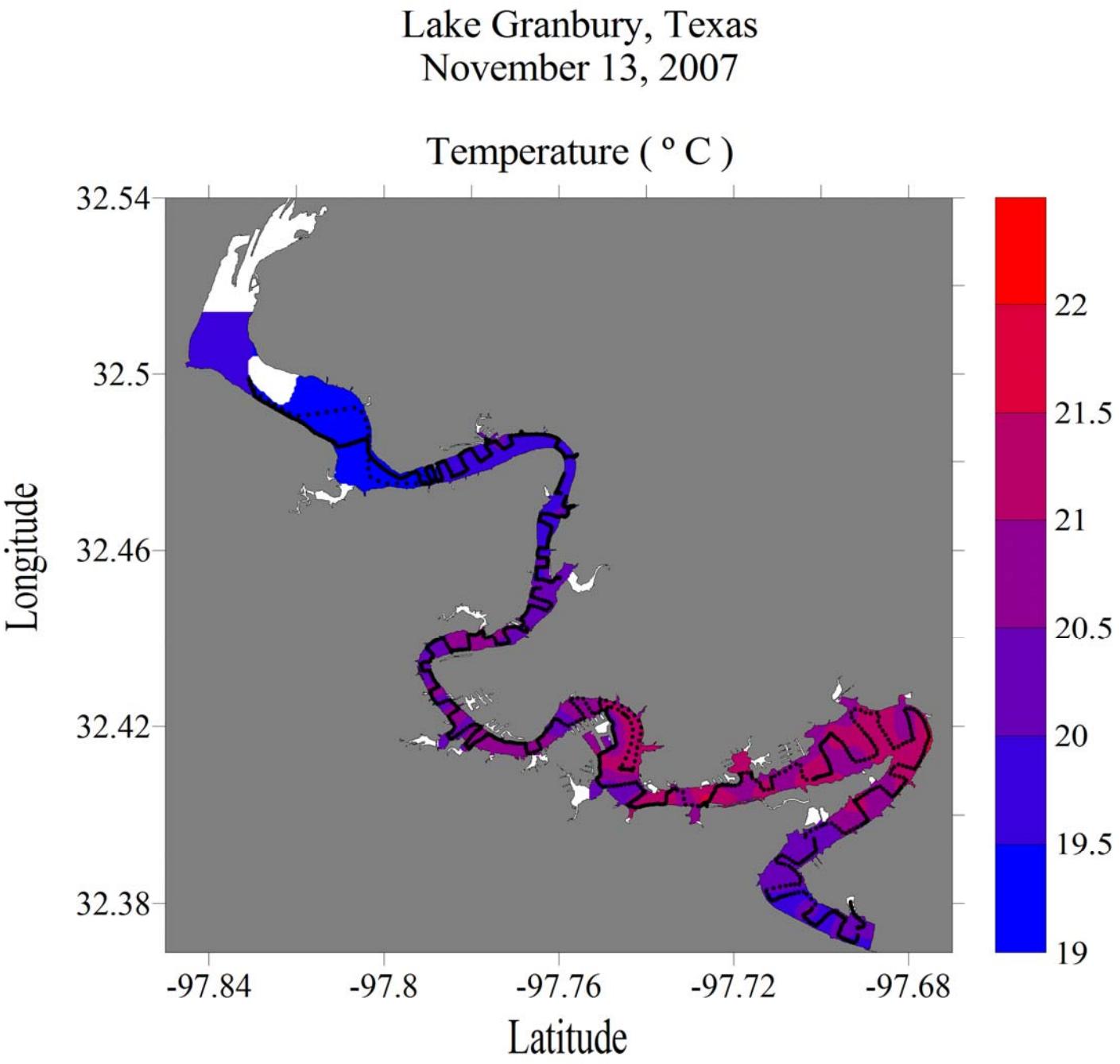

Figure E-44. Temperature dataflow map for Lake Granbury

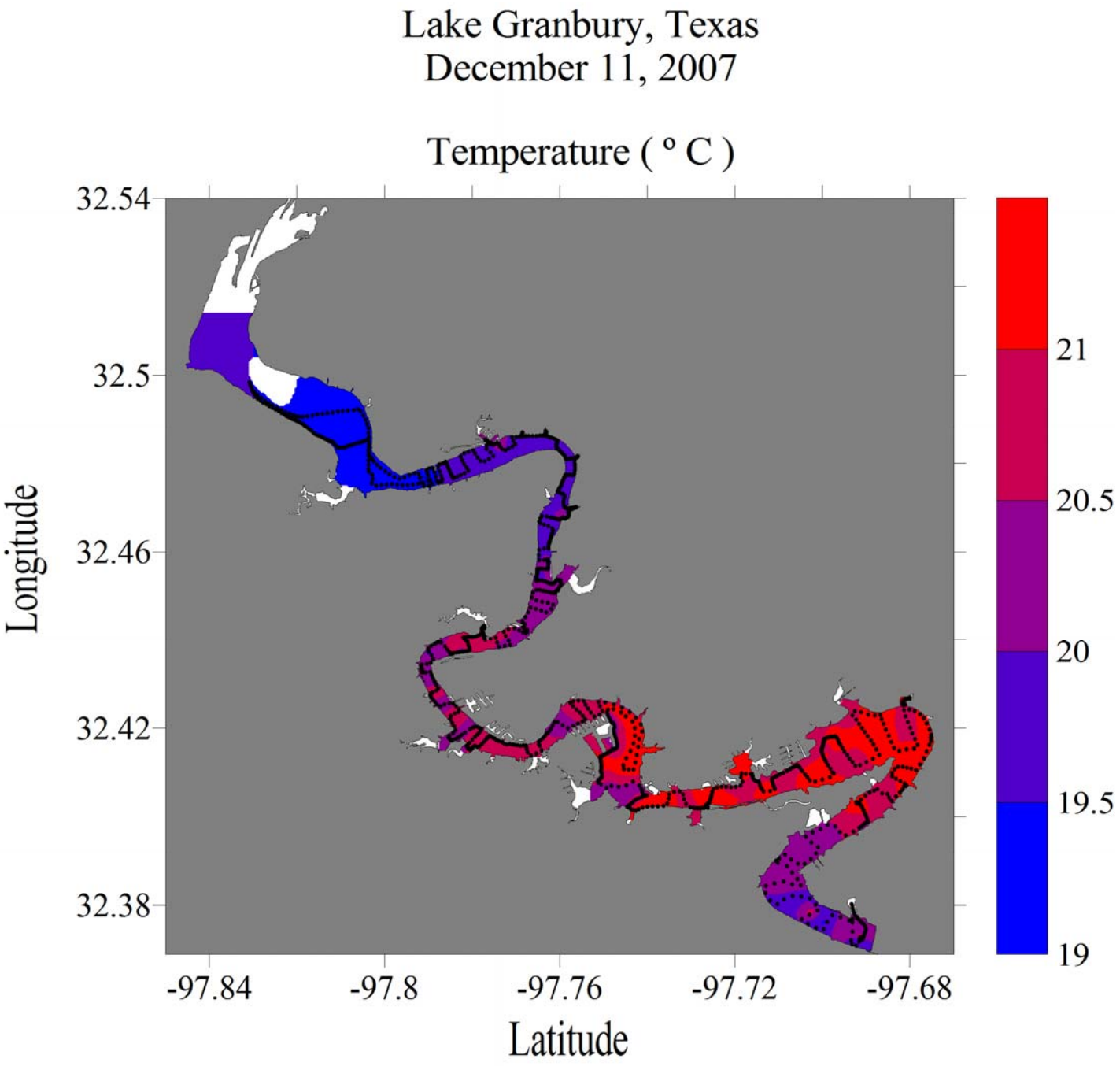

Figure E-45. Temperature dataflow map for Lake Granbury

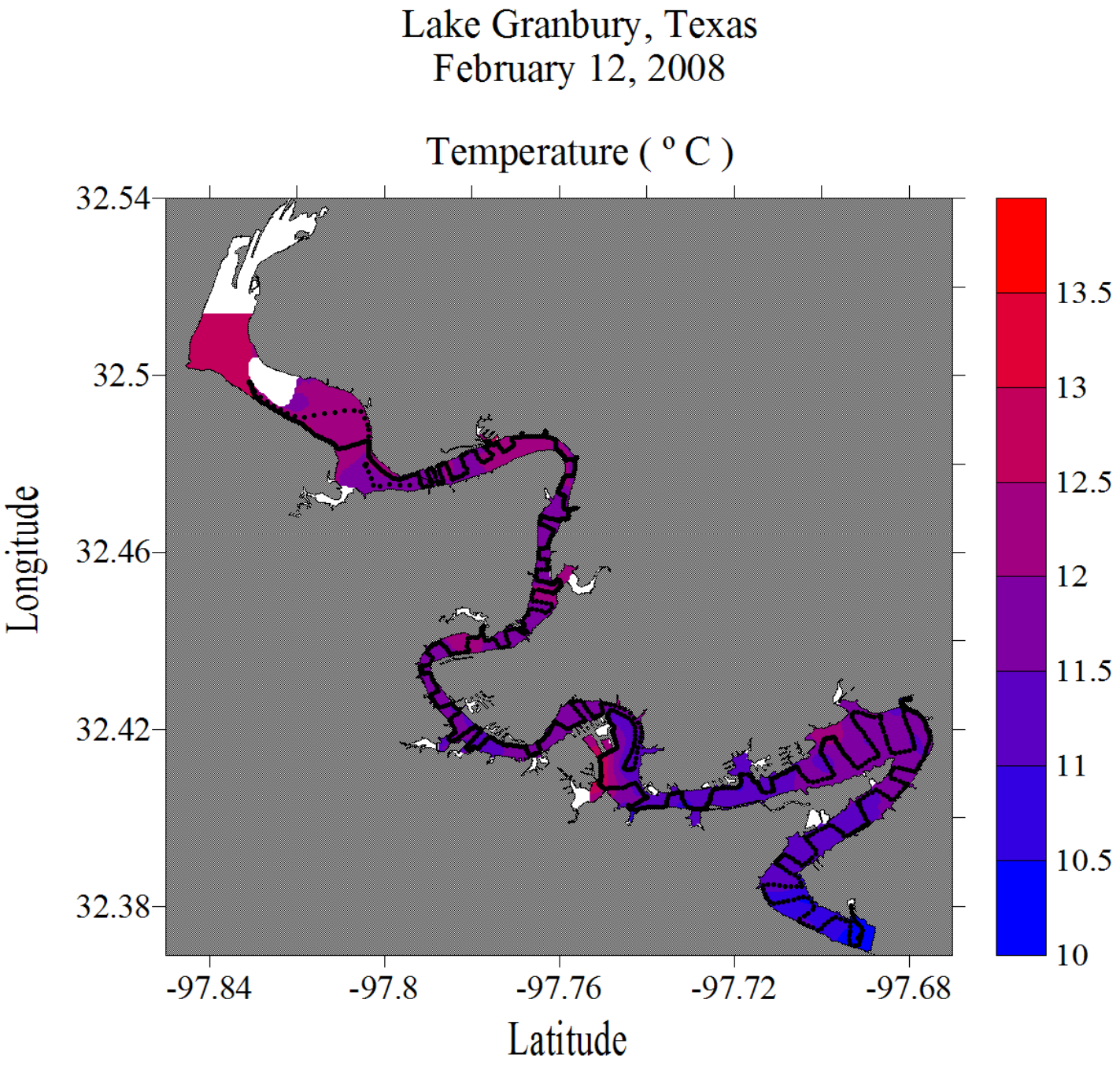

Figure E-46. Temperature dataflow map for Lake Granbury

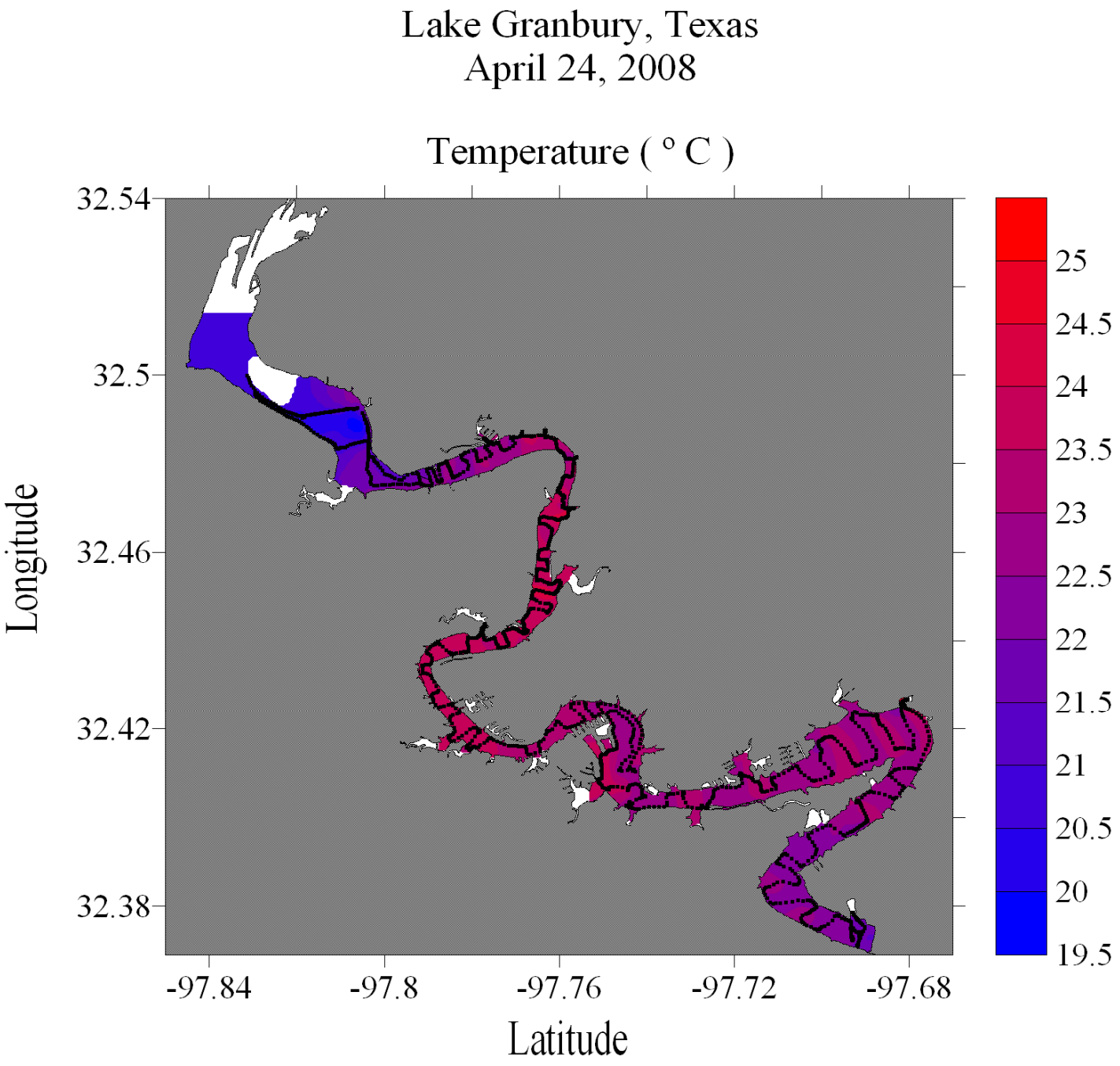

Figure E-47. Temperature dataflow map for Lake Granbury

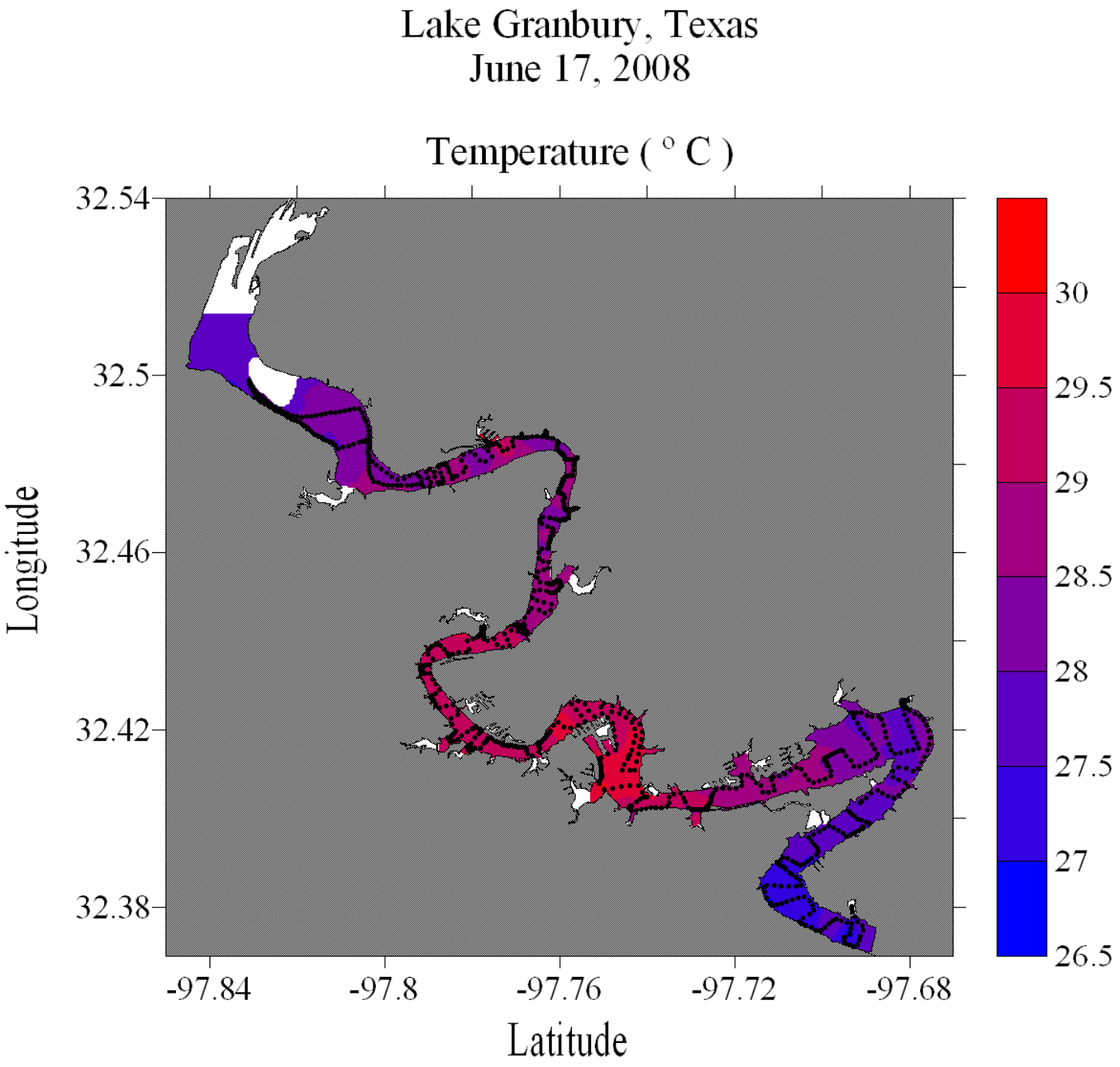

Figure E-48. Temperature dataflow map for Lake Granbury

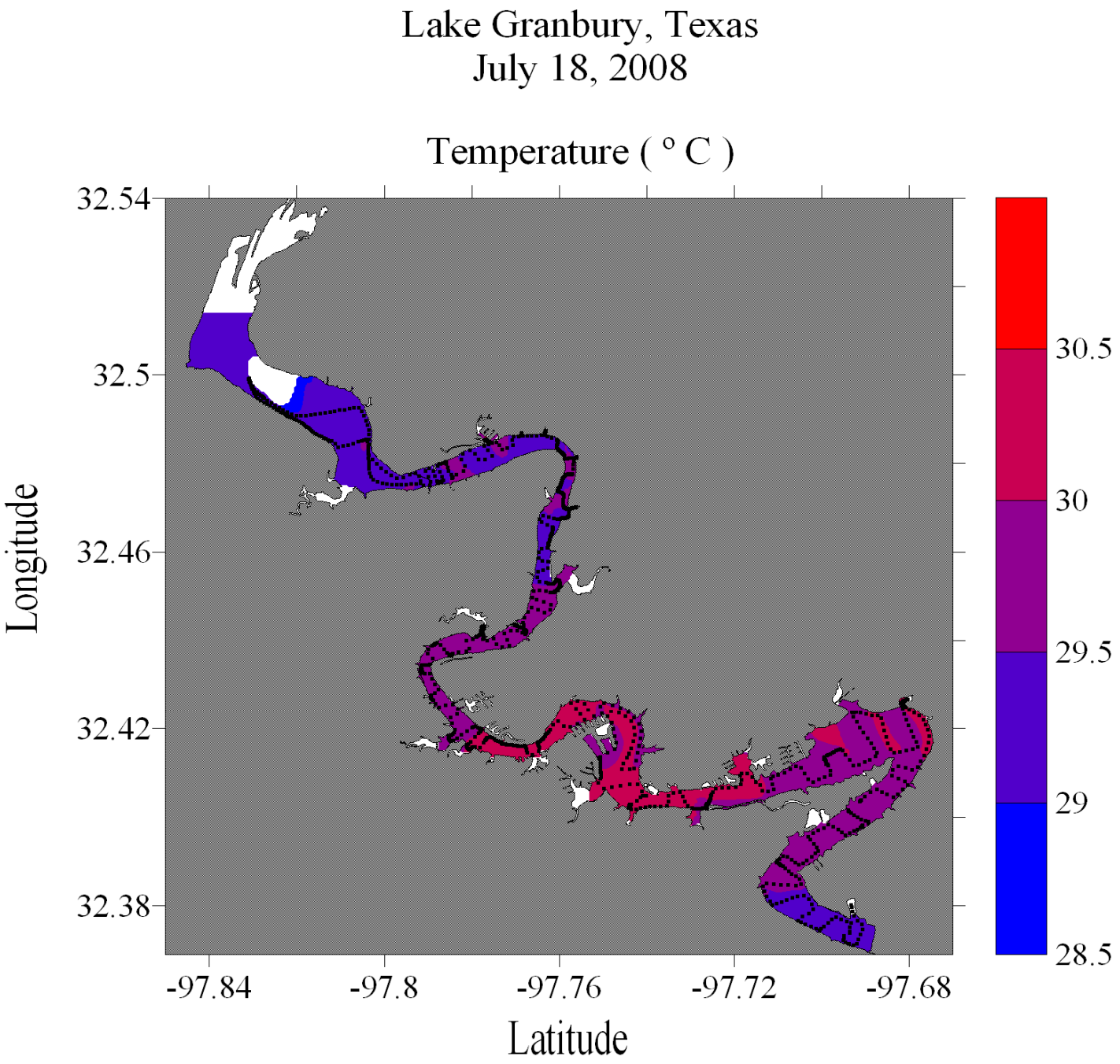

Figure E-49. Temperature dataflow map for Lake Granbury

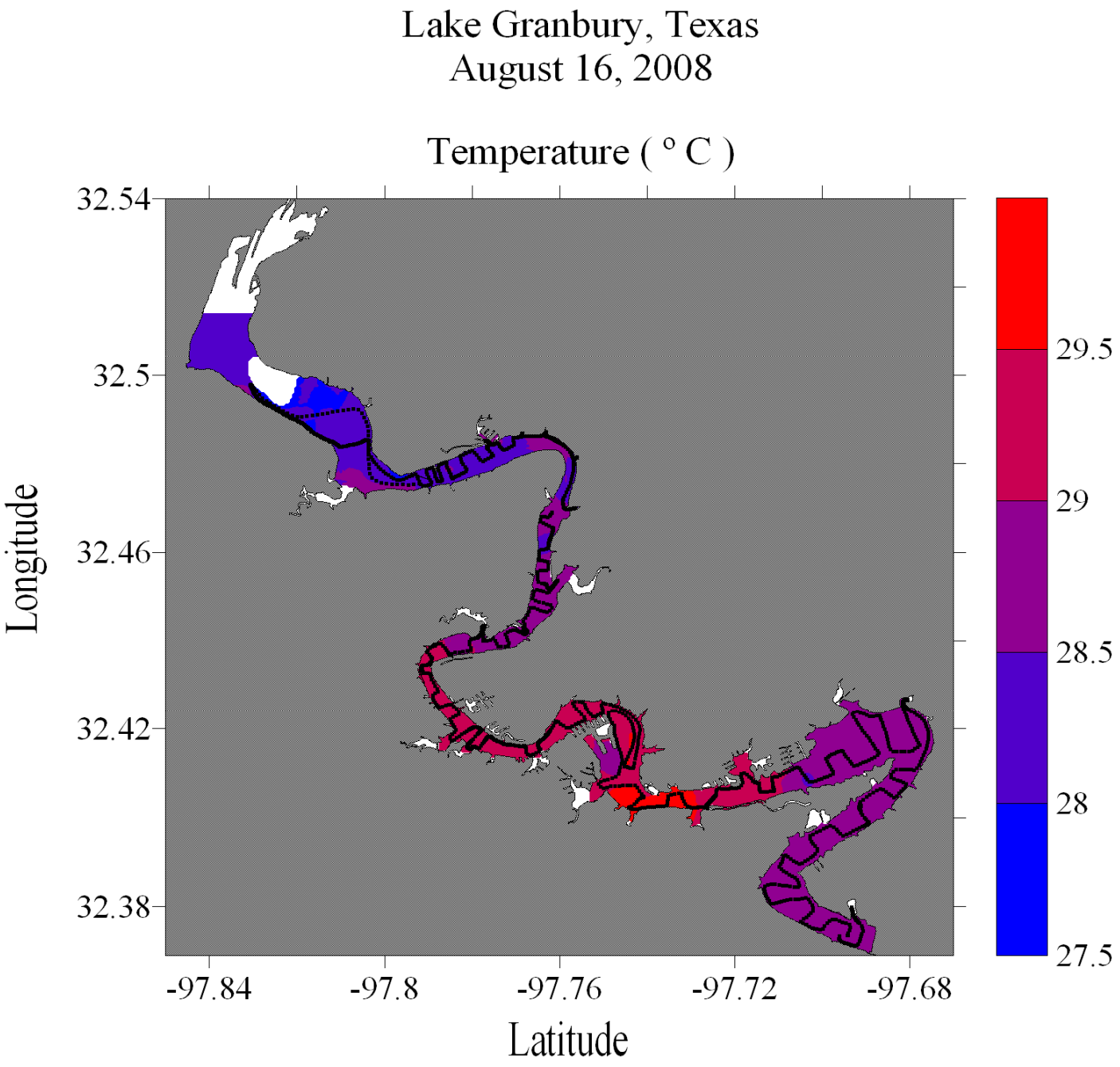

Figure E-50. Temperature dataflow map for Lake Granbury

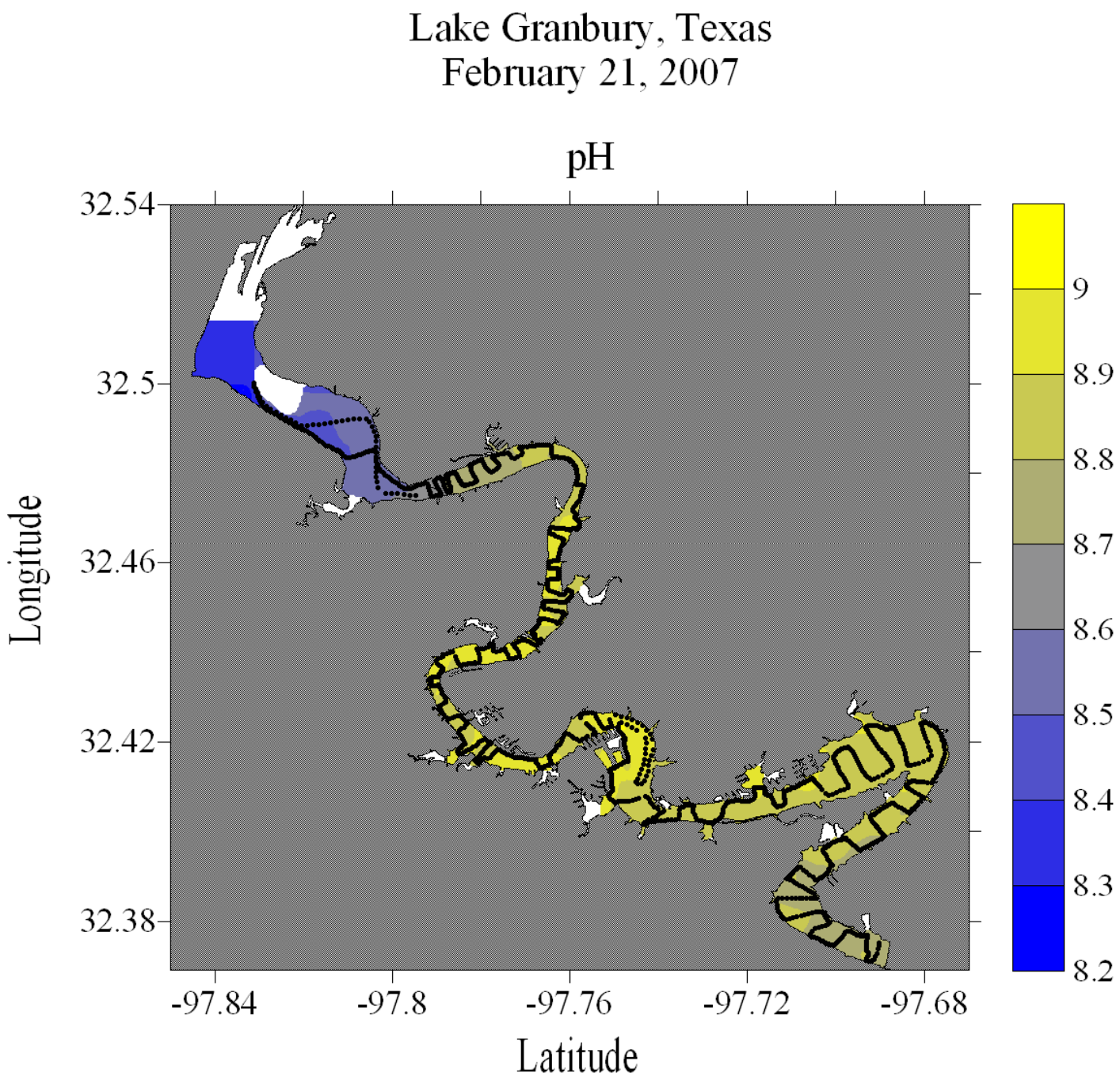

Figure E-51. pH dataflow map for Lake Granbury

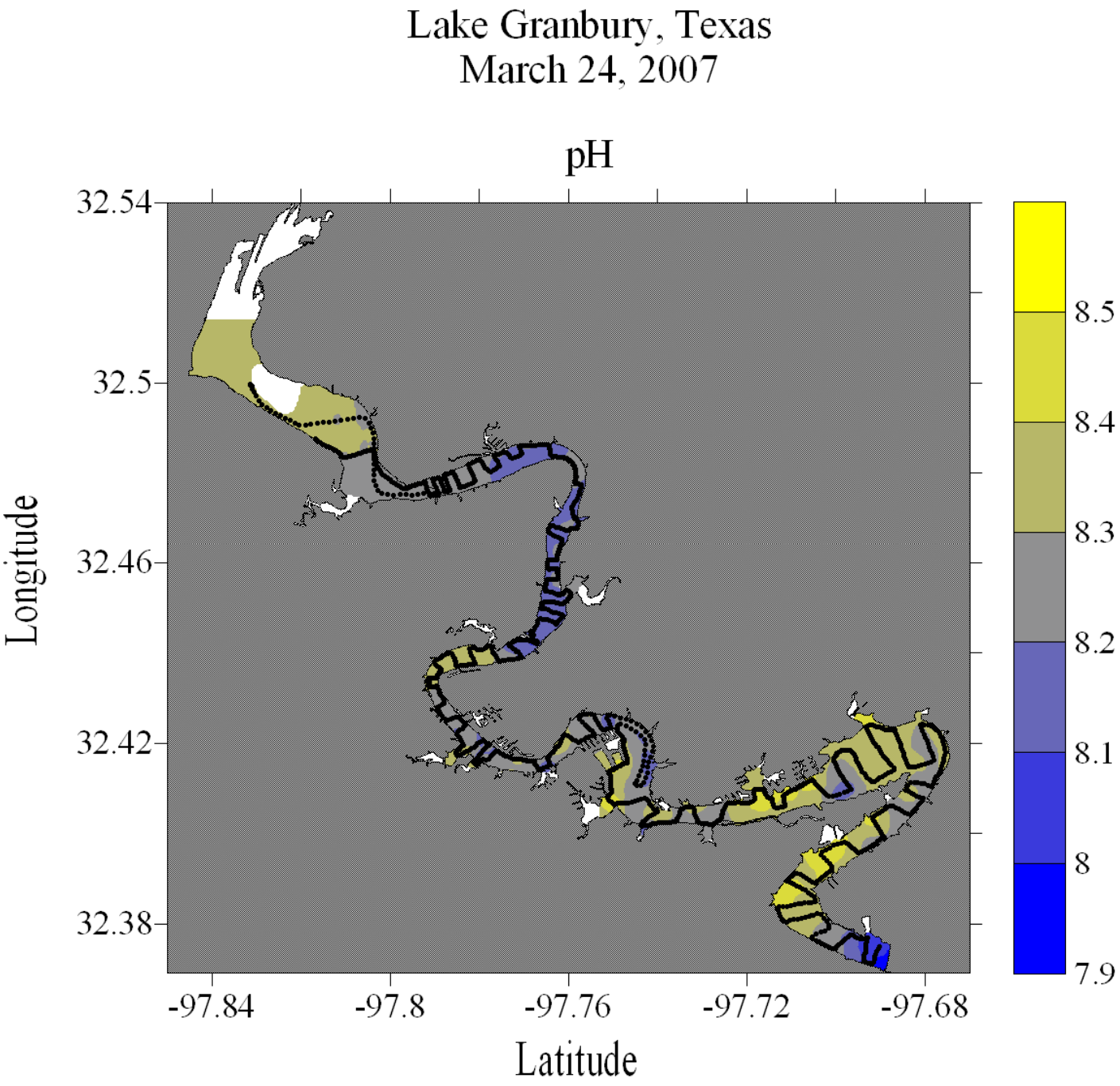

Figure E-52. pH dataflow map for Lake Granbury

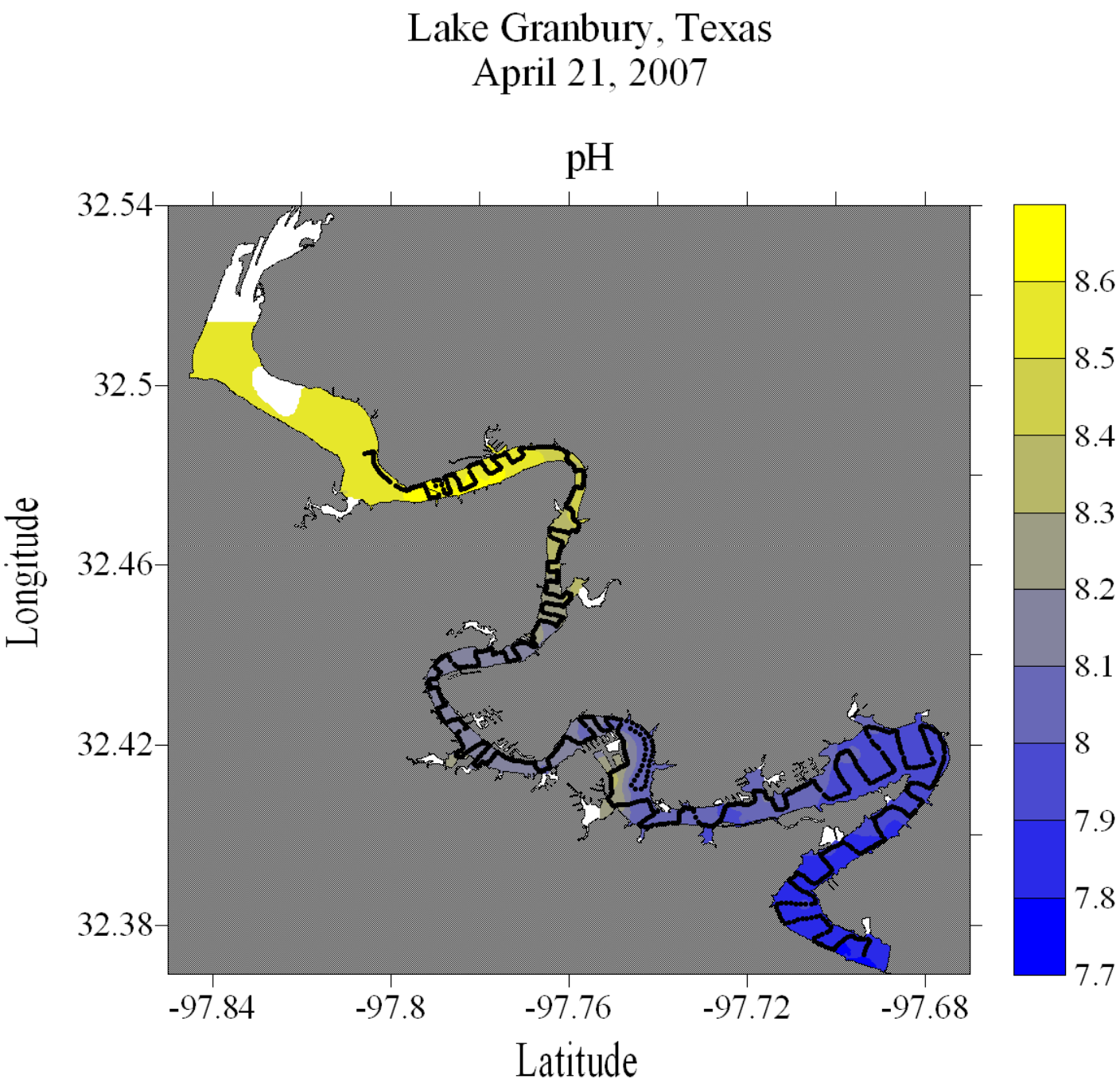

Figure E-53. pH dataflow map for Lake Granbury

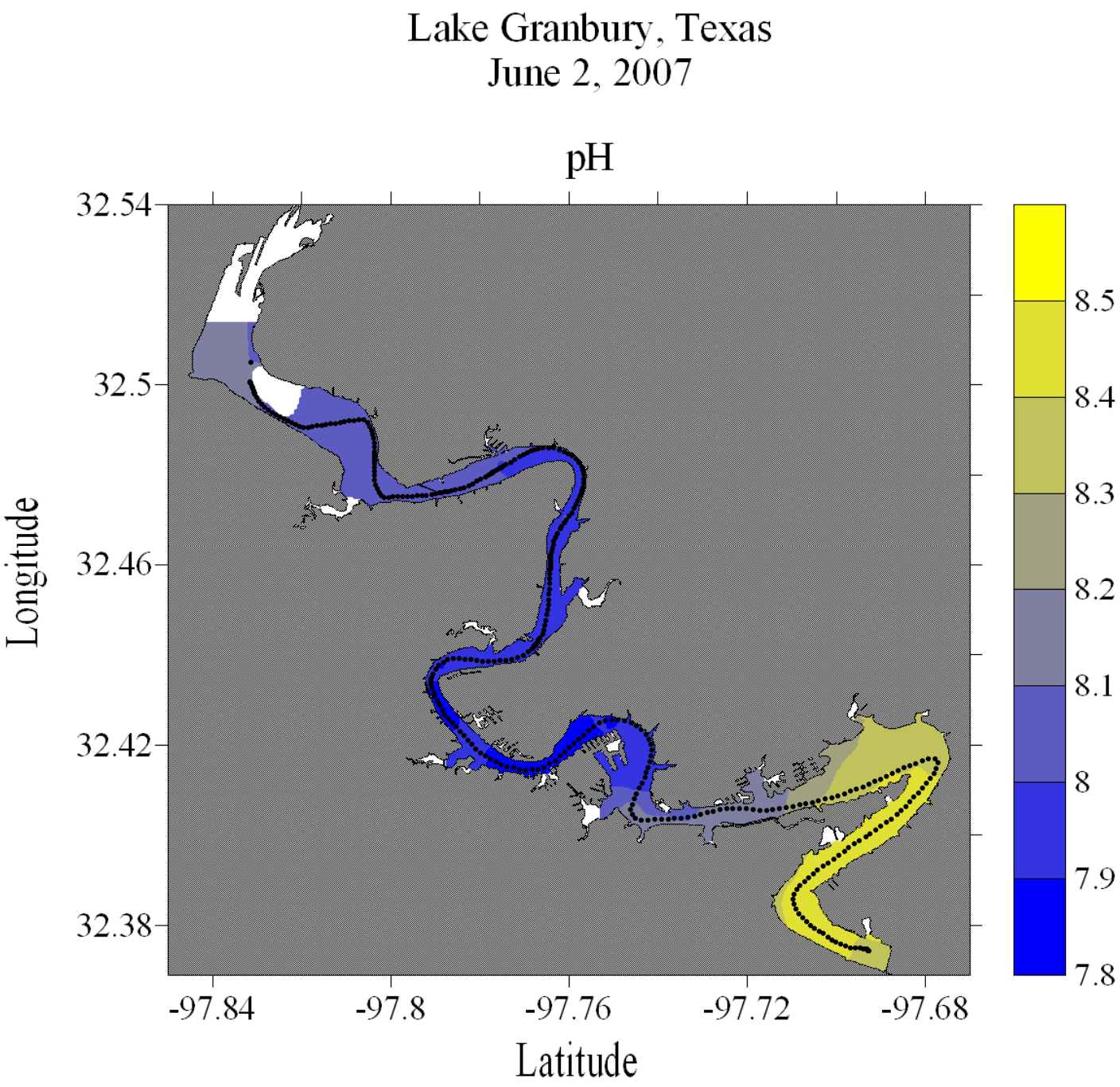

Figure E-54. pH dataflow map for Lake Granbury

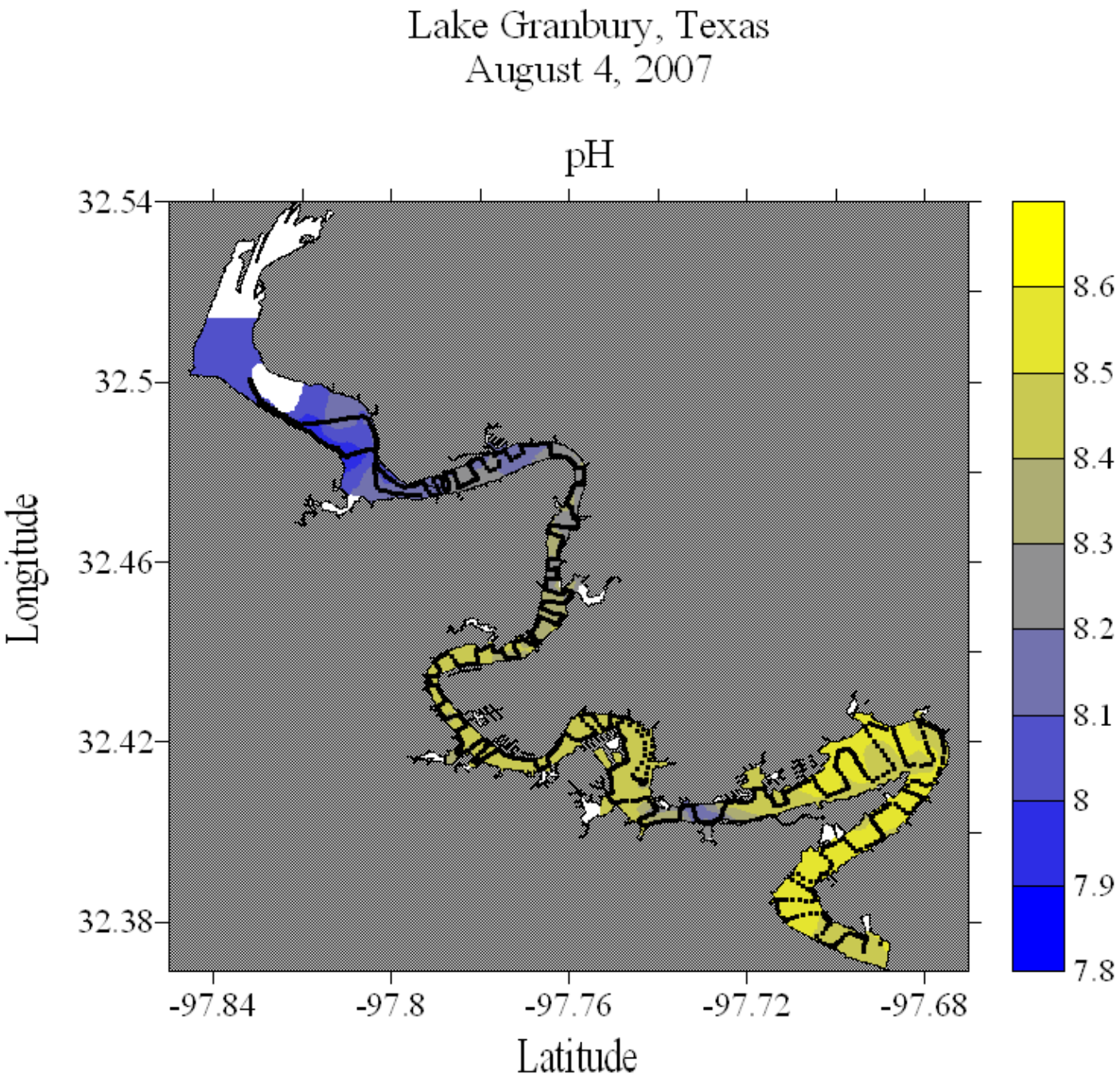

Figure E-55. pH dataflow map for Lake Granbury

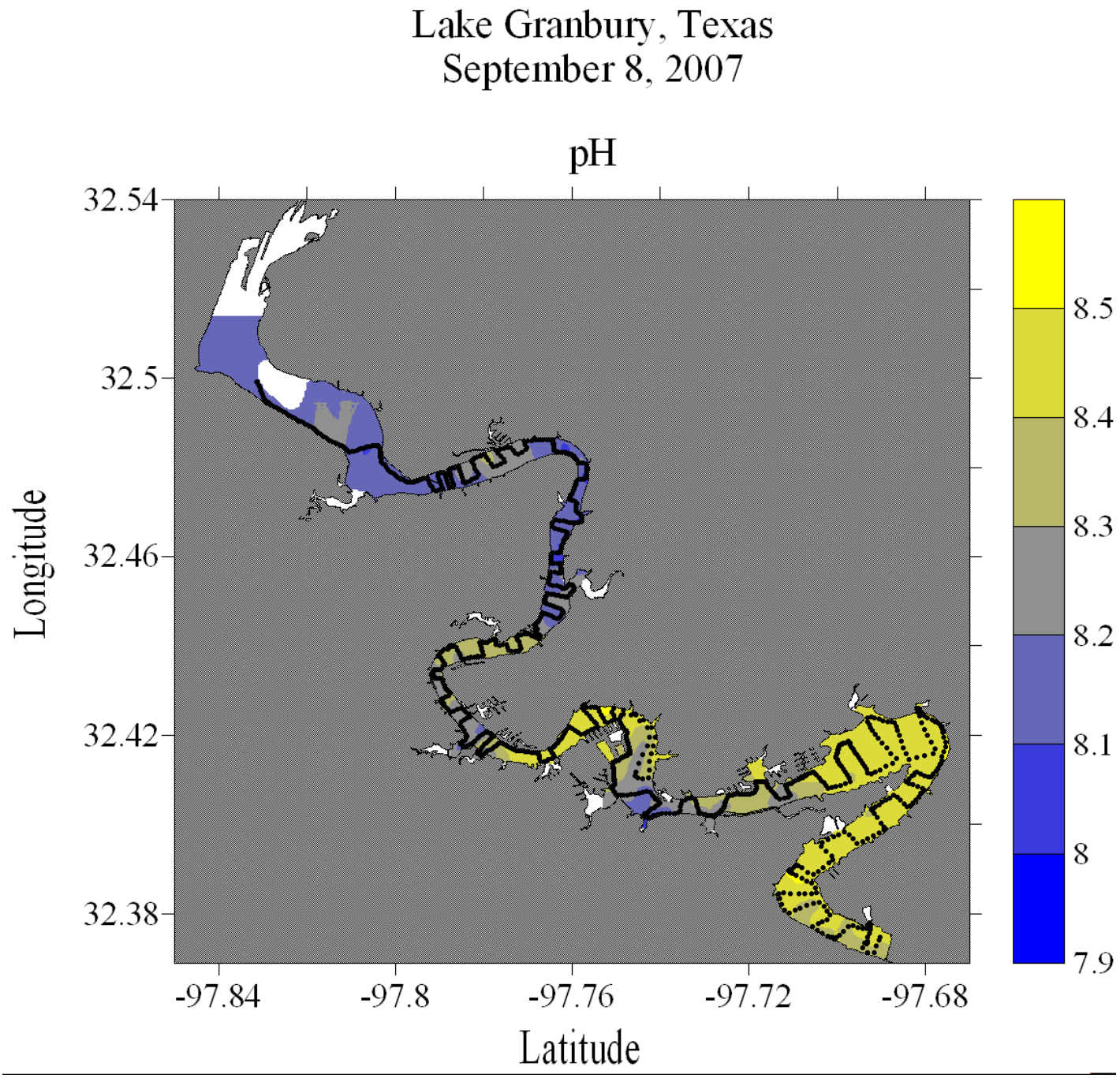

Figure E-56. pH dataflow map for Lake Granbury

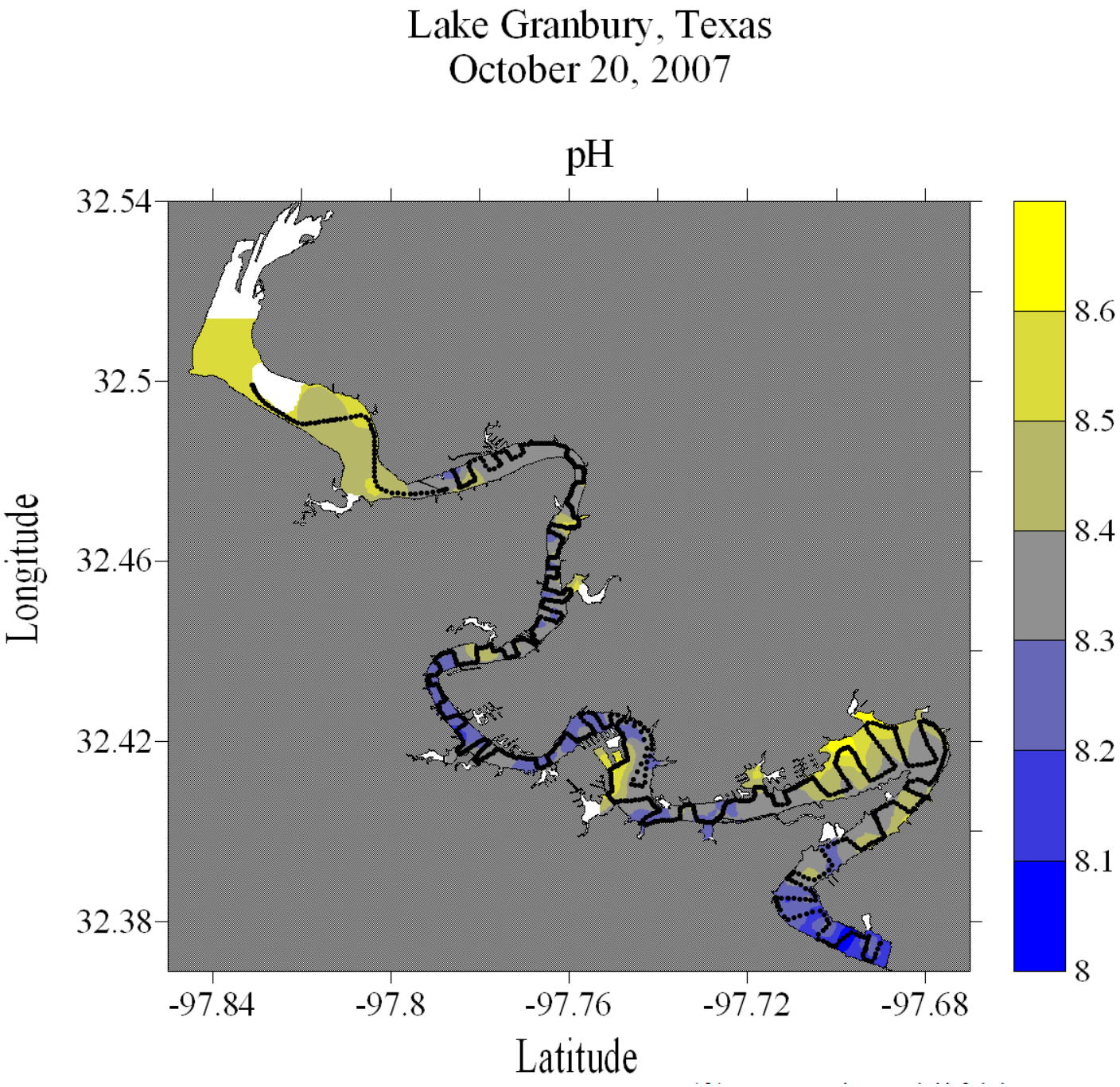

Figure E-57. pH dataflow map for Lake Granbury

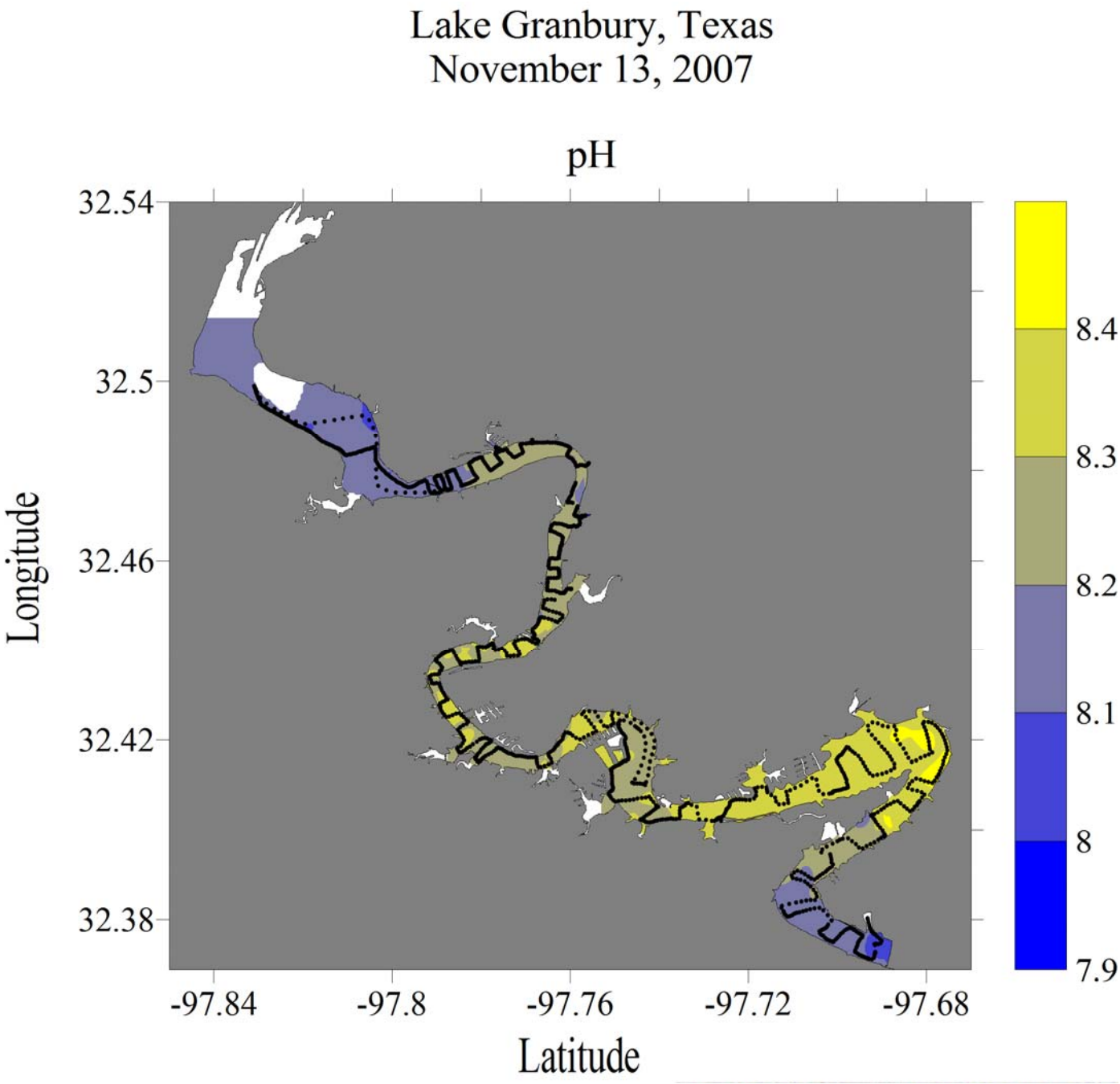

Figure E-58. pH dataflow map for Lake Granbury

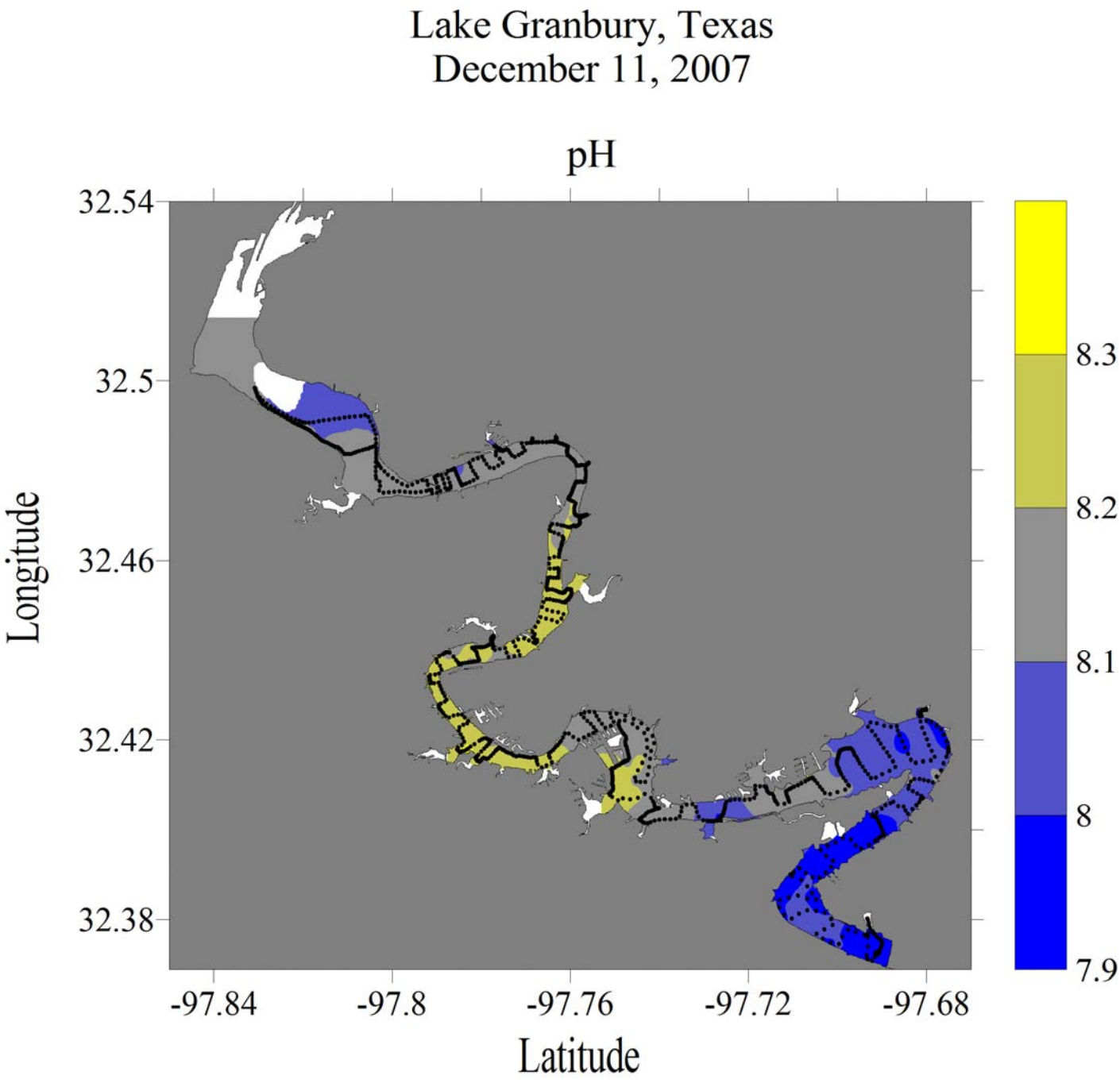

Figure E-59. pH dataflow map for Lake Granbury

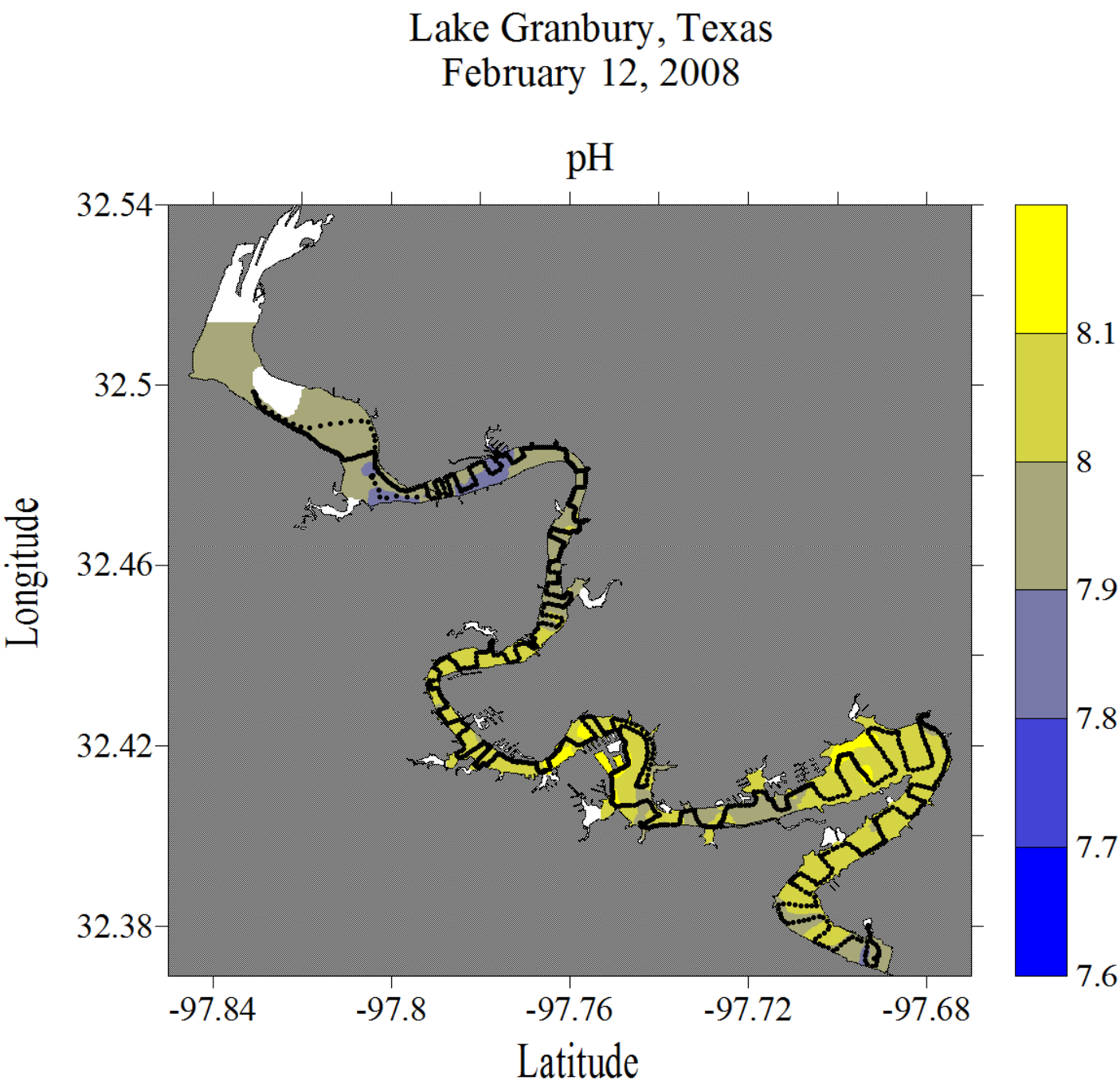

Figure E-60. pH dataflow map for Lake Granbury

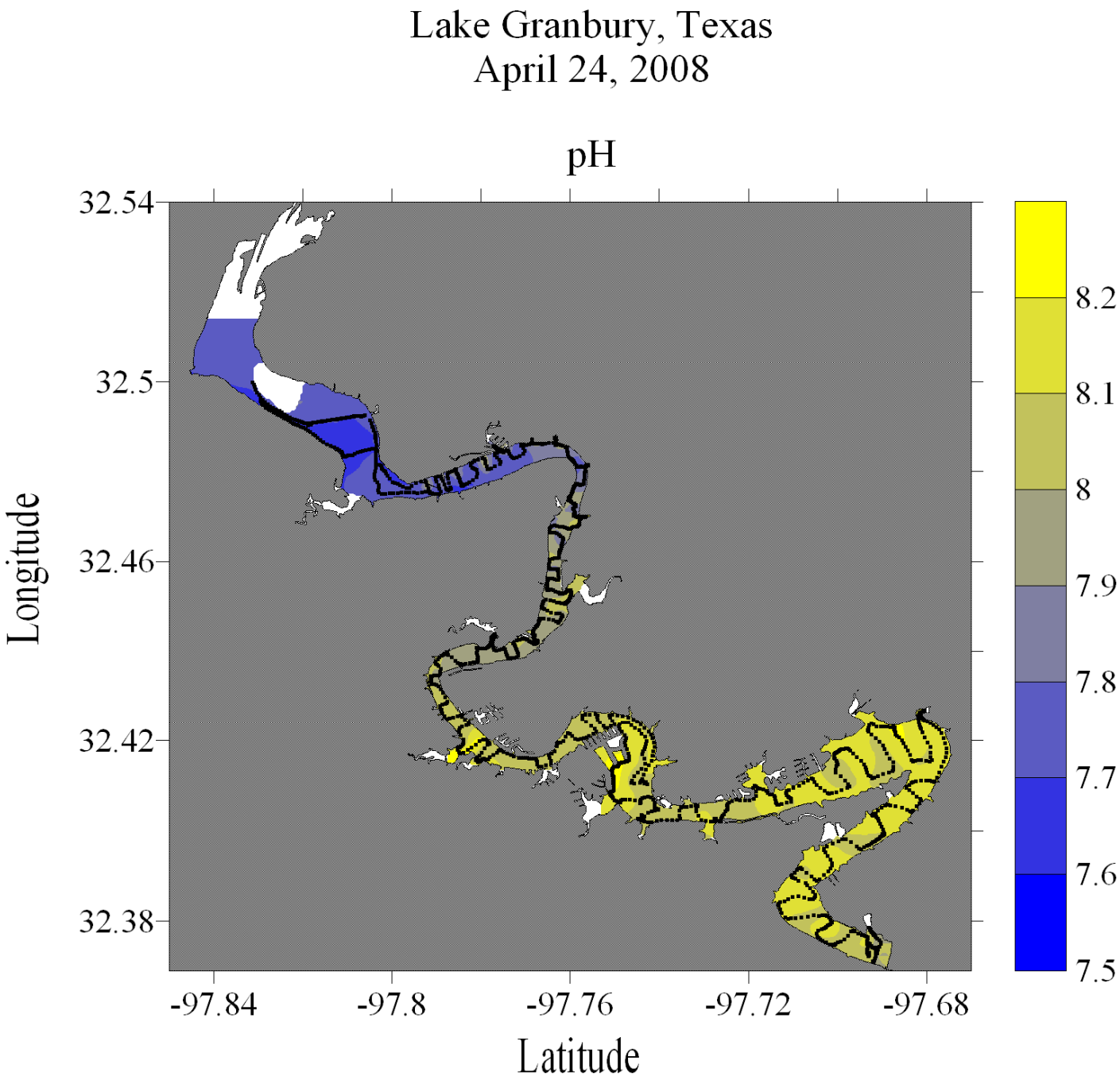

Figure E-61. pH dataflow map for Lake Granbury

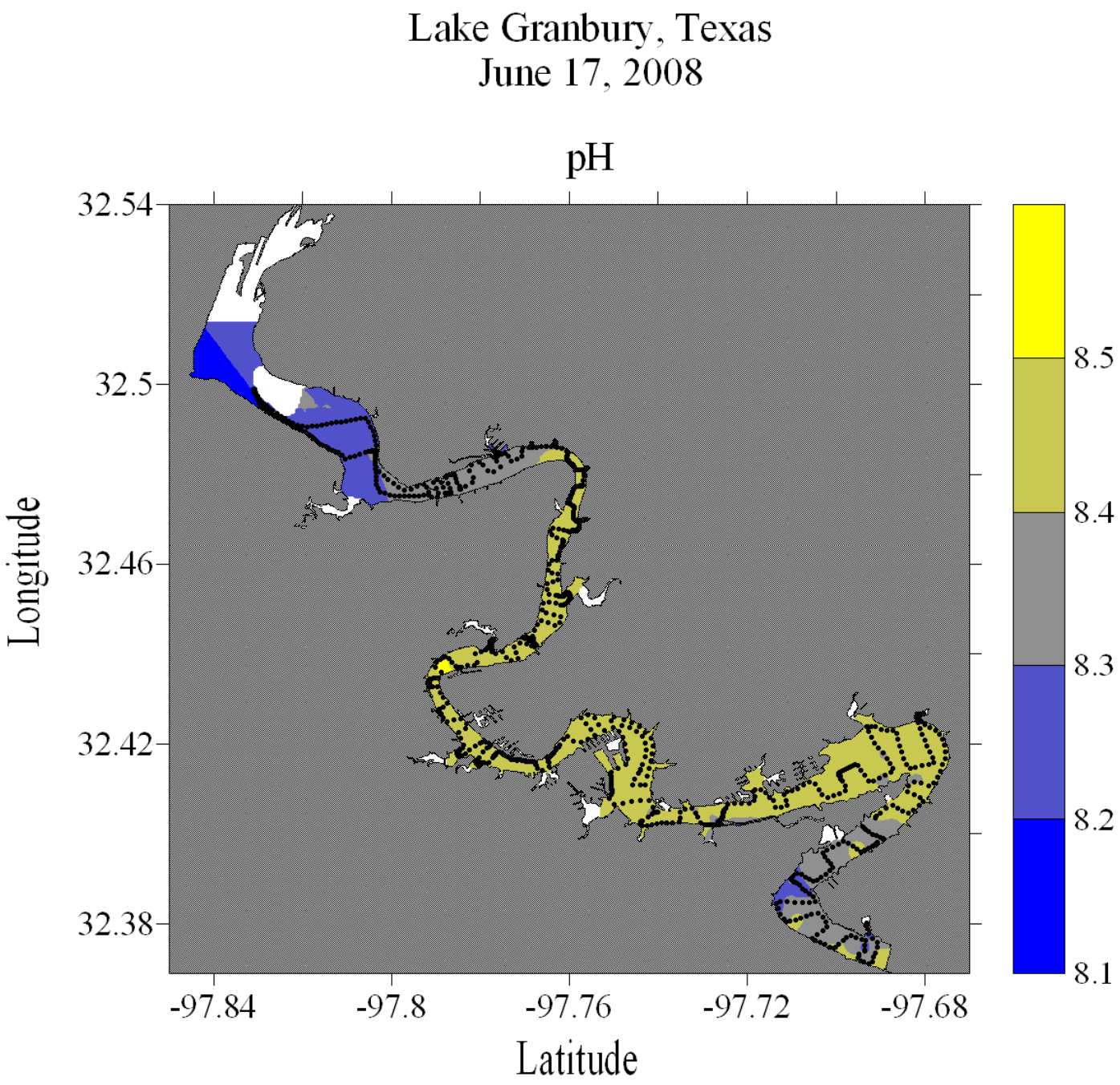

Figure E-62. pH dataflow map for Lake Granbury

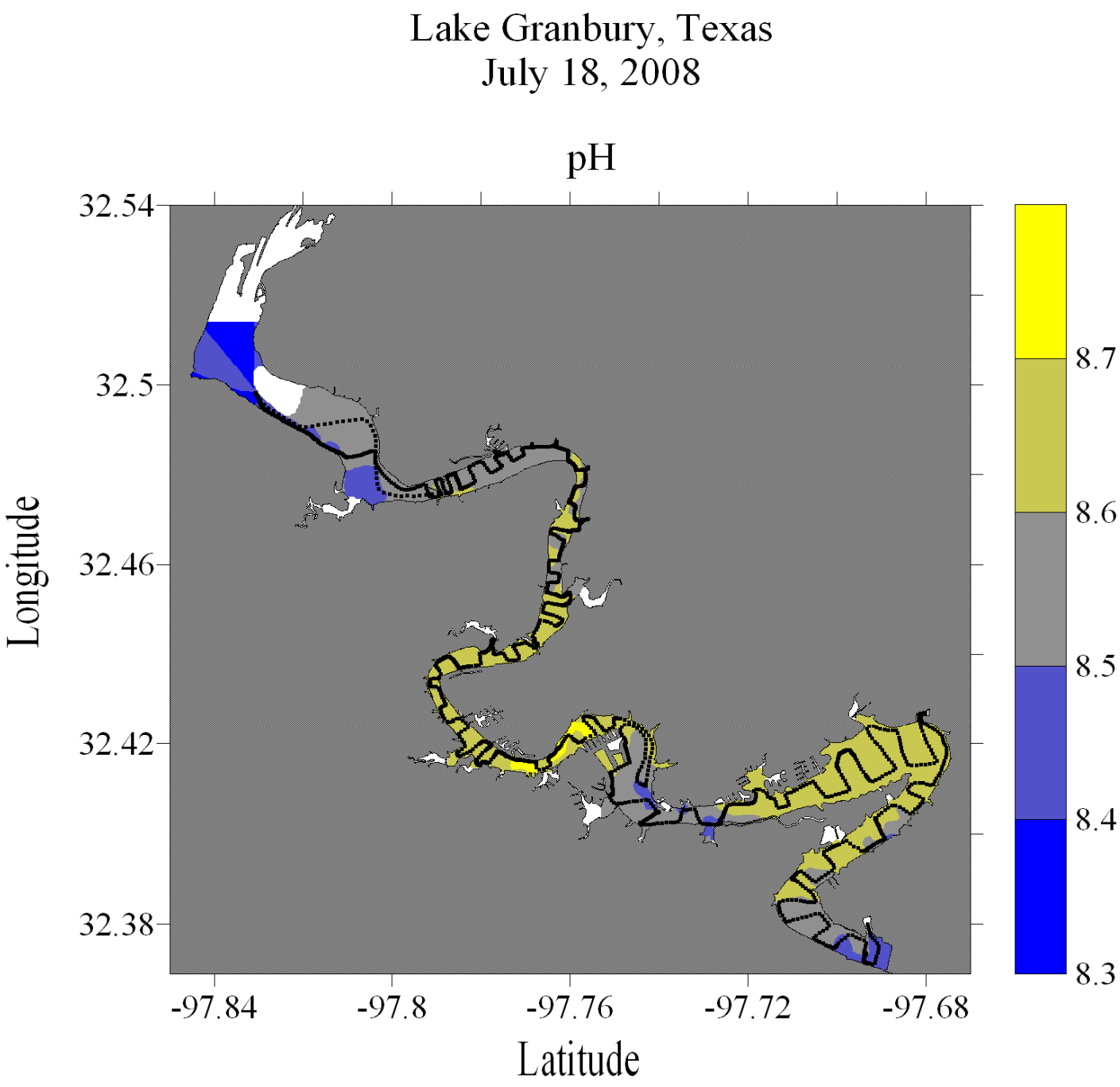

Figure E-63. pH dataflow map for Lake Granbury

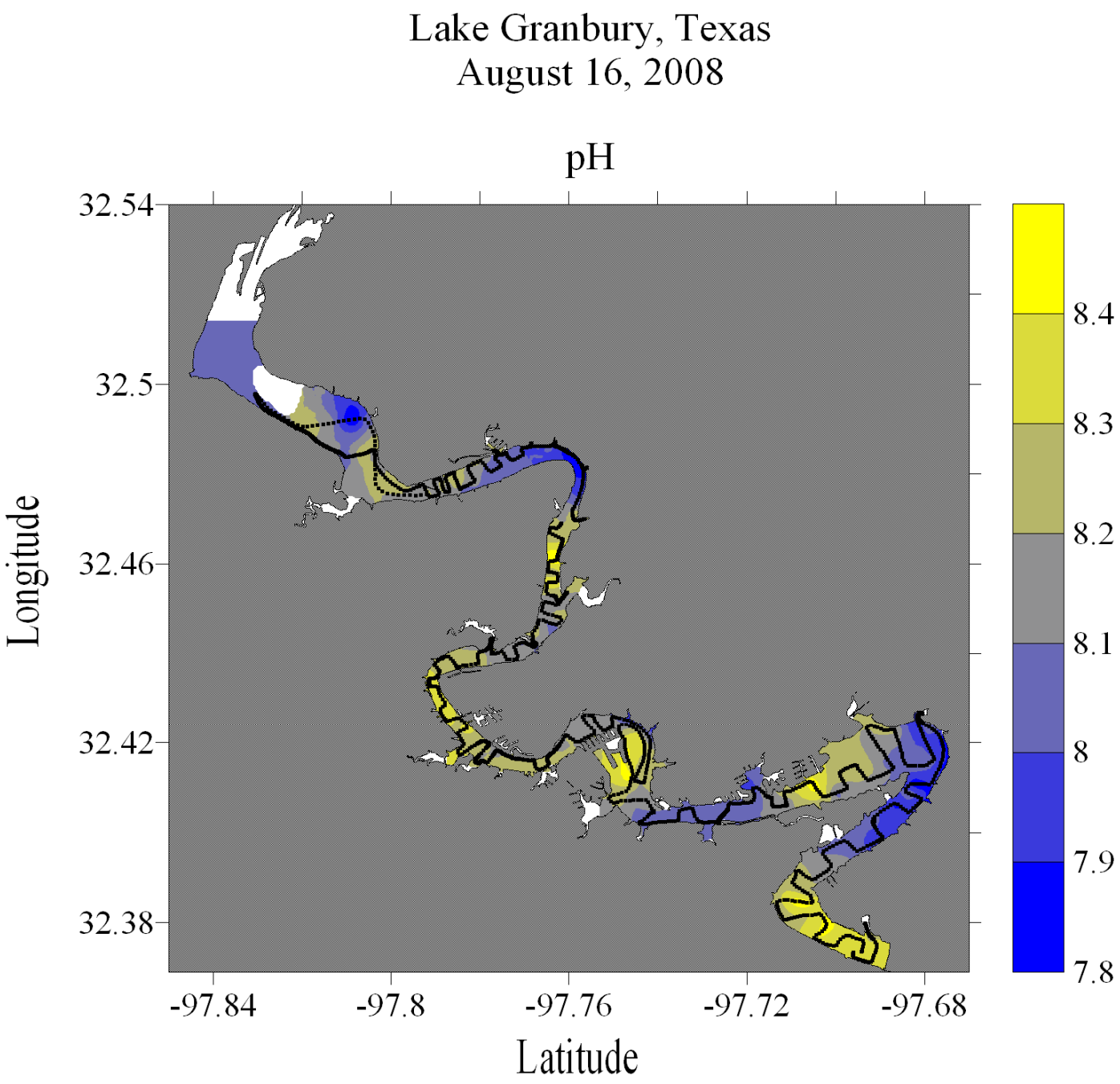

Figure E-64. pH dataflow map for Lake Granbury

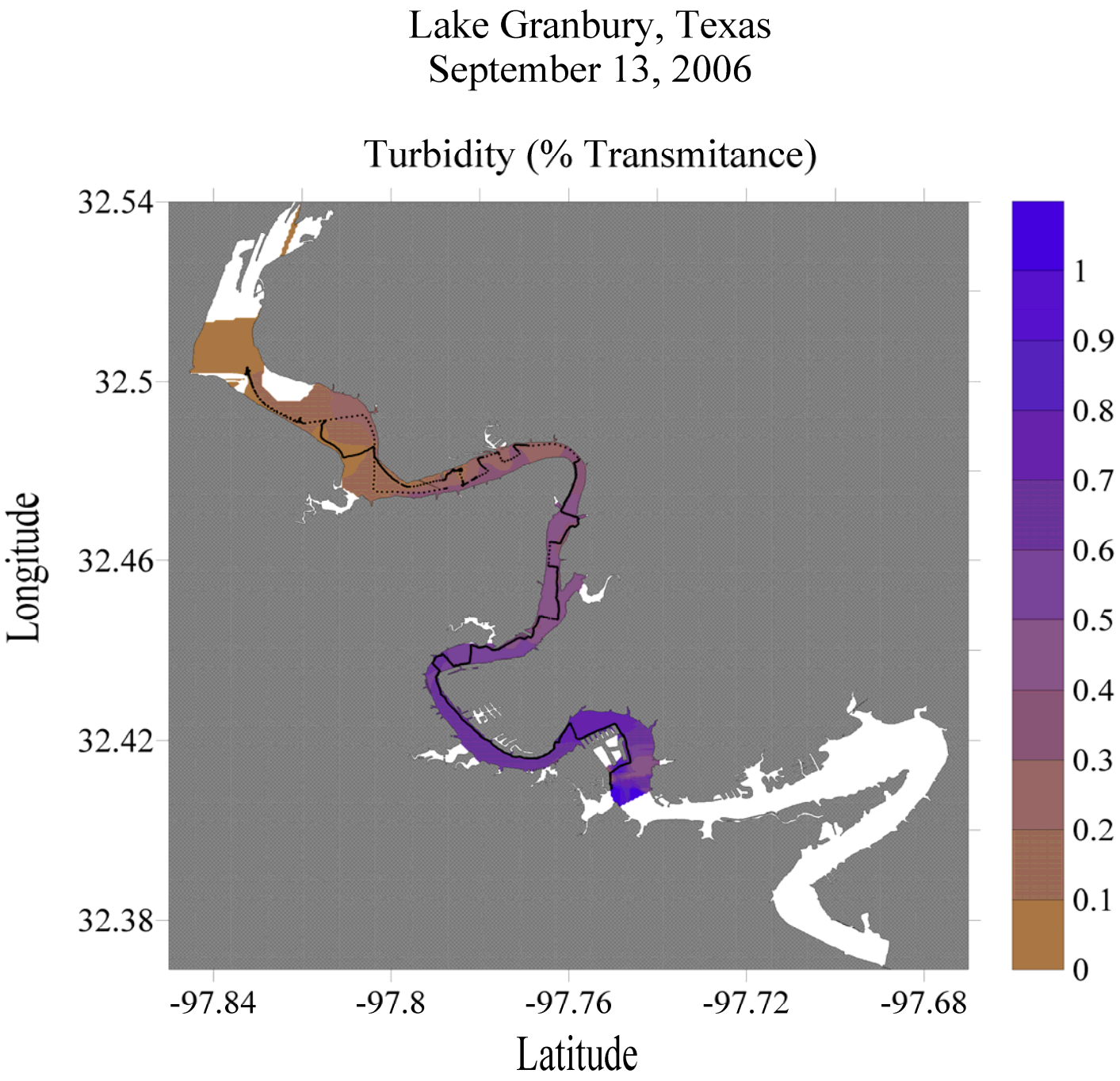

Figure E-65. Turbidity dataflow map for Lake Granbury

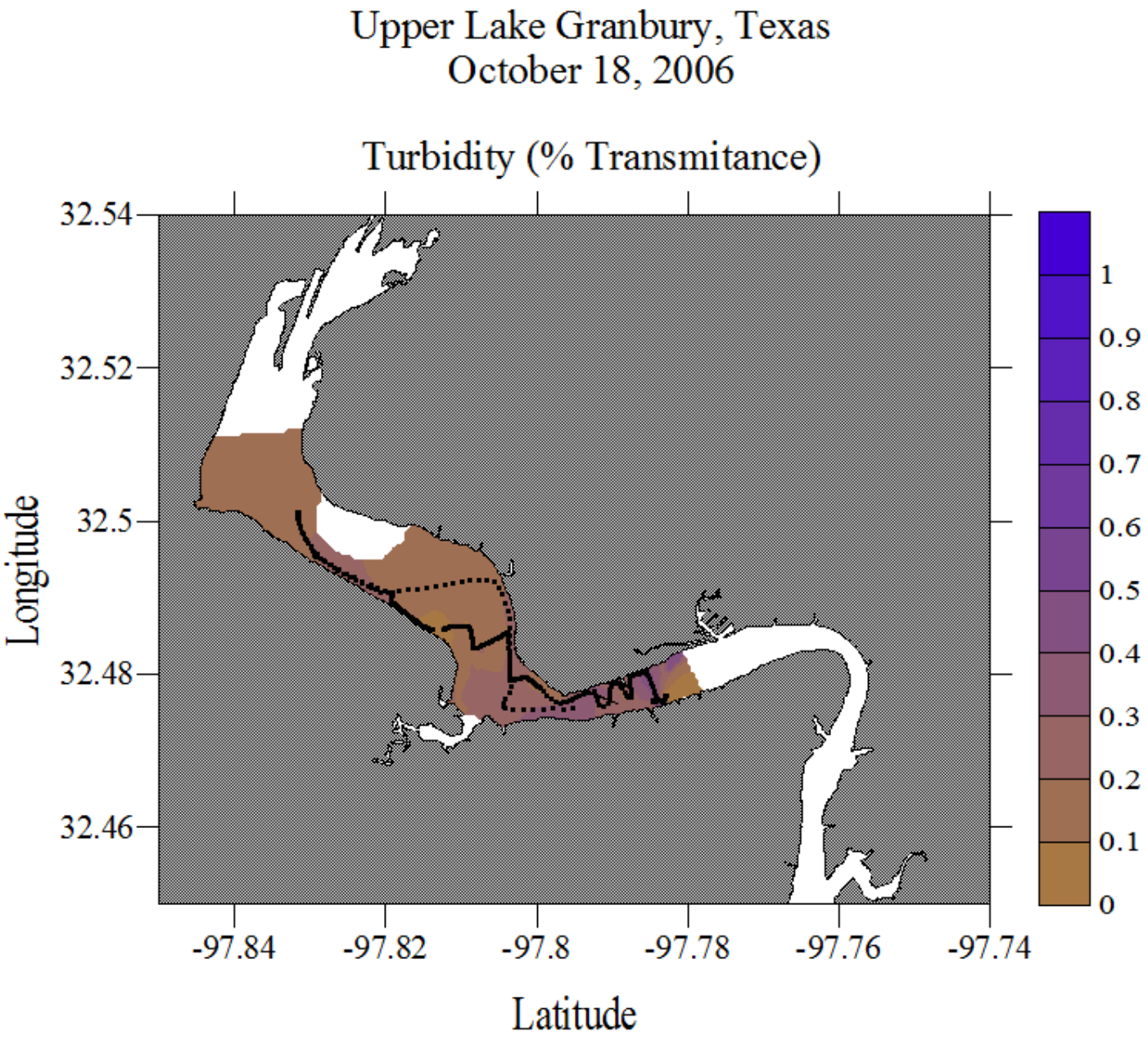

Figure E-66. Turbidity dataflow map for Lake Granbury

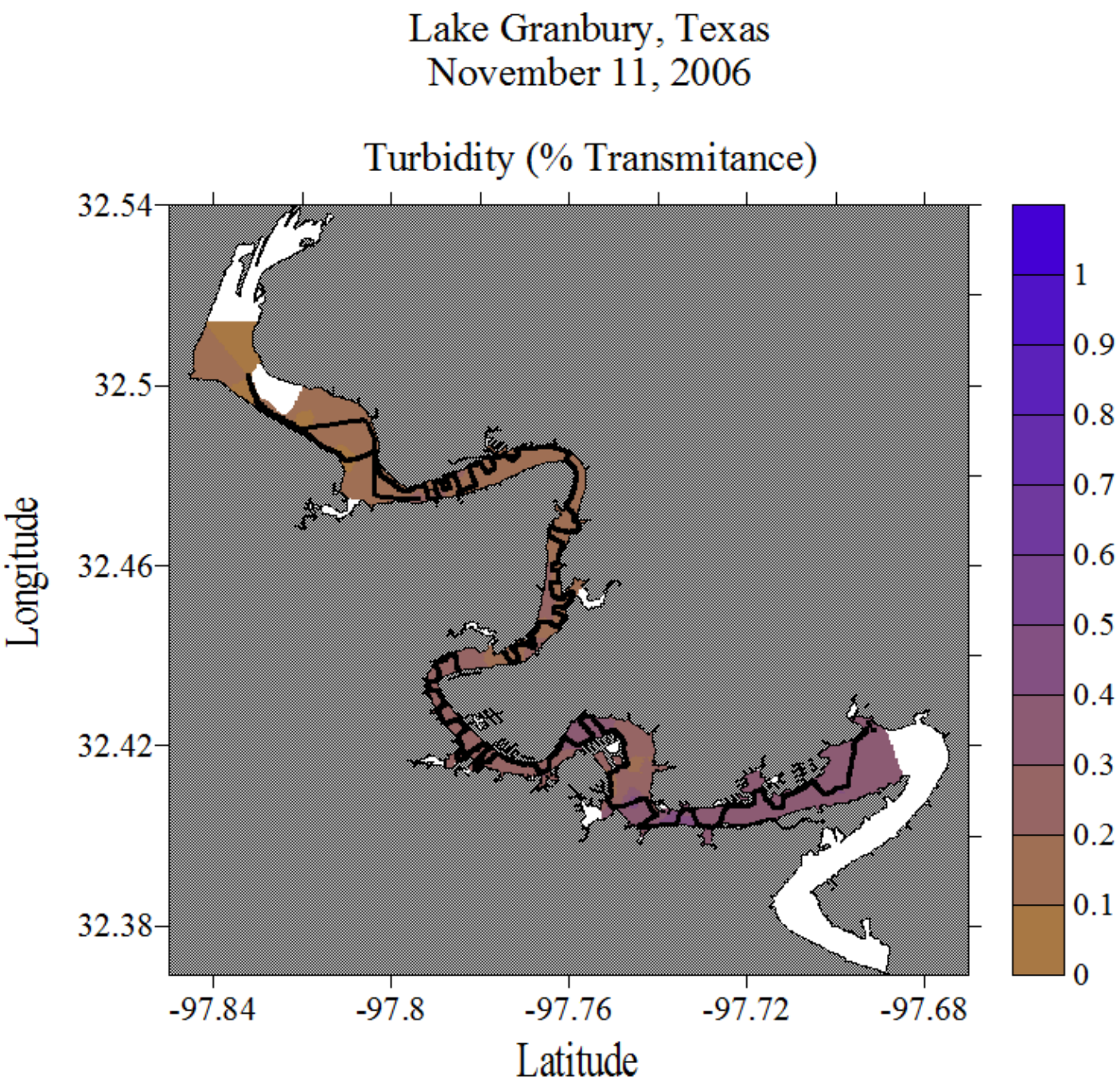

Figure E-67. Turbidity dataflow map for Lake Granbury

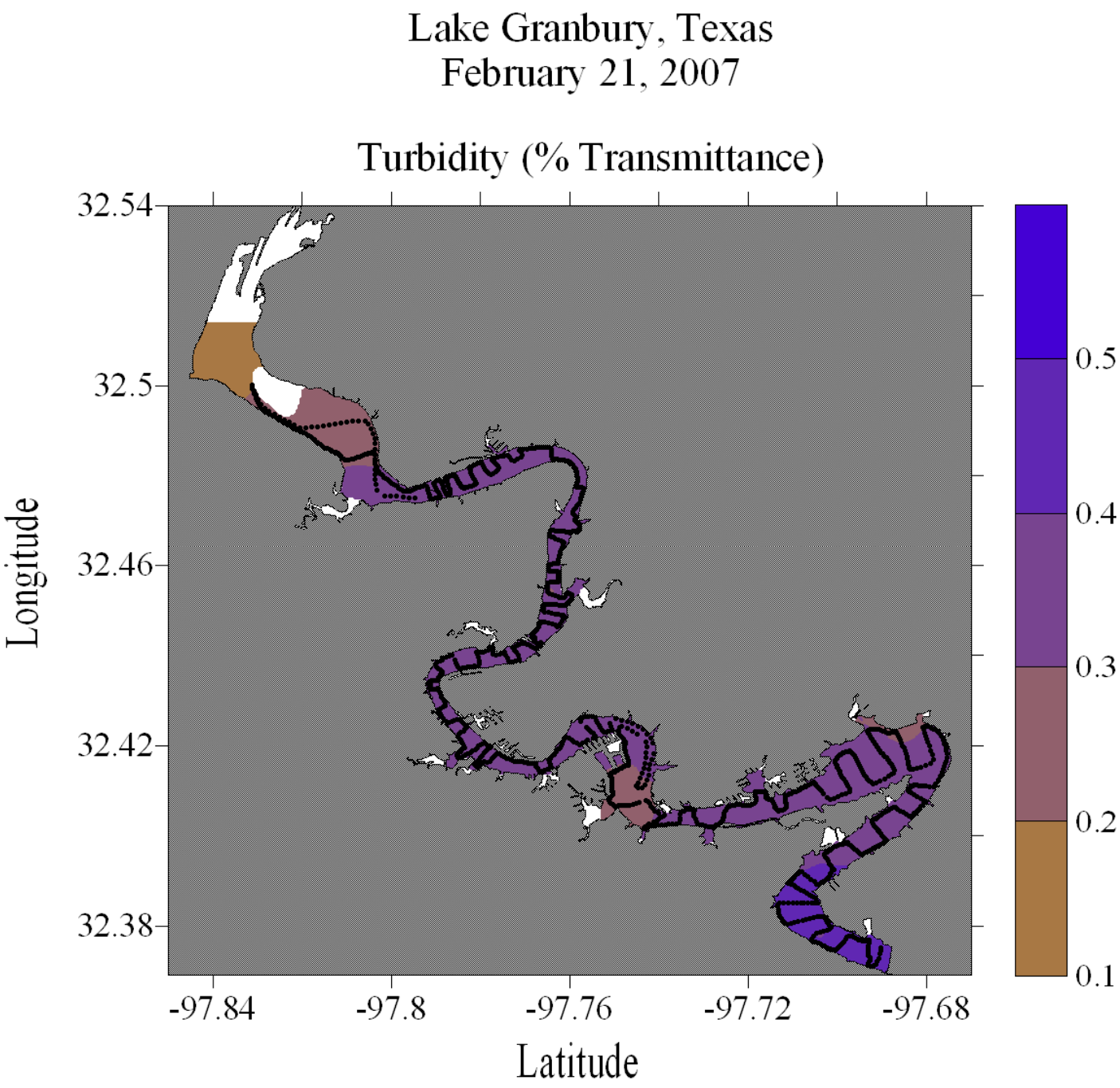

Figure E-68. Turbidity dataflow map for Lake Granbury

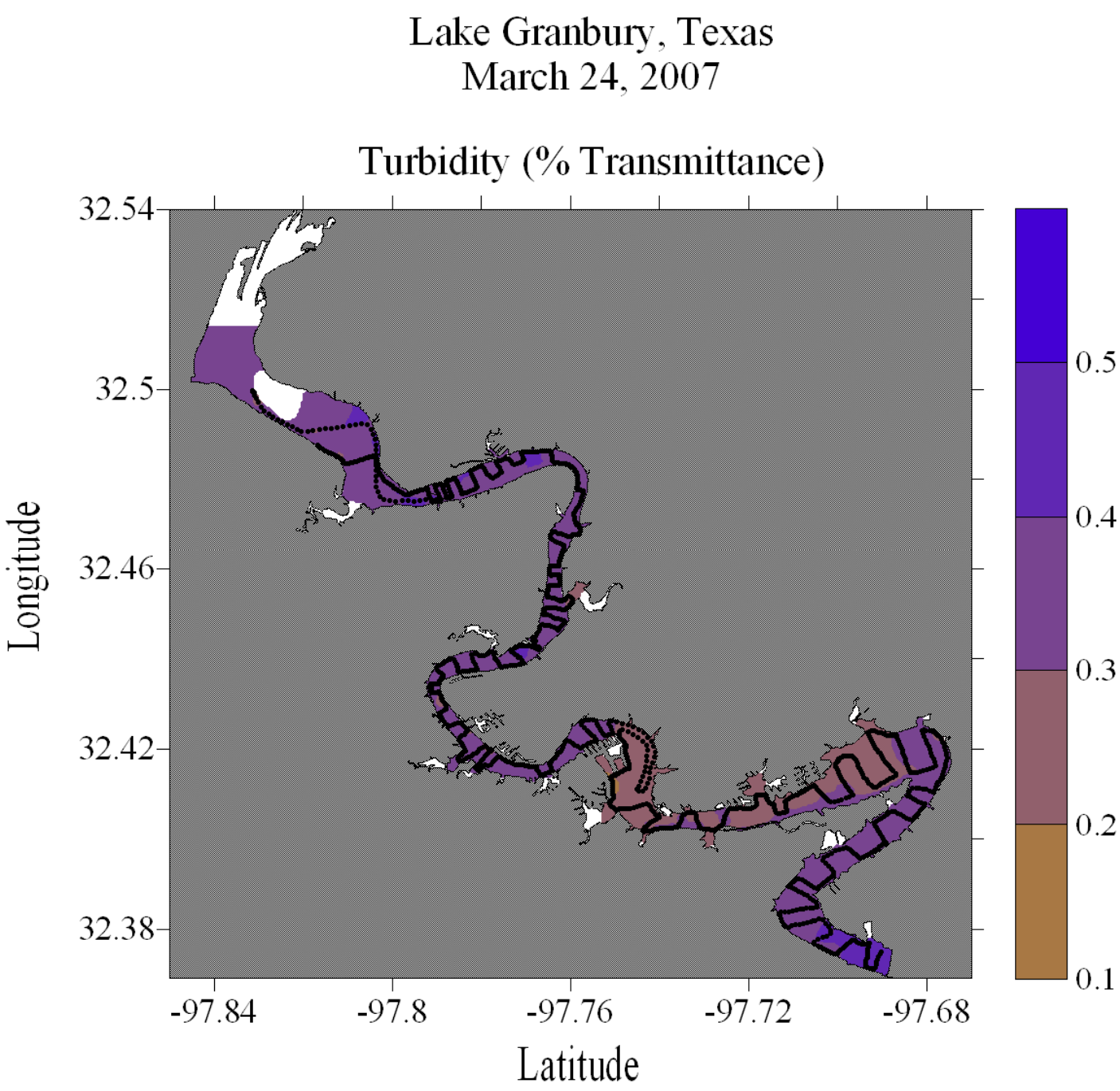

Figure E-69. Turbidity dataflow map for Lake Granbury

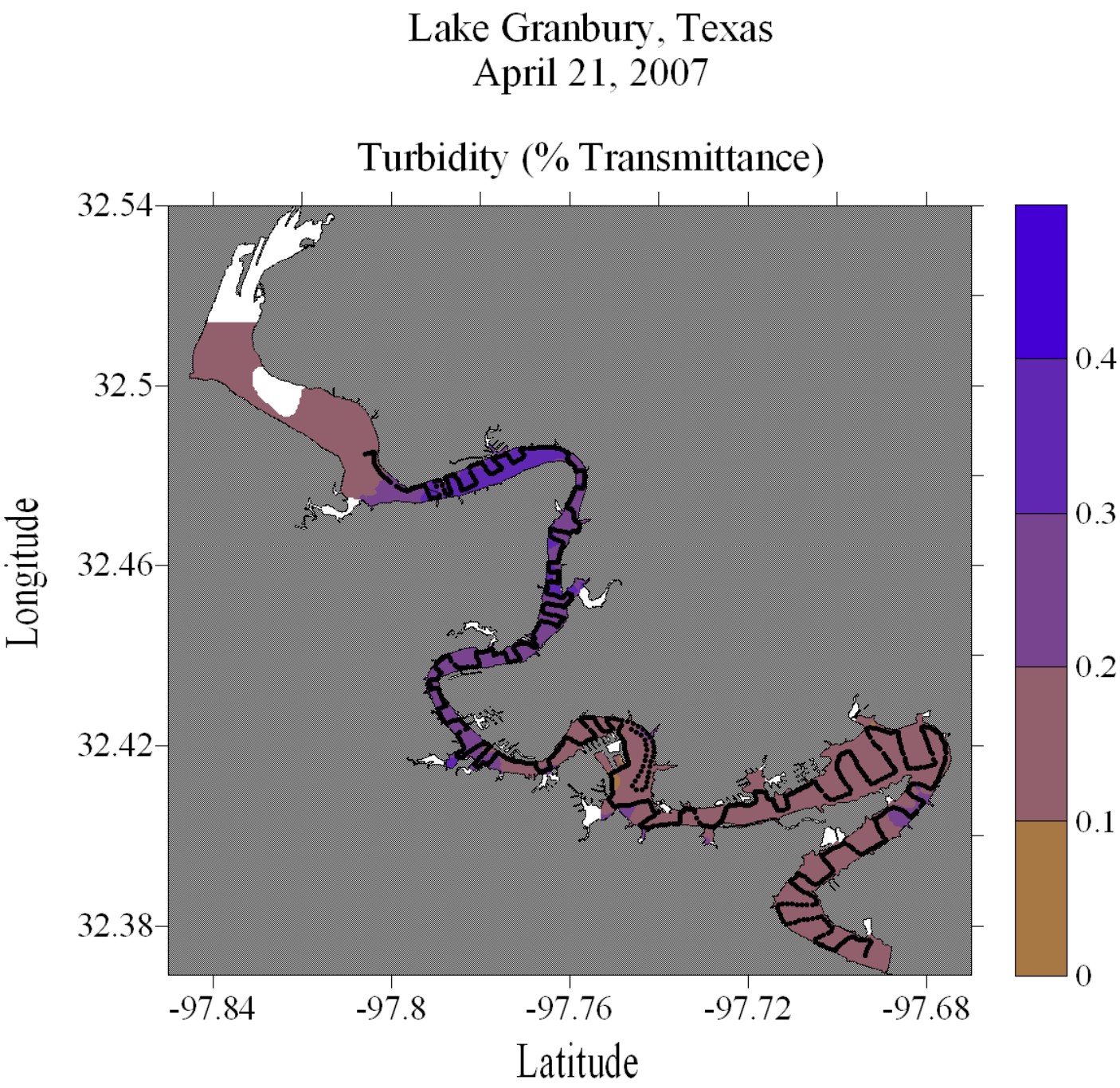

Figure E-70. Turbidity dataflow map for Lake Granbury

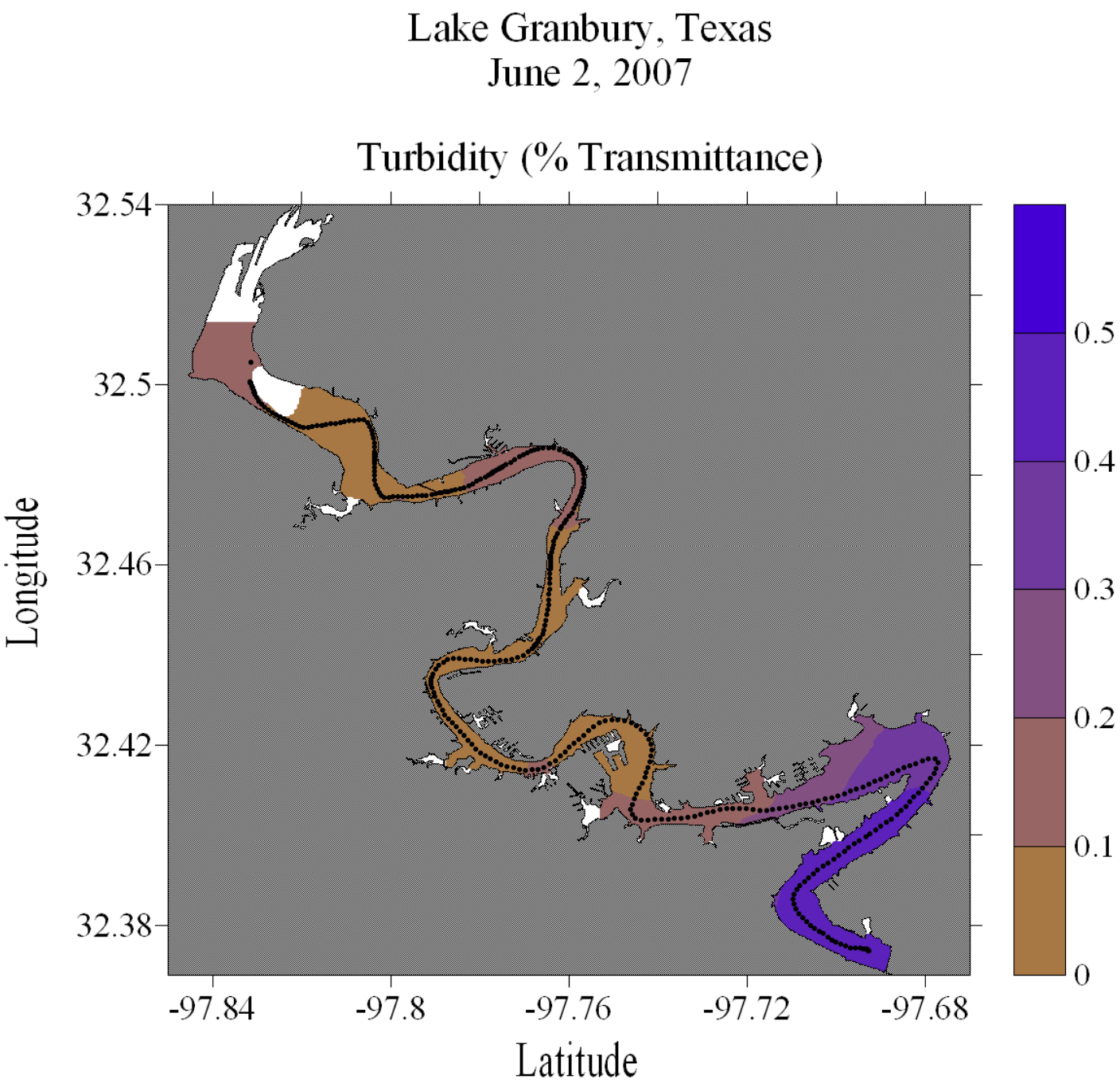

Figure E-71. Turbidity dataflow map for Lake Granbury

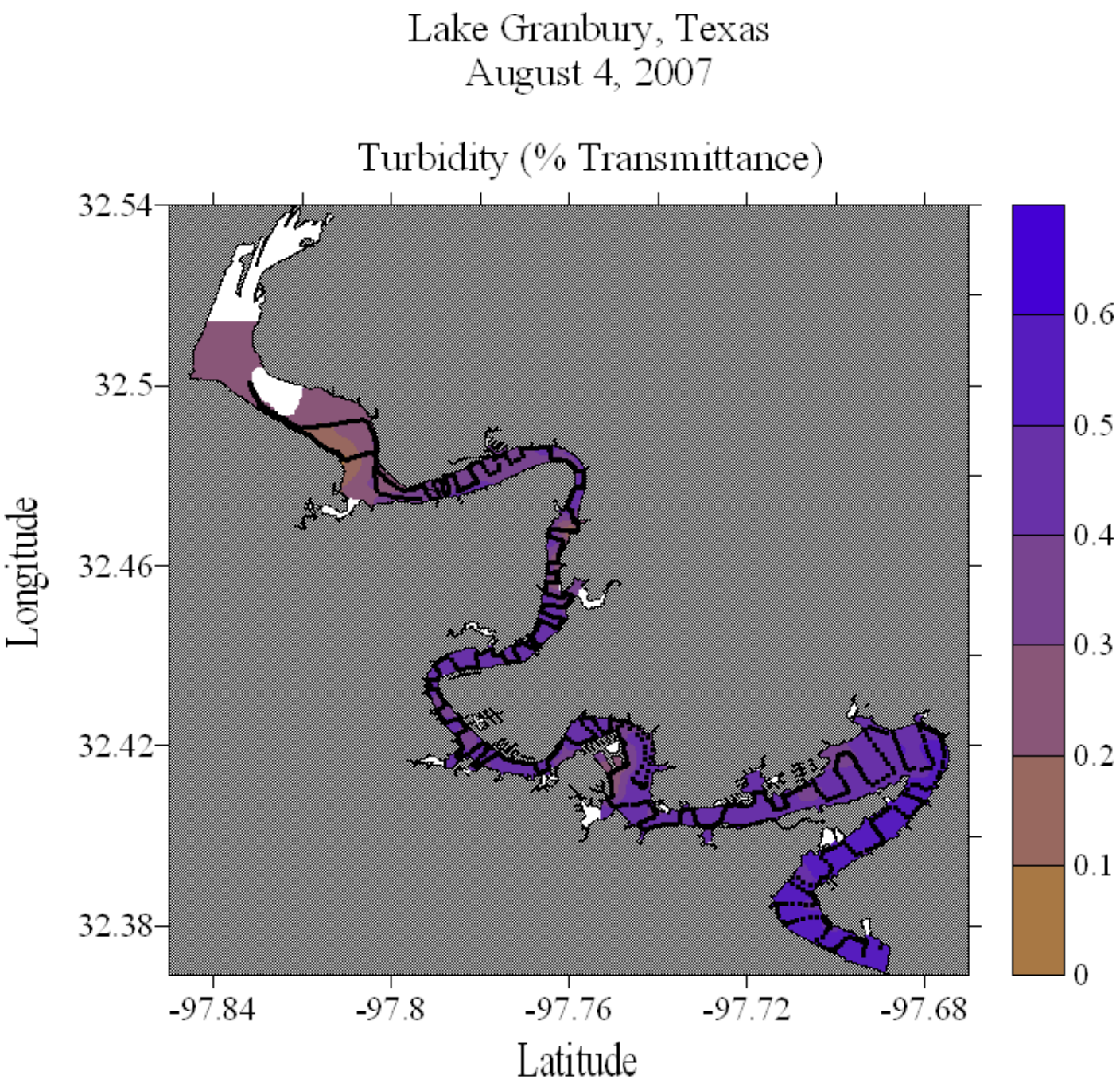

Figure E-72. Turbidity dataflow map for Lake Granbury

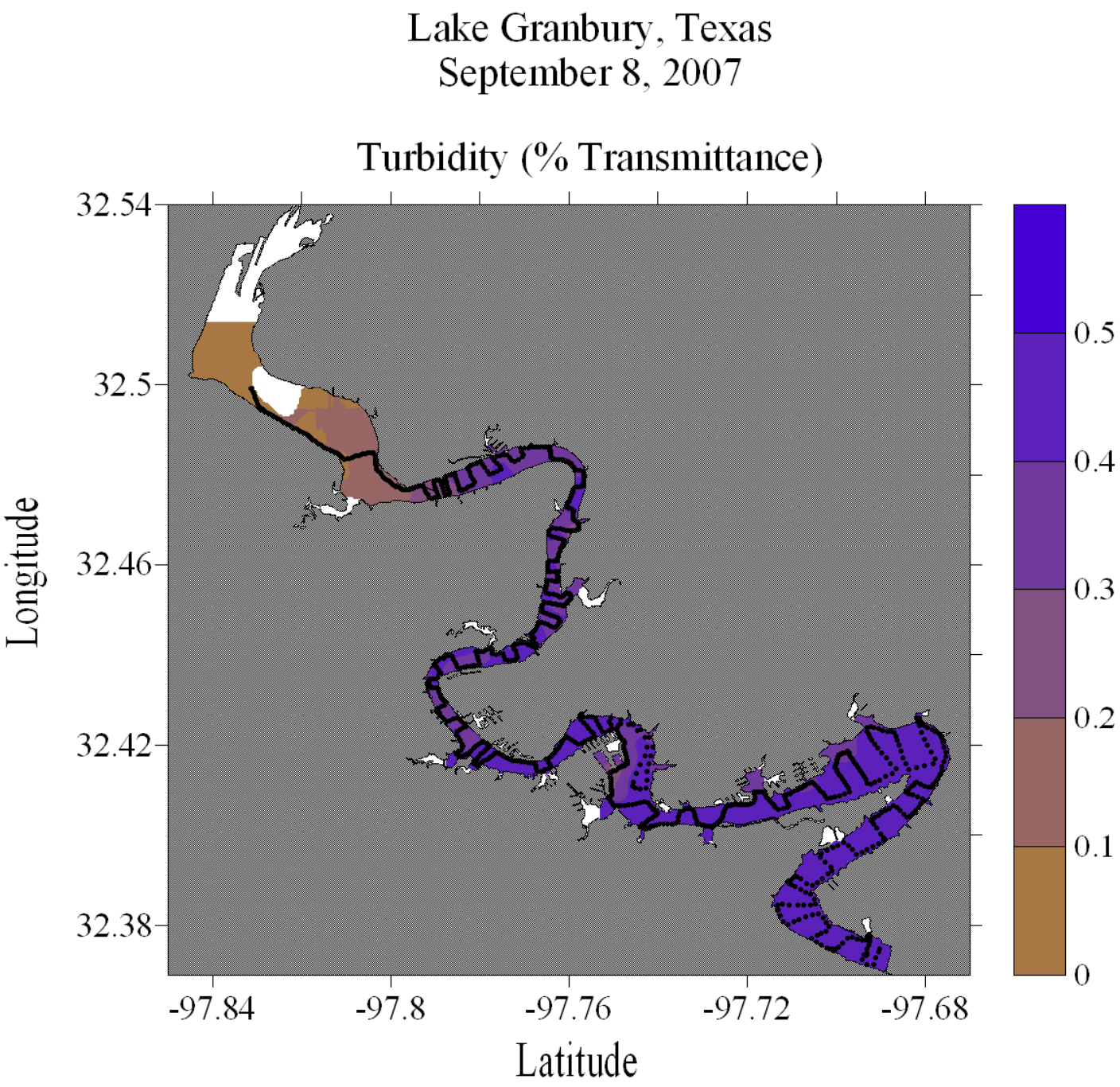

Figure E-73. Turbidity dataflow map for Lake Granbury

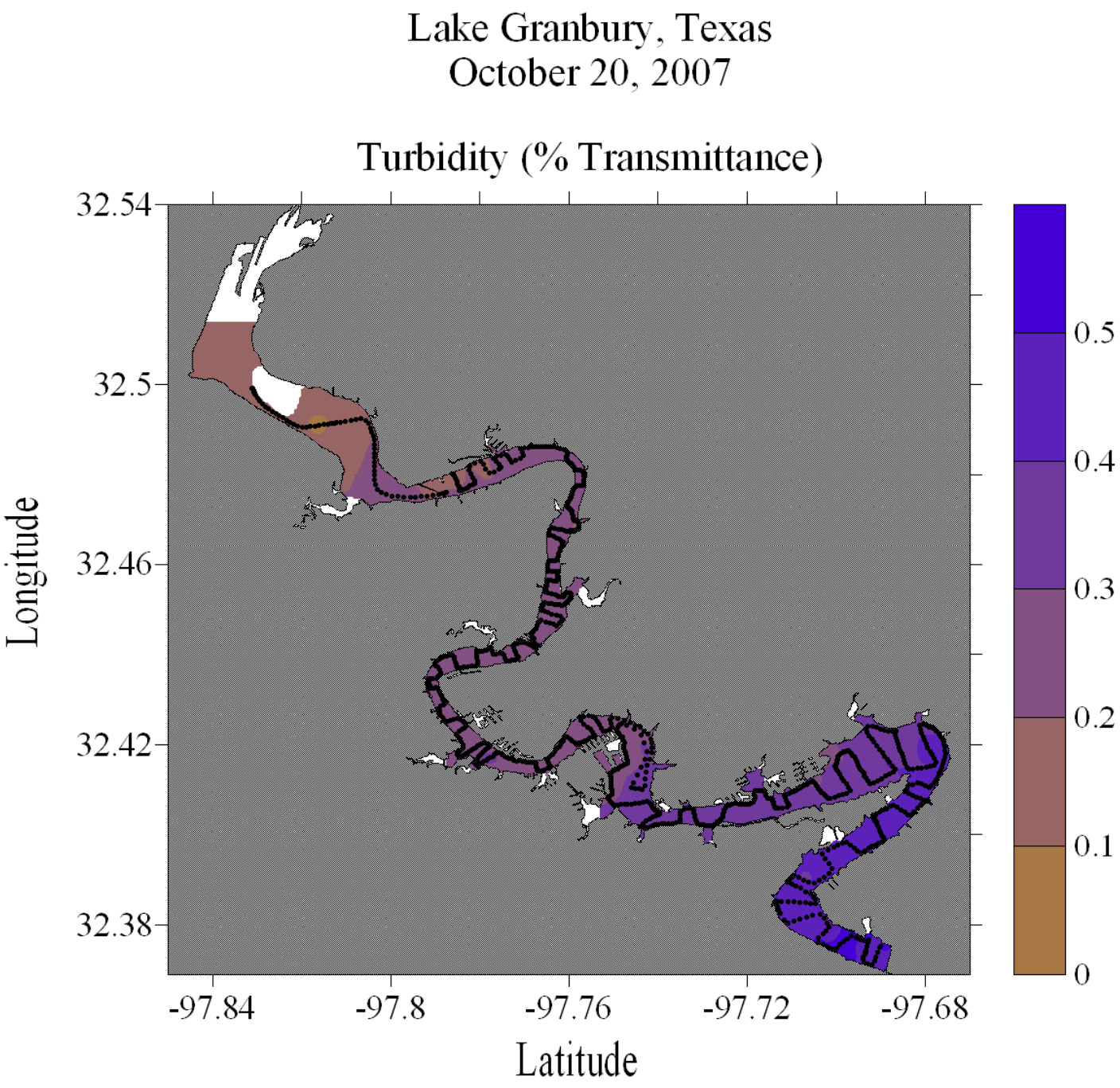

Figure E-74. Turbidity dataflow map for Lake Granbury

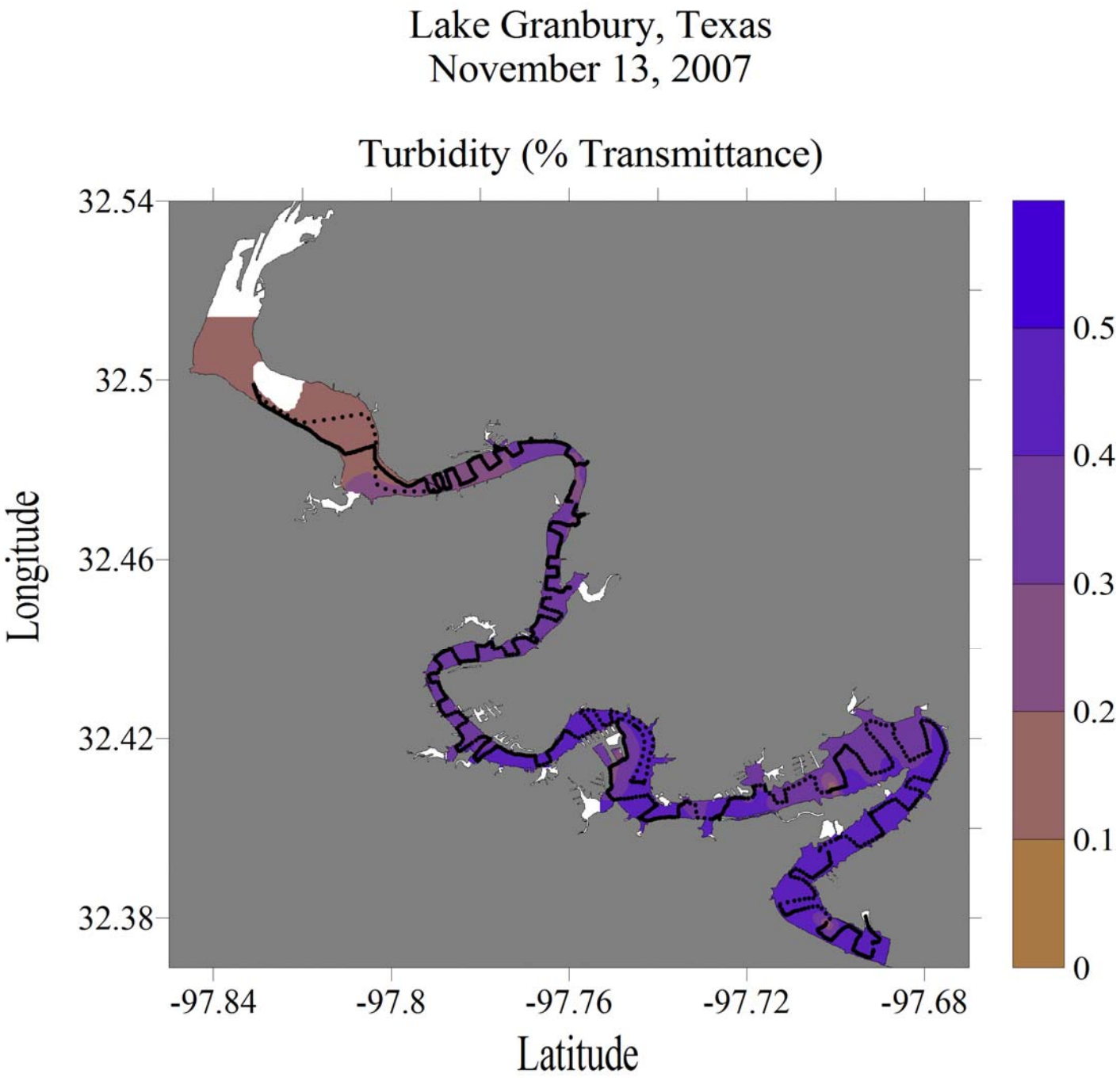

Figure E-75. Turbidity dataflow map for Lake Granbury

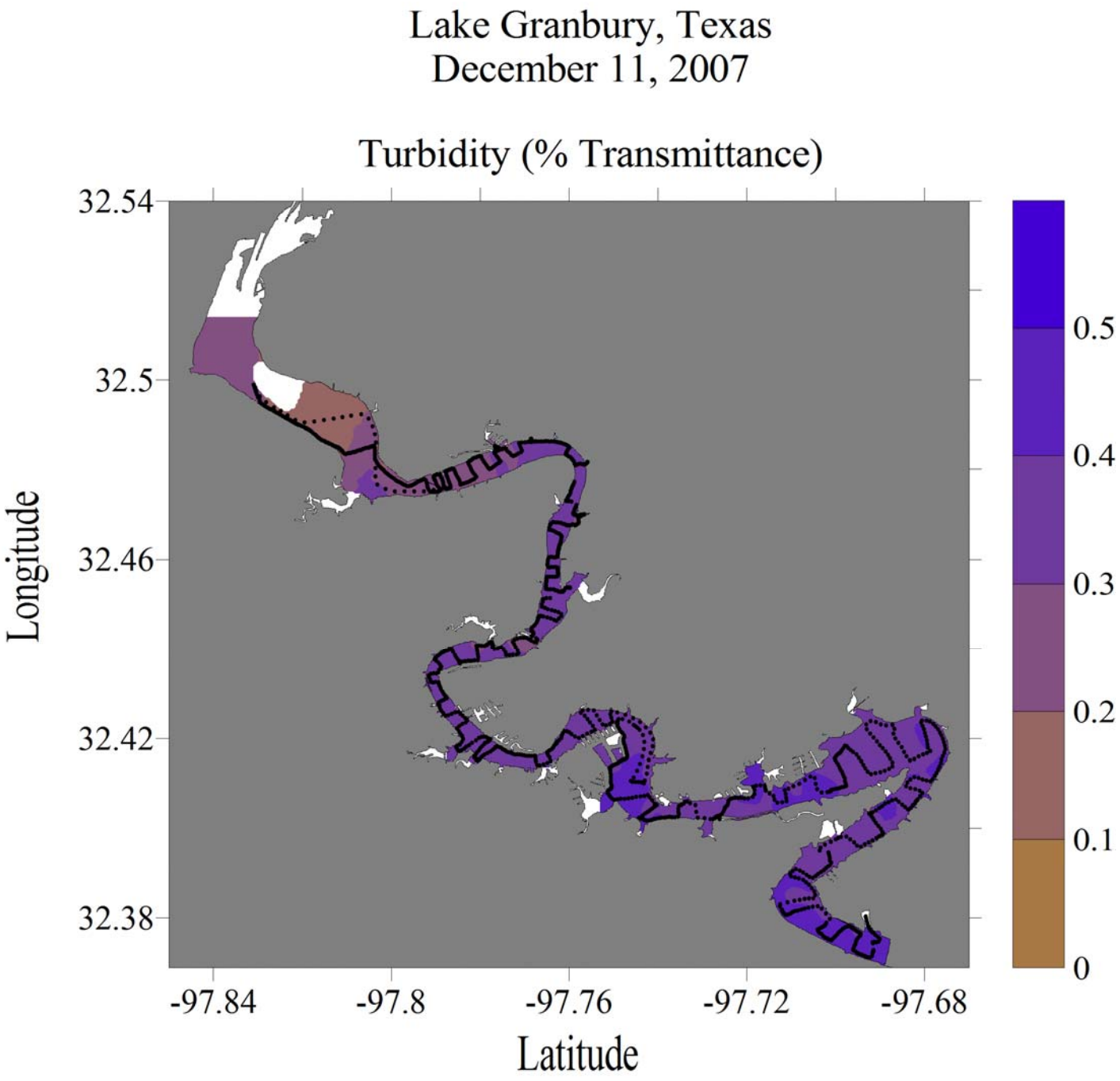

Figure E-76. Turbidity dataflow map for Lake Granbury

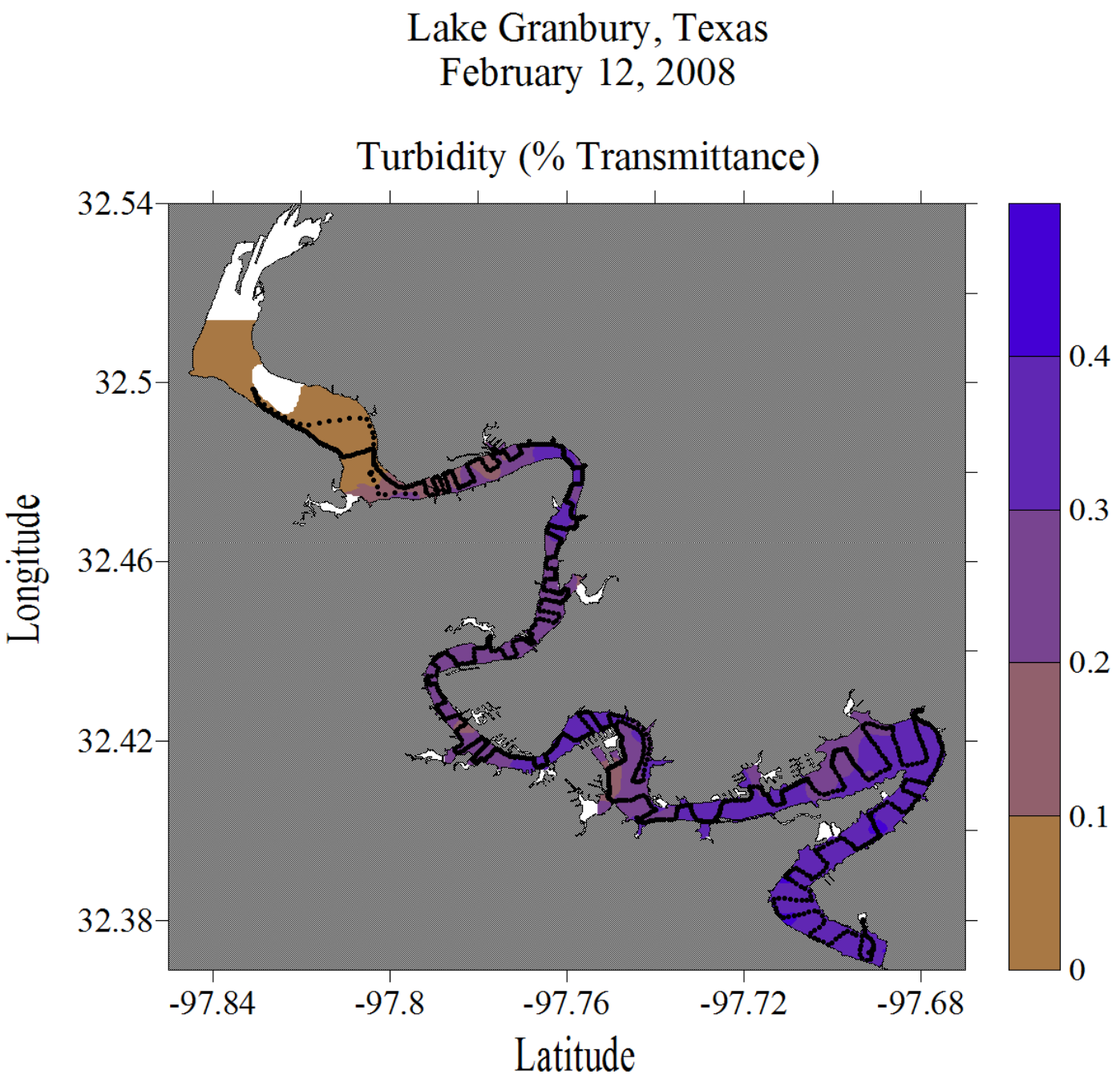

Figure E-77. Turbidity dataflow map for Lake Granbury

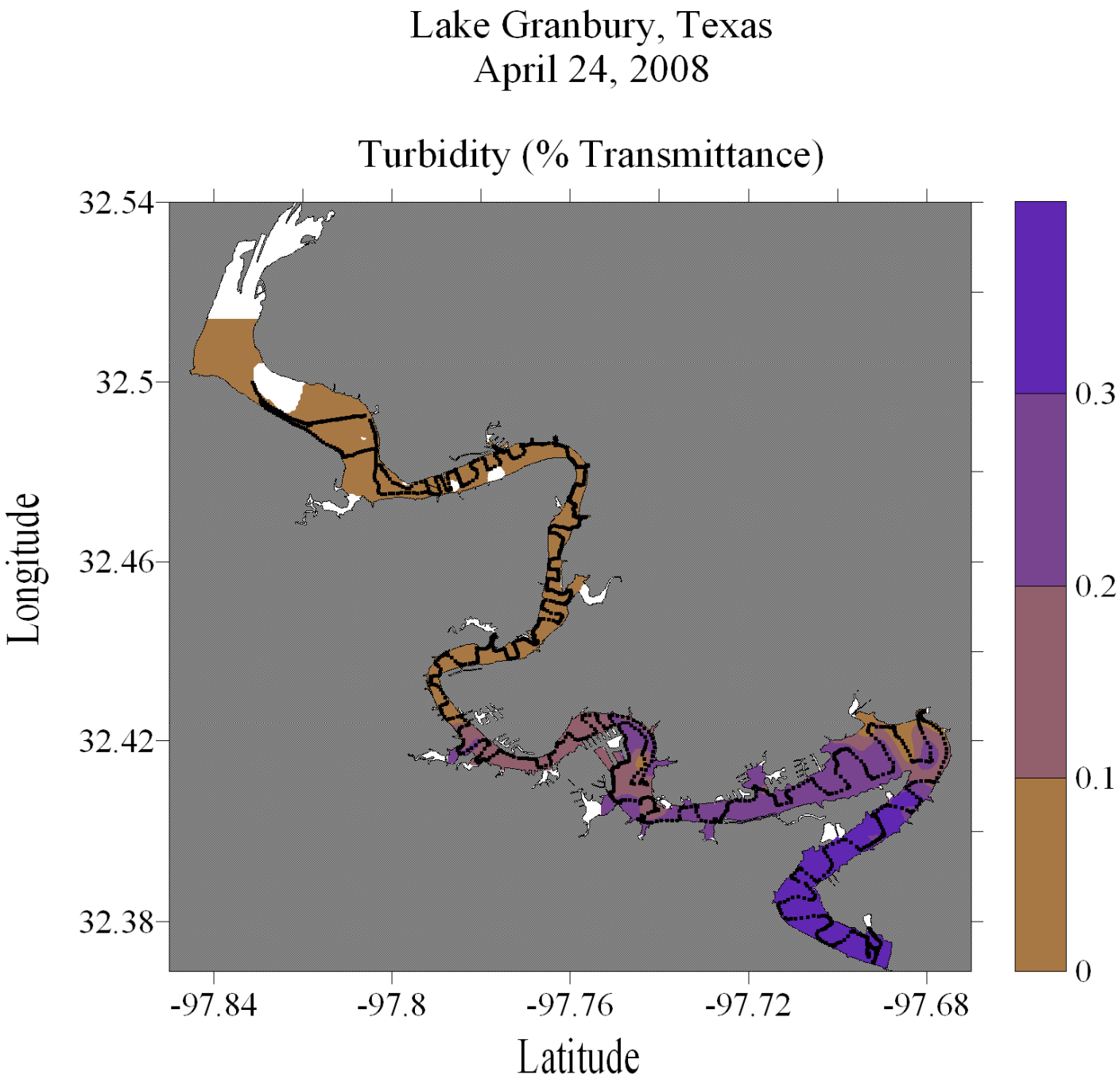

Figure E-78. Turbidity dataflow map for Lake Granbury

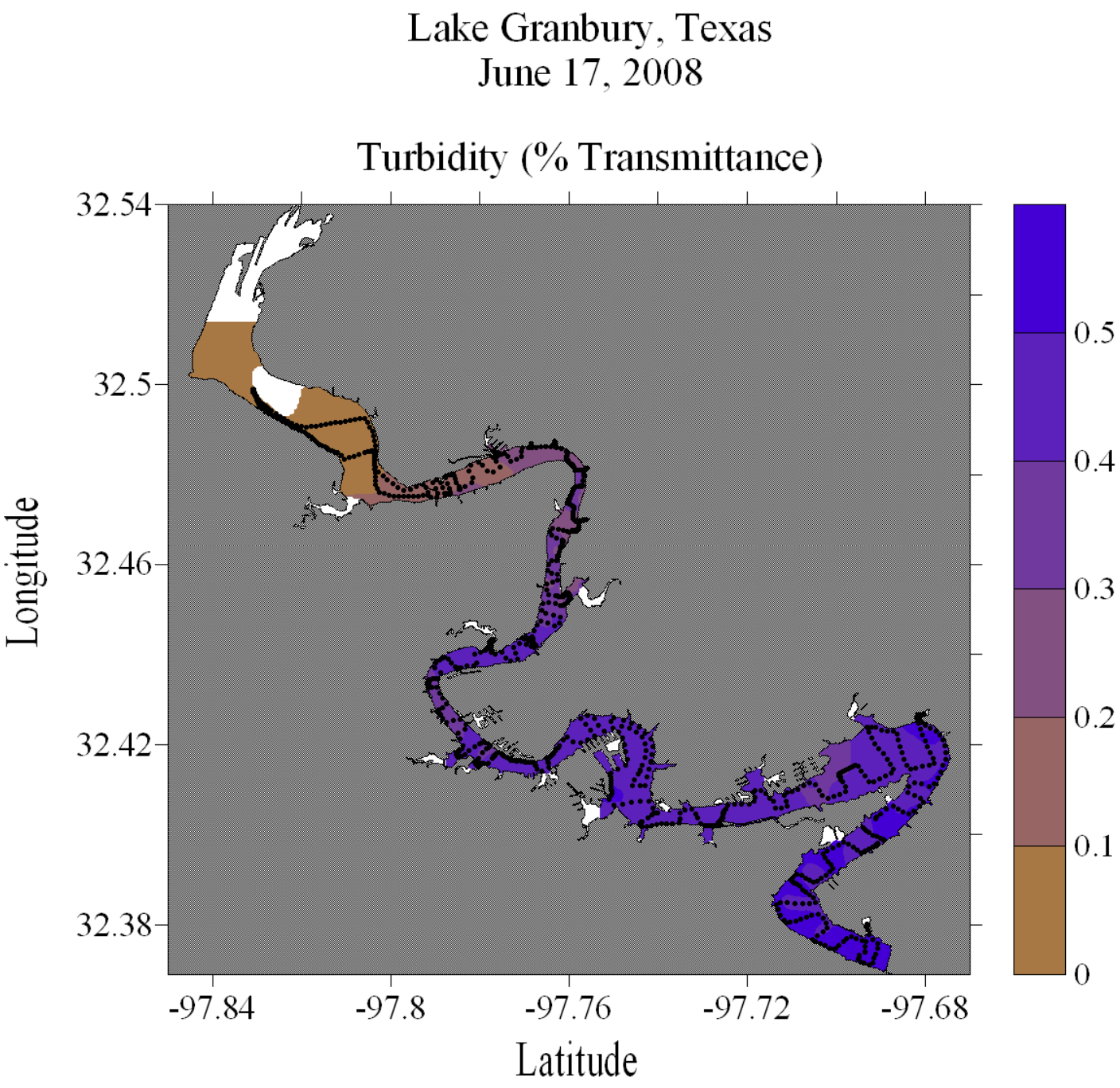

Figure E-79. Turbidity dataflow map for Lake Granbury

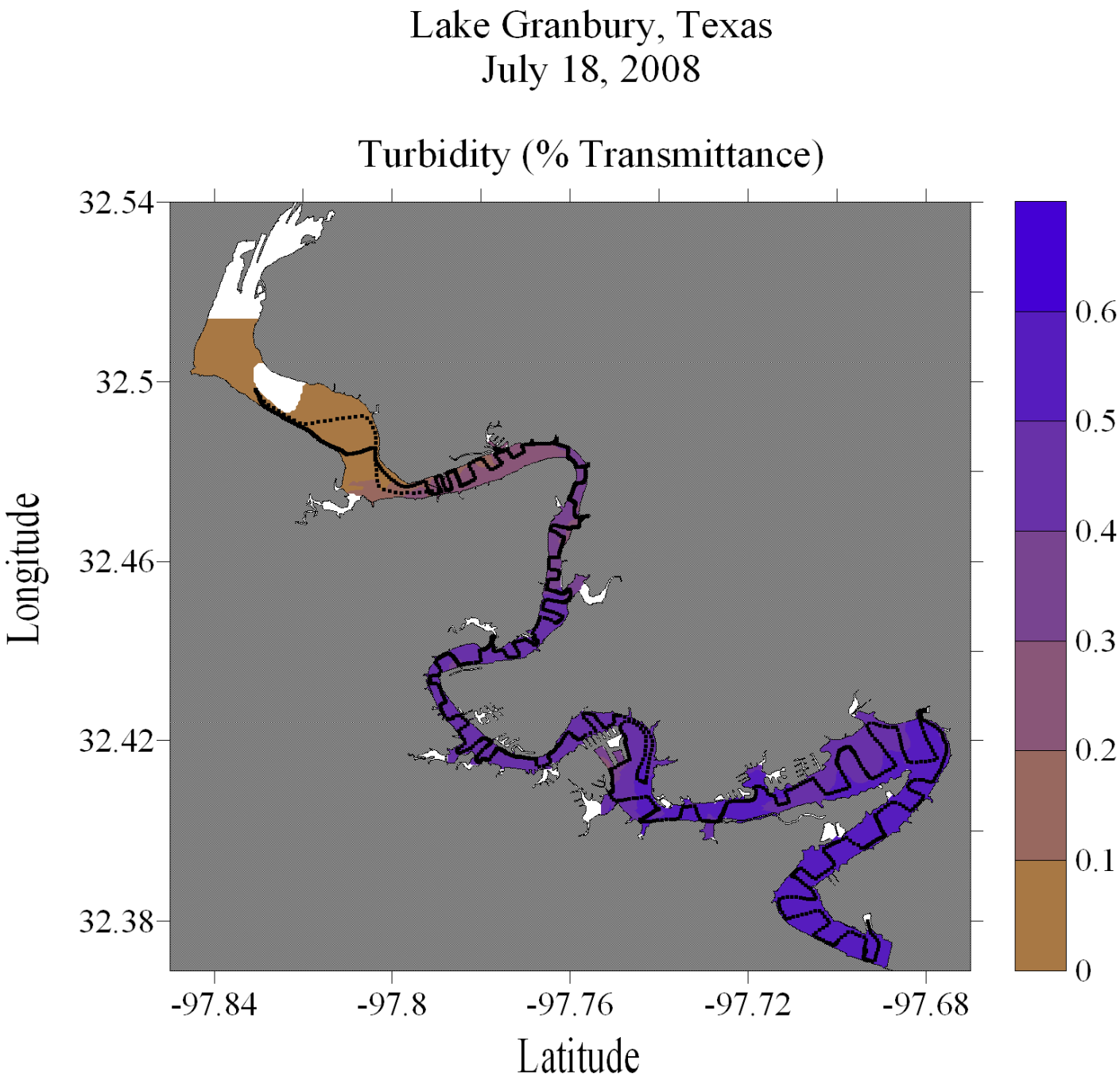

Figure E-80. Turbidity dataflow map for Lake Granbury

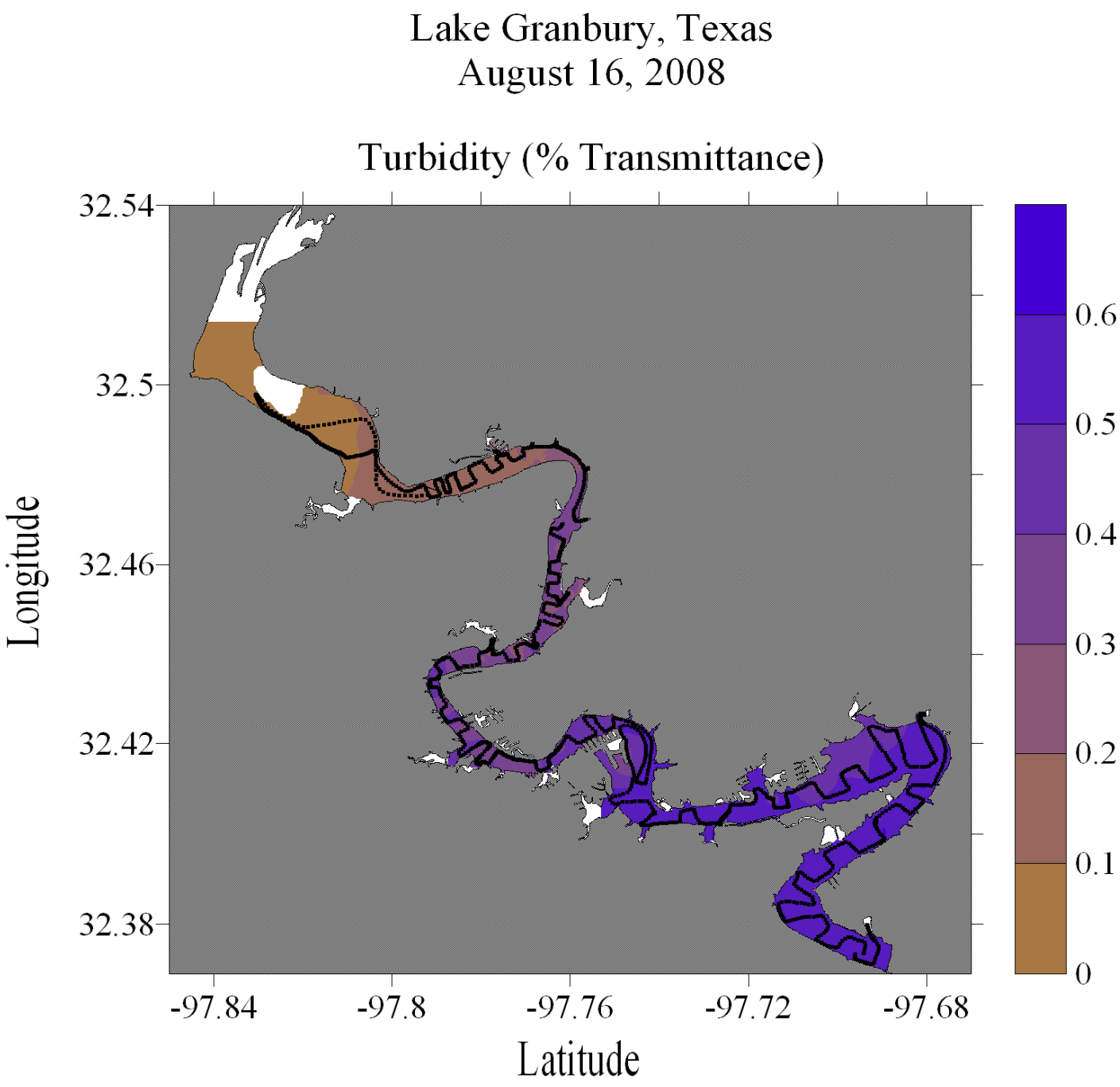

Figure E-81. Turbidity dataflow map for Lake Granbury

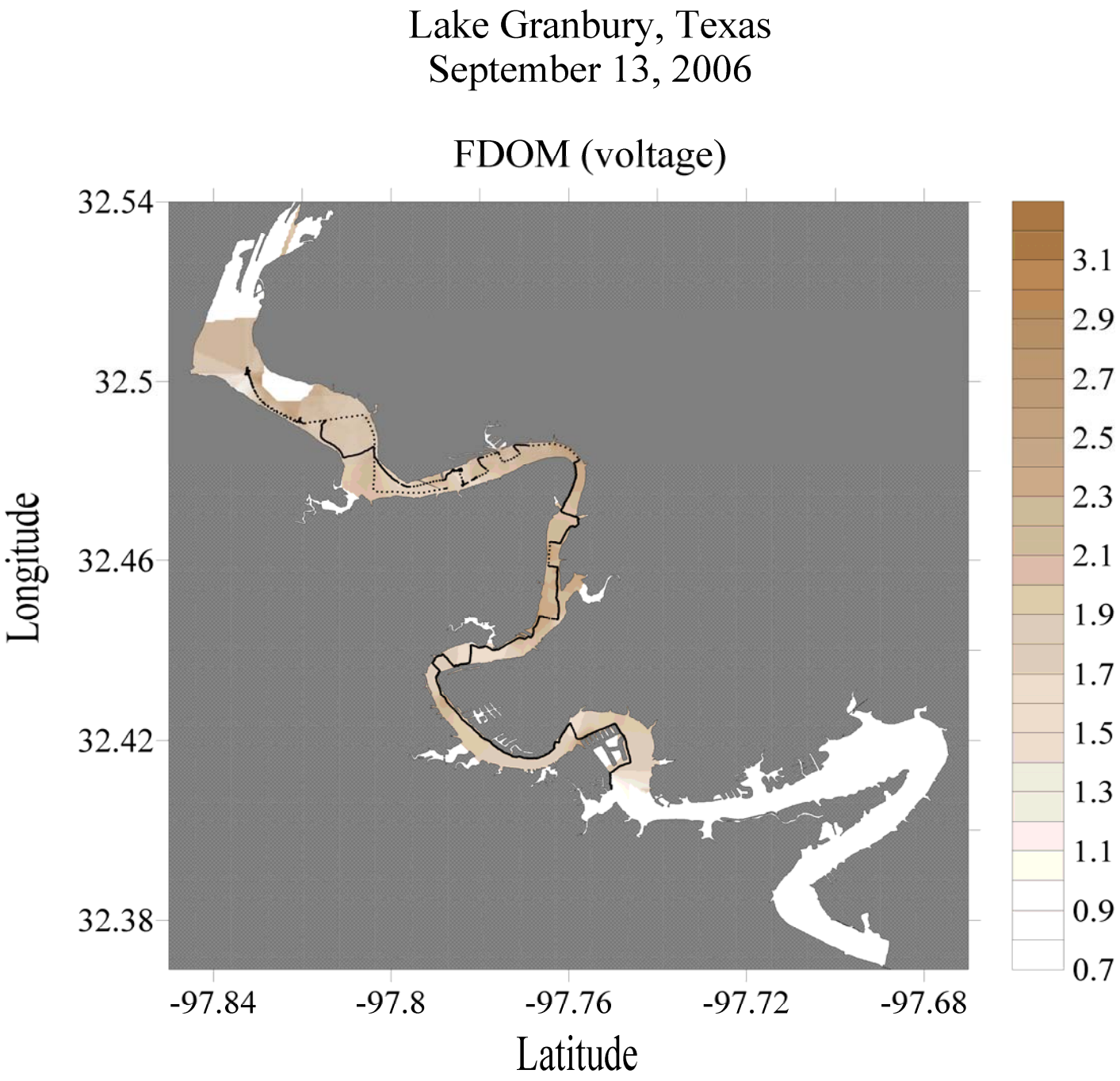

Figure E-82. Dissolved organic matter dataflow map for Lake Granbury

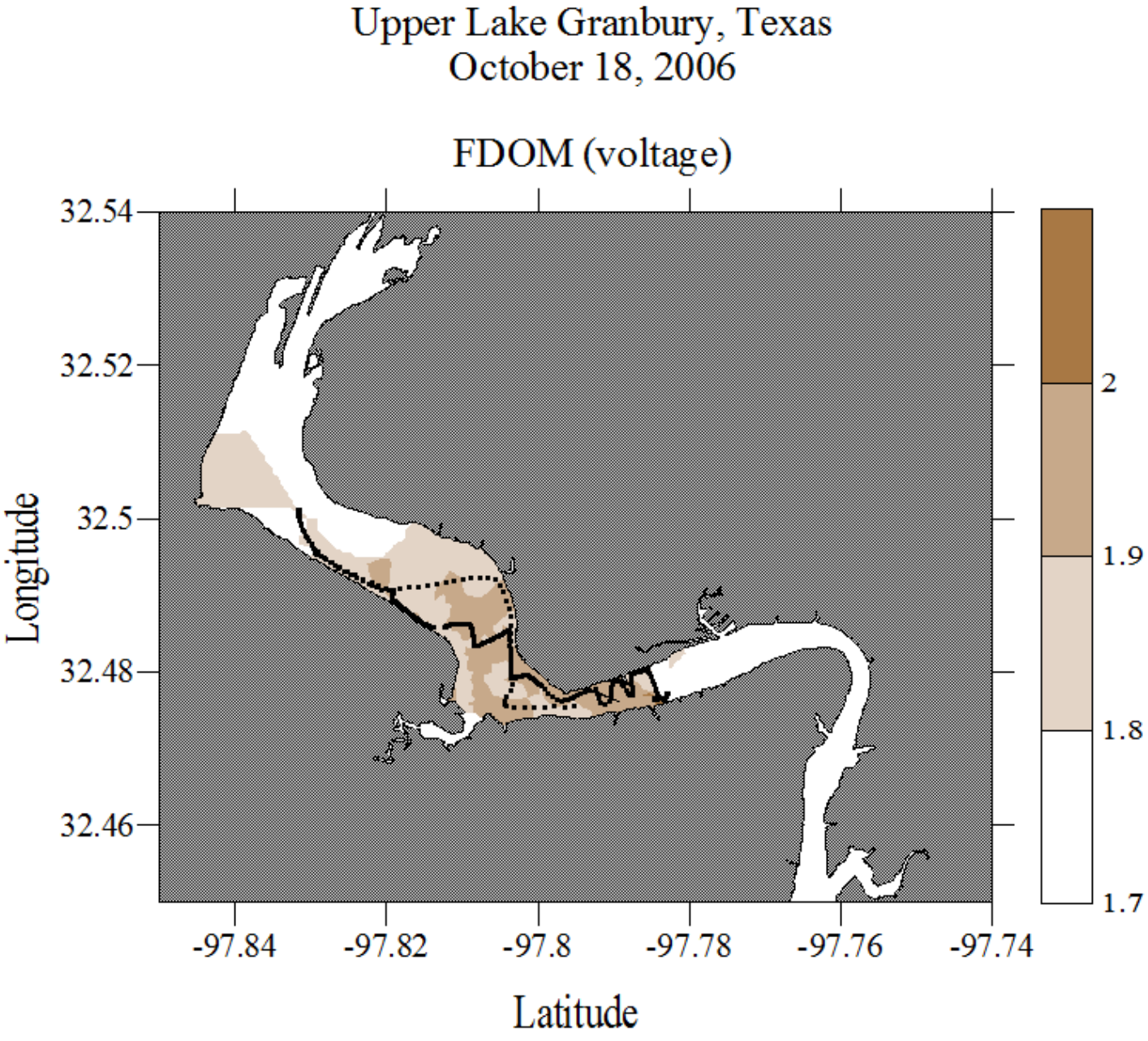

Figure E-83. Dissolved organic matter dataflow map for Lake Granbury

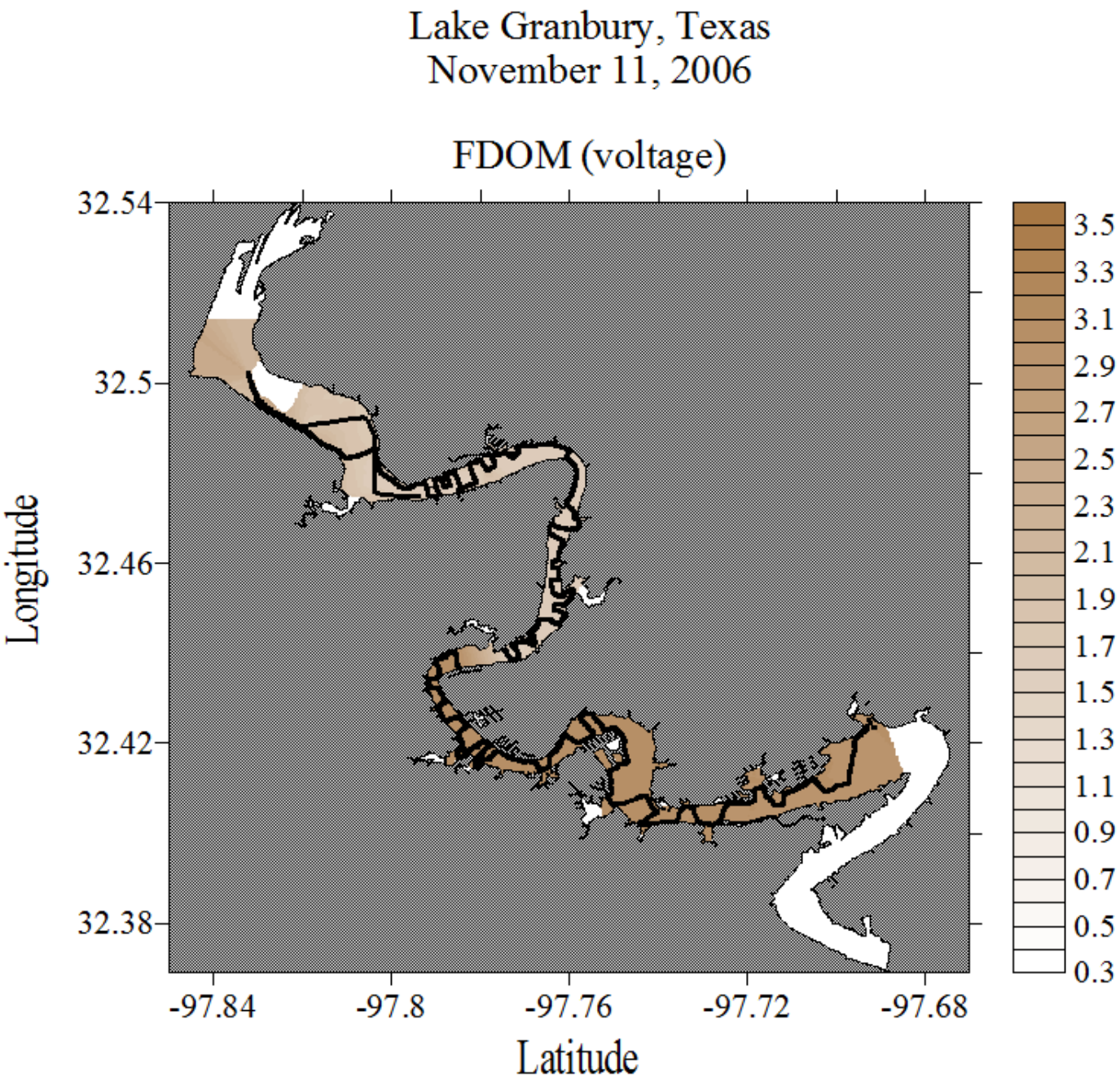

Figure E-84. Dissolved organic matter dataflow map for Lake Granbury

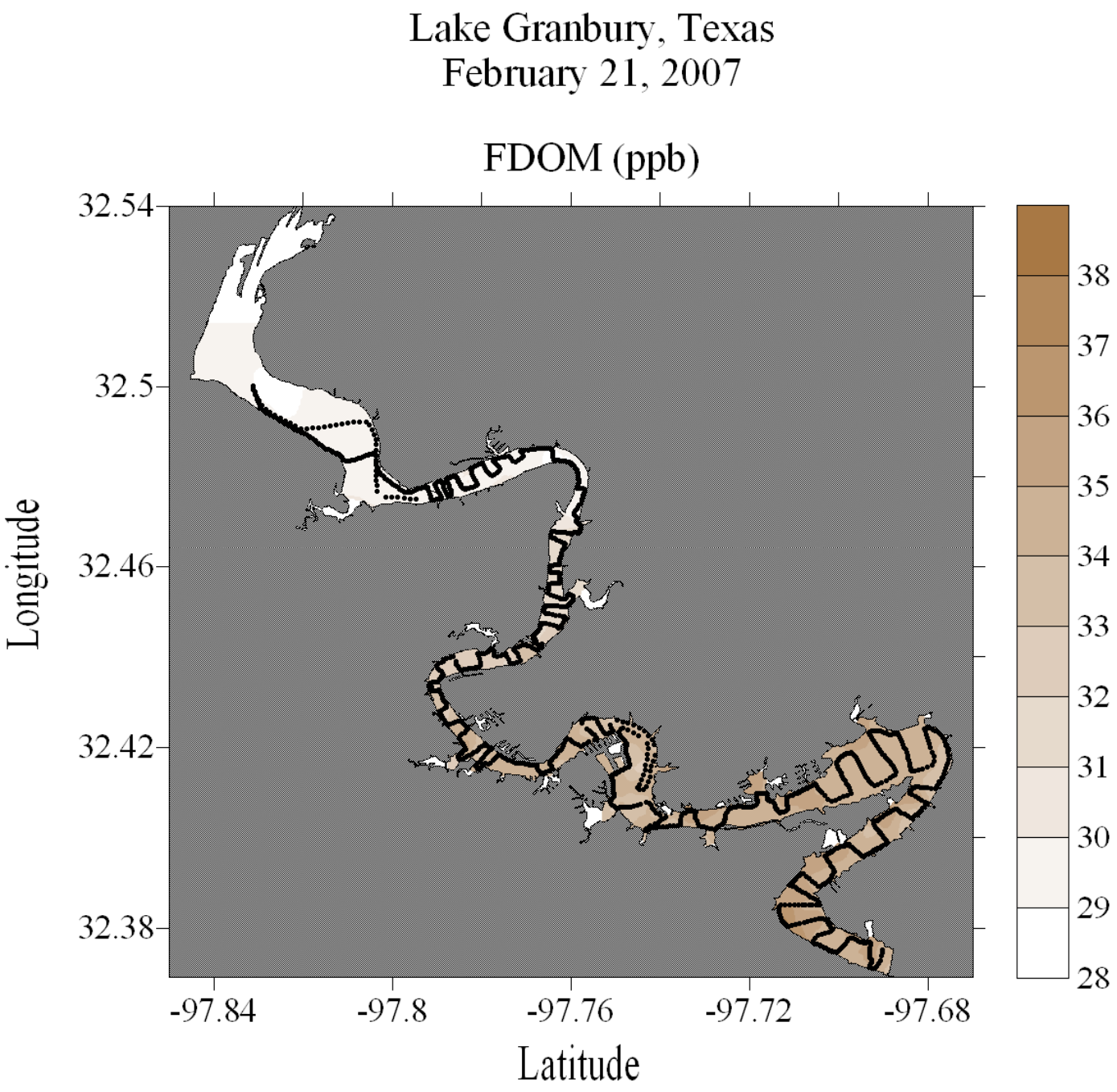

Figure E-85. Dissolved organic matter dataflow map for Lake Granbury

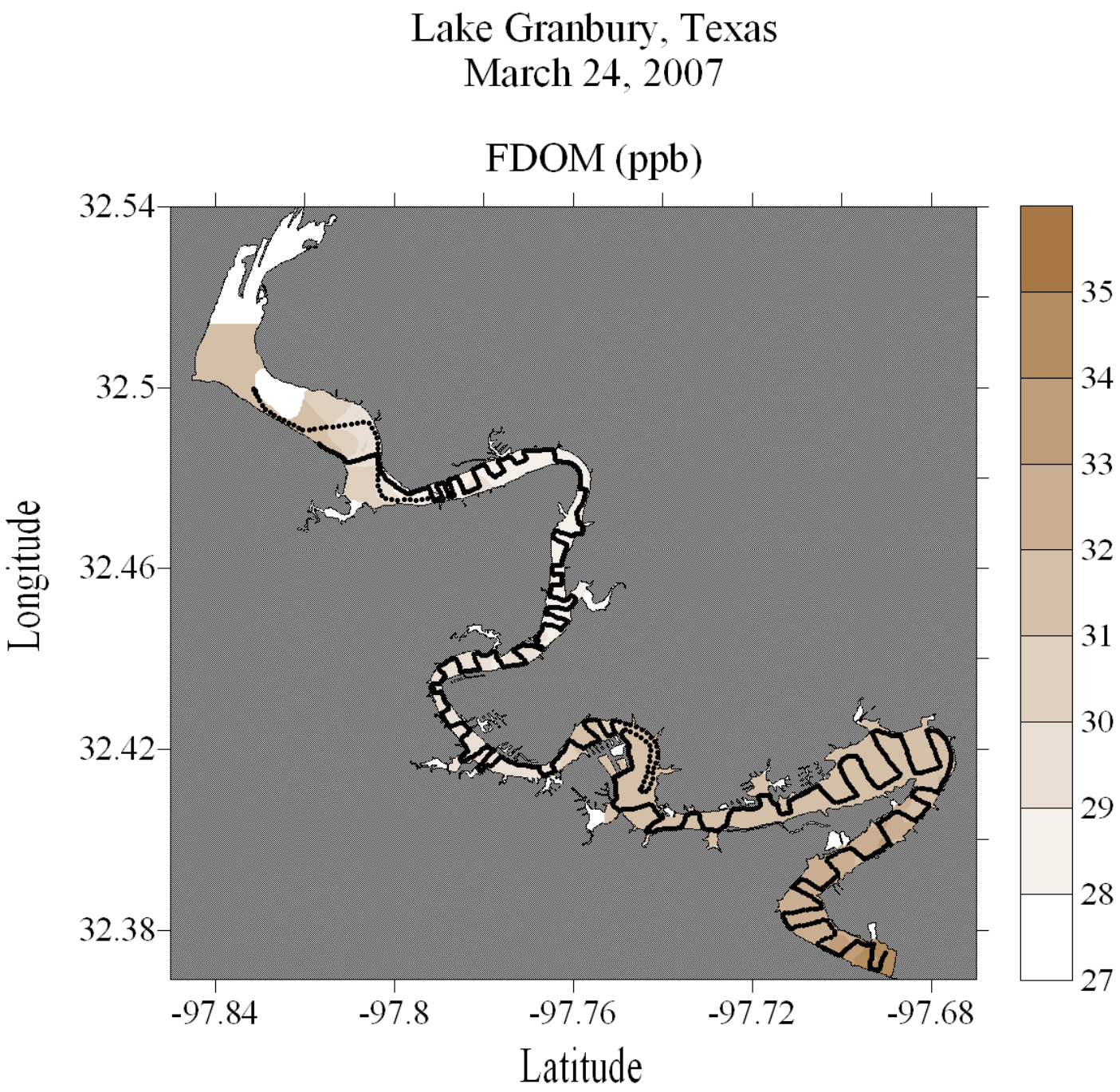

Figure E-86. Dissolved organic matter dataflow map for Lake Granbury

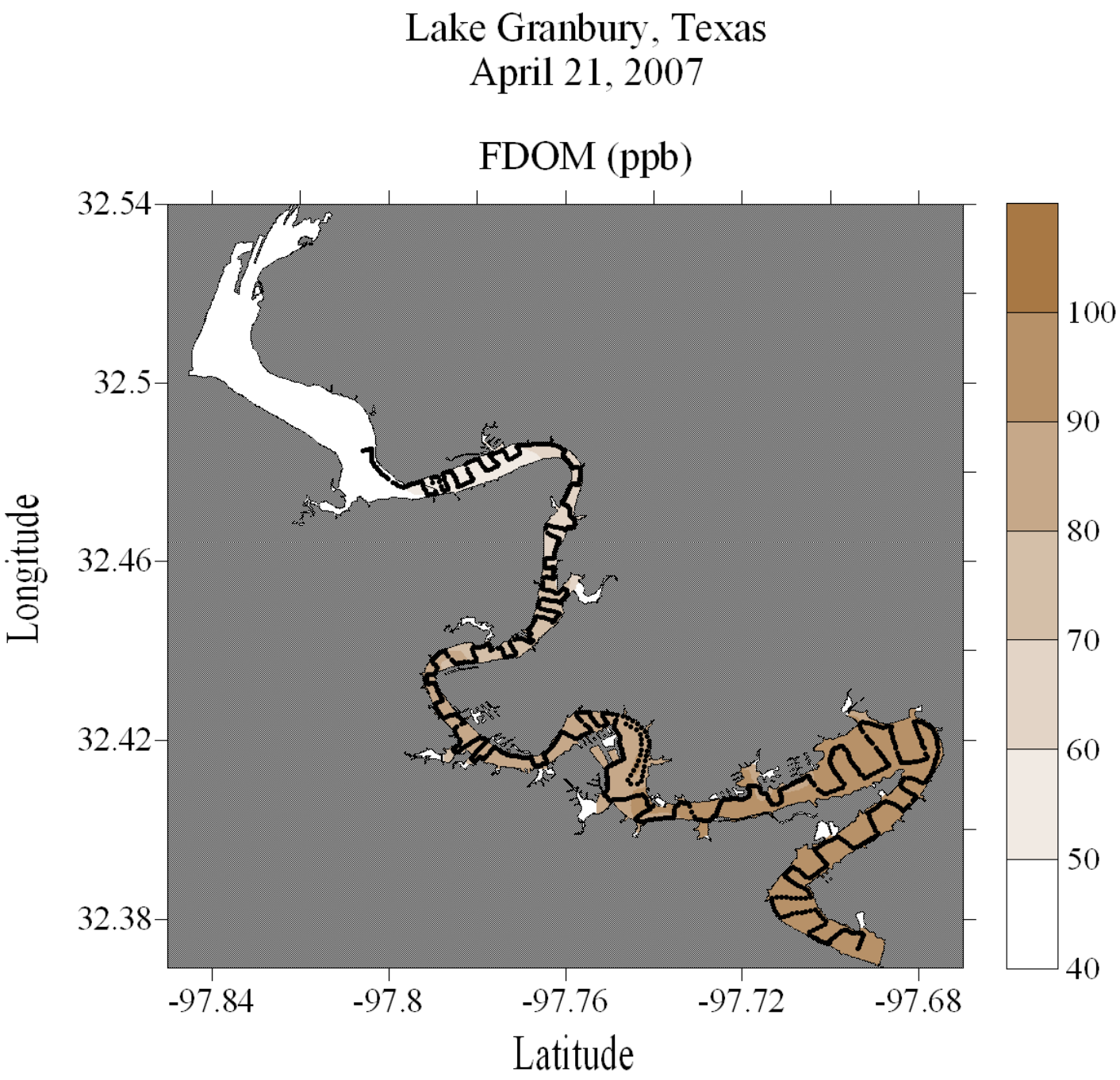

Figure E-87. Dissolved organic matter dataflow map for Lake Granbury

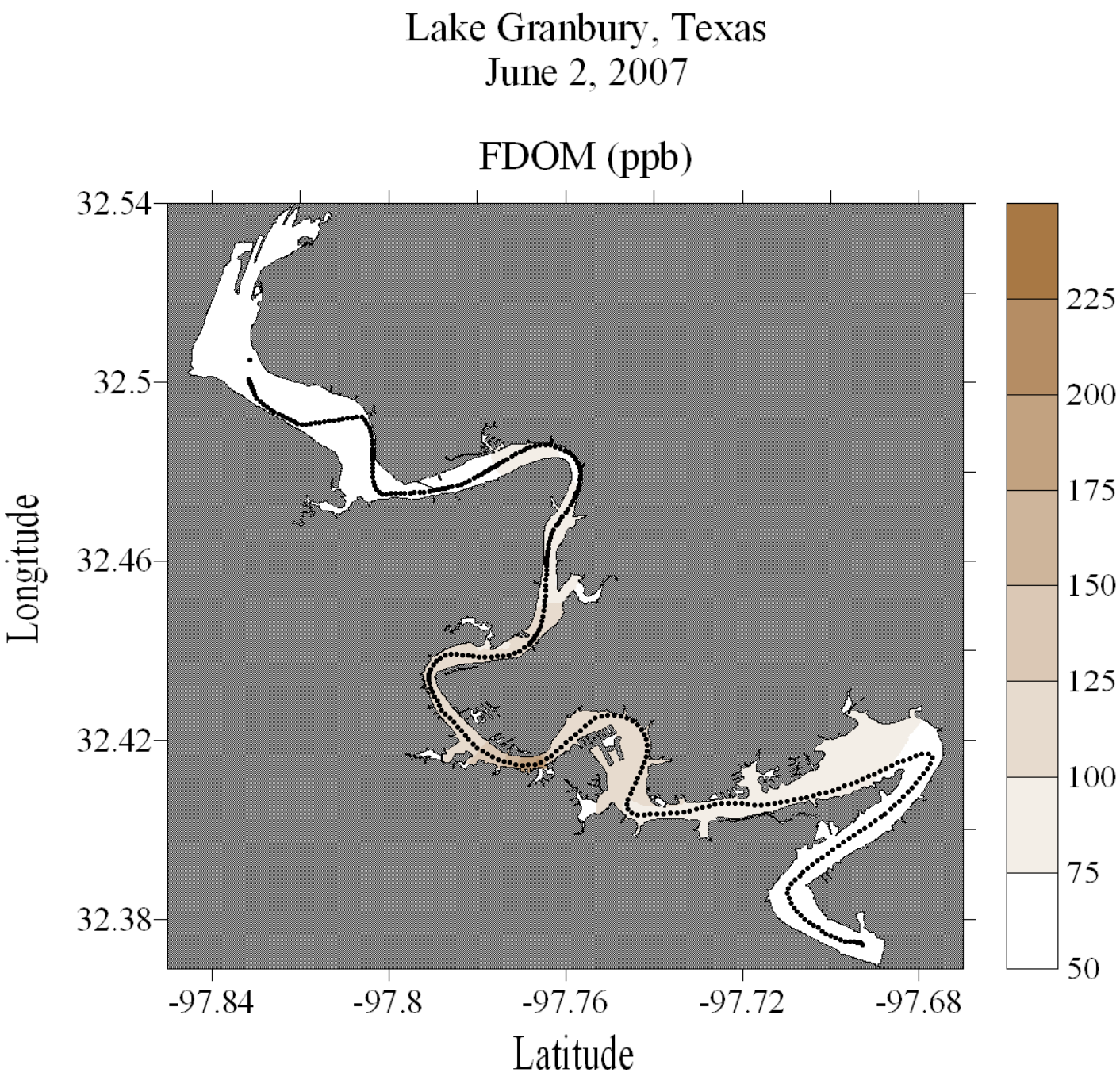

Figure E-88. Dissolved organic matter dataflow map for Lake Granbury

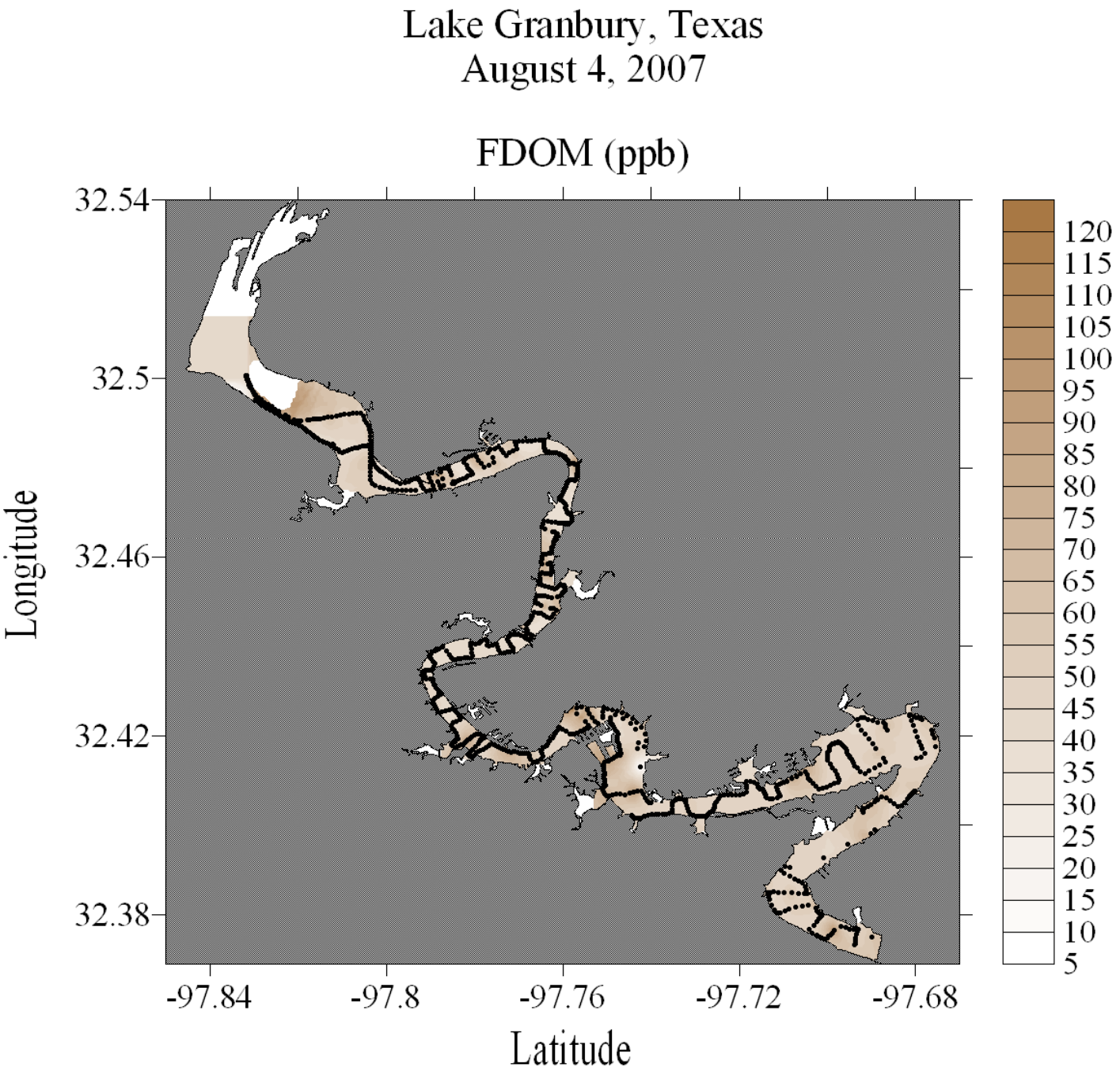

Figure E-89. Dissolved organic matter dataflow map for Lake Granbury

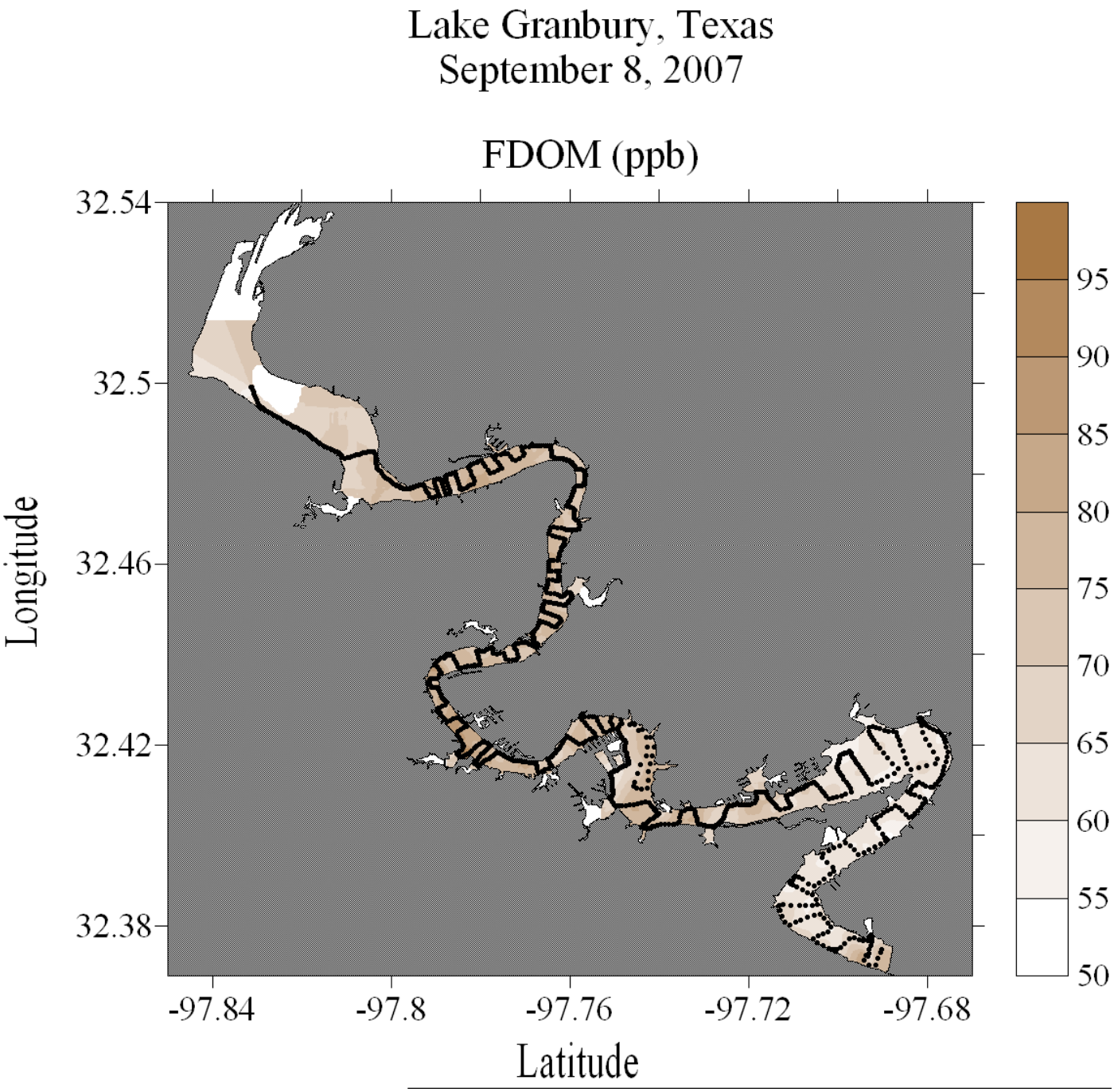

Figure E-90. Dissolved organic matter dataflow map for Lake Granbury

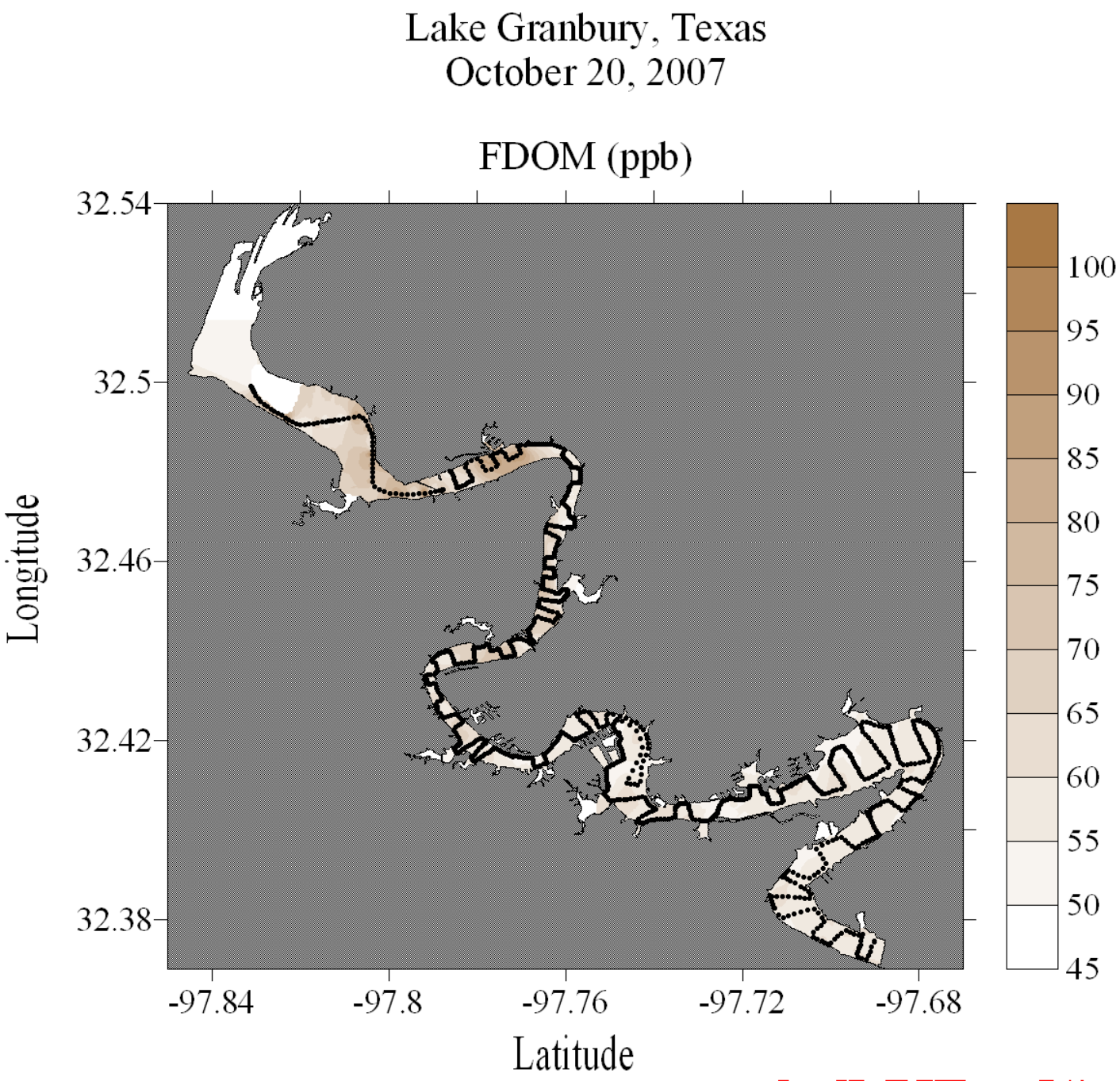

Figure E-91. Dissolved organic matter dataflow map for Lake Granbury

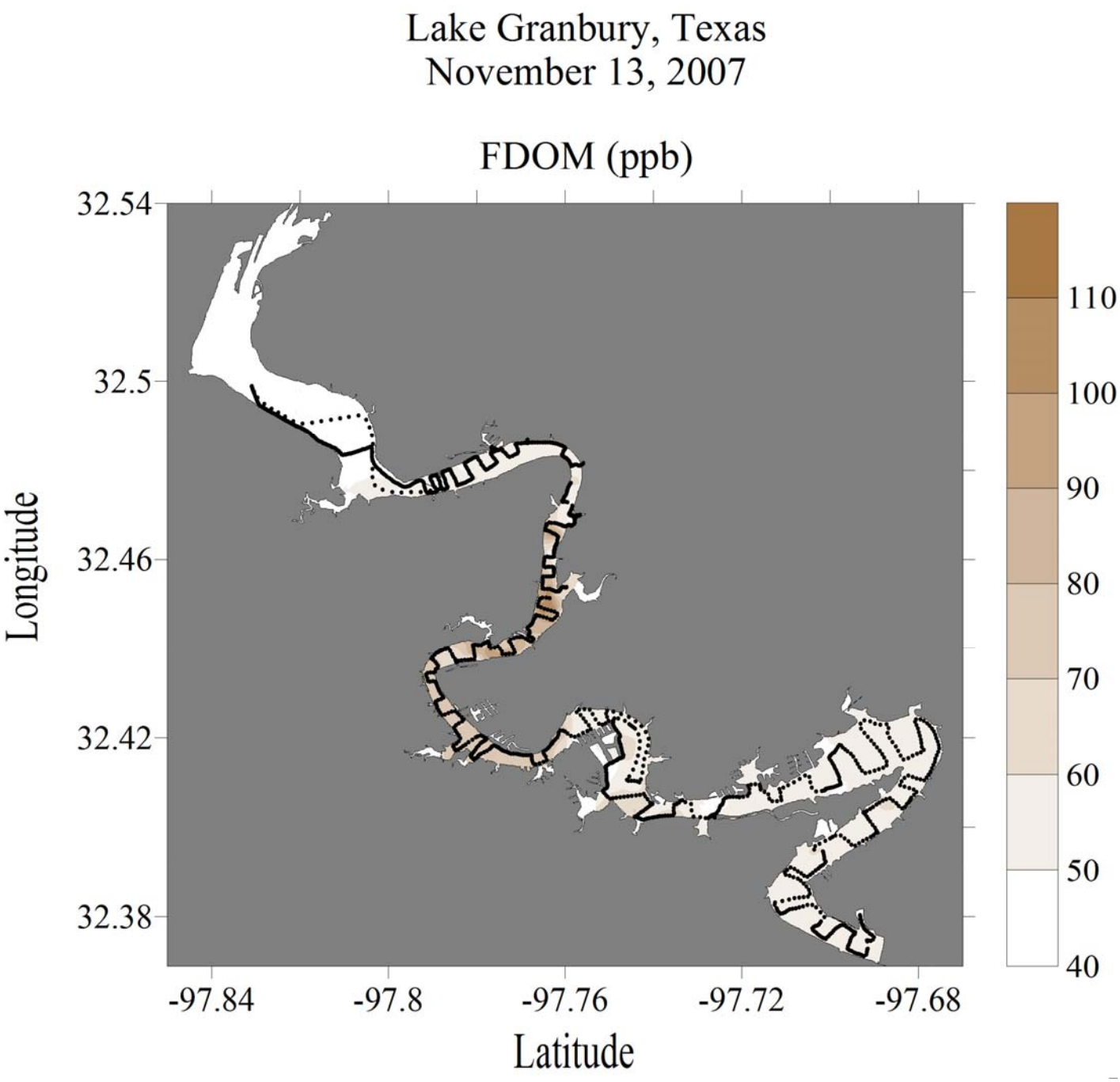

Figure E-92. Dissolved organic matter dataflow map for Lake Granbury

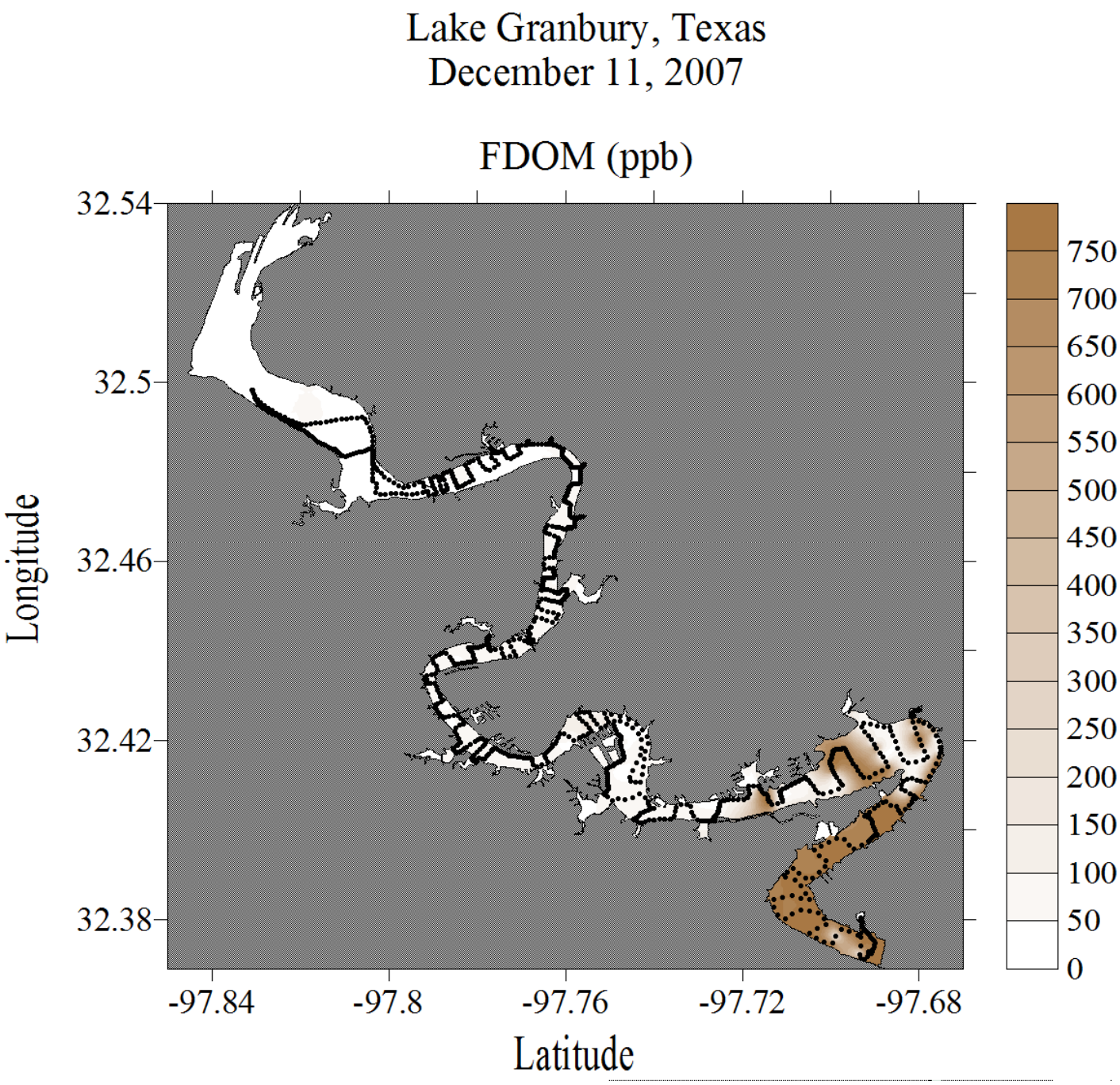

Figure E-93. Dissolved organic matter dataflow map for Lake Granbury

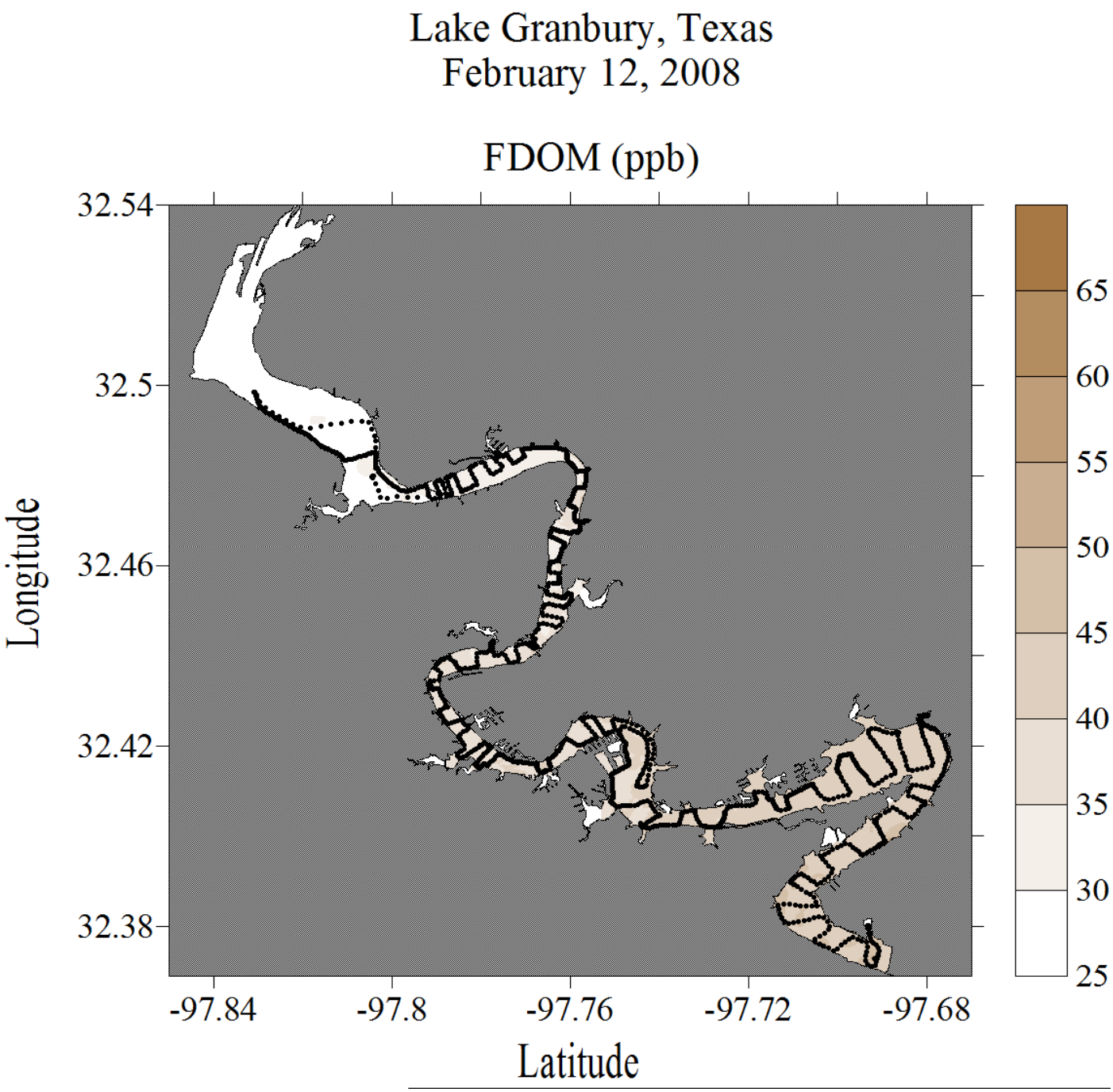

Figure E-94. Dissolved organic matter dataflow map for Lake Granbury

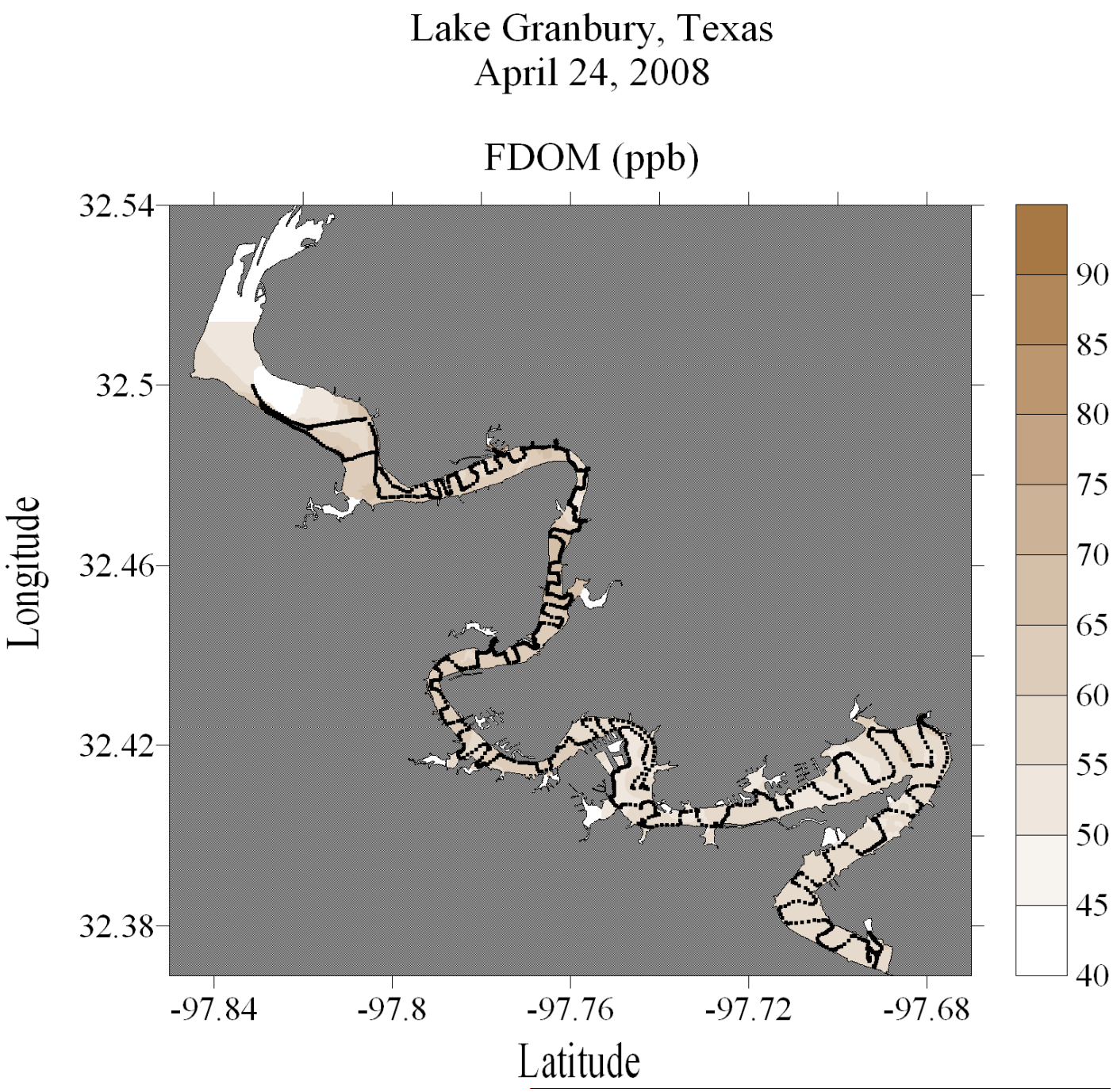

Figure E-95. Dissolved organic matter dataflow map for Lake Granbury

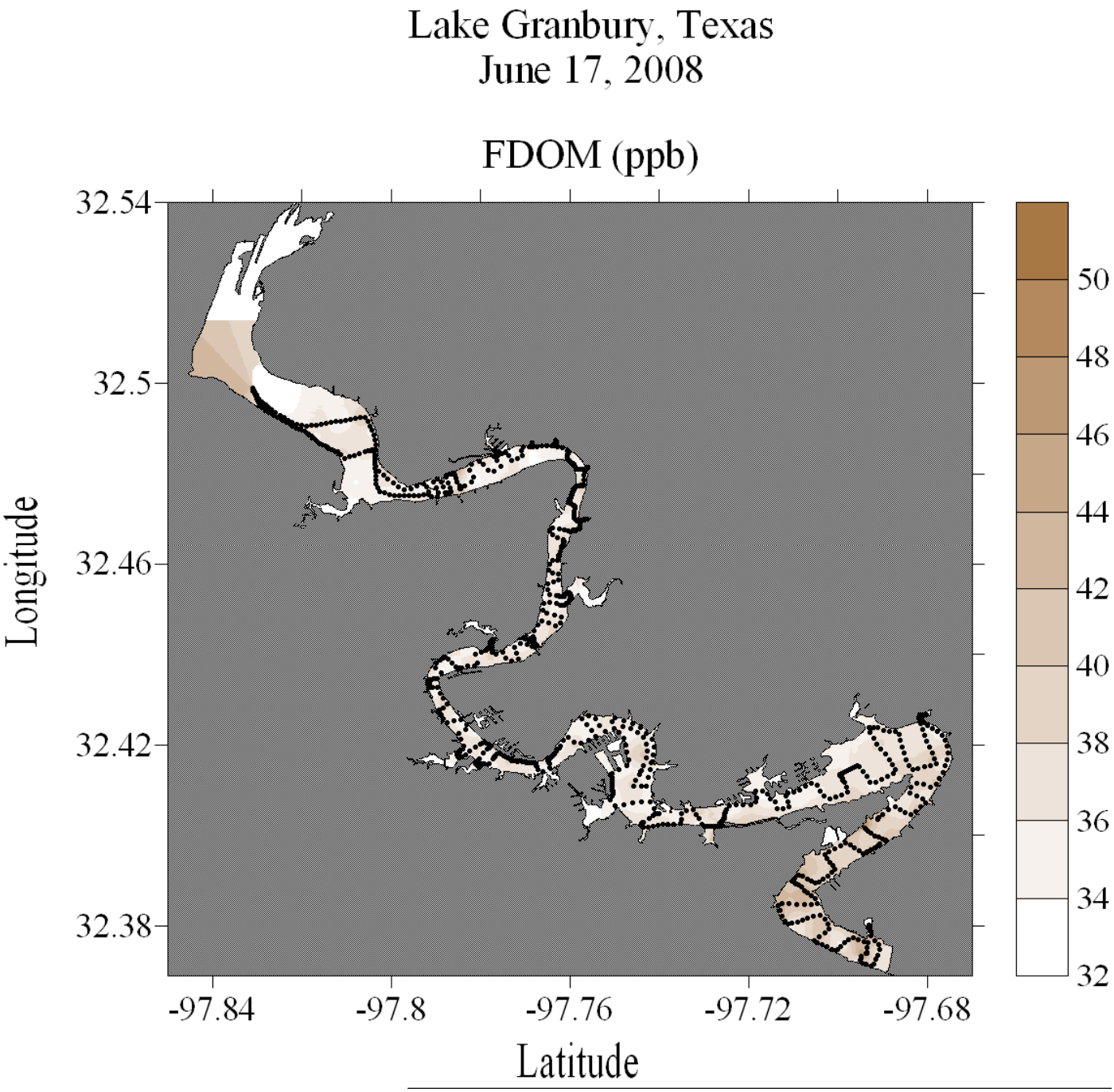

Figure E-96. Dissolved organic matter dataflow map for Lake Granbury

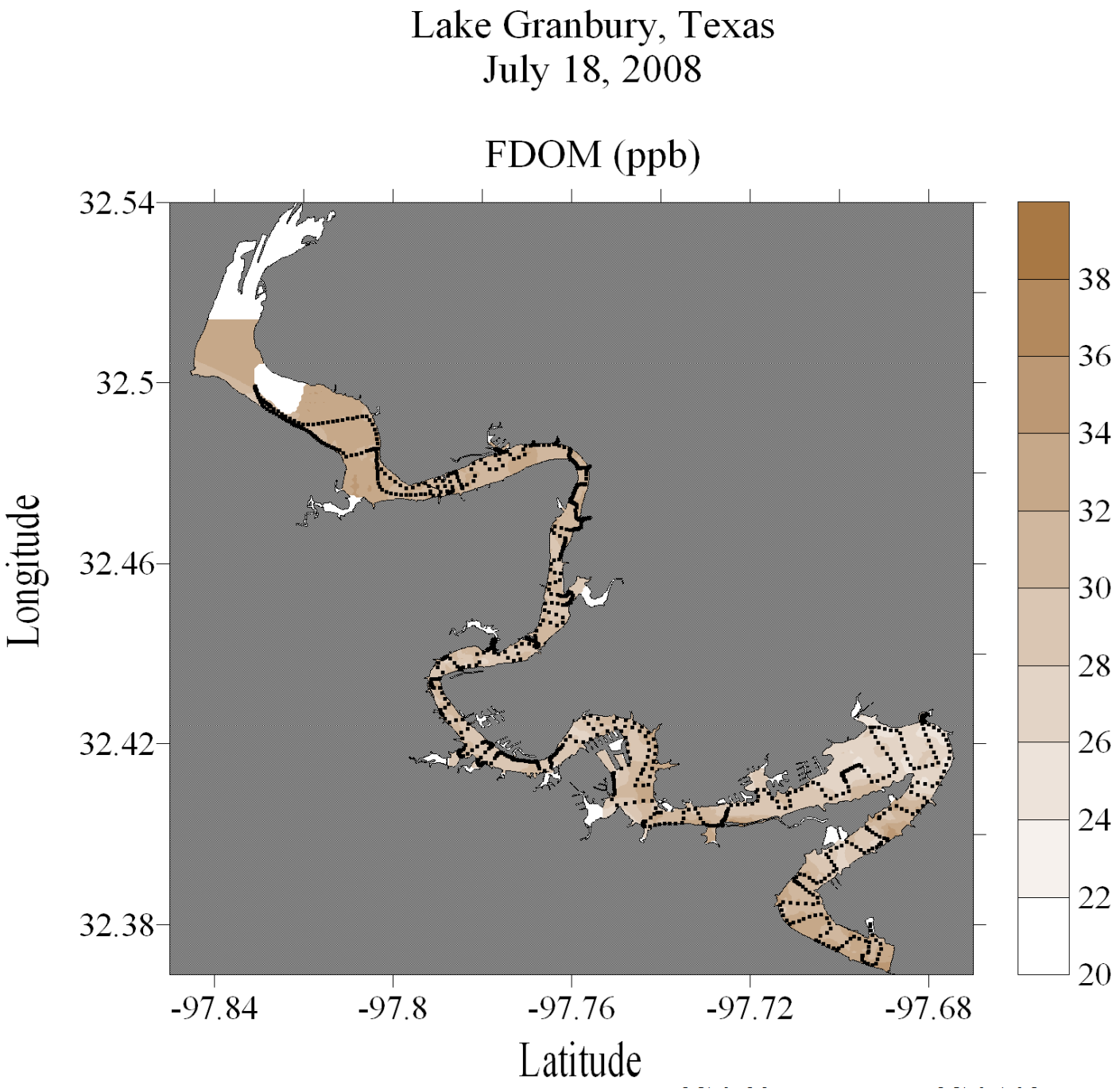

Figure E-97. Dissolved organic matter dataflow map for Lake Granbury

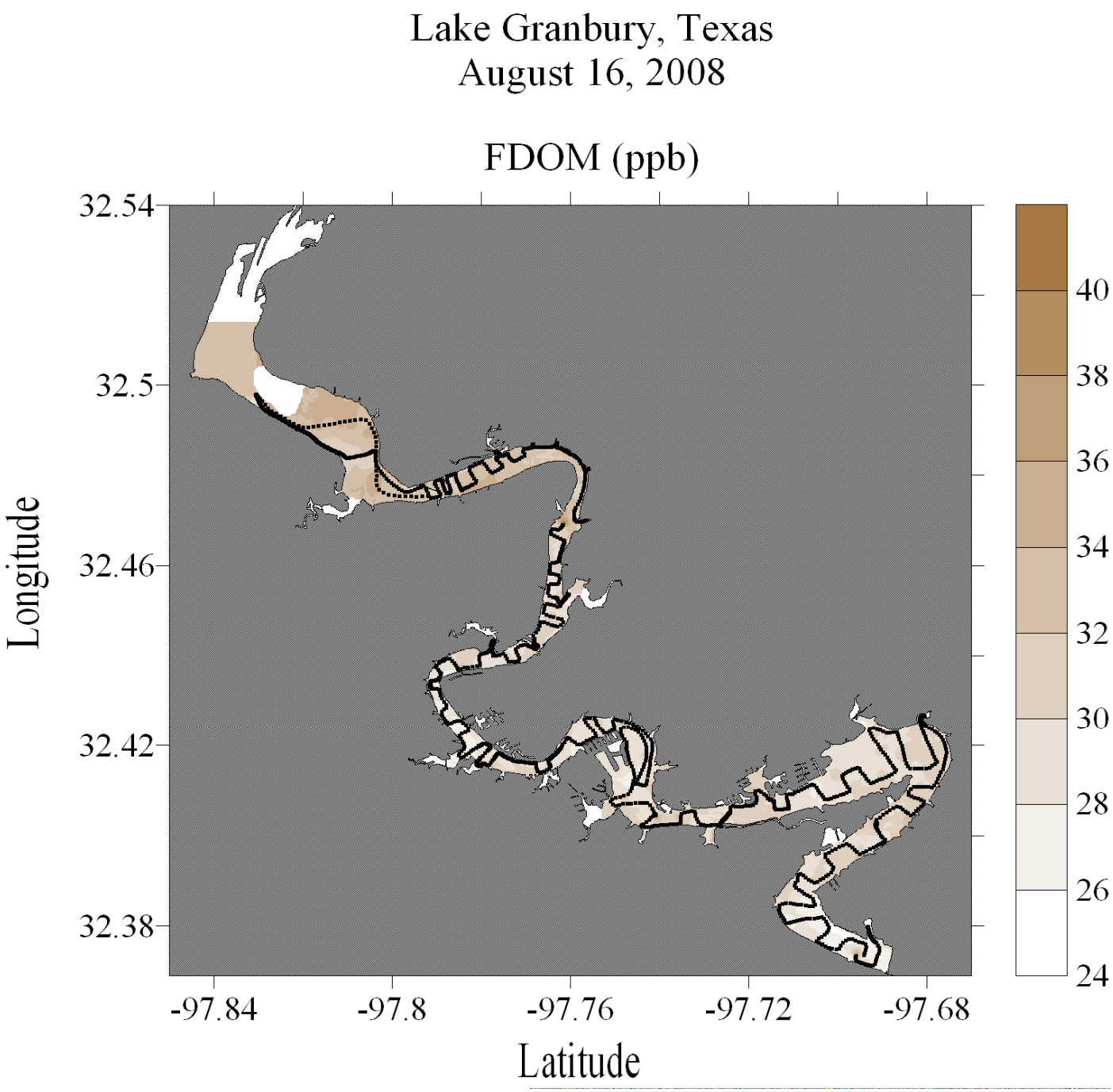

Figure E-98. Dissolved organic matter dataflow map for Lake Granbury

Appendix F

Lake Waco

Fixed station data from the both heads of the reservoir, and the location of the dam (stations 1 (head), 2, 3, 4 (dam), 5, 6, 7 (head).

The data collection involved monthly trips over a period from November 2007 to August 2008.

Figures F-1 through F-3 - Chlorophyll a, P. parvum, toxicity
Figures F-4 through F-8 – pH, temperature, salinity, Secchi depth, turbidity
Figures F-9 through F-13 – Cladoceran, copepod adult and nauplii, total rotifers, protozoan
Figures F-14 through F-15 – Phospahate, dissolved inorganic nitrogen
Figure F-16 – Dissolved organic carbon

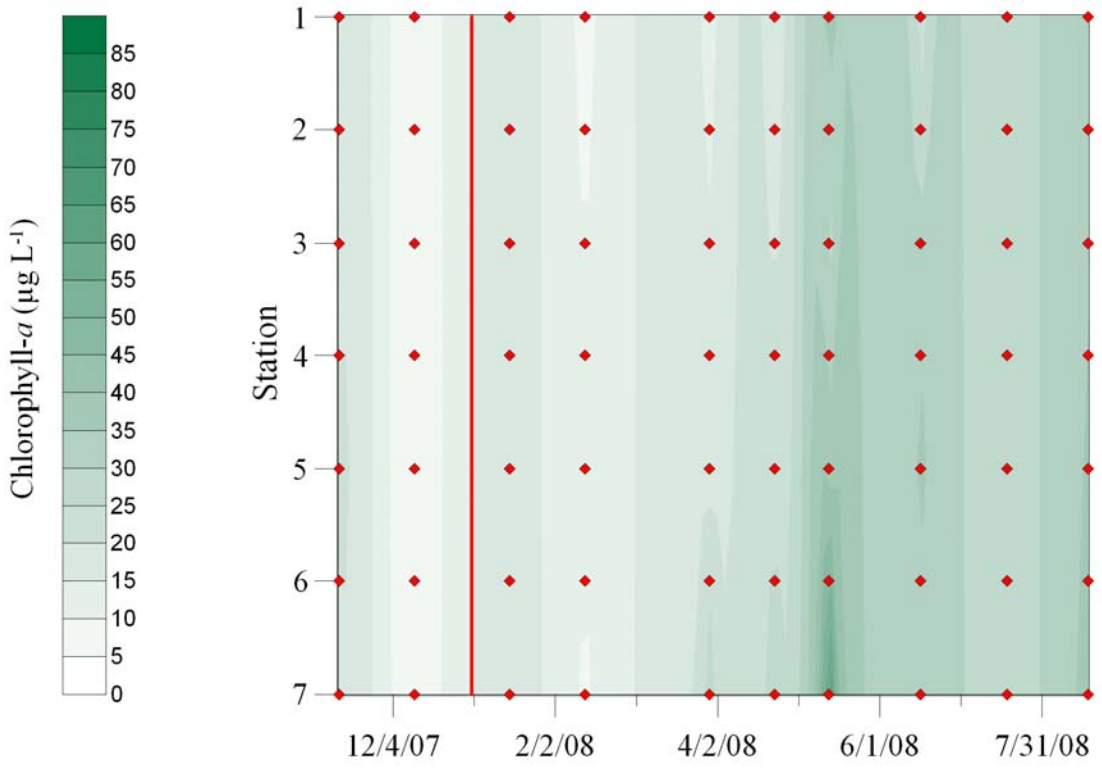

Figure F1. Phytoplankton biomass approximated using chlorophyll *a* for a period spanning November, 2007 through August, 2008.

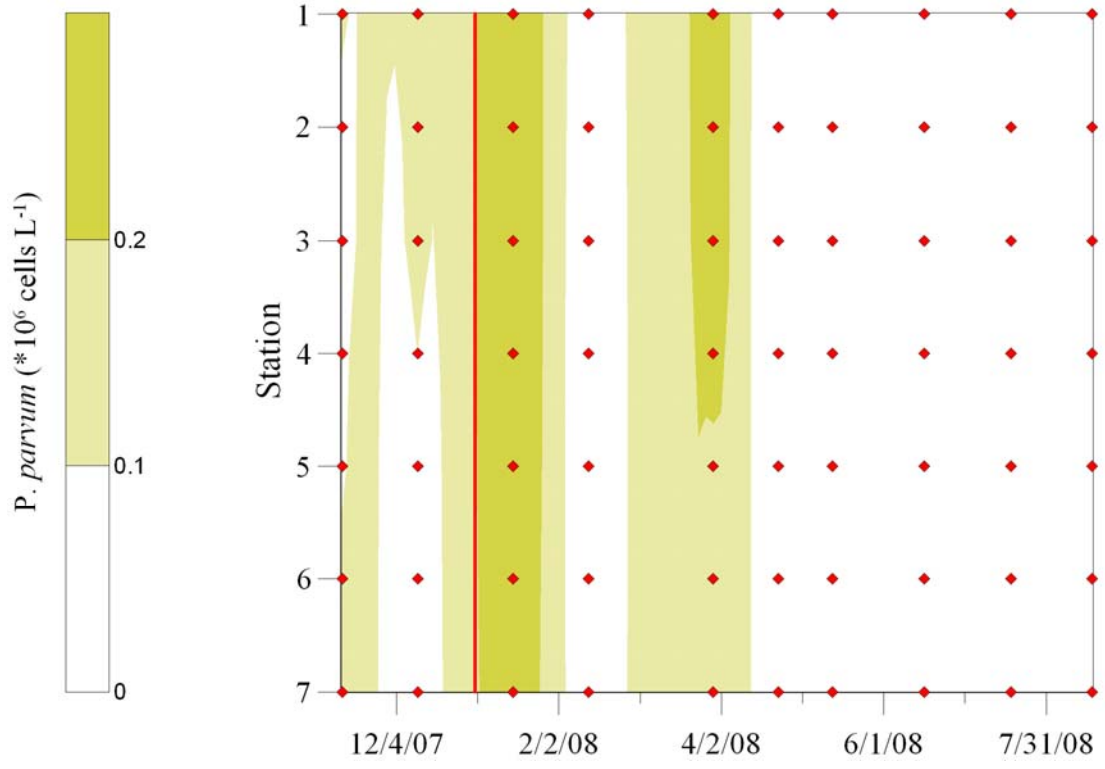

Figure F2. *Prymnesium parvum* population density for a period spanning November, 2007 through August, 2008.

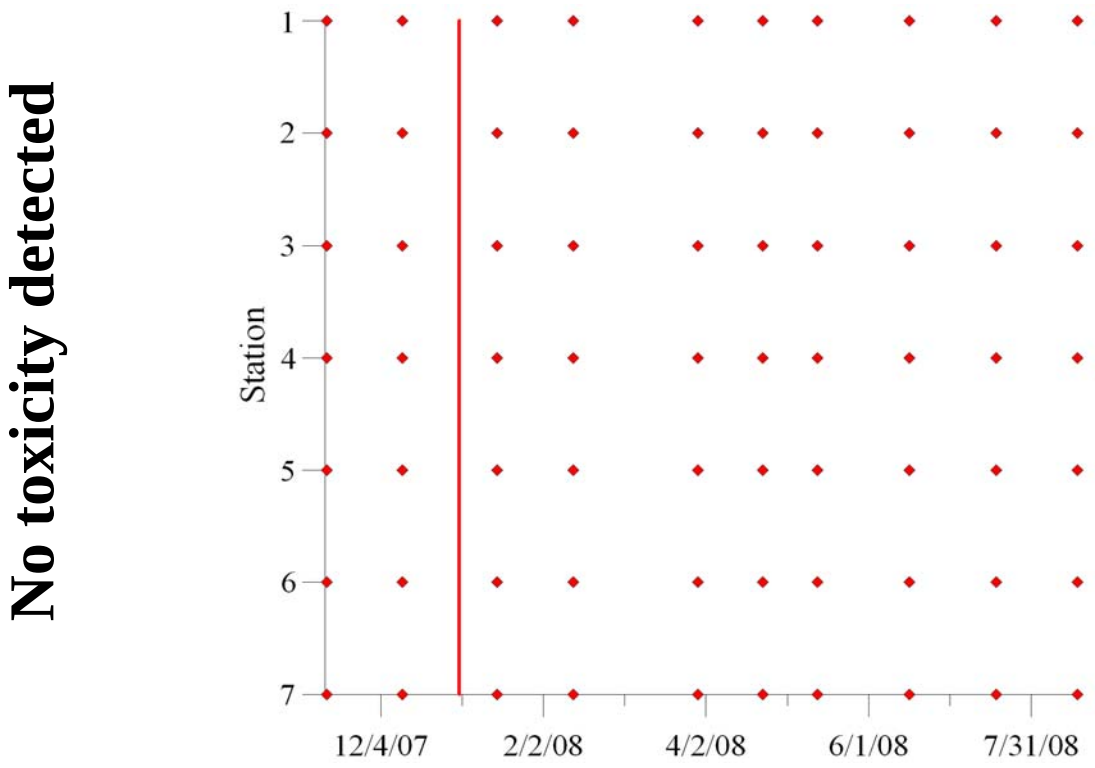

Figure F3. Ambient toxicity estimated using fish bioassays for a period spanning November, 2007 through August, 2008.

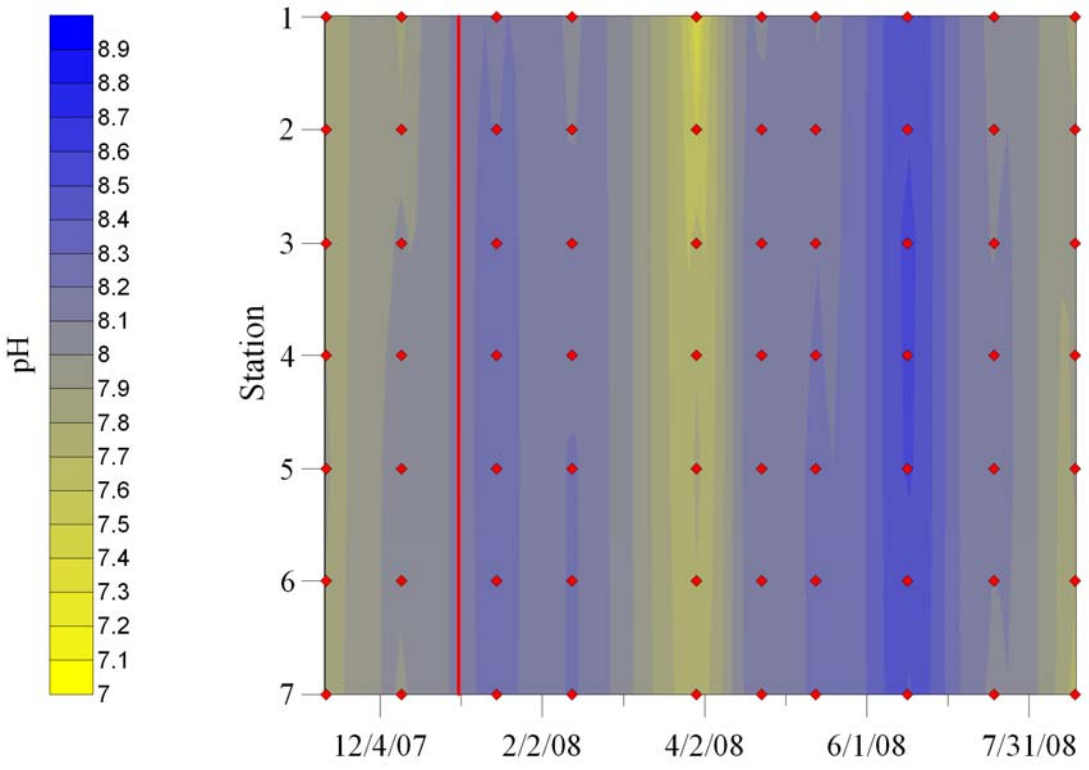

Figure F4. Surface water pH for a period spanning November, 2007 through August, 2008.

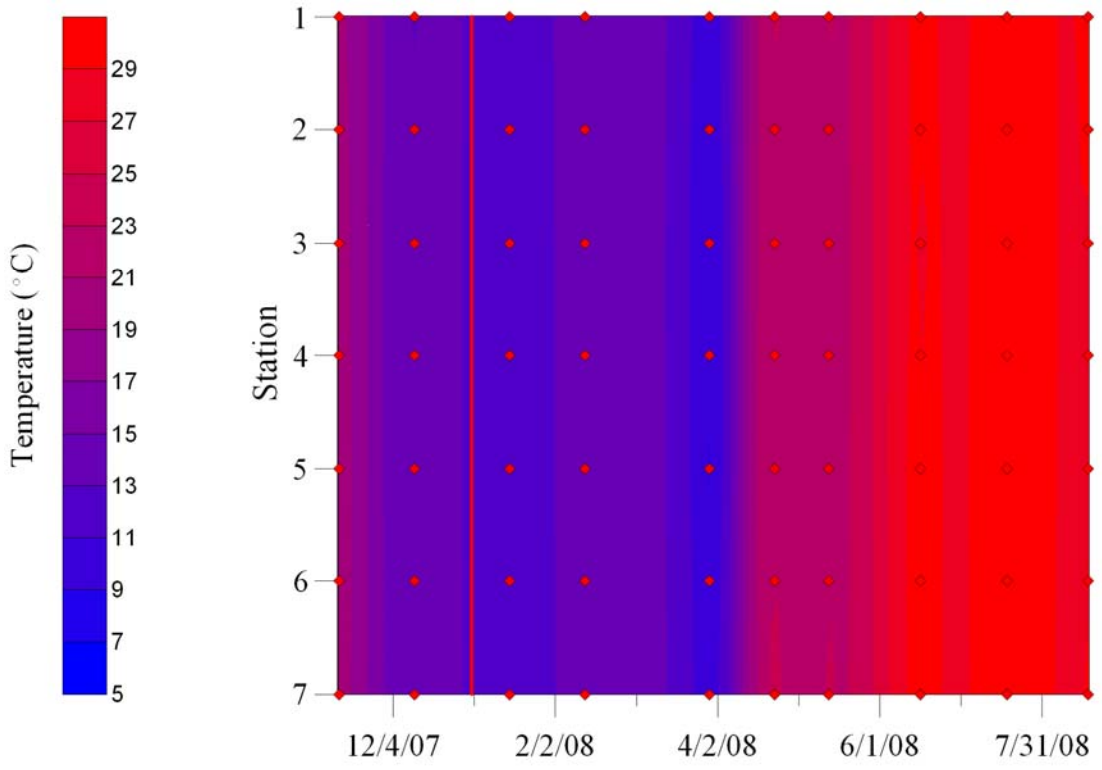

Figure F5. Surface water temperature for a period spanning November, 2007 through August, 2008.

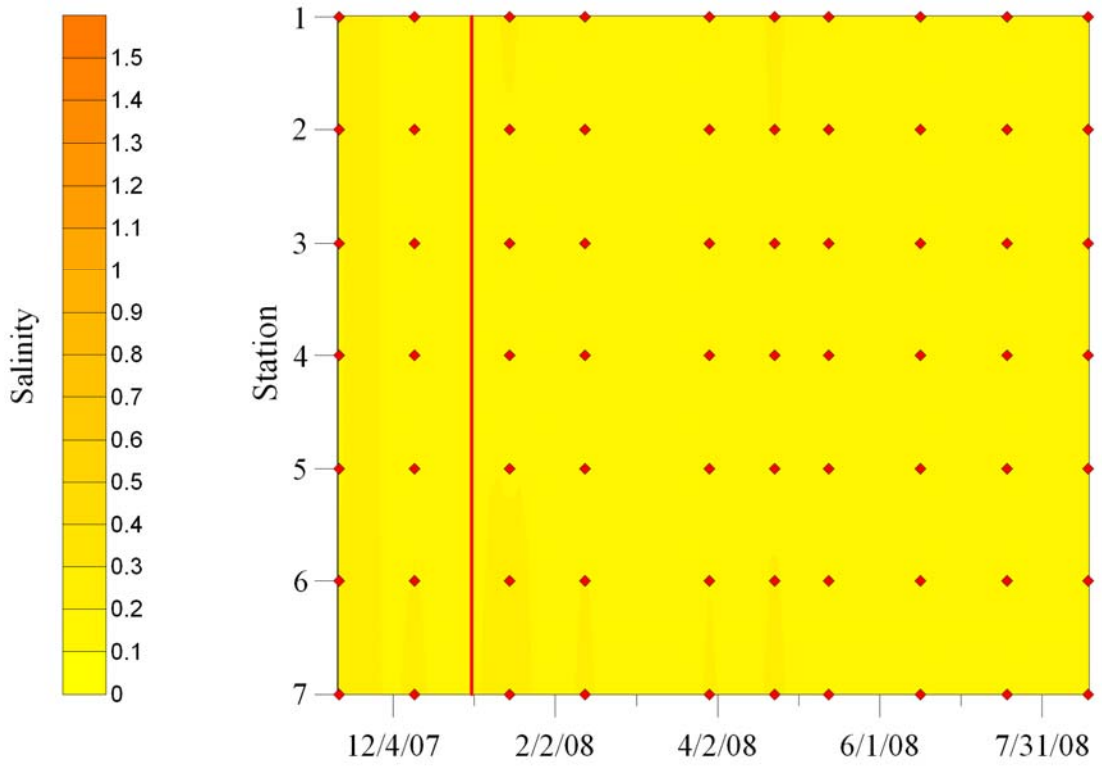

Figure F6. Surface water salinity for a period spanning November, 2007 through August, 2008.

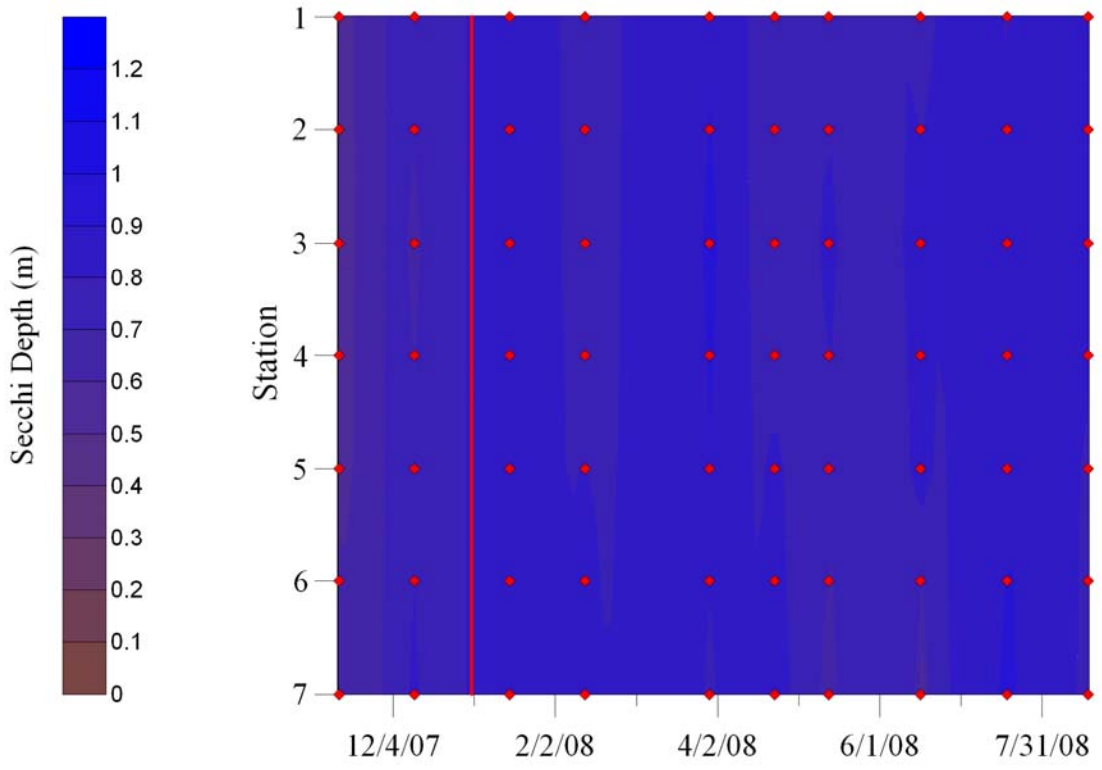

Figure F7. Secchi depth for a period spanning November, 2007 through August, 2008.

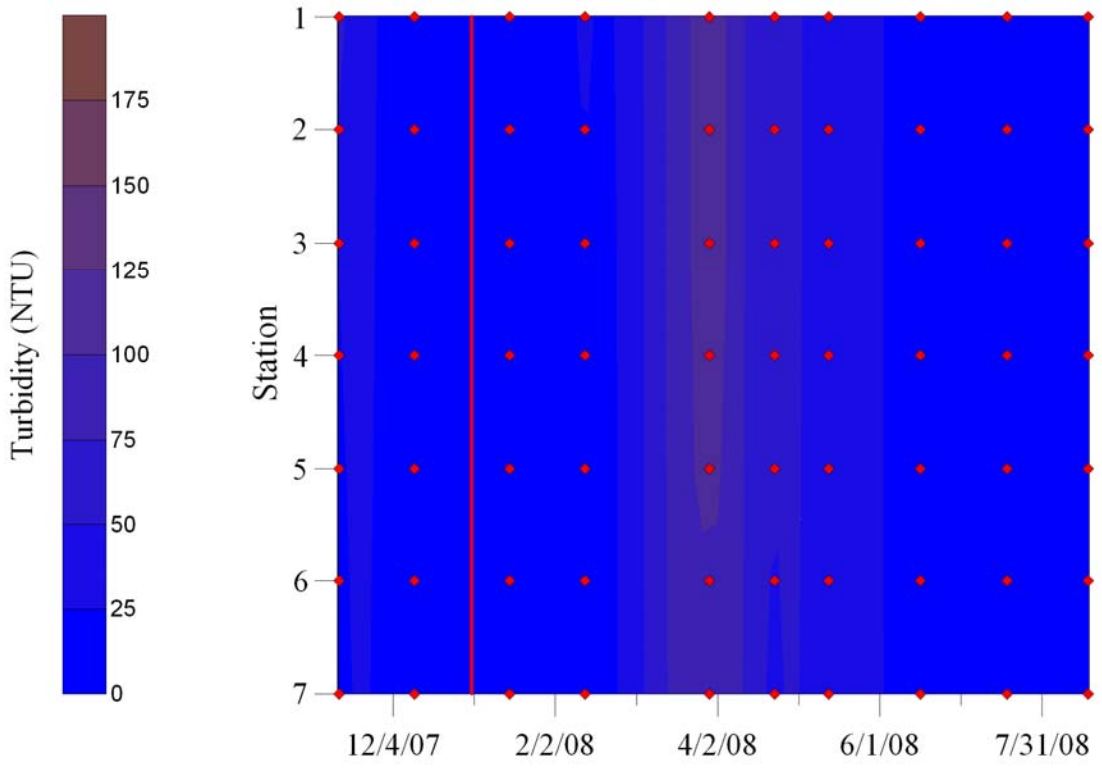

Figure F8. Surface water turbidity for a period spanning November, 2007 through August, 2008.

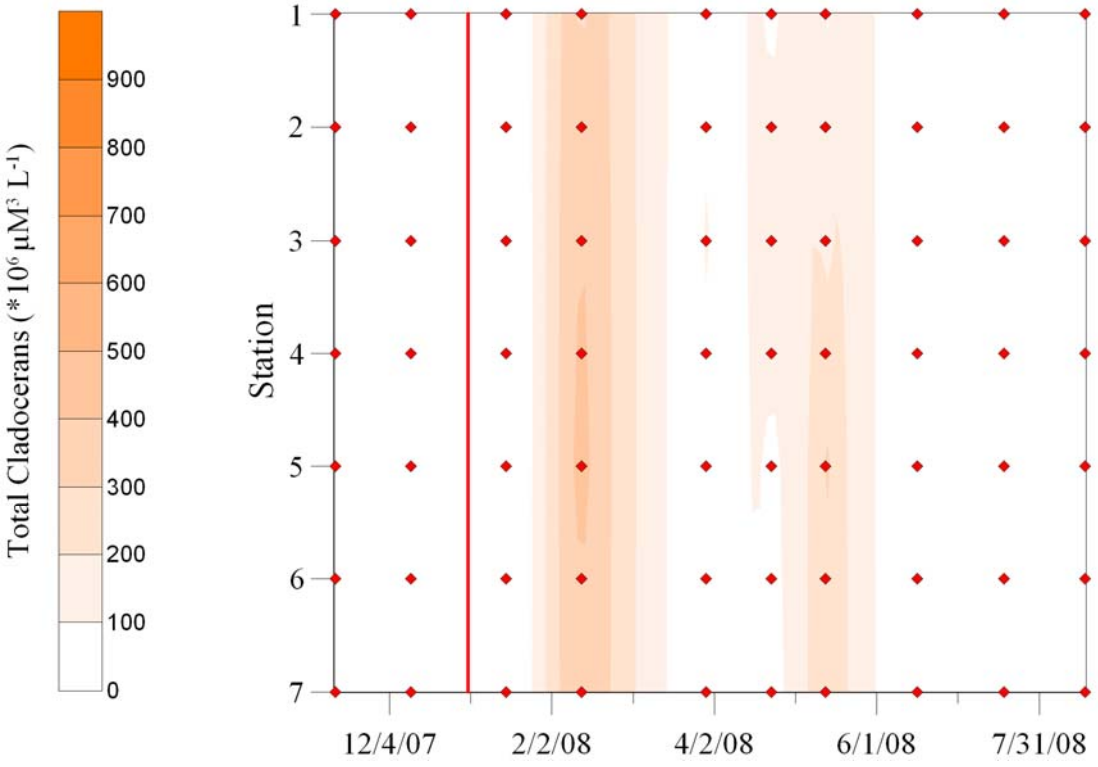

Figure F9. Total cladoceran biovolume for a period spanning November, 2007 through August, 2008.

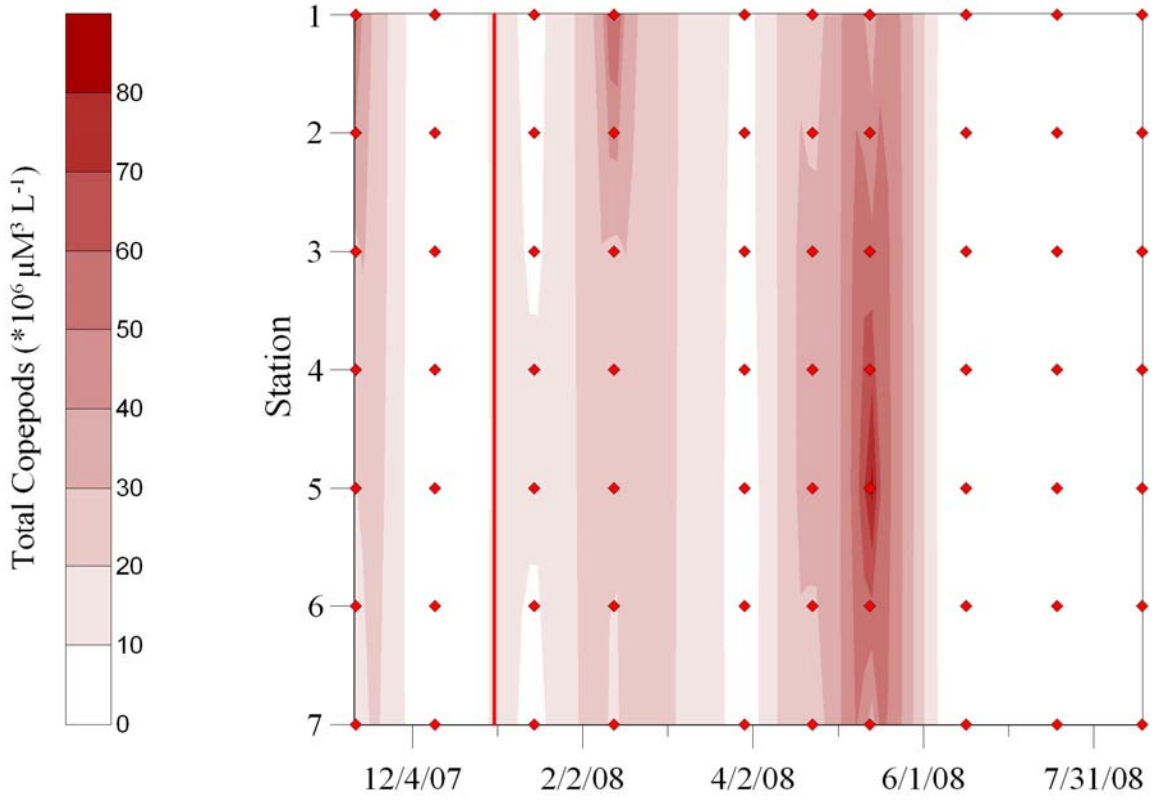

Figure F10. Total copepod biovolume for a period spanning November, 2007 through August, 2008.

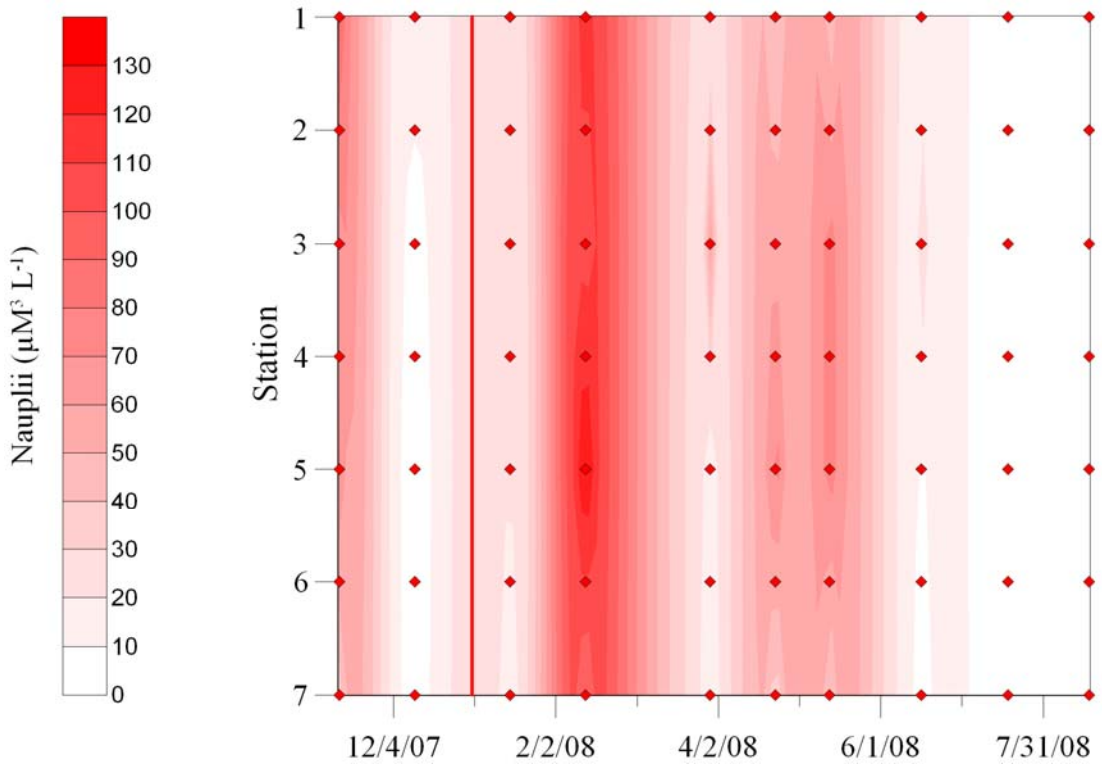

Figure F11. Total copepod nauplii biovolume for a period spanning November, 2007 through August, 2008.

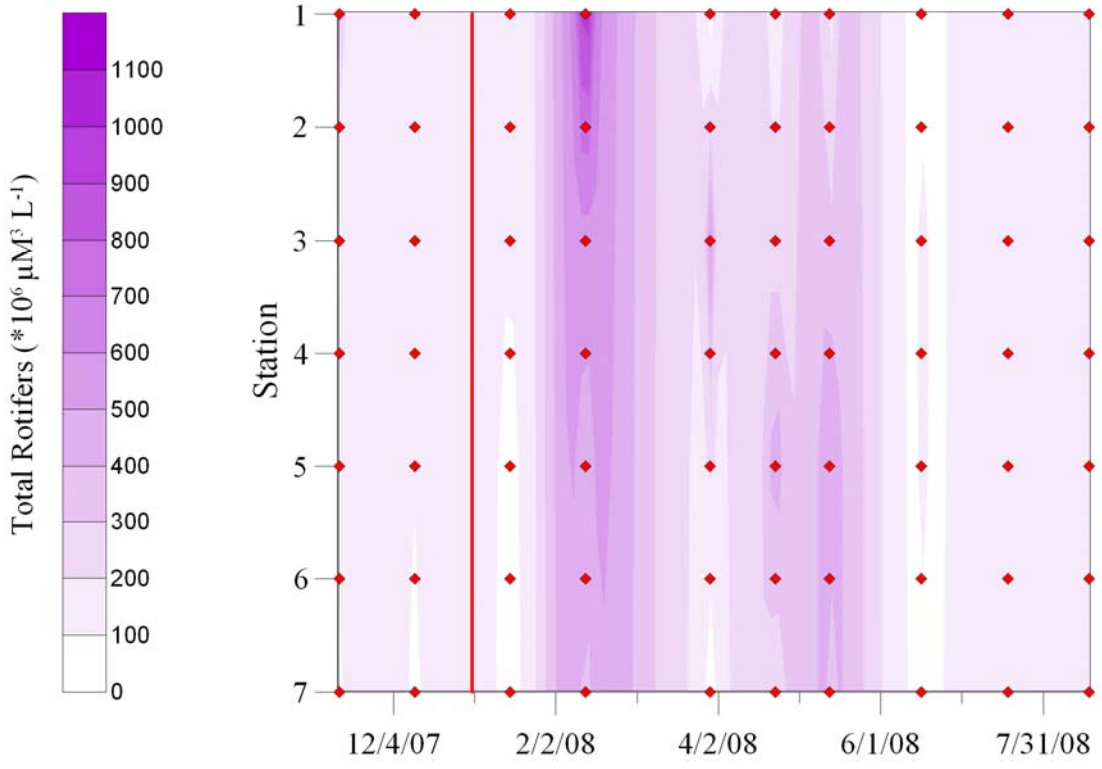

Figure F12. Total rotifer biovolume for a period spanning November, 2007 through August, 2008.

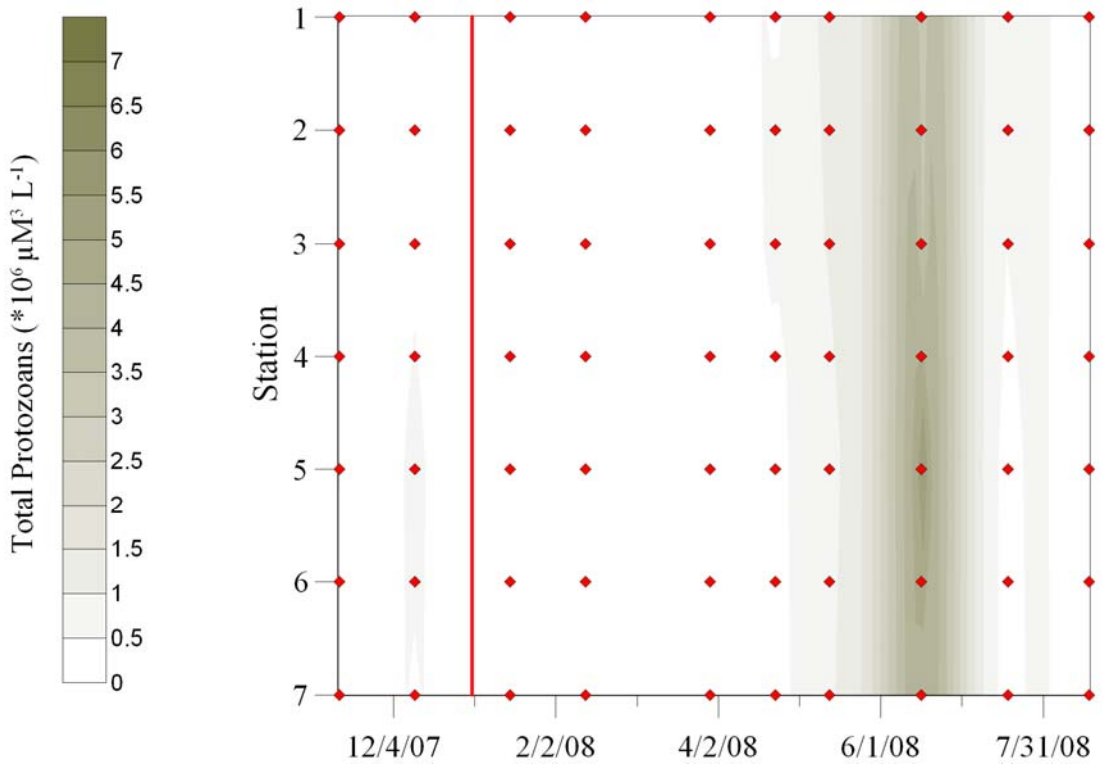

Figure F13. Total protozoan biovolume for a period spanning November, 2007 through August, 2008.

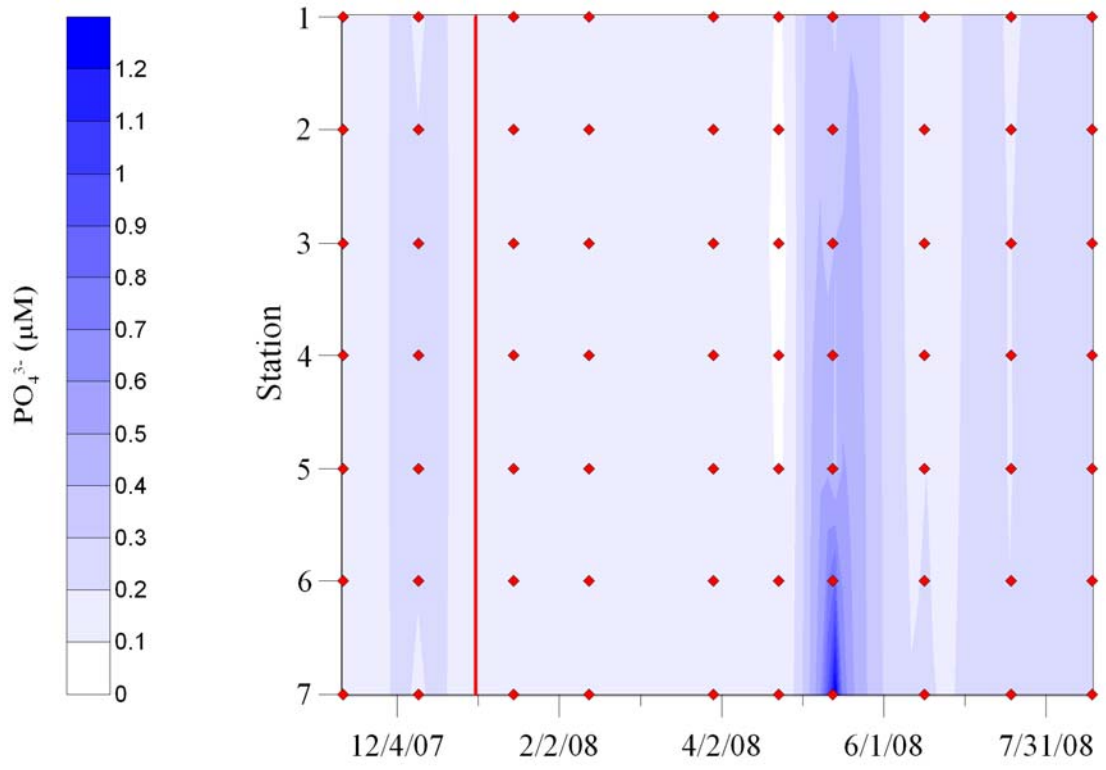

Figure F14. Phosphorus concentration for a period spanning November, 2007 through August, 2008.

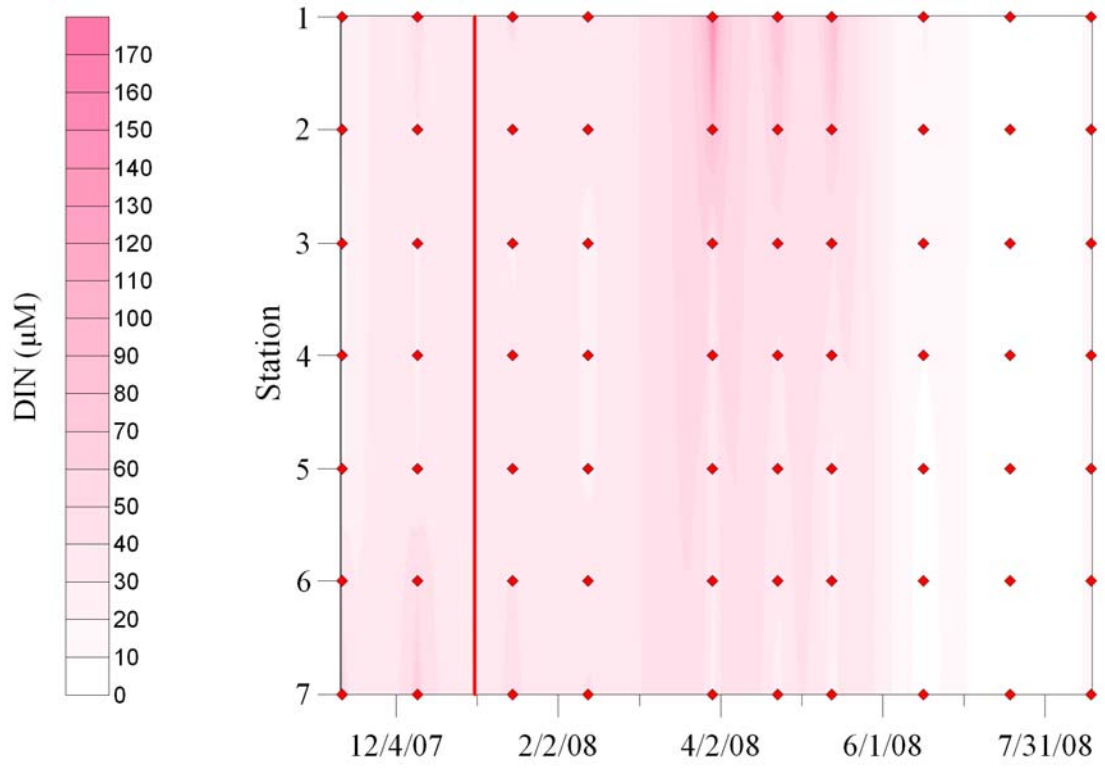

Figure F15. Dissolved inorganic nitrogen concentration for a period spanning November, 2007 through August, 2008.

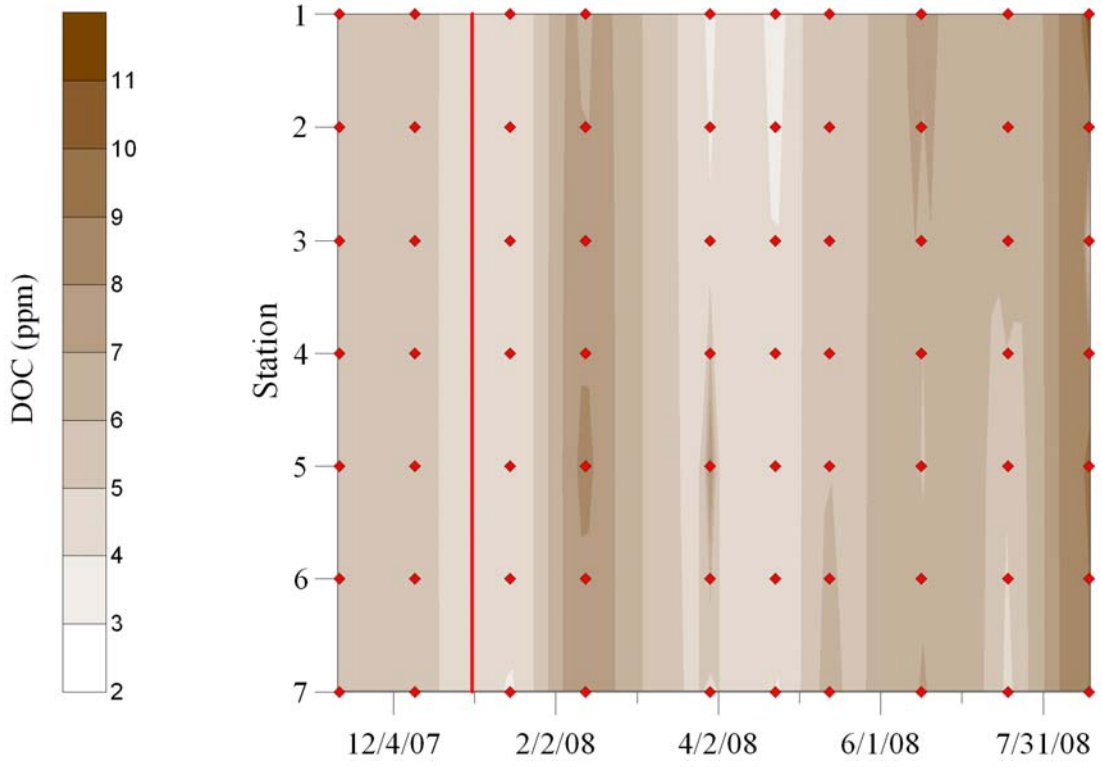

Figure F16. Dissolved organic carbon concentration for a period spanning November, 2007 through August, 2008.

Appendix G

Dataflow maps for Lake Waco

Monthly sampling from November 2007 through August, 2008.

Figures G-1 through G-9 - Chlorophyll *a*
Figures G-10 through G-18 - Salinity
Figures G-19 through G-27 - Temperature
Figures G-28 through G-36 - pH
Figures G-37 through G-45 - Turbidity
Figures G-46 through G-54 - Dissolved Organic Carbon

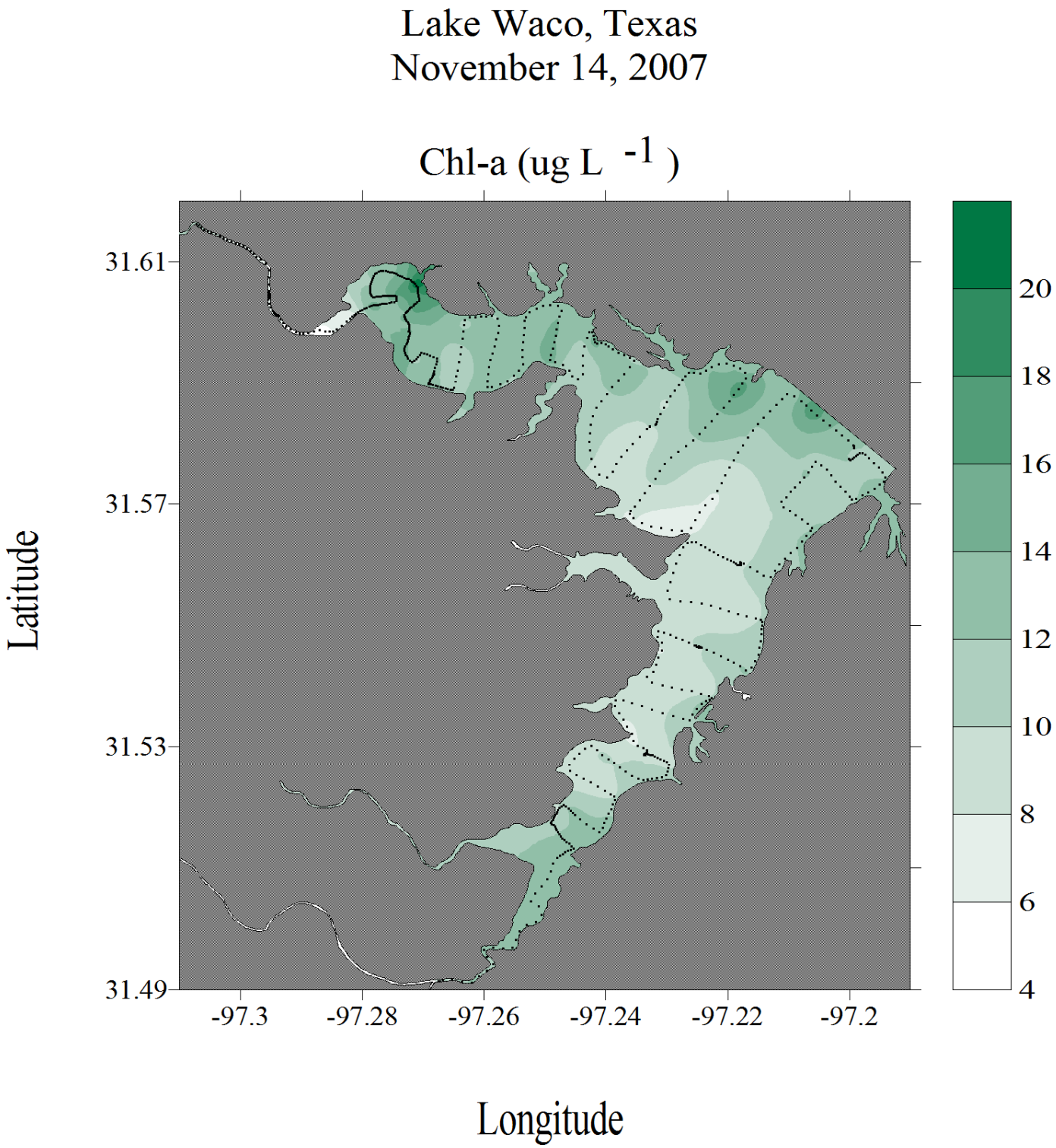

Figure G-1. Chlorophyll *a* dataflow map for Lake Waco

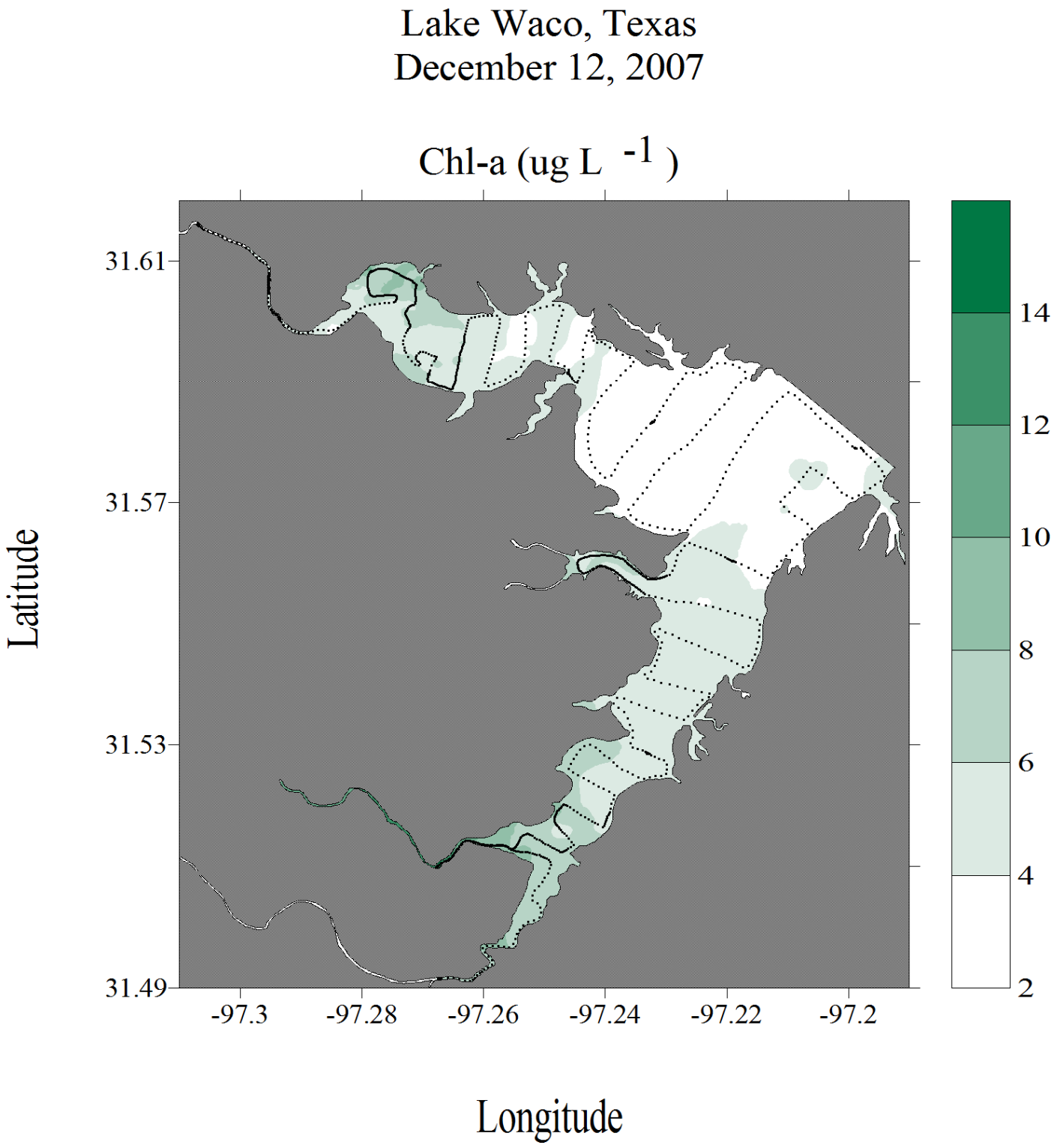

Figure G-2. Chlorophyll *a* dataflow map for Lake Waco

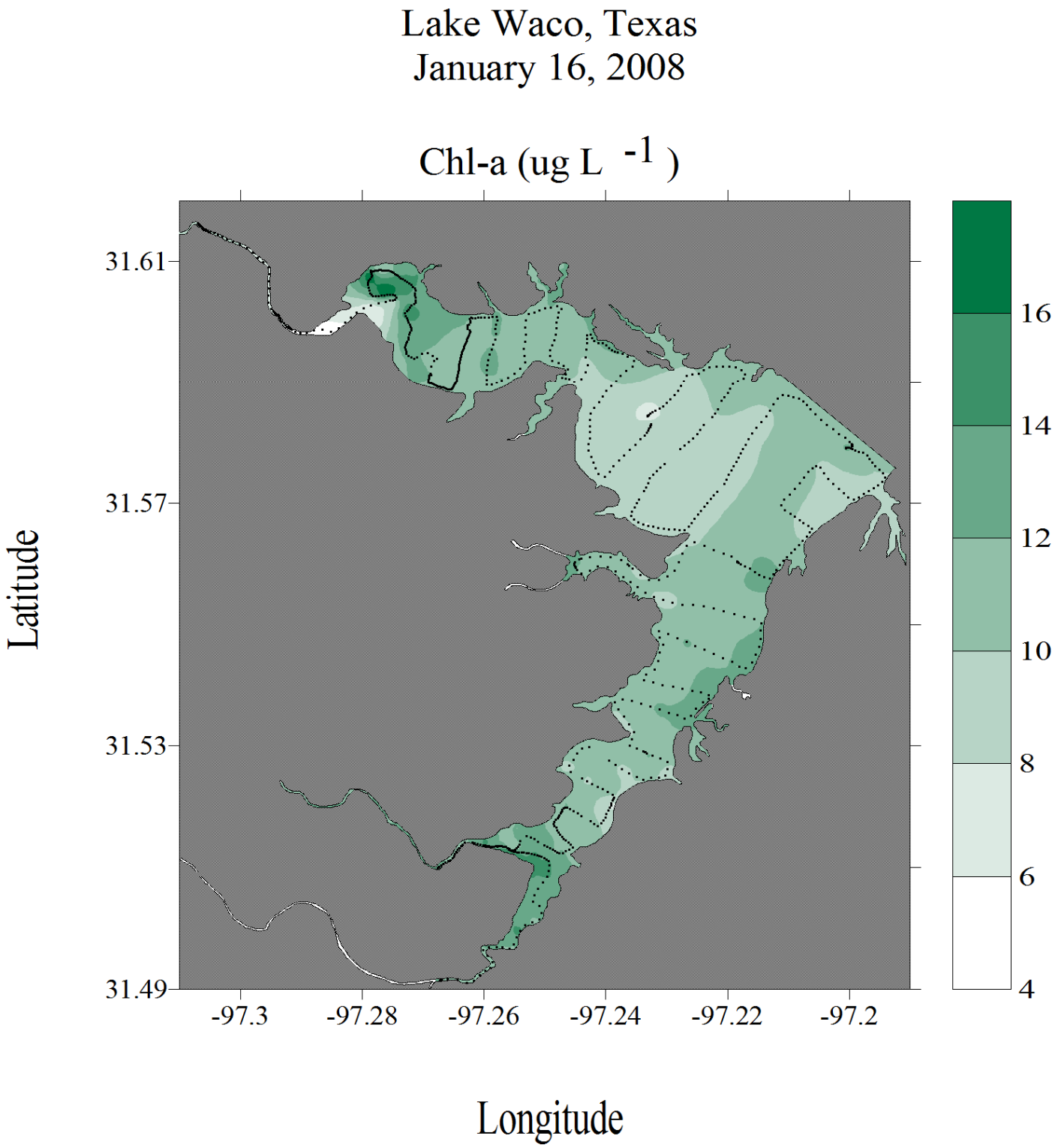

Figure G-3. Chlorophyll *a* dataflow map for Lake Waco

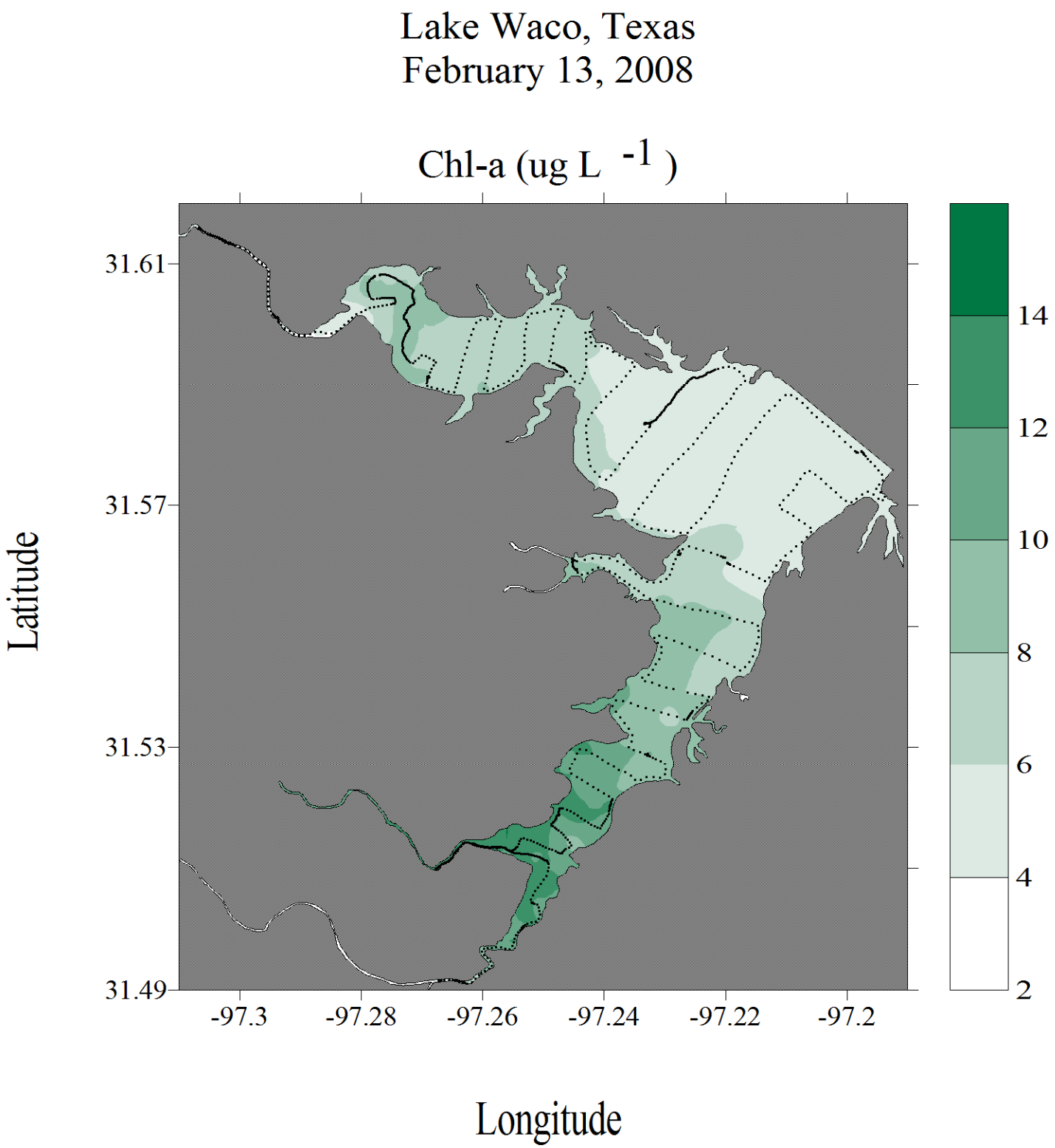

Figure G-4. Chlorophyll *a* dataflow map for Lake Waco

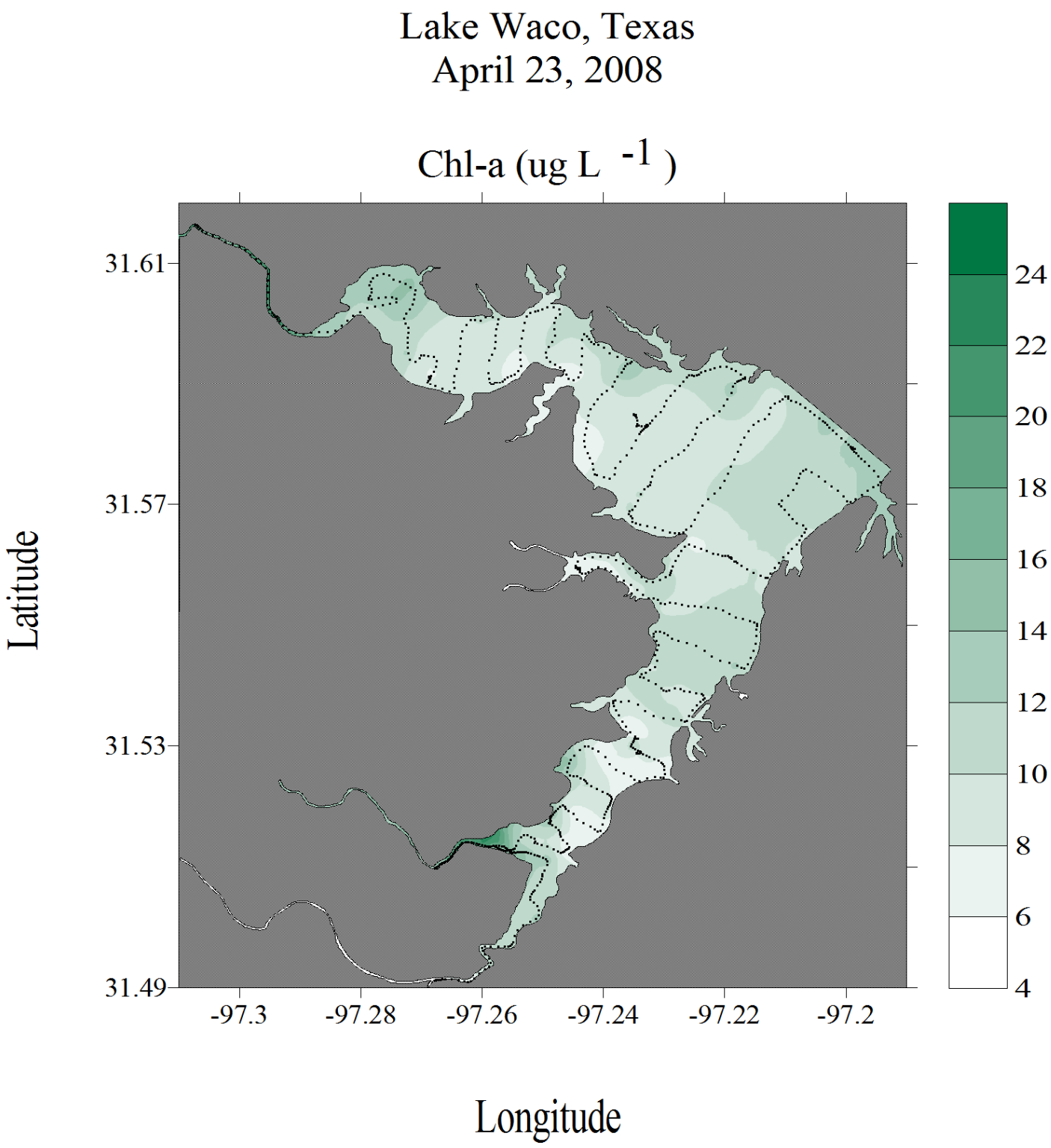

Figure G-5. Chlorophyll *a* dataflow map for Lake Waco

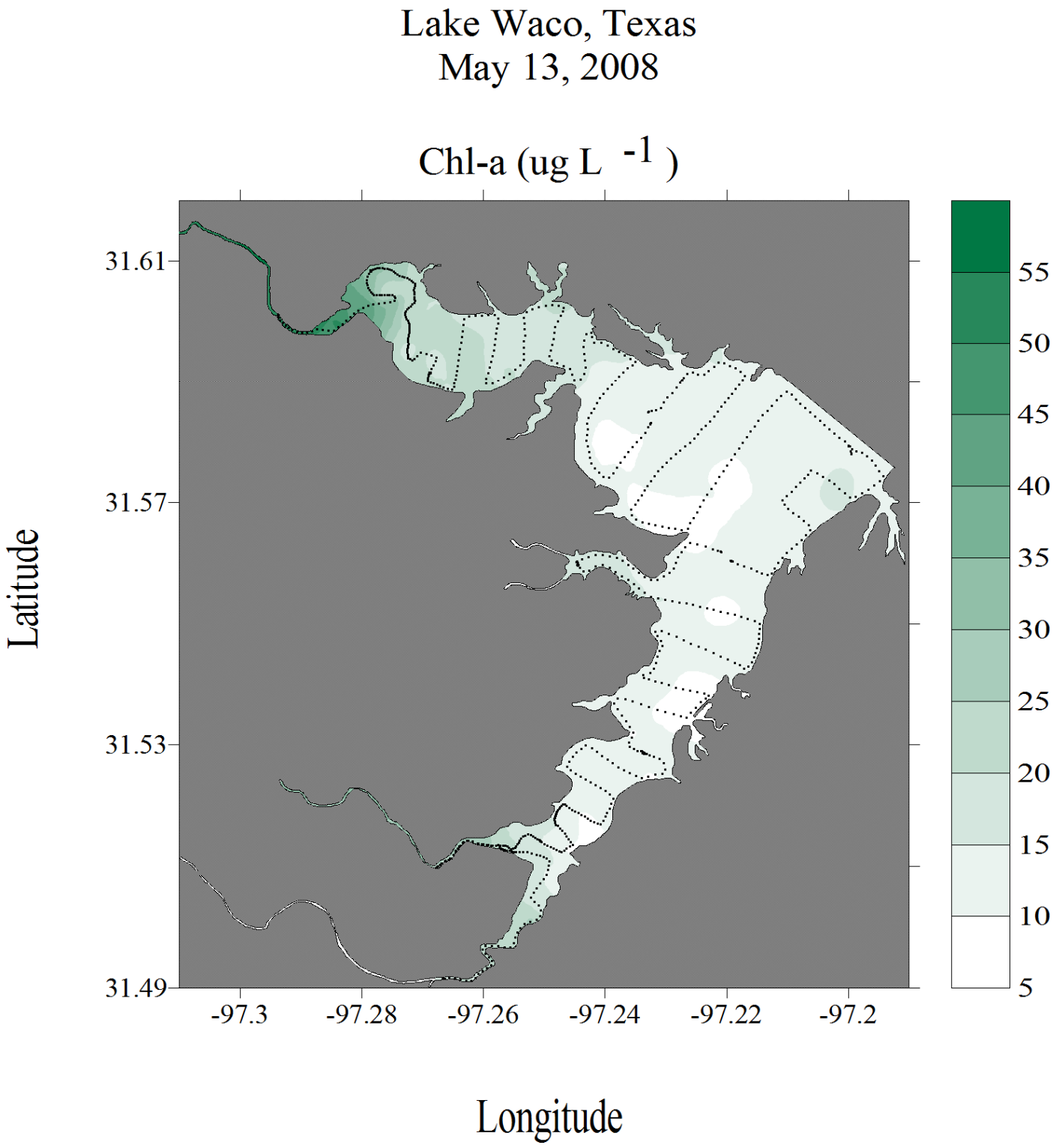

Figure G-6. Chlorophyll *a* dataflow map for Lake Waco

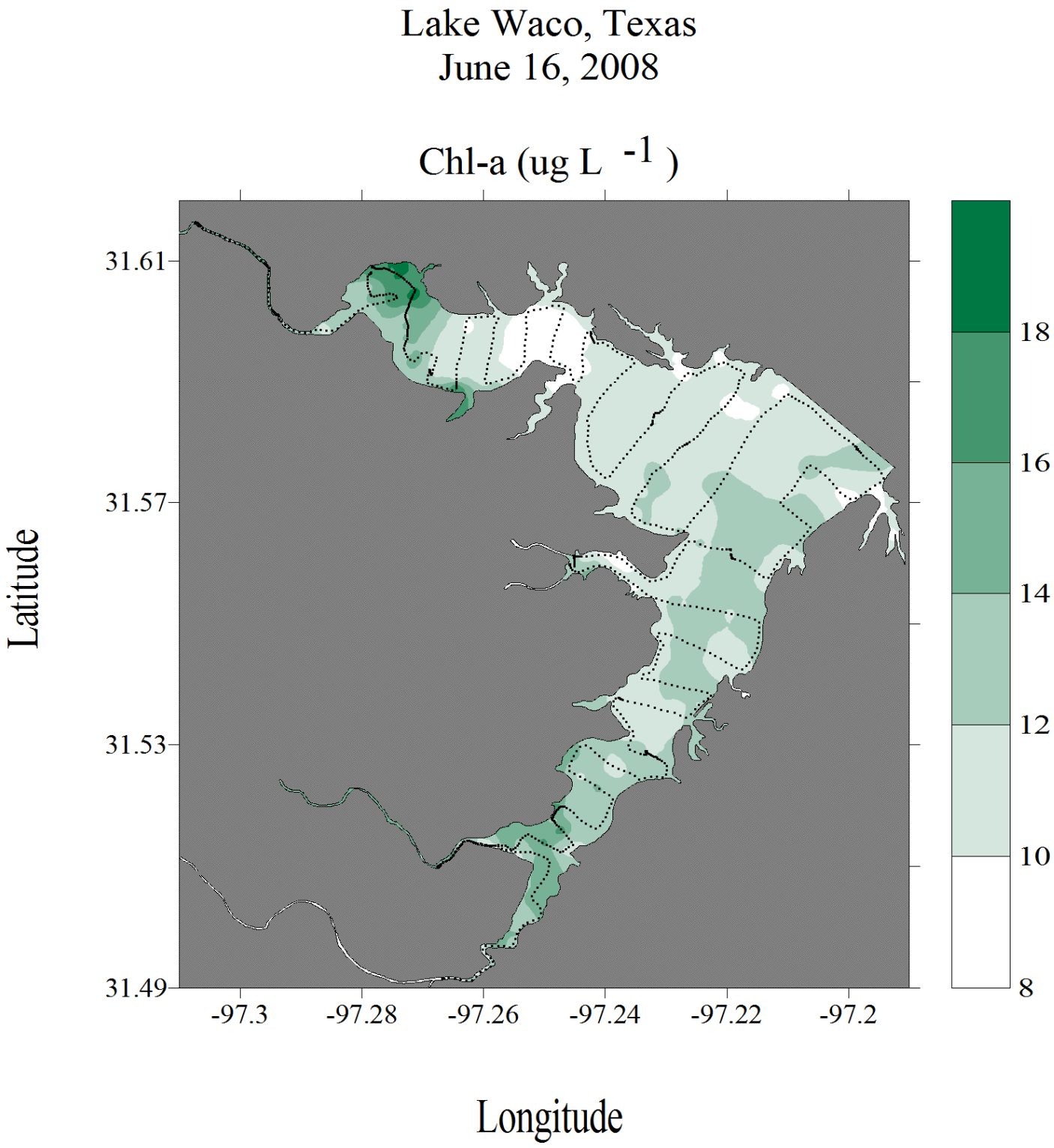

Figure G-7. Chlorophyll *a* dataflow map for Lake Waco

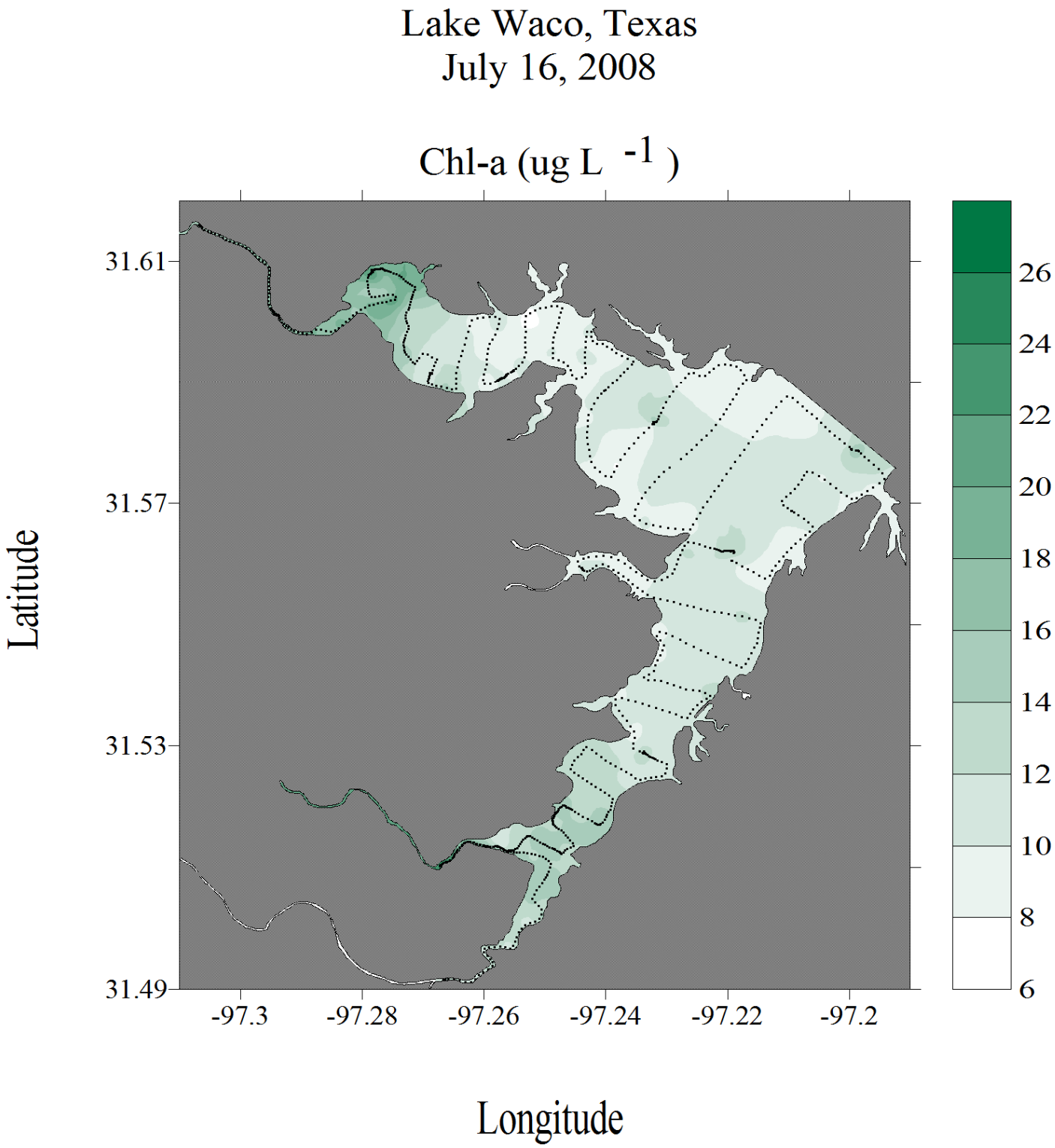

Figure G-8. Chlorophyll *a* dataflow map for Lake Waco

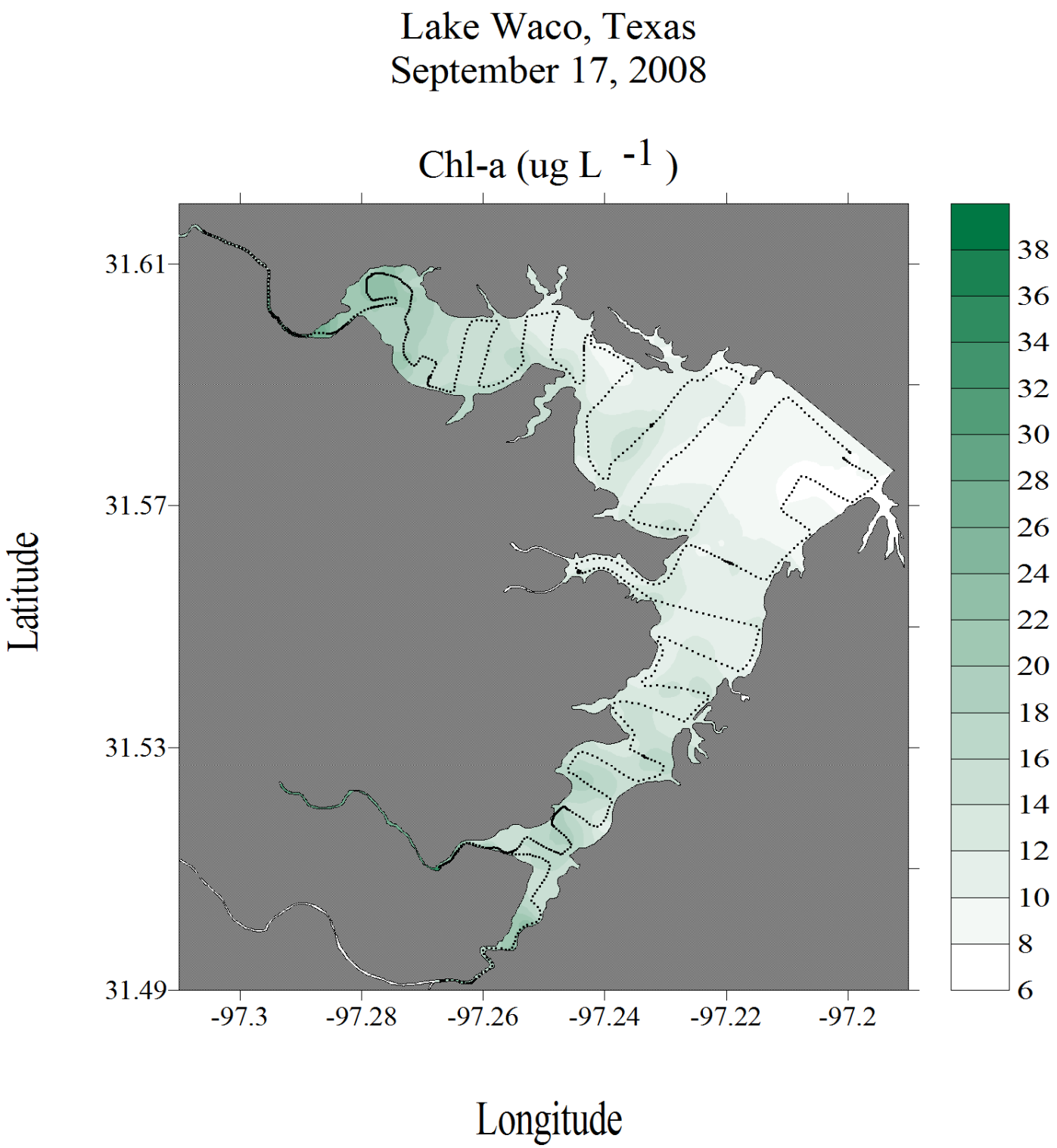

Figure G-9. Chlorophyll *a* dataflow map for Lake Waco

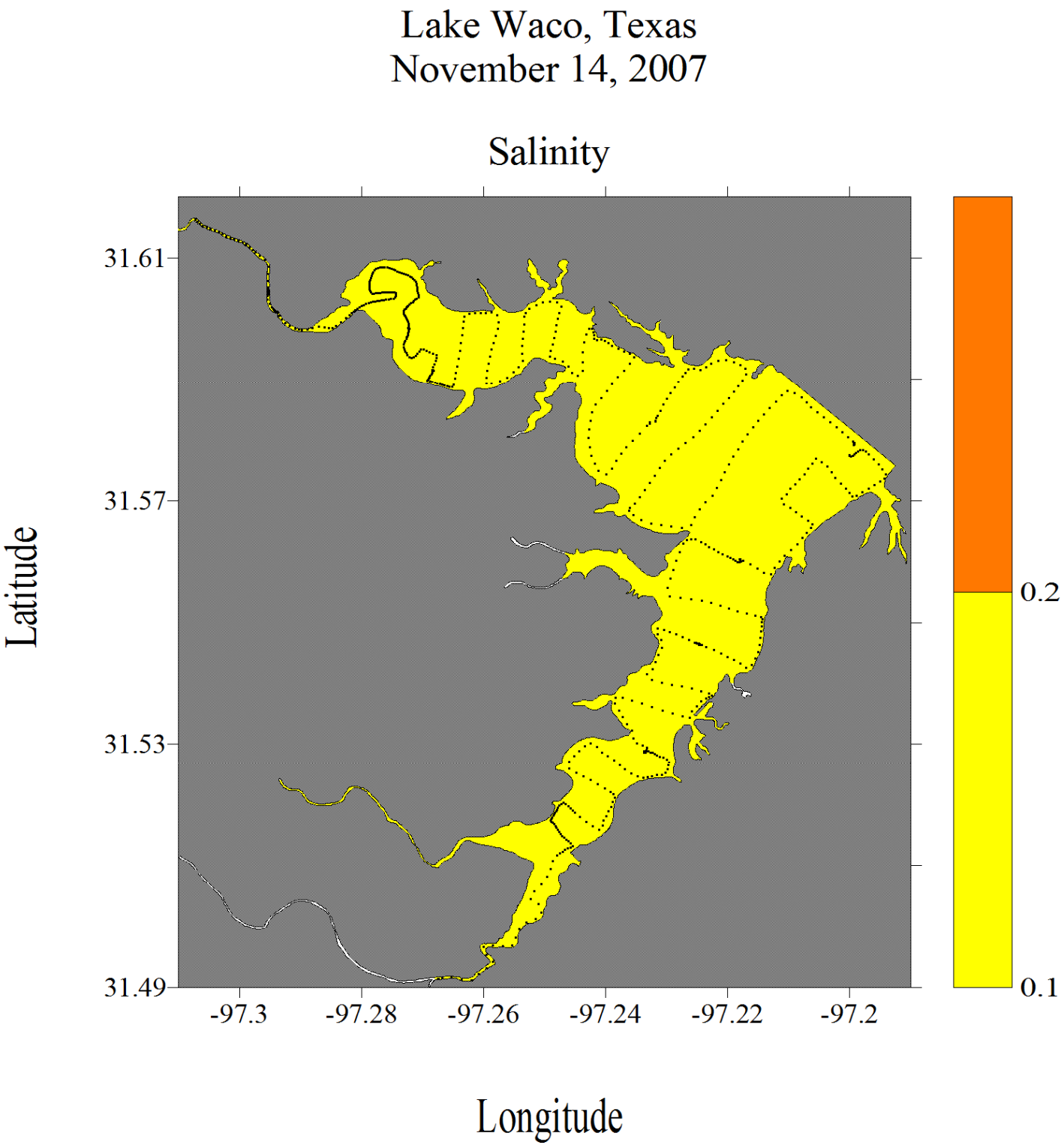

Figure G-10. Salinity dataflow map for Lake Waco

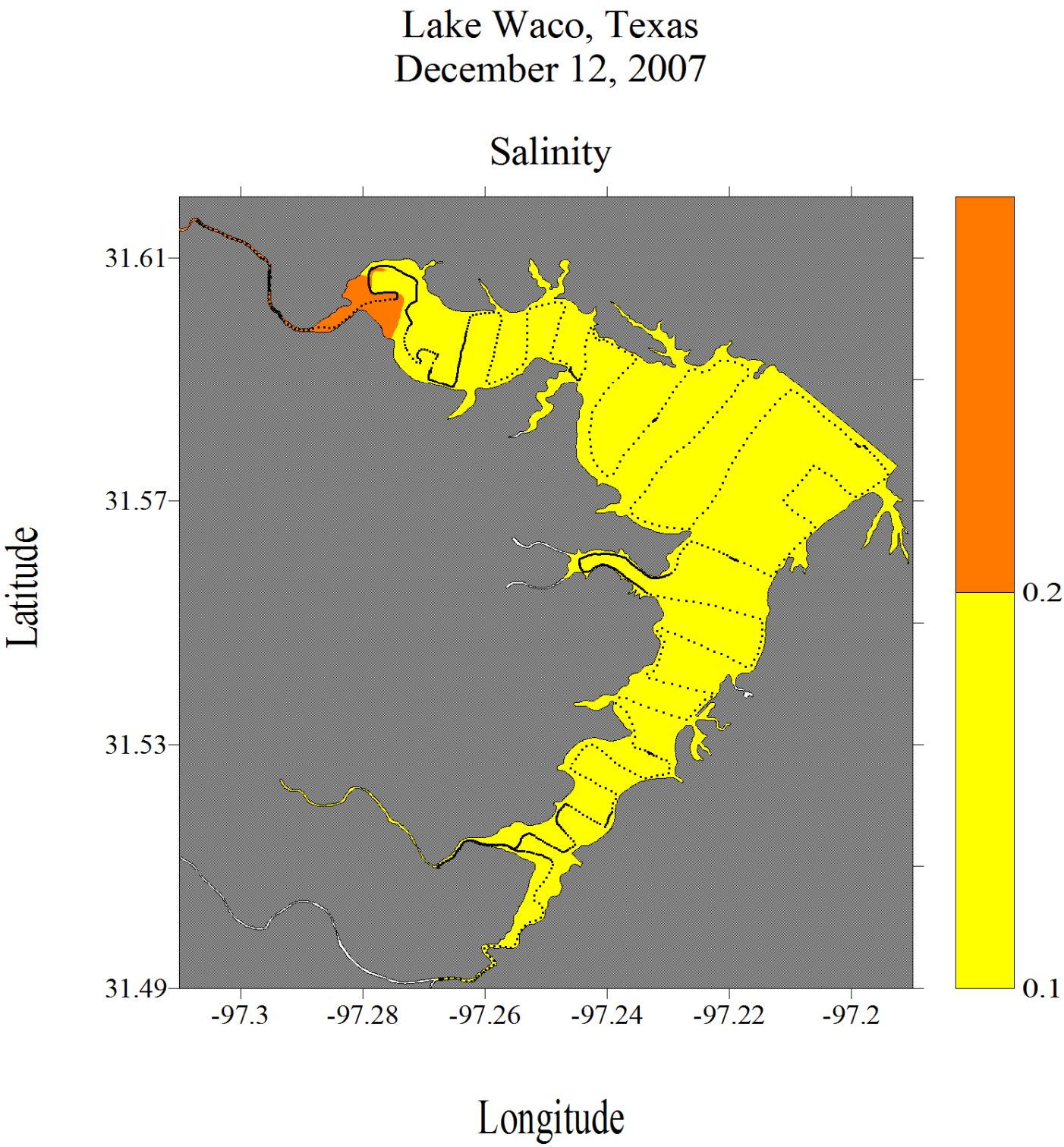

Figure G-11. Salinity dataflow map for Lake Waco

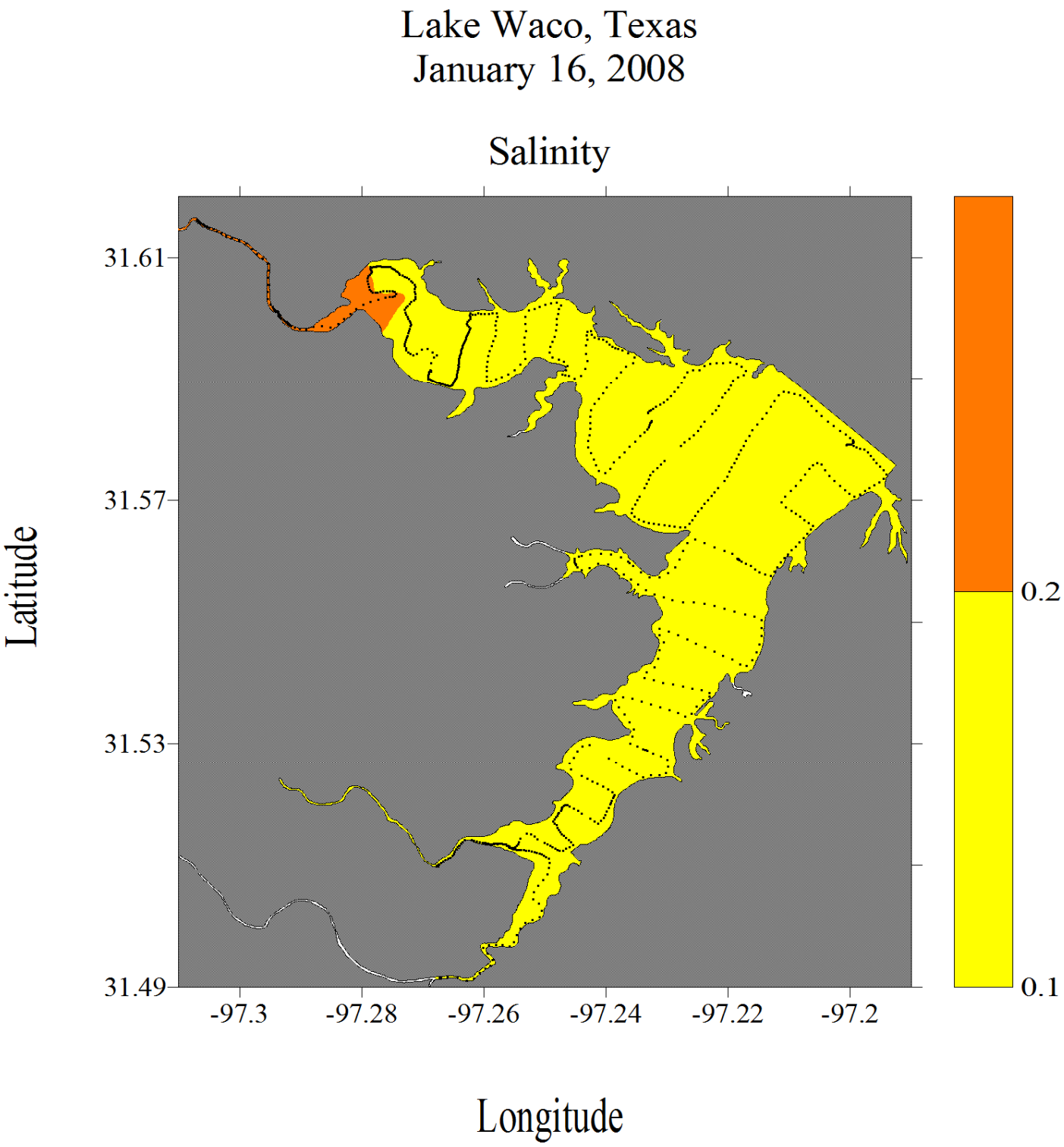

Figure G-12. Salinity dataflow map for Lake Waco

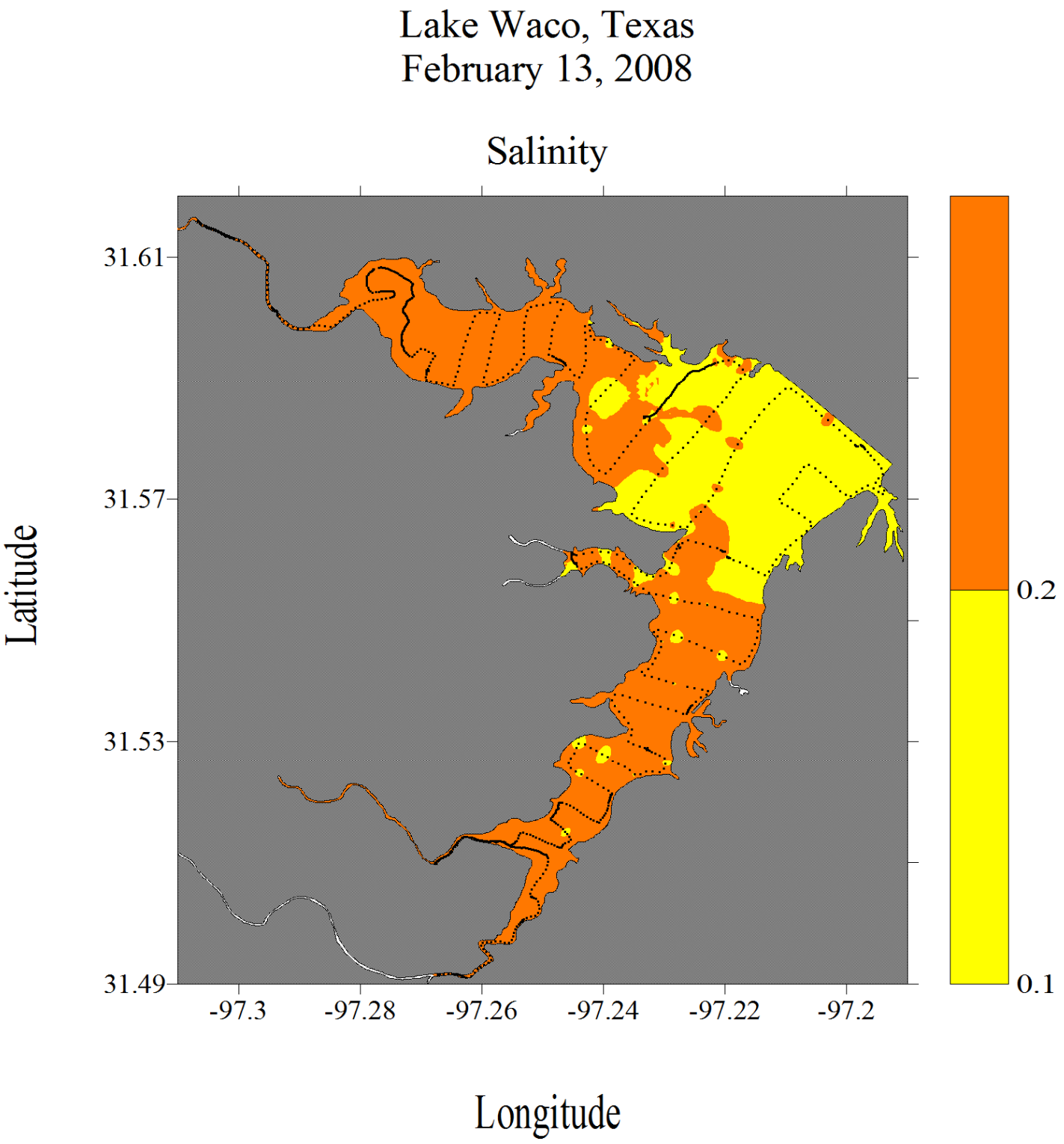

Figure G-13. Salinity dataflow map for Lake Waco

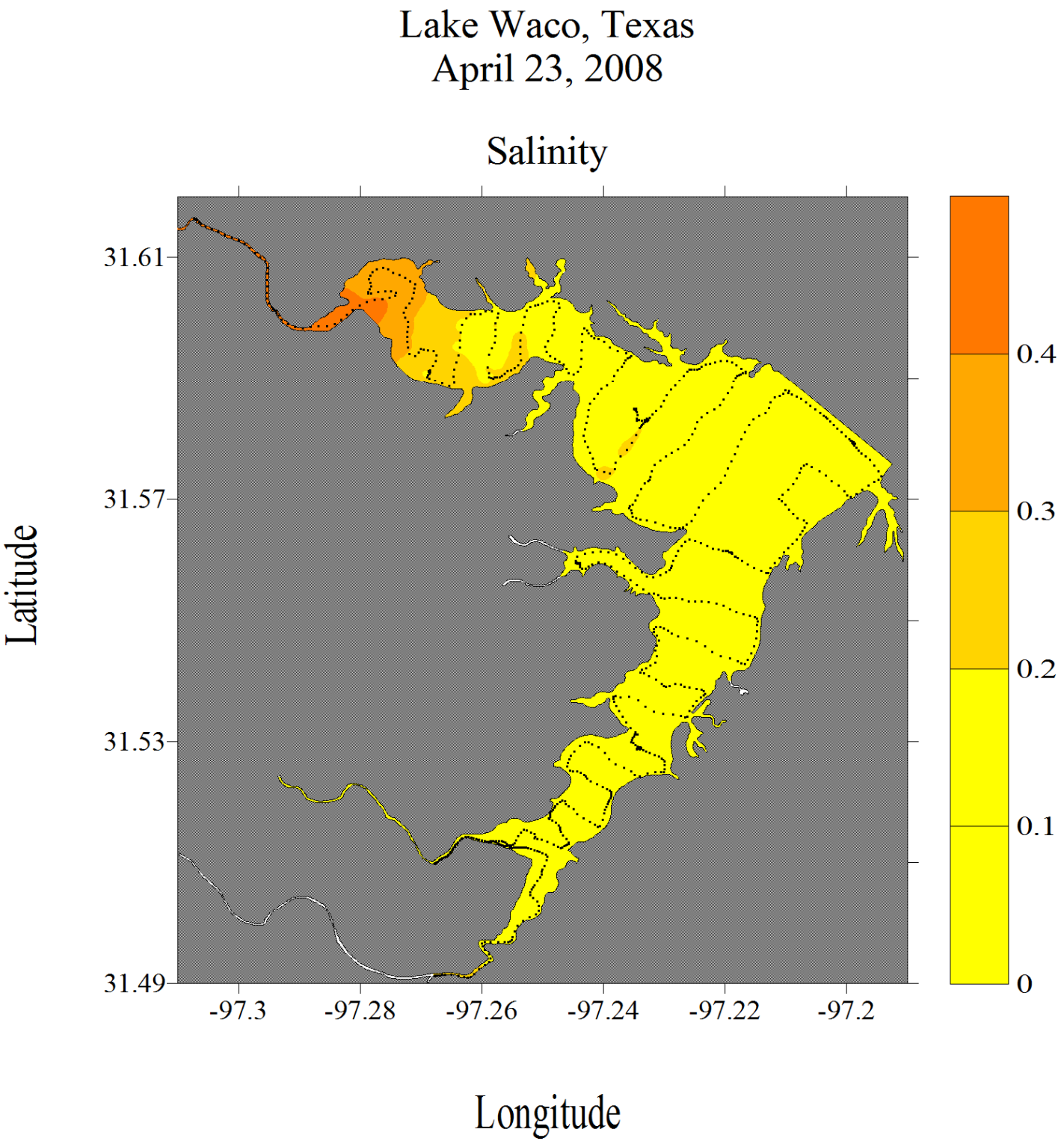

Figure G-14. Salinity dataflow map for Lake Waco

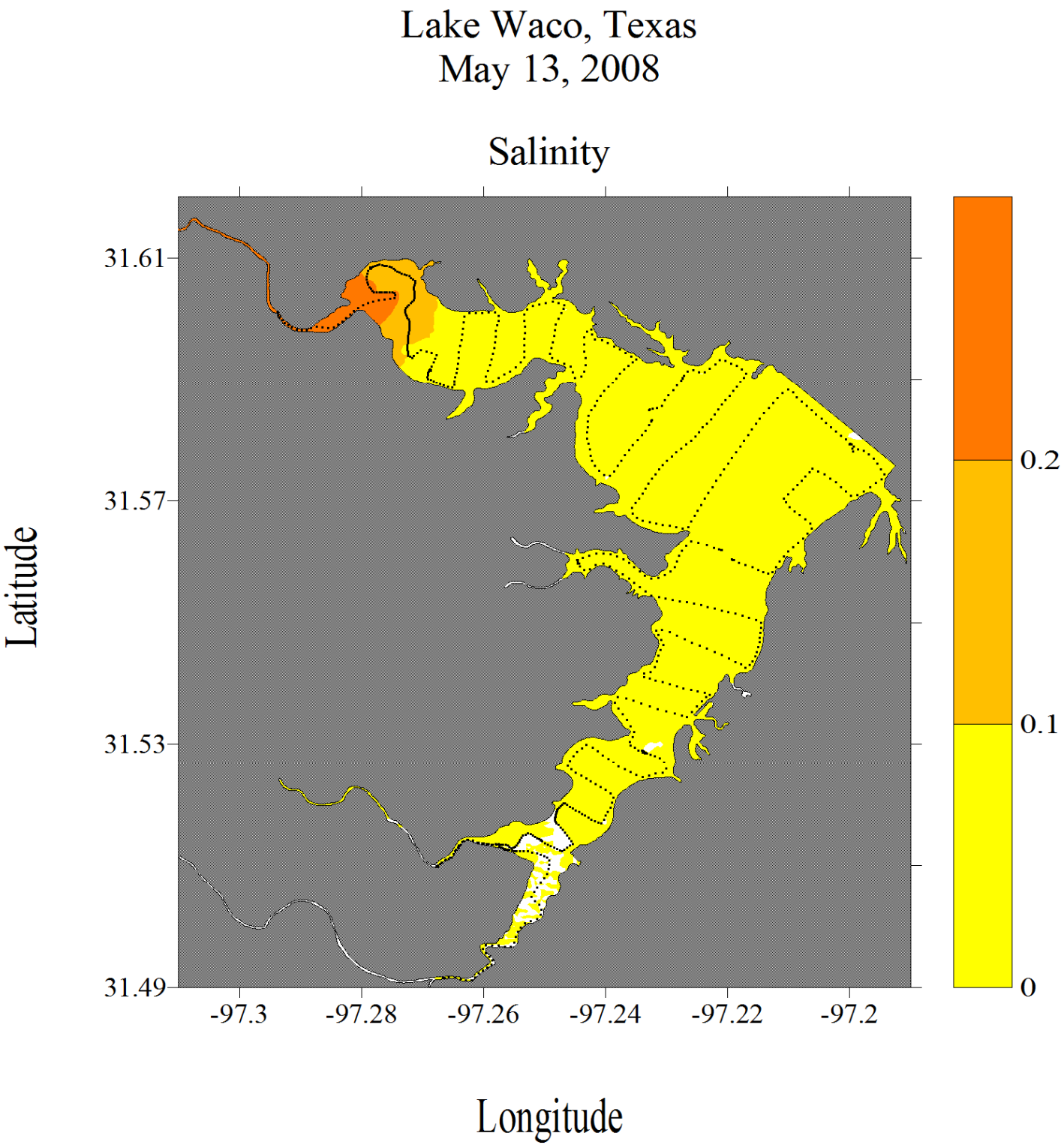

Figure G-15. Salinity dataflow map for Lake Waco

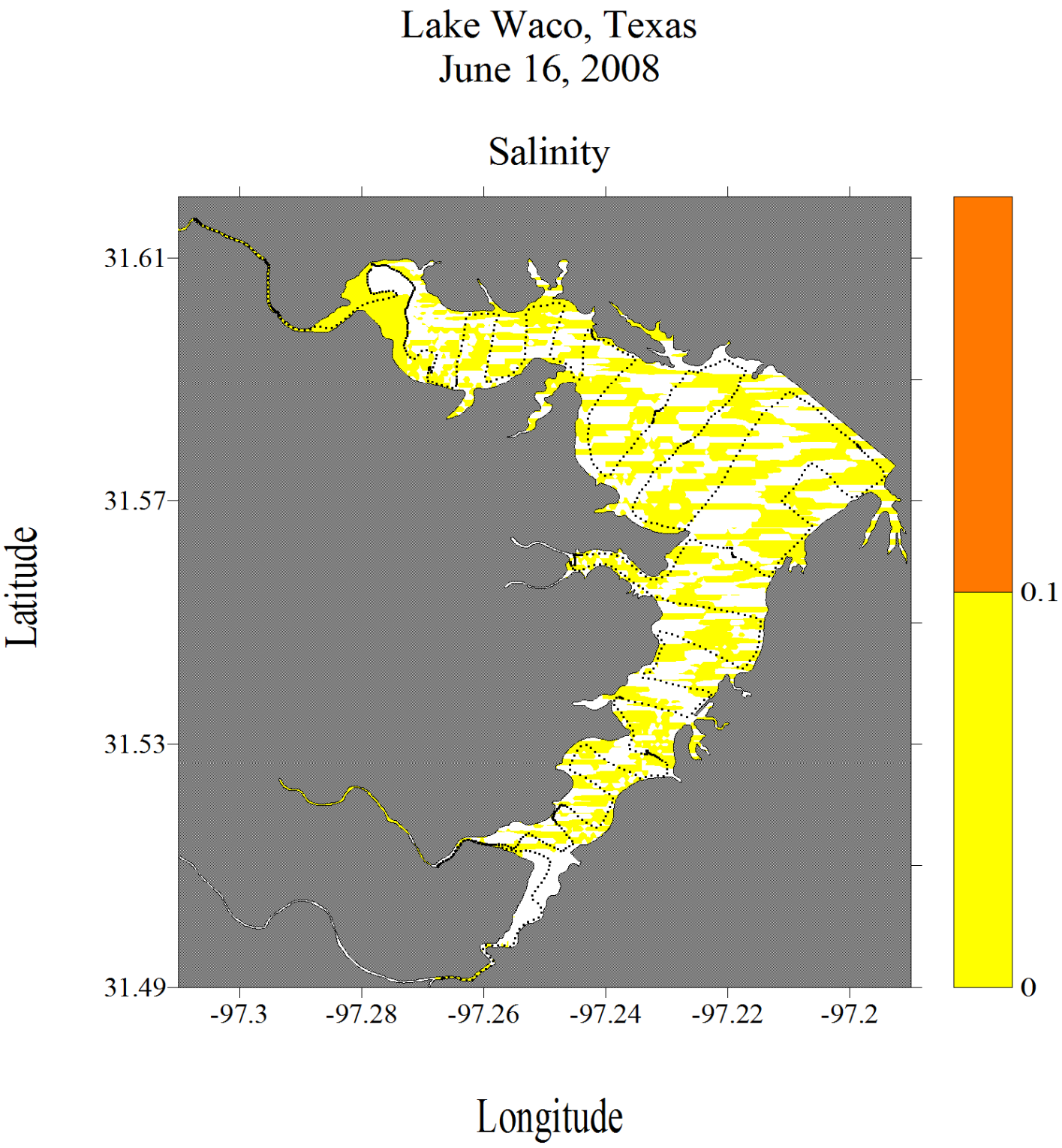

Figure G-16. Salinity dataflow map for Lake Waco

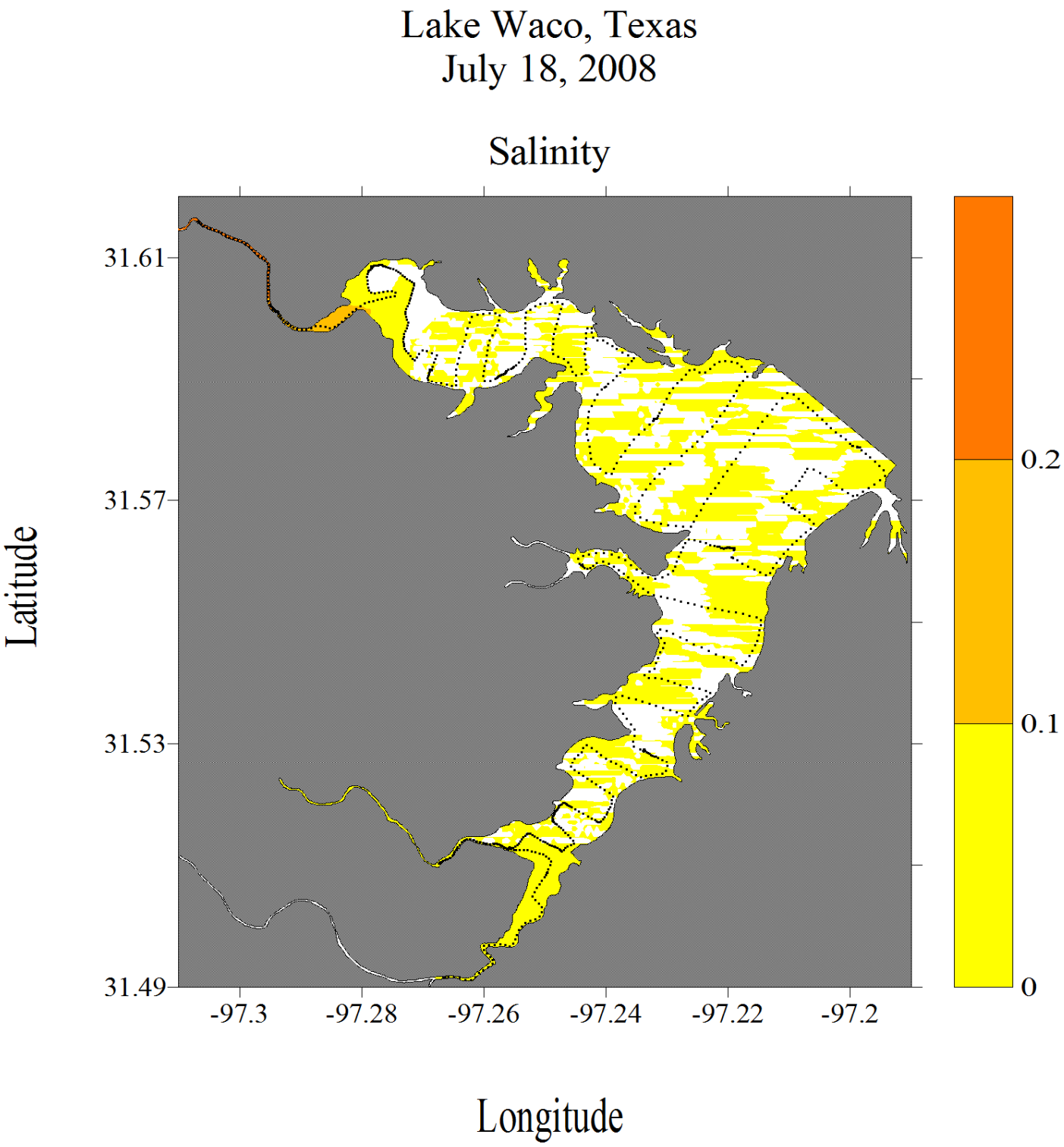

Figure G-17. Salinity dataflow map for Lake Waco

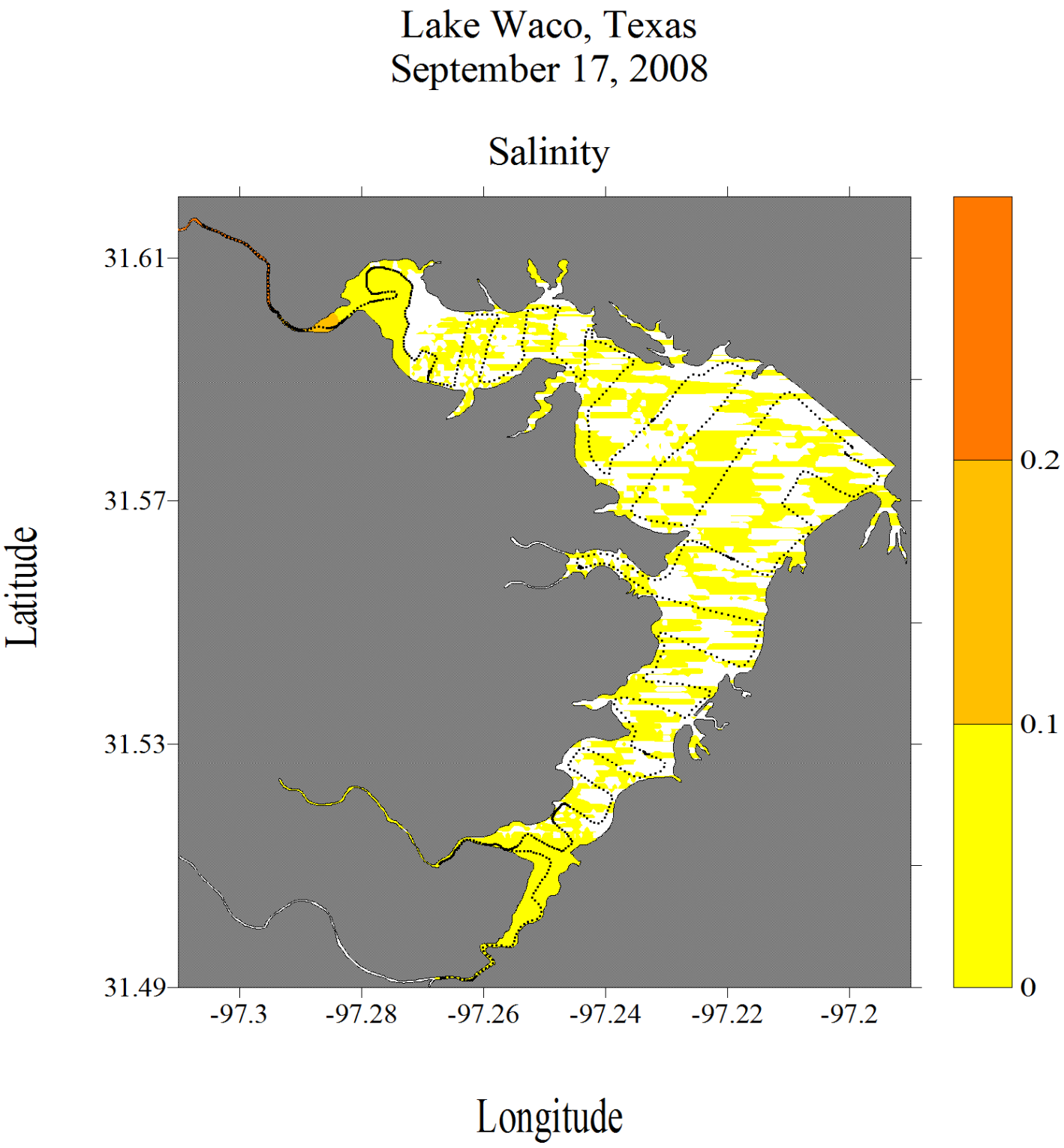

Figure G-18. Salinity dataflow map for Lake Waco

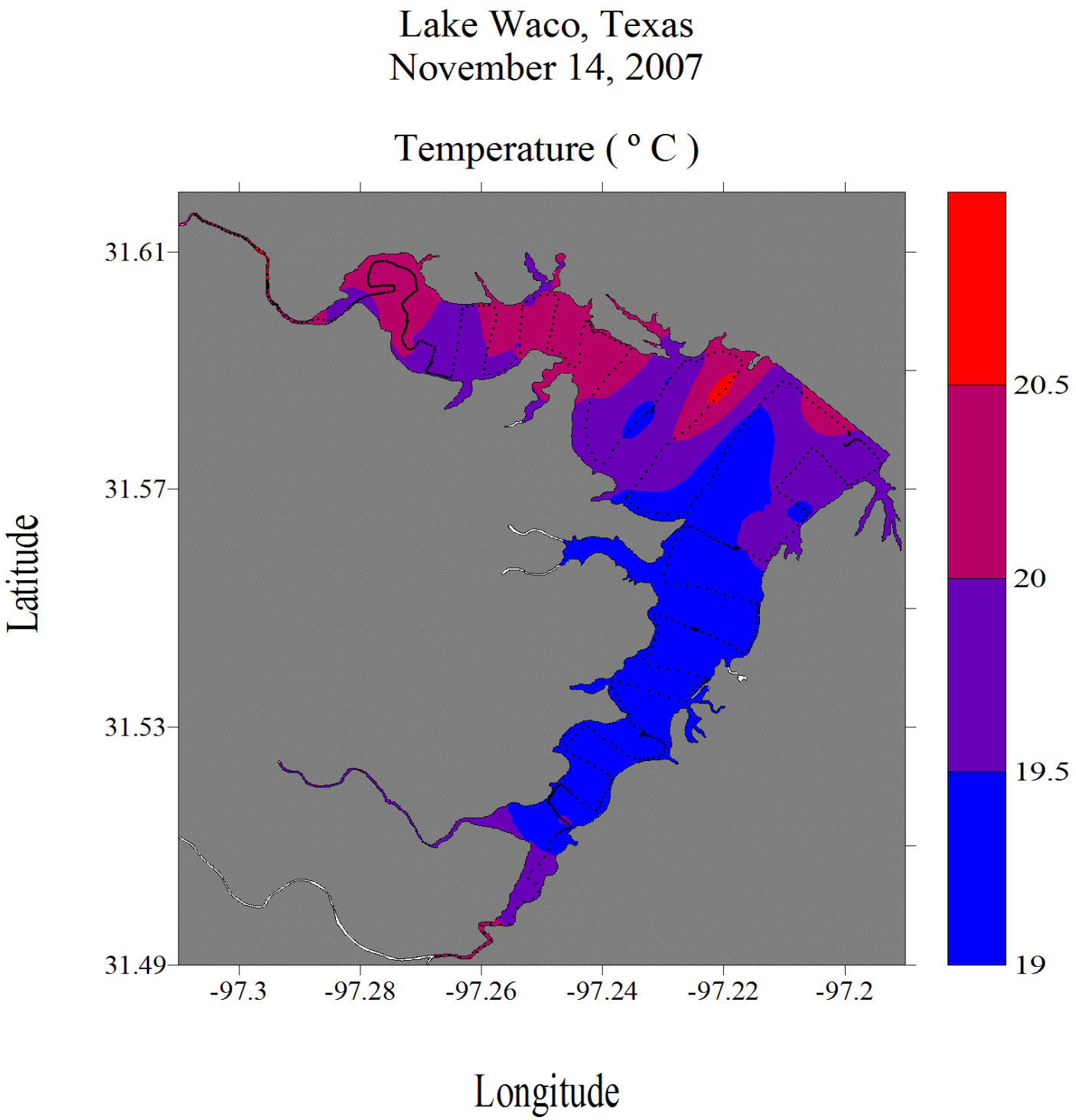

Figure G-19. Temperature dataflow map for Lake Waco

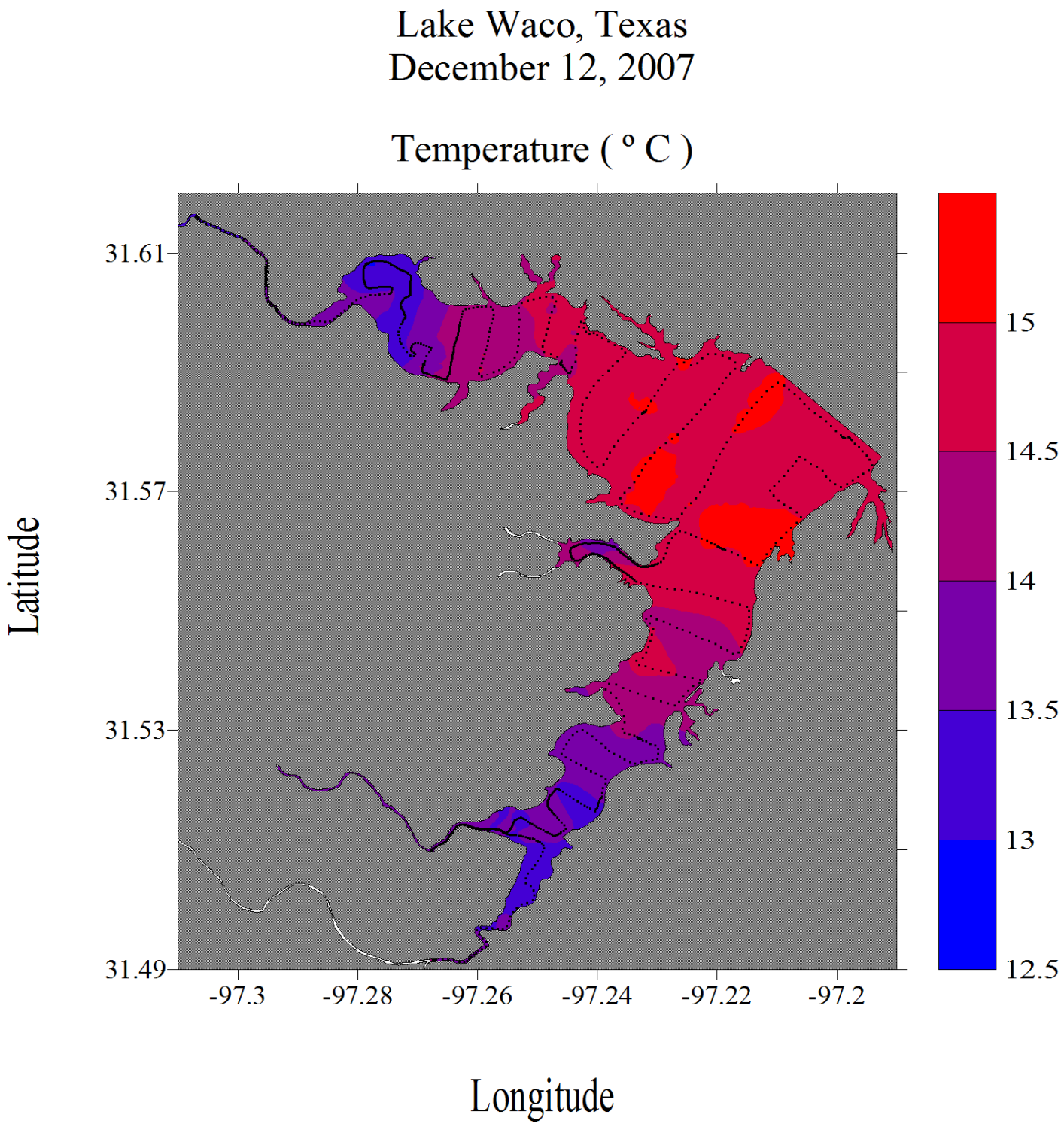

Figure G-20. Temperature dataflow map for Lake Waco

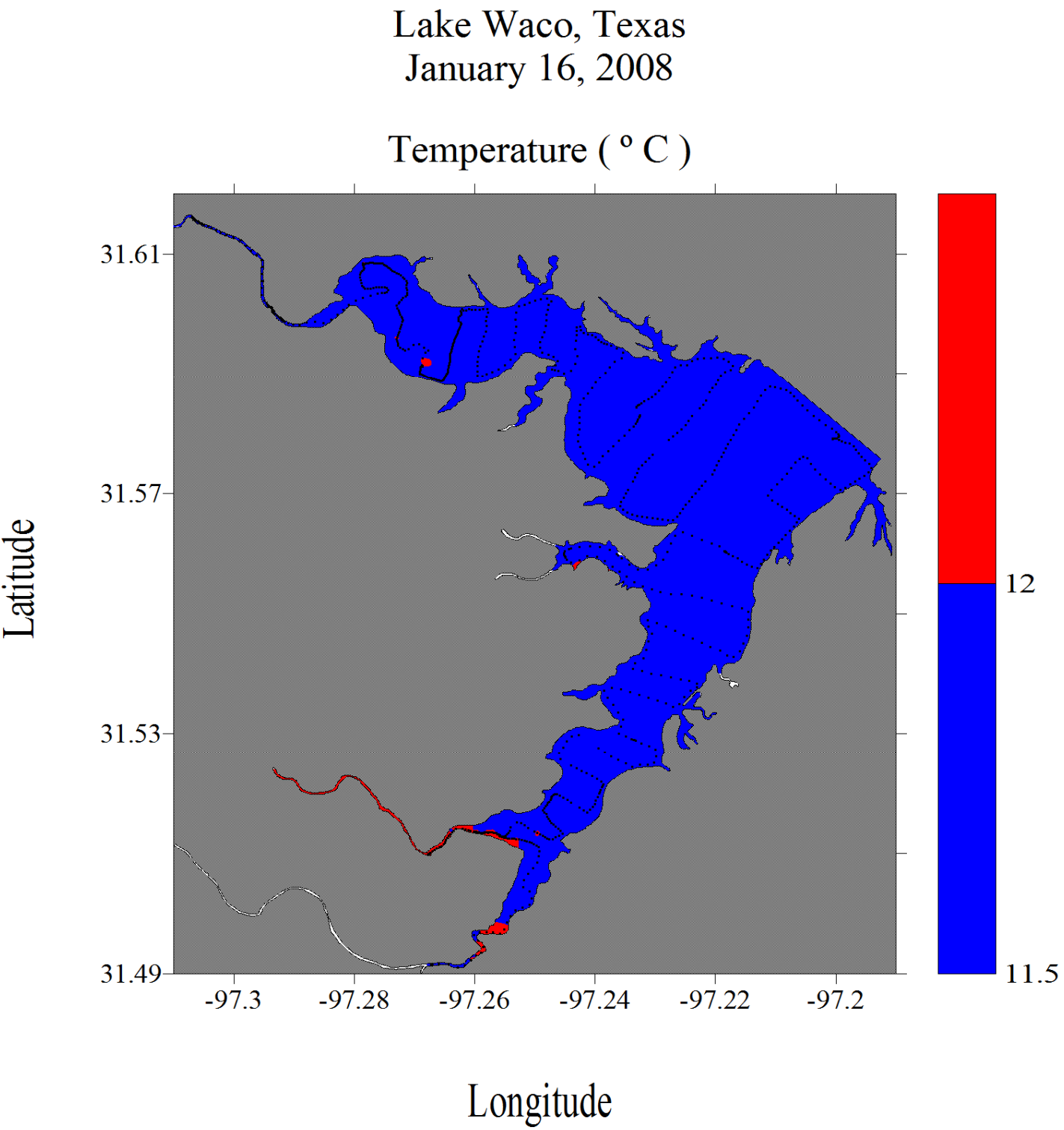

Figure G-21. Temperature dataflow map for Lake Waco

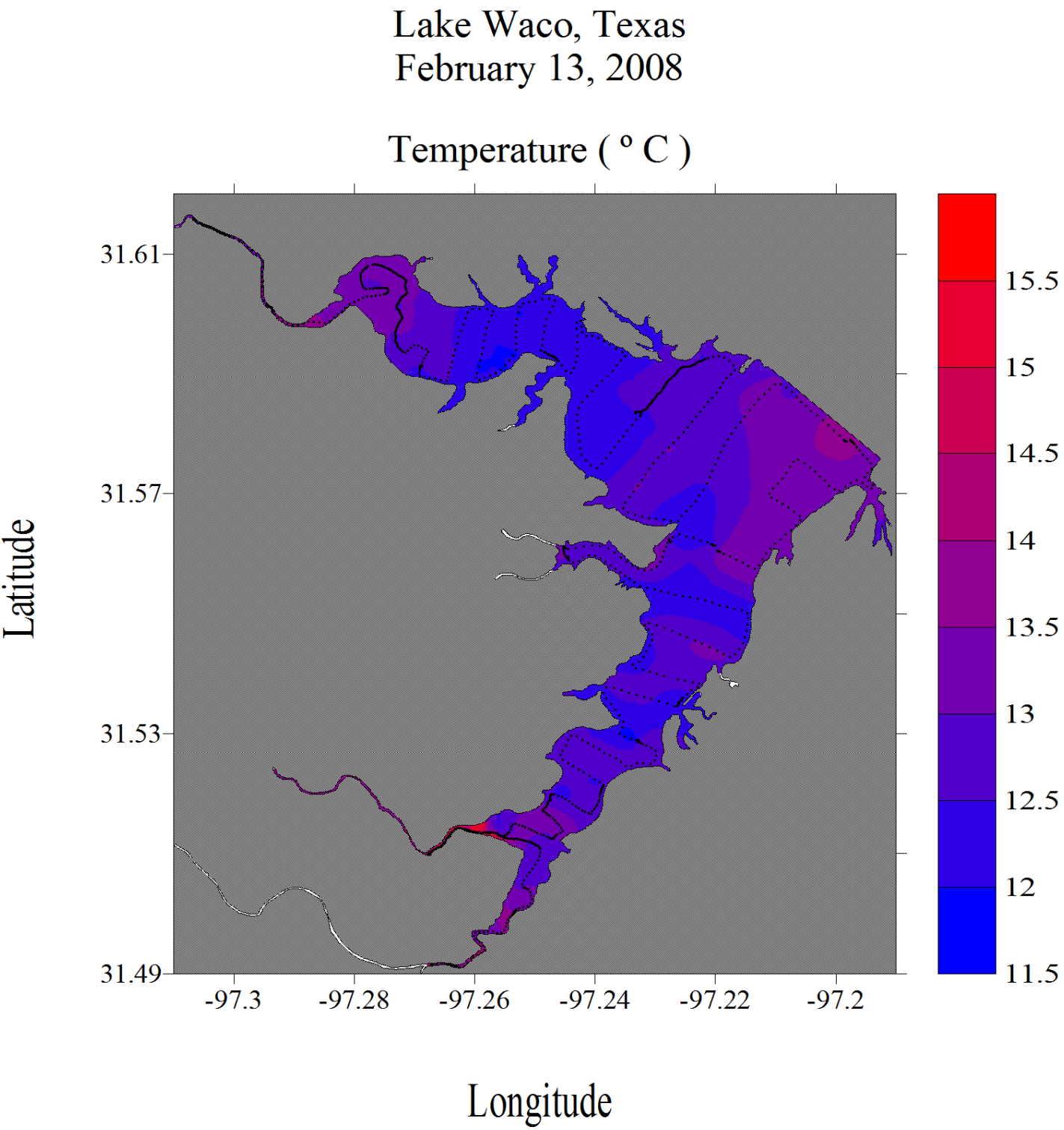

Figure G-22. Temperature dataflow map for Lake Waco

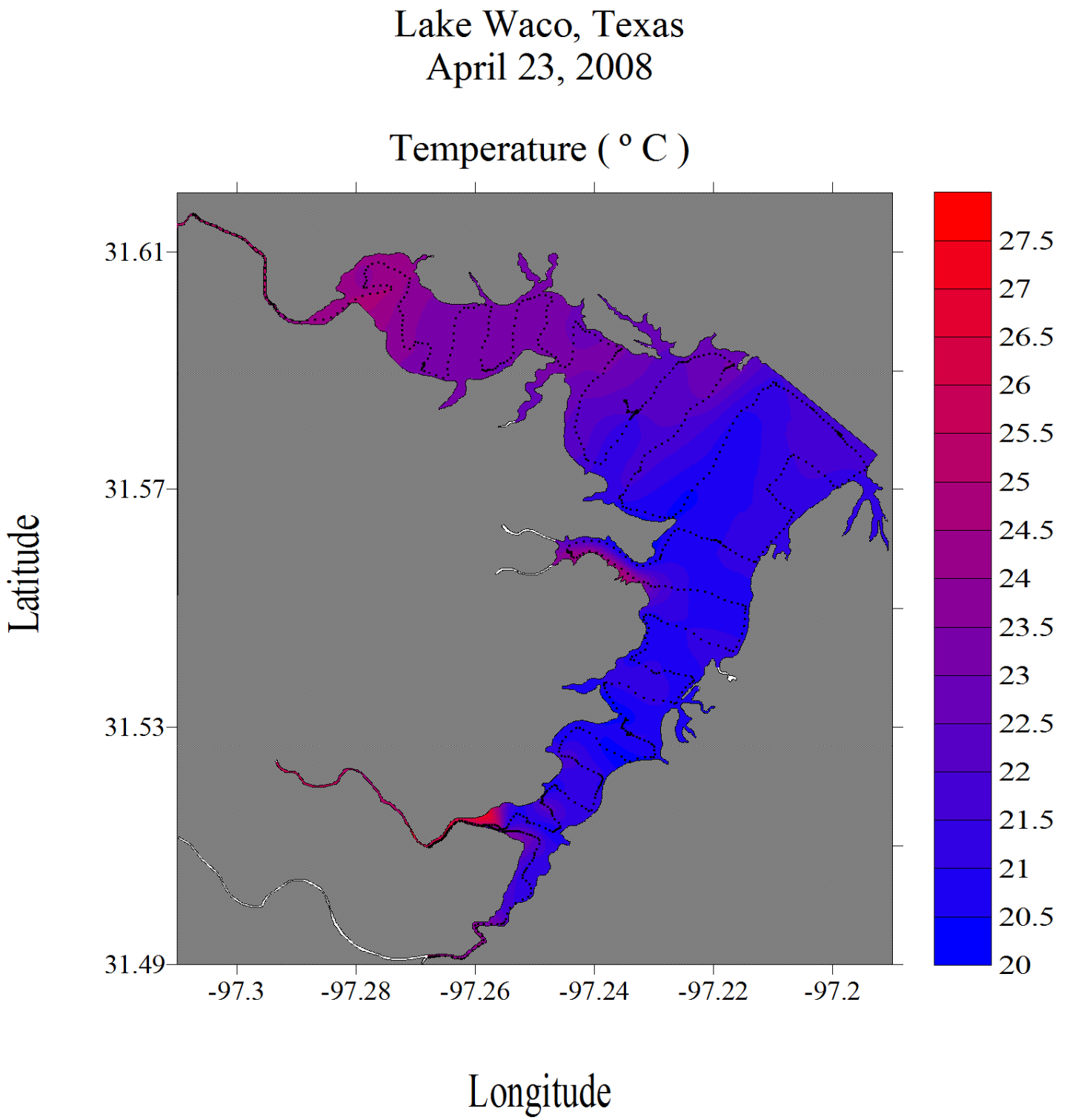

Figure G-23. Temperature dataflow map for Lake Waco

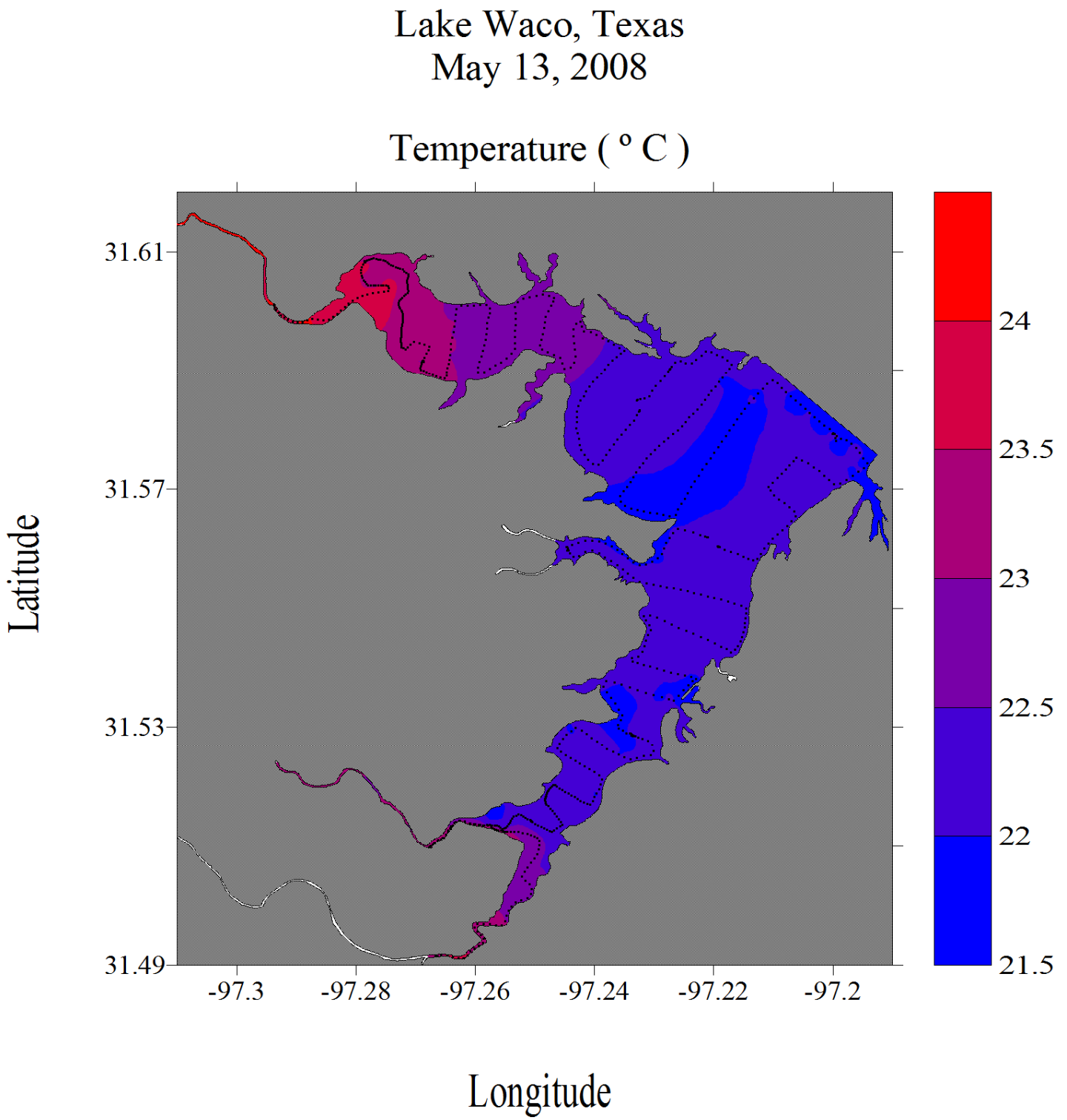

Figure G-24. Temperature dataflow map for Lake Waco

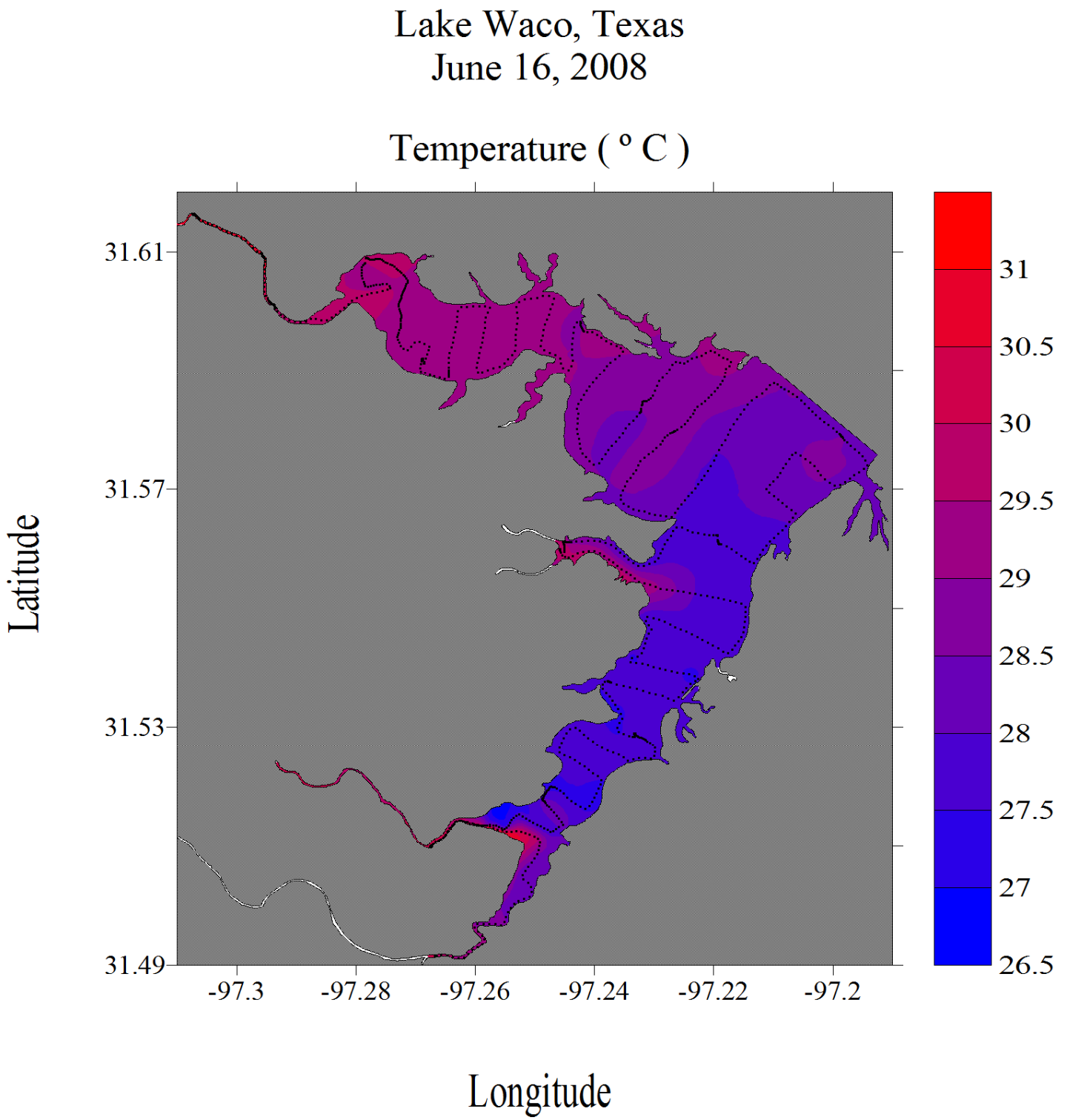

Figure G-25. Temperature dataflow map for Lake Waco

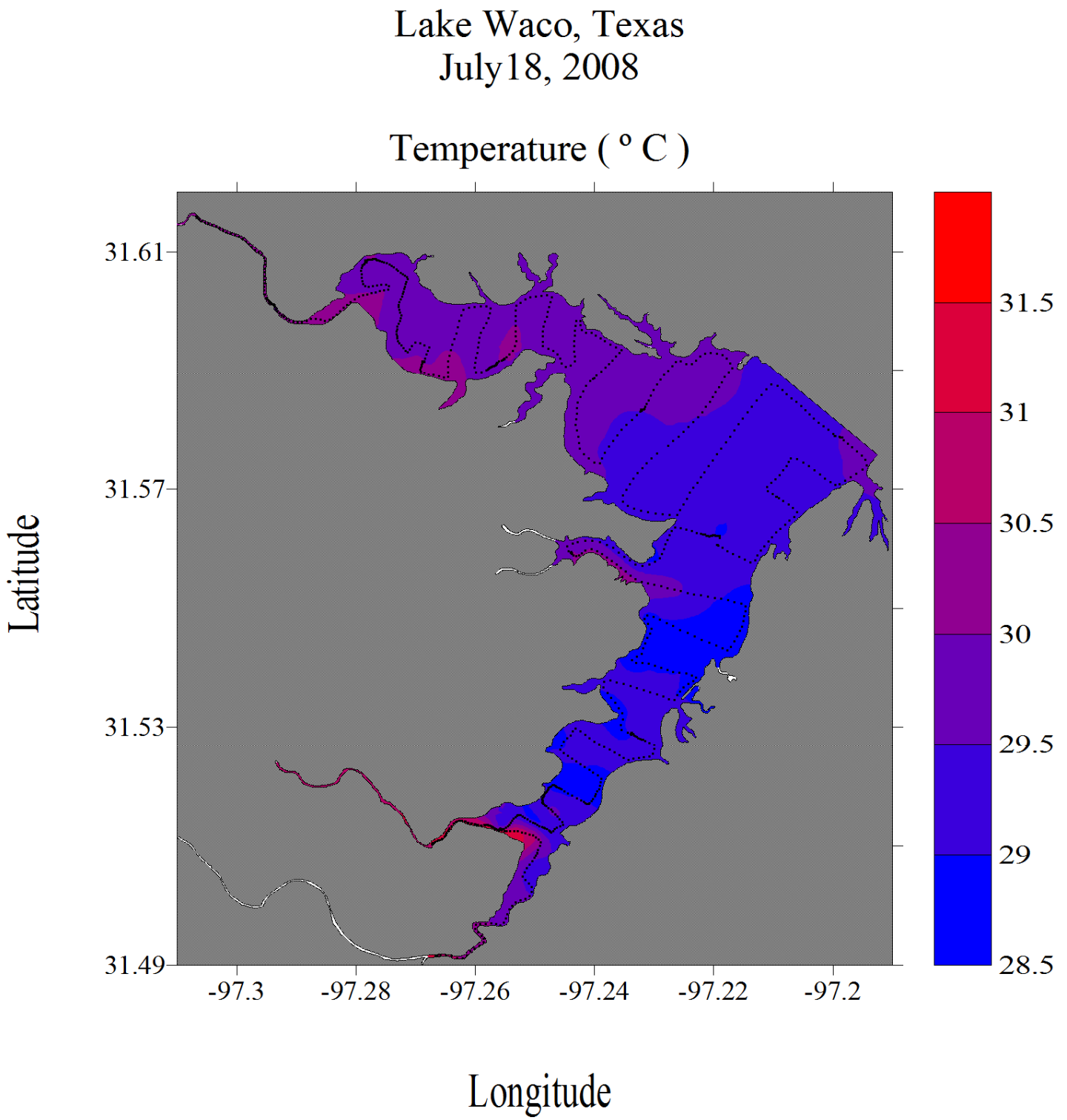

Figure G-26. Temperature dataflow map for Lake Waco

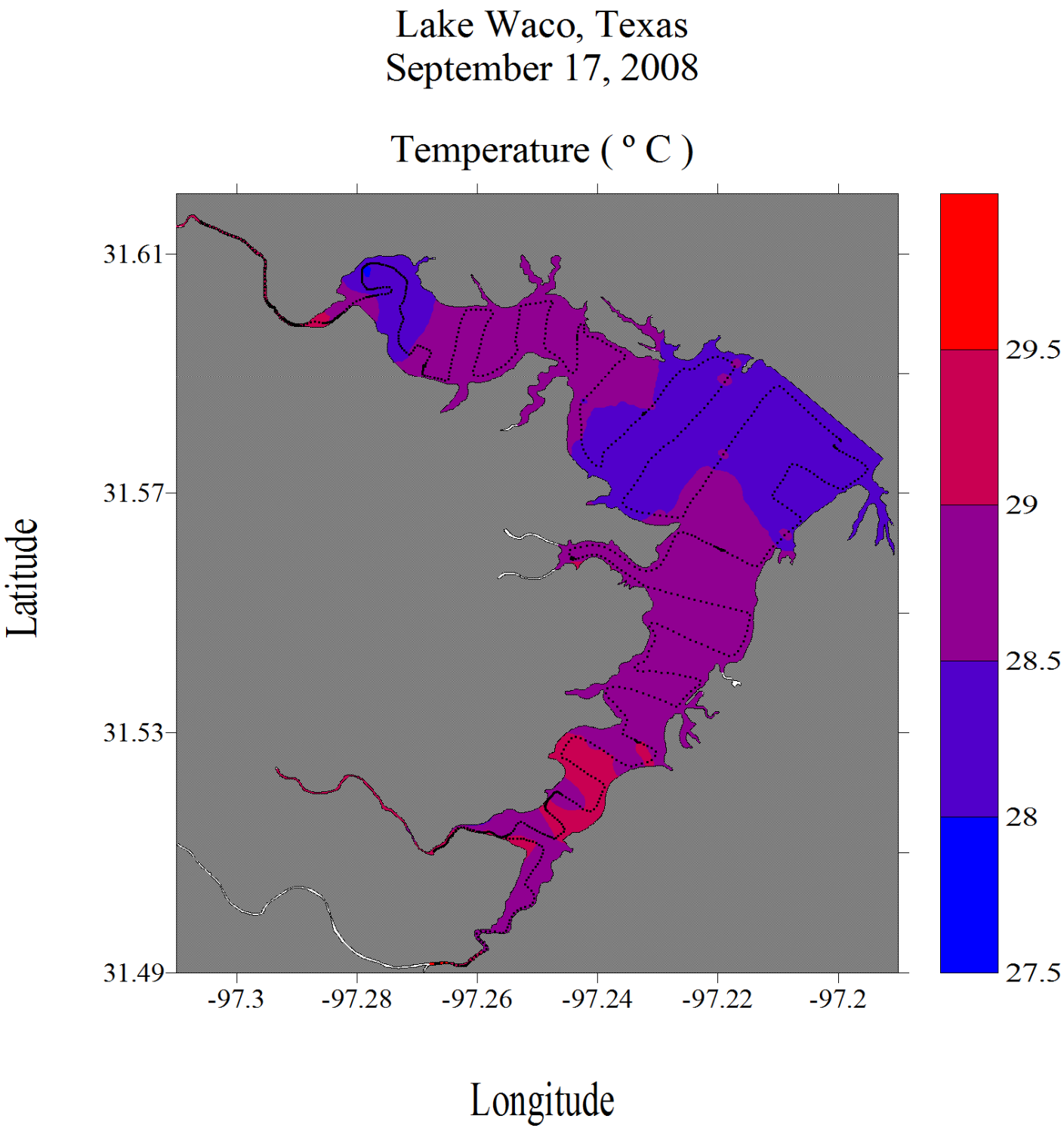

Figure G-27. Temperature dataflow map for Lake Waco

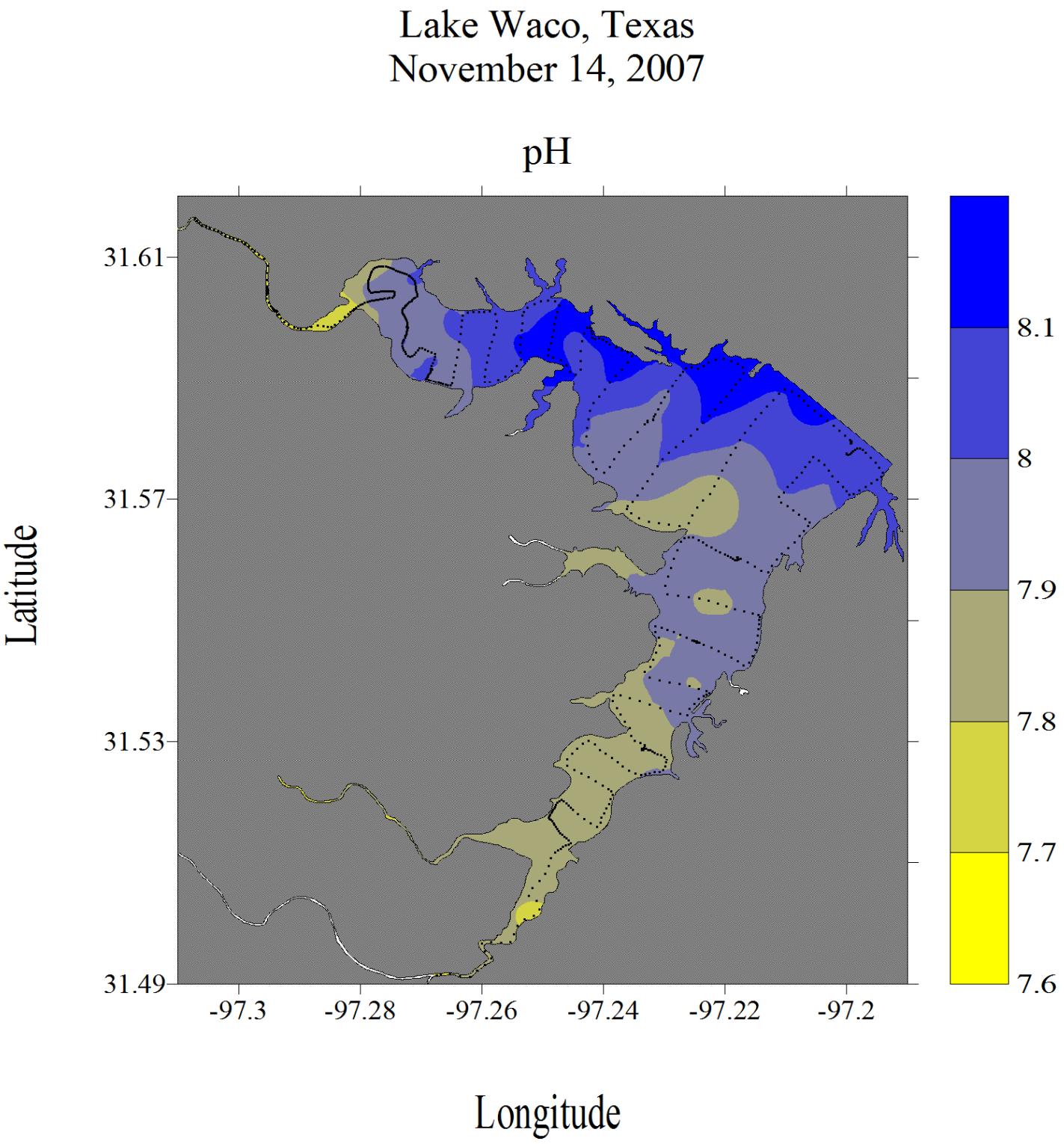

Figure G-28. pH dataflow map for Lake Waco

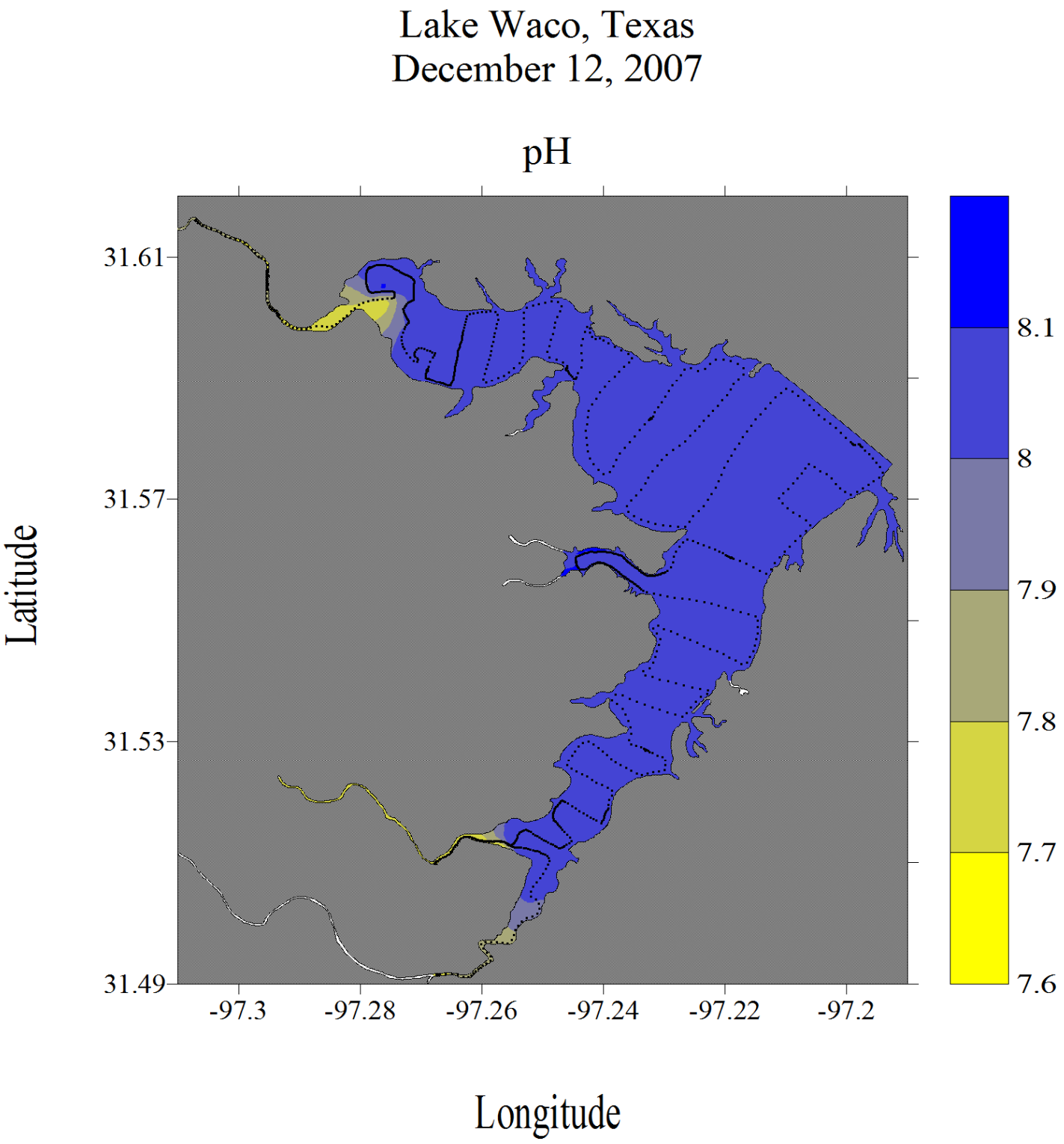

Figure G-29. pH dataflow map for Lake Waco

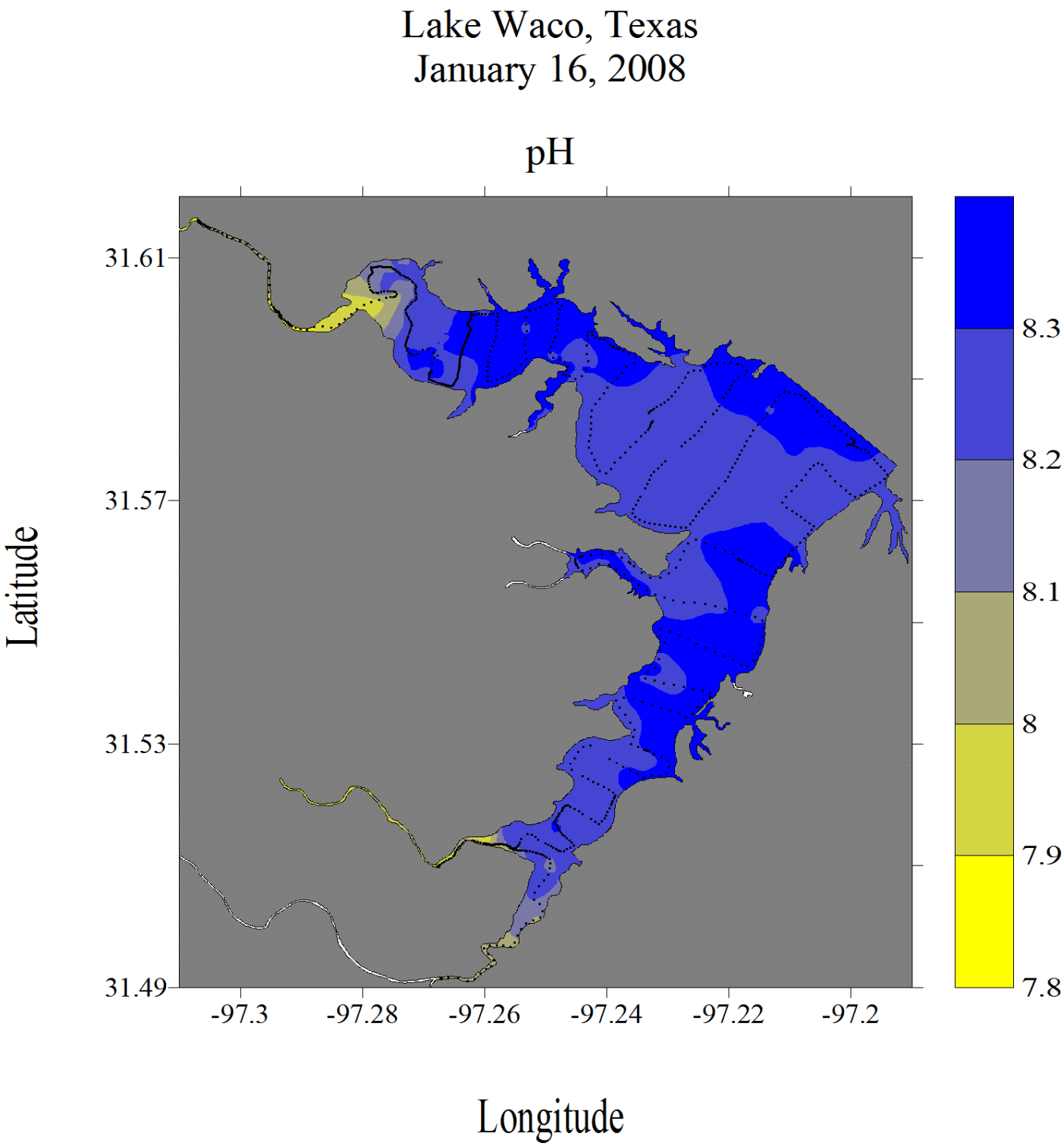

Figure G-30. pH dataflow map for Lake Waco

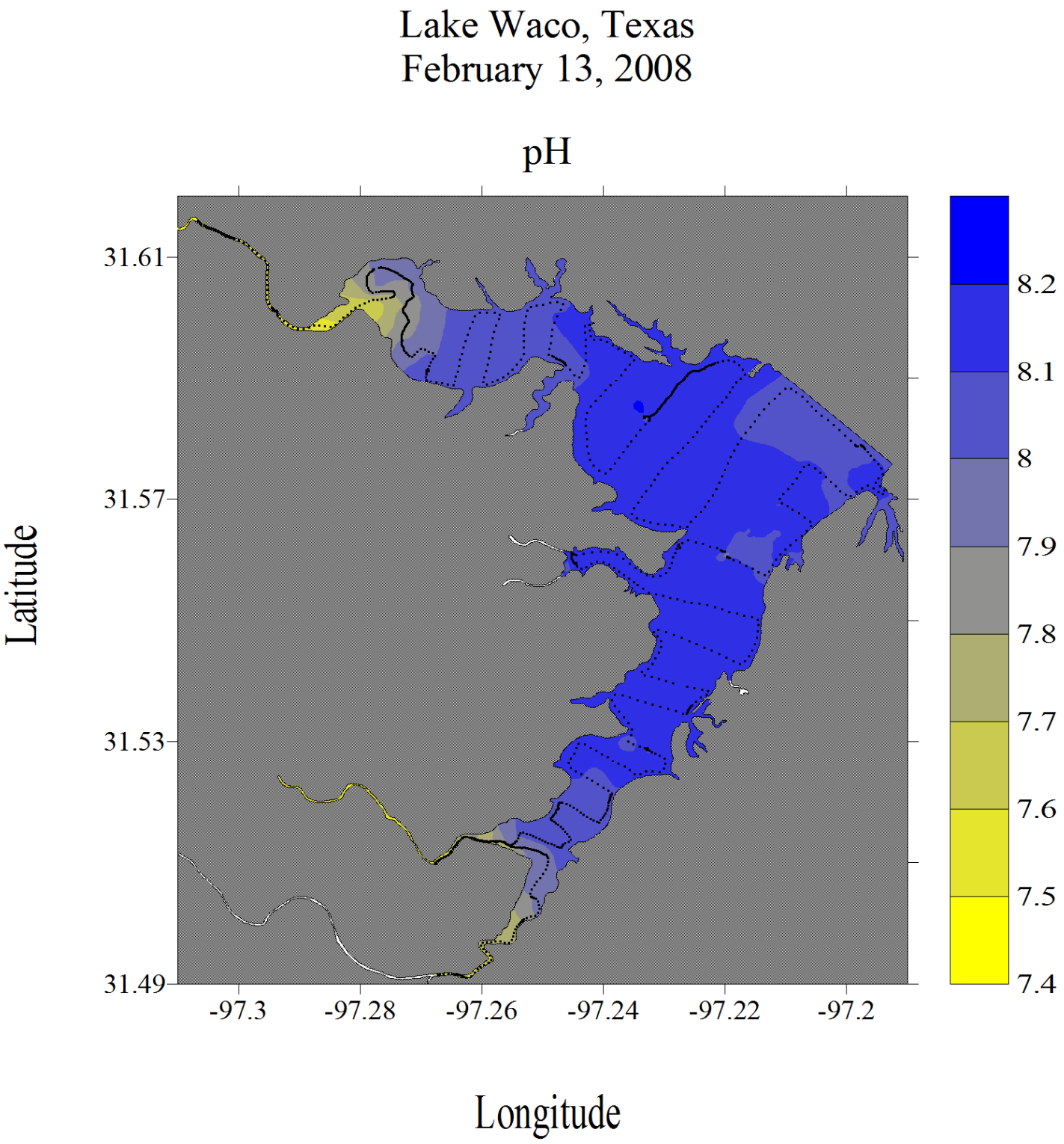

Figure G-31. pH dataflow map for Lake Waco

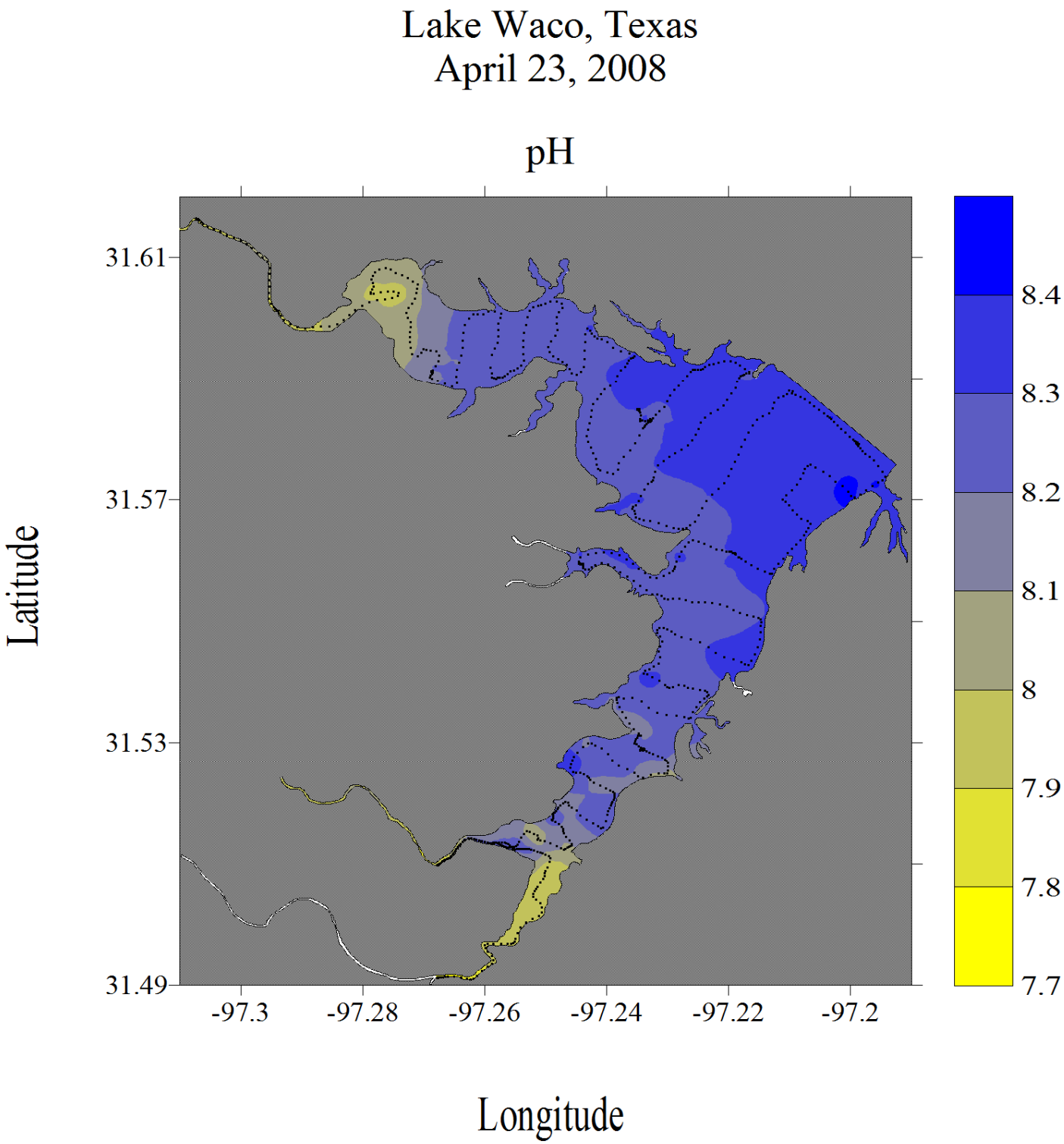

Figure G-32. pH dataflow map for Lake Waco

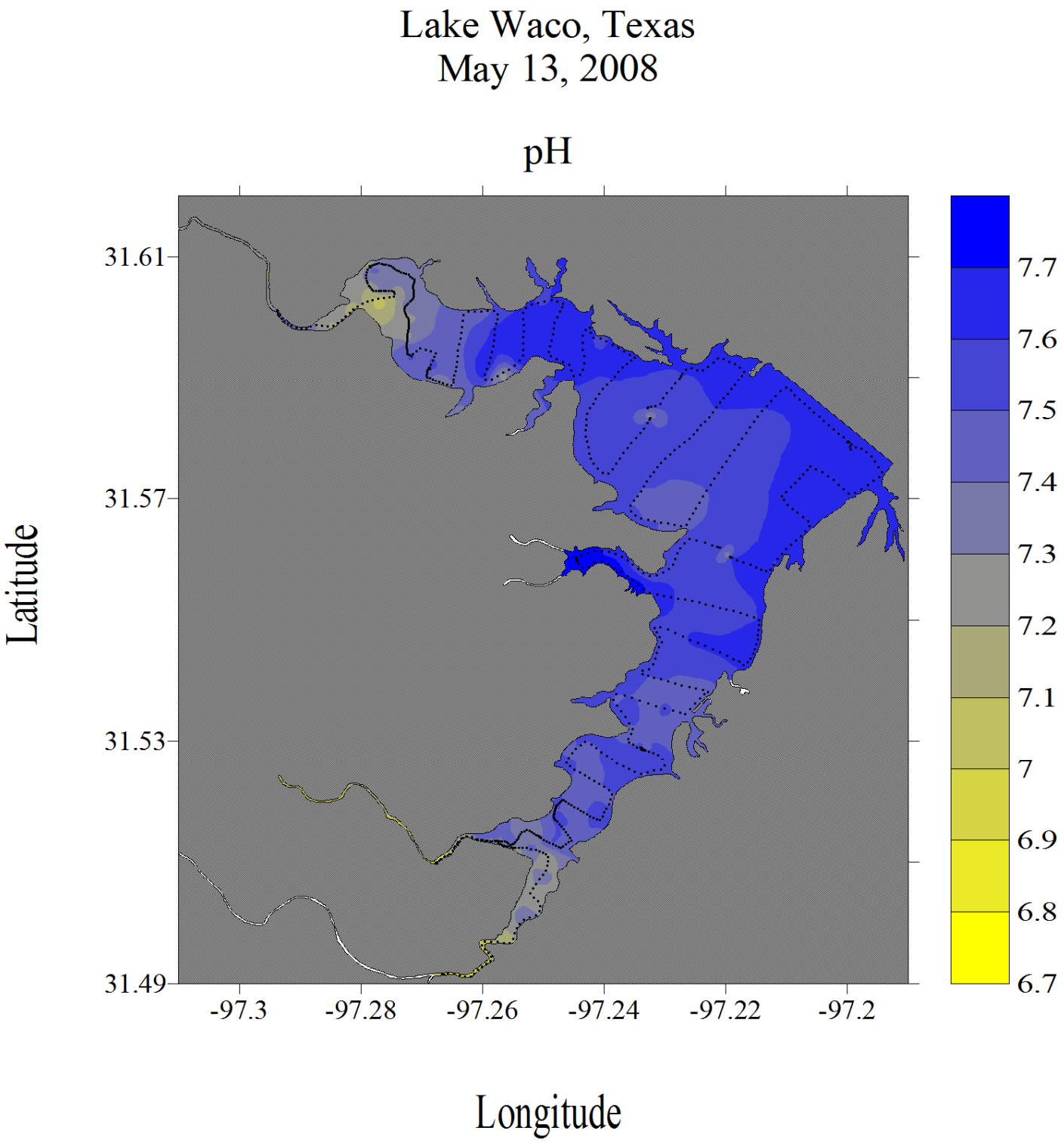

Figure G-33. pH dataflow map for Lake Waco

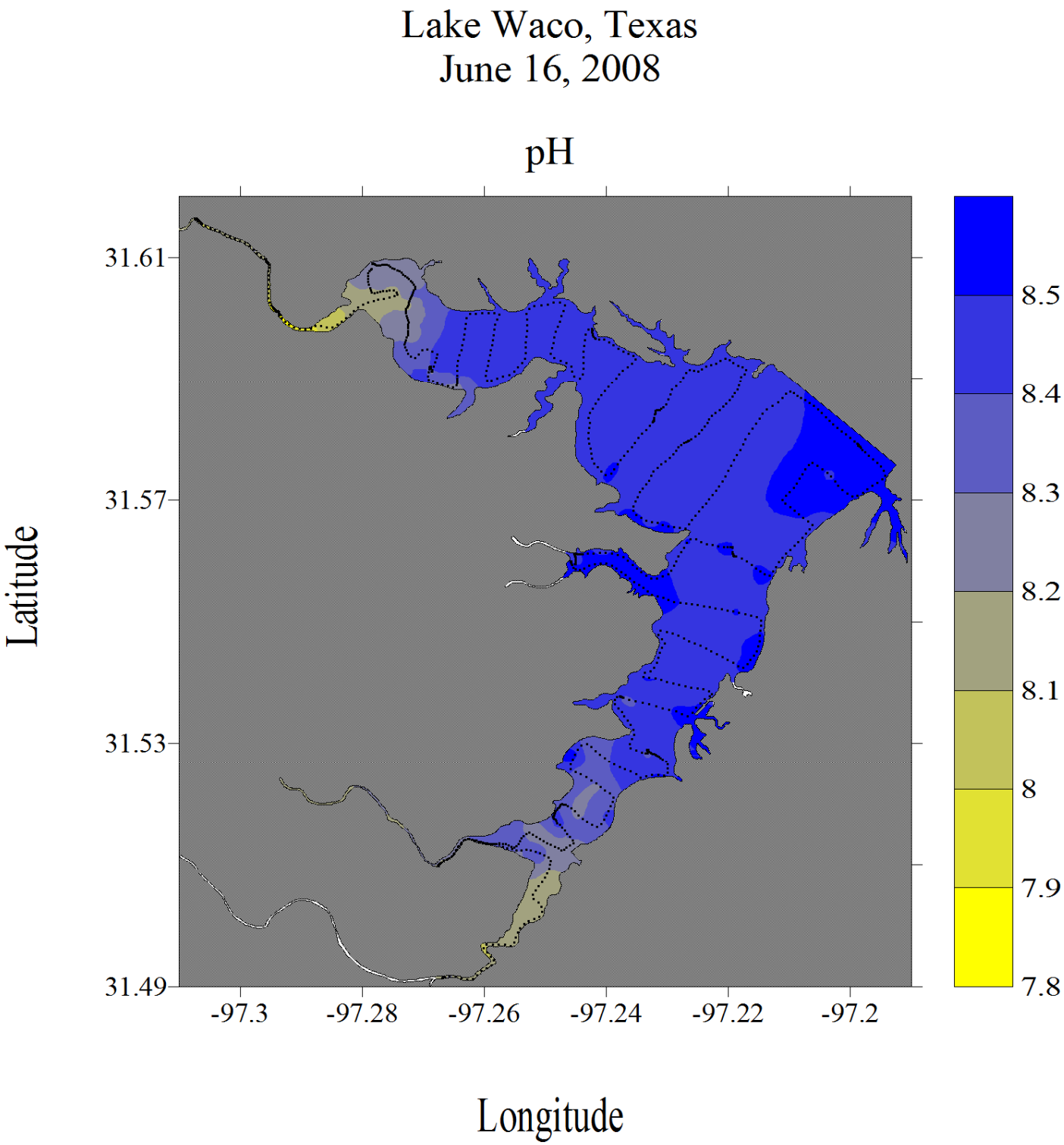

Figure G-34. pH dataflow map for Lake Waco

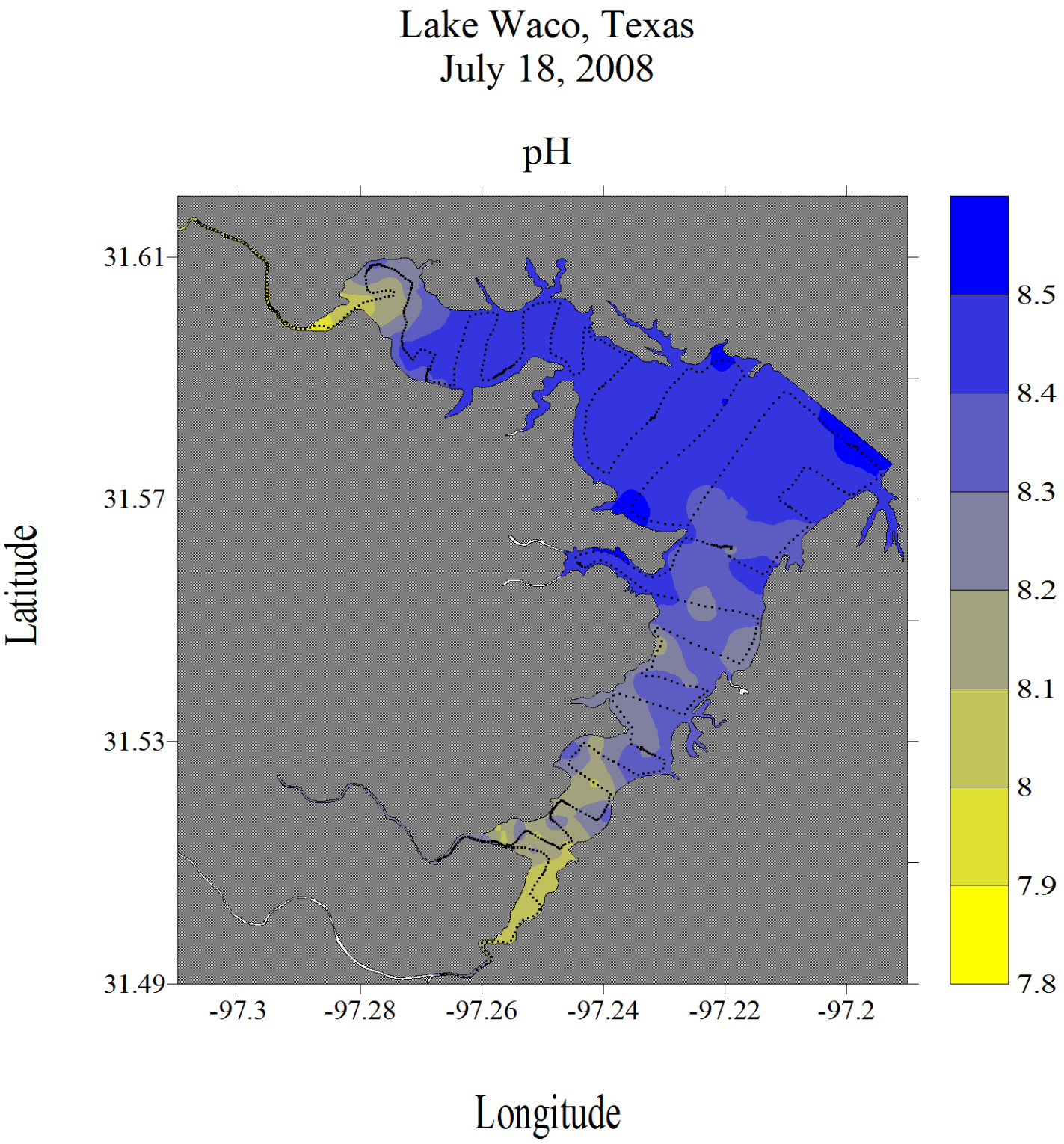

Figure G-35. pH dataflow map for Lake Waco

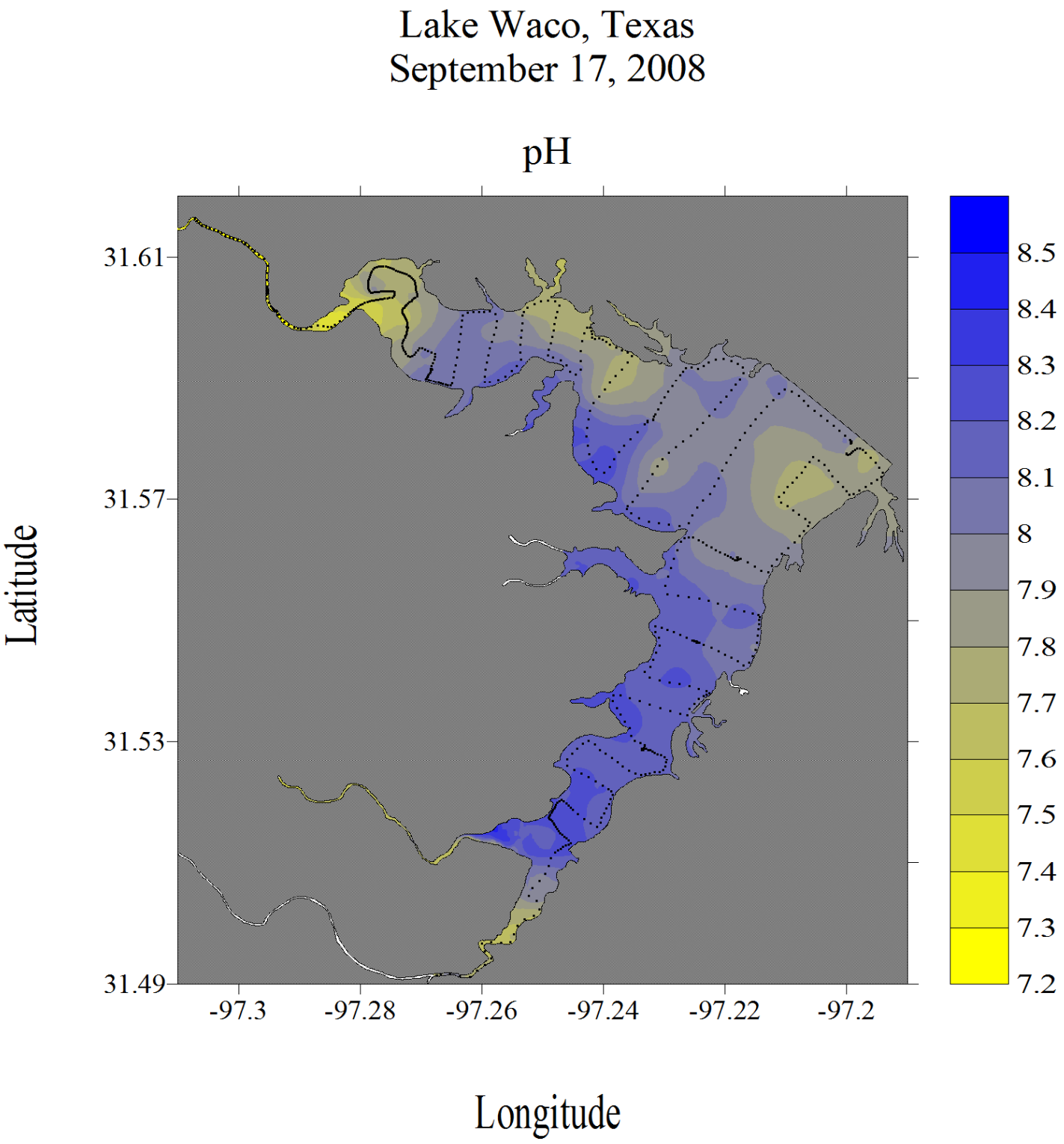

Figure G-36. pH dataflow map for Lake Waco

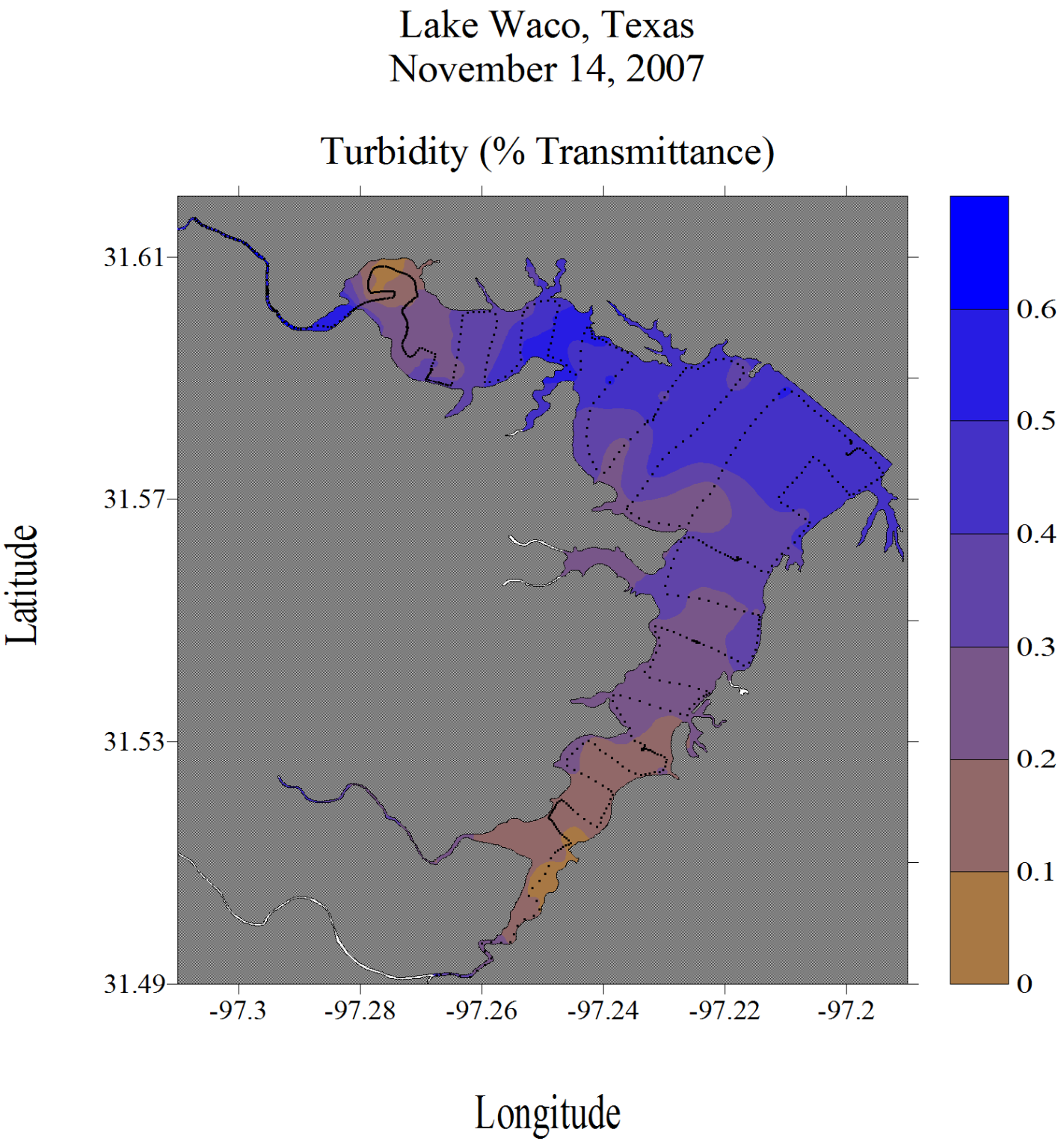

Figure G-37. Turbidity dataflow map for Lake Waco

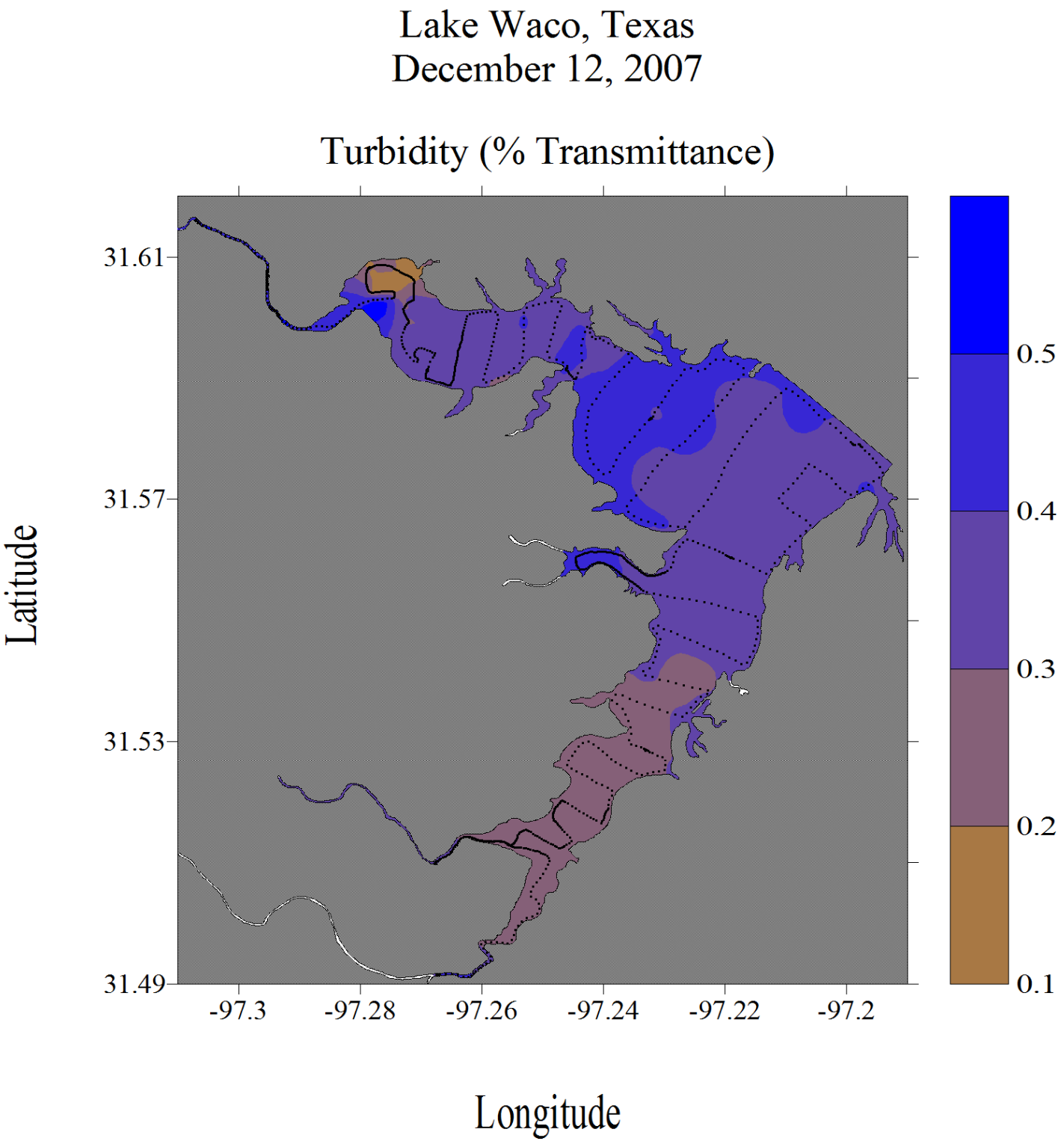

Figure G-38. Turbidity dataflow map for Lake Waco

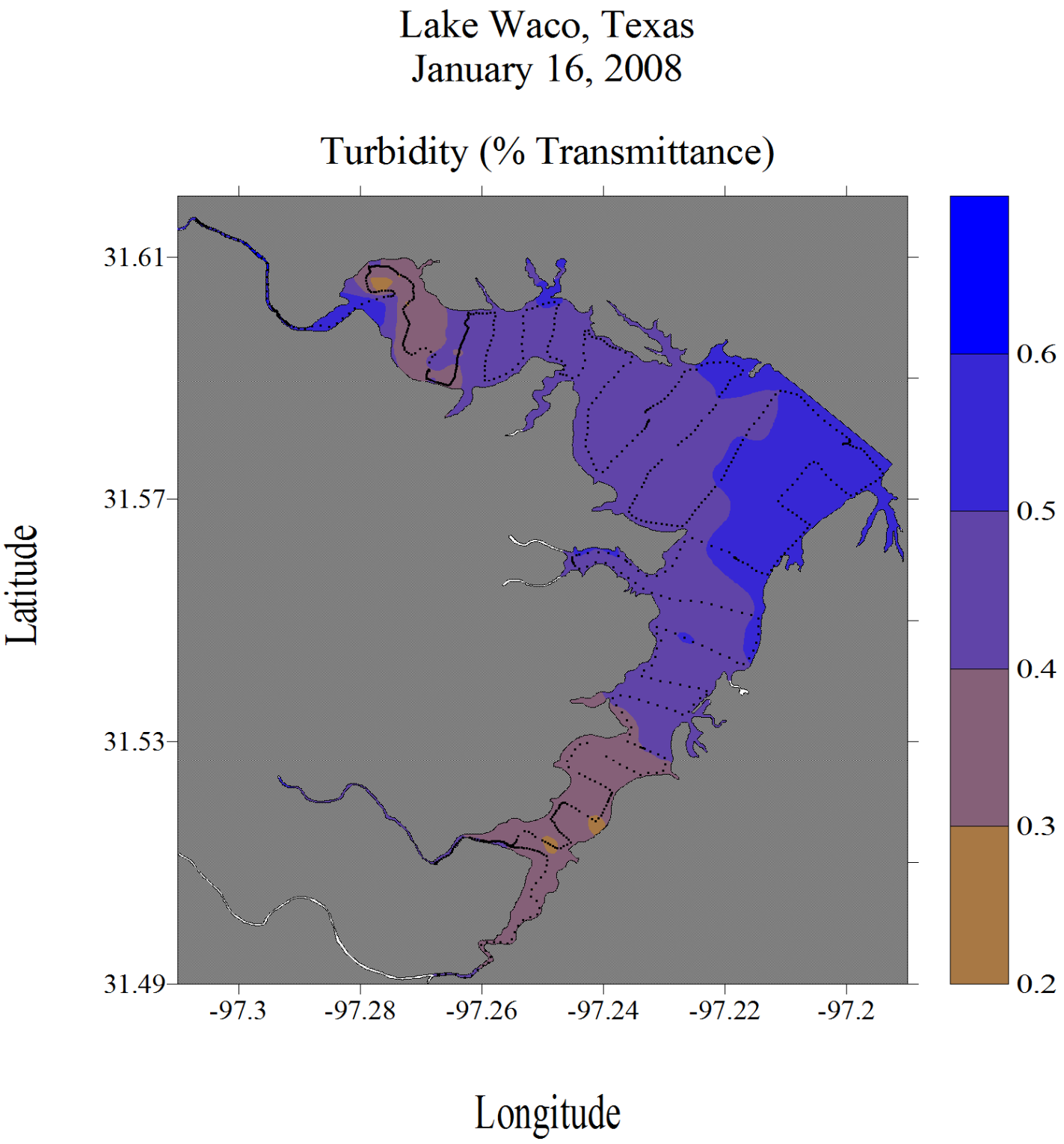

Figure G-39. Turbidity dataflow map for Lake Waco

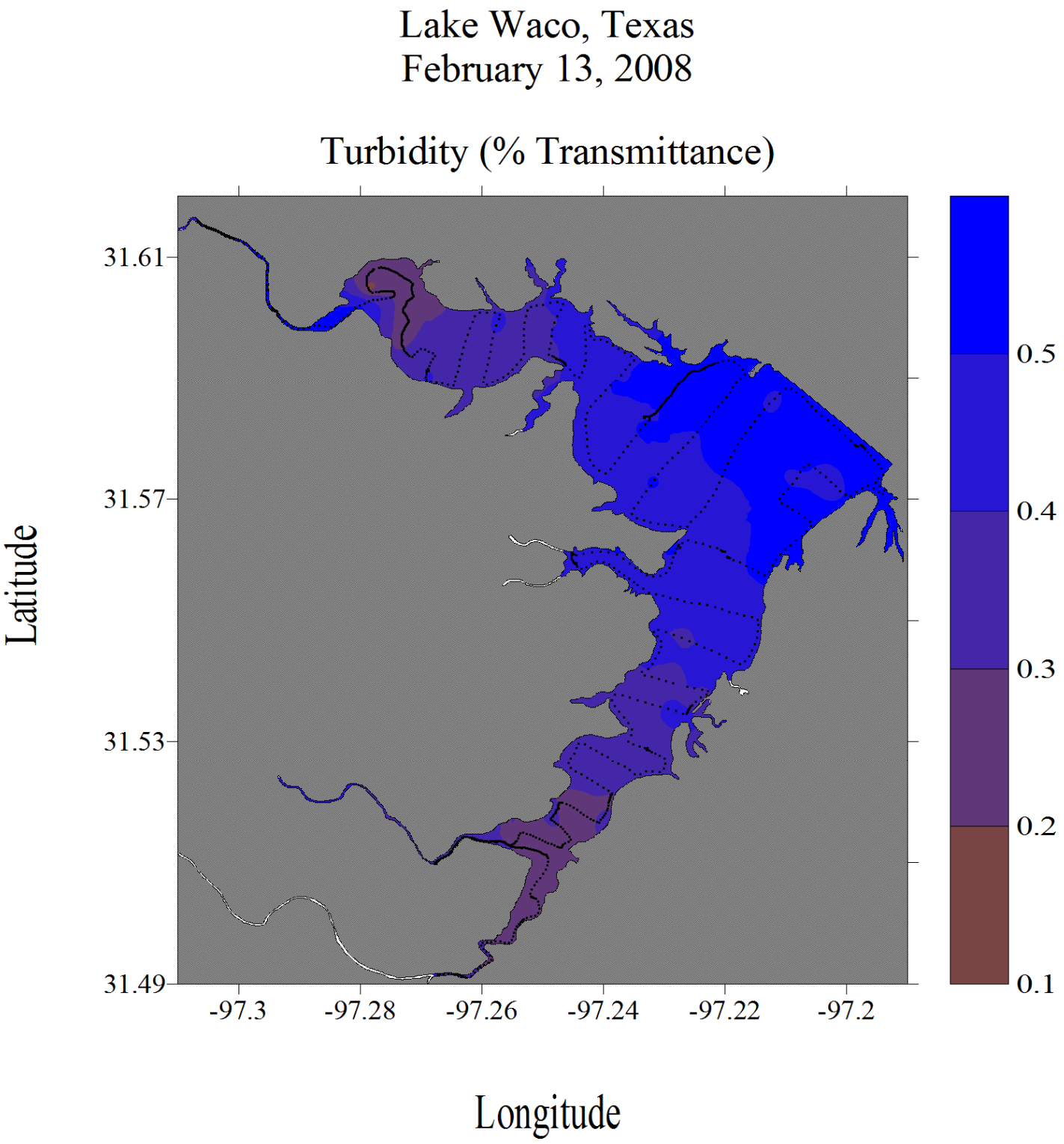

Figure G-40. Turbidity dataflow map for Lake Waco

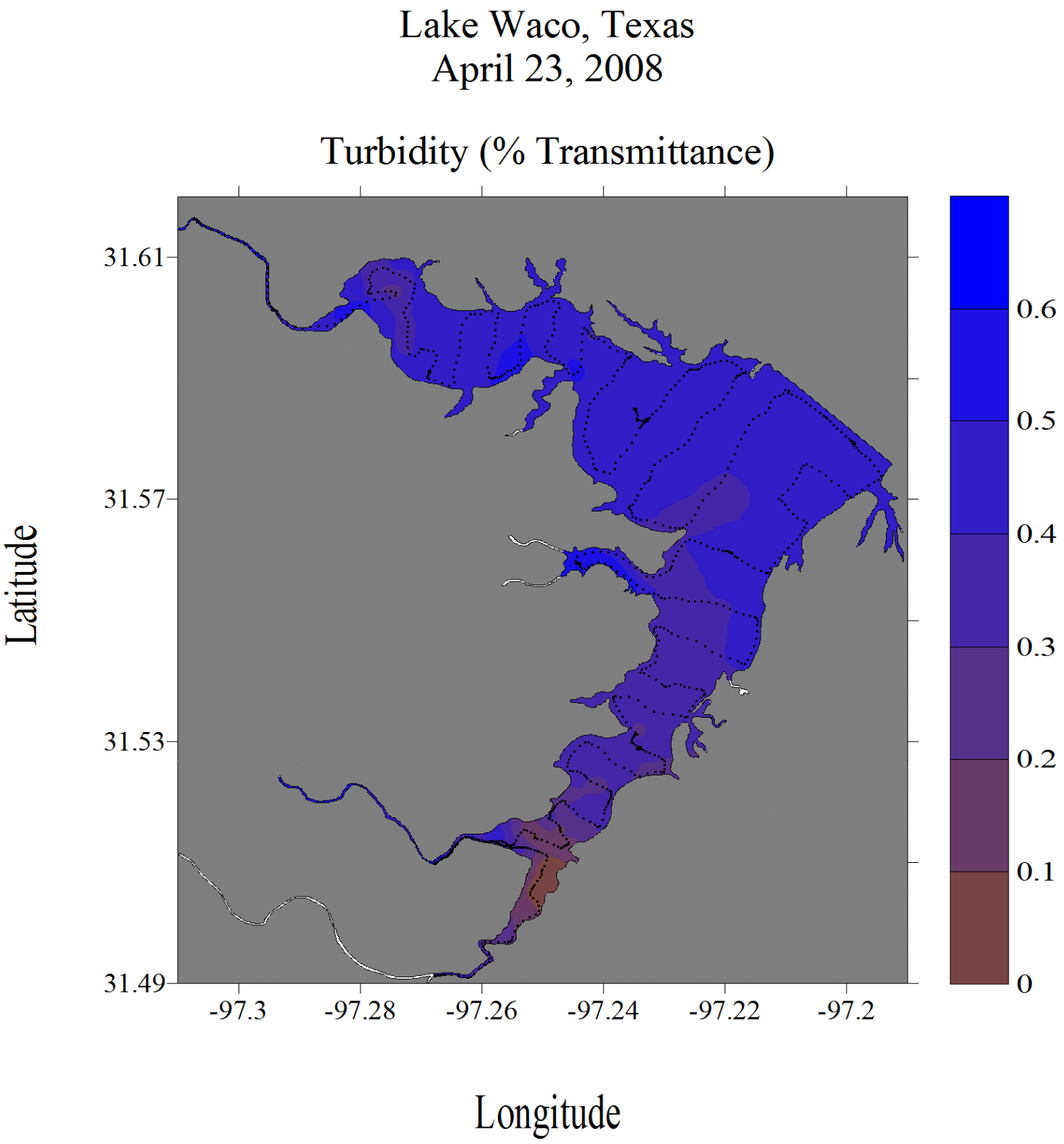

Figure G-41. Turbidity dataflow map for Lake Waco

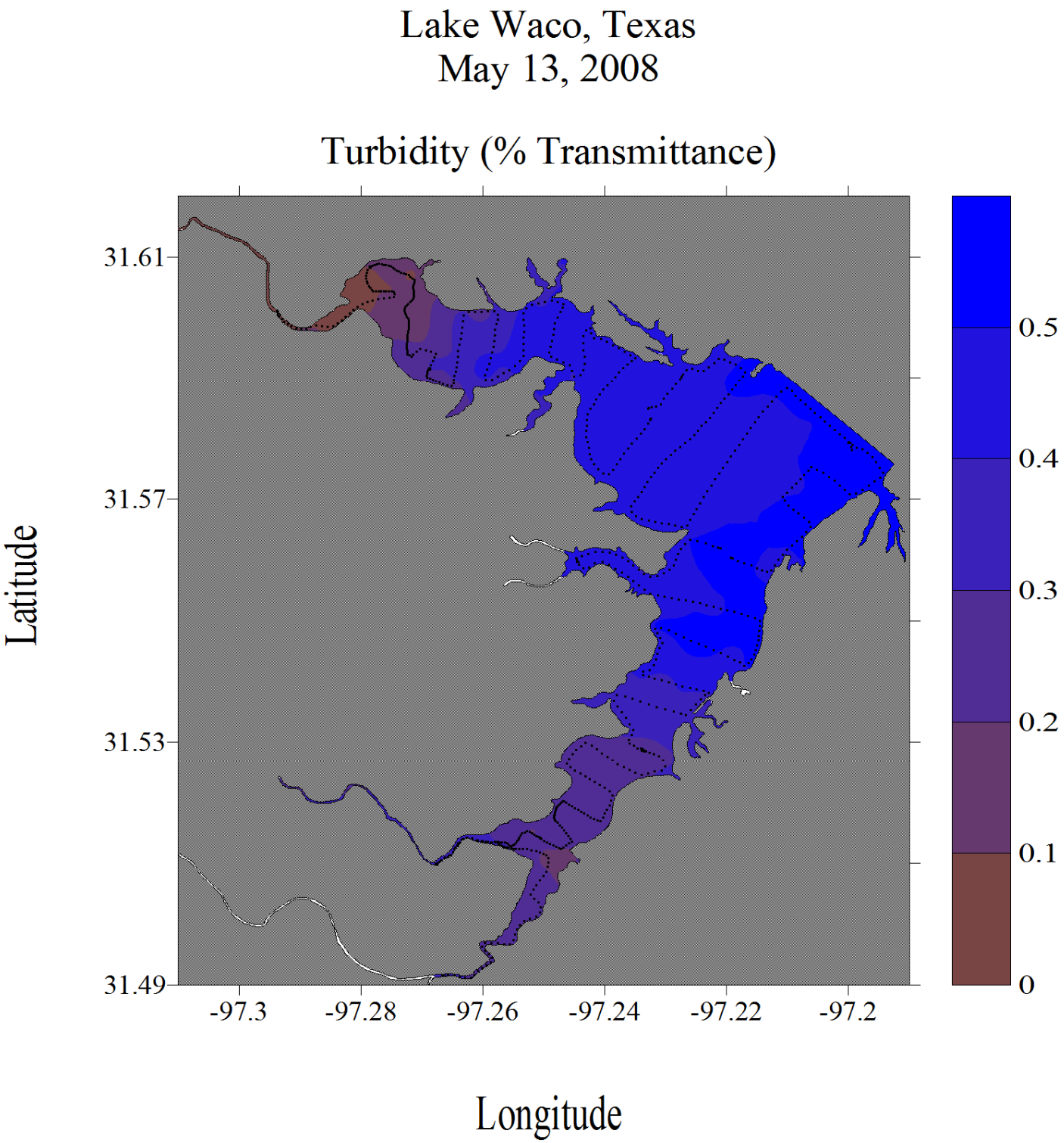

Figure G-42. Turbidity dataflow map for Lake Waco

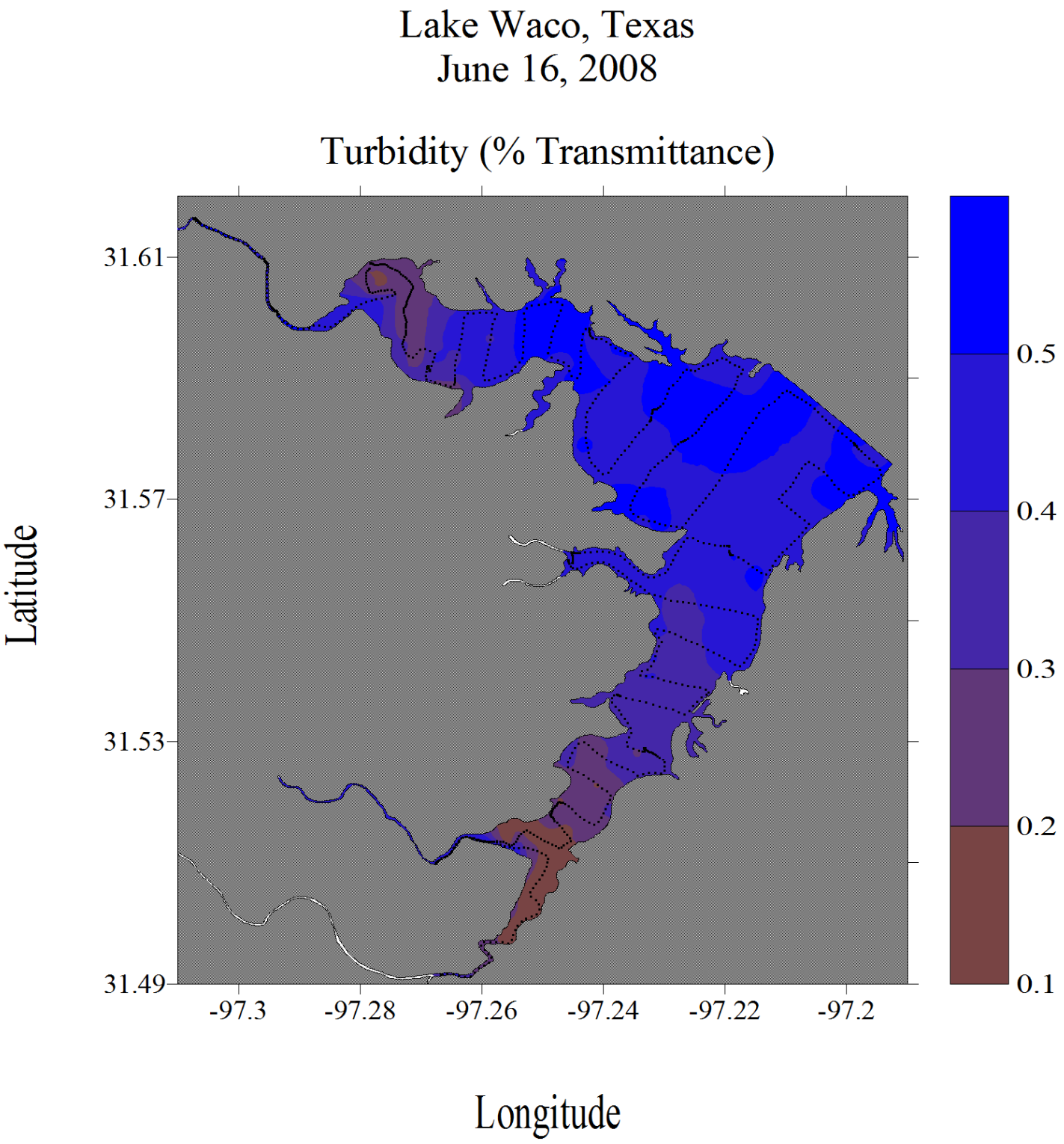

Figure G-43. Turbidity dataflow map for Lake Waco

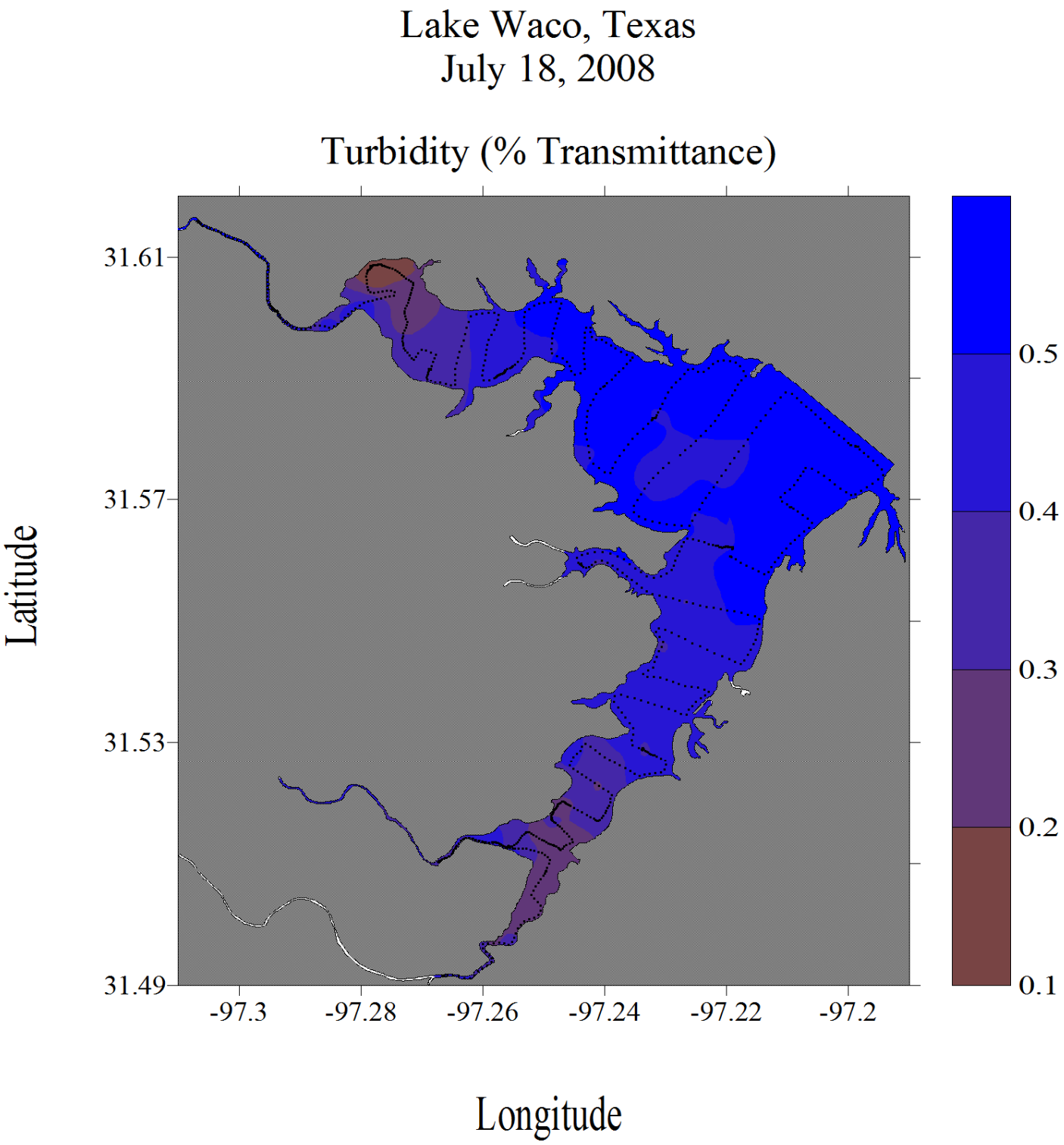

Figure G-44. Turbidity dataflow map for Lake Waco

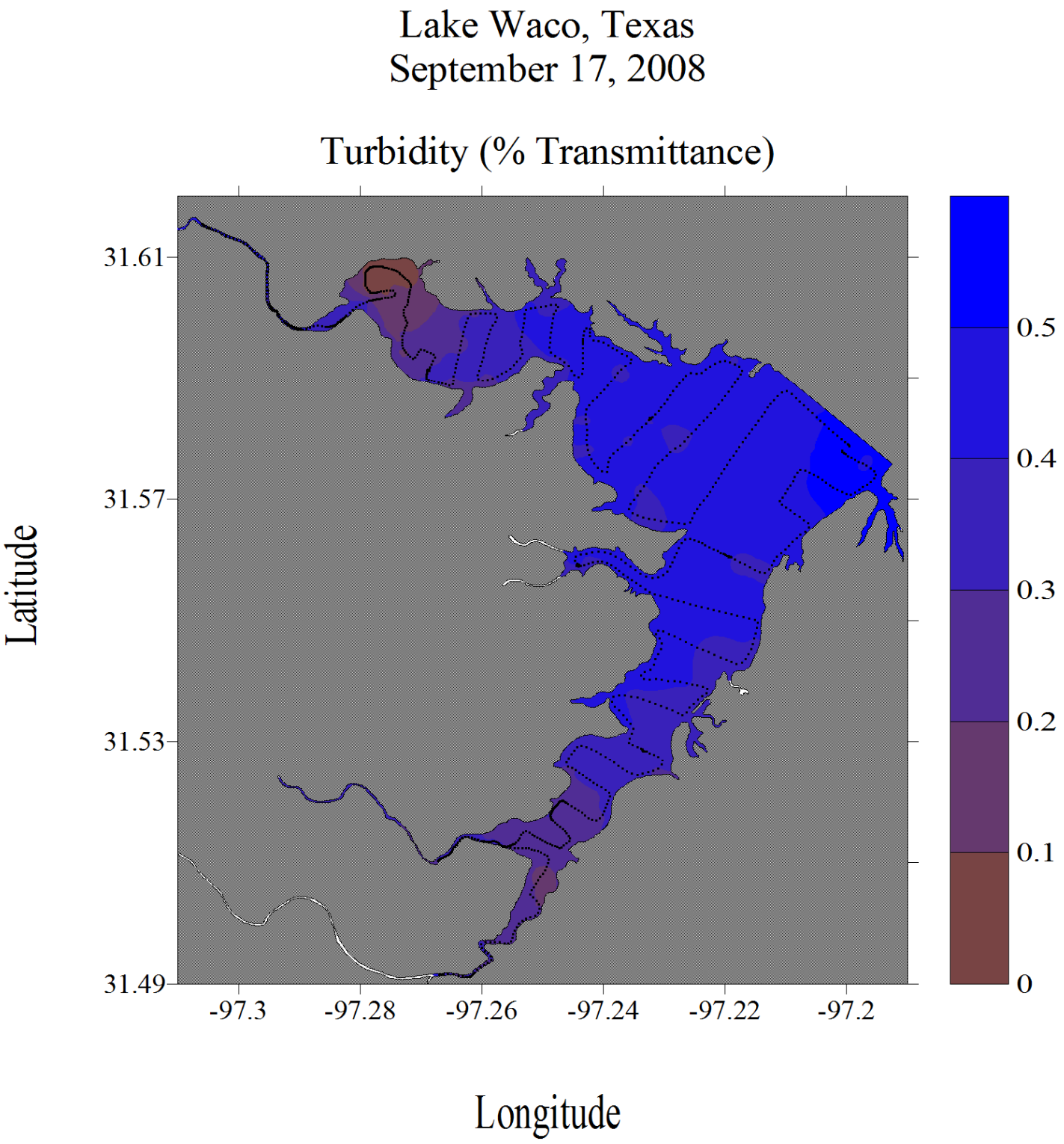

Figure G-45. Turbidity dataflow map for Lake Waco

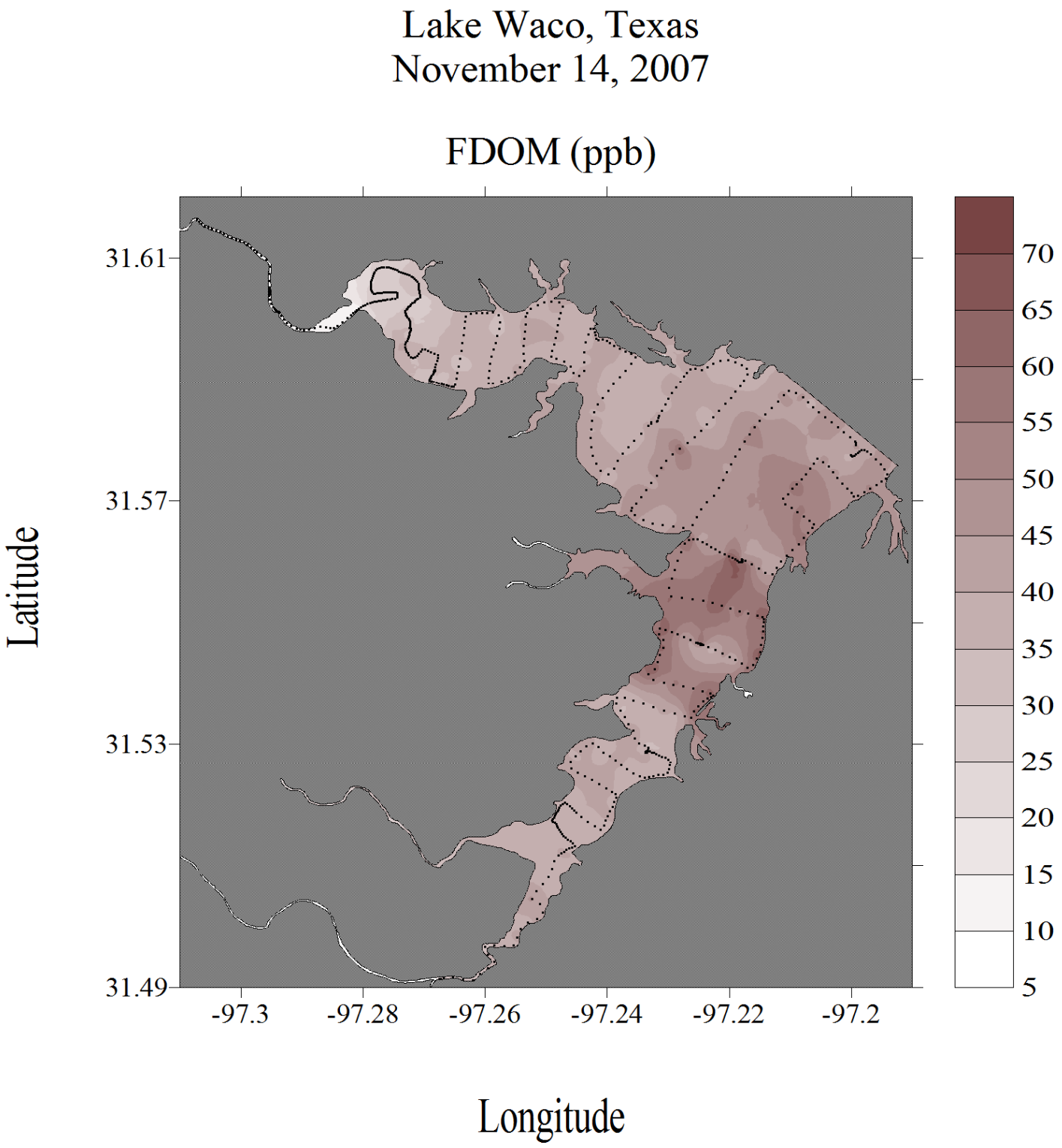

Figure G-46. Dissolved organic matter dataflow map for Lake Waco

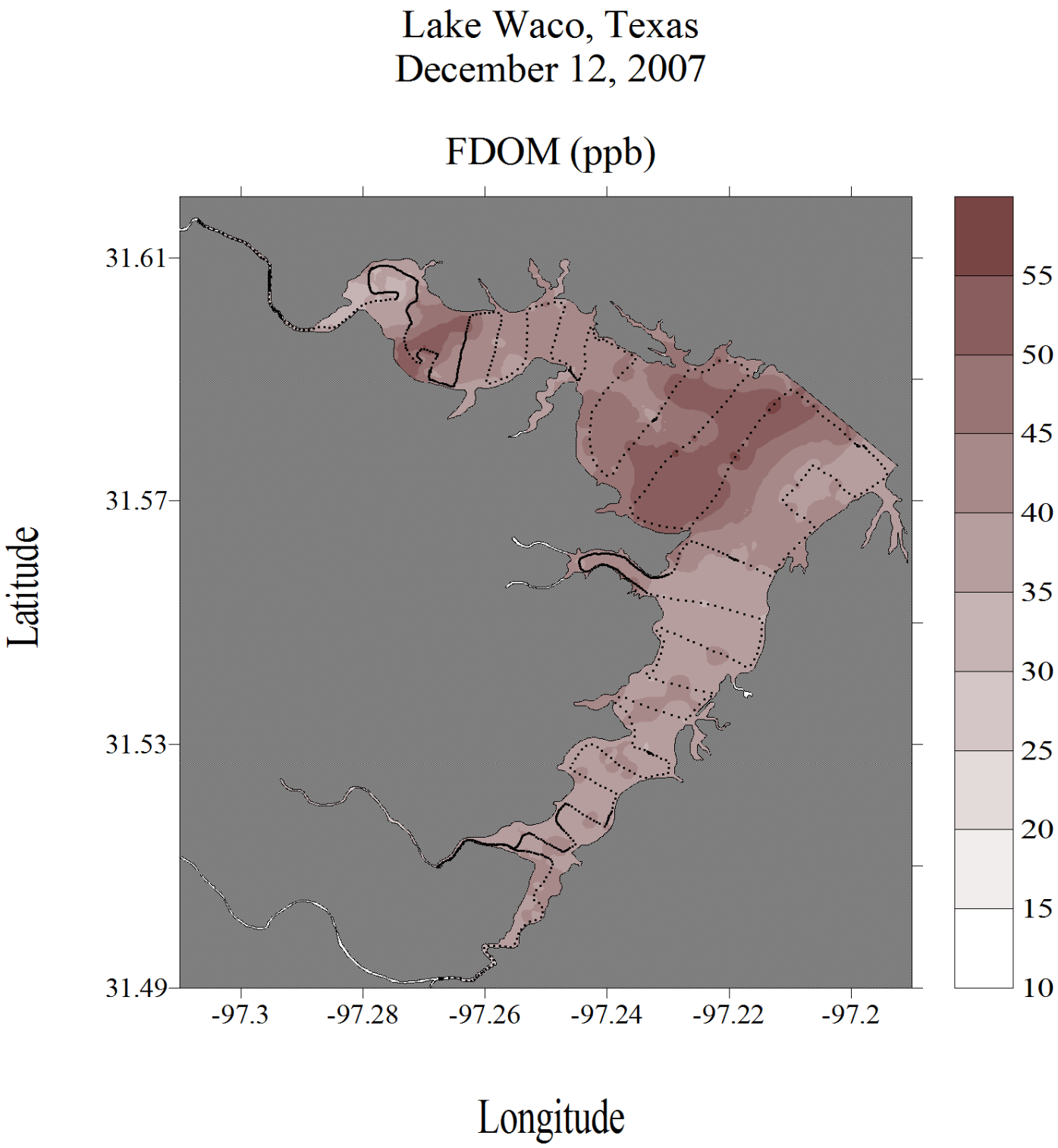

Figure G-47. Dissolved organic matter dataflow map for Lake Waco

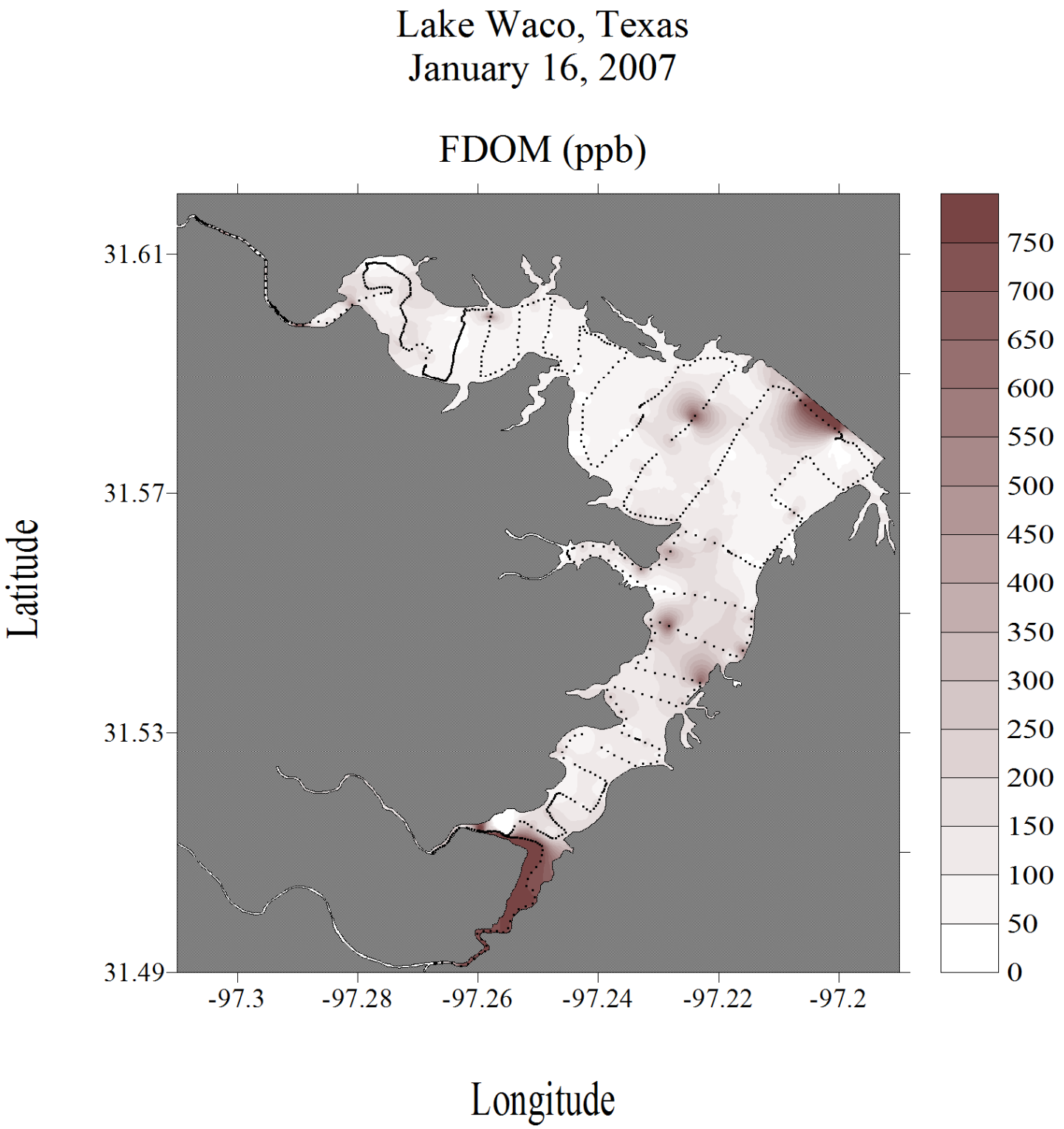

Figure G-48. Dissolved organic matter dataflow map for Lake Waco

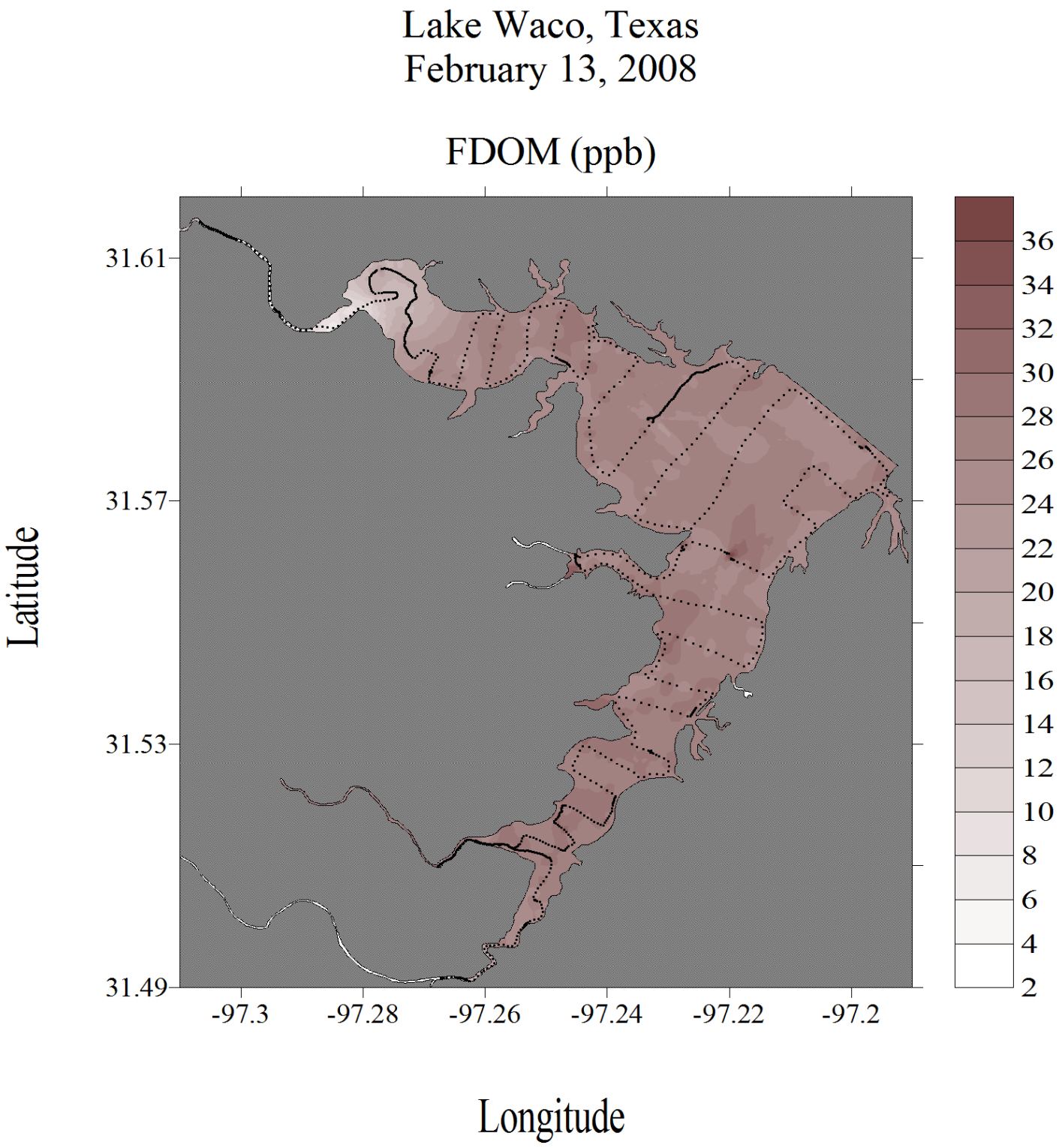

Figure G-49. Dissolved organic matter dataflow map for Lake Waco

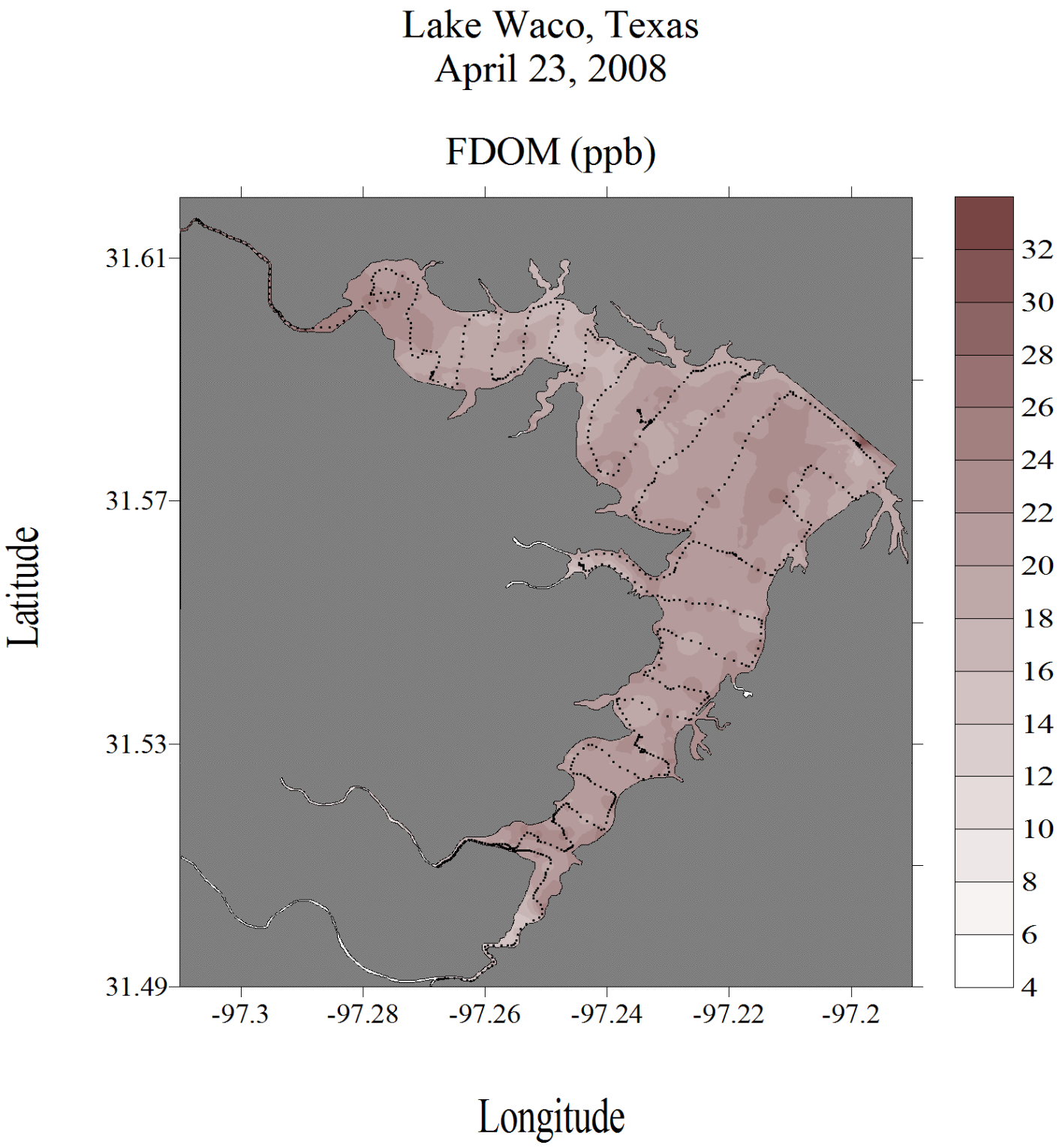

Figure G-50. Dissolved organic matter dataflow map for Lake Waco

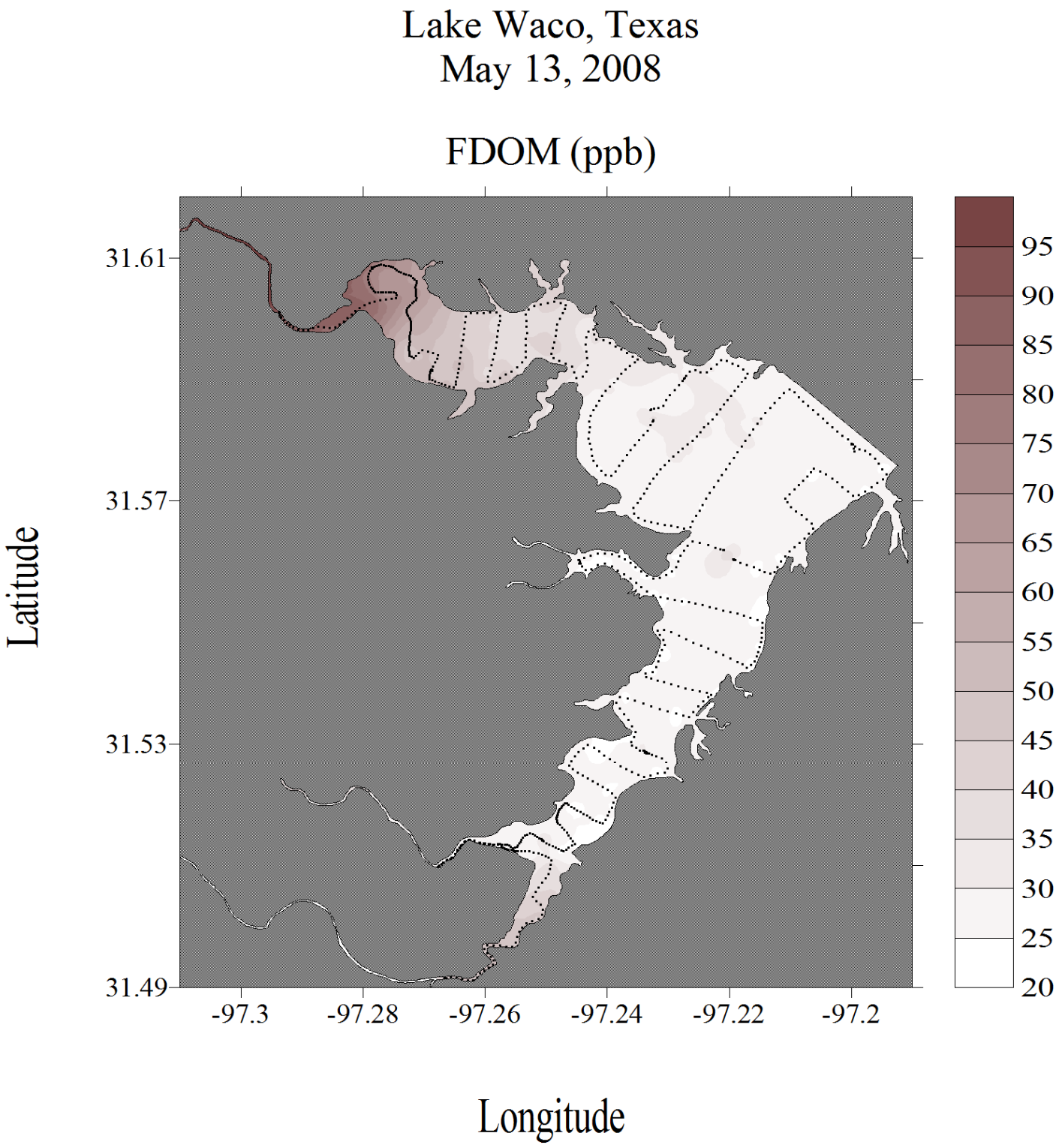

Figure G-51. Dissolved organic matter dataflow map for Lake Waco

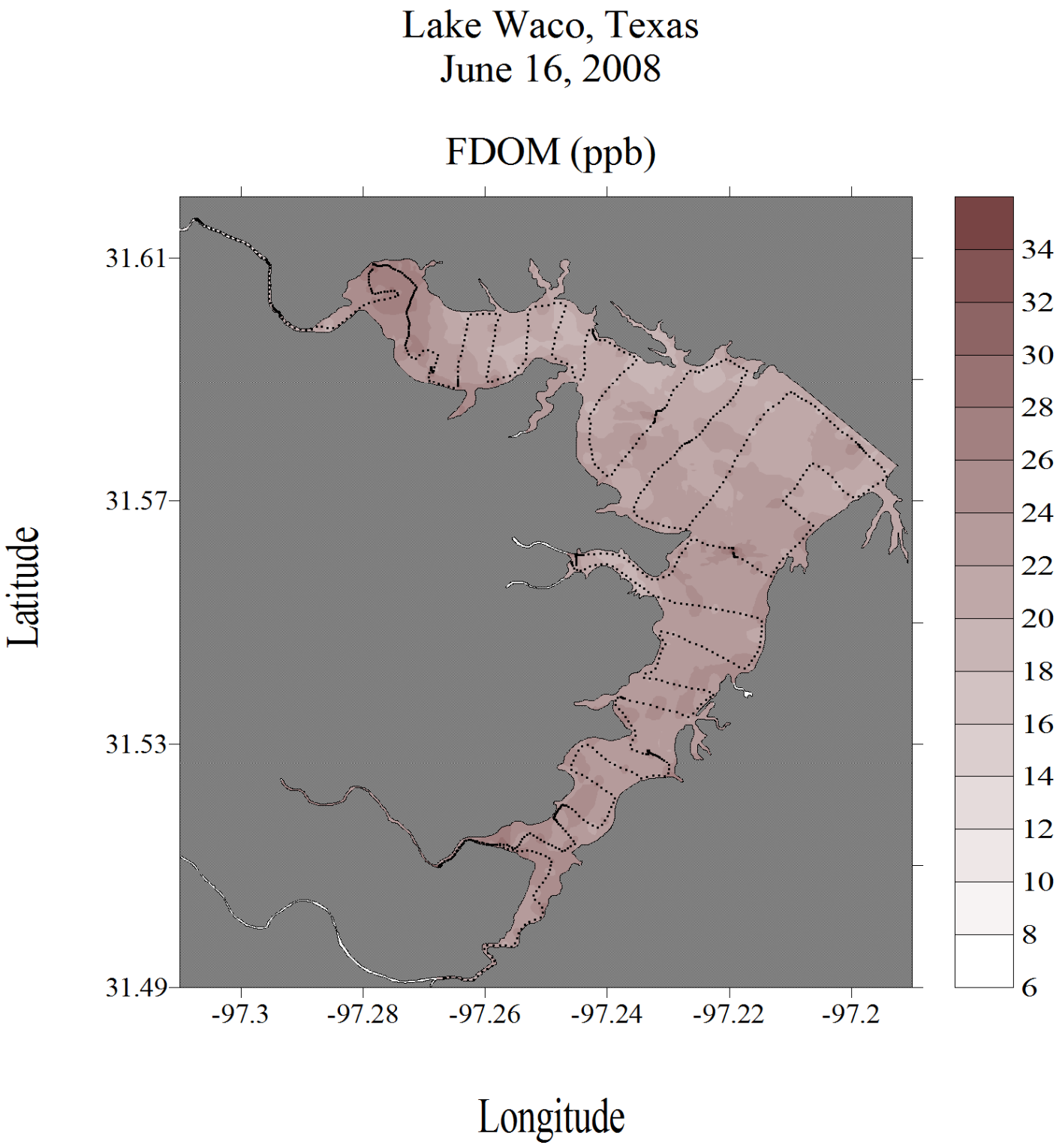

Figure G-52. Dissolved organic matter dataflow map for Lake Waco

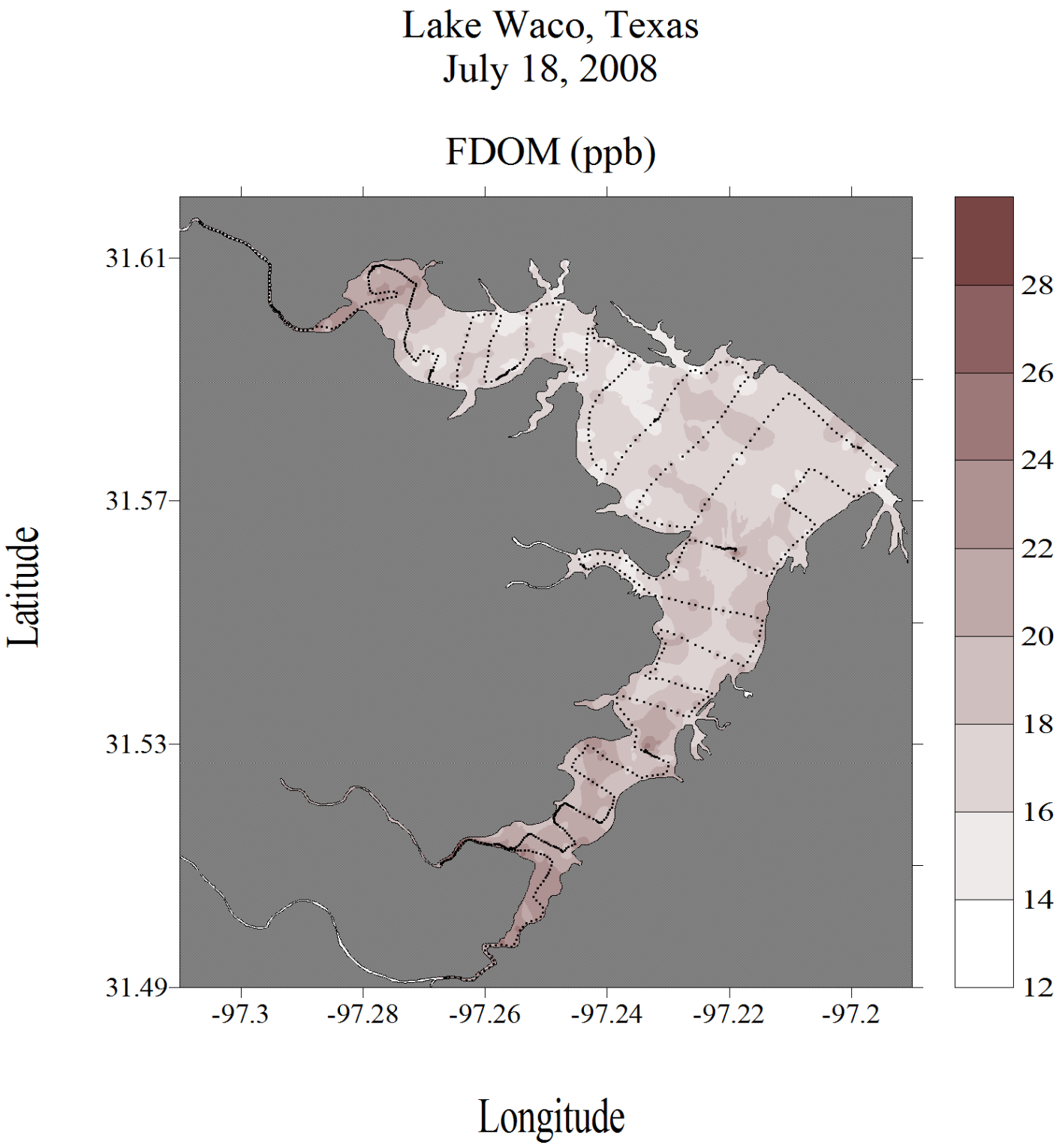

Figure G-53. Dissolved organic matter dataflow map for Lake Waco

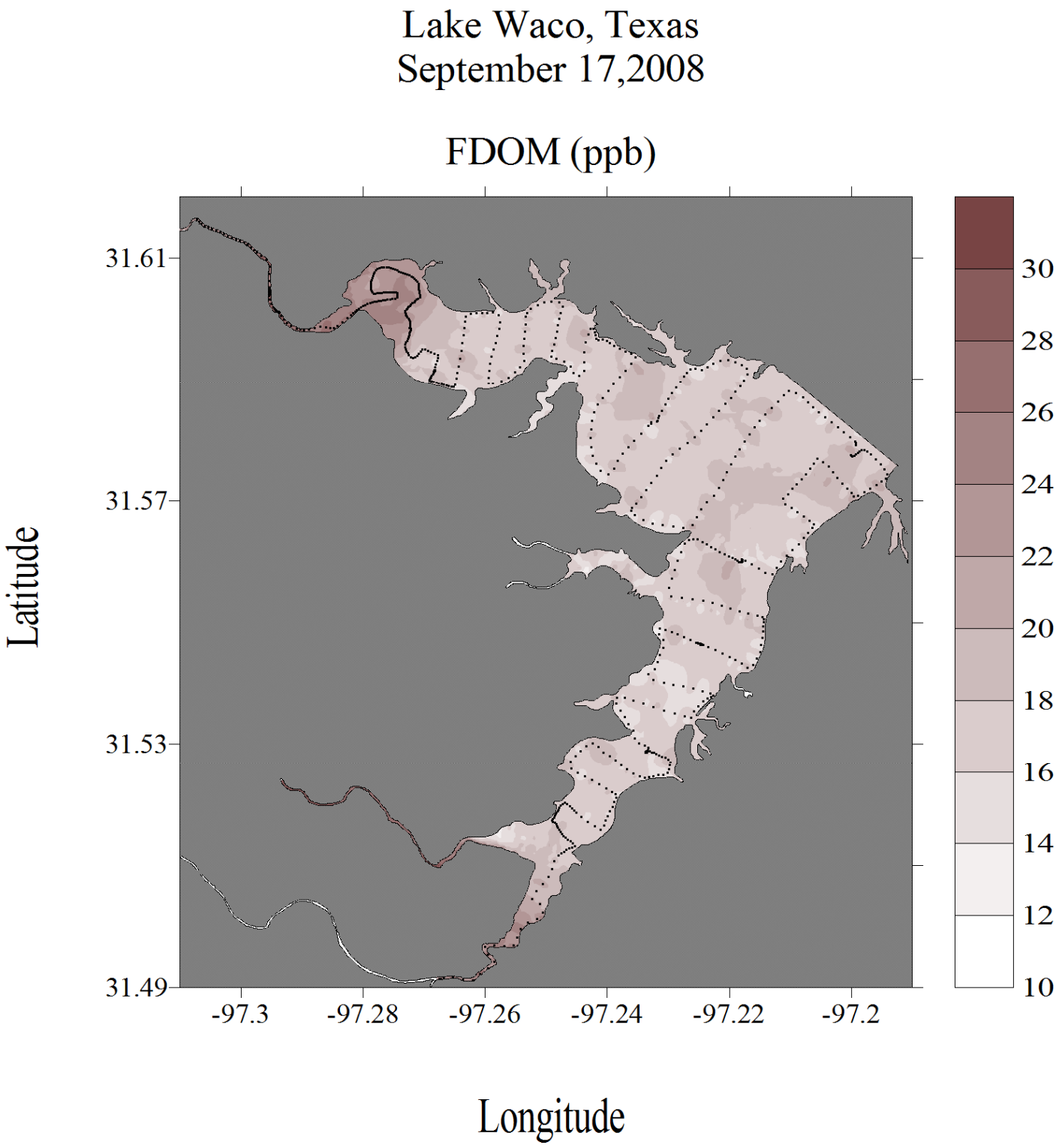

Figure G-54. Dissolved organic matter dataflow map for Lake Waco

Appendix H. Modeling Overview

This appendix is a brief guide to the other appendices that document modeling work. Zero- and 1-dimensional models were constructed in which the population dynamics of *P. parvum* were coupled to those of nutrients (nitrate, phosphate). A suite of five 0-dimensional models was developed, which differed in the number of algal populations competing with *P. parvum* (0, 1, or 4) and whether the competitor types included cyanobacteria exerting allelopathic effects on *P. parvum*. A single 1-dimensional model was developed, with no additional algal populations competing with *P. parvum*. All models take input data from observations of lake conditions (temperature, irradiance, salinity, zooplankton grazing, dilution by flows, nutrient supply) and produce predicted dynamics of *P. parvum* population density, densities of other algal populations (if present), and dissolved concentrations of nitrate and phosphate.

Population dynamics of *P. parvum* and other, competing algae are modeled as functions of physical factors such as temperature, irradiance, and salinity, and as functions of dissolved nitrate and phosphate concentration. Dynamics of these nutrients are coupled to population growth, so that large populations deplete nutrients leading to competition within and between populations. All algal populations suffer losses due to flow (washout from the habitat), grazing by zooplankton, and sinking in the case of diatoms. Some models also assume that a cyanobacterial population, competing with *P. parvum*, produces a toxin that reduces the growth rate of *P. parvum*.

Zero-dimensional models were based on coupled ordinary differential equations similar to those used in many water quality models that simulate algal and nutrient dynamics (Thomann and Mueller, 1987; Chapra, 1997). The formulation of these model equations is presented in **Appendix 2. Draft Modeling Manuscript**. A well tested $4^{th}/5^{th}$ order Runge-Kutta algorithm with adaptive step size was used for numerical simulations based on these differential equations (Press et al., 1986). One-dimensional models were based on partial differential equations (reaction-diffusion-advection equations), numerically simulated with the MacCormack algorithm, as modified by Chapra (1997). The formulation of these model equations is described in a Microsoft Word document in the **Electronic Appendix** (1-d Reservoir Model 1.doc).

The models constructed here take input data from observations of lake conditions (temperature, irradiance, salinity, zooplankton grazing, dilution by flows, nutrient supply) and produce predicted dynamics of *P. parvum* population density, densities of other algal populations (if present), and dissolved concentrations of nitrate and phosphate. One year of observational data from Lake Granbury was available to use as input and simulations of dynamics over multiple years were obtained by repeating these inputs as an annual cycle. Simulations quickly converged to annually periodic dynamics that were taken as predictions. These predictions were then compared to observations of *P. parvum* population densities taken at the same time the input data were collected. Three error metrics were used for quantitative comparison of predictions and observations, which measure the performance of the models in predicting the magnitude and timing of *P. parvum* population density during winter, the period of time when fish-killing blooms occur in Texas lakes. These models can also be modified to accept input data from multiple years or from other lakes when these become available, to enable more extensive predictions of *P. parvum* dynamics.

All numerical algorithms were coded in Fortran 77, and compiled with the Digital Visual Fortan compiler, version 6. Numerical work was done on several IBM PC type computers with Pentium 4 or higher processors. However, the program code is portable to a wide range of hardware for which Fortran compilers are available. The programs use only simple ASCII text files for input and output and thus can be used on a wide range of hardware enabling use of this file format. Implementation of the models requires a working knowledge of Fortran 77, and an appropriate compiler. Modifications to parameters, inputs, or equations require rewriting necessary lines of code and recompiling. All source code is provided in the **Electronic Appendix**.

Appendix I. Draft Modeling Manuscript

This is a manuscript entitled "Mathematical models of population dynamics of *Prymnesium parvum* in inland waters", submitted in August, 2008 to the *Journal of the American Water Resources Association* for publication as part of a special collection on "golden algae" to be issued in conjunction with an international symposium on this topic to take place in January, 2009. This manuscript is undergoing peer review and the published version might differ from the draft provided here. However, the manuscript provides an accurate summary of the zero-dimensional models developed for this project. The **Electronic Appendix** provides much more extensive documentation of the work described in the manuscript.

Abstract from the draft manuscript: Blooms of the harmful alga *Prymnesium parvum* have apparently increased in frequency in inland waters of the U.S., especially in western Texas. A suite of mathematical models was developed based on a chemostat (or CSTR) framework. Models for reservoirs were calibrated with data from Lake Granbury, Texas. Inputs include data on flows, salinity, irradiance, temperature, zooplankton grazing, and nutrients. Parameterization incorporates recent laboratory studies relating the specific growth rate of *P. parvum* to such factors. Specific models differ in whether and how interactions with competing algae are represented. These models address a mismatch between the fundamental ecophysiological niche of *P. parvum*, which grows best in relatively warm and salty waters, and the seasonal occurrence in Texas of blooms in relatively cool weather and more dilute, brackish waters. Sensitivity analyses suggest two approaches leading to predicted seasonal dynamics of *P. parvum* that resemble observations. The first is to align the fundamental and realized niches of *P. parvum* represented in models by designating a low optimal temperature for growth, an approach that disagrees with laboratory experiments. The second is to postulate that allelopathy resulting from cyanobacterial toxins reduces the growth rate of *P. parvum*, which has tentative support from field experiments.

Electronic Appendix

This is a CD-ROM containing electronic files providing further documentation of model development, program versions, and simulation runs that were done. Microsoft Word files are provided with several documents summarizing aspects of model development and results. Microsoft Excel files are provided containing input and output data, and source code files are provided.

Microsoft Word documentation files:

Files describing 0-dimensional models:

Lake Granbury chemostat notes.doc
Lake Granbury competition notes.doc
Lake Granbury general competitor notes.doc
Lake Granbury allelopathy notes.doc
Lake Granbury general allelopathy notes.doc

Lake Granbury forced cyanobacteria notes.doc
Lake Granbury grazer inhibition notes.doc
Lake Granbury toxicity index notes.doc

File describing 1-dimensional model:

1-d Reservoir Model.doc

Microsoft Excel data files:

Files with data from 0-dimensional models:

Competitor parameters.xls
Chl yields.xls
Granbury Allelopathy Baseline 1.xls
Granbury Allelopathy Baseline 2.xls
Granbury Allelopathy Sensitivity Analysis 1.xls
Granbury Allelopathy Sensitivity Analysis 1b.xls
Granbury Allelopathy Sensitivity Analysis 1c.xls
Granbury Allelopathy Sensitivity Analysis 2.xls
Granbury Allelopathy Sensitivity Analysis 2b.xls
Granbury Allelopathy Sensitivity Analysis 2c.xls
Granbury Baseline 1.xls
Granbury Calibration 1.xls
Granbury Calibration 2.xls
Calibration 3.xls
Granbury Chemostat Best.xls
Granbury Chemostat Inhibition 1.xls
Granbury Comp Allelo Inhibition 1.xls
Granbury Comp Allelo Inhibition 2.xls
Granbury Competition Baseline.xls
Granbury Competition Calibration 1.xls
Granbury Competition Inhibition 1.xls
Granbury Competition Sensitivity Analysis 1.xls
Granbury Competition Sensitivity Analysis 1b.xls
Granbury Competition Sensitivity Analysis 2.xls
Granbury Competition Sensitivity Analysis 2b.xls
Granbury Competition Sensitivity Analysis 3.xls
Granbury Competition Sensitivity Analysis 3b.xls
Granbury cyano calculations.xls
Granbury Cyano Pred vs Obs.xls
Granbury Forced Cyano Sensitivity Analysis 1.xls
Granbury Forced Cyano Sensitivity Analysis 1b.xls
Granbury Forced Cyanobacteria Baseline.xls
Granbury forcing data summary.xls
Granbury Generalized Alellopathy Baseline.xls

Granbury Generalized Alelo Inhibitor 1.xls
Granbury Generalized Alelo Inhibitor 2.xls
Granbury Generalized Allelo Sensitivity Analysis 1.xls
Granbury Generalized Allelo Sensitivity Analysis 1b.xls
Granbury Generalized Allelo Sensitivity Analysis 2.xls
Granbury Generalized Allelo Sensitivity Analysis 2b.xls
Granbury Generalized Comp Sensitivity Analysis 1.xls
Granbury Generalized Comp Sensitivity Analysis 1b.xls
Granbury Generalized Competition Baseline.xls
Granbury Generalized Inhibitor 1.xls
Granbury hydrology data.xls
Granbury light calculations.xls
Granbury Low T-ref.xls
Granbury observation data.xls
Granbury P parvum counts.xls
Granbury P parvum tox indices.xls
Granbury pigment calculations.xls
Granbury Reservoir Data.xls
Granbury salinity calculations.xls
Granbury Sensitivity Analysis 1.xls
Granbury temperature calculations.xls
Granbury TN calculations.xls
Granbury TN-TP ratios.xls
Granbury TP calculations.xls
Granbury zoop calculations.xls

Files with data from 1-dimensional model:

Granbury spatial forcing data.xls
Initial 1-d runs.xls

Source code files (Fortran 77):

gacoin.for
gacoins.for
gacom2.for
gacom3.for
gacom4.for
gacomp.for
gacyan1.for
gacys1.for
gaga1.for
gaga2.for
gagain.for
gagain2.for
gagains.for
gagains2.for
gagas1.for
gagas2.for
gagen1.for
gagen2.for
gagenin.for
gagenins.for
gagens1.for
gall1.for
gall2.for
gallin.for
gallin2.for
gallins.for
gallins2.for
galls1.for
galls2.for
gasenc3.for
gasenc4.for
gasens1.for
gasensc.for
gayear2.for
gayear3.for
xyear2.for
xyear3.for
xyear4.for

Title: Mathematical models of population dynamics of *Prymnesium parvum* in inland waters

Authors: James P. Grover[1], Jason W. Baker[2], Daniel L. Roelke[3], Bryan W. Brooks[4]

[1]Professor, Department of Biology, and Director, Program in Environmental and Earth Sciences, University of Texas at Arlington, Arlington, TX 76019; E-mail: grover@uta.edu; Phone: 817-272-2405 (corresponding author).

[2]Research Associate, Program in Environmental and Earth Sciences, University of Texas at Arlington, Arlington, TX 76019.

[3]Associate Professor, Departments of Wildlife and Fisheries Sciences, and Oceanography, Texas A&M University, College Station, TX 77843-2258.

[4]Associate Professor, Department of Environmental Science and Center for Reservoir and Aquatic Systems Research, Baylor University, One Bear Place #97266, Baylor University, Waco, TX 76798.

Abstract: Blooms of the harmful alga *Prymnesium parvum* have apparently increased in frequency in inland waters of the U.S., especially in western Texas. A suite of mathematical models was developed based on a chemostat (or CSTR) framework. Models for reservoirs were calibrated with data from Lake Granbury, Texas. Inputs include data on flows, salinity, irradiance, temperature, zooplankton grazing, and nutrients. Parameterization incorporates recent laboratory studies relating the specific growth rate of *P. parvum* to such factors. Specific models differ in whether and how interactions with competing algae are represented. These models address a mismatch between the fundamental ecophysiological niche of *P. parvum*, which grows best in relatively warm and salty waters, and the seasonal occurrence in Texas of blooms in relatively cool weather and more dilute, brackish waters. Sensitivity analyses suggest two approaches leading to predicted seasonal dynamics of *P. parvum* that resemble observations. The first is to align the fundamental and realized niches of *P. parvum* represented in models by designating a low optimal temperature for growth, an approach that disagrees with laboratory experiments. The second is to postulate that allelopathy resulting from cyanobacterial toxins reduces the growth rate of *P. parvum*, which has tentative support from field experiments.

Key terms: algae, aquatic ecology, harmful algal blooms, lakes, *Prymnesium parvum*

INTRODUCTION

Harmful algal blooms (HAB) emerged as a notable water quality issue towards the end of the last century, and have apparently increased in frequency and intensity over the last several decades, worldwide in both coastal and inland waters (Hallegraeff, 1993; Van Dolah et al., 2000; Sellner et al., 2003). Although many HABs have direct implications for human health, others are harmful primarily for their disruption of aquatic ecosystems and food webs (ecosystem disruptive algal blooms sensu Sunda et al., 2006). This study focuses on an example of the latter type, blooms of the haptophyte alga *Prymnesium parvum* (Edvardsen and Paasche, 1998; Edvardsen and Imai, 2006). Originally described from coastal waters (Carter, 1937; Otterstrøm and Steeman Nielsen, 1940), this species also inhabits brackish inland waters and blooms have become common in western Texas and other parts of the American Southwest, where it is referred to as golden algae. The principal impact of these blooms has been large fish kills, with an estimated $10^5 – 10^6$ dead fish in single events.

The perceived increase in HABs has often been attributed to eutrophication and changes in nutrient supply ratios (Smayda, 1989; Paerl, 1997; Cloern et al., 2001), although additional causes are possible, including climate change (Van Dolah et al., 2000), transport of harmful species to new habitats (Hallegraeff and Gollasch, 2006), changes in agricultural practices and land use (Paerl, 1998; Glibert et al., 2006), toxic pollutants (Paerl, 1998), inhibition of grazing on HAB species (Buskey et al, 1997; Turner and Tester, 1997), and natural processes (Sellner et al., 2003). For *P. parvum* and other HAB species in waters of varying salinity, changes in this parameter could be as important as changes in nutrient regimes.

In water quality modeling, eutrophication is a mature subject, but to address HABs the conventional approaches provide only a starting point. Models for HABs must address the species level, rather than using an aggregated approach wherein only a single algal population, or a few major functional types of algae are represented. In many eutrophication models, the main processes affecting algal population dynamics are nutrient-dependent reproductive growth and competition for nutrients, sinking, grazing by zooplankton, and transport. Emerging understanding of the chemical ecology of HABs suggests considering additional biological processes, which can include allelopathy, here meaning the production of toxins that impair competitors (Legrand et al., 2003; Babica, 2006; Granéli and Hansen, 2006), inhibition of grazers by toxins (Sunda et al., 2006), and possibly signaling within and between species (Lewis, 1986; Pohnert et al., 2007).

This paper reports construction and calibration of models focused on *P. parvum* blooms in Texas inland waters, as part of an integrated research program addressing this problem (Baker et al., 2007, unpublished; Roelke et al., 2007; Grover et al., 2007; Errera et al., in press; Roelke et al., unpublished; Schwierzke et al., unpublished; Valenti et al., unpublished; Brooks et al., this volume; Roelke et al., this volume; Schug et al., this volume). Formulations of biological processes were the primary goal, based on recent experimental studies of this species (Baker et al., 2007, unpublished), and thus representation of hydrodynamics was intentionally highly simplified. Several models were developed, differing in the number of competing algal types interacting with the focal HAB species, *P. parvum*, and in the biological processes represented. The simplest model represented only the population of *P. parvum*, growing in relation to nutrients,

other physical factors, and grazing. Models were also constructed with one and four additional populations of algae to represent algal functional types competing for nutrients with *P. parvum*. In two additional models one of the competing algal types also produced an allelopathic toxin inhibiting the growth of the focal species, *P. parvum*. These latter models were inspired by recent field experiments suggesting that cyanobacteria present in some Texas inland waters suppress the growth of *P. parvum* via an unidentified dissolved cyanotoxin (Roelke et al., this volume).

FIELD SITE

Calibration data for this study were obtained from Lake Granbury, Texas (97.8 °W, 32.4 °N), a reservoir on the Brazos River impounded in 1969. The lake has a volume (conservation storage) of 167.4 Mm^3, an area of 3378 ha, and a mean depth of 4.98 m. The shoreline follows the meandering river channel with an elongated, sinuous basin oriented northwest to southeast, 45 km long with an average width of 0.6 km. The lake has intakes for municipal water supply and power plant cooling.

From August 2006 to August 2007 samples were taken monthly at ten fixed stations and a number of routine water quality parameters were determined, along with zooplankton and phytoplankton community composition and population densities of *P. parvum* (Roelke et al., unpublished). During the period of observations, volume varied up to 5% below conservation storage. The lake was also eutrophic during this period, with mean total phosphorus of 1.63 μmo/l, mean chlorophyll *a* of 39.8 μg/l, and mean Secchi depth of 0.65 m. Conductometric salinity during this period averaged 1.15 psu, paired deep and shallow stations differed by 0.011 psu on average, and relative longitudinal variation in salinity at different sampling times ranged 2-50% (standard deviation/mean). Similarly low spatial variation for other water quality parameters suggests strong horizontal mixing during the period of the study. Profiles of the upper 15 meters obtained during monthly sampling never revealed vertical thermal stratification. The salinity of Lake Granbury is sufficient to permit growth of *P. parvum*, and large fish-killing blooms occurred in January to June of 2001 and February to April of 2003. Since then, large populations have regularly occurred in cooler weather, with varying degrees of toxicity.

MODEL FORMULATION

A chemostat or continuously-stirred tank reactor (CSTR) was chosen as the modeling framework for two reasons. First, the goal here is to develop descriptions of biological processes influencing the population dynamics of *P. parvum*, rather than develop accurate physical models of flows and chemical water quality. Second, the sampling program that provided calibration data revealed vigorous mixing in Lake Granbury. Model formulation thus began with conventional differential equations for coupled dynamics of algae and two dissolved nutrients in a chemostat (Thomann and Mueller, 1987; Chapra, 1997):

$$\frac{dN_i}{dt} = \mu_i(R,S;\sigma,I,T)N_i - m_iN_i - v_iN_i - D\left(N_i - N_{in}\right) \quad (1)$$

$$\frac{dR}{dt} = D(R_{in} - R) - \sum_i \left[\mu_i(R,S;\sigma,I,T) N_i / Y_{R,i} - rm_i N_i / Y_{R,i} \right] \quad (2)$$

$$\frac{dS}{dt} = D(S_{in} - S) - \sum_i \left[\mu_i(R,S;\sigma,I,T) N_i / Y_{S,i} - rm_i N_i / Y_{S,i} \right] \quad (3)$$

Here, N_i is the population density of algal type *i*. Up to five algal types are represented in the models considered here, indexed by subscript *i*: *p* – *P. parvum*; *c* – cyanobacteria; *d* – diatoms; *f* – flagellated algae other than *P. parvum* (including chrysophytes, cryptophytes, dinophytes, and euglenophytes); and *g* – chlorophytes. Apart from *P. parvum*, populations of other algal types are functional groups composed of many species. Three models were constructed: one with only a population of *P. parvum* and no competitors, one with a single competitor type (cyanobacteria) and one with all four types of competitors (Table 1).

Table 1. Models examined in this study.

Designation	Definition
PP0	Only the population of *P. parvum* is represented
PP1	*P. parvum* and one competitor type, cyanobacteria, are represented
PP4	*P. parvum* and four competitor types are represented
PP1A	*P. parvum* and one competitor type, cyanobacteria, are represented; allelopathy is included as cyanotoxin production
PP4A	*P. parvum* and four competitor types are represented; allelopathy is included as cyanotoxin production

Variables *R* and *S* are the concentrations of dissolved inorganic phosphorus and nitrogen, respectively. Inorganic nitrogen species (NO_3^-, NO_2^-, NH_4^+) are not resolved and are assumed to affect algal growth equivalently. Although NH_4^+ at concentrations exceeding 10 μmol/l are toxic to *P. parvum* (Barkoh et al., 2003; Grover et al., 2007), concentrations in the focal lake for this study, Lake Granbury, averaged only 2.4 μmol/l during the period of examined here and did not exceed 6.5 μmol/l.

The population growth rate of algal type *i* is governed by the function μ_i

$$\mu_i(R,S;\sigma,I,T) = \mu_{\max,i}(\sigma,I,T) \min\left\{ \frac{R}{K_{R,i}+R}, \frac{S}{K_{S,i}+S} \right\} \quad (4)$$

where $\mu_{\max,i}$ is a nutrient-saturated, maximal growth rate that depends on salinity (σ), irradiance (I), and temperature (T), which are time-dependent parameters based on observations, as described below in the section *Forcing Data*. The section *Initial Parameterization* specifies the $\mu_{\max,i}$ functions used for each algal type. Liebig's law of the minimum applies to the dependence of growth on the two nutrients (Rhee, 1982), and

growth rate in relation to concentration follows a rectangular hyperbola with half-saturation constants $K_{R,i}$ and $K_{S,i}$ for nitrogen and phosphorus, respectively.

The parameter m_i is mortality rate due to zooplankton grazing, which is a time-dependent function developed from observational data. The parameter v_i is mortality rate due to sinking, given by

$$v_i = u_i / h \tag{5}$$

where u_i is sinking speed and h is mean depth, which is taken here as a constant given the relatively small variations in volume that occurred during the study. Additionally, flow was parameterized by the dilution rate D, another time-dependent function developed from observations. The final term in Equation (1) includes an inflow of algal type i at concentration N_i, assigned a value of 100 cells/ml to specify a small amount of algal immigration. This immigration stabilized against competitive exclusion of any algal type, and was not included in model PP0.

Nutrient dynamics are governed by Equations (2) and (3), which have supply terms with input concentrations R_{in} and S_{in} for phosphorus and nitrogen, respectively. Remaining terms couple nutrient dynamics to algal populations. Nutrient uptake is proportional to population growth with yield coefficients $Y_{R,i}$ and $Y_{S,i}$ for phosphorus and nitrogen, respectively. Nutrient recycling is proportional to the mortality due to zooplankton grazing, with a recycling efficiency r specifying the proportion of grazed nutrient content that is recycled.

Allelopathy

Field experiments suggest that competition from cyanobacteria mediated by allelopathic substances might strongly influence dynamics of *P. parvum* (Roelke et al., this volume). To explore this hypothesis, models PP4A and PP1A were constructed with an equation added to represent the dynamics of a cyanotoxin with concentration (C). Production of the cyanotoxin is assumed to be proportional to the growth of the cyanobacteria population with coefficient ε_C. First-order decay of the cyanotoxin, due to photolysis and other processes, is assumed with a rate constant k_C. Thus the governing equation for cyanotoxin dynamics is

$$\frac{dC}{dt} = \mu_c N_c \varepsilon_C - k_C C \tag{6}$$

Inhibition of growth rate for *P. parvum* by cyanotoxin was suggested in field experiments, and is here represented by a modified equation for population dynamics:

$$\frac{dN_p}{dt} = \mu_p N_p \left(\frac{K_C^I}{C + K_C^I} \right) - m_p N_p - v_p N_p - D N_p \tag{7}$$

The inhibition term in parentheses is analogous to those used in enzyme kinetics, and the parameter K_C^I is the cyanotoxin concentration that produces a 50% reduction in growth

rate. For simplicity, cyanotoxin was assumed not to affect the growth of algal types other than *P. parvum.*

Forcing Data

Eight quantities were taken as time-dependent forcing functions and developed from observational data to represent environmental conditions affecting algal population dynamics: dilution rate (D), salinity (σ), irradiance (I), temperature (T), supply concentrations of nitrogen and phosphorus (R_{in}, S_{in}), mortality due to zooplankton grazing (m_i), and the nutrient recycling efficiency of grazing (r). For this study, the time period from August 1, 2006 to August 31, 2007 was considered. Most of the necessary data was obtained from monthly sampling of Lake Granbury with daily values calculated by linear interpolation. Numerical integration of the model equations was implemented for successive days with these daily values treated as fixed; i.e. integration was restarted every day with new values. Model runs of several years duration were obtained by repeating the annual period of input data as needed.

Lake Granbury was assumed to have constant volume at conservation storage, with flow dominated by discharge of the Brazos River. Daily discharge values were obtained from two USGS gauges: 08090800, about 40 km upstream of the headwaters, and 08091000, about 60 km downstream of the dam. Daily dilution rates were calculated from discharges at each station, and these two estimates were averaged to obtain the time series used for model forcing (Fig 1A). For the annual period modeled, high dilution rates occurred from spring to summer, which was a period of unusually wet weather.

Salinity data were averaged at each monthly sampling date for the ten stations and interpolated to obtain daily values (Fig. 1B). For the annual period modeled, low salinity of 0.6 – 1 psu occurred during the spring-summer period of high dilution, with higher salinity of about 1.4 psu otherwise.

To estimate the average water column irradiance, exponential attenuation over the mean depth of 5.0 m was assumed. Data on Secchi depth (h_{SD}) were averaged at each monthly sampling date for the ten stations and interpolated to obtain daily values. Secchi depth was then converted to attenuation coefficient (ε) with the formula $\varepsilon = 1.7 / h_{SD}$ (Idso and Gilbert, 1974), and interpolated to obtain daily values. Irradiance just under the water surface (I_0) was calculated from solar declination and day length (Kirk, 1983), assuming a surface reflectance of 6.5% (Wetzel, 2001). This result was then averaged over the photoperiod, and expressed as the photon flux that would deliver the same irradiance over 12 hours just under the water surface. This scaling of photoperiod was used because the laboratory experiments parameterizing the dependence of *P. parvum* growth on irradiance used a 12-hour photoperiod (Baker et al., 2007). Finally, the depth-averaged irradiance was calculated as

$$I = \frac{I_0}{\varepsilon h}\left(1 - e^{-\varepsilon h}\right) \tag{8}$$

For the annual period modeled, high irradiances occurred in late winter and in midsummer (Fig. 1C). Irradiance was reduced in spring and early summer due to high turbidity associated with high flows.

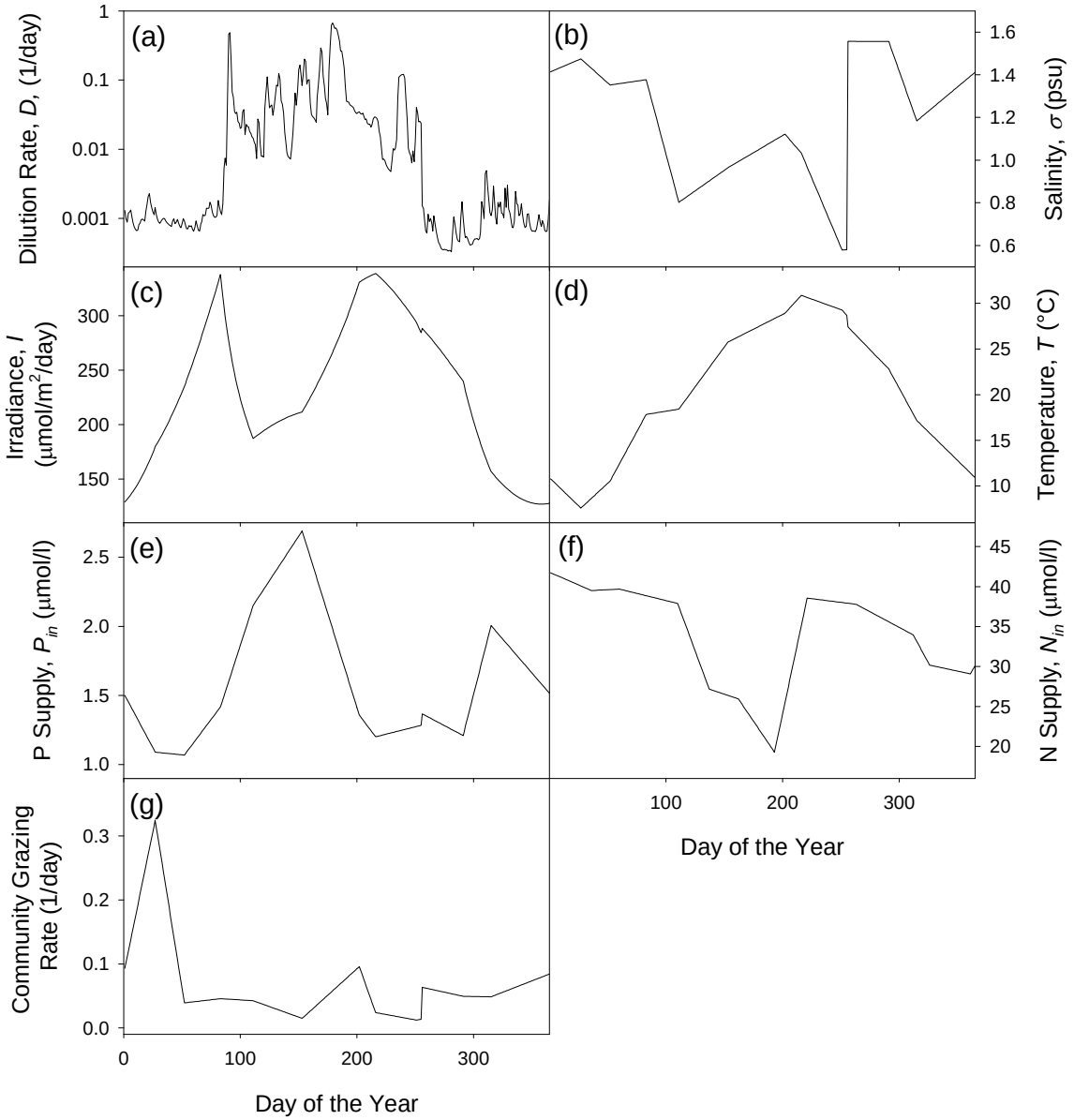

Figure 1. Forcing data from Lake Granbury, Texas: (a) dilution rate; (b) salinity; (c) irradiance; (d) temperature; (e) phosphorus supply concentration; (f) nitrogen supply concentration; (g) community grazing rate for zooplankton.

Temperature data were averaged at each monthly sampling date for the ten stations and interpolated to obtain daily values (Fig. 1D). For the annual period modeled, temperature varied approximately sinusoidally from 7.6°C to 30.9°C.

Ideally, supply concentrations for phosphorus and nitrogen would be estimated from loading studies, but such data are not available. Theoretically, for a chemostat at steady state, total nutrient concentration approaches the supply concentration (Grover, 1997). Therefore, total phosphorus (TP) and total nitrogen (TN) observations from the monthly monitoring program were taken as estimates of supply concentrations. These

values were averaged at each monthly sampling date for the ten stations and interpolated to obtain daily values (Fig. 1E, F). For the annual period modeled, TP averaged 1.6 μmol/l (range: 1.1 – 2.7 μmol/l) and TN averaged 34 μmol/l (range: 19 – 41 μmol/l); the TN:TP molar ratio averaged 30 (range: 18 – 66).

Estimates of mortality due to zooplankton grazing were developed from data on zooplankton populations obtained by microscopy. Community grazing rates (*CGR*) were calculated from population densities of zooplankton taxa, using literature to estimate volumes (Wetzel and Likens, 1991) and volume-specific clearance rates (Hansen et al., 1997) of each taxon. As with other data, *CGR* was averaged at each monthly sampling date for the ten stations and interpolated to obtain daily values (Fig. 1G). *CGR* estimates the total grazing activities of all zooplankton, but not all algal types are equally susceptible to grazing (Sterner, 1989). The mortality rate for each algal type was calculated as

$$m_i = w_i \cdot CGR \tag{9}$$

where w_i is a susceptibility parameter on the interval (0,1). Although w_i could vary with time due to changes in zooplankton community composition and grazing behavior, for simplicity it was assumed to be constant for a given algal type. Over most of the annual period modeled, *CGR* ranged 0.02 – 0.1 1/d, but much higher grazing rates occurred during mid-winter, when rotifers (*Brachionus* and *Keratella*) were abundant. The models constructed here permit input of the recycling efficiency (r) as a forcing function, because in principle it can vary with composition of the zooplankton and algal communities. Exploratory work suggested results were very insensitive to reasonable assignments of this parameter and given lack of adequate data, this quantity was taken as constant at a value of 0.5 (Sterner, 1989).

Initial Parameterization

For *P. parvum*, maximal growth rate as a function of salinity, irradiance and temperature was based on recent laboratory studies of a strain originating in Texas (Baker et al., 2007, unpublished). Baker et al. (unpublished) cultured this strain under conditions representative of Texas reservoirs where blooms have occurred, fitting the nutrient-saturated growth rate to salinity and temperature by multiple regression. Baker et al. (2007) conducted a similar study under higher salinity conditions but also at a range of irradiances. In that latter study, regression terms describing the response to light were additive to those for responses to temperature and salinity, so a hybrid model was adopted using regression terms for the responses to temperature and salinity from Baker et al. (unpublished) and regression terms for the response to irradiance from Baker et al. (2007). In full, the equation used is

$$\mu_{\max}(\sigma, I, T) = \max\left\{0, \beta_0 + \beta_1(\sigma - \sigma_{\text{ref}}) + \beta_2 e^{\left[0.7\left(\frac{T-T_{\text{ref}}}{T_{\text{ref}}}\right)\right]} + \beta_3(I - I_{\text{ref}})\right.$$
$$+ \beta_4(\sigma - \sigma_{\text{ref}})^2 + \beta_5 e^{\left[1.4\left(\frac{T-T_{\text{ref}}}{T_{\text{ref}}}\right)\right]} + \beta_6(I - I_{\text{ref}})^2 \qquad (10)$$
$$\left. + \beta_7(\sigma - \sigma_{\text{ref}}) e^{\left[0.7\left(\frac{T-T_{\text{ref}}}{T_{\text{ref}}}\right)\right]}\right\}$$

where terms β_j are regression coefficients, and σ_{ref}, I_{ref}, and T_{ref} are reference values of salinity, irradiance and temperature based on the experimental designs used (Table 2). Equation (10) describes response to salinity, irradiance, and temperature as unimodal, with an interaction such that the optimal temperature for growth declines with salinity (Fig. 2A).

Table 2. Parameters of the maximal growth function for *P. parvum*.

Parameter	Value	Parameter	Value
β_0	-3.531	β_6	-0.00000573
β_1	0.02534	β_7	0.1697
β_2	7.468	σ_{ref}	1.833
β_3	0.000611	I_{ref}	222
β_4	-0.06311	T_{ref}	20
β_5	-3.414		

For the remaining algal types, salinity-dependence of maximal growth rates was assumed negligible. Few data are available on the salinity responses of algal species common in inland waters. Additionally it may be assumed that species capable of growth under prevailing salinities are present in the species pools represented by the broadly defined algal types modeled. For these algal types, dependence of growth on temperature and irradiance was modeled as a product function

$$\mu_{\max,i}(I, T) = \mu_{\text{opt},i}\, g_i(I)\, f_i(T) \qquad (11)$$

where $\mu_{\text{opt},i}$ is the maximal growth rate at optimal irradiance and temperature, and functions f_i and g_i vary between 0 and 1. Values for $\mu_{\text{opt},i}$ (Table 3) were taken as the highest nutrient-saturated growth rates observed for species of each algal type in a dilution culture study of algae sampled from Texas reservoirs (Grover et al., 1999). Temperature responses (Fig. 2B) were modeled as piecewise linear functions based on Chapra (1997). Light responses (Fig. 2C) were also modeled as unimodal, piecewise linear functions for diatoms and flagellates, constructed as visual approximations to curves illustrated in Thomann and Mueller (1987). For chlorophytes, the photoinhibition at relatively low irradiance depicted by their curve was not observed in studies of algae from Texas reservoirs (Grover et al. 1999), so a rectangular hyperbola was adopted with a

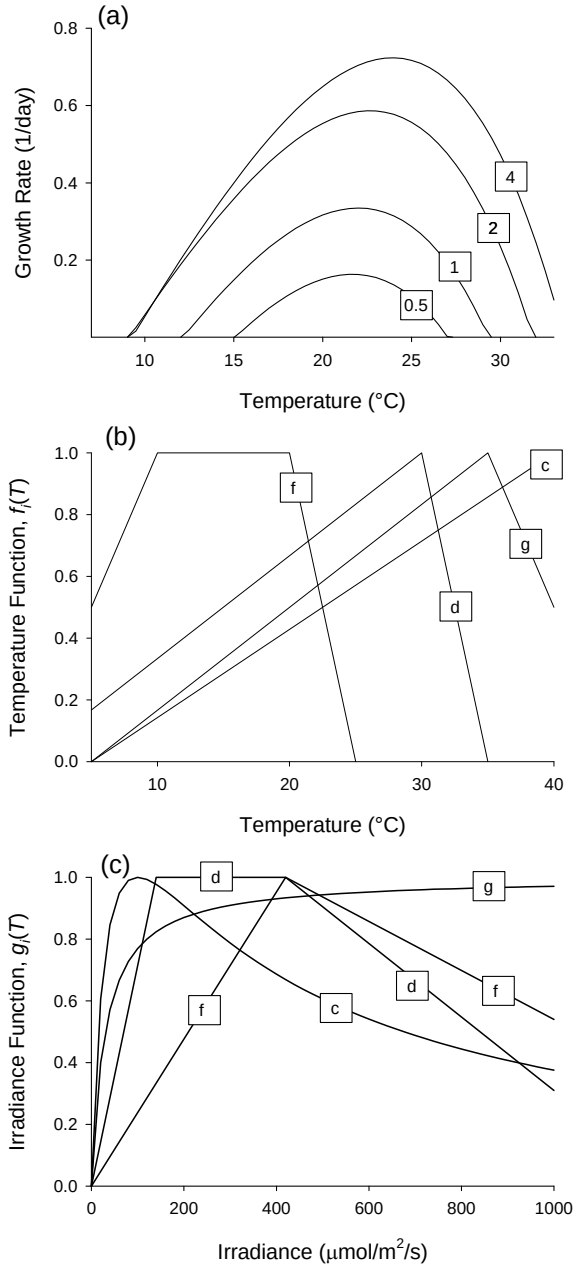

Figure 2. Functions describing maximal growth rates of algal populations. (a) *P. parvum*: curves show growth rates for an irradiance of 222 μmol photons/m^2/s as a function of temperature for salinities (psu) given in boxes. (b) Functions $f_i(T)$ governing growth responses to temperature for four types of algae (*c* – cyanobacteria; *d* – diatoms; *f* – flagellates; *g* – chlorophytes). (c) Functions $g_i(I)$ governing growth responses to light for the same four types of algae.

half-saturation constant of 30 μmol photons/m^2/d. For cyanobacteria, the function suggested by Litchman (2000) was used

$$g_c(I) = \max\left\{0, \frac{1.683I}{33.33 + I + I^2/300} - 0.01\right\} \quad (12)$$

with numerical values assigned to produce a curve peaking at 1, having a shape resembling her experimental data for cyanobacteria and those of Lee and Rhee (1999).

Table 3. Initial assignments of parameter values specific to algal types.

	Algal type				
Parameter	*P. parvum* (*p*)	Cyanobacteria (*c*)	Diatoms (*d*)	Flagellates (*f*)	Chlorophytes (*g*)
$\mu_{opt,i}$	NA*	1.52	1.87	0.79	1.25
$K_{R,i}$	0.009	0.166	0.14	0.02	0.15
$K_{S,i}$	0.01	3.686	0.04	3.31	1.15
$Y_{R,i}$	7.2×10^8	3.5×10^8	4.0×10^7	8.3×10^7	2.0×10^8
$Y_{S,i}$	3.125×10^7	3.08×10^7	4.4×10^6	7.5×10^6	7.1×10^6
w_i	0.5	0.49	0.8	1.0	0.64
v_i	0	0	0.18	0	0

*Not Applicable given definition of functions used.

The half-saturation constant for phosphorus-dependent growth of *P. parvum* was assigned as the average of several estimates obtained under low salinity in laboratory experiments (Baker et al., unpublished), and the half-saturation constant for nitrogen-dependent growth was assigned to an arbitrary low value consistent with laboratory observations saturated growth at very low concentrations (Baker, 2007) (Table 3). Half-saturation constants for nutrient-dependent growth of other algal types were assigned based on estimates for algae sampled from Texas reservoirs (Grover et al., 1999). Because these parameters strongly influence outcomes of competition for nutrients (Grover, 1997), some further adjustments were made during exploratory simulations of model PP4 without *P. parvum*. These adjustments successfully obtained seasonal patterns of abundance resembling those documented in Texas reservoirs, where cyanobacteria dominate in summer with other algal types having greatest relative abundance in cooler weather (Grover et al., 1999; Roelke et al., 2004; Grover and Chrzanowski, 2005). All such initial calibrations were done prior to obtaining data from Lake Granbury to construct the forcing functions described above, so data from another Texas reservoir were used, Joe Pool Lake (Grover and Chrzanowski, 2004, 2005).

Yield coefficients for *P. parvum* were assigned initial values within the ranges observed in the laboratory (Baker et al., 2007, unpublished), which were adjusted during exploratory simulations of model PP0 so that peak populations were of the same order of magnitude as the largest populations observed in the field (which can exceed 10^5 cells/ml). Yield coefficients for other algal types were taken from published laboratory studies of nutrient-limited representatives of each type: Hu and Zhang (1993) for

cyanobacteria and diatoms; and Gotham and Rhee (1981a, b) for chlorophytes. For flagellates, the value for yield of a *Cryptomonas* sp. on phosphorus (Grover, 1989) was used to calculate yield on nitrogen from a value for the cellular N:P ratio (Sommer, 1991).

Grazing susceptibility parameters were assigned initial values based on expectations that *P. parvum*, flagellates, and diatoms would have moderate to high susceptibility while cyanobacteria and chlorophytes would have low to moderate susceptibility (Sterner, 1989). Adjustments were then made during exploratory simulations of models PP0 (for *P. parvum* alone) and PP4 (run for other algal types without *P. parvum*). Reservoirs in Texas are often well-mixed vertically (Grover and Chrzanowski, 2004; Roelke et al., 2004), so it was initially assumed that sinking mortality would be negligible. During exploratory simulations, however, it was found that diatoms reached unrealistic abundances unless a modest sinking mortality was imposed, corresponding to a sinking speed of 0.9 m/d in Lake Granbury, a value near the average reported for several diatoms (Reynolds, 2006).

Parameterization of terms relating to cyanotoxin is based on considering the steady state concentration predicted by Equation (6):

$$C^* = \frac{\mu_c N_c^* \varepsilon_C}{k_C} \tag{13}$$

where the asterisk denotes a steady state value. When cyanobacteria are abundant, dissolved concentrations of cyanotoxins such as nodularin and microcystin are about 1 μg/l (Heresztyn and Nicholson, 1997; Park et al., 1998; Fromme, 2000), which is assumed to represent a quasi-steady state. A first-order decay rate for the cyanotoxin (k_C) of 0.5 d^{-1} is assumed, broadly consistent with observed degradation of cyanotoxins in natural waters (Cousins et al., 1996; Heresztyn and Nicholson, 1997). Then, taking a cyanobacteria population density of 2×10^4 cells/ml with a growth rate or 0.1 d^{-1} as representative of summertime in Texas lakes (Grover et al., 1999), the value of the production coefficient ε_C must be 2.5×10^{-7} μg/cell to produce a steady state concentration of 1 μg/l. With these parameter values, simulations of model PP4A with all four types of algal competitors predicted cyanotoxin concentrations during summer in the expected range of about 1 μg/l. However, simulations of model PP1A with one type of competitor parameterized as cyanobacteria led to much higher cyanotoxin concentrations. So for model PP1A a lower value for ε_C of 12.5×10^{-8} μg/cell was adopted, producing predicted cyanotoxin concentrations during summer of about 1 μg/l. The value of the growth inhibition parameter for *P. parvum* (K_C^I) is assigned to be 0.1 μg/l, so that the cyanotoxin concentrations simulated should strongly inhibit growth of *P. parvum*, consistent with field experiments (Roelke et al., this volume).

MODEL RESULTS AND CALIBRATION

Overview

Numerical integrations of models were obtained using a fourth-order Runge-Kutta algorithm with adaptive step size (Press et al., 1986). Using the initial parameters, integrations of each model were implemented for five (model PP0) or twenty simulated years (other models). Simulations were initialized with competitor populations, if present, and nutrient concentrations at the January 1 values obtained for long term simulations without *P. parvum* present. *P. parvum* was then initialized at a low density of 100 cells/ml and simulations run for the specified times. All simulations became annually periodic over the times specified, displaying seasonal oscillations forced by the annual time series of environmental inputs. Predicted dynamics of *P. parvum* in the last simulated year were compared to observations obtained by direct microscopic count of monthly samples taken from Lake Granbury at the ten sampling stations described above.

An extensive sensitivity analysis was then conducted for each model using protocols described below in the section *Sensitivity analyses*. Model performance with alternative parameter values was screened using error metrics described below and for selected parameter values, the predicted dynamics of *P. parvum* were visually compared to observations. Additional modifications to some models were explored less thoroughly.

Error Metrics

Three error metrics were developed to screen model performance, based on a broad goal of accurately simulating dynamics of *P. parvum* during cool weather, when blooms typically occur in Texas inland waters. The first metric (M_1) is the relative error in predicted peak density over the year calculated as

$$M_1 = \left| \frac{N_{\max,p} - \hat{N}_{\max,p}}{\hat{N}_{\max,p}} \right| \tag{14}$$

where $\hat{N}_{\max,p}$ is the predicted peak population density and $N_{\max,p}$ is the observed peak population density. The second metric (M_2) is the relative error in the average natural logarithm of population density over the first 100 days of the year (January 1 to April 9) when fish-killing blooms of *P. parvum* are most commonly observed, and when the highest abundance was observed during the year of calibration data.

$$M_2 = \left| \frac{\left\langle \ln N_p \right\rangle - \left\langle \ln \hat{N}_p \right\rangle}{\left\langle \ln \hat{N}_p \right\rangle} \right| \tag{15}$$

where $\hat{N}_p$ is predicted population density and N_p is observed population density, and angle brackets indicate a time-average. The third metric (M_3) is the difference timing

between the predicted and observed peaks of population density, relative to the length of a year:

$$M_3 = \min\left\{\left|\frac{t_{\max} - \hat{t}_{\max}}{365}\right|, \frac{365 + t_{\max} - \hat{t}_{\max}}{365}\right\} \quad (16)$$

where $\hat{t}_{\max}$ is the time of the predicted peak population density and $t_{\max}$ is the time of the observed peak population density.

Model Results for Initial Parameters

With the initial parameterization, none of predicted dynamics of *P. parvum* agreed well with observations for any of the models (Table 4, Fig. 3). Model PP0 (Fig. 3A), without competing algal populations, predicted two seasonal peaks for the *P. parvum* population, one in spring (April to June) and one in autumn (September to December). Minima were predicted in February, at the time of the observed maximum, and during summer (July to August). Model PP0 had low error in its prediction of the average natural log density of *P. parvum* in winter (metric M_2), but this was accomplished essentially by over-predicting the density of *P. parvum* at all other times of year.

Table 4. Error metrics comparing predicted and observed dynamics of *P. parvum* for the initial parameterization of the models examined.

Model	Error in peak density, M_1	Error in average winter natural log density, M_2	Error in peak timing, M_3
PP0	96%	3%	14%
PP1	94%	160%	33%
PP4	99%	227%	30%
PP1A	6425%	415%	23%
PP4A	2934%	392%	21%

Models PP1 and PP4 (Figs. 3B, C) included one and four competing populations of algae, and both models predicted similar dynamics for *P. parvum*. A seasonal maximum was predicted in late spring (early June), with a secondary peak predicted in late autumn (August). Predicted minima again occurred in February, at the time of the observed maximum, and in late summer (early September). In both of these models, competing populations reduced the nutrients available to *P. parvum*, reducing its predicted density, and to some extent correcting the problem of over-prediction for model PP0, from which competitors were absent.

Models PP1A and PP4A (Figs. 3 D, E) also included competing populations of algae, but one of these (cyanobacteria) produced an allelopathic toxin inhibiting growth of *P. parvum*. Both models predicted similar dynamics for *P. parvum*. A single seasonal maximum was predicted in late autumn (early December), with a predicted minimum in February at the time of the observed maximum. Compared to other models, this one

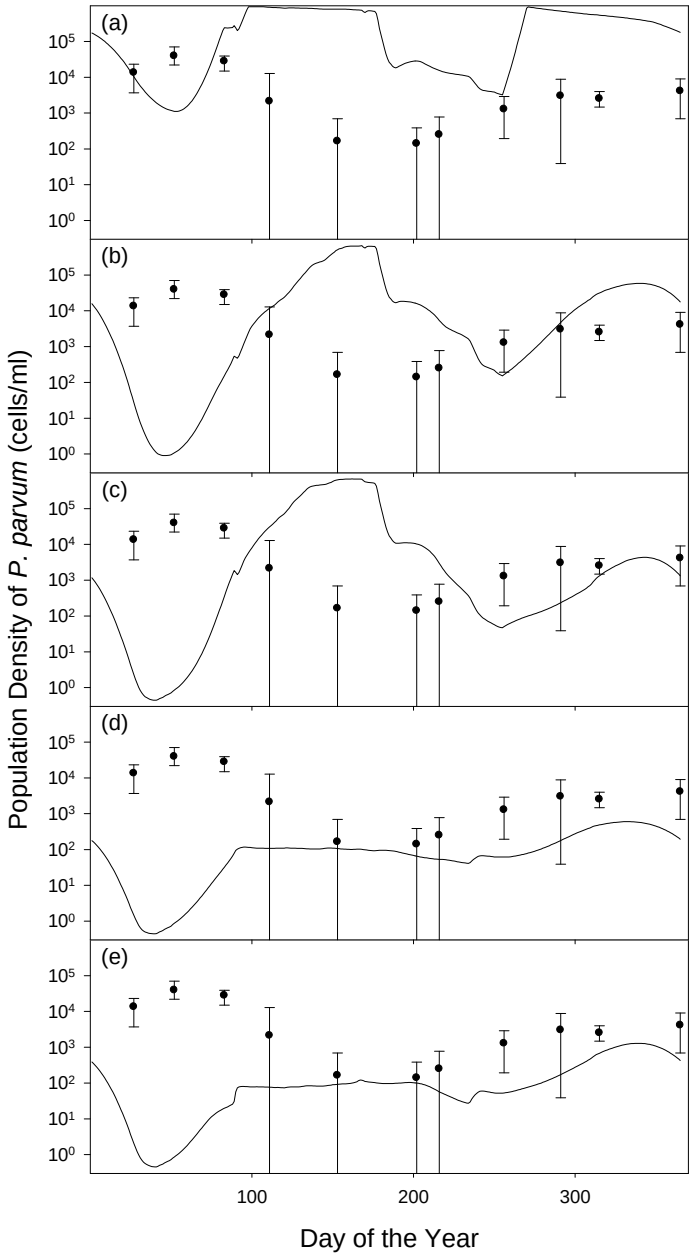

Figure 3. Predicted and observed population dynamics of *P. parvum* in Lake Granbury with initial parameterization for all models. Solid line shows predicted values; symbols show observed values as the average of ten sampling stations. Whiskers show range of sampling stations; when zero observations occurred at some stations, whiskers extend to the bottom of the figure. (a) Model PP0. (b) Model PP1. (c) Model PP4. (d) Model PP1A. (e) Model PP4A.

included two interactions by which other algal populations negatively affected *P. parvum*: competition for nutrients, and allelopathy. Consequently the population density of *P. parvum* was under-predicted over the course of the year.

In summary, none of the models provided convincing simulations of the seasonal dynamics of *P. parvum*, using the initial parameterization. All models predicted a minimum population at the time of the observed maximum in February. At this time, temperature reached its seasonal minimum while grazing mortality reached its maximum. All models predicted an increase of the population of *P. parvum* through the spring, though this increase did not lead to a high predicted population in late spring for models PP1A and PP4A because the allelopathic effects of cyanobacteria became strong. Otherwise, models PP0, PP1 and PP4 predicted seasonal population peaks of *P. parvum* in late spring, at a time when the observed population was low. All models predicted a late summer minimum for *P. parvum*, followed by population increases in autumn. The improved growth predicted in autumn was associated with reduced inflow, high salinity, low grazing mortality, and moderate (though falling) temperature. Improved growth in autumn is perhaps the one feature of the observed seasonal dynamics of *P. parvum* successfully predicted by these models, although timing of initiation and rate of growth were not predicted precisely.

Sensitivity Analyses and Modified Parameter Sets

To see whether alternative parameter assignments would produce better predictions of the seasonal dynamics of *P. parvum*, a sensitivity analysis was conducted for each model. Most parameters were varied through a range of 0.3× - 3× the initial value, except that grazing susceptibilities (w_i) and the recycling parameter (r) were truncated at 1. Sensitivity analysis was implemented differently for the functions governing responses to temperature, light and salinity, by perturbing the overall shape of the function rather than individual parameters. For algal types other than *P. parvum*, the height of the response function was varied through a range of 0.3× - 3× by changing the growth rate under optimal conditions (μ_{opt}). For *P. parvum*, the response function (Equation 10) is parameterized in terms regression coefficients and reference levels (T_{ref} for temperature, I_{ref} for light, and σ_{ref} for salinity). The regression intercept (β_0) was varied to produce a change in elevation of the growth response. Reference levels T_{ref}, I_{ref} and s_{ref} were also varied, producing rigid translations of the response surfaces for light and salinity along the respective axis. Due to the nonlinearity of the temperature response, similar variations in T_{ref} both translated the response, shifting the optimal temperature, and squeezed or stretched the shape of the response along the temperature axis. For the other taxa, responses to temperature and light were not parameterized in terms of reference values, so shifts in optimum values along with stretching and squeezing were implemented by transforming the forcing data multiplicatively through the range 0.3× - 3×. In addition to truncating some parameter variations at the biologically meaningful limit of 1, the range of 0.3× - 3× was truncated in other instances where very high values of error metrics indicated large errors.

Using the error metrics as screening tools, alternative parameter assignments were selected for further examination if they reduced at least one error metric to below 20% without large increases in other metrics (Table 5). For models PP0, PP1, and PP4,

adjustment of the reference temperature (T_{ref}) for the growth response of *P. parvum* to abiotic conditions (Equation 10) led to predictions that shared several features (Figs. 4A-C): a peak population occurring in late winter and early spring, shortly after the observed peak; a summer minimum population falling far below the observed minimum; and a population increase in autumn and early winter that began later and rose more rapidly than the observed increase at this time. For model PP0, without competitors, the late winter-spring bloom of *P. parvum* was predicted to persist longer than was observed. With competitors, models PP1 and PP4 both predicted termination of the bloom shortly after the time that low populations began to occur in observations. There was little difference between the dynamics predicted by models PP1 and PP4, with parameter T_{ref} decreased (Figs. 4B, C).

Table 5. Error metrics comparing predicted and observed dynamics of *P. parvum* using adjusted parameters as in Fig. 4.

Model	Error in peak density, M_1	Error in average winter natural log density, M_2	Error in peak timing, M_3
PP0	95%	16%	0%
PP1	60%	5%	10%
PP4	50%	0%	10%
PP1A	39%	29%	10%
PP4A	70%	16%	10%

For models PP0, PP1, and PP4, reduction of T_{ref} to values in a range of 6 - 15 °C led to dynamics similar to those illustrated for a value of T_{ref} = 12.5 °C (Fig. 4A-C). The illustrated value severely distorts of the growth response of *P. parvum* to temperature (Fig. 5): for low salinities, growth is impossible above about 20 °C. This distortion strongly contradicts laboratory experiments (Baker et al., 2007, unpublished; Grover et al., 2007), which have consistently shown strong growth potential at temperatures of 20 – 30 °C for salinities down to 1 psu. The very low population density of *P. parvum* predicted during summer by these models with low T_{ref} results directly from this lack of growth at warm temperatures.

For models PP1A and PP4A, in which both allelopathy and resource competition affect *P. parvum*, improved agreement between predicted dynamics and observations was obtained by increasing the parameter β_0 in the growth response of *P. parvum* to abiotic conditions (Equation 10). For model PP1A, an increase of 0.161 d^{-1} to β_0 = -3.37 minimized error metric M_1, and was close to minimal for metrics M_2 and M_3. For model PP4A, an increase of 0.131 d^{-1} to β_0 = -3.4 minimized error metric M_3, and was close to minimal for metrics M_1 and M_2. These changes led to similar predictions of *P. parvum* dynamics (Figs. 4D and E): a peak of population density occurred in late spring – early summer, coming later than the observed peak; although the predicted decline to a summer minimum also came later than the observed decline, the minimum population level in summer broadly agreed with observations; and a population increase was predicted to occur through autumn and early winter, which began later than the observed increase and was somewhat faster. These models with adjusted values of β_0 also predicted a minimum population density for *P. parvum* in mid-winter, at the time of the observed peak.

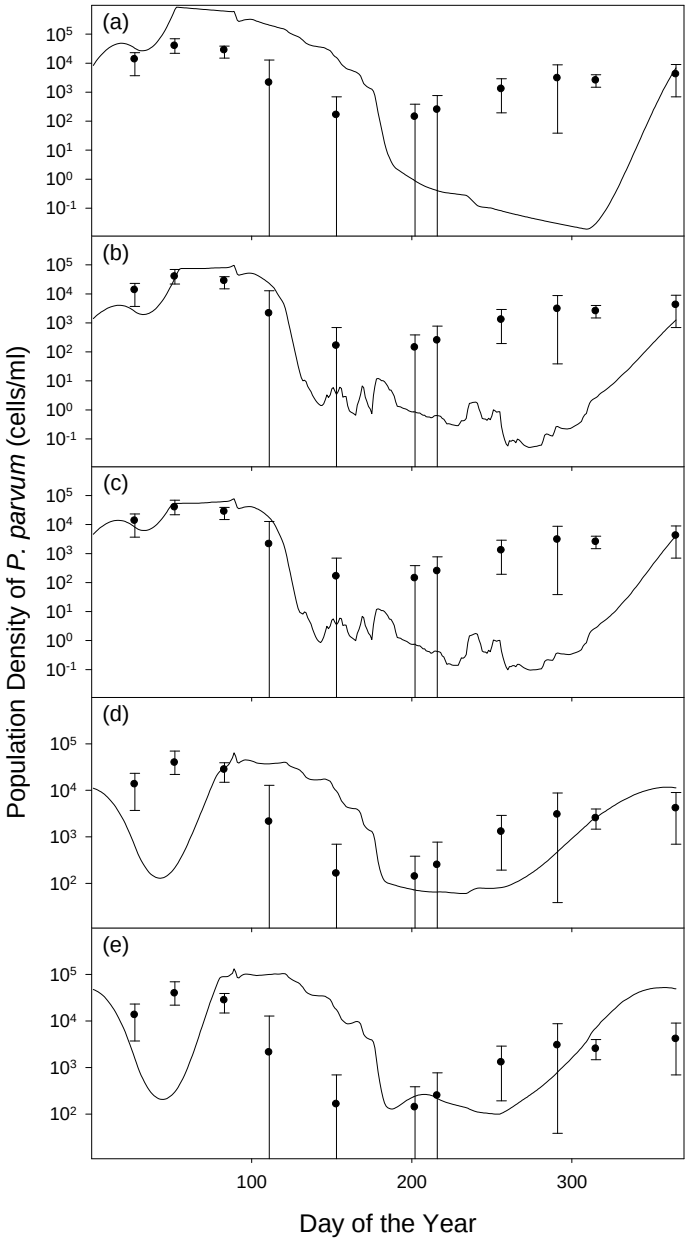

Figure 4. Predicted and observed population dynamics of *P. parvum* in Lake Granbury with modified parameter sets explained in the text. Solid line shows predicted values; symbols show observed values as the average of ten sampling stations. Whiskers show range of sampling stations; when zero observations occurred at some stations, whiskers extend to the bottom of the figure. (a) Model PP0. (b) Model PP1. (c) Model PP4. (d) Model PP1A. (e) Model PP4A.

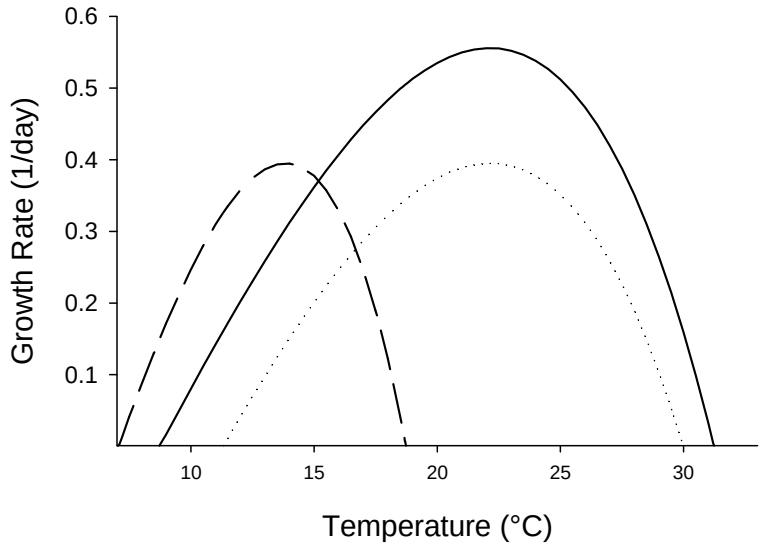

Figure 5. Maximal growth functions for P. parvum in relation to temperature calculated for an irradiance of 222 μmol photons/m^2/s and a salinity of 1.2 psu: dotted line – initial parameterization; dashed line – modified parameterization with reference temperature T_{ref} reduced to 12.5 °C; solid line – modified parameterization with intercept β_0 increased to -3.37 1/d.

For models PP1A and PP4A, increasing β_0 to the values indicated above increase the growth rate of *P. parvum* under all conditions of temperature, irradiance and salinity. The magnitude of this increase is moderate, however (Fig. 5), and is within the experimental and statistical errors arising in the laboratory experiments used to derive Equation (10) describing the growth of *P. parvum* (Baker et al., 2007, unpublished). Higher growth rates than indicated by Equation (10) would also be consistent with the acclimation to temperature and salinity suggested to occur over scales of several weeks by Baker et al. (unpublished). For models PP1A and PP4A, improved agreement between predicted dynamics and observations could also be obtained by decreasing the parameter T_{ref}, as was done for other models, but only if very low and biologically implausible values were used (< 6 °C).

Predictions of all models were sensitive to parameters other than those adjusted to produce Fig. 4. Generally the most influential parameters were those of the functions describing the growth response of *P. parvum* to temperature, light and salinity (Equation 10). In most cases, similar improvements in model performance could be achieved by adjustments of β_0, T_{ref} or σ_{ref}. For models without allelopathy (PP0, PP1, PP4) adjusting T_{ref} produced the greatest agreement with observations, while for those with allelopathy (PP1A, PP4A) adjusting β_0 produced the greatest improvement. Other influential parameters included grazing susceptibilities (w_i) and yields on phosphorus ($Y_{R,i}$). These were left at values determined during initial parameterization because these produced low values for error metrics in all cases examined. In some models, parameters describing the

growth of competing algal types or production of cyanotoxin were influential, but changes from the initially assigned values were associated with tradeoffs in which one error metric declined while another increased.

Further Modifications

The models studied here were constructed to complement an observational study in which abundances of algae other than *P. parvum* are estimated by analysis of phytopigments. The similarity of predictions between models with one other type of algae, parameterized as cyanobacteria, and those with four types, suggests that these particular algae could have a critical influence on the dynamics of *P. parvum*. To explore this idea further, a modification of models PP1A was developed to use observed, monthly cyanobacterial abundances as forcing data. These observations were averaged spatially among the ten sampling stations in Lake Granbury and interpolated daily between sampling dates, as for other forcing data. Observations consisted of the estimated biomass density of cyanobacteria as chlorophyll *a*, so conversion was necessary for model parameters based on cell population densities. The typical cell volume for cyanobacteria in Texas reservoirs was estimated as 35 μm^3, the geometric mean from a database of cell sizes developed during previous studies (Grover and Chrzanowski, 2004, 2005). From this a conversion of 0.2 pg C / μm^3 (Rocha and Duncan, 1985) was used to estimate 7 pg C / cell for cyanobacteria. Because nutrient limitation in field populations of algae typically reduces chlorophyll-to-carbon ratios a relatively low value of 10 μg chl *a* / mg C was adopted here (Chapra, 1997), producing a conversion of 70 fg chl *a* / cell.

The dynamics predicted for *P. parvum* when observations of cyanobacteria are treated as forcing data strongly resemble those predicted by models PP1 and PP4 with initial parameter assignments (Fig. 6A). Results of a sensitivity analysis were also very similar to those models. The best improvements in model performance resulted from adjusting the reference temperature T_{ref} to 12.5 °C in the growth function of *P. parvum*. After this adjustment, predicted dynamics resembled those of models PP1 and PP4 with T_{ref} adjusted (Fig. 6B).

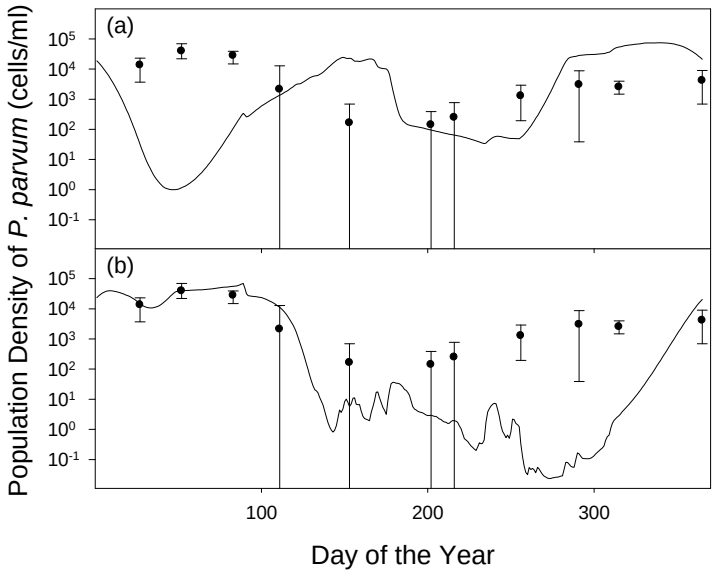

Figure 6. Predicted and observed population dynamics of *P. parvum* in Lake Granbury using observed cyanobacteria abundance as forcing data for model PP1A. Solid line shows predicted values; symbols show observed values as the average of ten sampling stations. Whiskers show range of sampling stations; when zero observations occurred at some stations, whiskers extend to the bottom of the figure. (a) Initial parameterization. (b) Modified parameterization with reference temperature T_{ref} reduced to 12.5 °C.

DISCUSSION

Calibration of the models examined here relates to a paradox long evident in studying blooms of *P. parvum* in Texas inland waters. This species grows optimally at relatively warm temperatures of 25 – 30 °C (Larsen et al., 1993; Larsen and Bryant, 1993; Baker et al., 2007; unpublished), and thus blooms should occur primarily in summer. Yet, blooms in Texas have occurred primarily in winter. Ecologists are familiar with the tendency for species to occur in the field under narrower and usually lower temperatures than those permitting growth in the laboratory (Magnuson et al., 1979). This phenomenon is usually attributed to lack of competition and other biological interactions in the laboratory, and the restrictive action of these processes in natural settings (Hutchinson, 1959). The fundamental niche refers to growth responses to temperature and other factors obtained in the laboratory, while the realized niche refers to those found in nature.

The fundamental niche of *P. parvum* is expressed graphically by Fig. 2A, and models based on this niche err in their predictions (Fig. 3), due to the much different realized niche. Constructing models PP1 and PP4 with competing populations of algae examined the classical expectation that competition for nutrient resources would suffice to alter the fundamental niche and restrict *P. parvum* to occurring under cool temperatures. That expectation was not met, so models PP1A and PP4A were constructed to examine whether an additional process, allelopathy from the competing algae, would

restrict *P. parvum* to cooler temperatures. Without additional adjustments identified during calibration, that expectation was also not met.

Calibration identified two parameter adjustments bringing predicted dynamics of *P. parvum* into closer agreement with observations: (1) modifying the temperature response of *P. parvum* by reducing the parameter T_{ref}, essentially aligning it with the realized niche; and (2) raising the growth rate of *P. parvum* under all conditions, which was effective only for models with allelopathy. Both of these modifications have advantages and disadvantages.

The first alternative is a strong distortion of the temperature response of *P. parvum*. Though it contradicts laboratory data, this distortion accommodates the general notion that the realized niche differs from the fundamental niche, and is a convenient way to improve model predictions when lacking specific knowledge of the ecological processes causing this niche restriction. With this adjustment, models PP1 and PP4 successfully simulate the winter bloom of *P. parvum* in the calibration data and predict its termination at about the right time. The cost of this success comes in summer, when the adjusted temperature response predicts no growth and much lower population density than observed. As a result of under-predicting the population density in summer, the predicted rise of *P. parvum* in autumn is later and faster than observed. This first alternative also violates the spirit of mechanistic modeling – it is an ad hoc adjustment that improves predictions, but whose basis and robustness are unclear.

The second alternative proposes that allelopathy from cyanobacteria negatively impacts *P. parvum*, and calibration further suggests that a modest increase in the growth response of this species brings improves the agreement of predictions with observations. To that extent, this exercise supports the hypothesis that allelopathy from cyanobacteria influences the population dynamics of *P. parvum* in Texas inland waters. The adjustment of the growth response during calibration is within the likely experimental error of the studies supporting the growth response, and has a plausible basis of acclimation that could occur in natural populations experiencing variations in temperature that are slow compared to growth dynamics. Allelopathy models adjusted after calibration successfully simulate the low population density of *P. parvum* during summer and mimic the autumn rise better than models with a distorted temperature response. However, dynamics during winter are not as well simulated. A drop in population density is predicted during the lowest temperatures in February in sharp disagreement with observations. Although this drop is followed by a recovery to near the observed population densities, the resulting spring bloom is predicted to last longer than observed.

Additionally, the mechanistic basis for modeling allelopathy as done here is weak, and the formulation adopted is largely conjectural. Cyanobacteria produce many toxins (Codd et al., 2005). To our knowledge no purified cyanotoxins have been tested for effects on *P. parvum* in laboratory experiments, though culture filtrates from three species of cyanobacteria did not inhibit growth of *P. parvum* (Suikkanen et al., 2004). The models constructed here assume that cyanotoxin production is proportional to the product of population density and growth rate, so that production could be limited either by a low population or by reduced growth, e.g. by nutrient limitation (Orr and Jones, 1998). However, there is evidence that at least one cyanotoxin, nodularin, can be produced by non-growing, nutrient-limited populations (Stolte et al., 2002). The models also attribute toxin production to the entire assemblage of cyanobacteria. In reality, only

particular species and strains of cyanobacteria produce toxins and toxin dynamics are correlated to the waxing and waning of these particular populations (Kardinaal and Visser, 2005). Further information on the susceptibility of *P. parvum* to cyanotoxins, and on cyanotoxin dynamics in Texas inland waters, is required to evaluate and refine (or abandon) this process in models focusing on *P. parvum* blooms.

A number of other model improvements could be contemplated. The representation of grazing mortality in the models presented here is based on the total grazing activity of zooplankton and constant susceptibility coefficients. However, different zooplankton species vary widely in their predation upon different algal species, so constant susceptibilities are unrealistic. As modeled here, the grazing mortality rate is independent of algal population density. This is unlikely to be true, especially for *P. parvum*, where there is evidence that dense, toxic populations inhibit or even kill several types of zooplankton (Tillman, 2003; Sopanen et al., 2006, 2008; Roelke et al., 2007; Brooks et al., this volume). Finally, the use of observational inputs to drive grazing mortality could be problematic in some applications. The detailed information on taxonomic composition required to calculate the community grazing rate is not obtained in many monitoring programs. A simple alternative would be to use proxy data representing typical zooplankton dynamics for the type of habitat being modeled. A more complex alternative would be to simulate the population dynamics of zooplankton, coupled to those of algae, which would require considerable effort for calibration and validation.

The models presented here did not explicitly address the toxicity of *P. parvum*, because of several current uncertainties. It is common to observe dense populations that are not toxic to fish (Roelke et al., unpublished). One class of toxins has been characterized (Murata and Yasumoto, 2000), but there may be others, and little is known of the molecular regulation of toxin production. Toxin production is increased by stresses such as nutrient limitation (Johansson and Granéli, 1999; Granéli and Johansson, 2003) and suboptimal temperature and salinity (Baker et al., 2007), and toxicity to fish but not hemolytic activity correlates with high pH (Shilo and Aschner, 1953; Ulitzur and Shilo, 1964; Padilla 1970; Grover, 2007; Valenti et al., unpublished). However, available information does not provide a strong basis for quantitative model formulation. Fortunately, knowledge of the ecological toxicology of *P. parvum* is advancing rapidly (Granéli and Flynn, 2006; Brooks et al., this volume; Schug et al., this volume).

Mixotrophy on the part of *P. parvum* might also be related to its toxicity. Ingestion of bacteria has been observed under nutrient-limited conditions (Nygaard and Tobiesen, 1993; Legrand et al., 2001), and toxins produced by *P. parvum* can lyse larger microorganisms, making their cellular contents available for ingestion (Skovgaard and Hansen, 2003; Tillman, 2003). Conceivably, mixotrophy could boost the growth rate of *P. parvum* under the cool and dark conditions of winter when pure phototrophy is less favored. For Lake Granbury in particular, water quality concerns also focus on high densities of *E. coli*, which is likely correlated to inputs of organic matter that could stimulate mixotrophic growth. *P. parvum* also forms cysts (Carter, 1937), and like other harmful algae blooms could be related to germination of these resting stages (Sellner et al., 2003), but no information is currently available on factors that regulate encystment and germination in this species.

In conclusion, some first steps in model construction and calibration have been taken to address blooms of *P. parvum* in Texas inland waters. To date, modeling highlights a contradiction between the fundamental niche of this harmful alga, predicting growth under warm temperatures, and the realized niche, wherein high population densities are observed in cool weather. Competition from other algae might partly explain this discrepancy, and the similarity between models with one and four competing populations suggests that it is most important to represent cyanobacteria, and less important to represent other types of algae. Calibration suggests, however, that models with competing algal populations simulate the observed dynamics of *P. parvum* only when adjusted in one of two ways: either allelopathy from cyanobacteria must be included, or the temperature response of *P. parvum* must be altered from laboratory-based expectations to align with the realized niche. The models constructed and calibrated here remain to be evaluated against further data, which is being collected from ongoing studies of Lake Granbury and other Texas lakes. They also serve as a basis for incorporating other processes affecting the population dynamics and toxicity of *P. parvum* as research on this species advances.

ACKNOWLEDGMENTS

This material is based upon work supported by several grants from the Texas Parks and Wildlife Department, Congressional funding through the U.S. Department of Energy, and the U.S. Fish and Wildlife Service. This material is also based upon work supported by the National Science Foundation under Grant No. DEB-0444844.

NOTATION

N_i	Population density of algal type *i* (cells/ml)
i	Index for algal type: *p* – *P. parvum*; *c* – cyanobacteria; *d* – diatoms; *f* – flagellates; *g* – chlorophytes
R	Concentration of dissolved inorganic phosphorus (μmol/l)
S	Concentration of dissolved inorganic nitrogen (μmol/l)
C	Concentration of cyanotoxin (μg/l)
$\mu_i(R,S;\sigma,I,T)$	Population growth rate of algal type *i* as a function of nutrients and environmental conditions (1/d)
$\mu_{maxi}(\sigma,I,T)$	Maximal population growth rate of algal type *i* as a function of environmental conditions (1/d)
$f_i(T)$	Temperature response function for algal type *i* (dimensionless)
$g_i(I)$	Irradiance response function for algal type *i* (dimensionless)
σ	Salinity (practical salinity units, psu)
I	Average water column irradiance (μmol photons/m^2/s)
T	Surface water temperature (°C)
$K_{R,i}$, $K_{S,i}$	Half-saturation constants for phosphorus- and nitrogen-dependent growth of algal type *i*, respectively (μmol/l)
$Y_{R,i}$, $Y_{S,i}$	Yield coefficients on phosphorus and nitrogen for algal type *i*, respectively (cells/μmol)
v_i	Sinking mortality for algal type *i* (1/d)

u_i	Sinking speed for algal type *i* (m/d)
h	Mean depth (m)
m_i	Mortality due to zooplankton grazing for algal type *i* (1/d)
D	Dilution rate (1/d)
R_{in}, S_{in}	Supply concentrations of nitrogen and phosphorus, respectively (μmol/l)
r	Recycling efficiency of zooplankton grazing (dimensionless)
ε_C	Production coefficient for cyanotoxin (μg/cell)
k_C	Decay coefficient for cyanotoxin (1/d)
K_C^I	Inhibition parameter for effect of cyanotoxin on growth of *P. parvum* (μg/l)
h_{SD}	Secchi depth (m)
ε	Vertical attenuation coefficient for irradiance (1/m)
I_0	Irradiance just under the water surface (μmol photons/m^2/s)
CGR	Community grazing rate (1/d)
w_i	Grazing susceptibility parameter for algal type i (dimensionless)
β_j	Coefficients of maximal growth function for *P. parvum* (various dimensions)
σ_{ref}, I_{ref}, T_{ref}	Reference levels of salinity, irradiance and temperature in maximal growth function for *P. parvum* (psu, μmol photons/m^2/s, °C)
$\mu_{\text{opt},i}$	Maximal growth rate of algal type *i* under optimal conditions (1/d)
$f_i(T)$	Temperature response of growth for algal type *i* (dimensionless)
$g_i(I)$	Irradiance response of growth for algal type *i* (dimensionless)

LITERATURE CITED

Babica, P., L. Bláha, and B. Maršálek, 2006. Exploring the Natural Role of Microcystins – A Review of Effects on Photoautotrophic Organisms. Journal of Phycology 42:9-20.

Baker, J.W., 2007. Basic Ecology and Mathematical Modeling of Prymnesium parvum, "Golden Algae", in Texas. Ph.D. Dissertation, The University of Texas at Arlington, Arlington, Texas, USA. Chap. 4.

Baker, J.W., J.P. Grover, B.W. Brooks, F. Ureña-Boeck, D.L. Roelke, R. Errera, and R.L. Kiesling, 2007. Growth and Toxicity of *Prymnesium parvum* (Haptophyta) as a Function of Salinity, Light and Temperature. Journal of Phycology 43:219-227.

Baker, J.W., J.P. Grover, R. Ramachandrannair, C. Black, T.W. Valenti, Jr., B.W. Brooks, and D.L. Roelke, unpublished. Dynamics at the Edge of the Niche: An Experimental Study of the Harmful Alga *Prymnesium parvum*. Submitted to Limnology and Oceanography.

Barkoh, A., D.G. Smith, and J.W. Schlechte, 2003. An effective minimum concentration of un-ionized ammonia nitrogen for controlling *Prymnesium parvum*. North American Journal of Aquaculture 65:220-225.

Buskey, E.J., P.A. Montagna, A.F. Amos, and T.E. Whitledge, 1997. Disruption of Grazer Populations as a Contributing Factor to the Initiation of the Texas Brown Tide Algal Bloom. Limnology and Oceanography 42(5, part 2):1215-1222.

Chapra, S.C. 1997. Surface Water Quality Modeling. McGraw-Hill, New York, USA. Chaps. 33-35.

Carter, N., 1937. New or Interesting Algae from Brackish Water. Archiv für Protistenkunde 90:1-68.

Cloern, J.E., 2001. Our Evolving Conceptual Model of the Coastal Eutrophication Problem. Marine Ecology Progress Series 210:223-253.

Codd, G.A., J. Lindsay, F.M. Young, L.F. Morrison, and J.S. Metcalf, 2005. Harmful Cyanobacteria: From Mass Mortalities to Management Measures. *In:* Harmful Cyanobacteria, Huisman, J., H.C.P. Matthijs, and P.M. Visser (Editors). Springer, Dordrecht, The Netherlands, pp. 1-23.

Cousins, I.T., D.J. Bealing, H.A. James, and A. Sutton, 1996. Biodegradation of Microcystin-LR by Indigenous Mixed Bacterial Populations. Water Research 30(2):481-485.

Edvardsen, B. and I. Imai, 2006. The Ecology of Harmful Flagellates within Prymnesiophyceae and Raphidophyceae. *In:* Ecology of Harmful Algae, Granéli, E. and J.T. Turner (Editors), Springer-Verlag, Berlin, Germany, pp. 67-79.

Edvardsen, B. and E. Paasche, 1998. Bloom Dynamic and Physiology of *Prymnesium* and *Chrysochromulina*. *In:* Physiological Ecology of Harmful Algal Blooms, Anderson, D.M., A.D. Cembella, and G.M. Hallegraeff (Editors). Springer-Verlag, Berlin, Germany, pp. 193-208.

Errera, R.M., D.L. Roelke, R.L. Kiesling, B.W. Brooks, J.P. Grover, L. Schwierzke, F. Ureña-Boeck, J.W. Baker, and J.L. Pinckney, 2008. Effect of Imbalanced Nutrients and immigration on *Prymnesium parvum* Community Dominance and Toxicity: Results from In-Lake Microcosm Experiments. Aquatic Microbial Ecology, in press.

Fromme, H., A. Köhler, R. Krause, and D. Führling, 2000. Occurrence of Cyanobacterial Toxins – Microcystins and Anatoxin-a – in Berlin Water Bodies with Implications to Human Health and Regulations. Environmental Toxicology 15:120-130.

Glibert, P.M., J. Harrison, C. Heil, and S. Seitzinger. 2006. Escalating Worldwide Use of Urea – A Global Change Contributing to Coastal Eutrophication. Biogeochemistry 77:441-463.

Gotham, I.J. and G-Y. Rhee, 1981a. Comparative Kinetic Studies of Phosphate-Limited Growth and Phosphate Uptake in Phytoplankton in Continuous Culture. Journal of Phycology 17:257-265.

Gotham, I.J. and G-Y. Rhee, 1981b. Comparative Kinetic Studies of Nitrate-Limited Growth and Nitrate Uptake in Phytoplankton in Continuous Culture. Journal of Phycology 17:309-314..

Granéli, E. and K. Flynn, 2006. Chemical and Physical Factors Influencing Toxin Content. *In:* Ecology of Harmful Algae, Granéli, E. and J.T. Turner (Editors), Springer-Verlag, Berlin, Germany, pp. 229-241..

Granéli, E. and P.J. Hansen, 2006. Allelopathy in Harmful Algae: A Mechanism to Compete for Resources? *In:* Ecology of Harmful Algae, Granéli, E. and J.T. Turner (Editors), Springer-Verlag, Berlin, Germany, pp. 189-201.

Granéli, E., and N. Johansson, 2003. Effects of the Toxic Haptophyte *Prymnesium parvum* on the Survival and Feeding of a Ciliate: The Influence of Different Nutrient Conditions. Marine Ecology Progress Series 254:49-56.

Grover, J.P. 1989. Phosphorus-Dependent Growth Kinetics of 11 Species of Freshwater Algae. Limnology and Oceanography 34:339-346.
Grover, J.P., 1997. Resource Competition. Chapman and Hall, London, UK. Chap. 2.
Grover, J.P., J.W. Baker, F. Ureña-Boeck, B.W. Brooks, R.M. Errera, D.L. Roelke, and R.L. Kiesling, 2007. Laboratory Tests of Ammonium and Barley Straw Extract as Agents to Suppress Abundance of the Harmful Alga *Prymnesium parvum* and its Toxicity to Fish. Water Research 41:2503-2512.
Grover, J.P. and T.H. Chrzanowski, 2004. Limiting Resources, Disturbance, and Diversity in Phytoplankton Communities. Ecological Monographs 74:533-551.
Grover, J.P. and T.H. Chrzanowski, 2005. Seasonal Dynamics of Phytoplankton in Two Warm Temperate Reservoirs: Association of Taxonomic Composition with Temperature. Journal of Plankton Research 27:1-17.
Grover, J.P., R.W. Sterner, and J.L. Robinson, 1999. Algal Growth in Warm Temperate Reservoirs: Nutrient-Dependent Kinetics of Individual Taxa and Seasonal Patterns of Dominance. Archiv für Hydrobiology 145:1-23.
Hallegraeff, G.M., 1993. A Review of Harmful Algal Blooms and Their Apparent Global Increase. Phycologia 32(2):79-99.
Hallegraeff, G.M. and S. Gollasch, 2006. Anthropogenic Introductions of Microalgae. *In:* Ecology of Harmful Algae, Granéli, E. and J.T. Turner (Editors), Springer-Verlag, Berlin, Germany, pp. 380-390.
Hansen, P.J., P.K. Bjørnsen, and B.W. Hansen, 1997. Zooplankton Grazing and Growth: Scaling Within the 2 – 2,000-μm Body Size Range. Limnology and Oceanography 42(4):687-704.
Heresztyn, T. and B.C. Nicholson. 1997. Nodularin Concentrations in Lakes Alexandrina and Albert, South Australia, During a Bloom of the Cyanobacterium (Blue-Green Alga) *Nodularia spumigena* and Degradation of the Toxin. Environmental Toxicology and Water Quality 12 (4):273-282.
Hu, S. and D.-Y. Zhang, 1993. The Effects of Initial Population Density on the Competition for Limiting Nutrients in Two Freshwater Algae. Oecologia 96:569-574.
Hutchinson, G.E. Concluding Remarks. Cold Spring Harbor Symposia on Quantitative Biology 22:415-427.
Idso, S.B. and R.G. Gilbert, 1974. On the Universality of the Poole and Atkins Secchi Disk – Light Extinction Equation. Journal of Applied Ecology 11:399-401.
Johansson, N., and E. Granéli, 1999. Influence of Different Nutrient Conditions on Cell Density, Chemical Composition and Toxicity of *Prymnesium parvum* (Haptophyta) in Semi-Continuous Cultures). Journal of Experimental Marine Biology and Ecology 239:243-258.
Kardinaal, W.E.A. and P.M. Visser, 2005. Dynamics of Cyanobacterial Toxins: Sources of Variability in Microcystin Concentrations. *In:* Harmful Cyanobacteria, Huisman, J., H.C.P. Matthijs, and P.M. Visser (Editors). Springer, Dordrecht, The Netherlands, pp. 41-63.
Kirk, J.T.O., 1983. Light and Photosynthesis in Aquatic Ecosystems. Cambridge University Press, Cambridge, UK. Chap. 2.

Larsen, A., and S. Bryant, 1998. Growth Rate and Toxicity of *Prymnesium parvum* and *Prymnesium patelliferum* (Haptophyta) in Response to Changes in Salinity, Light and Temperature. Sarsia 83:409-418.

Larsen, A., W. Eikrem, and E. Paasche, 1993. Growth and Toxicity in *Prymnesium patelliferum* (Prymnesiophyceae) Isolated From Norwegian Waters. Canadian .Journal of Botany 71:1357-1362.

Lee, D.-Y. and G-Y. Rhee. 1999. Kinetics of Growth and Death in *Anabaena flos-aquae* (Cyanobacteria) Under Light Limitation and Supersaturation. Journal of Phycology 35(4):700-709.

Legrand, C., N. Johansson, G. Johnsen, K.Y. Borsheim, and E. Granéli, 2001. Phagotrophy and Toxicity Variation in the Mixotrophic *Prymnesium parvum* (Haptophyceae). Limnology and Oceanography 46(5):1208-1214.

Legrand, C., K. Rengefors, G.O. Fistarol, and E. Granéli, 2003. Allelopathy in Phytoplankton – Biochemical, Ecological, and Evolutionary Aspects. Phycologia 42(4):405-419.

Lewis, W.M., Jr., 1986. Evolutionary Interpretations of Allelochemical Interactions in Phytoplankton Algae. American Naturalist 127(2):184-194.

Litchman, E., 2000. Growth Rates of Phytoplankton Under Fluctuating Light. Freshwater Biology 44(2):223-235.

Magnuson, J.J., L.B. Crowder, and P.A. Medvick, 1979. Temperature as an Ecological Resource. American Zoologist 19:331-343.

Murata, M. and T. Yasumoto, 2000. The Structure Elucidation and Biological Activities of High Molecular Weight Algal Toxins: Maitotoxins, Prymnesins and Zooxanthellatoxins. Natural Products Reports 17:293-314.

Nygaard, K. and A. Tobiesen. 1993. Bacterivory in Algae: A Survival Strategy During Nutrient Limitation. Limnology and Oceanography 38(2):273-279.

Orr, J.T. and G.J. Jones. 1998. Relationship Between Microcystin Production and Cell Division Rates in Nitrogen-Limited *Microcystis aeruginosa* Cultures. Limnology and Oceanography 43(7):1604-1614.

Otterstrøm, C.V. and E. Steeman Nielsen, 1940. Two Cases of Extensive Mortality in Fishes Caused by the Flagellate *Prymnesium parvum* (Carter). Report of the Danish Biological Station 44:1-24.

Padilla, G.M. 1970. Growth and toxigenesis of the chrysomonad *Prymnesium parvum* as a function of salinity. Journal of Protozoology 17: 546-462.

Paerl, H.W., 1997. Coastal Eutrophication and Harmful Algal Blooms: Importance of Atmospheric Deposition and Groundwater as "New" Nitrogen and Other Nutrient Sources. Limnology and Oceanography 42(5, part 2):1154-1165.

Paerl, H.W., 1998. Structure and Function of Anthropogenically Altered Microbial Communities in Coastal Waters. Current Opinion in Microbiology 1:296-302.

Park, H.-D., C. Iwami, M.F. Watanabe, K.-I. Harada, T. Okino, and H. Hayashi. 1998. Temporal Variabilities of the Concentrations of Intra- and Extracellular Microcystin and Toxic *Microcystis* Species in a Hypereutrophic Lake, Lake Suwa, Japan (1991-1994). Environmental Toxicology and Water Quality 13:61-72.

Pohnert, G., M. Steinke, and R. Tollrian, 2007. Chemical Cues, Defense Metabolites and the Shaping of Pelagic Interspecific Interactions. Trends in Ecology and Evolution 22(4):198-204.

Press, W.H., B.P. Flannery, S.A. Teukolsky, and W.T. Vetterling, 1986. Numerical Recipes: The Art of Scientific Computing, Cambridge University Press, Cambridge, UK. Chap. 15.

Reynolds, C.S. 2006. The Ecology of Phytoplankton. Cambridge University Press, Cambridge, UK. Chap. 2.

Rhee, G-Y., 1982. Effects of Environmental Factors and Their Interactions on Phytoplankton Growth. Advances in Microbial Ecology 6:33-74.

Rocha, O. and A. Duncan, 1985. The Relationship Between Cell Carbon and Cell Volume in Freshwater Algal Species Used in Zooplanktonic Studies. Journal of Plankton Research 7:279-294.

Roelke, D., Y. Buyukates, M. Williams, and J. Jean. 2004. Interannual Variability in the Seasonal Plankton Succession of a Shallow, Warm-Water Lake. Hydrobiologia 513:205-218.

Roelke, D.L., R.M. Errera, R. Kiesling, B.W. Brooks, J.P. Grover, L. Schwierzke, F. Ureña-Boeck, J. Baker, and J.L. Pinckney, 2007. Effects of Nutrient Enrichment on *Prymneisum parvum* Population Dynamics and Toxicity: Results from Field Experiments, Lake Possum Kingdom, USA. Aquatic Microbial Ecology 46:125-140.

Schwierzke, L., D.L. Roelke, B.W. Brooks, J.P. Grover, and J.L. Pinckney, unpublished. The Role of Grazers and Virus in *Prymnesium parvum* Bloom Termination: In-Lake Experiments from Lake Whitney (Texas, USA). Submitted to Harmful Algae?

Sellner, K.G., G.J. Doucette, and G.J. Kirkpatrick, 2003. Harmful Algal Blooms: Causes, Impacts, and Detection. Journal of Industrial Microbiology and Biotechnology 30:383-406.

Shilo, M. and M. Aschner, 1953. Factors governing the toxicity of cultures containing the phytoflagellate *Prymnesium parvum* Carter. Journal of General Microbiology 8:333-343.

Skovgaard, A. and P.J. Hansen, 2003. Food Uptake in the Harmful Alga Prymnesium parvum Mediated by Excreted Toxins. Limnology and Oceanography 48(3):1161-1166.

Smayda, T.J., 1989. Primary Production and the Global Epidemic of Phytoplankton Blooms in the Sea: A Linkage? *In:* Novel Phytoplankton Blooms, Cosper, E.M., V.M. Bricelj, and E.J. Carpenter (Editors). Springer-Verlag, Berlin, Germany, pp. 449-483.

Sommer, U., 1991. A Comparison of the Droop and the Monod Models of Nutrient Limited Growth Applied to Natural Populations of Phytoplankton. Functional Ecology 5:535-544.

Sopanen, S., M. Koski, P. Kuuppo, P. Uronen, C. Legrand, and T. Tamminen. 2006. Toxic Haptophyte Prymnesium parvum Affects Grazing, Survival, Egestion and Egg Production of the Calanoid Copepods *Eurytemora affinis* and *Acartia bifilosa*. Marine Ecology Progress Series 327:223-232.

Sopanen, S., M. Koski, P. Uronen, P. Kuuppo, S. Lehtinen, C. Legrand, and T. Tamminen, 2008. *Prymnesium parvum* Exotoxins Affect the Grazing and Viability of the Calanoid Copepod *Eurytemora affinis*. Marine Ecology Progress Series 361:191-202.

Sterner, R.W., 1989. The Role of Grazers in Phytoplankton Succession. *In:* Plankton Ecology: Succession in Plankton Communities, Sommer, U. (Editor). Springer-Verlag, Berlin, Germany, pp 107-170.

Stolte, W., C. Karlsson, P. Carlsson, and E. Granéli, 2002. Modeling the Increase in Nodularin Content in Baltic Sea *Nodularia spumigena* During Stationary Phase in Phosphorus-Limited Batch Cultures. FEMS Microbiology Ecology 41:211-230.

Suikkanen, S., G.O. Fistarol, and E. Granéli. 2004. Allelopathic Effects of the Baltic Cyanobacteria *Nodularis spumigena*, *Aphanizomenon flos-aquae*, and *Anabaena lemmermanii* on Algal Monocultures. Journal of Experimental Marine Biology and Ecology 308:85-101.

Sunda, W.G., E. Granéli, and C.J. Gobler, 2006. Positive Feedback and the Development and Persistence of Ecosystem Disruptive Algal Blooms. Journal of Phycology 42:963-974.

Thomann, R.V. and J.A. Mueller, 1987. Principles of Surface Water Quality Modeling and Control. HarperCollins, New York, USA. Chap. 7.

Tillman, U., 2003. Kill and Eat Your Predator: A Winning Strategy of the Planktonic Flagellate *Prymnesium parvum*. Aquatic Microbial Ecology 32:73-84.

Turner, J.T. and P.A. Tester, 1997. Toxic Marine Phytoplankton, Zooplankton Grazers, and Pelagic Food Webs. Limnology and Oceanography 42(5, part 2):1203-1214.

Ulitzur, S. and M. Shilo. 1964. A sensitive assay system for determination of the ichthyotoxicity of *Prymnesium parvum*. Journal of General Microbiology 36: 161-169.

Van Dolah, F.M., 2000. Marine Algal Toxins: Origins, Health Effects, and Their Increased Occurrence. Environmental Health Perspectives 108(supplement 1):133-141.

Wetzel, R.G. 2001. Limnology, 3rd ed. Academic Press, San Diego, California, USA. Chap. 5.

Wetzel, R.G. and G.E. Likens, 1991. Limnological Analyses, 2nd ed. Springer-Verlag, Berlin, Germany. Chap. 11.